

# **$\beta$ -FUNCTIONALIZED CHLORINS AND PORPHYRINS: SYNTHESIS, SPECTRAL AND REDOX PROPERTIES**

**PH. D. THESIS**

*by*

**NIVEDITA CHAUDHRI**



**DEPARTMENT OF CHEMISTRY  
INDIAN INSTITUTE OF TECHNOLOGY ROORKEE  
ROORKEE-247667 (INDIA)  
MARCH, 2018**

# **$\beta$ -FUNCTIONALIZED CHLORINS AND PORPHYRINS: SYNTHESIS, SPECTRAL AND REDOX PROPERTIES**

**A THESIS**

*Submitted in partial fulfilment of the  
Requirement for the award of the degree*

*of*

**DOCTOR OF PHILOSOPHY**

*in*

**CHEMISTRY**

*by*

**NIVEDITA CHAUDHRI**



**DEPARTMENT OF CHEMISTRY  
INDIAN INSTITUTE OF TECHNOLOGY ROORKEE  
ROORKEE-247667 (INDIA)  
MARCH, 2018**



**©INDIAN INSTITUTE OF TECHNOLOGY ROORKEE ROORKEE-2018  
ALL RIGHTS RESERVED**



# INDIAN INSTITUTE OF TECHNOLOGY ROORKEE ROORKEE

## CANDIDATE'S DECLARATION

I hereby certify that the work which is being presented in the thesis entitled “ **$\beta$ -FUNCTIONALIZED CHLORINS AND PORPHYRINS: SYNTHESIS, SPECTRAL AND REDOX PROPERTIES**” in partial fulfilment of the requirements for the award of the Degree of Doctor of Philosophy and submitted in the Department of Chemistry of the Indian Institute of Technology Roorkee, Roorkee is an authentic record of my own work carried out during a period from January, 2013 to March, 2018 under the supervision of Dr. M. Sankar, Associate Professor, Department of Chemistry, Indian Institute of Technology Roorkee, Roorkee.

The matter presented in the thesis has not been submitted by me for the award of any other degree of this or any other Institute.

(Nivedita Chaudhri)

This is to certify that the above statement made by the candidate is correct to the best of my knowledge.

(M. Sankar)  
Supervisor

The PhD Viva-Voce Examination of **Miss Nivedita Chaudhri**, Research Scholar, has been held on 04.05.2018.

Chairman, SRC

Signature of External Examiner

This is to certify that the student has made all the corrections in the thesis.

Signature of Supervisor

Head of the Department



## ACKNOWLEDGEMENTS

---

*Completion of this doctoral dissertation was not possible without support of several people. It is very difficult to thank everyone individually but I would like to express my deep gratitude to all of them who have directly or indirectly helped me throughout my doctoral program.*

*First of all I bow my head in front of almighty GOD for all his divine blessings showered on me to reach at this brink of giving a final shape of my dream. My first and foremost thank and humble reverence goes to my Ph.D. supervisor Dr. M. SANKAR, who allowed me to work in his research group and exemplified to me the meaning of research. I feel equally glad for the motivation, guidance, valuable suggestions and feedback that he has provided throughout my research career at IIT Roorkee. I deeply thank him for his encouragement that carried me on through difficult times and for his insights and useful suggestions that helped to shape my research skills. He has always made himself available to clarify my doubts despite his busy schedules and I consider it as a great opportunity to do my doctoral program under his guidance and to learn from his research expertise. I am highly indebted for his gentle and benign behavior and his patience in correcting mistakes during my research work. I am also heartily thankful to Mrs. Ananthalakshmi Sankar, for her care, love and kindness towards me and providing homely environment throughout my Ph. D. duration.*

*I am very thankful to Prof. M. R. Maurya, Head of the Department (HOD) Chemistry to arranging the necessary infrastructures and his kind support to pursue my research work successfully. Besides my supervisor, I would like to thank my student research committee (SRC): Dr. P. Jeevanandam (SRC Chairman), Dr. R. K. Peddintti (Internal Expert), and Dr. P Gopinath (External Expert) not only for their insightful comments and encouragement but also for the hard question which incited me to widen my research from various perspectives.*

*I am grateful to Prof. U. P. Singh and Dr. Neetu Singh for their generous help in Single crystal XRD data collection. I am thankful to Dr. Kiran Ambatipudi and Prof. R. Prasad, Department of Biotechnology, IIT Roorkee, for their kind help in MALDI-TOF measurements. I am also expressing my thanks to Dr. Bhupendra singh, Institute Instrument Centre, IIT Roorkee, for collecting fluorescence lifetime data.*

*A good support system is important to surviving and staying sane in any institution. I was lucky to have two seniors cum friends in IIT Roorkee and they are Dr. Nitika Grover and Dr. Sweety Rathi. They formed the core of my research time and I feel cheerful to the wonderful time especially tea time and all the fun what we had in IITR. Dr. Grover is a wonderful and generous friend without her support it was not possible for me to complete my dissertation. I admire her positive outlook.*

*My heartfelt thanks to my present and former labmates Dr. Ravi Kumar, Dr. Pinky Yadav, Dr. Mandeep K. Chahal, Dr. Nidhi Sharma, Kamal Prakash, Tawseef A. Dar, Pinki Rathi, Gaurav, Sandeep, Renu, Inderpal, Chitranjan, Amit Tyagi, Amit Kumar, B. Madhusudan, Upasna, Anshul, Mandeep Khan and Neeraj for their untiring and continued support during my work.*

*My sincere thanks are extended to my dear friends especially Dr. Manisha Singh, Ranjana Kumari, Mrs. Anshul Chaudhary, Kuldeep Singh, Munindra Singh. Their love, timely help and friendship will always be remembered. I also cherish my friendship with Neha Taneja, Sapna Singh, V. Joseph. Neetu Yadav, Shweta Kaushik and Shilpi Pal for their kindness, well wishes and constant prayers*

*“At the end of the day, the most overwhelming key to a child's success is the positive involvements of parents” My words are not enough to express my love, reverence for my parents Mr. Ravindra Singh and Mrs. Vimlesh Devi for their unconditional love, blessings and sacrifices what they rendered to me. Side by side, or far apart our grandparents are always in our heart. My beloved grandparents late Mr. Ramnath Singh and Mrs. Nawab Kaur deserve a special line of respect and sincere gratitude for their unending love and care. I owe my deep gratitude to my other grandparents Mr. Prakash Singh and Mrs. Saroj Devi for their love and encouragement in all the time. The most precious gifts from my parents and GOD are my sister and brother. I express my heartfelt thanks to my dearest sister and brother-in-law Mrs. Poonam and Mr. Sumit Chaudhary for their love, motivation and care. I am in dearth of proper words to express my abounding feeling to my younger brother Mr. Vineet for his constant support, love and affection throughout my life.*

*A special mention goes to my joyful and lovely nephew Divyansh (Laddu), niece (Manya) and all my little cousins Nidhi, Prachi, Shivansh and Devansh for their love. In their company I forget all worries.*

*Finally, an honorable mention goes to my all family members and relatives for their love and prayers. I was extraordinary fortunate to having father like uncles especially Mr. Virendra Singh and Dharamveer Singh Sindhu. I thanks to them from bottom of my heart for their endless motivation, support and love. I owe my deep gratitude to my aunty Mrs. Renu for her motherly love and care. Many thanks to my all cousins and I would like to especially thank Monika Sindhu and Soni Sindhu for their encouragement and love.*

*I express my regards and respect to all the teachers who have ever taught me. Without their prior teaching, blessings and motivation I could not able to start and embarked the research. Thanks for planting the seeds of Knowledge.*

*The final assistance provided by Council of Scientific & Industrial Research (CSIR), India, that made my research work very smooth and prompt, is gratefully acknowledged.*

*I greatly appreciate the help and co-operation extended by nonteaching and technical staff in IIT Roorkee. I am extremely thankful to those people whose names have been unknowingly left. For that I apologize and believe that they will be always with me.*

*Last but not the least I feel privileged for my stay at IIT Roorkee and providing me a great work culture and a wonderful ambience.*

**Nivedita Chaudhri**



## ABSTRACT

---

Porphyrins are naturally occurring tetrapyrroles and utilized as model compounds for many biological and material applications. Due to their conformational flexibility, porphyrins can adopt a range of nonplanar conformations which is needed for a variety of biological functions.  $\beta$ -Functionalization of porphyrins results into varying degrees of porphyrin core confirmation, intriguing photophysical and electrochemical redox properties. Herein, we focused on the synthesis of  $\beta$ -functionalized novel chlorins, porphyrins and benzoporphyrins derived from 2-nitroporphyrin in order to tune their structural, photophysical and electrochemical redox properties. The proposed thesis will be consisting of the following chapters.

**Chapter 1** deals with the general introduction to tetrapyrroles, laboratory synthesis of porphyrin,  $\beta$ -functionalized porphyrinoids and their potential applications in dye-sensitized solar cells (DSSCs), photodynamic therapy (PDT), chemosensing, nonlinear optics (NLO) and catalysis.

**Chapter 2** describes about the versatile synthetic route for  $\beta$ -functionalized chlorins and porphyrins by varying the size of Michael donors. Size dependent approach was applied for the fine-tuning of product formation from porphyrins to chlorins. Notably, we were able to isolate mono/trisubstituted porphyrin and/or di/tetra-substituted chlorin from one-pot synthesis. Single-crystal X-ray diffraction analysis revealed the quasiplanar to moderate nonplanar conformation of chlorins due to *trans* orientation of the  $\beta$ -substituents, whereas porphyrins exhibited higher mean plane deviation of 24-atom core ( $\Delta_{24}$ ) as compared to chlorins.  $\beta$ -Functionalized chlorins exhibited lower protonation constants and much higher deprotonation constants as compared to porphyrins revealing the combined effect of the conformation of macrocyclic core and the electronic nature of  $\beta$ -substituents. Facile synthesis of porphyrins and/or chlorins based on the size of Michael donor employed and in turn resulted in tunable photophysical and electrochemical redox properties are the significant features of the present work.

**Chapter 3** describes the facile selective conversion of planar *trans*-chlorins into highly twisted doubly fused-porphyrins or -chlorins *via* oxidative fusion.  $\beta$ -to-*ortho*-phenyl doubly fused-porphyrins (DFPs) or -chlorins (DFCs) were regioselectively synthesized in good to excellent yields (70-92%) under mild reaction conditions with high atom economy. The product selectivity was controlled by the presence or absence of Ni(II) ion in the macrocyclic core. Ni(II) *trans*-chlorins selectively yielded Ni(II) difused porphyrins NiDFPs whereas free base *trans*-chlorins

afforded only free base difused chlorins H<sub>2</sub>DFCs. The synthesized fused porphyrinoids exhibited significantly red-shifted spectral features ( $\Delta\lambda_{\text{max}} = 16\text{-}53\text{ nm}$ ) of Soret band due to extended  $\pi$ -conjugation and highly twisted macrocyclic conformation (twist angle  $\sim 20\text{-}34^\circ$ ) with tunable electrochemical redox properties. Inner core NHs of fused chlorins exhibited tremendous downfield shift ( $\Delta\delta = 1.71\text{-}2.02\text{ ppm}$ ) as compared to their precursors. The overall protonation constants for H<sub>2</sub>DFC(IND)(X)<sub>2</sub> (X = H, Br, Ph) were profoundly higher ( $\sim 40\text{-}60$  folds) as compared to H<sub>2</sub>DFC(MN)(X)<sub>2</sub> (X = H, Br, Ph) due to the combined effect of electronic nature of the substituents and nonplanarity of the macrocyclic core. Overall this chapter describes the facile synthetic routes to electronically tunable  $\beta$ -modified porphyrins and chlorins.

**Chapter 4** deals with nickel acetate catalyzed autoxidation of free base *trans*-chlorins into monofused Ni(II) porphyrins. One flask synthesis of  $\beta$ -to-*ortho*-phenyl monofused porphyrins with indanedione functionalities has been achieved *via* metal mediated oxidative fusion of free base *trans*-chlorins. Extended  $\pi$ -conjugation of porphyrins aromatic circuit was accomplished by connecting  $\beta$ -pyrrolic indanedione groups with *meso-ortho*-phenyls. Compared to the unfused precursors i.e. *trans*-chlorins, these monofused porphyrins and their Co(II), Ni(II), Cu(II) and Zn(II) complexes have shown a spectacular bathochromic shift of Soret as well as the longest wavelength bands in the absorption spectra. NiMFP(IND)R<sub>2</sub> (where R = H and Ph) were best described as typically *ruffled* due to their high  $\Delta 24$  and  $\Delta C_\beta$  as compared to the Zinc(II) complexes. Notably, Ni(II) complexes NiMFP(IND) (**1**) and NiMFP(IND)Ph<sub>2</sub> (**3**) exhibited metal centered oxidation (Ni<sup>II</sup>/Ni<sup>III</sup>) due to extended  $\pi$ -conjugation and electronic nature of  $\beta$ -substituents. Monofused Ni(II) complexes (Ni(II)MFP(IND)s) have shown slightly higher HOMO-LUMO gap (80-150 mV) as compared to corresponding difused porphyrins (Ni(II)DFP(IND)<sub>2</sub>s).

**Chapter 5** describes the synthesis of 2-nitro-benzoporphyrin using Heck coupling reaction of NiTPP(NO<sub>2</sub>)Br<sub>2</sub> which further treated with active methylene compounds (malononitrile and indane-1,3-dione) to obtain the corresponding *trans*-benzochlorins. The oxidative fusion of benzochlorins using DDQ resulted into triply fused porphyrins. These doubly fused benzoporphyrins exhibited broadened and red-shifted UV-Vis spectra as compared to simple difused systems due to extended  $\pi$ -conjugation and enhanced nonplanarity provided by fused benzene ring at  $\beta$ - $\beta'$  position. In contrast to planar *trans*-chlorins or simple doubly fused porphyrins, a nice alteration in Q/B ratio was observed for antipodal  $\beta$ - $\beta'$  fused porphyrins. The



values for Q/B ratio have been found very high in these *meso*- $\beta$ ,  $\beta$ - $\beta'$  fused porphyrins which again described the impact of enhanced nonplanarity on the electronic properties of the macrocyclic skeleton.

**Chapter 6** deals with the synthesis of  $\beta$ -trisubstituted “push-pull” porphyrins. NiTPP(NO<sub>2</sub>)R<sub>2</sub> (where R = Br and Ph) have shown nitroalkene type reactivity towards active methylene compounds (acetylacetone and ethyl acetoacetate) for Michael addition reactions to obtain corresponding porphyrins. Notably, in case of ethyl acetoacetate appended porphyrin, the high temperature favors the rapid cleavage of C-C bond which resulted into the dissociation of COCH<sub>3</sub> group and formation of ester appended porphyrins instead of desired product. The diketone or ester has little influence on the absorption and fluorescence profiles inducing small bathochromic shifts and slight decrement in fluorescence intensity and quantum yield as compared to the precursor 2-nitroporphyrin whereas a noticeable effect of acetylacetone group on the redox properties have been observed. Diketone appended porphyrins have shown multiple oxidation and reduction due to the presence of keto-enol tautomerism. The impact of the antipodal  $\beta$ -substituent on the redox potentials has also been observed.

**Chapter 7** describes about the facile synthesis of perchloro-2-nitro-*meso*-tetraphenylporphyrin and its metal complexes (Co<sup>II</sup>, Ni<sup>II</sup>, Cu<sup>II</sup> and Zn<sup>II</sup>). The data compared with homosubstituted porphyrins i.e. MTPPCl<sub>8</sub> to highlight the effect of nitro group over their conformation as well as their spectral properties. Nitro bearing porphyrins exhibited 10-15 nm red shifts in the electronic spectra and dramatic anodic shift in the reduction potentials. Free base perhaloporphyrins exhibited colorimetric responses toward highly basic anions such as CN<sup>-</sup>, F<sup>-</sup>, CH<sub>3</sub>COO<sup>-</sup> and H<sub>2</sub>PO<sub>4</sub><sup>-</sup> ions and being able to detect these anions in nanomolar concentration. The red-shifted electronic spectral features, the higher  $\beta_2$  values for deprotonation and anion recognition were interpreted in terms of enhanced nonplanarity and electron withdrawing effect of NO<sub>2</sub> and/or halo substituents. The large anodic shift in voltammetric studies and disappearance of <sup>1</sup>H NMR signals of imino protons strongly support the anion induced deprotonation. The electron deficient Co(II) perhaloporphyrins were utilized as sensors for the selective rapid visual detection of cyanide ions for the first time in porphyrin chemistry.

**Chapter 8** concludes the results obtained in the proposed thesis with future perspectives.





## List of publications Published/Communicated

1. **Nivedita Chauhri**, Nitika Grover and M. Sankar\* Versatile Synthetic Route for  $\beta$ -Functionalized Chlorins and Porphyrins by Varying the Size of Michael Donors: Syntheses, Photophysical, and Electrochemical Redox Properties. *Inorg. Chem.* **2017**, *56*, 11532-11545 (*Highlighted as HOT paper*).
2. Nitika Grover<sup>§</sup>, **Nivedita Chaudhri**<sup>§</sup> and M. Sankar\* Facile Conversion of Ni(II) Cyclopropylchlorins into Novel  $\beta$ -Substituted Porphyrins through Acid-Catalyzed Ring-Opening Reaction. *Inorg. Chem.* **2017**, *56*, 424-437 (*Highlighted as HOT paper*).  
<sup>§</sup>contributed equally to this work.
3. **Nivedita Chaudhri**, Nitika Grover, and M. Sankar\* Selective Conversion of Planar *trans*-Chlorins into Highly Twisted Doubly Fused-Porphyrins or -Chlorins *via* Oxidative Fusion. *Inorg. Chem.* **2018**, (*Manuscript revised and submitted*).
4. **Nivedita Chaudhri**, Nitika Grover, and M. Sankar\* Nickel Acetate Induced Skeleton Rearrangement of Free Base *trans*-Chlorins into Monofused Ni<sup>II</sup> Porphyrins by One Pot Synthesis. *Inorg. Chem.* **2018**, (*Manuscript revised and submitted*).
5. **Nivedita Chaudhri** and M. Sankar\* Colorimetric “Naked Eye” Detection of CN<sup>-</sup>, F<sup>-</sup>, CH<sub>3</sub>COO<sup>-</sup> and H<sub>2</sub>PO<sub>4</sub><sup>-</sup> Ions by Highly Nonplanar Electron Deficient Perhaloporphyrins. *RSC Adv.* **2015**, *5*, 3269-3275.
6. **Nivedita Chaudhri**, Ray J. Butcher, and M. Sankar\* Synthesis, Structural, Photophysical, Electrochemical Redox and Axial Ligation Properties of Highly Electron Deficient Perchlorometalloporphyrins and Selective CN<sup>-</sup> Sensing by Co(II) Complexes. *New J. Chem.* **2018** (DOI:10.1039/C7NJ04418F).
7. **Nivedita Chaudhri**, Nipun Sawhney, Bijjam Madhusudhan, Anubhav Raghav, M. Sankar\* and S. Satapati\* Effect of Functional Groups on Sensitization of Dye Sensitized Solar Cells using Free Base Porphyrins. *J. Porphyrins Phthalocyanines* **2017**, *21*, 222-230.
8. **Nivedita Chaudhri**, Nitika Grover, and M. Sankar\* Asymmetrically  $\beta$ -Substituted Porphyrins and Chlorins: Synthesis, Spectroscopic and Electrochemical Redox Properties. *ECS Trans.* **2015**, *66*, 11-20 (*Invited Article*).
9. Ravi Kumar, **Nivedita Chaudhri** and M. Sankar\* Ratiometric and Colorimetric “Naked Eye” Selective Detection of CN<sup>-</sup> Ions by Electron Deficient Ni(II) Porphyrins and Their Reversibility Studies. *Dalton Trans.* **2015**, *44*, 9149-9157 (*One of the "Most accessed articles" during April 2015*).

10. Upasana Sah, Kajal Shrama, **Nivedita Chaudhri**, M. Sankar\* and P. Gopinath\* Antimicrobial Photodynamic Therapy: Single-walled Carbon Nanotube (SWCNT)-Porphyrin Conjugate for Visible Light Mediated Inactivation of *Staphylococcus aureus*. *Colloids and Surfaces B: Biointerfaces* **2018**, 162, 108-117.
11. **Nivedita Chaudhri** and M. Sankar\* Synthesis and Oxidative Fusion of *Trans*-Benzochlorins into Difused Benzoporphyrins: Synthesis and Anion Sensing Properties (*Submitted for publication*).
12. **Nivedita Chaudhri**, Nitika Grover, Kumari Anshul, and M. Sankar\* Synthesis, Structural, Photophysical and Electrochemical Redox Studies of  $\beta$ -Trisubstituted Porphyrins Derived From 2-Nitroporphyrins (*Submitted for publication*).



## **PRESENTATION IN THE INTERNATIONAL/NATIONAL CONFERENCES**

1. **Nivedita Chaudhri**, N. Grover, K. Anshul and M. Sankar\* Facile Synthesis of Unsymmetrical  $\beta$ -Substituted Porphyrins *via* Nucleophilic Substitution Reactions. Poster presentation at the 9<sup>th</sup> International Conference on Porphyrins and Phthalocyanines (ICPP-9) held at Nanjing, China during July 3-8, 2016.
2. **Nivedita Chaudhri** and M. Sankar\* Synthesis, Spectral and Electrochemical Redox Properties of Porphyrin-based Schiff Bases. Poster Presentation at 6<sup>th</sup> EuCheMS Conference on Nitrogen Ligands, held at Beaune, France during September 13-17, 2015.
3. **Nivedita Chaudhri** and M. Sankar\* Selective Anion Sensing by Electron Deficient Porphyrins. Poster presentation at the 8<sup>th</sup> International Conference on Porphyrins and Phthalocyanines (ICPP-8) held at Istanbul, Turkey during June 22-27, 2014.
4. **Nivedita Chaudhri**, N. Grover, and M. Sankar Synthesis, Structural and Intriguing Electrochemical Redox properties of  $\beta$ -Functionalized 'Push-Pull' Porphyrins and Chlorins. Poster presentation at ACS meeting held at IIT Roorkee, Roorkee, India on 7<sup>th</sup> February 2018.
5. N. Grover, **Nivedita Chaudhri**, and M. Sankar\* Facile Synthesis, Structural, Photophysical and Intriguing Electrochemical Redox properties of  $\beta$ -Functionalized 'Push-Pull' Porphyrins and Chlorins. Poster Presentation at the 17<sup>th</sup> Symposium on Modern Trends in Inorganic Chemistry (MTIC-XVII), December 12-14, 2017 at IISER Pune and NCL Pune, Pune.
6. **Nivedita Chaudhri**, N. Sawhney, B. Madhusudhan, M. Sankar\* and S. Satapathi\* Effect of Functional Groups on Sensitization of Dye Sensitized Solar Cells using Free Base Porphyrins. Poster presentation at the international conference on advanced materials for energy, environment and health (ICAM-2016) held at IIT Roorkee, Roorkee, India during March 4-7, 2016.
7. **Nivedita Chaudhri** and M. Sankar\* Synthesis, Spectral and Electrochemical Redox Properties of Porphyrin-based Schiff Bases. Poster Presentation at 6<sup>th</sup> EuCheMS Conference on Nitrogen Ligands, held at Beaune, France during September 13-17, 2015.
8. **Nivedita Chaudhri**, N. Grover, K. Anshul and M. Sankar\* Synthesis, Structures and Electrochemical Redox Properties of Asymmetrically  $\beta$ -Substituted Porphyrins' Poster Presentation at the 16<sup>th</sup> Symposium on Modern Trends in Inorganic Chemistry (MTIC-XVI), December 3-5, 2015 at Jadavpur University, Kolkata.
9. **Nivedita Chaudhri** and M. Sankar\* Synthesis and Studies on Sterically Crowded Porphyrins. Poster presented at the 16<sup>th</sup> National Symposium in Chemistry organized by Chemical Research Society of India (CRSI), February 7-9, 2014 at IIT Bombay, India.

10. R. Kumar, **Nivedita Chaudhri** and M. Sankar  $\beta$ -Substituted Porphyrins as  $\text{CN}^-$  Sensors. Presented at Royal Society Chemistry (RSC) India Roadshow held at IIT Delhi on 5th Nov 2014.
11. R. Kumar, **Nivedita Chaudhri**, M. K. Chahal and M. Sankar Ratiometric and Colorimetric 'Naked-eye' Selective Detection of  $\text{CN}^-$  ions by Porphyrinic Chemosensors and their Reversibility Studies. Oral presentation at 6<sup>th</sup> EuCheMS Conference on Nitrogen Ligands, September 13-17, 2015 at Beaune, France.
12. M. K. Chahal, **Nivedita Chaudhri**, K. Prakash, R. Kumar, N. Grover, P. Yadav and M. Sankar Naked-eye Detection of Toxic Anions using Porphyrinoid Chemosensors and their Reusability Studies. Invited oral presentation at the 9<sup>th</sup> International Conference on Porphyrins and Phthalocyanines (ICPP-9) held at Nanjing, China during July 3-8, 2016.



# TABLE OF CONTENTS

Title	Page No.
Candidate's Declaration	
Acknowledgements	i
Abstract	v
List of Publications	ix
List of Conferences	xi
Table of Contents	xiii
List of Charts	xxi
List of Schemes	xxii
List of Figures	xxiii
List of Tables	xxix
<b>CHAPTER 1. Introduction</b>	
1.1 Introduction to the Tetrapyrrolic Pigments	3
1.2 Synthetic Porphyrin Analogues	4
1.3 Laboratory Synthesis of Porphyrin	5
1.4 Functionalization of Porphyrin	6
1.5 Modification at $\beta$ -Pyrrolic Position	7
1.6 Various Applications of Porphyrinoids	9
1.6.1 Porphyrinoids in DDSC Application	9
1.6.2 Porphyrinoids as PDT Agents	11
1.6.3 Porphyrins as Ion Chemosensors	13
1.6.4 Porphyrins in Catalytic Application	15
1.6.5 Porphyrinoids as NLO Materials	17
1.7 Objectives and Future Scope of the Present Work	19
1.8 References	21

## CHAPTER 2. Versatile Synthetic Route for $\beta$ -Functionalized Chlorins and Porphyrins by Varying The Size of Michael Donors: Syntheses, Photophysical and Electrochemical Redox Properties

2.1 Introduction	37
2.2 Experimental Section	39
2.2.1 Chemicals	39
2.2.2 Instrumentation and Methods	40
2.2.3 General Synthetic Procedure for The Preparation of $H_2TPP(R)X_2$ ; X = H, Br and R = CHD and DMBA)	40
2.2.4 General Synthetic Procedure for The Preparation of $H_2TPC(R)_2X_2$ ; X = H, Br and R = BENAC and IND)	43
2.2.5 Synthesis of 2-(2'-Cyclohexane-1',3'-dione)-5,10,15,20-tetraphenylporphyrinato Nickel (II) NiTPP(CHD) ( <b>1a</b> )	45
2.2.6 Synthesis of 2-(2'-Cyclohexane-1',3'-dione)-12,13-dibromo-5,10,15,20-tetraphenylporphyrinato Nickel (II) NiTPPBr <sub>2</sub> (CHD) ( <b>2a</b> )	45
2.2.7 Synthesis of 2-(1',3'-dimethyl-5'-barbituric acid)-5,10,15,20-tetraphenylporphyrinato Nickel (II) NiTPP(DMBA) ( <b>3a</b> )	46
2.2.8 Synthesis of 2-(1',3'-dimethyl-5'-barbituric acid)-12,13-dibromo-5,10,15,20-tetraphenylporphyrinato Nickel (II) NiTPPBr <sub>2</sub> (DMBA) ( <b>4a</b> )	46
2.2.9 Synthesis of 2-(1'-cyano-3'-oxo-3'-phenyl-2'-propanenitrile)-5,10,15,20-tetraphenylporphyrinato Ni(II) NiTPP(BENAC) ( <b>5</b> ) and 2,3-Di-(1'-cyano-3'-oxo-3'-phenyl-2'-propanenitrile)-5,10,15,20-tetraphenylchlorinato Ni(II) NiTPC(BENAC) <sub>2</sub>	46
2.2.10 Synthesis of 2-(1'-cyano-3'-oxo-3'-phenyl-2'-propanenitrile)-12,13-dibromo-5,10,15,20-tetraphenylporphyrinato Nickel (II) NiTPPBr <sub>2</sub> (BENAC) ( <b>6</b> ) and 2,3-Di-(1'-cyano-3'-oxo-3'-phenyl-2'-propanenitrile)-12,13-dibromo-5,10,15,20-tetraphenylchlorinato Nickel (II) NiTPCBr <sub>2</sub> (BENAC) <sub>2</sub> ( <b>9a</b> )	47
2.2.11 Synthesis of 2,3-Di-(5'-indane-1',3'-dione)-5,10,15,20-tetraphenylchlorinato Nickel (II) NiTPC(IND) <sub>2</sub> ( <b>10a</b> )	48
2.2.12 Synthesis of 2,3-Di-(5'-indane-1',3'-dione)-12,13-dibromo-5,10,15,20-tetraphenylchlorinato Nickel (II) NiTPCBr <sub>2</sub> (IND) <sub>2</sub> ( <b>11a</b> )	49
2.2.13 General Procedure for the Synthesis of Zn(II) Complexes from Free Base Porphyrins	49

2.3 Results and Discussion	52
2.3.1 Synthesis and Characterization	52
2.3.2 Crystal Structure Discussion	55
2.3.3 DFT Studies	58
2.3.4 Absorption Spectral Studies	59
2.3.5 Fluorescence Spectral Studies	61
2.3.6 <sup>1</sup> H NMR and Mass Spectrometric Studies	64
2.3.7 Protonation and Deprotonation Studies	66
2.3.8 Electrochemical Redox Properties	70
2.4 Conclusions	73
2.5 References	73
<b>CHAPTER 3. Regioselective Conversion of Planar <i>Trans</i>-Chlorins into Highly Twisted Doubly Fused-Porphyrins (DFPs) or -Chlorins (DFCs) via Oxidative Fusion</b>	
3.1 Introduction	79
3.2 Experimental Section	80
3.2.1 Chemicals	80
3.2.2 Instrumentation and Methods	80
3.2.3 General Procedure for the Synthesis of Ni(II) Doubly Fused Porphyrins (NiDFPs)	81
3.2.4 General Synthetic Procedure for the Synthesis of Free Base Doubly Fused Chlorins (H <sub>2</sub> DFCs)	83
3.3 Results and Discussion	85
3.3.1 Synthesis and Characterization	85
3.3.2 <sup>1</sup> H NMR and Mass Spectrometric Studies	88
3.3.3 Crystal Structure Discussion	89
3.3.4 DFT Studies	93
3.3.5 Electronic Spectral Studies	94

3.3.6 Electrochemical Redox Properties	96
3.3.7 Protonation-Deprotonation Studies	98
3.4 Conclusions	100
3.5 References	101

**CHAPTER 4. One-Pot Synthesis of Ni(II) Monofused Porphyrins (NiMFPs) via Nickel Acetate Catalyzed Oxidation of Free Base *trans*-Chlorins**

4.1 Introduction	107
4.2 Experimental Section	109
4.2.1 Chemicals	109
4.2.2 Instrumentation and Methods	109
4.2.3 General Procedure for the Synthesis of Ni(II) Monofused porphyrins (NiMFPs)	109
4.2.4 Synthesis of Free Base Mono-fused porphyrins (H <sub>2</sub> MFPs)	111
4.2.5 General Procedure for the Synthesis of Metal Complexes of Monofused Porphyrins [(M(II)MFPs) (M = Co(II), Cu(II), and Zn(II))]	112
4.3 Results and Discussion	113
4.3.1 Synthesis and Characterization	113
4.3.2 <sup>1</sup> H NMR and Mass Spectrometric Studies	116
4.3.3 X-Ray Crystal Structure Discussion	118
4.3.4 DFT Studies	122
4.3.5 Electronic Spectral Studies	123
4.3.6 Electrochemical Redox Properties	125
4.4 Conclusions	128
4.5 References	128

**CHAPTER 5. Triply Fused Porphyrins: Synthesis, Spectral, Electrochemical Redox and Anion Sensing Properties**

5.1 Introduction	135
5.2 Experimental Section	136



5.2.1 Chemicals	136
5.2.2 Instrumentation and Methods	137
5.2.3 General Procedure for the Synthesis of <i>trans</i> -Benzochlorins NiTPC(IND) <sub>2</sub> (Benzo) (1) and NiTPC(MN) <sub>2</sub> (Benzo) (2)	137
5.2.4 Synthetic Procedure for Oxidative Fusion of <i>trans</i> -Benzochlorins into difused Benzoporphyrins NiDFP(IND) <sub>2</sub> (Benzo) and NiDFP(MN) <sub>2</sub> (Benzo) (3 and 4)	138
5.2.5 Synthetic Procedure for NiTPCBr <sub>4</sub> (IND) <sub>2</sub> (Benzo) (5)	138
5.3 Results and Discussion	139
5.3.1 Synthesis and Characterization	139
5.3.2 <sup>1</sup> H NMR and Mass Spectrometric Studies	140
5.3.3 DFT Calculation	142
5.3.4 Absorption Studies	143
5.3.5 Electrochemical Studies	145
5.3.6 Anion Sensing Properties	148
5.3.7 Selective Detection of Cyanide Ion by NiDFP(MN) <sub>2</sub> (Benzo) (4)	149
5.4 Conclusions	152
5.5 References	153
 <b>CHAPTER 6. Synthesis, Structural, Photophysical and Electrochemical Redox Studies of β-Trisubstituted Porphyrins</b>	
6.1 Introduction	159
6.2 Experimental Section	161
6.2.1 Chemicals	161
6.2.2 Instrumentation and Methods	161
6.2.3 Synthetic Procedures	161
6.2.3.1 General Synthetic Procedure for the Preparation of 2-(1-Acetyl-2'-oxopropyl)- 12,13-dibromo/diphenyl-5,10,15,20-tetraphenyl Porphyrinato Nickel(II); NiTPP[CH(COCH <sub>3</sub> ) <sub>2</sub> ]R <sub>2</sub> (where R = Br or Ph)	161
6.2.3.2 General Synthetic Procedures for the Preparation of 2-(1-Acetyl-1-	162

ethoxycarbonylmethyl)-12,13-dibromo/diphenyl-5,10,15,20-tetraphenyl Porphyrinato Nickel(II); NiTPP[CH<sub>2</sub>COOC<sub>2</sub>H<sub>5</sub>]R<sub>2</sub> (Where R = Br or Ph)

6.2.3.3 Synthesis of H<sub>2</sub>TPP[CH(COCH<sub>3</sub>)<sub>2</sub>]R<sub>2</sub> (**1** and **2**), H<sub>2</sub>TPP[CH<sub>2</sub>COOC<sub>2</sub>H<sub>5</sub>]R<sub>2</sub> (3 and 4) (where R = Br or Ph) and Their Metal Complexes (**1a-1d** and **2a-2d**) 164

6.3 Results and Discussion 167

6.3.1 Synthesis and Characterization 167

6.3.2 <sup>1</sup>H NMR and Mass Spectrometric Studies 169

6.3.3 Single Crystal X-ray Structures 171

6.3.4 DFT Studies 174

6.3.5 Photophysical Studies 175

6.3.6 Electrochemical Redox Studies 178

6.4 Conclusions 181

6.5 References 181

## **Chapter 7. Perhaloporphyrins: Synthesis, Structural, Electrochemical Redox and Anion Sensing Properties**

7.1 Introduction 187

7.2 Experimental Section 189

7.2.1 Chemicals 189

7.2.2 Instrumentation and Methods 189

7.2.3 Synthetic Procedures 190

7.2.3.1 Synthetic Procedures for NiTPP(NO<sub>2</sub>)Cl<sub>7</sub> 190

7.2.3.2 Synthesis of H<sub>2</sub>TPP(NO<sub>2</sub>)Cl<sub>7</sub> (**1**) 190

7.2.3.3 General Procedure for the Synthesis of MTPP(NO<sub>2</sub>)Cl<sub>7</sub> and MTPPCl<sub>8</sub> (where M = Co<sup>II</sup>, Cu<sup>II</sup> and Zn<sup>II</sup>) 191

7.3 Results and Discussion 192

7.3.1 Synthesis and Characterization 192

7.3.2 Crystal Structures Discussion 193

7.3.3 <sup>1</sup>H NMR and Mass Spectrometric Studies 195

7.3.4 Electronic Spectral Studies	197
7.3.5 Electrochemical Studies	199
7.3.6 Protonation and Deprotonation Studies of <b>1-4</b>	201
7.3.7 Detection of Basic Anions by <b>1-4</b> through Anion Induced Deprotonation	202
7.3.8 Axial Ligation Studies of Zn(II) Complexes	208
7.3.9 Selective Cyanide Sensing by Cobalt (II) Complexes	212
7.3.10 DFT Studies	215
7.4 Conclusions	217
7.5 References	218
<b>Chapter 8. Summary and Conclusions</b>	<b>225</b>
Appendix-I	233
Appendix-II	257
Appendix-III	273
Appendix-IV	285
Appendix-V	293
Appendix-VI	303



## List of Charts

	<b>Page</b>
<b>CHAPTER 2</b>	<b>No.</b>
Chart 2.1 Molecular Structures of Synthesized Porphyrins.	38
Chart 2.2 Molecular Structures of Synthesized Chlorins.	39
<b>CHAPTER 3</b>	
Chart 3.1 Molecular Structures of Synthesized Doubly Fused Porphyrins and Chlorins.	80
<b>CHAPTER 4</b>	
Chart 4.1 Molecular Structures of Synthesized Fused Porphyrins.	108
<b>CHAPTER 5</b>	
Chart 5.1 Molecular Structures of Synthesized Porphyrinoids.	136
<b>CHAPTER 6</b>	
Chart 6.1 Molecular Structures of Synthesized $\beta$ -Tri-substituted Porphyrins MTPP[CH(COCH <sub>3</sub> ) <sub>2</sub> ]R <sub>2</sub> and MTPP[CH <sub>2</sub> COOC <sub>2</sub> H <sub>5</sub> ]R <sub>2</sub> (where R = Br and Ph).	160
<b>CHAPTER 7</b>	
Chart 7.1 Molecular Structures of Synthesized Porphyrins.	188

## List of Schemes

	<b>Page</b>
	<b>No.</b>
<b>CHAPTER 2</b>	
Scheme 2.1 Synthetic Routes for the Preparation of Di/tetra- $\beta$ -Substituted Tetraphenylchlorins.	53
Scheme 2.2 Synthetic Route for the Preparation of Mono/tri- $\beta$ -Substituted Tetraphenylporphyrins.	54
Scheme 2.3 The Plausible Mechanism for the Synthesis of Porphyrins and Chlorins.	55
<b>CHAPTER 3</b>	
Scheme 3.1 Synthetic Routes to NiDFP(IND) <sub>2</sub> X <sub>2</sub> and H <sub>2</sub> DFC(IND) <sub>2</sub> X <sub>2</sub> (where X = H, Br, Ph).	85
Scheme 3.2 Synthetic Routes to NiDFP(MN) <sub>2</sub> X <sub>2</sub> and H <sub>2</sub> DFC(MN) <sub>2</sub> X <sub>2</sub> (where X = H, Br, Ph).	86
Scheme 3.3 The proposed Mechanism for Ring Fusion.	87
<b>CHAPTER 4</b>	
Scheme 4.1 Synthetic Route to M(II)MFP(IND)R <sub>2</sub> (where M(II) = 2H, Co(II), Ni(II), Cu(II), Zn(II) and X = H, Br, Ph).	114
Scheme 4.2 The plausible Mechanistic Pathway for Mono-Fused Porphyrins.	114
<b>CHAPTER 5</b>	
Scheme 5.1 Synthetic Route to Benzochlorins and Difused Benzoporphyrins.	140
Scheme 5.2 Plausible Mechanism for the Detection of Basic Anions through <i>trans</i> -Chlorins.	149
Scheme 5.3 The Schematic representation of Binding of CN <sup>-</sup> Ion to <b>4</b> and its Reversibility in Presence of Trifluoroacetic Acid.	152
<b>CHAPTER 6</b>	
Scheme 6.1 Michael Addition of 1,3-Diketone and 3-ketoester with $\beta$ -Nitroporphyrins.	168
Scheme 6.2 Plausible Mechanism for the Synthesis of Asymmetrically Substituted Porphyrins.	169
<b>CHAPTER 7</b>	
Scheme 7.1 Facile Synthetic Route to Mixed $\beta$ -substituted Perchlorometalloporphyrins.	192
Scheme 7.2 Plausible Mechanism for the Detection of Anions by <b>1-4</b> .	207
Scheme 7.3 The plausible Mechanism for Cyanide Ion Sensing.	215

## List of Figures

<b>CHAPTER 1</b>	<b>Page No.</b>
Figure 1.1 Molecular Structures of Naturally Occurring Tetrapyrrole Pigments.	3
Figure 1.2 Synthetic Porphyrin Analogues.	4
Figure 1.3 Functionalization of Porphyrin by Positions.	6
Figure 1.4 Functionalization of Porphyrins.	7
Figure 1.5 Modification of Porphyrin Skeleton at $\beta$ -Pyrrolic position.	8
Figure 1.6 <i>Meso</i> -Substituted Highly Efficient Porphyrin Based Sensitizers having PCE up to 14%.	10
Figure 1.7 Highly Efficient $\beta$ -Substituted Dyes.	10
Figure 1.8 Mechanisms of Photodynamic Reactions Involved in Photodynamic Therapy.	11
Figure 1.9 Photosensitizers Approved by Different Health Organizations to Use in Human Clinical Trials.	12
Figure 1.10 Porphyrin Based Anion Sensors.	14
Figure 1.11 Porphyrin Based Cation Sensors.	14
Figure 1.12 Sterically Hindered $\beta$ -Substituted Metalloporphyrin as Catalysts.	15
Figure 1.13 Molecular Structures of Highly Efficient Porphyrin Based Catalysts Utilized in Various Catalytic Applications.	16
Figure 1.14 Molecular Structures of Functionalized Porphyrins Used in NLO Applications.	18
 <b>CHAPTER 2</b>	
Figure 2.1 ORTEP Diagrams Showing Top and Side Views of NiTPPBr <sub>2</sub> (CHD) ( <b>2a</b> ) (a and b) NiTPC(BENAC) <sub>2</sub> ( <b>8a</b> ) (d and e) and H <sub>2</sub> TPCBr <sub>2</sub> (BENAC) <sub>2</sub> ( <b>9</b> ) (g and h), Respectively. Solvates are Not Shown for Clarity, the $\beta$ -Substituents and $\beta$ -/ <i>meso</i> -Phenyls are Omitted for Clarity in Side View. (c), (f) and (i) Showing Numbering of Carbon Atoms in the Skeleton.	56
Figure 2.2 Packing Diagram Showing O $\cdots$ O Interaction between the Nearest CHDs in NiTPPBr <sub>2</sub> (CHD) ( <b>2a</b> ).	58

Figure 2.3	Pictorial Representation of Frontier Molecular Orbitals (FMOs) of H <sub>2</sub> TPP(CHD) ( <b>1</b> ).	59
Figure 2.4	Electronic Absorption Spectra of Synthesized Free Base Porphyrins/Chlorins in CH <sub>2</sub> Cl <sub>2</sub> . Circled Area Shows the Absorption due to BENAC and IND.	60
Figure 2.5	Fluorescence Spectra of Synthesized Free Base Complexes.	61
Figure 2.6	Fluorescence Lifetime Decay Profiles of (a) H <sub>2</sub> TPP(CHD) ( <b>1</b> ) and H <sub>2</sub> TPC(BENAC) <sub>2</sub> ( <b>8</b> ) (b) H <sub>2</sub> TPC(BENAC) <sub>2</sub> ( <b>8</b> ) and H <sub>2</sub> TPCBr <sub>2</sub> (BENAC) <sub>2</sub> .	62
Figure 2.7.	<sup>1</sup> H NMR Spectrum of H <sub>2</sub> TPC(IND) <sub>2</sub> ( <b>10</b> ) in CDCl <sub>3</sub> at 298 K.	65
Figure 2.8	Representative <sup>1</sup> H NMR Spectra of Imino Proton Region of Synthesized Free Base Porphyrins and Chlorins.	66
Figure 2.9	UV-vis spectral titration of (a) H <sub>2</sub> TPPBr <sub>2</sub> (DMBA) ( <b>4</b> ) and (b) H <sub>2</sub> TPCBr <sub>2</sub> (IND) <sub>2</sub> ( <b>11</b> ) in Toluene at 298 K; Insets show the Corresponding Hill Plots.	67
Figure 2.10	UV-vis. Spectral Changes of (a) H <sub>2</sub> TPP(DMBA) ( <b>3</b> ) and (b) H <sub>2</sub> TPC(IND) <sub>2</sub> ( <b>10</b> ) While Increasing [TBAOH] in Toluene at 298 K; Insets Show The Corresponding Hill Plots.	68
Figure 2.11	<sup>1</sup> H NMR Spectral Changes of H <sub>2</sub> TPCBr <sub>2</sub> (IND) <sub>2</sub> ( <b>11</b> ) Upon Addition of TBAOH in CDCl <sub>3</sub> at 298 K.	70
Figure 2.12	Comparative Cyclic Voltammograms of (a) Ni(II) Chlorins and (b) Zn(II) Chlorins.	71
<b>CHAPTER 3</b>		
Figure 3.1	Comparative <sup>1</sup> H NMR Spectra of (a) NiTPC(IND) <sub>2</sub> and NiDFP(IND) <sub>2</sub> (b) H <sub>2</sub> TPC(IND) <sub>2</sub> and H <sub>2</sub> DFC(IND) <sub>2</sub> .	88
Figure 3.2	Comparative Chemical Shifts of Core Imino Protons of Free Base Fused Chlorins.	88
Figure 3.3	MALDI-TOF Mass Spectrum of H <sub>2</sub> DFC(IND) <sub>2</sub> ( <b>4</b> ).	89
Figure 3.4	ORTEP Showing Top and Side Views of (a and e) NiDFP(IND) <sub>2</sub> ( <b>1</b> ); (b and f) H <sub>2</sub> DFC(IND) <sub>2</sub> Br <sub>2</sub> ( <b>5</b> ); (c and g) NiDFP(MN) <sub>2</sub> Br <sub>2</sub> ( <b>8</b> ) and NiDFC(MN) <sub>2</sub> Br <sub>2</sub> <b>8a</b> (d and h).	90
Figure 3.5	ORTEP Diagrams (a) NiDFP(IND) <sub>2</sub> ( <b>1</b> ) and (b) NiDFP(MN) <sub>2</sub> Br <sub>2</sub> ( <b>8</b> ) Showing the Bond Angles for Fused Tetrahedral Carbon.	93
Figure 3.6	Frontier Molecular Orbitals of H <sub>2</sub> DFC(MN) <sub>2</sub> ( <b>10</b> ).	94



Figure 3.7	(a) Comparative Absorption Spectra of H <sub>2</sub> DFC(IND) <sub>2</sub> ( <b>4</b> ) and H <sub>2</sub> TPC(IND) <sub>2</sub> . (b) Comparative Emission Spectra of H <sub>2</sub> DFC(IND) <sub>2</sub> ( <b>4</b> ) and H <sub>2</sub> TPC(IND) <sub>2</sub> .	95
Figure 3.8	Comparative CVs of (a) NiDFP(MN) <sub>2</sub> X <sub>2</sub> (b) H <sub>2</sub> DFC(MN) <sub>2</sub> X <sub>2</sub> (where X = H, Br, Ph) in CH <sub>2</sub> Cl <sub>2</sub> .	96
Figure 3.9	Plot of HOMO-LUMO Trend in Ni(II)DFPs.	98
Figure 3.10	UV-vis. Spectral Changes of H <sub>2</sub> DFC(MN) <sub>2</sub> ( <b>10</b> ) while Increasing the Conc. of (a) TFA (b) TBAOH in CH <sub>2</sub> Cl <sub>2</sub> at 298 K; Insets Show the Corresponding Hill Plots.	99
<b>CHAPTER 4</b>		
Figure 4.1	<sup>1</sup> H NMR Spectrum of H <sub>2</sub> MFP(IND) ( <b>1</b> ) in CDCl <sub>3</sub> .	116
Figure 4.2	Comparative <sup>1</sup> H NMR Spectra of Precursor (H <sub>2</sub> TPC(IND) <sub>2</sub> ) and Ni(II) Mono-Fused Porphyrin (Ni(II)MFP(IND)).	117
Figure 4.3	MALDI-TOF-MS Spectrum of H <sub>2</sub> MFP(IND) ( <b>1</b> ) in CH <sub>2</sub> Cl <sub>2</sub> .	117
Figure 4.4	ORTEP Showing Top and Side Views of (a and e) NiMFP(IND) ( <b>1b</b> ); (b and f) ZnMFP(IND)•Py ( <b>1d</b> •Py); (c and g) NiMPF(IND)Ph <sub>2</sub> ( <b>3b</b> ), and (d and h) ZnMFP(IND)Ph <sub>2</sub> •CH <sub>3</sub> OH ( <b>3d</b> •CH <sub>3</sub> OH). Phenyl rings in the side views are omitted for clarity.	118
Figure 4.5	(a) Numbering of Carbon Atoms in the Macrocyclic Skeleton; (b) ORTEP Showing the <i>sp</i> <sup>3</sup> Hybridized Carbon with Deformed Tetrahedral Geometry.	121
Figure 4.6	Frontier Molecular Orbitals of H <sub>2</sub> MFP(IND) ( <b>1</b> ) Using B3LYP/6-31G Basis Sets.	122
Figure 4.7	Frontier Molecular Orbitals of The Two Highest Energy Filled (HOMOs) and Two Lowest Energy Unfilled (LUMOs) Orbitals of Precursor (H <sub>2</sub> TPC(IND) <sub>2</sub> ) and Product H <sub>2</sub> MFP(IND) ( <b>1</b> ). The Orbitals were Generated Based on a Density Functional Calculation (B3LYP) Using a 6-31G Basis Set. The Energies are given in eV units.	123
Figure 4.8	(a) Comparative absorption spectra of synthesized free base porphyrins in CH <sub>2</sub> Cl <sub>2</sub> . (b) The comparative emission spectra of synthesized free base monofused porphyrins in CH <sub>2</sub> Cl <sub>2</sub> .	124
Figure 4.9	Comparative Cyclic Voltammograms of (a) NiMFP(IND)R <sub>2</sub> (b) CuMFP(IND)R <sub>2</sub> (where R = H, Br, and Ph) in CH <sub>2</sub> Cl <sub>2</sub> using 0.1 M TBAPF <sub>6</sub> .	126

## CHAPTER 5

- Figure 5.1  $^1\text{H}$  NMR Spectrum of NiTPC(IND) $_2$ (Benzo) (**1**) in  $\text{CDCl}_3$  at 298 K. 141
- Figure 5.2  $^1\text{H}$  NMR Spectrum of NiDFP(IND) $_2$ (Benzo) (**3**) in  $\text{CDCl}_3$  at 298 K. 142
- Figure 5.3 MALDI-TOF-Mass Spectrum of NiDFP(IND) $_2$ (Benzo) (**3**) in positive ion mode. 142
- Figure 5.4 Frontier Molecular Orbitals of NiDFP(IND) $_2$ (Benzo) (**3**). 143
- Figure 5.5 (a) Comparative Absorption Spectra of Synthesized *trans*-Benzochlorins; (b) Synthesized Difused Benzoporphyrins in  $\text{CH}_2\text{Cl}_2$  at 298 K. 144
- Figure 5.6 Comparative Cyclic Voltammograms of Synthesized Porphyrinoids in  $\text{CH}_2\text{Cl}_2$  at 298 K using 0.1M TBAPF $_6$ . 146
- Figure 5.7 Variations in HOMO-LUMO Gap. 147
- Figure 5.8 UV-Visible Spectral Changes of NiTPC(IND) $_2$ (Benzo) (**1**) while Sequential Addition of Cyanide Ion in  $\text{CH}_2\text{Cl}_2$  at 298 K. 148
- Figure 5.9 (a) Colorimetric Response of **4** with Tested Anions in  $\text{CH}_2\text{Cl}_2$ ; (b) UV-Vis Spectral Changes of **4** ( $1.08 \times 10^{-5}$  M) upon Addition of Excess of Tested Anions in The Form of TBA in  $\text{CH}_2\text{Cl}_2$  298 K; (c) UV-visible Spectral Titrations of **4** (10  $\mu\text{M}$ ) upon Sequential Addition of TBACN (0.018 M) in  $\text{CH}_2\text{Cl}_2$ , Inset Shows Corresponding Hill Plot. 150
- Figure 5.10 (a) Picture of Test Strips of **4** (5 mM) for Detection of Cyanide ion in  $\text{CH}_2\text{Cl}_2$ . (b) Sigmoidal Curve for **4** Representing Graph between  $[\text{CN}^-]$  vs  $\Delta A$  Indicating Positive Cooperative Behavior. (c) Ratiometric Absorbance Ratio ( $A_{524}/A_{478}$ ) of **4** (10  $\mu\text{M}$ ) upon Addition of 2 eq. of  $\text{CN}^-$  and 10 eq. of Other Interfering Anions. 151
- Figure 5.11 (a) The Colorimetric and UV-Visible Spectral Changes of **4** for Reversibility Test; (b) The Stability Test of **4**. $2\text{CN}^-$  adduct observed for 300 min. 151

## CHAPTER 6

- Figure 6.1  $^1\text{H}$  NMR Spectrum of  $\text{H}_2\text{TPP}[\text{CH}(\text{COCH}_3)_2]\text{Ph}_2$  (**2**) in  $\text{CDCl}_3$ . 170
- Figure 6.2 MALDI-TOF Mass Spectrum of  $\text{H}_2\text{TPP}[\text{CH}(\text{COCH}_3)_2]\text{Ph}_2$  (**2**) in Positive Ion Mode. 171
- Figure 6.3 ORTEP Diagrams Showing Top and Side Views of (a and d) NiTPP[CH(COCH $_3$ ) $_2$ ]Br $_2$  (**1b**); (b and e)  $\text{H}_2\text{TPP}[\text{CH}_2\text{COOC}_2\text{H}_5]\text{Br}_2$  (**3**) and (c and f) ZnTPP[CH $_2$ COOC $_2$ H $_5$ ]Ph $_2$ •Py (**4d**•Py). (g-i) Displacement of Porphyrin 24-core Atoms (in Å) from The Mean Plane. 172

Figure 6.4	Frontier Molecular Orbitals of H <sub>2</sub> TPP[CH(COCH <sub>3</sub> ) <sub>2</sub> ]Ph <sub>2</sub> ( <b>2</b> ).	174
Figure 6.5	(a) Comparative UV-Visible Spectra of Synthesized Free Base Porphyrins in CH <sub>2</sub> Cl <sub>2</sub> at 298K. (b) Comparative Emission Spectra of Free Base Complexes in CH <sub>2</sub> Cl <sub>2</sub> at 298K.	175
Figure 6.6	Comparative Cyclic Voltammograms of Synthesized (a) Co(II) complexes, and (b) Ni(II) Complexes in CH <sub>2</sub> Cl <sub>2</sub> at 298 K.	179

## CHAPTER 7

Figure 7.1	ORTEP Diagrams Showing Top Views of (a) ZnTPP(NO <sub>2</sub> )Cl <sub>7</sub> ( <b>1d</b> ) and; (b) ZnTPPCl <sub>8</sub> ( <b>2d</b> ). (c, d) Displacement of Porphyrin Core Atoms (Å) from the Mean Plane for <b>1d</b> and <b>2d</b> .	194
Figure 7.2	Packing Diagram of CoTPP(NO <sub>2</sub> )Cl <sub>7</sub> ( <b>1a</b> ) in a Unit Cell.	195
Figure 7.3	<sup>1</sup> H NMR Spectrum of NiTPP(NO <sub>2</sub> )Cl <sub>7</sub> ( <b>2b</b> ) in CDCl <sub>3</sub> at 298 K.	195
Figure 7.4	Negative Ion Mode ESI Mass Spectrum of H <sub>2</sub> TPPNO <sub>2</sub> Cl <sub>7</sub> ( <b>1</b> ) in CH <sub>3</sub> CN.	196
Figure 7.5	(a) UV-Vis. Absorption Spectra of <b>1</b> and <b>3</b> and (b) Fluorescence Spectra of <b>1-4</b> in Toluene at 298 K.	197
Figure 7.6	(a) Electronic Absorption Spectra of <b>1d</b> and <b>2d</b> in CH <sub>2</sub> Cl <sub>2</sub> , Inset Shows Expanded Region for Q bands. (b) Electronic Emission Spectra of <b>1d</b> and <b>2d</b> in CH <sub>2</sub> Cl <sub>2</sub> at 298 K.	198
Figure 7.7	CVs and DPVs of <b>1-4</b> in CH <sub>2</sub> Cl <sub>2</sub> Containing 0.1 M TBAPF <sub>6</sub> at 298 K.	199
Figure 7.8	UV-Visible Spectral Titrations of <b>1</b> with TFA (a) and TBAOH (b) in Toluene at 298 K. Insets Shows the Corresponding Hill Plots.	201
Figure 7.9	Colorimetric Response of <b>1</b> with Tested Anions (a). Optical Absorption Spectra of <b>1</b> with Tested Anions (b), and UV-Visible Spectral Titration of <b>1</b> with CN <sup>-</sup> ions (C) in Toluene.	203
Figure 7.10	(a) Bar graph constructed log β <sub>2</sub> vs. [Anions] for <b>1-4</b> in Toluene at 298K. (b) Sigmoidal Curve for <b>1-4</b> , ΔA vs. [TBAF] Indicating Positive Cooperative Behavior.	204
Figure 7.11	DPV Traces of <b>1</b> While Increasing Concentration of F <sup>-</sup> Ion in CH <sub>2</sub> Cl <sub>2</sub> Containing 0.1 M TBAPF <sub>6</sub> at 298 K.	206
Figure 7.12	(a) Colorimetric Response of <b>1</b> for Reversibility and Reusability Test with CN <sup>-</sup> (b) Reversibility test: Treatment of The Complex <b>1</b> •2CN <sup>-</sup> with a Solution of TFA.	208
Figure 7.13	(a) Axial Ligation of Pyridine to <b>1d</b> (8.29×10 <sup>-6</sup> M) in Toluene at 298K. (b) Axial Ligation of CN <sup>-</sup> Ion to <b>1d</b> (8.29×10 <sup>-6</sup> M) in Toluene. Main Plots	209

Show the Spectral Changes in Soret Region and Insets Show Plot [Pyridine] vs. [Pyridine]/ $\Delta A$ .

- Figure 7.14 (a) Comparative Plot of  $\log K_{eq}$  vs  $pK_a$  is given for **1d** and **2d**. (b) Comparative Plot of  $\log K_{eq}$  vs  $pK_a$  is given for ZnTPP(NO<sub>2</sub>)Br<sub>7</sub> and ZnTPPBr<sub>8</sub>. 210
- Figure 7.15 (a) Colorimetric Changes of **1a** with Tested Anions in Toluene. (b) UV-vis. Spectral Changes of **1a** upon Addition of Excess of Anions in Toluene. (c) UV-visible Spectral Changes of **1a** ( $1.04 \times 10^{-5}$  M) upon Sequential Addition of CN<sup>-</sup> ion. Insight Shows a Plot between [CN<sup>-</sup>]<sup>2</sup> and [CN<sup>-</sup>]<sup>2</sup>/ $\Delta A$ . 212
- Figure 7.16 (a) DPV (in V vs Ag/ AgCl) Traces Recorded for **1a** and **1a**.2CN<sup>-</sup> in CH<sub>2</sub>Cl<sub>2</sub> Containing 0.1M TBAPF<sub>6</sub> with a scan rate of 0.1 V/s at 298 K. (b) Ratiometric Absorbance Changes ( $A_{490}/A_{447}$ ) of **1a** ( $1.04 \times 10^{-5}$  M) on Addition of 1-2 Equiv. of CN<sup>-</sup> and 10 Equiv. of Other Anions. 213
- Figure 7.17 Reversible Studies of **1a** Using 1mM Solution of TFA in Toluene at 298 K. 214
- Figure 7.18 Fully Optimized Geometries of (a and c) Top and Side Views of CoTPP(NO<sub>2</sub>)Cl<sub>7</sub> (**1a**), (b and d) Top and Side Views of CoTPP(NO<sub>2</sub>)Cl<sub>7</sub>.CN<sup>-</sup> (**1a**.CN<sup>-</sup>).H Atoms in Top Views and Phenyl Rings in Side Views are Omitted for Clarity. 215
- Figure 7.19 The Pictorial representation of frontier molecular orbitals of (a) CoTPP(NO<sub>2</sub>)Cl<sub>7</sub> (b) CoTPP(NO<sub>2</sub>)Cl<sub>7</sub> (**1a**.CN<sup>-</sup>). 216
- Figure 7.20 (a) The Experimental UV-Vis. Spectrum and (b) The Theoretical UV-Vis. Spectrum of CoTPP(NO<sub>2</sub>)Cl<sub>7</sub>.CN<sup>-</sup> (**1a**.CN<sup>-</sup>). 217

## List of Tables

	<b>Page No.</b>
<b>CHAPTER 2</b>	
Table 2.1 Photophysical Properties of Synthetic Chlorins and Porphyrins.	62
Table 2.2 Photophysical Properties of Synthetic Chlorins and Porphyrins.	63
Table 2.3 Protonation and Deprotonation Constants ( $\log \beta_2$ ) of Free Base Mixed Substituted Chlorins and Porphyrins in Toluene at 298 K	67
Table 2.4 Electrochemical Redox Data of Porphyrinoids in $\text{CH}_2\text{Cl}_2$ at 298 K.	72
<b>CHAPTER 3</b>	
Table 3.1 Crystal Structure Data of NiDFP(IND) ( <b>1</b> ), $\text{H}_2\text{DFC}(\text{IND})_2\text{Br}_2$ ( <b>5</b> ), $\text{H}_2\text{TPC}[\text{CH}(\text{CN})_2]_2$ , NiDFP(MN) $_2\text{Br}_2$ ( <b>8</b> ) and NiDFC(MN) $_2\text{Br}_2$ ( <b>8a</b> ).	91
Table 3.2 Selected Average Bond Lengths and Bond Angles of NiDFP(IND) ( <b>1</b> ), $\text{H}_2\text{DFC}(\text{IND})_2\text{Br}_2$ ( <b>5</b> ), $\text{H}_2\text{TPC}[\text{CH}(\text{CN})_2]_2$ , NiDFP(MN) $_2\text{Br}_2$ ( <b>8</b> ) and NiDFC(MN) $_2\text{Br}_2$ ( <b>8a</b> ).	92
Table 3.3 Absorption Spectral Data of $\text{H}_2\text{DFCs}$ in $\text{CH}_2\text{Cl}_2$ .	95
Table 3.4 Redox Potentials of Synthesized $\text{H}_2\text{DFCs}$ and NiDFPs in $\text{CH}_2\text{Cl}_2$ at 298 K	97
Table 3.5 Protonation and Deprotonation Constants ( $\log \beta_2$ ) of synthesized $\text{H}_2\text{DFCs}$ in $\text{CH}_2\text{Cl}_2$ at 298 K.	100
<b>CHAPTER 4</b>	
Table 4.1 Crystal Structure Data of NiMFP(IND) ( <b>1b</b> ), ZnMFP(IND) ( <b>1d</b> ), NiMFP(IND)Ph $_2$ ( <b>3b</b> ), and ZnMFP(IND)Ph $_2$ ( <b>3d</b> ).	119
Table 4.2 Selected Average Bond Lengths and Bond Angles.	120
Table 4.3 Photophysical Data of Synthesized Free base Mono-fused Porphyrins and Their Corresponding Zn(II) complexes in $\text{CH}_2\text{Cl}_2$ .	125
Table 4.4 Electrochemical Redox Data of Mono-fused Porphyrins in $\text{CH}_2\text{Cl}_2$ at 298 K.	127
<b>CHAPTER 5</b>	
Table 5.1 Electronic Spectral Data of Synthesized Porphyrinoids in $\text{CH}_2\text{Cl}_2$ at 298 K.	145
Table 5.2 Comparative Electrochemical Redox Data of Synthesized Porphyrinoids in $\text{CH}_2\text{Cl}_2$ at 298 K.	147

## CHAPTER 6

Table 6.1	Selected Bond Lengths ( $\text{\AA}$ ) and Bond Angles ( $^\circ$ ) of Crystallized Compounds	173
Table 6.2	Spectroscopic Data of <b>1-4</b> and Corresponding Zn(II) Complexes ( <b>1d-4d</b> ) in $\text{CH}_2\text{Cl}_2$ .	176
Table 6.3	Photophysical Data of Synthesized Free base and their Zn(II) Complexes.	176
Table 6.4	Electrochemical Redox Data in $\text{CH}_2\text{Cl}_2$ at 298K using $\text{TBAPF}_6$ as Supporting Electrolyte.	180

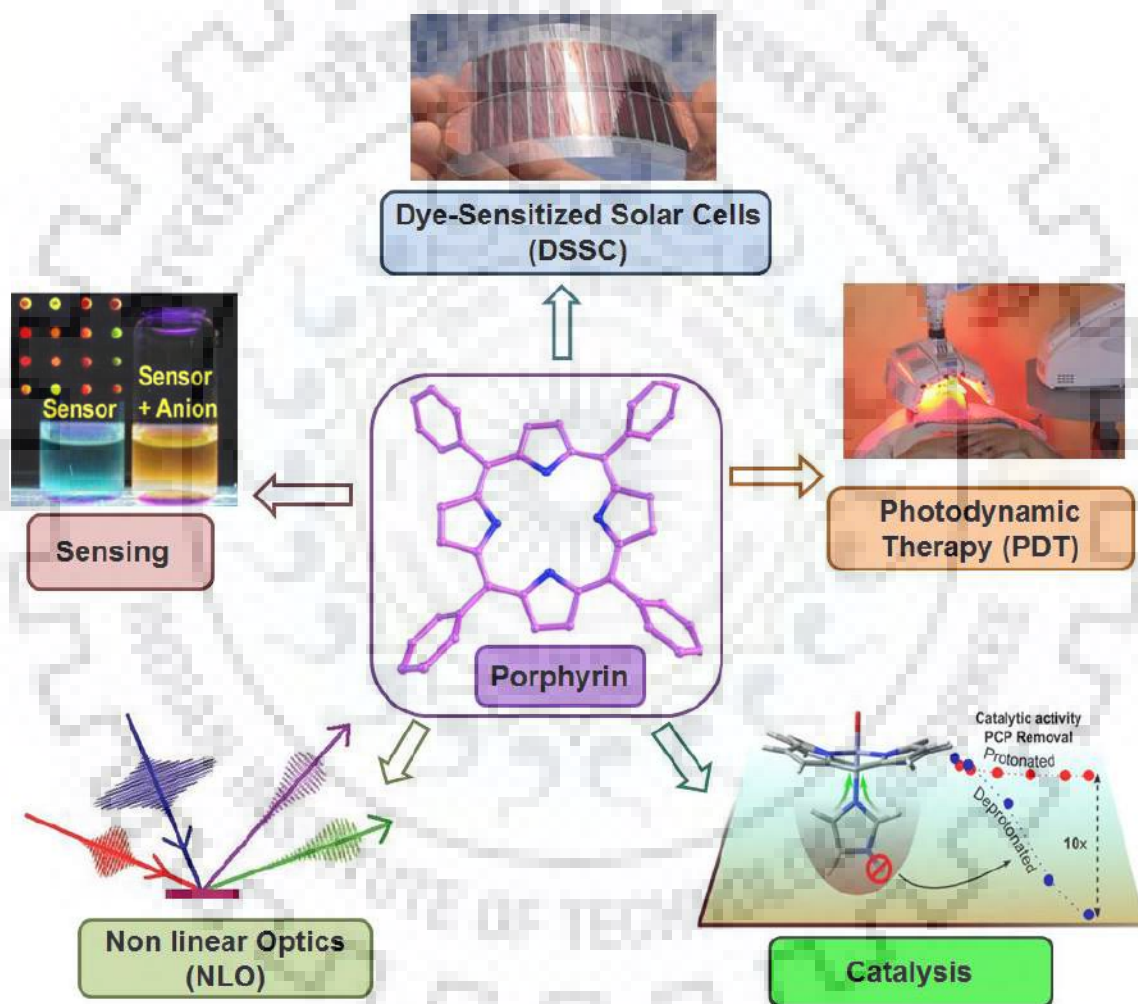
## CHAPTER 7

Table 7.1	UV-Visible and Fluorescence Spectral Data of <b>1-4</b> in Toluene at 298 K.	197
Table 7.2	Optical Absorption and Emission Spectral Data of $\text{MTPP}(\text{NO}_2)\text{Cl}_7$ and $\text{MTPP}\text{Cl}_8$ .	198
Table 7.3	Electrochemical Redox Data of Synthesised Porphyrins in $\text{CH}_2\text{Cl}_2$ at 298 K.	200
Table 7.4	Protonation and Deprotonation Constants ( $\beta_2$ and $\log \beta_2$ ) of <b>1-4</b> in Toluene.	201
Table 7.5	Association Constants of <b>1-4</b> with Various Anions in Toluene.	204
Table 7.6	The Detection Limits (LOD) and Quantification Limits (LOQ) of Anions by <b>1-4</b> in Toluene at 298 K.	205
Table 7.7	Equilibrium Constants ( $K_{\text{eq}}$ ) for The Ligation of Nitrogenous Bases With Zn(II) Complexes of Perchloroporphyrins in Toluene at 298 K.	210
Table 7.8	The Overall Binding Constants ( $\beta_2$ ) for the Ligation of Basic Anions with Zn(II) Complexes of Perchloroporphyrins in Toluene at 298 K.	211



# CHAPTER I

## “Introduction”







## CHAPTER 1

## INTRODUCTION

## 1.1 INTRODUCTION TO THE TETRAPYRROLIC PIGMENTS

Tetrapyrroles are the most abundant naturally occurring pigments that accomplish diverse biochemical functions and are essential in most of the known living organisms [1-4]. Tetrapyrrolic pigments consist of four pyrrole rings, interconnected through methine or methylene bridges except corrin ring system [5,6]. The naturally occurring tetrapyrroles mainly differ in their ring substituents, oxidation state of their ring system, and nature of the chelated metal ion [1-8]. The widely known members of this group are heme (responsible for the red color of blood) and chlorophyll (contributes to the observed green color of most of the plants, algae and some bacteria) (Figure 1.1) [9,10].

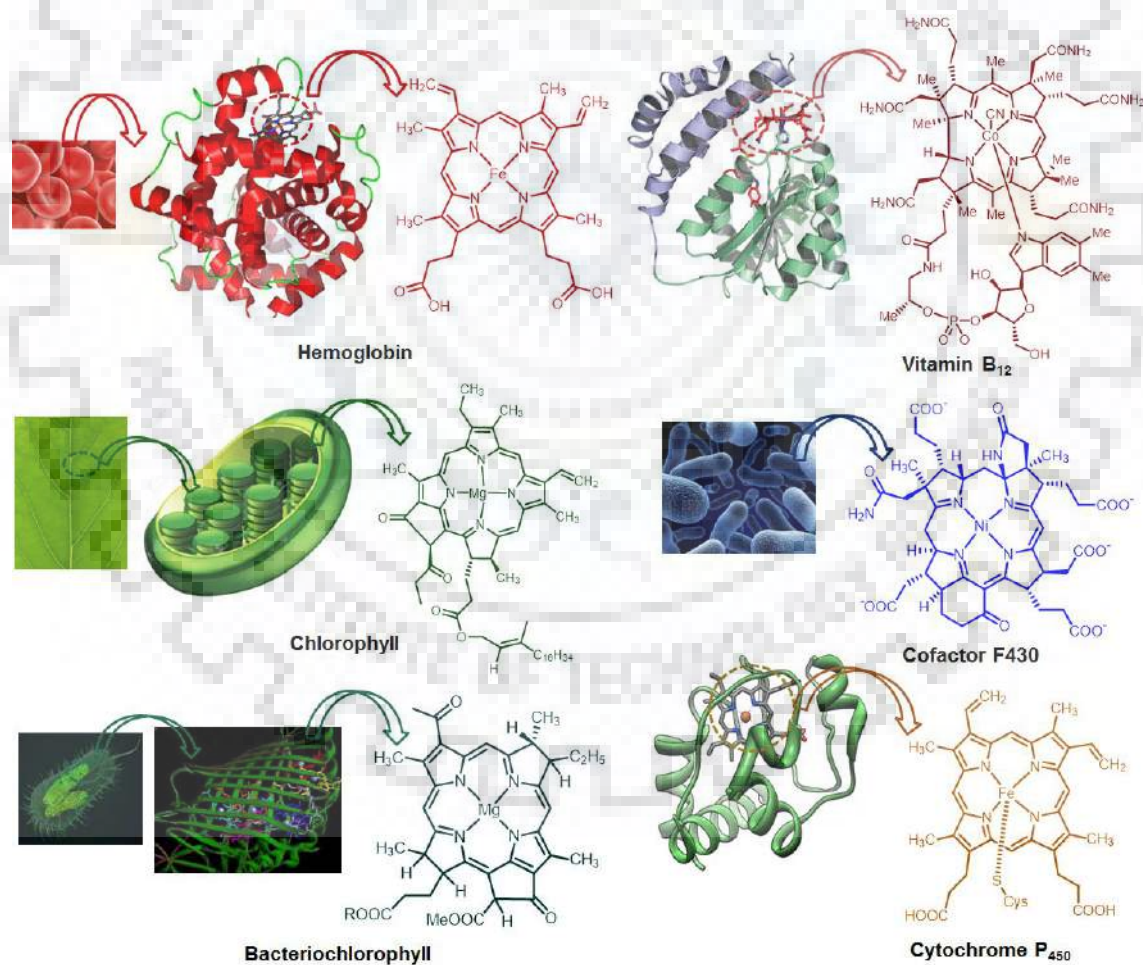


**Figure 1.1** Molecular Structures of Naturally Occurring Tetrapyrrole Pigments.

Among all, some biologically important and widespread naturally occurring tetrapyrroles are: vitamin B<sub>12</sub>, cytochrome P<sub>450</sub>, bacteriochlorophyll and coenzyme F430. The macrocyclic skeleton of heme is commonly known as porphyrin [11] whereas the tetrapyrrolic skeleton of chlorophyll and bacteriochlorophyll are known as chlorin and bacteriochlorin, respectively [12, 13]. The basic skeleton without any substitution is called porphine.

This introductory chapter includes a review of porphyrin literature on the *meso*/ $\beta$ -functionalized porphyrins, synthetic modification and utilization of the porphyrinoids in various application including dye-sensitized solar cells (DSSCs), photodynamic therapy (PDT), ion sensing, catalysis, and nonlinear optics (NLO).

## 1.2 SYNTHETIC PORPHYRIN ANALOGUES

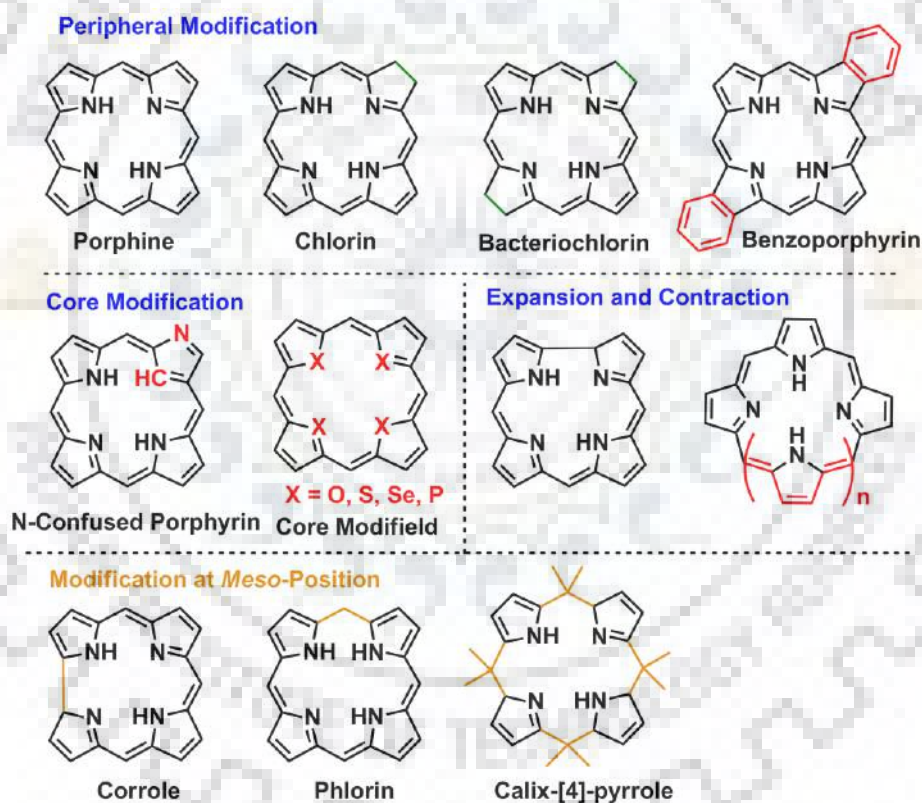


Figure 1.2 Synthetic Porphyrin Analogues.

Porphyrins are tetrapyrrolic 18- $\pi$  electron aromatic, highly conjugated macrocycles which undoubtedly represent one of the most widely studied of all known macrocyclic ring systems [14-16]. The advantage with porphyrin ligands is their conformational flexibility which allows them to adopt a wide range of nonplanar conformations. The chemical richness of this

macrocycle has inspired the study of a wide range of porphyrin analogues in recent years. Their electronic properties can be easily tuned by suitable structural modifications at the macrocyclic skeleton. Figure 1.2 shows the four following ways to modify the porphyrin skeleton: (a) modification at the periphery of the porphyrin which leads to the synthesis of a number of porphyrin analogues including  $\beta$ /*meso*-substituted porphyrins [17,18], chlorins [19], bacteriochlorins [20] and benzoporphyrins [21,22]. (b) One of the most attractive strategies to modify porphyrin skeleton is the replacement of one or two pyrrole N's with C and other heteroatoms such as O, S, Se, Te, Si, and P. The resulting class of modified porphyrins is known as N-confused porphyrins [23] or core-modified porphyrins [24,25]. (c) Synthetic modification *via* contraction or expansion of macrocycle or annulation of additional rings onto the porphyrin periphery often leads to contracted, expanded and annulated isomeric porphyrins [26-28]. (d) Modification over the bridging units which are connecting two pyrrole rings leads to different class of porphyrin analogues for examples phlorin and corroles [29,30].

### 1.3 LABORATORY SYNTHESIS OF PORPHYRIN

In 1967, Adler and Longo have reported the one pot synthesis of *meso*-substituted tetraarylporphyrins by allowing pyrrole and substituted aldehydes to react for 30 min. in refluxing propionic acid (141 °C) in open air [31]. This was the modified version of sealed tube reaction given by Rothmund in 1963 [32]. This reaction has allowed a wide range of substituted benzaldehydes to be converted into corresponding tetraphenylporphyrins [33]. Nonetheless this methodology was facing some vexing problems. First, the acid sensitive aldehydes were not stable towards it. Second, the formation of high level tar was creating purification problems. Third, this method was quite suitable for the synthesis of symmetrically substituted porphyrins ( $A_4$ ). While the condensation of two different aldehydes with pyrrole in a required ratio was producing a number of fractions with asymmetrically substituted porphyrins like  $A_4$ ,  $A_3B$ , *cis*- $A_2B_2$ , *trans*- $A_2B_2$ ,  $AB_3$  and  $B_4$ . Notably the purification of required product was quite tedious. Thus, to overcome these problems in 1980's, Lindsey and coworkers provided the milder reaction conditions for large scale syntheses of unsymmetrically *meso*-substituted porphyrins [34,35]. This methodology was not only appropriate for the preparation of tetraphenylporphyrins in high yields but also helpful in the synthesis of those substituted porphyrins which were inaccessible *via* alternative synthetic routes. The basic skeleton of porphyrin contains eight  $\beta$ -

positions, four *meso*-positions and four inner core nitrogen atoms for further functionalization (Figure 1.3) [36,37].

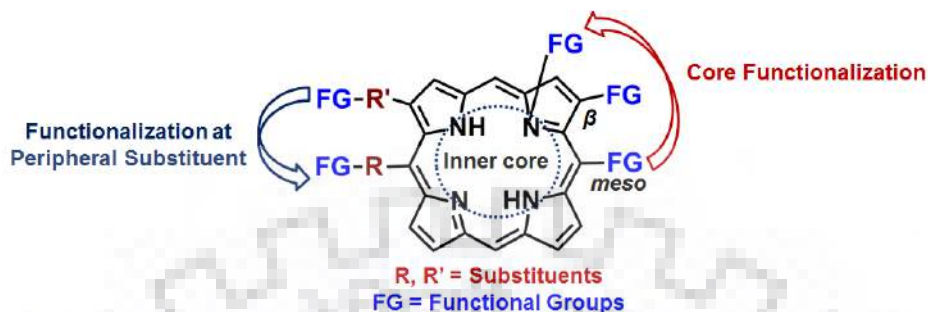


**Figure 1.3** Functionalization of Porphyrin by Positions.

## 1.4 FUNCTIONALIZATION OF PORPHYRIN

The syntheses of *meso*/ $\beta$ -functionalized porphyrins can be achieved by adopting two widespread ways (Figure 1.4). First consider the condensation of functionalized pyrrole with prior substituted aldehydes or condensing  $\beta$ -functionalized dipyrromethanes with substituted aldehydes [38,39]. Second includes the introduction of functional groups or substituents after construction of the macrocyclic core that is called post functionalization [37,40]. Furthermore the post functionalization can be achieved by two following methodologies: (a) core functionalization, and; (b) insertion of functional groups at the peripheral substituents. The condensation of substituted pyrroles with aldehydes is economically challengeable. The insertion of various functional groups through post functionalization involved a variety of chemical reactions including electrophilic addition or substitution [41], nucleophilic substitution [42], functional group transformation [43] and metal catalyzed cross coupling reactions [37,44,45]. Since the electronic properties of the porphyrin macrocycle can be modulated through functionalization at the  $\beta$  and/or *meso*-positions. In particular, the functionalization at  $\beta$ -pyrrolic position exerts pronounced steric and electronic effects on the porphyrin  $\pi$ -system as compared to *meso*-position [46-48].

The naturally occurring tetrapyrroles are  $\beta$ -substituted. The porphyrins with unsymmetrical  $\beta$ -substitutions are of special interest because they can mimic the naturally occurring porphyrinoids which are also having unsymmetrical  $\beta$ -substitution. Numerous varieties of  $\beta$ -substituted porphyrins are reported in literature [45-48] which have been derived *via* substitution, cross coupling reaction and free radical mechanism.



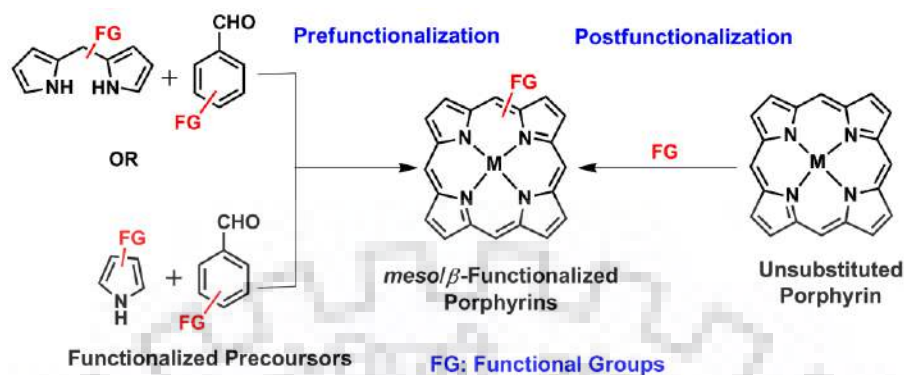


**Figure 1.4** Functionalization of Porphyrins.

## 1.5 MODIFICATION AT $\beta$ -PYRROLIC POSITION

Porphyrin can easily undergo a wide variety of electrophilic substitution reactions including nitration, formylation, halogenation etc. which lead to the synthesis of a library of  $\beta$ -functionalized porphyrins [49-51]. The resulting porphyrins further undergo many functional group transformations. Figure 1.4 shows the possible synthetic routes for the modification of  $\beta$ -pyrrolic position. The formyl and nitro groups are important attachment to the porphyrin ring as they can be easily modify and elaborated into other useful functionalities [52,53].

Initially in 1994, Crossley and coworkers have shown the nitroalkenes type reactivities of 2-nitroporphyrins in their reaction profiles and expediently used them for  $\beta$ -functionalization of tetrapyrroles [54]. In light of these findings, in the late of 1990s Smith and coworkers have effectively utilized 2-nitroporphyrin for the synthesis of a variety of dihydroporphyrins (chlorins), fused pyrroloporphyrins and naphthochlorins [55,56]. In 1996, Smith *et al.* have reported the first synthesis of pyrroloporphyrin based on Barton Zard condensation reaction [57], whereas Cavaleiro and coworkers have used 2-formylporphyrins for the synthesis of mono and di-pyrroloporphyrins [53]. The oxidation of  $\beta$ -pyrrole using  $\text{OsO}_4$  to provide diols have become an important tool for pyrrole modified approach (PMP approach) (Figure 1.5) [58]. The breaking and mending principle given by Brückner *et al.* has been proved as a versatile way for the generation of a large number of pyrrole modified porphyrins including 4, 5, 6 and 7-membered heterocyclic rings [59]. The reduction of one  $\beta$ -pyrrolic C-C double bond generally leads to the synthesis of chlorins, whereas the reduction of two opposite  $\beta$ - $\beta'$  double bonds leads to the synthesis of bacteriochlorins [13]. On the other hand, the reduction of two  $\beta$ -pyrrolic carbon-

carbon double bonds of parallel sides gives isobacteriochlorins [60]. Some of the pioneer research groups provided novel synthetic path to reach a wide range of tetraphenylchlorins [13].

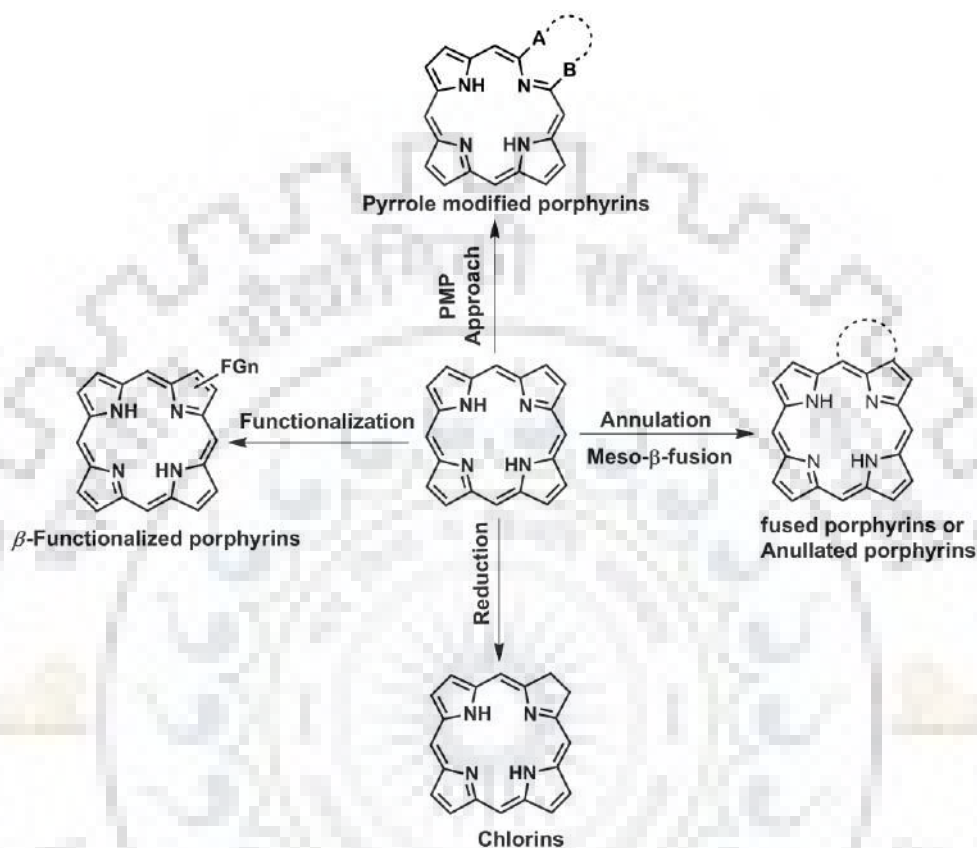


**Figure 1.5** Modification of Porphyrin Skeleton at  $\beta$ -Pyrrolic Positions.

Annulation of a ring onto the porphyrin periphery is also an important pathway to obtain a variety of modified porphyrin skeleton with tunable photophysical and electrochemical properties [61,62]. On the other hand, due to the unique photophysical and electrochemical redox properties which acquire from fused  $\pi$ -conjugated systems, the intramolecular fusion of porphyrin aromatic circuit has been an exciting subject from the last decade. Osuka and co-workers are the pioneer researchers who have synthesized a wide variety of *meso-meso*, *meso- $\beta$*  and  *$\beta$ - $\beta'$*  fused porphyrin systems using different strategies [63,64]. In 2013, Kojima and coworkers synthesized multiply fused porphyrins which described the effects of extended  $\pi$ -conjugation on the optical and electrochemical properties [65].

## 1.6 VARIOUS APPLICATIONS OF PORPHYRINOIDS

Synthetic porphyrinoids have been widely utilized for various applications due to their outstanding properties such as strong absorption in visible region, varying degree of  $\pi$ -conjugated nonplanar conformations, high thermal stability and good coordination ability. Some of the useful applications of porphyrins are described in details.

### 1.6.1 Porphyrinoids in DDSC Application

Due to the continuous growth in population and economy the world's limited energy resources will be exhausted in the coming future. Since various environmental problems are emerging day by day because of over consumption of fossil fuel, therefore artificial photosynthesis and photovoltaic are highly desirable technologies in this context because clean sun light harvesting is substantially inexhaustible. Dye-sensitized solar cells (DSSCs) have gained much attention in research over silicon-based solar cells due to their potential advantages of low-cost, easy production and high power conversion efficiencies [66,67]. In recent years, ruthenium based sensitizers and organic dyes have been effectively utilized for DSSC application [68,69]. Despite their overwhelming performance they encountered some vexing problems such as high cost, environmental concern, tiresome synthesis and low absorption in the red region which limit the large scale syntheses and bound the prospective for wide applications of these compounds. As DSSC mimics the natural photosynthesis thus the first report where chlorophyll was examined to function as photosensitizer on ZnO semiconductor for solar cell application was published by Tributsch in 1972 [70]. Later in 1993, Grätzel and coworker have used the chlorophyll derivatives and related natural porphyrins with TiO<sub>2</sub> solar cell for artificial photosynthesis where they achieved maximum power conversion efficiency of 2.6% [71]. *Meso*-substituted  $\pi$ -extended porphyrins with suitable donor and anchor groups have been largely explored and have proven excellent photosensitizers in DSSC application [72]. In 2011, Grätzel and coworkers have reported the D- $\pi$ -A type *meso*-substituted Zn<sup>II</sup> porphyrin based dye (**YD2-o-C8**) with 12.3% PCE (Figure 1.6) [73]. In extension of this potential work later in 2014, same group achieved the highest power conversion efficiency of 13% using porphyrin sensitizers (**SM371**, **SM315**) [74]. Recently in 2017, Kim and coworkers have been successful to increase the PCE value up to 14% for dye **SGT-021** by using tandem solar cell employing cobalt electrolyte in the top and bottom

cell [75]. This is the highest efficiency ever achieved for porphyrin based DSSC. Over past few years, the porphyrin sensitizer containing strong donor group such as diarylamino group and ethynylcarboxyphenyl group as an anchor are known to be the best performing sensitizer in the field of porphyrin chemistry [72]. Wang *et al.* introduced the thiophene-carboxylic instead of benzoic acid as an anchor group and ethynyl substituted donor where they have achieved the efficiency of 9.53% (Figure 1.6) [76].

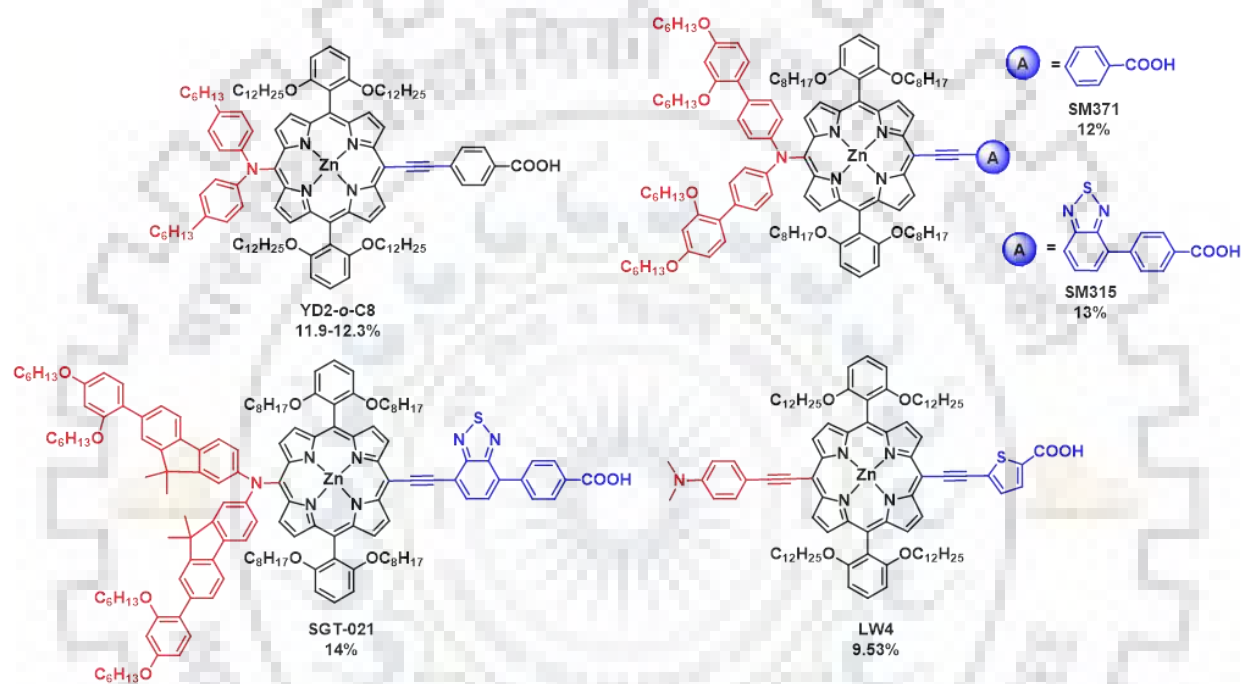


**Figure 1.6** *Meso*-substituted Highly Efficient Porphyrin based Sensitizers having PCE up to 14%.

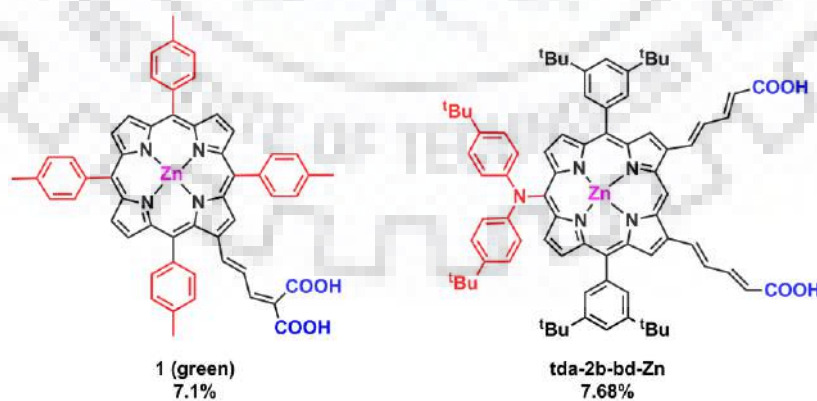


**Figure 1.7** Highly Efficient  $\beta$ -substituted Dyes.



Apart from *meso*-substituted porphyrins, in the past few decades a number of research groups have devoted many efforts to design “push-pull” kind of  $\beta$ -substituted Zn(II) tetraarylporphyrins which have an appropriate functional group at the  $\beta$ -pyrrolic position such as  $\pi$ -ethynyl system carrying a carboxylic group at the end (Figure 1.7) [77]. Already in 2007, Officer and coworkers have been achieved an encouraging efficiency of 7.1% for a pale green dye [78]. Later Kim *et al.* slightly improved the PCE value up to 7.68% for **tda-2b-bd-Zn** dye where they used diamine donor groups at the *meso*-position and two conjugated carboxylic acid groups at the  $\beta$ -pyrrolic positions [79]. Unlike porphyrins, chlorins are rarely used for DSSC application due to their synthetic difficulties [80].

On the basis of published results, one can clearly say that extended  $\pi$ -conjugated “push-pull” type porphyrins consist of strong electron donor groups and suitable anchor groups will shape the future for highly efficient photosensitizers in DSSC application.

### 1.6.2 Porphyrinoids as PDT Agents

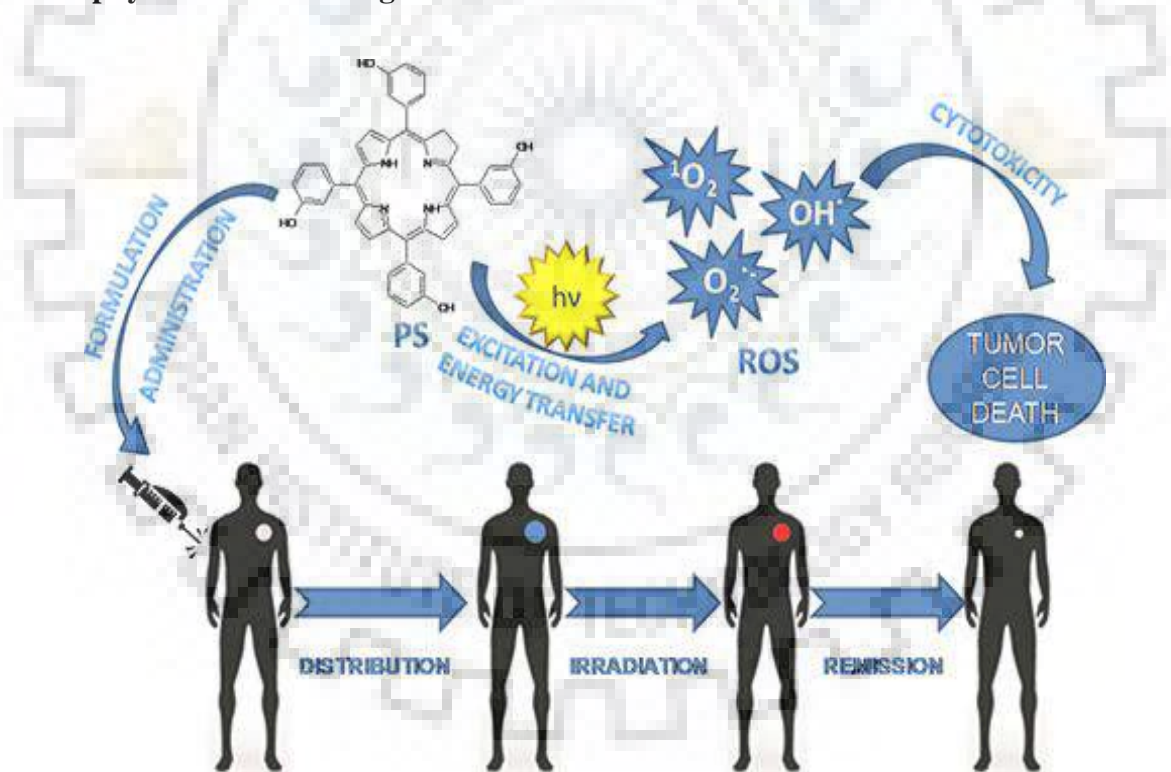


**Figure 1.8** Mechanisms of Photodynamic Reactions Involved in Photodynamic Therapy. (Copyright 2017 Intech).

Cancer is one of the death causing diseases. Now-a-days it is growing in much faster rate due to the common use of exposures such as toxic chemical, harmful radiations, or by natural mutation. Some traditional cancer treatment modalities are available which include surgery, chemotherapy and radiation therapy but they have the following side effects and drawbacks: (a) surgery can't be performed at every part of the body; (b) chemotherapy leads to vomiting, nausea, hair loss and sometimes leading to depress the immune system which causes immune disorders; (c) normal cells also getting affected which leads to low the normal organ function; (d) old aged patients who have weak immune systems can't bear the pain; (e) radiation destroys the epithelial surfaces and also causes swelling of soft tissues and infertility. In contrast, photodynamic therapy (PDT) is more controllable and does not exhibit other organ toxicity [81, 82]. It is capable to selectively destroy the malignant cells. PDT involves singlet oxygen as cytotoxic agent which is responsible for the selective destruction of tumor cells (Figure 1.8).

Some porphyrinoids including porphyrin, benzoporphyrins, texaphyrins, pthalocyanin, naphthalocyanins, chlorins and bacteriochlorins have been effectively utilized as PDT agents [83-87] for human clinic trails and approved by different health organization (Figure 1.9).

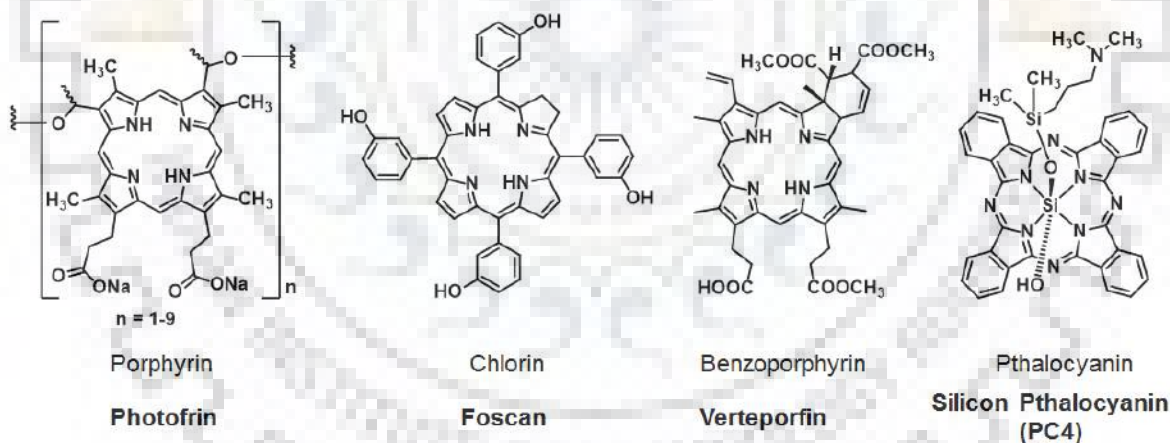


**Figure 1.9** Photosensitizers Approved by Different Health Organizations to Use in Human Clinical Trials.

In late of 1970s, Dougherty and his coworkers have introduced haematoporphyrin derivative; **HpD** (mixture of water soluble porphyrins) as the first photosensitizer, later the more purified version was named as **Photofrin** [88]. Pandey *et al.* are the pioneer researchers who are excellently working on the PDT applications of the porphyrin based photosensitizers [89,90].

Recently in 2016, they have explained the effect of metallation of porphyrin based sensitizers on the tumor imaging and photodynamic therapy where In(III) complex of **HPPH-CD** showed the best cancer imaging and PDT efficacy [91]. Though porphyrin based PSs performed well for cancer imaging still they have limitation to detect deeply seated tumor because of their small Stokes shifts which limits their application in fluorescence imaging. Therefore, still there is a requirement to develop bifunctional agents which can provide a unique approach to detect and cure the deeply seated tumor cells. The second major concern of the medical community is to use PDT for the treatment of infectious diseases which are untreatable by antibiotics. In this context, some cationic photosensitizers as a simple and highly effective antimicrobial PDT agent are being explored [92].

### 1.6.3 Porphyrins as Ion Chemosensors

The sensing of anions, neutral molecules, and cations has attracted substantial attention because of their prevalent distribution in environment and biological processes [93,94]. Porphyrinoids have a unique structural diversity which effectively helps them to show inherent advantages for ion recognition study *via* different sensing behavior. The inner core nitrogens are properly arranged for the recognition of basic anions. Hill, D'Souza, and coworkers explained that the anion binding to inner core protons led to the large cathodic shifts which empowered its application as an excellent electrochemical anion chemosensors [95]. Additionally they can chelate a wide variety of metals. Functionalization of porphyrin macrocyclic unit with specific ion receptors has also been proved one of the effective ways to recognize the biologically important ions [96]. In order to attain selectivity and enhanced sensitivity towards a particular ion especially anion, proper orientate of binding sites is required which is often difficult because of their different geometries, shape, and size. Over the past few decades, porphyrinoids such as phlorins [97], calixpyrroles [98], oxoporphyrinogens [99], saphyrins [100] and porphyrins [101] etc. have been proved outstanding multifunctional sensors for a variety of anions by different sensing strategies including chemosensing and chemodosimetry (Figure 1.10). The selective sensing of any target analyte can be achieved either by chemical bond formation/cleavage i.e. chemodosimetry or through supramolecular interactions i.e. chemosensing. Dicyanovinyl appended porphyrinoids have been proved the promising candidates for selective detection of cyanide ion through chemodosimetric methods [102]. Some of the pioneer research groups have

published few worthy reports which describe the dual sensing character of the macrocyclic skeletons [103, 104].

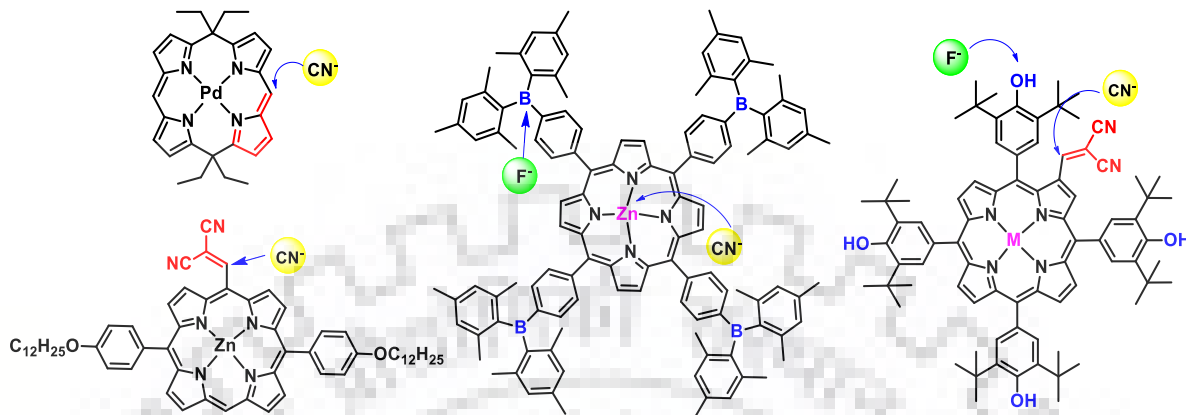


**Figure 1.10** Porphyrin Based Anion Sensors.

Metalloporphyrins have been extensively utilized for the selective detection of cyanide ion because metalloporphyrins show the Lewis acidic behavior due to the presence of metal ion in the macrocyclic core. Cyanide ion due to its intrinsic affinity; it binds to many metals such as copper, cobalt, rhodium and zinc through axial coordination [105]. Beer and coworkers developed several “picket fence” porphyrins with suitable anion-recognition arms connected to *meso*-positions of zinc porphyrin skeleton for modulating the anion binding strategies [106].

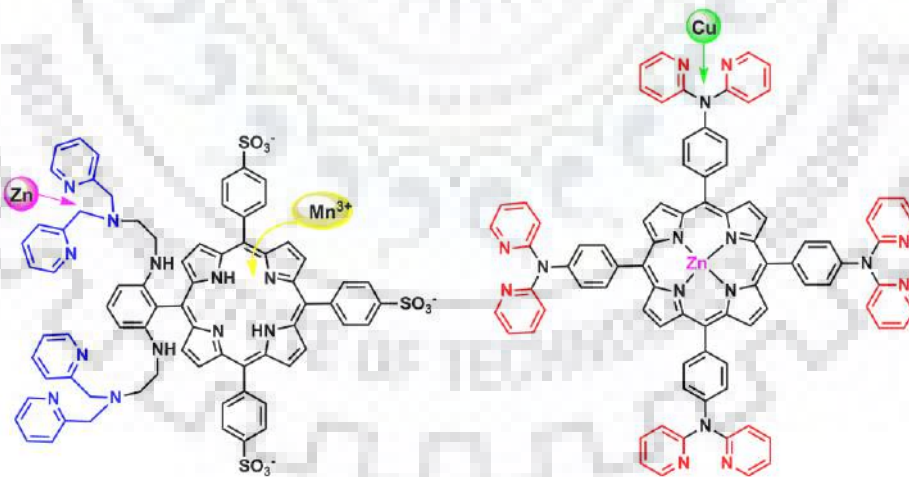


**Figure 1.11** Porphyrin Based Cation Sensors.

Till date, porphyrins periphery functionalized with different receptor units have been reported for the detection of a wide variety of cations such as  $\text{Cd}^{2+}$ ,  $\text{Cu}^{2+}$ ,  $\text{Zn}^{2+}$ ,  $\text{Pb}^{2+}$ ,  $\text{Hg}^{2+}$ ,  $\text{Mn}^{3+}$ , and  $\text{Y}^{3+}$  [107]. In addition, the chelation ability of porphyrins towards different metal ions can also be

considered as metal ion sensing ability (Figure 1.11). Wang, Lv, and coworkers demonstrated that the introduction of a triamino unit to the porphyrin periphery do not only enhanced its solubility in water but also designed a proper binding site for the selective detection of  $Zn^{2+}$  metal ion [108].

In spite of outstanding performance of porphyrin-based ion chemosensors in nonaqueous media, this research area is still at a growing stage because natural and biochemical analytes are most often present in aqueous media therefore the research on water soluble porphyrin sensors is required. At the other extreme, polymer-containing porphyrinic sensors are also in demand to make practical applications more useful.

#### 1.6.4 Porphyrins in Catalytic Application

Synthetic metalloporphyrins are the analogues of prosthetic groups of heme containing enzyme (cytochrome P450 enzyme) which catalyze various oxidation reaction with the same macrocyclic skeleton (protoporphyrin IX) where oxidation of organic substrates into water soluble products occurs [109,110]. Inspired by the mysteries surrounding the nature of reactive intermediates and high utilities of these organic transformations, many research groups explored the synthesis of several model metalloporphyrins that have successfully mimicked many aspects of the biological systems [111-113]. The first report based on metalloporphyrin catalyzed oxidation was given by Groves *et al.* in 1979 where iron-porphyrin complex ( $Fe(TPP)Cl$ ) catalyzed the hydroxylation and epoxidation of alkenes [114]. Iron and manganese complexes of porphyrins are known to be superior homogeneous catalyst for the oxygen transfer or oxygenation reactions [115,116].

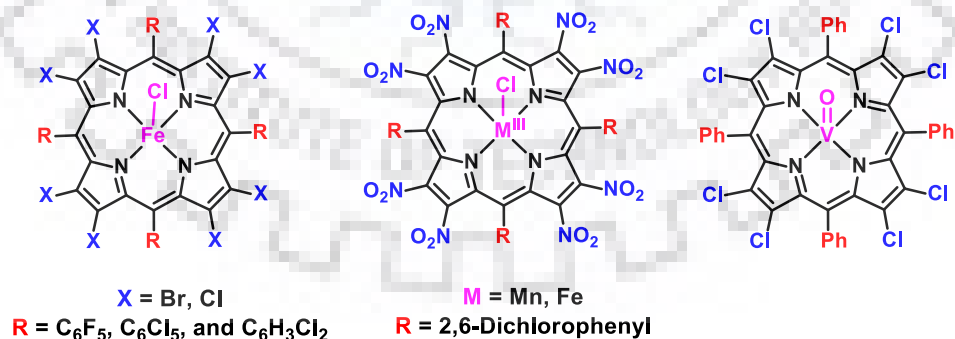


**Figure 1.12** Sterically Hindered  $\beta$ -Substituted Metalloporphyrin as Catalysts.



Highly  $\beta$ -substituted porphyrins have also been effectively utilized in catalytic oxygenation of alkenes and they have shown very high turnover numbers (TON) (Figure 1.12) [117]. For examples, perhalogenated porphyrins with phenyl, pentafluorophenyl, mesityl and 2,6-dichlorophenyl *meso*-substituents have been proven highly efficient robust catalysts [117,118]. Other than iron and manganese porphyrins, vanadyl porphyrins have also been used for catalytic application in oxidation of cyclohexane but the selectivity was not observed there. In this context, in 2015 our research group has used the vanadyl complex of perchloroporphyrin for the selective epoxidation of olefins [119]. It is observed that the high valent metalloporphyrins form oxido-peroxido species which react with organic substrates and transfer the oxygen to the substrate. Due to the steric strain between  $\beta$ -substituent these highly  $\beta$ -substituted porphyrins is prevented towards oxidative degradation which occurs through bimolecular attack.

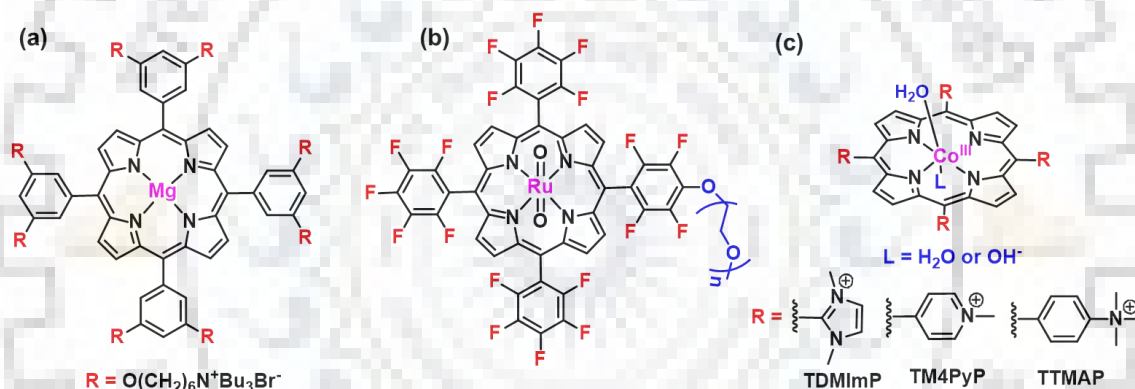


**Figure 1.13** Molecular Structures of Highly Efficient Porphyrin Based Catalysts Utilized in Various Catalytic Applications.

Apart from  $\beta$ -substituted porphyrins, sterically hindered *meso*-substituted porphyrins have also been used as efficient oxidative catalysts for epoxidation and hydroxylation reactions like Halterman porphyrins are a class of sterically hindered porphyrins which have proved to be good catalysts for alkene oxidation reaction [120]. Some recent advancement involved the synthesis of some water soluble porphyrins so that the catalytic application can be carried out in aqueous media. In 2006, Che and coworkers reported a unique water-soluble oxometalloporphyrin catalyst  $[\text{Ru}^{\text{VI}}(\text{F}_{20}\text{tp})\text{O}_2]\text{-PEG}$  which was reactive towards benzylic hydroxylation of ethylbenzene in both organic and aqueous media (Figure 1.13b) [121]. In 2013, Groves and Wang have used homogeneous cationic cobalt porphyrins for a very interesting water oxidation

reaction [122]. Very recently, Hasegawa and coworkers prepared bifunctional  $\text{Mg}^{\text{II}}$  porphyrin catalysts which have been effectively utilized for the solvent-free synthesis of cyclic carbonates from epoxides and  $\text{CO}_2$  [123].

### 1.6.5 Porphyrinoids as NLO Materials

Nonlinear optics deals with the phenomena which arise from the interaction of matter with intense radiation. In general, the optical properties of any system usually defined by the optical susceptibility  $\chi$  which is related to the refractive index and the dielectric constant. For an isolated molecule the molecular polarization is given by:

$$P = \alpha E + \beta EE + \gamma EEE \quad \text{Eq.1}$$

Where  $\alpha$  = linear polarizability,  $\beta$  = second order hyperpolarizability;  $\gamma$  = cubic hyperpolarizability and E is the applied electric field.

For an array of molecules, the polarization can be given as:

$$P = \chi^{(1)}E + \chi^{(2)}EE + \chi^{(3)}EEE \quad \text{Eq.2}$$

Where  $\chi^{(1)}$  = linear susceptibility,  $\chi^{(2)}$  = second order susceptibility and  $\chi^{(3)}$  third-order susceptibility.

In small electric field the second and third term are negligible so the molecule shows linear optical behavior however when molecule is irradiated with high electric field then 2<sup>nd</sup> and 3<sup>rd</sup> term become more evident and hence describes the nonlinear behavior so it is safe to say that nonlinearity of any molecule is only observed in intense field.

Porphyrins have rich photophysical properties and their excited state properties can easily be modulated through conformational changes of macrocyclic skeleton, symmetry of molecule, metal complexation, orientation and strength of the dipole moment. By modulating the degree of  $\pi$ -conjugation and introducing suitable donor-acceptor substituents at porphyrin periphery, the ground state absorption can be tuned with fine tuning of NLO properties [124]. All these aspects make them good candidates for NLO materials [125]. Since the optical materials have high dissipative optical nonlinearity, rapid response time, large dynamic range and a broadband spectral response. For a high nonlinear response, the material should have the effective delocalization of  $\pi$ -electron cloud. In this context, tetrapyrrolic aromatic systems are extremely useful because they consist of delocalized 18- $\pi$  electron system and show very good thermal

stability. A lot of efforts have been made to develop modern photonic devices based on porphyrins which exhibited outstanding NLO properties (Figure 1.15) [125,126].

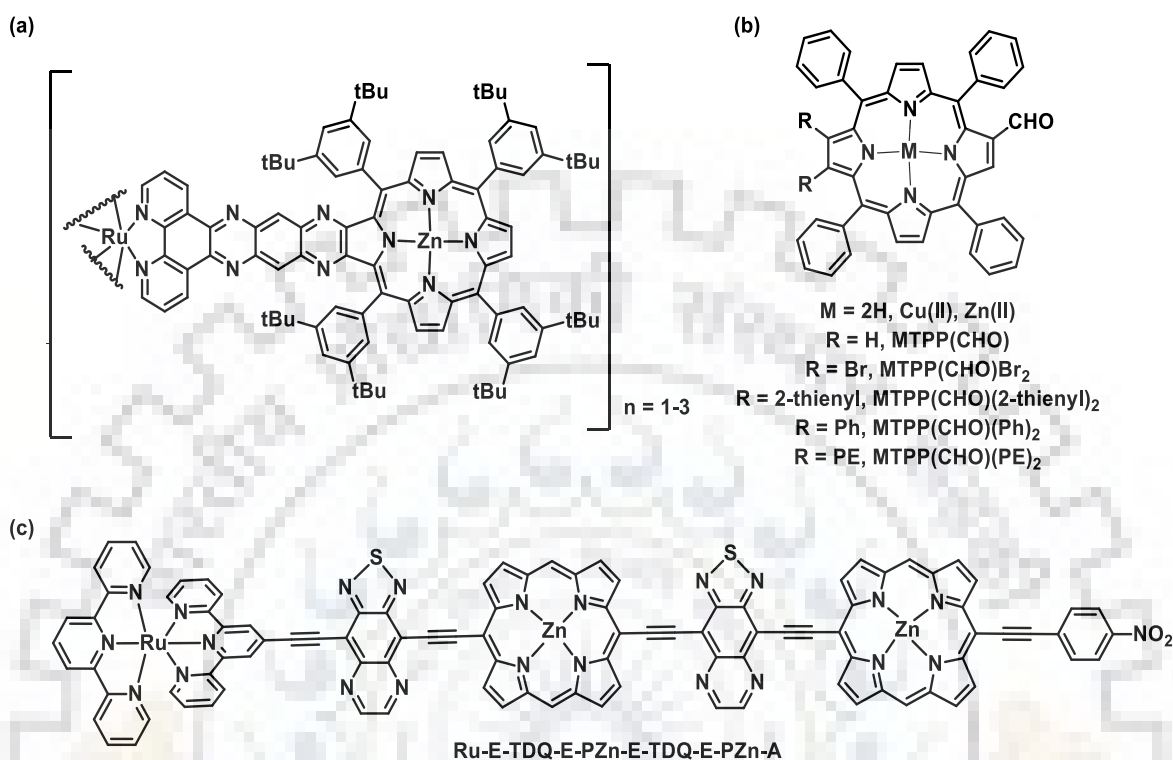


**Figure 1.14** Molecular Structures of Functionalized Porphyrins Used in NLO Applications.

The first NLO study of *meso*-substituted “push-pull” type porphyrins was established by Suslick and coworkers in early 1990s [127]. They used nitro group as an acceptor and diaminophenyl groups as donor at the *para*-positions of *meso*-phenyl rings. Later, Sen and coworkers investigated the “push-pull” type fluoroarylporphyrins containing 2-nitro group at the  $\beta$ -position and N,N-dimethylamino groups at *para* position of *meso*-phenyls for NLO applications [128]. The porphyrin oligomers are also known to be most promising candidate for NLO materials [124]. In 2012, Beratan *et al.* designed some coupled porphyrin chromophores with ruthenium complex which have shown unusually high hyperpolarizabilities [129]. Rely in 2015, Nolte and coworkers have synthesized zinc porphyrin dimers and trimers where two porphyrins were connected *via* ruthenium metal core and exhibited large third-order nonlinear optical absorption coefficients and refractive indices [130].



## 1.7 OBJECTIVES AND FUTURE SCOPE OF THE PRESENT WORK

$\beta$ -Substitution of porphyrin macrocycle is of growing interest because a limited number of reports are available in the literature for synthetic methodologies of  $\beta$ -substituted porphyrins. Since asymmetrically  $\beta$ -substituted porphyrins have immense variety of applications such as nonlinear optical (NLO) materials, sensitizers in DSSC, PDT agents, anion and cation sensors and as efficient catalysts which can mimic the metalloenzymes. The introduction of nitro group at the  $\beta$ -pyrrolic position is of particular interest because a variety of chemical reaction can be performed on 2-nitroporphyrins. Furthermore 2-nitroporphyrins due to their facile synthesis and ease of conversion into different function groups have been proved superior starting material for further functionalization. Nucleophilic substitution of 2-nitroporphyrin by various Michael donors provided a variety of  $\beta$ -substituted porphyrins or chlorins with tunable photophysical and electrochemical redox properties. Porphyrins with mixed substitution have been widely explored whereas the studies on mixed substituted chlorins have not been reported. In addition the modification of  $\beta$ -pyrrolic position *via* different chemical reaction is again an area of important research because it further changes the electronic of the macrocyclic system.

Fusion onto the porphyrin periphery is one of the modest ways to obtain a large number of modified porphyrins. Herein, we have synthesized *meso-o*-phenyl doubly fused porphyrins or doubly fused chlorins from *trans*-chlorins by adopting a facile synthetic route. The fused porphyrins have been widely explored by some pioneer research groups. On contrary, chlorins have reduced  $\beta$ -pyrroles thus the extension of  $\pi$ -conjugation by utilizing chlorins is still a challenging task.

The conversion of chlorins into metalloporphyrins is largely unexplored. We utilized one pot, one step synthesis of monofused nickel porphyrins which were derived from free base *trans*-chlorins. Generally fusion required a couple of reactions involving coupling, addition and substitution reactions but herein, free base *trans*-chlorins autoxidized into mono fused porphyrins. Metal catalyzed oxidation is common in organic synthesis but in porphyrin chemistry it is largely unexplored.

$\pi$ -Extension onto the porphyrin macrocycle upon  $\beta$ - $\beta'$  fusion has considerable attention owing to their potential application in optoelectronics, organic electronics, and photo medicines due to

their unique combination of photophysical and physicochemical properties. Heck coupling in porphyrins is quite difficult because it leads to the low yield in case of  $\beta$ - $\beta'$ -fused porphyrins i.e. benzoporphyrins. Further  $\beta$ -substitution of benzoporphyrins is of growing interest because a limited number of research articles are available in literature which describes the syntheses of mixed  $\beta$ -substituted benzoporphyrins. Still there is a space to introduce a simplest method to reach benzochlorins and explore the fusion chemistry of these benzochlorins. In this regards, we have synthesized and characterized some *trans*-benzochlorins and converted them into highly twisted  $\beta$ -to-*meso*-*o*-phenyl doubly fused benzoporphyrins. The highly electron deficient nonplanar conformation of macrocycles primed them suitable to display anion sensing properties through axial ligation.

$\beta$ -Nitroporphyrins are versatile starting material for further functionalization. Numerous porphyrin derivatives have been prepared by Smith, Cavaleiro and others. Often their structural, photophysical and electrochemical redox properties are unexplored. The  $\beta$ -nitro-tetraphenylporphyrins have been extensively utilized for synthesis of  $\beta$ -functionalized tri-substituted porphyrins. Further, we explored their spectroscopic and electrochemical redox properties.

Fully  $\beta$ -substituted electron deficient porphyrins are widely explored in literature due to their unique photochemical, stereochemical and redox properties. Further, these sterically crowded porphyrins have shown interesting catalytic application. But the use of these porphyrins in sensing applications is relatively new in the research field. In 2015, our research group has highlighted the ligation behavior of electron deficient metalloporphyrins towards cyanide ion. As continuous effort, we are presenting the use of highly nonplanar electron deficient porphyrins for the colorimetric detection of basic anions through anion induced deprotonation. Further Co(II) perchloroporphyrins have been used for the selective detection of cyanide ion.

The present thesis consists of following eight chapters:

*Chapter 1* deals with the general introduction about naturally occurring tetrapyrrolic pigments. It describes different synthetic routes for the synthetic analogues of porphyrins. Further it highlights functionalization of the macrocyclic core and different material and biological applications of the porphyrinoids.

Chapter 2 shows the various synthetic routes for  $\beta$ -substituted porphyrins or chlorins from 2-nitroporphyrin by varying the size of Michael donors. Further it describes the structural, photophysical and electrochemical redox properties of the synthesized porphyrinoids.

Chapter 3 describes the facile regioselective conversion of planar *trans*-chlorin in highly twisted doubly fused porphyrins (DFPs) or doubly fused chlorins (DFCs).

Chapter 4 deals with the Ni(II) acetate catalyzed auto-oxidation of free base *trans*-chlorins into Ni(II) mono-fused porphyrins Ni(II)MPPs.

Chapter 5 introduces the synthesis of nonplanar electron deficient benzochlorins and their oxidative fusion into triply fused  $\beta$ - $\beta'$  and *meso*- $\beta$ -fused porphyrins. Further it highlights the anion sensing properties of these newly synthesized porphyrinoids.

Chapter 6 includes the synthesis, structural, photophysical and electrochemical redox properties of mixed  $\beta$ -trisubstituted porphyrins derived from 2-nitroporphyrins.

Chapter 7 describes the colorimetric “Naked Eye” detection of basic anions by highly nonplanar electron deficient perhaloporphyrins. It also deals with the selective cyanide sensing by metal complexes of perchloroporphyrins.

Chapter 8 summaries the research work carried out in this thesis with future perspectives.

## 1.8 REFERENCES

1. Lippard, S. J.; Berg, J. M. “*Principles of Bioinorganic Chemistry*” University Science Books, Mill Valley, California, **1994**.
2. Battersby, A. R. Tetrapyrroles: The Pigments of Life. *Nat. Prod. Rep.* **2000**, *17*, 507-526.
3. Dolphin, D. “*The Porphyrins*” Academic Press, New York, **1979**.
4. Kadish, K. M.; Smith, K. M.; Guilard, R. Eds.; In *The Porphyrin Handbook*; Academic Press: New York, **2000**; Vol. 4
5. Burnham, B. F.; Plane, R. A. Studies on the Biosynthesis of the Corrin Ring of Vitamin B12. *Biochem. J.* **1966**, *98*, 13c-15c.

6. Halpern, J. Chemistry and Significance of Vitamin B12 Model System. In “*B12*” Dolphin, D. Eds.; John Wiley, New York, **1982**, Vol 1, pp. 501-542.
7. Kadish, K. M.; Smith, K. M.; Guilard, R. Eds.; In the Porphyrin Handbook; Academic Press: New York, **2000**; Vol. 3.
8. Kaim, W.; Schwederski, B. Bioinorganic Chemistry: Inorganic Elements in the Chemistry of Life: An Introduction and Guide. John Wiley & Sons, **1987**.
9. Jones, D. R.; Summerville, D. A.; Basolo, F. Synthetic Oxygen Carriers Related to Biological Systems. *Chem. Rev.* **1979**, *79*, 139-179.
10. Seely, G. R. The Structural and Chemistry of Functional Groups. In *The Chlorophyll*; Vernon, L. P.; Seely, G. R. Eds.; Academic Press: New York, **1966**, pp 67-109.
11. Poulos, T. L. Heme Enzyme Structure and Function. *Chem. Rev.* **2014**, *114*, 3919-3962.
12. Mass, O.; Taniguchi, M.; Ptaszek, M.; Springer, J. W.; Faries, K. M.; Diers, J. R.; Bocian, D. F.; Holten, D.; Lindsey, J. S. Structural and Characteristics that Make Chlorophylls Green: Interplay of Hydrocarbon Skeleton and Substituents. *New J. Chem.* **2011**, *35*, 76-88.
13. Taniguchi, M.; Lindsey, J. S. Synthetic Chlorins, Possible Surrogates for Chlorophylls, Prepared by Derivatized of Porphyrins. *Chem. Rev.* **2017**, *117*, 344-535.
14. Kadish, K. M.; Smith, K. M.; Guilard, R. Eds.; The Porphyrin Handbook, Academic Press, San Diego, **2000**.
15. Chatterjee, T.; Shetti, V. S.; Sharma, R.; Ravikanth, M. Heteroatom-Containing Porphyrin Analogues. *Chem. Rev.* **2017**, *117*, 3254-3328.
16. Fuhrhop, J.-H.; Smith, K. M. “*Laboratory methods*”. pp. 757-870. Smith, K.M. Ed., In Porphyrins and metalloporphyrins, Elsevier, Amsterdam, **1975**.
17. Hiroto, S.; Miyake, Y.; Shinokubo, H. Synthesis and Functionalization of Porphyrins through Organometallic Methodologies. *Chem. Rev.* **2017**, *117*, 2910-3043.
18. Kadish, K. M.; Smith, K. M.; Guilard, R., Eds., “Handbook of Porphyrin Science”, World Scientific Publishing Co. Inc., New Jersey, Vol. 1-25, **2012** and Vol. 25-35, **2014**.

19. Tome, A. C.; Lacerda, P. S. S.; Neves, M. G. P. M. S.; Cavaleiro, J. A. S. *Meso-Arylporphyrins as Dienophiles in Diels-Alder reactions: A Novel Approach to the Synthesis of Chlorins, Bacteriochlorins and Naphthoporphyrins.* *Chem. Commun.* **1997**, 1199-1200.
20. Chen, C.-Y.; Bocian, D. F.; Lindsey, J. S.; Synthesis of 24 Bacteriochlorin Isotopologues, Each Containing a Symmetrical Pair of  $^{13}\text{C}$  or  $^{15}\text{N}$  Atoms in the Inner Core of the Macrocycle. *J. Org. Chem.* **2014**, *79*, 1001-1016.
21. Jiao, L.; Hao, E.; Fronczek, F. R.; Vicente, M. G. H.; Smith, K. M. Benzoporphyrins via an Olefin Ring-Closure Metathesis Methodology. *Chem. Commun.* **2006**, 3900-3902.
22. Carvalho, C. M. B.; Santos, S. M.; Neves, M. G. P. M. S.; Tome, A. C.; Silva, A. M. S.; Rocha, J.; Cavaleiro, J. A. S. *Meso-Tetraphenylbenzoporphyrin-2<sup>2</sup>,2<sup>3</sup>-dicarboxylic Anhydride: A Platform to Benzoporphyrin Derivatives.* *J. Org. Chem.* **2013**, *78*, 6622-6631.
23. Hiroyuki Furuta, Tsutomu Asano, and Takuji Ogawa "N-Confused Porphyrin": A New Isomer of Tetraphenylporphyrin. *J. Am. Chem. Soc.* **1994**, *116*, 767-768.
24. Narayanan, S. J.; Sridevi, B.; Chandrashekar, T. K.; Vij, A.; Roy, R. Novel Core-Modified Expanded Porphyrins with *meso*-Aryl Substituents: Synthesis, Spectral and Structural Characterization. *J. Am. Chem. Soc.* **1999**, *121*, 9053-9068.
25. Maeda, C.; Yoneda, T.; Aratani, N.; Yoon, M.-C.; Lim, J. M.; Kim, D.; Yoshioka, N.; Osuka, A. Synthesis of Carbazole-Containing Porphyrinoids by a Multiple Annulation Strategy: A Core-Modified and  $\pi$ -Expanded Porphyrin. *Angew. Chem., Int. Ed.* **2011**, *50*, 5691-5694.
26. Sessler, J. L.; Seidel, D. Synthetic Expanded Porphyrin Chemistry. *Angew. Chem. Int. Ed.* **2003**, *42*, 5134-5175.
27. Sessler, J. L.; Gross, Z.; Furuta, H. Introduction: Expanded, Contracted, and Isomeric Porphyrins. *Chem. Rev.* **2017**, *117*, 2201-2202.
28. Sarma, T.; Panda, P. K. Annulated Isomeric, Expanded, and Contracted Porphyrins. *Chem. Rev.* **2017**, *117*, 2785-2838.

29. Kim, D.; Chun, H.-J.; Donnelly, C. C.; Geier, G. R. Two-Step, One-Flask Synthesis of a *Meso*-Substituted Phlorin. *J. Org. Chem.* **2016**, *81*, 5021-5031.
30. R. Orłowski, D. Gryko, D. T. Gryko, Synthesis of Corroles and Their Heteroanalogs. *Chem. Rev.* **117**, *4*, 3102-3137.
31. Adler, A. D.; Longo, F. R.; Finarelli, J. D.; Goldmacher, J.; Assour, J.; Korsakoff, L. A Simplified Synthesis for *Meso*-tetraphenylporphine. *J. Org. Chem.* **1967**, *32*, 476-476.
32. Rothmund, P. Formation of Porphyrins from Pyrrole and Aldehydes. *J. Am. Chem. Soc.* **1935**, *57*, 2010-2011.
33. Adler, A. D.; Longo, F. R.; Shergalis, W. Mechanistic Investigations of Porphyrin Syntheses. I. Preliminary Studies on *meso*-Tetraphenylporphin. *J. Am. Chem. Soc.* **1964**, *86*, 3145-3149.
34. Lindsey, J. S.; Schreiman, I. C.; Hsu, H. C.; Kearney, P. C.; Marguerettaz, A. M. Rothmund and Adler-Longo Reactions Revisited: Synthesis of Tetraphenylporphyrins under Equilibrium Conditions. *J. Org. Chem.* **1987**, *52*, 827-836.
35. Lindsey, J. S. Synthesis of *meso*-Substituted Porphyrins. In *The Porphyrin Handbook*; Kadish, K. M., Smith, K. M., Guillard, R., Eds.; Academic Press: San Diego, CA, **2000**, Vol. 1, pp 45-118.
36. Kalisch, W. W.; Senge, M. O. Facile *meso*-Functionalization of Porphyrins by Nucleophilic Substitution with Organolithium Reagents. *Angew. Chem., Int. Ed.* **1998**, *37*, 1107-1109.
37. Hiroto, S; Miyake, Y; Shinokubo, H. Synthesis and Functionalization of Porphyrins through Organometallic Methodologies. *Chem. Rev.* **2017**, *117*, 2910-3043.
38. Temelli, B.; Unaleroglu, C. Synthesis of *meso*-Tetraphenyl porphyrins via Condensation of Dipyrromethanes with N-tosyl Imines. *Tetrahedron* **2009**, *65*, 2043-2050.
39. Hao, E.; Fronczek, F. R.; Graca, M.; Vicente, H. Carborane Functionalized Pyrroles and Porphyrins via the Suzuki Cross Coupling Reaction. *Chem. Commun.* **2006**, 4900-4902.



40. Birin, K. P.; Gorbunova, Y. G.; Tsivadze, A. Y. New Approach for Post-Functionalization of *meso*-Formylporphyrins. *RSC Adv.* **2015**, *5*, 67242-67246.
41. Senge, M. O.; Gerstung, V.; Senge, K. R.; Runge, S.; Lehmann, I. Non-Planar Porphyrins with Mixed Substituent Pattern: Bromination and Formylation of Ethyl-Substituted Tetraphenylporphyrins and Tetraalkylporphyrins. *J. Chem. Soc. Dalton Trans.* **1998**, *24*, 4187-4199.
42. Senge, M. O. Nucleophilic Substitution as a Tool for the Synthesis of Unsymmetrical Porphyrins. *Acc. Chem. Res.* **2005**, *38*, 733-743.
43. Serra, V. I. V.; Pires, S. M. G.; Alonso, C. M. A.; Neves, M. G. P. M. S.; Tome, A. C.; Cavaleiro, J. A. S. *Meso*-tetraarylporphyrins Bearing Nitro or Amino Groups: Synthetic Strategies and Reactivity Profiles. *Top. Heterocycl. Chem.* **2014**, *33*, 35-78.
44. Mitchell, T. N. Organotin Reagents in Cross-Coupling Reactions, in *Metal-Catalyzed Cross-Coupling Reactions*. (Eds. de Meijere, A.; Diederich, F.), Wiley-VCH, Weinheim, **2004**, pp 125-161.
45. Kostas, I. D.; Coutsolelos, A. G.; Charalambidis, G.; Skondra, A. The First Use of Porphyrins as Catalysts in Cross-Coupling Reactions: a Water-Soluble Palladium Complex with a Porphyrin Ligand as an Efficient Catalyst Precursor for the Suzuki-Miyaura Reaction in Aqueous Media under Aerobic Conditions. *Tetrahedron Lett.* **2007**, 486688-486691.
46. Kalnoor, B. S.; Bisht, P. B.; Jena, K. C.; Velkannan, V.; Bhyrappa, P. Mixed  $\beta$ -Pyrrole Substituted *Meso*-Tetraphenylporphyrins and Their Metal Complexes: Optical Nonlinearity Using Degenerate Four Wave Mixing Technique. *J. Phys. Chem. A* **2013**, *117*, 8216-8221.
47. Kumar, R.; Sankar, M. Synthesis, Spectral, and Electrochemical Studies of Electronically Tunable  $\beta$ -Substituted Porphyrins with Mixed Substituent Pattern. *Inorg. Chem.* **2014**, *53*, 12706-12719.

48. Grover, N.; Song, Y.; Sankar, M.; Kasish, K. M. Asymmetrically Crowded “Push-Pull” Octaphenylporphyrins with Modulated Frontier Orbitals: Syntheses, Photophysical, and Electrochemical Redox Properties. *Inorg. Chem.* **2016**, *55*, 584-597.
49. Moura, N. M. M.; Faustino, M. A. F.; Neves, M. G. P. M. S.; Duarte, A. C.; Cavaleiro, J. A. S. Vilsmeier-Haack Formylation of Cu(II) and Ni(II) Porphyrin Complexes Under Microwaves Irradiation. *J. Porphyrins Phthalocyanines* **2011**, *15*, 652-658.
50. Giraudeau, A.; Callot, H. J.; Jordan, J.; Ezhar, I.; Gross, M. Substituent Effects in the Electroreduction of Porphyrins and Metalloporphyrins. *J. Am. Chem. Soc.* **1979**, *101*, 3857-3862.
51. Chumakov, D. E.; Khoroshutin, A. V.; Anisimov, A. V.; Kobrakov, K. I. Bromination of Porphyrins (Review). *Chem. Heterocycl. Compd.* **2009**, *45*, 259-283.
52. Crossley, M. J.; Sheehan, C. S.; Khoury, T.; Reimers, J. R.; Santic, P. J. Construction of Building Blocks For Extended Porphyrin Arrays by Nitration of Porphyrin-2, 3-diones and Quinoxalino[2,3-b]Porphyrins. *New J. Chem.* **2008**, *32*, 340-352.
53. Silva, A. M. G.; Faustino, M. A. F.; Tomé, A. C.; Neves, M. G. P. M. S.; Silva, A. M. S.; Cavaleiro, J. A. S. A Novel Approach to the Synthesis of Mono- and Dipyrroloporphyrins. *J. Chem. Soc., Perkin Trans. 1*, **2001**, 2752-2753.
54. Crossley, M. J.; Harding, M. M.; Tansey, C. W. A Convenient Synthesis of 2-Alky1-5,10,15,20-tetraphenylporphyrins: Reaction of Metallo-2-nitro-5,10,15,20-Tetraphenylporphyrins with Grignard and Organolithium Reagents. *J. Org. Chem.* **1994**, *59*, 4433-4437.
55. Shea, K. M.; Jaquinod, L.; Khoury, R. G.; Smith, K. M. Dodecasubstituted Metallochlorens (Metallodihydroporphyrins). *Chem. Commun.* **1998**, 759-760.
56. Shea, K. M.; Jaquinod, L.; Smith, K. M. Dihydroporphyrin Synthesis: New Methodology. *J. Org. Chem.* **1998**, *63*, 7013-7021.
57. Jaquinod, L.; Gros, C.; Olmstead, M. M.; Antolovich, M.; Smith, K. M. First Syntheses of Fused Pyrroloporphyrins. *Chem. Commun.* **1996**, 1475-1476.



58. Banerjee, S.; Zeller, M.; Brückner, C. OsO<sub>4</sub>-Mediated Dihydroxylation of *meso*-Tetraphenylporphyrin N-Oxide and Transformation of the Resulting Diolchlorin N-Oxide Regioisomers, *J. Org. Chem.* **2010**, *75*, 1179-1187.
59. Bruckner, C.; The Breaking and Mending of *meso*-Tetraarylporphyrins: Transmuting the Pyrrolic Building Blocks. *Acc. Chem. Res.* **2016**, *49*, 1080-1092.
60. Singh, S.; Aggarwal, A.; Thompson, S.; Tome, J. P. C.; Zhu, X.; Samaroo, D.; Vinodu, M.; Gao, R.; Drain, C. M. Synthesis and Photophysical Properties of Thioglycosylated Chlorins, Isobacteriochlorins, and Bacteriochlorins for Bioimaging and Diagnostics. *Bioconjugate Chem.* **2010**, *21*, 2136-2146.
61. C. Maeda, H. Shinokubo, A. Osuka, Synthesis of *meso*-5-Azaindolyl-Appended Zn(II) Porphyrins via Pd-Catalyzed Annulation. *Org. Lett.* **2007**, *9*, 2493-2496.
62. Shimizu, S.; Ito, Y.; Oniwa, K.; Hirokawa, S.; Miura, Y.; Matsushita, O.; Kobayashi, N. Synthesis of 5,10,15-Triazaporphyrins-Effect of Benzo-annulation on the Electronic Structures. *Chem. Commun.* **2012**, *48*, 3851-3853.
63. Fukui, N.; Cha, W.; Shimizu, D.; Oh, J.; Furukawa, K.; Yorimitsu, H.; Kim, D.; Osuka, A. Highly Planar Diarylamine-Fused Porphyrins and Their Remarkably Stable Radical Cations. *Chem. Sci.* **2017**, *8*, 189-199.
64. Nakamura, Y.; Aratani, N.; Shinokubo, H.; Takagi, A.; Kawai, T.; Matsumoto, T.; Yoon, Z. S.; Kim, D. Y.; Ahn, T. K.; Kim, D.; Muranaka, A.; Kobayashi, N.; Osuka, A. A Directly Fused Tetrameric Porphyrin Sheet and Its Anomalous Electronic Properties That Arise from the Planar Cyclooctatetraene Core. *J. Am. Chem. Soc.* **2006**, *128*, 4119-4127.
65. Ishizuka, T.; Saegusa, Y.; Shiota, Y.; Ohtake, K.; Yoshizawa, K.; Kojima, T. Multiply-Fused Porphyrins-Effects of Extended  $\pi$ -Conjugation on the Optical and Electrochemical Properties. *Chem. Commun.* **2013**, *49*, 5939-5941.
66. Grätzel, M. Recent Advances in Sensitized Mesoscopic Solar Cells. *Acc. Chem. Res.* **2009**, *42*, 1788-1798.

67. Han, L.; Islam, A.; Chen, H.; Malapaka, C.; Chiranjeevi, B.; Zhang, S.; Yang, X.; Yanagida, M. High-Efficiency Dye-Sensitized Solar Cell With A Novel Co-Adsorbent *Energy Environ. Sci.* **2012**, *5*, 6057-6060.
68. Chen, C.; Wang, M.; Li, J.; Pootrakulchote, N.; Alibabaei, L.; Ngoc-le, C.-H.; Decoppet, J.; Tsai, J.; Grätzel, C.; Wu, C.; Zakeeruddin, S. M.; Grätzel, M.; Highly Efficient Light-Harvesting Ruthenium Sensitizer for Thin-Film Dye-Sensitized Solar Cells. *ACS Nano* **2009**, *3*, 3103-3109.
69. Huang, J.; Wang, H.; Yan, K.; Zhang, X.; Chen, H.; Li, C.-Z.; Yu, J. Highly Efficient Organic Solar Cells Consisting of Double Bulk Heterojunction Layers. *Adv. Mater.* **2017**, *29*, 1606729(1-9).
70. Tributsch, H. Reaction of Excited Chlorophyll Molecules at Electrodes and In Photosynthesis. *J. Photochem. Photobiol.* **1972**, *16*, 261-269.
71. Kay, A.; Grätzel, M. Artificial Photosynthesis. 1. Photosensitization of Titania Solar Cells with Chlorophyll Derivatives and Related Natural Porphyrins. *J. Phys. Chem.* **1993**, *97*, 6272-6277.
72. Higashino, T.; Imahori, H. Porphyrins as Excellent Dyes for Dye-Sensitized Solar Cells: Recent Developments and Insights. *Dalton Trans.* **2015**, *44*, 448-463.
73. Yella, A.; Lee, H.-W.; Tsao, H. N.; Yi, C.; Chandiran, A. K.; Nazeeruddin, M. K.; Diao, E. W.-G.; Yeh, C.-Y.; Zakeeruddin, S. M.; Grätzel, M. Porphyrin-Sensitized Solar Cells with Cobalt<sup>(II/III)</sup>-Based Redox Electrolyte Exceed 12 Percent Efficiency. *Science* **2011**, *334*, 629-634.
74. Mathew, S.; Yella, A.; Gao, P.; Humphry-Baker, R.; Curchod, B. F. E.; Ashari-Astani, N.; Tavernelli, I.; Rothlisberger, U.; Nazeeruddin, M. K.; Grätzel, M. Dye-Sensitized Solar Cells With 13% Efficiency Achieved Through The Molecular Engineering of Porphyrin Sensitizers. *Nat. Chem.* **2014**, *6*, 242-247.
75. Kang, S. H.; Jeong, M. J.; Eom, Y. K.; Choi, I. T.; Kwon, S. M.; Yoo, Y.; Kim, J.; Kwon, J.; Park, J. H.; Ki, H. K. Porphyrin Sensitizers with Donor Structural Engineering for

- Superior Performance Dye-Sensitized Solar Cells and Tandem Solar Cells for Water Splitting Applications. *Adv. Mater.* **2017**, *7*, 1602117 (1-10).
76. Lu, J.; Xu, X.; Cao, K.; Cui, J.; Zhang, Y.; Shen, Y.; Shi, X.; Liao, L.; Cheng, Y.; Wang, M. D- $\pi$ -A Structured Porphyrins for Efficient Dye-Sensitized Solar Cells *J. Mater. Chem. A*, **2013**, *1*, 10008-10015.
77. Carlo, G. D.; Biroli, A. O.; Tessore, F.; Caramori, S.; Pizzotti, M.  $\beta$ -Substituted Zn<sup>II</sup> Porphyrins as Dyes for DSSC: A Possible Approach to Photovoltaic Windows. *Coord. Chem. Rev.* **2018**, *358*, 153-177.
78. Campbell, W. M.; Jolley, K. W.; Wagner, P.; Wagner, K.; Walsh, P. J.; Gordon, K. C.; Schmidt-Mende, L.; Nazeeruddin, M. K.; Wang, Q.; Gratzel, M.; Officer, D. L. Highly Efficient Porphyrin Sensitizers for Dye-Sensitized Solar Cells. *J. Phys. Chem. C* **2007**, *111*, 1760-1762.
79. Ishida, M.; Park, S. W.; Hwang, D.; Koo, Y. B.; Sessler, J. L.; Kim, D.Y.; Kim, D. Donor-Substituted  $\beta$ -Functionalized Porphyrin Dyes on Hierarchically Structured Mesoporous TiO<sub>2</sub> Spheres. *J. Phys. Chem. C* **2011**, *115*, 19343-19354.
80. Li, Y.-C.; Feng, Y.-Q.; Wang, Y.-T.; Fan, C.-C.; Liu, X.-J.; Li, X.-G.; Zhang, B. Design of High-Performance Chlorin Type Dyes for Dye-Sensitized Solar Cells. *Int. J. Quantum Chem.* **2014**, *114*, 222-232.
81. Macdonald, I. J.; Dougherty, T. J. Basic Principles of Photodynamic Therapy. *J. Porphyrins Phthalocyanines* **2001**, *5*, 105-129.
82. Pandey, R. K. Recent Advances in Photodynamic Therapy. *J. Porphyrins Phthalocyanines* **2000**, *4*, 368-373.
83. Ethirajan, M.; Chen, Y.; Joshi, P.; Pandey, R. K. The Role of Porphyrin Chemistry in Tumor Imaging and Photodynamic Therapy. *Chem. Soc. Rev.* **2011**, *40*, 340-362.
84. Chan, W. M.; Lim, T. H.; Pece, A.; Silva, R.; Yoshimura, N. Verteporfin PDT for Non-Standard Indications-A Review of Current Literature. *Graefes Arch. Clin. Exp. Ophthalmol.* **2010**, *248*, 613-626.

85. Pandey, R. K.; Bellnier, D. A.; Smith, K. M.; Dougherty, T. J. Chlorin and Porphyrin Derivatives as Potential Photosensitizers in Photodynamic Therapy. *Photochem. Photobiol.* **1991**, *53*, 65-72.
86. Sternberg, E. D.; Dolphin, D.; Brückner, C. Porphyrin Based Photosensitizers for Use in Photodynamic Therapy. *Tetrahedron* **1998**, *54*, 4151-4202.
87. Anderson, C. Y.; Freye, K.; Tubesing, K. A.; Li, Y. S.; Kenney, M. E.; Mukhtar, H.; Elmets, C. A. A. Comparative Analysis of Silicon Phthalocyanine Photosensitizers for In Vivo Photodynamic Therapy of RIF-1 Tumors in C3H mice. *Photochem. Photobiol.* **1998**, *67*, 332-336.
88. Dolmans, D. E.; Fukumura, D.; Jain, R. K. Photodynamic Therapy for Cancer. *Nat. Rev. Cancer*, **2003**, *3*, 380-387.
89. Chen, Y.; Sajjad, M.; Wang, Y.; Batt, C.; Nabi, H. A.; Pandey, R. K. TSPO 18 kDa (PBR) Targeted Photosensitizers for Cancer Imaging (PET) and PDT. *ACS Med. Chem. Lett.* **2011**, *2*, 136-141.
90. Gil, M.; Bieniasz, M.; Seshadri, M.; Fisher, D.; Ciesielski, M. J.; Chen, Y.; Pandey, R. K.; Kozbor, D. Photodynamic Therapy Augments The Efficacy of Oncolytic Vaccinia Virus Against Primary and Metastatic Tumours in Mice. *Br. J. Cancer* **2011**, *105*, 1512-1521.
91. Patel, N. J.; Chen, Y.; Joshi, P.; Pera, P.; Baumann, H.; Missert, J. R.; Ohkubo, K.; Fukuzumi, S.; Nani, R. R.; Schnermann, M. J.; Chen, P.; Zhu, J.; Kadish, K. M.; Pandey, R. K. Effect of Metalation on Porphyrin-Based Bifunctional Agents in Tumor Imaging and Photodynamic Therapy. *Bioconjugate Chem.* **2016**, *27*, 667-680.
92. Hamblin, M. R.; Hasan, T. Photodynamic Therapy: A New Antimicrobial Approach to Infectious Disease? *Photochem Photobiol Sci.* **2004**, *3*, 436-450.
93. Ueno, T.; Nagano, T. Fluorescent Probes for Sensing and Imaging. *Nat. Methods* **2011**, *8*, 642-645.
94. Carter, K. P.; Young, A. M.; Palme, A. E. Fluorescent Sensors for Measuring Metal Ions in Living Systems. *Chem. Rev.* **2014**, *114*, 4564-4601.

95. Schumacher, A. L.; Hill, J. P.; Ariga, K.; D'Souza, F. Highly Effective Electrochemical Anion Sensing Based on Oxoporphyrinogen. *Electrochem. Commun.* **2007**, *9*, 2751-2754.
96. Ding, Y.; Zhu, W.-H.; Xie, Y. Development of Ion Chemosensors Based on Porphyrin Analogues. *Chem. Rev.* **2017**, *117*, 2203-2256.
97. Pistner, A. J.; Lutterman, D. A.; Ghidui, M. J.; Ma, Y.-Z.; Rosenthal, J. Synthesis, Electrochemistry and Photophysics of a Family of Phlorin Macrocycles that Display Cooperative Fluoride Binding. *J. Am. Chem. Soc.* **2013**, *135*, 6601-6607.
98. Nishiyabu, R.; Anzenbacher, P. 1,3-Indane-Based Chromogenic Calixpyrroles with Push-Pull Chromophores: Synthesis and Anion Sensing. *Org. Lett.* **2006**, *8*, 359-362.
99. Hill, J. P.; Schumacher, A. L.; D'Souza, F.; Labuta, J.; Redshaw, C.; Elsegood, M. R. J.; Aoyagi, M.; Nakanishi, T.; Ariga, K. Chromogenic Indicator for Anion Reporting Based on an N-Substituted Oxoporphyrinogen. *Inorg. Chem.* **2006**, *45*, 8288-8296.
100. Sessler, J. L.; Davis, J. M. Sapphyrins: Versatile Anion Binding Agents. *Acc. Chem. Res.* **2001**, *34*, 989-997.
101. Kubo, Y.; Yamamoto, M.; Ikeda, M.; Takeuchi, M.; Shinkai, S.; Yamaguchi, S.; Tamao, K. A Colorimetric and Ratiometric Fluorescent Chemosensor with Three Emission Changes: Fluoride Ion Sensing by a Triarylborane-Porphyrin Conjugate. *Angew. Chem., Int. Ed.* **2003**, *42*, 2036-2040.
102. Chahal, M. K.; Sankar, M. Switching between Porphyrin, Porphodimethene and Porphyrinogen Using Cyanide and Fluoride Ions Mimicking Volatile Molecular Memory and the 'NOR' logic gate. *Dalton Trans.* **2016**, *45*, 16404-16412.
103. Li, Y.; Cao, L.; Tian, H. Fluoride Ion-Triggered Dual Fluorescence Switch Based on Naphthalimides Winged Zinc Porphyrin. *J. Org. Chem.* **2006**, *71*, 8279-8282.
104. Swamy, P. C. A.; Mukherjee, S.; Thilagar, P. Dual Binding Site Assisted Chromogenic and Fluorogenic Recognition and Discrimination of Fluoride and Cyanide by a Peripherally Borylated Metalloporphyrin: Overcoming Anion Interference in Organoboron Based Sensors. *Anal. Chem.* **2014**, *86*, 3616-3624.

105. Kumar, R.; Chaudhri, N.; Sankar, M. Ratiometric and Colorimetric “Naked Eye” Selective Detection of CN<sup>-</sup> Ions by Electron Deficient Ni(II) Porphyrins and Their Reversibility Studies. *Dalton Trans.* **2015**, *44*, 9149-9157.
106. Cormode, D. P.; Murray, S. S.; Cowley, A. R.; Beer, P. D. Sulfate Selective Anion Recognition by a Novel tetra-Imidazolium Zinc Metalloporphyrin Receptor. *Dalton Trans.* **2006**, 5135-5140.
107. Okamoto, K.; Fukuzumi, S. An Yttrium Ion-Selective Fluorescence Sensor Based on Metal Ion-Controlled Photoinduced Electron Transfer in Zinc Porphyrin-Quinone Dyad. *J. Am. Chem. Soc.* **2004**, *126*, 13922-13923.
108. Lv, Y.; Cao, M.; Li, J.; Wang, J. A Sensitive Ratiometric Fluorescent Sensor for Zinc(II) with High Selectivity. *Sensors* **2013**, *13*, 3131-3141.
109. Cytochrome P-450; Structure, Mechanism and Biochemistry; Ortiz de Montellano, P., Ed.; Plenum Press: New York, 1985.
110. Meunier, B.; de Visser, S. P.; Shaik, S. Mechanism of Oxidation Reactions Catalyzed by Cytochrome P450 enzymes. *Chem. Rev.* **2004**, *104*, 3947-3980.
111. Meunier, B. Metalloporphyrins as Versatile Catalysts for Oxidation Reactions and Oxidative DNA Cleavage. *Chem. Rev.* **1992**, *92*, 1411-1456.
112. Che, C. M.; Lo, V. K. Y.; Zhou, C. Y.; Huang, J. S. Selective Functionalization of Saturated C-H Bonds with Metalloporphyrin Catalysts. *Chem. Soc. Rev.* **2011**, *40*, 1950-1975.
113. Groves, J. T.; Watanabe, Y. Heterolytic and Homolytic O-O Bond-Cleavage Reactions of (Acylperoxo)Manganese(III) Porphyrins. *Inorg. Chem.* **1986**, *25*, 4808-4810.
114. Groves, J. T.; Nemo, T. E.; Myers, R. S. Hydroxylation and Epoxidation Catalyzed by Iron-Porphine Complexes. Oxygen Transfer from Iodosylbenzene. *J. Am. Chem. Soc.* **1979**, *101*, 1032-1033.
115. Green, M. T.; Dawson, J. H.; Gray, H. B. Oxoiron(IV) in Chloroperoxidase Compound II is Basic: Implications for P450 Chemistry. *Science* **2004**, *304*, 1653-1656.



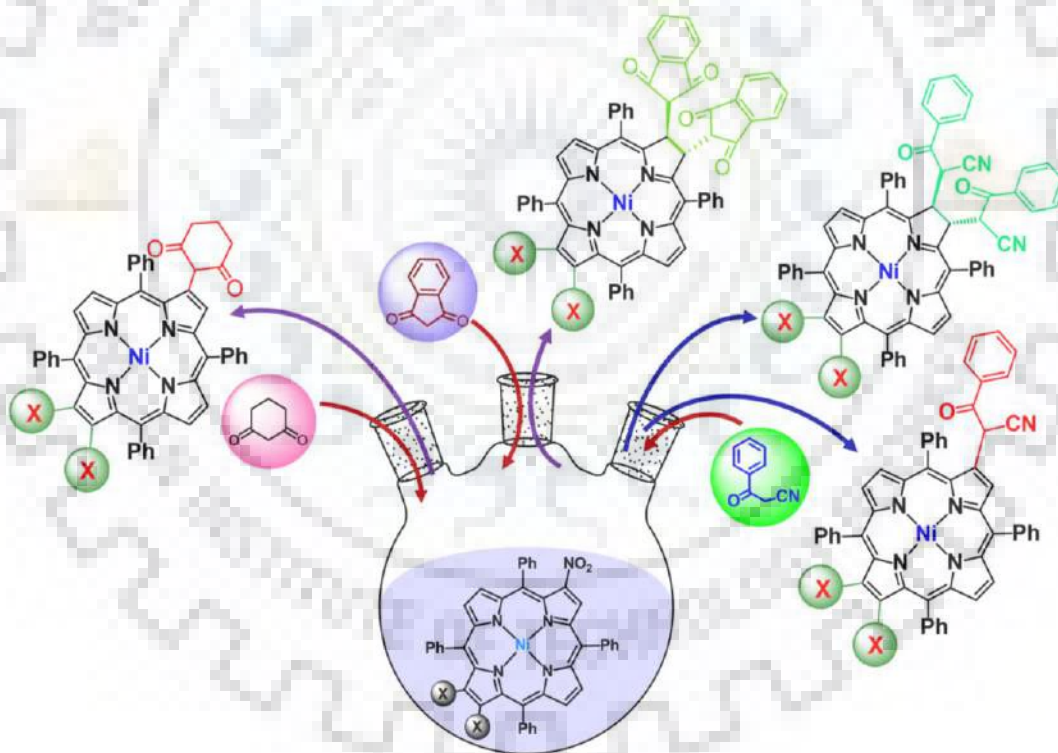
116. Liu, W.; Groves, J. T. Manganese Catalyzed C-H Halogenation. *Acc. Chem. Res.* **2015**, *48*, 1727-1735.
117. Grinstaff, M. W.; Hill, M. G.; Labinger, L. A.; Gray H. B. Mechanism of Catalytic Oxygenation of Alkanes by Halogenated Iron Porphyrins. *Science* **1994**, *264*, 1311-1313.
118. Dolphin, D.; Traylor, T. G.; Xie, L. Y. Polyhaloporphyrins: Unusual Ligands for Metals and Metal-Catalyzed Oxidations. *Acc. Chem. Res.* **1997**, *30*, 251-259.
119. Kumar, R.; Chaudhary, N.; Sankar, M.; Maurya, M. R. Electron Deficient Nonplanar  $\beta$ -Octachlorovanadylporphyrin as a Highly Efficient and Selective Epoxidation Catalyst for Olefins. *Dalton Trans.* **2015**, *44*, 17720-17729.
120. Lai, T.-S.; Chan, F.-Y.; So, P.-K.; Ma, D.-L.; Wong, K.-Y. Che, C.-M. Alkene Cyclopropanation Catalyzed by Halterman Iron Porphyrin: Participation of Organic Bases as Axial Ligands. *Dalton Trans.* **2006**, 4845-4851.
121. Zhang, J.-L.; Huang, J.-S.; Che, C.-M. Oxidation Chemistry of Poly(ethylene glycol)-Supported Carbonylruthenium(II) and Dioxoruthenium(VI) *meso*-Tetrakis(pentafluorophenyl)porphyrin. *Chem.-Eur. J.* **2006**, *12*, 3020-3031.
122. Wang D.; Groves, J. T. Efficient Water Oxidation Catalyzed by Homogeneous Cationic Cobalt Porphyrins with Critical Roles for the Buffer Base. *Proc. Natl. Acad. Sci.* **2013**, *110*, 15579-15584.
123. Ema, T.; Miyazaki, Y.; Shimonishi, J.; Maeda, C.; Hasegawa, J.-Y. Bifunctional Porphyrin Catalysts for the Synthesis of Cyclic Carbonates from Epoxides and CO<sub>2</sub>: Structural Optimization and Mechanistic Study. *J. Am. Chem. Soc.* **2014**, *136*, 15270-15279.
124. Tanaka, T.; Osuka, A. Conjugated Porphyrin Arrays: Synthesis, Properties and Applications for Functional Materials. *Chem. Soc. Rev.* **2015**, *44*, 943-969.
125. Senge, M. O.; Fazekas, M.; Notaras, E. G. A.; Blau, W. J.; Zawadzka, M.; Locos, O. B.; Ni Mhuircheartaigh, E. M. Nonlinear Optical Properties of Porphyrins. *Adv. Mater.* **2007**, *19*, 2737-2774.

126. Kalnoor, B. S.; Bisht, P. B.; Jena, K. C.; Velkannan, V.; Bhyrappa, P. Mixed  $\beta$ -Pyrrole Substituted meso-Tetraphenylporphyrins and Their Metal Complexes: Optical Nonlinearity Using Degenerate Four Wave Mixing Technique. *J. Phys. Chem. A* **2013**, *117*, 8216-8221.
127. Suslick, K. S.; Chen, C.-T.; Meredith, G. R.; Cheng, L.-T. Push-Pull Porphyrins as Nonlinear Optical Materials. *J. Am. Chem. Soc.* **1992**, *114*, 6930-6931.
128. Sen, A.; Ray, P. C.; Das, P. K.; Krishnan, V. Metalloporphyrins for Quadratic Nonlinear Optics. *J. Phys. Chem.* **1996**, *100*, 19611-19613.
129. Jiang, N.; Zuber, G.; Keinan, S.; Nayak, A.; Yang, W.; Therien, M. J.; Beratan, D. N. Design of Coupled Porphyrin Chromophores with Unusually Large Hyperpolarizabilities. *J. Phys. Chem. C* **2012**, *116*, 9724-9733.
130. de Torres, M.; Semin, S.; Razdolski, I.; Xu, J.; Elemans, J. A. A. W.; Rasing, T.; Rowan, A. E.; Nolte, R. J. M. Extended  $\pi$ -Conjugated Ruthenium Zinc-Porphyrin Complexes with Enhanced Nonlinear-Optical Properties. *Chem. Commun.* **2015**, *51*, 2855-2858.



## CHAPTER 2

“Versatile Synthetic Route for  $\beta$ -Functionalized Chlorins and Porphyrins by Varying the Size of Michael Donors: Syntheses, Photophysical and Electrochemical Redox Properties”





## CHAPTER 2

**VERSATILE SYNTHETIC ROUTE FOR  $\beta$ -FUNCTIONALIZED CHLORINS AND PORPHYRINS BY VARYING THE SIZE OF MICHAEL DONORS: SYNTHESSES, PHOTOPHYSICAL AND ELECTROCHEMICAL REDOX PROPERTIES****2.1 INTRODUCTION**

*Meso*-tetraarylporphyrins are widely explored due to their facile synthesis, characteristic deep colors, intense fluorescence, high photochemical stability, and also their ability to chelate a wide variety of metal ions in their inner core [1,2]. Therefore, they have wide-range of utilities in biology and material chemistry [3-5] such as artificial photosynthesis [6], catalysis [7], DSSC [8], nonlinear optics [9], and chemosensing [10]. In most of these applications, it is enviable to tune the optical properties of porphyrin  $\pi$ -system by the modification of macrocyclic core [11-13]. Several methods have been reported in literature for the conversion of porphyrins into chlorins [13-15]. The insertion of single nitro group at the  $\beta$ -pyrrolic position of porphyrin is one of the successful examples that have been widely used to obtain chlorins [16]. MTPP(NO<sub>2</sub>) undergoes a variety of S<sub>N</sub>Ar reaction with a wide range of nucleophiles and reveals the Michael acceptor character of this macrocycle. Generally, S<sub>N</sub>Ar reactions are preferred with electron-deficient aromatic compounds. For that purpose, synthetically accessible  $\beta$ -nitroporphyrins would be the better applicant over halogenated porphyrins. The electronic properties of chlorins allows them to capture more light of longer wavelength region for light harvesting [17], PDT [18], and singlet oxygen generation [19].

Recently, Brückner *et al.* have reported the synthesis of various pyrrole modified porphyrins by formal replacement of a pyrrole with several types of fused rings for e.g. carbaporphyrinoids, benziporphyrins, oxypyriporphyrins, indaphyrins and indachlorins etc. [20-22]. However, still there is a space to introduce cyclic moiety through C-C bond formation at reduced or conjugated  $\beta$ -pyrrole without breaking or mending the pyrrole ring. This inspired us to perform functionalization at the  $\beta$ -pyrrole positions of TPP derivatives, which led to the synthesis of  $\beta$ -functionalized porphyrins and/or chlorins.

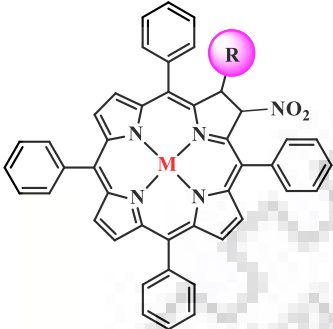
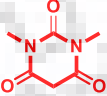
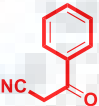
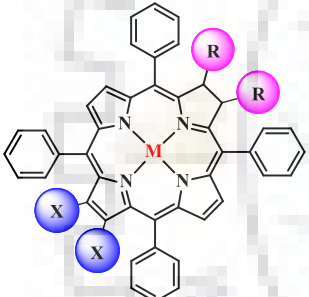
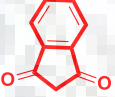
Herein, eight new families of  $\beta$ -substituted porphyrins and chlorins have been synthesized in which each chlorin bears vicinal groups at the reduced pyrrole ring whereas each porphyrin bears mono-substituent at the  $\beta$ -position (Charts 2.1 and 2.2).

Three distinct methods have been developed for the synthesis of chlorins and porphyrins bearing cyclic-1,3-dione derivatives. (a) Reaction of relatively small size cyclic-1,3-dione (cyclohexane-1,3-dione (CHD) and 1,3-dimethylbarbituric acid (DMBA)) with MTPP(NO<sub>2</sub>) and MTPP(NO<sub>2</sub>)Br<sub>2</sub> where M = 2H and Ni(II) yielded mono and tri- $\beta$ -substituted porphyrins, respectively. (b) Reaction of relatively moderate sized nucleophile such as benzoylacetonitrile (BENAC) with NiTPP(NO<sub>2</sub>) and NiTPP(NO<sub>2</sub>)Br<sub>2</sub> afforded mono- and tri-  $\beta$ - substituted porphyrins and di-/tetra-substituted chlorins. (c) Reaction of relatively large size active methylene compound such as indane-1,3-dione (IND) with MTPP(NO<sub>2</sub>) and MTPP(NO<sub>2</sub>)Br<sub>2</sub> where M = 2H, Ni(II) yielded di-/tetra-substituted chlorins. However, no porphyrin formation was observed in the last case. Cyclic-1,3-diones are widely used in heterocyclic synthesis [23]. Therefore, the introduction of these substituents at  $\beta$ -position of porphyrins makes them good substrates for further functionalization.

**Chart 2.1** Molecular Structures of Synthesized Porphyrins.

Porphyrins	R	X	M	Name	Code	% Yield
		H	2H	H <sub>2</sub> TPP(CHD)	<b>1</b>	78
		Ni(II)		NiTPP(CHD)	<b>1a</b>	65
		Zn(II)		ZnTPP(CHD)	<b>1b</b>	80
		Br	2H	H <sub>2</sub> TPPBr <sub>2</sub> (CHD)	<b>2</b>	72
		Ni(II)		NiTPPBr <sub>2</sub> (CHD)	<b>2a</b>	70
		Zn(II)		ZnTPPBr <sub>2</sub> (CHD)	<b>2b</b>	77
		H	2H	H <sub>2</sub> TPP(DMBA)	<b>3</b>	63
		Ni(II)		NiTPP(DMBA)	<b>3a</b>	60
		Zn(II)		ZnTPP(DMBA)	<b>3b</b>	77
		Br	2H	H <sub>2</sub> TPPBr <sub>2</sub> (DMBA)	<b>4</b>	87
		Ni(II)		NiTPPBr <sub>2</sub> (DMBA)	<b>4a</b>	58
		Zn(II)		ZnTPPBr <sub>2</sub> (DMBA)	<b>4b</b>	84
	H	Ni(II)	NiTPP(BENAC)	<b>5</b>	26	
	Br	Ni(II)	NiTPPBr <sub>2</sub> (BENAC)	<b>6</b>	23	

**Chart 2.2** Molecular Structures of Synthesized Chlorins.

Chlorins	R	X	M	Name	Code	% Yield
			2H	H <sub>2</sub> TPC(NO <sub>2</sub> )(DMBA)	<b>7</b>	10
			2H	H <sub>2</sub> TPC(BENAC) <sub>2</sub>	<b>8</b>	80
		H	Ni(II)	NiTPC(BENAC) <sub>2</sub>	<b>8a</b>	37
			Zn(II)	ZnTPC(BENAC) <sub>2</sub>	<b>8b</b>	80
			2H	H <sub>2</sub> TPCBr <sub>2</sub> (BENAC) <sub>2</sub>	<b>9</b>	77
		Br	Ni(II)	NiTPCBr <sub>2</sub> (BENAC) <sub>2</sub>	<b>9a</b>	41
			Zn(II)	ZnTPCBr <sub>2</sub> (BENAC) <sub>2</sub>	<b>9b</b>	87
		H	2H	H <sub>2</sub> TPC(IND) <sub>2</sub>	<b>10</b>	69
			Ni(II)	NiTPC(IND) <sub>2</sub>	<b>10a</b>	67
			Zn(II)	ZnTPC(IND) <sub>2</sub>	<b>10b</b>	77
			2H	H <sub>2</sub> TPCBr <sub>2</sub> (IND) <sub>2</sub>	<b>11</b>	84
		Br	Ni(II)	NiTPCBr <sub>2</sub> (IND) <sub>2</sub>	<b>11a</b>	69
			Zn(II)	ZnTPCBr <sub>2</sub> (IND) <sub>2</sub>	<b>11b</b>	87

## 2.2 EXPERIMENTAL SECTION

### 2.2.1 Chemicals

Pyrrole, 1,3-indanedione, benzoylacetonitrile and 1,3-dimethylbarbituric acid were purchased from Alfa Aesar, UK and used as received. Benzaldehyde, N-bromosuccinimide (NBS), Zn(OAc)<sub>2</sub>•2H<sub>2</sub>O, K<sub>2</sub>CO<sub>3</sub>, TBAPF<sub>6</sub>, CaH<sub>2</sub> and P<sub>2</sub>O<sub>5</sub> were purchased from HiMedia, India. 1,3-cyclohexanedione, and Ni(OAc)<sub>2</sub>•4H<sub>2</sub>O were purchased from Sigma-Aldrich, India and used without further purification. Silica gel (100-200 mesh) and DMSO purchased from Thomas

Baker, India and used as received. All the solvents employed in this work were distilled and dried before use. NBS was recrystallized from hot water and dried for 6 h at 70 °C under vacuum. TBAPF<sub>6</sub> was recrystallized twice from hot ethanol and dried under vacuum for 2 days at 25 °C. H<sub>2</sub>TPP, H<sub>2</sub>TPP(NO<sub>2</sub>), H<sub>2</sub>TPP(NO<sub>2</sub>)Br<sub>2</sub>, and their metal complexes were synthesized according to the literature methods [24-26].

### 2.2.2 Instrumentation and Methods

The electronic absorption spectra were recorded on Agilent Cary 100 spectrophotometer using a pair of quartz cells of 10 mm path length and 3.5 ml volume. The emission spectra were recorded on Hitachi F-4600 spectrofluorometer using a quartz cell of 10 mm path length. All the NMR studies have been carried out on JEOL ECX 400 MHz using CDCl<sub>3</sub> and DMSO-d<sub>6</sub> as a solvent at 298 K. MALDI-TOF-MS spectra were recorded on Bruker UltrafleXtreme-TN MALDI-TOF/TOF spectrometer using 2-(4-hydroxyphenylazo)benzoic acid (HABA) as a matrix in positive ion mode. The X-ray quality single crystals of NiTPPBr<sub>2</sub>(CHD) (**2a**) were obtained by vapor diffusion of CH<sub>3</sub>OH into the toluene solution of porphyrinoids whereas X-ray quality single crystals of H<sub>2</sub>TPCBr<sub>2</sub>(BENAC)<sub>2</sub> (**9**) and NiTPC(BENAC)<sub>2</sub> (**8a**) by vapor diffusion of hexane into the CHCl<sub>3</sub> solution of chlorin. X-ray quality single crystals of ZnTPCBr<sub>2</sub>(IND)<sub>2</sub> (**11b**) were obtained by diffusion of hexane into the CHCl<sub>3</sub> solution of chlorin along with few drops of pyridine. The single-crystal X-ray diffraction data was collected on a Bruker Apex-II CCD diffractometer. In case of NiTPPBr<sub>2</sub>(CHD) (**2a**) SQUEEZE procedure [27] was applied in order to correct electron density contribution from disordered solvent molecules. The cyclic voltammetric studies were carried out using CH instruments (CHI 620E). A three electrode assembly was used consisted of a Platinum working electrode, Ag/AgCl as a reference electrode and a Pt-wire as a counter electrode. The porphyrin concentration was maintained ~1 mM during electrochemical measurements. The whole experiment was performed under inert atmosphere.

### 2.2.3 General Synthetic Procedure for the Preparation of H<sub>2</sub>TPP(R)X<sub>2</sub>; X = H, Br and R = CHD and DMBA):

10 eq. of K<sub>2</sub>CO<sub>3</sub> and active methylene compounds (CHD or DMBA) were taken in 4.5 ml of DMSO and stirred for 10 min under inert atmosphere at reflux. To this solution, 100 mg of H<sub>2</sub>TPP(NO<sub>2</sub>)X<sub>2</sub> (where X = H or Br) was added and further refluxed for 2.5-3.0 h. The



completion of the reaction was monitored by TLC. The reaction mixture was cooled to room temperature and diluted with  $\text{CHCl}_3$ . The organic layer was washed with brine ( $2 \times 100$  ml) and finally with distilled water (100 ml). The organic layer was passed over anhydrous  $\text{Na}_2\text{SO}_4$  and dried using rotatory evaporator. The crude porphyrin was purified by column chromatography using  $\text{CHCl}_3$  to  $\text{CHCl}_3$ :acetone (99:1, v/v) mixture to afford the title compound as a bright purple solid.

**2-(2'-Cyclohexane-1', 3'-dione)-5,10,15,20-tetraphenylporphyrin  $\text{H}_2\text{TPP}(\text{CHD})$  (1):** Yield: 78% (86 mg, 0.12 mmol). Melting Point  $> 315$  °C. UV/vis ( $\text{CH}_2\text{Cl}_2$ ):  $\lambda_{\text{max}}(\text{nm})(\log \epsilon)$  419(5.49), 518(4.18), 552(3.76), 591(3.68), 648(3.66).  $^1\text{H}$  NMR (400 MHz,  $\text{CDCl}_3$ )  $\delta$  (ppm): 8.85-8.79(m, 4H,  $\beta$ -H), 8.75(d,  $^3J_{\text{H,H}} = 8$  Hz, 1H,  $\beta$ -H), 8.68(s, 1H,  $\beta$ -H), 8.55(d,  $^3J_{\text{H,H}} = 8$  Hz, 1H,  $\beta$ -H), 8.27-8.12(m, 6H, *meso*-*o*-Ph), 8.04(d,  $^3J_{\text{H,H}} = 8$  Hz, 2H, *meso*-*o*-Ph), 7.78-7.59(m, 12H, *meso*-*m,p*-Ph), 3.01(s, 1H, -CH), 1.96-1.91(m, 2H, - $\text{CH}_2$ ), 1.79-1.71(m, 2H, - $\text{CH}_2$ ), 1.31(t, 2H,  $^3J_{\text{H,H}} = 8$  Hz, - $\text{CH}_2$ ), -2.71(s, 2H, NH).  $^{13}\text{C}$  NMR (100 MHz,  $\text{CDCl}_3$ )  $\delta$  (ppm): 218.3, 142.2, 141.9, 134.7, 134.6, 128.1, 127.8, 126.9, 126.8, 126.8, 126.7, 120.5, 120.3, 120.1, 20.0, 19.9. MALDI-TOF-MS ( $m/z$ ): found 725.949  $[\text{M} + \text{H}]^+$ , calcd 725.291. Anal. Calcd for  $\text{C}_{50}\text{H}_{36}\text{N}_4\text{O}_2 \cdot 0.5\text{CHCl}_3$ : C, 77.31; H, 4.69; N, 7.14. Found: C, 77.09; H, 4.55; N, 6.95.

**2-(2'-Cyclohexane-1',3'-dione)-12,13-dibromo-5,10,15,20-tetraphenylporphyrin**

**$\text{H}_2\text{TPPBr}_2(\text{CHD})$  (2):** Yield: 72% (89 mg, 0.101 mmol.) Melting Point  $> 310$  °C. UV/vis ( $\text{CH}_2\text{Cl}_2$ ):  $\lambda_{\text{max}}(\text{nm})(\log \epsilon)$  422(5.41), 519(4.13), 550(3.43), 598(3.51), 655(3.61).  $^1\text{H}$  NMR (400 MHz,  $\text{CDCl}_3$ )  $\delta$  (ppm): 8.88 (s, 1H,  $\beta$ -H), 8.83-8.77(m, 2H,  $\beta$ -H), 8.60-8.51(m, 2H,  $\beta$ -H), 8.23-7.99(m, 8H, *meso*-*o*-Ph), 7.77-7.63(m, 12H, *meso*-*m,p*-Ph), 4.71(s, 1H, -CH), 2.40-2.10(m, 4H, - $\text{CH}_2$ ), 1.93-1.70(m, 4H, - $\text{CH}_2$ ), -2.85(s, 2H, NH).  $^{13}\text{C}$  NMR (100 MHz,  $\text{CDCl}_3$ )  $\delta$  (ppm): 141.8, 141.7, 141.2, 140.9, 140.8, 134.6, 128.3, 128.2, 128.0, 127.9, 127.4, 127.1, 127.0, 126.9, 126.7, 19.98. MALDI-TOF-MS ( $m/z$ ): found 804.059  $[\text{M} + \text{H}]^+ - \text{Br}$ , calcd 804.209. Anal. Calcd for  $\text{C}_{50}\text{H}_{34}\text{N}_4\text{O}_2\text{Br}_2 \cdot \text{CH}_3\text{OH}$ : C, 66.97; H, 4.19; N, 6.13. Found: C, 67.15; H, 4.36; N, 6.27.

**2-(1',3'-dimethyl-5'-barbituric acid)-5,10,15,20-tetraphenylporphyrin  $\text{H}_2\text{TPP}(\text{DMBA})$  (3):**

The residue was chromatographed to afford a trace amount (10% of the total) of nitro chlorin followed by the title compound as a purple solid. Yield:  $\text{H}_2\text{TPC}(\text{NO}_2)(\text{DMBA})$  (10%, 12 mg, 0.015 mmol),  $\text{H}_2\text{TPP}(\text{DMBA})$  (63%, 73 mg, 0.095 mmol). Melting Point  $> 310$  °C.

**H<sub>2</sub>TPC(NO<sub>2</sub>)(DMBA):** UV/vis (CH<sub>2</sub>Cl<sub>2</sub>):  $\lambda_{\max}$ (nm)(log  $\epsilon$ ) 435(5.46), 537(4.03), 580(4.29), 618(3.64), 675(4.00). <sup>1</sup>H NMR (400 MHz, CDCl<sub>3</sub>)  $\delta$  (ppm): 9.72(d, <sup>3</sup>J<sub>H,H</sub> = 4 Hz, 1H,  $\beta$ -H), 8.92(d, <sup>3</sup>J<sub>H,H</sub> = 4 Hz, 1H,  $\beta$ -H), 8.76(q, <sup>3</sup>J<sub>H,H</sub> = 4 Hz, 2H,  $\beta$ -H), 8.66(q, <sup>3</sup>J<sub>H,H</sub> = 4 Hz, 2H,  $\beta$ -H), 8.59(d, <sup>3</sup>J<sub>H,H</sub> = 8 Hz, 1H, *meso-o*-Ph), 8.41(s, 1H, *meso-o*-Ph), 8.20-8.13(m, 6H, *meso-o*-Ph), 7.81-7.71(m, 12H, *meso-m,p*-Ph), 7.58 (d, <sup>3</sup>J<sub>H,H</sub> = 8 Hz, 1H,  $\beta$ -H), 7.52(t, <sup>3</sup>J<sub>H,H</sub> = 8 Hz, 1H,  $\beta$ -H), 3.49(s, 6H, -CH<sub>3</sub>), 2.17(s, 1H, -CH), -1.77(s, 1H, -NH). <sup>13</sup>C NMR (100 MHz, CDCl<sub>3</sub>)  $\delta$  (ppm): 169.4, 151.3, 141.8, 141.6, 141.1, 139.1, 134.7, 134.5, 134.3, 129.5, 128.0, 127.9, 127.8, 127.0, 126.9, 126.8, 122.0, 121.1, 120.2, 110.9, 60.0, 29.6. MALDI-TOF-MS (*m/z*): found 768.423 [M]<sup>+</sup>-HNO<sub>2</sub>, calcd 768.285. Anal. Calcd for C<sub>50</sub>H<sub>37</sub>N<sub>7</sub>O<sub>5</sub>: C, 73.61; H, 4.57; N, 12.02. Found: C, 73.96; H, 4.61; N, 11.97.

**H<sub>2</sub>TPP(DMBA):** UV/vis (CH<sub>2</sub>Cl<sub>2</sub>):  $\lambda_{\max}$ (nm)(log  $\epsilon$ ) 419(5.50), 515(4.18), 550(3.71), 595(3.65), 648(3.54). <sup>1</sup>H NMR (400 MHz, CDCl<sub>3</sub>)  $\delta$  (ppm): 9.24(s, 1H,  $\beta$ -H), 8.86-8.82(m, 2H,  $\beta$ -H), 8.76(dd, <sup>3</sup>J<sub>H,H</sub> = 4 Hz, 12 Hz, 2H,  $\beta$ -H), 8.68(d, <sup>3</sup>J<sub>H,H</sub> = 4 Hz, 1H,  $\beta$ -H), 8.29(d, <sup>3</sup>J<sub>H,H</sub> = 4 Hz, 1H,  $\beta$ -H), 8.27(d, <sup>3</sup>J<sub>H,H</sub> = 4 Hz, 1H, *meso-o*-Ph), 8.22(dd, <sup>3</sup>J<sub>H,H</sub> = 4 Hz, 8Hz, 2H, *meso-o*-Ph), 8.18-8.15(m, 3H, *meso-o*-Ph), 7.98-7.95(m, 2H, *meso-o*-Ph), 7.76-7.61(m, 12H, *meso-m,p*-Ph), 3.69(s, 1H, -CH), 3.29(s, 6H, -CH<sub>3</sub>), -2.64(d, 2H, -NH). <sup>13</sup>C NMR (100 MHz, CDCl<sub>3</sub>)  $\delta$  (ppm): 168.7, 136.9, 134.8, 134.7, 134.6, 134.5, 127.9, 126.9, 126.8, 126.7, 126.0, 29.17, 27.71. MALDI-TOF-MS (*m/z*): found 786.171 [M+NH<sub>4</sub>]<sup>+</sup> calcd 786.319. Anal. Calcd for C<sub>50</sub>H<sub>36</sub>N<sub>6</sub>O<sub>3</sub>: C, 78.11; H, 4.74; N, 10.93. Found: C, 78.42; H, 4.96; N, 11.14.

**2-(1',3'-dimethyl-5'-barbituric acid)-12,13-dibromo-5,10,15,20-tetraphenylporphyrin**

**H<sub>2</sub>TPPBr<sub>2</sub>(DMBA) (4):** The resulting solid was chromatographed and eluted using CHCl<sub>3</sub> to 2% MeOH in CHCl<sub>3</sub> to give titled porphyrin. Yield: 87% (99 mg, 0.106 mmol). Melting Point > 300 °C. UV/vis (CH<sub>2</sub>Cl<sub>2</sub>):  $\lambda_{\max}$ (nm)(log  $\epsilon$ ) 428(5.37), 525(4.12), 600(3.53), 670(3.79). <sup>1</sup>H NMR (400 MHz, CDCl<sub>3</sub>)  $\delta$  (ppm): 9.04(s, 1H,  $\beta$ -H), 8.82(d, <sup>3</sup>J<sub>H,H</sub> = 4 Hz, 1H,  $\beta$ -H), 8.78(d, <sup>3</sup>J<sub>H,H</sub> = 4 Hz, 1H,  $\beta$ -H), 8.62(d, <sup>3</sup>J<sub>H,H</sub> = 4 Hz, 1H,  $\beta$ -H), 8.31-8.28(m, 2H,  $\beta$ -H, *meso-o*-Ph), 8.18-8.12(m, 5H, *meso-o*-Ph), 8.0-7.98(m, 2H, *meso-o*-Ph), 7.80-7.74(m, 9H, *meso-m,p*-Ph), 7.67-7.62(m, 3H, *meso-m,p*-Ph), 3.42(s, 1H, -CH), 3.27(s, 6H, -CH<sub>3</sub>), -2.73(d, 2H, -NH). <sup>13</sup>C NMR (100 MHz, CDCl<sub>3</sub>)  $\delta$  (ppm): 168.2, 137.1, 135.5, 135.4, 135.3, 127.5, 127.4, 127.2, 126.8, 126.7, 126.6,

29.93. MALDI-TOF-MS ( $m/z$ ): found 947.885  $[M+Na]^+$ , calcd 947.095. Anal. Calcd for  $C_{50}H_{34}N_6O_3Br_2 \cdot 0.5CH_3OH$ : C, 64.34; H, 3.85; N, 8.92. Found: C, 64.13; H, 3.72; N, 8.82.

### 2.2.4 General Synthetic Procedure for The Preparation of $H_2TPC(R)_2X_2$ ; X = H, Br and R = BENAC and IND):

A solution of 10 eq.  $K_2CO_3$  and 10 eq. of active methylene compound (benzoylacetonitrile or indane-1,3-dione) in 5 ml of DMSO was stirred for 15 min under inert atmosphere at reflux. To this, 100 mg of  $H_2TPP(NO_2)X_2$  (where X = H, Br) was added and refluxed further for 2-3 h. The completeness of the reaction was monitored by TLC. After completion of the reaction, the reaction mixture was diluted with  $CHCl_3$ . The organic layer was separated and washed twice with brine solution and dried over anhydrous sodium sulphate. The solvent was removed by rotatory evaporation and the resulting residue was dissolved in minimum amount of  $CHCl_3$  and subjected to silica gel column. The titled compound was eluted using  $CHCl_3$  as eleuent.

#### 2,3-Di-(1'-cyano-3'-oxo-3'-phenyl-2'-propanenitrile)-5,10,15,20-tetraphenylchlorin

**$H_2TPC(BENAC)_2$  (8)**: Yield: 80% (109 mg, 0.12 mmol). Melting Point > 310 °C. UV/vis ( $CH_2Cl_2$ ):  $\lambda_{max}(nm)(\log \epsilon)$  255(4.56), 416(5.34), 516(4.21), 544(4.18), 593(3.88), 646(4.47).  $^1H$  NMR (400 MHz,  $CDCl_3$ )  $\delta$  (ppm): 8.70(dd,  $^3J_{H,H} = 8$  Hz, 16 Hz, 4H,  $\beta$ -H), 8.49(s, 2H,  $\beta$ -H), 8.27(d,  $^3J_{H,H} = 8$ Hz, 4H, *meso-o*-Ph), 8.09(dd,  $^3J_{H,H} = 8$  Hz, 20 Hz, 4H, *meso-o*-Ph), 8.02-7.97(m, 4H, *meso-m,p*-Ph), 7.88(t,  $^3J_{H,H} = 8$  Hz, 2H, *meso-m,p*-Ph), 7.76-7.69 (m, 8H, *meso-m,p*-Ph), 7.63(t,  $^3J_{H,H} = 8$ Hz, 2H,  $\beta$ -*p*-Ph(BENAC), 7.30(t,  $^3J_{H,H} = 8$ Hz, 4H,  $\beta$ -*m*-Ph(BENAC), 6.69 (d,  $^3J_{H,H} = 8$ Hz, 4H,  $\beta$ -*o*-Ph(BENAC), 5.59(d,  $^3J_{H,H} = 4$ Hz, 2H,  $\beta$ -H), 5.05(d,  $^3J_{H,H} = 4$ Hz, 2H, -CH), -1.62(s, 1H, -NH).  $^{13}C$  NMR (100 MHz,  $CDCl_3$ )  $\delta$  (ppm): 189.1, 158.4, 153.6, 142.1, 141.9, 141.4, 136.1, 134.2, 132.8, 129.9, 128.6, 128.4, 127.9, 124.1, 115.2, 112.1, 48.9, 48.9, 44.5, 44.4. MALDI-TOF-MS ( $m/z$ ): found 942.927  $[M+K]^+$ , calcd 942.132; found 760.073  $[M+H]^+$  - BENAC, calcd 760.307. Anal. Calcd for  $C_{62}H_{42}N_6O_2$ : C, 82.46; H, 4.69; N, 9.31. Found: C, 81.97; H, 4.37; N, 8.97.

#### 2,3-Di-(1'-cyano-3'-oxo-3'-phenyl-2'-propanenitrile)-12,13-dibromo-5,10,15,20-

**tetraphenylchlorin  $H_2TPCBr_2(BENAC)_2$  (9)**: Yield: 77% (99 mg, 0.094 mmol). Melting Point > 310 °C. UV/vis ( $CH_2Cl_2$ ):  $\lambda_{max}(nm)(\log \epsilon)$  256(4.52), 423(5.27), 525(4.13), 595(3.97), 645(4.09).  $^1H$  NMR (400 MHz,  $CDCl_3$ )  $\delta$  (ppm): 8.68(d,  $^3J_{H,H} = 8$  Hz, 2H,  $\beta$ -H), 8.64-8.62(m,

2H,  $\beta$ -H), 8.19(d,  $^3J_{\text{H,H}} = 4$  Hz, 2H, *meso*-*o*-Ph), 8.09-8.04(m, 5H, *meso*-*o*-Ph), 7.97 (t,  $^3J_{\text{H,H}} = 8$  Hz, 3H, *meso*-Ph), 7.87(t,  $^3J_{\text{H,H}} = 8$  Hz, 3H, *meso*-*m,p*-Ph), 7.76-7.72(m, 7H, *meso*-*m,p*-Ph), 7.63(t,  $^3J_{\text{H,H}} = 8$  Hz, 2H,  $\beta$ -*p*-Ph(BENAC), 7.30(t,  $^3J_{\text{H,H}} = 8$  Hz, 4H,  $\beta$ -*m*-Ph(BENAC), 6.68 (d,  $^3J_{\text{H,H}} = 8$  Hz, 4H,  $\beta$ -*o*-Ph(BENAC), 5.52(d,  $^3J_{\text{H,H}} = 4$  Hz, 2H,  $\beta$ -H), 5.00(d,  $^3J_{\text{H,H}} = 4$  Hz, 2H, -CH), -1.63(s, 1H, -NH).  $^{13}\text{C}$  NMR (100 MHz,  $\text{CDCl}_3$ )  $\delta$  (ppm): 188.9, 159.5, 145.2, 142.8, 141.3, 141.0, 134.7, 134.0, 132.6, 129.0, 128.8, 128.5, 123.7, 115.0, 112.3, 48.7, 44.0. MALDI-TOF-MS ( $m/z$ ): found 1061.360  $[\text{M}+\text{H}]^+$  calcd 1061.835; found 918.622  $[\text{M}+\text{H}]^+$ -BENAC, calcd 918.693; found 813.436  $[\text{M}+\text{K}]^+$ -2BENAC, calcd 813.641. Anal. Calcd for  $\text{C}_{62}\text{H}_{40}\text{N}_6\text{O}_2\text{Br}_2 \cdot 2\text{CHCl}_3$ : C, 59.51; H, 3.26; N, 6.47. Found: C, 59.21; H, 3.00; N, 6.17.

**2,3-Di-(2'-indane-1',3'-dione)-5,10,15,20-tetraphenylchlorin  $\text{H}_2\text{TPC}(\text{IND})_2$  (10):** Yield: 69% (94 mg, 0.104 mmol). Melting Point > 300 °C. UV/vis ( $\text{CH}_2\text{Cl}_2$ ):  $\lambda_{\text{max}}(\text{nm})(\log \epsilon)$  229(4.80), 419(5.18), 518(4.08), 545(3.97), 595(3.71), 649(4.31).  $^1\text{H}$  NMR (400 MHz,  $\text{CDCl}_3$ )  $\delta$  (ppm): 8.61(d,  $^3J_{\text{H,H}} = 8$  Hz, 2H,  $\beta$ -H), 8.47(s, 2H,  $\beta$ -H), 8.25(s, 2H,  $\beta$ -H), 8.20(d,  $^3J_{\text{H,H}} = 4$  Hz, 2H, *meso*-*o*-Ph), 8.02(d,  $^3J_{\text{H,H}} = 8$  Hz, 4H, *meso*-*o*-Ph), 7.90(t,  $^3J_{\text{H,H}} = 8$  Hz, 2H, *meso*-*o*-Ph), 7.83(t,  $^3J_{\text{H,H}} = 8$  Hz, 2H, *meso*-*m,p*-Ph), 7.73-7.67(m, 10H, *meso*-*m,p*-Ph), 7.54(d,  $^3J_{\text{H,H}} = 8$  Hz, 2H,  $\beta$ -Ph-H(IND), 7.51-7.43(m, 4H,  $\beta$ -Ph(IND), 7.28(d,  $^3J_{\text{H,H}} = 4$  Hz, 1H,  $\beta$ -Ph(IND), 7.24(d,  $^3J_{\text{H,H}} = 4$  Hz, 1H,  $\beta$ -Ph(IND), 4.88(d,  $^3J_{\text{H,H}} = 4$  Hz, 2H,  $\beta$ -H), 3.27(d,  $^3J_{\text{H,H}} = 4$  Hz, 2H, -CH), -1.58(s, 2H, -NH). MALDI-TOF-MS ( $m/z$ ): found 906.998  $[\text{M}+\text{H}]^+$ , calcd 906.012 ; found 760.242  $[\text{M}]^+$ -IND, calcd 760.284. Anal. Calcd for  $\text{C}_{62}\text{H}_{40}\text{N}_4\text{O}_4 \cdot \text{CH}_3\text{OH}$ : C, 80.75; H, 4.73; N, 5.98 Found: C, 80.52; H, 4.58; N, 5.76.

**2,3-Di-(2'-indane-1',3'-dione)-12,13-dibromo-5,10,15,20-tetraphenylchlorin**

**$\text{H}_2\text{TPCBr}_2(\text{IND})_2$  (11):** Yield 84% (98 mg, 0.092 mmol). Melting Point > 300 °C. UV/vis ( $\text{CH}_2\text{Cl}_2$ ):  $\lambda_{\text{max}}(\text{nm})(\log \epsilon)$  230(4.91), 427(5.27), 527(4.16), 596(3.90), 648(4.12).  $^1\text{H}$  NMR (400 MHz,  $\text{CDCl}_3$ )  $\delta$  (ppm): 8.56(d,  $^3J_{\text{H,H}} = 8$  Hz, 2H,  $\beta$ -H), 8.12(d,  $^3J_{\text{H,H}} = 8$  Hz, 2H,  $\beta$ -H), 8.00(d,  $^3J_{\text{H,H}} = 8$  Hz, 2H, *meso*-*o*-Ph), 7.89(t,  $^3J_{\text{H,H}} = 8$  Hz, 3H, *meso*-*o*-Ph), 7.84(t,  $^3J_{\text{H,H}} = 8$  Hz, 3H, *meso*-*o*-Ph), 7.75-7.64(m, 12H, *meso*-*m,p*-Ph), 7.56(d,  $^3J_{\text{H,H}} = 8$  Hz,  $\beta$ -Ph(IND), 7.48(t,  $^3J_{\text{H,H}} = 8$  Hz, 2H,  $\beta$ -Ph(IND), 7.43(t,  $^3J_{\text{H,H}} = 8$  Hz, 2H,  $\beta$ -Ph(IND), 7.29(d,  $^3J_{\text{H,H}} = 8$  Hz, 2H,  $\beta$ -Ph(IND), 4.81(d,  $^3J_{\text{H,H}} = 4$  Hz, 2H,  $\beta$ -H), 3.23(d,  $^3J_{\text{H,H}} = 4$  Hz, 2H, -CH), -1.57(s, 2H, -NH).  $^{13}\text{C}$  NMR (100 MHz,  $\text{CDCl}_3$ )  $\delta$  (ppm): 197.9, 197.2, 163.8, 144.5, 143.1, 143.0, 142.6, 141.5, 140.8, 136.4,

136.0, 128.3, 127.4, 123.8, 122.8, 112.8, 112.6, 56.7, 56.6, 29.8. MALDI-TOF-MS ( $m/z$ ): found 1063.231  $[M+H]^+$ , calcd 1063.804 ; found 918.771  $[M]^+-IND$ , calcd 918.670. Anal. Calcd for  $C_{62}H_{38}N_4O_4Br_2 \cdot H_2O$ : C, 68.90; H, 3.73; N, 5.18 Found: C, 68.68; H, 3.52; N, 4.97.

### 2.2.5 Synthesis of 2-(2'-Cyclohexane-1',3'-dione)-5,10,15,20-tetraphenylporphyrinato Nickel (II) NiTPP(CHD) (1a)

50 mg (0.069 mmol) of NiTPP(NO<sub>2</sub>) was taken and the titled compound was prepared using similar method as described for **1**. Yield: 65% (35 mg, 0.045 mmol) UV/vis (CH<sub>2</sub>Cl<sub>2</sub>):  $\lambda_{max}(nm)(\log \epsilon)$  416(5.45), 533(4.25). Melting Point > 300 °C. <sup>1</sup>H NMR (400 MHz, CDCl<sub>3</sub>)  $\delta$  (ppm): 8.72(d, <sup>3</sup>J<sub>H,H</sub> = 8 Hz, 4H,  $\beta$ -H), 8.62(t, <sup>3</sup>J<sub>H,H</sub> = 4Hz, 2H,  $\beta$ -H), 8.48(d, <sup>3</sup>J<sub>H,H</sub> = 4 Hz, 1H,  $\beta$ -H), 7.99(t, <sup>3</sup>J<sub>H,H</sub> = 8 Hz, 6H, *meso-o*-Ph), 7.83(d, <sup>3</sup>J<sub>H,H</sub> = 4 Hz, 1H, *meso-o*-Ph), 7.76(d, <sup>3</sup>J<sub>H,H</sub> = 8 Hz, 1H, *meso-o*-Ph), 7.70-7.50(m, 12H, *meso-m,p*-Ph), 5.86(s, 1H, -CH), 2.38-2.28(m, 2H, -CH<sub>2</sub>), 2.20-2.01(m, 2H, -CH<sub>2</sub>), 1.90-1.66(m, 2H, -CH<sub>2</sub>). <sup>13</sup>C NMR (100 MHz, CDCl<sub>3</sub>)  $\delta$  (ppm): 197.3, 170.5, 143.5, 142.9, 142.7, 142.2, 140.6, 133.7, 132.9, 132.7, 132.5, 132.0, 127.8, 127.0, 119.2, 118.9, 116.3, 53.5, 27.6. MALDI-TOF-MS ( $m/z$ ): found 781.138  $[M+H]^+$ , calcd 781.210. Anal. Calcd for C<sub>50</sub>H<sub>34</sub>N<sub>4</sub>O<sub>2</sub>Ni : C, 76.84; H, 4.39; N, 7.17. Found: C, 76.38; H, 4.50; N, 7.07.

### 2.2.6 Synthesis of 2-(2'-Cyclohexane-1',3'-dione)-12,13-dibromo-5,10,15,20-tetraphenylporphyrinato Nickel (II) NiTPPBr<sub>2</sub>(CHD) (2a)

40 mg (0.046 mmol) of NiTPP(NO<sub>2</sub>)Br<sub>2</sub> was taken and the titled compound was prepared using similar procedure as described for **2**. Yield: 70% (30 mg, 0.032 mmol). UV/vis (CH<sub>2</sub>Cl<sub>2</sub>):  $\lambda_{max}(nm)(\log \epsilon)$  424(5.31), 540(4.16), 578(3.81). <sup>1</sup>H NMR (400 MHz, CDCl<sub>3</sub>)  $\delta$  (ppm): 8.68(d, <sup>3</sup>J<sub>H,H</sub>=4Hz, 1H,  $\beta$ -H), 8.58(dd, <sup>3</sup>J<sub>H,H</sub> = 4 Hz, 12 Hz, 2H,  $\beta$ -H), 8.53(s, 1H,  $\beta$ -H), 8.36(d, <sup>3</sup>J<sub>H,H</sub> = 4 Hz, 1H,  $\beta$ -H), 7.95-7.92(m, 3H, *meso-o*-Ph), 7.83-7.77(m, 5H, *meso-o*-Ph), 7.66-7.59(m, 12H, *meso-m,p*-Ph), 5.77(s, 1H, -CH), 2.37-2.17(m, 4H, -CH<sub>2</sub>), 2.03-1.86(m, 2H, -CH<sub>2</sub>). <sup>13</sup>C NMR (100 MHz, CDCl<sub>3</sub>)  $\delta$  (ppm): 144.0, 143.7, 143.4, 142.8, 141.5, 139.7, 139.4, 139.1, 137.2, 135.9, 135.4, 133.8, 133.7, 133.3, 132.8, 132.7, 128.3, 128.2, 127.2, 124.4, 119.2, 119.1, 118.2, 117.9, 29.8, 29.5, 19.8. MALDI-TOF-MS ( $m/z$ ): found 940.023  $[M+H]^+$ , calcd 940.323. Anal. Calcd for C<sub>50</sub>H<sub>32</sub>N<sub>4</sub>O<sub>2</sub>Br<sub>2</sub>Ni•C<sub>6</sub>H<sub>14</sub> : C, 65.59; H, 4.52; N, 5.46. Found: C, 65.73; H, 4.15; N, 5.68.



### 2.2.7 Synthesis of 2-(1', 3'-dimethyl-5'-barbituric acid)-5,10,15,20-tetraphenylporphyrinato Nickel (II) NiTPP(DMBA) (3a)

60 mg (0.084 mmol) of NiTPP(NO<sub>2</sub>) was taken and titled compound was prepared using a method as described for **3**. Yield: 60% (41 mg, 0.050 mmol). UV/vis (CH<sub>2</sub>Cl<sub>2</sub>):  $\lambda_{\max}$ (nm)(log  $\epsilon$ ) 416(5.25), 536(4.06), 592(3.52). <sup>1</sup>H NMR (400 MHz, CDCl<sub>3</sub>)  $\delta$  (ppm): <sup>1</sup>H NMR (400 MHz, CDCl<sub>3</sub>)  $\delta$ : 9.48(d, <sup>3</sup>J<sub>H,H</sub> = 4 Hz, 1H,  $\beta$ -H), 8.81(d, <sup>3</sup>J<sub>H,H</sub> = 8 Hz, 1H,  $\beta$ -H), 8.63(d, <sup>3</sup>J<sub>H,H</sub> = 4 Hz, 1H,  $\beta$ -H), 8.58(t, <sup>3</sup>J<sub>H,H</sub> = 4 Hz, 2H,  $\beta$ -H), 8.53(d, <sup>3</sup>J<sub>H,H</sub> = 4 Hz, 1H,  $\beta$ -H), 8.43(s, 1H,  $\beta$ -H), 8.11(d, <sup>3</sup>J<sub>H,H</sub> = 8 Hz, 1H, *meso*-*o*-Ph), 7.95-7.91(m, 7H, *meso*-*o*-Ph), 7.70-7.62(m, 12H, *meso*-*m,p*-Ph), 6.26(s, 6H, -CH<sub>3</sub>). MALDI-TOF-MS (*m/z*): found 825.138 [M+H]<sup>+</sup>, calcd 825.212. Anal. Calcd for C<sub>50</sub>H<sub>34</sub>N<sub>6</sub>O<sub>3</sub>Ni•0.5CHCl<sub>3</sub>: C, 68.52; H, 3.94; N, 9.49. Found: C, 68.23; H, 4.06; N, 9.25.

### 2.2.8 Synthesis of 2-(1',3'-dimethyl-5'-barbituric acid)-12,13-dibromo-5,10,15,20-tetraphenylporphyrinato Nickel (II) NiTPPBr<sub>2</sub>(DMBA) (4a)

60 mg (0.069 mmol) of NiTPP(NO<sub>2</sub>)Br<sub>2</sub> was taken and titled compound was prepared using a method as described for **4**. Yield: 58% (39 mg, 0.040 mmol). UV/vis (CH<sub>2</sub>Cl<sub>2</sub>):  $\lambda_{\max}$ (nm)(log  $\epsilon$ ) 426(5.33), 540(4.17), 582(3.88). <sup>1</sup>H NMR (400 MHz, CDCl<sub>3</sub>)  $\delta$  (ppm): 9.11(s, 1H,  $\beta$ -H), 8.65(d, <sup>3</sup>J<sub>H,H</sub> = 4Hz, 1H,  $\beta$ -H), 8.57(d, <sup>3</sup>J<sub>H,H</sub> = 4Hz, 1H,  $\beta$ -H), 8.49(d, <sup>3</sup>J<sub>H,H</sub> = 4Hz, 1H,  $\beta$ -H), 8.07-7.99(m, 5H,  $\beta$ -H and *meso*-*o*-Ph-H), 7.85(s, 1H, *meso*-*o*-Ph-H), 7.84-7.82(m, 2H, *meso*-*o*-Ph-H), 7.80(s, 1H, *meso*-*o*-Ph-H), 7.69-7.63(m, 12H, *meso*-*m,p*-Ph-H), 3.63(s, 1H, -CH), 3.22(s, 6H, -CH<sub>3</sub>). <sup>13</sup>C NMR (100 MHz, CDCl<sub>3</sub>)  $\delta$  (ppm): 134.1, 133.9, 133.7, 133.2, 128.3, 128.1, 127.4, 127.3, 127.2, 127.1, 126.0, 63.8, 63.7, 29.8, 22.7, 16.2, 16.1. MALDI-TOF-MS (*m/z*): found 984.343 [M+H]<sup>+</sup>, calcd 984.336; found 905.271 [M+H]<sup>+</sup>-Br, calcd 905.440. Anal. Calcd for C<sub>50</sub>H<sub>32</sub>N<sub>6</sub>O<sub>3</sub>Br<sub>2</sub>Ni: C, 61.07; H, 3.28; N, 8.55. Found: C, 60.92; H, 3.23; N, 8.10.

### 2.2.9 Synthesis of 2-(1'-cyano-3'oxo-3'-phenyl-2'-propanenitrile)-5,10,15,20-tetraphenylporphyrinato Nickel (II) NiTPP(BENAC) (5) and 2,3-Di-(1'-cyano-3'oxo-3'-phenyl-2'-propanenitrile)-5,10,15,20-tetraphenylchlorinato Nickel (II) NiTPC(BENAC)<sub>2</sub> (8a)

A solution of NiTPP(NO<sub>2</sub>) (100 mg, 0.139 mmol) in DMSO (5 ml) was treated with K<sub>2</sub>CO<sub>3</sub> (192 mg, 1.39 mmol) and benzoylacetonitrile (202 mg, 1.39 mmol). The resulting reaction mixture



was heated at 90 °C under inert atmosphere for 2.5 h. The reaction mixture was diluted with  $\text{CHCl}_3$  (~20 ml) and washed by the saturated aqueous NaCl. The organic layer was separated, dried over anhydrous  $\text{Na}_2\text{SO}_4$ , and concentrated. Column chromatography of the resulting solid provided the mono-substituted porphyrin as first fraction (red colored product) and di-substituted chlorin as second fraction (green colored product).

**NiTPP(BENAC) (5)** Yield: 26% (30 mg, 0.036 mmol) UV/vis ( $\text{CH}_2\text{Cl}_2$ ):  $^1\text{H}$  NMR (400 MHz,  $\text{CDCl}_3$ )  $\delta$  (ppm): 8.87(s, 1H,  $\beta$ -H), 8.76-8.66(m, 5H,  $\beta$ -H), 8.60(t,  $^3J_{\text{H,H}} = 4$  Hz, 1H,  $\beta$ -H), 8.01-7.97(m, 5H, *meso-o*-Ph), 7.72-7.64(m, 13H, *meso-o*, *m* and *p*-Ph), 7.52-7.45(m, 4H, *meso-m*, *p*-Ph and  $\beta$ -Ph(BENAC)), 7.40(t,  $^3J_{\text{H,H}} = 8$  Hz, 2H,  $\beta$ -Ph(BENAC)), 7.32(t,  $^3J_{\text{H,H}} = 8$  Hz, 1H,  $\beta$ -Ph(BENAC)), 5.91(s, 1H, -CH). MALDI-TOF-MS ( $m/z$ ): found 815.602  $[\text{M}+\text{H}]^+$ , calcd 815.562.  $^{13}\text{C}$  NMR (100 MHz,  $\text{CDCl}_3$ )  $\delta$  (ppm): 143.3, 143.0, 140.4, 140.0, 139.6, 128.6, 128.4, 128.2, 128.1, 128.0, 127.7, 127.2, 127.0, 53.5, 29.7. Anal. Calcd for  $\text{C}_{53}\text{H}_{33}\text{N}_5\text{ONi}$ : C, 78.15; H, 4.08; N, 8.60. Found: C, 78.33; H, 4.25; N, 8.37.

**NiTPC(BENAC)<sub>2</sub> (8a)** Yield: 37% (50 mg, 0.052 mmol) UV/vis ( $\text{CH}_2\text{Cl}_2$ ):  $\lambda_{\text{max}}$ (nm) (log  $\epsilon$ ) 253(4.65), 415(5.23), 506(3.71), 570(3.94), 608(4.46).  $^1\text{H}$  NMR (400 MHz,  $\text{CDCl}_3$ )  $\delta$ :  $^1\text{H}$  NMR (400 MHz,  $\text{CDCl}_3$ )  $\delta$  (ppm): 8.80(d,  $^3J_{\text{H,H}} = 8$  Hz, 2H,  $\beta$ -H), 8.32(d,  $^3J_{\text{H,H}} = 4$  Hz, 2H,  $\beta$ -H), 8.18(s, 2H,  $\beta$ -H), 8.00(t,  $^3J_{\text{H,H}} = 8$  Hz, *meso-o*-Ph), 7.83(d,  $^3J_{\text{H,H}} = 8$  Hz, 3H, *meso-o*-Ph), 7.79(d,  $^3J_{\text{H,H}} = 4$  Hz, *meso-o*-Ph), 7.63-7.56(m, 12H, *meso-m,p*-Ph), 7.31(d,  $^3J_{\text{H,H}} = 8$  Hz, 2H,  $\beta$ -*p*-Ph(BENAC)), 7.17-7.14(m, 4H, 4H,  $\beta$ -*m*-Ph(BENAC)), 6.63(d,  $^3J_{\text{H,H}} = 8$  Hz, 2H,  $\beta$ -*o*-Ph(BENAC)), 5.20(d,  $^3J_{\text{H,H}} = 4$  Hz, 2H,  $\beta$ -H), 4.58(d,  $^3J_{\text{H,H}} = 4$  Hz, 2H, -CH).  $^{13}\text{C}$  NMR (100 MHz,  $\text{CDCl}_3$ )  $\delta$  (ppm): 188.9, 147.7, 145.0, 141.7, 140.2, 140.1, 139.1, 134.7, 133.0, 132.4, 129.6, 129.4, 128.7, 128.4, 128.2, 127.9, 127.0, 114.4, 110.3, 46.6, 43.0. MALDI-TOF-MS ( $m/z$ ): found 959.599  $[\text{M}+\text{H}]^+$ , calcd 959.264; found 817.307  $[\text{M}+\text{H}]^+$ -BENAC, calcd 817.578; found 673.047  $[\text{M}+\text{H}]^+$ -2BENZAC, calcd 673.189. Anal. Calcd for  $\text{C}_{62}\text{H}_{40}\text{N}_6\text{O}_2\text{Ni}\cdot\text{H}_2\text{O}$ : C, 76.16; H, 4.33; N, 8.60. Found: C, 76.08; H, 4.65; N, 8.52.

**2.2.10 Synthesis of 2-(1'-cyano-3'-oxo-3'-phenyl-2'-propanenitrile)-12,13-dibromo-5,10,15,20-tetraphenylporphyrinato Nickel (II) NiTPPBr<sub>2</sub>(BENAC) (6) and 2,3-Di-(1'-cyano-3'-oxo-3'-phenyl-2'-propanenitrile)-12,13-dibromo-5,10,15,20-tetraphenylchlorinato Nickel (II) NiTPCBr<sub>2</sub>(BENAC)<sub>2</sub> (9a)**

A solution of NiTPP(NO<sub>2</sub>)Br<sub>2</sub> (150 mg, 0.171 mmol) in DMSO (5 ml) was treated with K<sub>2</sub>CO<sub>3</sub> (237 mg, 1.71 mmol) and benzoylacetonitrile (249 mg, 1.71 mmol). The resulting reaction mixture was heated at 90 °C under inert atmosphere for 2.5 h. The reaction mixture was diluted with CHCl<sub>3</sub> (~20 ml) and washed by the saturated aqueous NaCl and dried with Na<sub>2</sub>SO<sub>4</sub>. The crude porphyrinoid was chromatographed to afford tri-substituted porphyrin (first fraction, red colored) followed by the tetra-substituted chlorin (second fraction, green colored).

**NiTPPBr<sub>2</sub>(BENAC) (6)** Yield: 23% (38 mg, 0.039 mmol). <sup>1</sup>H NMR (400 MHz, CDCl<sub>3</sub>)  $\delta$  (ppm): 8.79(d, <sup>3</sup>J<sub>H,H</sub> = 4Hz, 1H,  $\beta$ -H), 8.69-8.61(m, 2H,  $\beta$ -H), 8.53-8.45(m, 2H,  $\beta$ -H), 8.21(d, <sup>3</sup>J<sub>H,H</sub> = 4Hz, 1H, *meso*-*o*-Ph), 7.98(d, <sup>3</sup>J<sub>H,H</sub> = 4Hz, 1H, *meso*-*o*-Ph), 7.87-7.78(m, 4H, *meso*-*o*-Ph), 7.70-7.63(m, 14H, *meso*-*o*, *m* and *p*-Ph), 7.53-7.449(m, 2H,  $\beta$ -Ph(BENAC)), 7.40-7.29(m, 3H,  $\beta$ -Ph(BENAC)), 5.63(s, 1H, -CH). <sup>13</sup>C NMR (100 MHz, CDCl<sub>3</sub>)  $\delta$  (ppm): 188.5, 144.0, 143.9, 143.3, 140.8, 139.2, 138.8, 137.9, 136.4, 134.3, 134.2, 133.9, 133.7, 133.5, 133.2, 133.1, 133.0, 132.7, 132.6, 129.1, 128.7, 128.6, 128.4, 127.9, 127.3, 124.8, 120.1, 118.5, 117.7, 41.9. MALDI-TOF-MS (*m/z*): found 973.014 [M+H]<sup>+</sup>, calcd 973.354; found 868.424 [M+H]<sup>+</sup>-PhCO, calcd 868.241. Anal. Calcd for C<sub>53</sub>H<sub>31</sub>N<sub>5</sub>OBr<sub>2</sub>Ni: C, 65.47; H, 3.21; N, 7.20. Found: C, 65.43; H, 3.48; N, 7.34.

**NiTPCBr<sub>2</sub>(BENAC)<sub>2</sub> (9a)** Yield: 41% (79 mg, 0.070 mmol). UV/vis (CH<sub>2</sub>Cl<sub>2</sub>):  $\lambda_{\max}$ (nm) (log  $\epsilon$ ) 255(4.64), 427(5.19), 520(3.76), 572(3.85), 610(4.24). <sup>1</sup>H NMR (400 MHz, CDCl<sub>3</sub>)  $\delta$  (ppm): 8.77(d, <sup>3</sup>J<sub>H,H</sub> = 8 Hz, 1H,  $\beta$ -H), 8.33(d, <sup>3</sup>J<sub>H,H</sub> = 4 Hz, 3H,  $\beta$ -H), 8.02-7.94(m, 2H, *meso*-*o*-Ph), 7.82(t, <sup>3</sup>J<sub>H,H</sub> = 8 Hz, 2H, *meso*-*o*-Ph), 7.74-7.71(m, 4H, *meso*-*o*-Ph), 7.64-7.36(m, 12H, *meso*-*m*, *p*-Ph), 7.27-7.23(m, 5H,  $\beta$ -Ph(BENAC)), 6.63(d, <sup>3</sup>J<sub>H,H</sub> = 8 Hz, 5H,  $\beta$ -Ph(BENAC)), 5.11(d, <sup>3</sup>J<sub>H,H</sub> = 4 Hz, 2H,  $\beta$ -H), 4.53(d, <sup>3</sup>J<sub>H,H</sub> = 4 Hz, 2H, -CH). <sup>13</sup>C NMR (100 MHz, CDCl<sub>3</sub>)  $\delta$  (ppm): 188.7, 148.4, 145.5, 139.9, 139.2, 139.0, 135.1, 134.8, 134.6, 133.1, 132.7, 132.3, 131.9, 129.7, 129.1, 128.6, 128.4, 128.3, 128.2, 127.2, 123.6, 120.5, 114.3, 110.5, 46.5, 42.7. MALDI-TOF-MS (*m/z*): found 1118.930 [M+H]<sup>+</sup>, calcd 1118.512; found 976.102 [M+H]<sup>+</sup>-BENAC, calcd 976.370; found 831.089 [M+H]<sup>+</sup>-2BENAC, calcd 831.221. Anal. Calcd for C<sub>62</sub>H<sub>38</sub>N<sub>6</sub>O<sub>2</sub>Br<sub>2</sub>Ni•CHCl<sub>3</sub>: C, 61.18; H, 3.18; N, 6.78. Found: C, 61.38; H, 3.25; N, 6.54.

### 2.2.11 Synthesis of 2,3-Di-(5'-indane-1',3'-dione)-5,10,15,20-tetraphenylchlorinato Nickel (II) NiTPC(IND)<sub>2</sub> (10a)

50 mg (0.069 mmol) of NiTPP(NO<sub>2</sub>) was taken and titled compound was prepared using methods as described for **10**. Yield: 67% (45 mg, 0.047 mmol) UV/vis (CH<sub>2</sub>Cl<sub>2</sub>):  $\lambda_{\max}$ (nm) (log  $\epsilon$ ) 230(4.94), 417(5.12), 505(3.78), 577(3.91), 615(4.34). <sup>1</sup>H NMR (400 MHz, CDCl<sub>3</sub>)  $\delta$  (ppm): 8.29(d, <sup>3</sup>J<sub>H,H</sub> = 4 Hz, 2H,  $\beta$ -H), 8.16(s, 2H,  $\beta$ -H), 7.77(d, <sup>3</sup>J<sub>H,H</sub> = 4 Hz, 6H,  $\beta$ -H, *meso-o*-Ph), 7.71-7.69(m, 7H, *meso-o,m,p*-Ph), 7.63-7.58(m, 9H, *meso-m,p*-Ph), 7.32-7.30(m, 4H,  $\beta$ -Ph(IND)), 7.21-7.18(m, 2H,  $\beta$ -Ph(IND)), 6.91(d, <sup>3</sup>J<sub>H,H</sub> = 4 Hz, 2H,  $\beta$ -Ph(IND)), 5.01(d, <sup>3</sup>J<sub>H,H</sub> = 8 Hz, 2H,  $\beta$ -H), 2.99(d, <sup>3</sup>J<sub>H,H</sub> = 8 Hz, 2H, -CH). <sup>13</sup>C NMR (100 MHz, CDCl<sub>3</sub>)  $\delta$  (ppm): 197.7, 196.8, 147.3, 147.1, 142.4, 141.6, 140.4, 139.4, 135.5, 133.8, 133.0, 128.9, 127.7, 127.5, 127.2, 127.0, 123.8, 123.4, 123.1, 53.8, 48.2, 47.2. MALDI-TOF-MS (*m/z*): found 961.759 [M+H]<sup>+</sup>, calcd 961.231; found 817.133 [M+H]<sup>+</sup>-IND, calcd 817.210. Anal. Calcd for C<sub>62</sub>H<sub>38</sub>N<sub>4</sub>O<sub>4</sub>Ni: C, 77.43; H, 3.98; N, 5.83. found: C, 77.13; H, 3.79; N, 5.63.

### 2.2.12 Synthesis of 2,3-Di-(5'-indane-1',3'-dione)-12,13-dibromo-5,10,15,20-tetraphenylchlorinato Nickel (II) NiTPCBr<sub>2</sub>(IND)<sub>2</sub> (**11a**)

60 mg (0.069 mmol) of NiTPP(NO<sub>2</sub>)Br<sub>2</sub> was taken and titled compound was prepared using methods as described for **4**. Yield: 69% (53 mg, 0.047 mmol). UV/vis (CH<sub>2</sub>Cl<sub>2</sub>):  $\lambda_{\max}$ (nm) (log  $\epsilon$ ) 230(4.99), 429(5.17), 515(3.79), 573(3.88), 617(4.27). <sup>1</sup>H NMR (400 MHz, CDCl<sub>3</sub>)  $\delta$  (ppm): 8.87(d, <sup>3</sup>J<sub>H,H</sub> = 4Hz, 2H,  $\beta$ -H), 7.79-7.75(m, 8H,  $\beta$ -H, *meso-o*-Ph), 7.69-7.58(m, 14H, *meso-o, m* and *p*-Ph), 7.32(s, 4H,  $\beta$ -Ph(IND)), 7.22-7.19(m, 2H,  $\beta$ -Ph(IND)), 6.91-6.84(m, 2H,  $\beta$ -Ph(IND)), 4.96(d, <sup>3</sup>J<sub>H,H</sub> = 8Hz, 2H,  $\beta$ -H), 2.95(d, <sup>3</sup>J<sub>H,H</sub> = 8Hz, 2H, -CH). <sup>13</sup>C NMR (100 MHz, CDCl<sub>3</sub>)  $\delta$  (ppm): 197.5, 196.6, 142.4, 142.3, 138.6, 135.7, 135.6, 134.4, 133.2, 128.3, 127.7, 123.5, 123.2, 111.9, 53.7, 29.5, 22.69. MALDI-TOF-MS (*m/z*): found 1120.830 [M+H]<sup>+</sup>, calcd 1120.482; found 975.914 [M]<sup>+</sup>-IND, calcd 975.348. Anal. Calcd for C<sub>62</sub>H<sub>36</sub>N<sub>4</sub>O<sub>4</sub>Br<sub>2</sub>Ni: C, 66.52; H, 3.24; N, 5.00. found: C, 66.33; H, 3.44; N, 5.24.

### 2.2.13 General Procedure for the Synthesis of Zn(II) Complexes From Free Base Porphyrins

30 mg free base tetraphenylporphyrins were dissolved in 15 ml of CHCl<sub>3</sub>. To this, 10 eq. of Zn(OAc)<sub>2</sub>•2H<sub>2</sub>O in 2mL of MeOH solution was added and the resulting mixture was refluxed for 30-45 min. The organic layer was washed with water and concentrated. The crude residual porphyrins were purified by column chromatography.

**2-(2'-Cyclohexane-1',3'-dione)-5,10,15,20-tetraphenylporphyrinato Zinc (II) ZnTPP(CHD)**

**(1b):** Yield: 80% (26 mg, 0.033). UV/vis (CH<sub>2</sub>Cl<sub>2</sub>):  $\lambda_{\max}$ (nm) (log  $\epsilon$ ) 420(5.53), 549(4.17), 586(3.54). <sup>1</sup>H NMR (400 MHz, DMSO-d<sub>6</sub>)  $\delta$  (ppm): 10.37(s, 1H, -OH), 8.78(d, <sup>3</sup>J<sub>H,H</sub> = 4Hz, 1H,  $\beta$ -H), 8.75-8.73(m, 2H,  $\beta$ -H), 8.67(d, <sup>3</sup>J<sub>H,H</sub> = 4Hz, 1H,  $\beta$ -H), 8.43(d, <sup>3</sup>J<sub>H,H</sub> = 4Hz, 1H,  $\beta$ -H), 8.32(d, <sup>3</sup>J<sub>H,H</sub> = 4Hz, 1H,  $\beta$ -H), 8.20-8.15(m, 6H,  $\beta$ -H, *meso-o*-Ph), 8.02-7.99(m, 1H, *meso-o*-Ph), 7.80-7.57(m, 14H, *meso-o*, *m* and *p*-Ph), 2.18-2.12(m, 2H, -CH<sub>2</sub>), 1.93-1.59(m, 4H, -CH<sub>2</sub>). <sup>13</sup>C NMR (100 MHz, CDCl<sub>3</sub>)  $\delta$  (ppm): 149.6, 149.4, 149.2, 148.7, 148.1, 143.6, 143.3, 142.8, 140.2, 135.5, 134.6, 133.5, 132.1, 132.0, 131.7, 127.9, 127.0, 125.8, 124.1, 121.3, 120.8, 120.5, 119.5, 115.7, 79.72, 20.1. MALDI-TOF-MS (*m/z*): found 787.125 [M+H]<sup>+</sup>, calcd 787.204. Anal. Calcd for C<sub>50</sub>H<sub>34</sub>N<sub>4</sub>O<sub>2</sub>Zn•CH<sub>3</sub>OH: C, 74.68; H, 4.67; N, 6.83. Found: C, 74.45; H, 4.68; N, 6.66.

**2-(2'-Cyclohexane-1',3'-dione)-12,13dibromo-5,10,15,20-tetraphenylporphyrinato Zinc (II)**

**ZnTPPBr<sub>2</sub>(CHD) (2b):** Yield: 77% (25 mg, 0.026). UV/vis (CH<sub>2</sub>Cl<sub>2</sub>):  $\lambda_{\max}$ (nm) (log  $\epsilon$ ) 423(5.45), 552(4.17), 590(3.71). <sup>1</sup>H NMR (400 MHz, CDCl<sub>3</sub>)  $\delta$  (ppm): 8.94-8.88(m, 2H,  $\beta$ -H), 8.68(d, <sup>3</sup>J<sub>H,H</sub> = 8Hz, 1H,  $\beta$ -H), 8.24-8.18(m, 2H,  $\beta$ -H), 8.10(s, 1H, *meso-o*-Ph), 8.04-7.92(m, 3H, *meso-o*-Ph), 7.84-7.74(m, 7H, *meso-o*, *m* and *p*-Ph), 7.70-7.65(m, 4H, *meso-m* and *p*-Ph), 7.54(t, <sup>3</sup>J<sub>H,H</sub> = 8Hz, 2H, *meso-m* and *p*-Ph), 7.14-6.99(m, 3H, *meso-m* and *p*-Ph), 5.48(s, 1H, -CH), 1.74-1.53(m, 2H, -CH<sub>2</sub>), 1.43-1.36(m, 4H, -CH<sub>2</sub>). MALDI-TOF-MS (*m/z*): found 867.105 [M+H]<sup>+</sup>-Br, calcd 867.006. Anal. Calcd for C<sub>50</sub>H<sub>32</sub>N<sub>4</sub>O<sub>2</sub>Br<sub>2</sub>Zn•C<sub>6</sub>H<sub>14</sub>: C, 65.16; H, 4.49; N, 5.43. Found: C, 65.21; H, 4.67; N, 5.72.

**2-(1',3'-Dimethyl-5'-barbituric acid)-5,10,15,20-tetraphenylporphyrinato Zinc (II)**

**ZnTPP(DMBA) (3b):** Yield: 77% (25 mg, 0.030). UV/vis (CH<sub>2</sub>Cl<sub>2</sub>):  $\lambda_{\max}$ (nm) (log  $\epsilon$ ) 420(5.63), 549(4.31), 587(3.71). <sup>1</sup>H NMR (400 MHz, CDCl<sub>3</sub>)  $\delta$  (ppm): 9.44(s, 1H,  $\beta$ -H), 8.93-8.88(m, 3H,  $\beta$ -H), 8.74(d, <sup>3</sup>J<sub>H,H</sub> = 8 Hz, 1H,  $\beta$ -H), 8.25-8.12(m, 7H,  $\beta$ -H, *meso-o*-Ph), 7.92(d, <sup>3</sup>J<sub>H,H</sub> = 8 Hz, 2H, *meso-o*-Ph), 7.78-7.54(m, 13H, *meso-o,m,p*-Ph), 4.01(s, 1H, -CH), 3.23(s, 6H, -CH<sub>3</sub>). <sup>13</sup>C NMR (100 MHz, CDCl<sub>3</sub>)  $\delta$  (ppm): 168.8, 150.3, 136.9, 136.8, 134.6, 134.5, 134.4, 132.7, 132.2, 131.7, 131.6, 126.6, 126.5, 125.7, 125.6, 53.5, 29.2. MALDI-TOF-MS (*m/z*): found 848.384 [M+NH<sub>4</sub>]<sup>+</sup>, calcd 848.232. Anal. Calcd for C<sub>50</sub>H<sub>34</sub>N<sub>6</sub>O<sub>3</sub>Zn•H<sub>2</sub>O: C, 70.63; H, 4.24; N, 9.88. Found: C, 70.68; H, 4.49; N, 9.95.

**2-(1', 3'-Dimethyl-5'-barbituric acid)-12,13-dibromo-5,10,15,20-tetraphenylporphyrinato Zinc (II) ZnTPPBr<sub>2</sub>(DMBA) (4b):** Yield: 84% (27 mg, 0.027 mmol). UV/vis (CH<sub>2</sub>Cl<sub>2</sub>):  $\lambda_{\max}$ (nm) (log  $\epsilon$ ) 426(5.57), 556(4.27), 592(3.85). <sup>1</sup>H NMR (400 MHz, CDCl<sub>3</sub>)  $\delta$  (ppm): 9.35(s, 1H,  $\beta$ -H), 8.81(s, 2H,  $\beta$ -H), 8.62(d, <sup>3</sup>J<sub>H,H</sub> = 4 Hz, 1H,  $\beta$ -H), 8.22(d, <sup>3</sup>J<sub>H,H</sub> = 8 Hz, 2H,  $\beta$ -H, *meso*-*o*-Ph), 8.07-7.99(m, 5H, *meso*-*o*-Ph), 7.90(d, <sup>3</sup>J<sub>H,H</sub> = 4 Hz, 2H, *meso*-*o*-Ph), 7.78-7.56(m, 12H, *meso*-*m,p*-Ph), 3.95(s, 1H, -CH), 3.23(s, 1H, -CH<sub>3</sub>). MALDI-TOF-MS (*m/z*): found 1009.228 [M+Na]<sup>+</sup>, calcd 1009.009. Anal. Calcd for C<sub>50</sub>H<sub>32</sub>N<sub>6</sub>O<sub>3</sub> Br<sub>2</sub>Zn•CH<sub>3</sub>OH: C, 59.93; H, 3.55; N, 8.22. Found: C, 59.84; H, 3.25; N, 8.02.

**2, 3-Di-(1'-cyano-3'-oxo-3'-phenyl-2'-propanenitrile)-5,10,15,20-tetraphenylchlorinato Zinc (II) ZnTPC(BENAC)<sub>2</sub> (8b):** Yield: 80% (26 mg, 0.027 mmol). UV/vis (CH<sub>2</sub>Cl<sub>2</sub>):  $\lambda_{\max}$ (nm) (log  $\epsilon$ ) 255(4.39), 419(5.21), 515(3.62), 588(3.86), 613(4.35). <sup>1</sup>H NMR (400 MHz, CDCl<sub>3</sub>)  $\delta$  (ppm): 8.61(d, <sup>3</sup>J<sub>H,H</sub> = 8 Hz, 2H,  $\beta$ -H), 8.55(d, <sup>3</sup>J<sub>H,H</sub> = 4 Hz, 2H,  $\beta$ -H), 8.40 (s, 2H,  $\beta$ -H), 8.18-8.16(m, 2H, *meso*-*o*-Ph), 8.12-7.99(m, 8H, *meso*-*o,m,p*-Ph), 7.93(t, <sup>3</sup>J<sub>H,H</sub> = 8 Hz, 2H, *meso*-*m,p*-Ph), 7.84(t, <sup>3</sup>J<sub>H,H</sub> = 8 Hz, 2H, *meso*-*m,p*-Ph), 7.71-7.67(m, 6H, *meso*-*m,p*-Ph), 7.61(t, <sup>3</sup>J<sub>H,H</sub> = 8 Hz, 2H,  $\beta$ -Ph(BENAC)), 7.28(d, <sup>3</sup>J<sub>H,H</sub> = 8 Hz, 3H,  $\beta$ -Ph(BENAC)), 7.25(s, 1H,  $\beta$ -Ph(BENAC)), 6.62(d, <sup>3</sup>J<sub>H,H</sub> = 4 Hz, 4H,  $\beta$ -Ph(BENAC)), 5.42(d, <sup>3</sup>J<sub>H,H</sub> = 4 Hz, 2H,  $\beta$ -H), 5.07(d, <sup>3</sup>J<sub>H,H</sub> = 4 Hz, 2H, -CH). <sup>13</sup>C NMR (100 MHz, CDCl<sub>3</sub>)  $\delta$  (ppm): 188.67, 154.6, 154.0, 148.5, 146.8, 142.6, 142.5, 124.6, 133.6, 132.5, 129.5, 129.0, 128.8, 126.6, 112.1, 47.7, 44.6, 29.7. MALDI-TOF-MS (*m/z*): found 1003.552 [M+K]<sup>+</sup>, calcd 1003.214; found 824.328 [M+H]<sup>+</sup>-BENAC Calcd 824.265. Anal. Calcd for C<sub>62</sub>H<sub>40</sub>N<sub>6</sub>O<sub>2</sub>Zn•CH<sub>3</sub>OH: C, 75.79; H, 4.44; N, 8.42. Found: C, 75.58; H, 4.26; N, 8.29.

**2,3-Di-(1'-cyano-3'-oxo-3'-phenyl-2'-propanenitrile)-12,13-dibromo-5,10,15,20-tetraphenylchlorinato Zinc (II) ZnTPCBr<sub>2</sub>(BENAC)<sub>2</sub> (9b):** Yield: 87% (30 mg, 0.027). UV/vis (CH<sub>2</sub>Cl<sub>2</sub>):  $\lambda_{\max}$ (nm) (log  $\epsilon$ ) 254(4.51), 427(5.36), 524(3.82), 563(3.88), 611(4.35). <sup>1</sup>H NMR (400 MHz, CDCl<sub>3</sub>)  $\delta$  (ppm): 8.57(d, <sup>3</sup>J<sub>H,H</sub> = 4 Hz, 2H,  $\beta$ -H), 8.44(d, <sup>3</sup>J<sub>H,H</sub> = 4 Hz, 2H,  $\beta$ -H), 8.04 (d, <sup>3</sup>J<sub>H,H</sub> = 4 Hz, 8H, *meso*-*o*-Ph), 7.94-7.78(m, 7H, *meso*-*m,p*-Ph), 7.73-7.67(m, 5H, *meso*-*m,p*-Ph), 7.61(t, <sup>3</sup>J<sub>H,H</sub> = 8 Hz, 4H,  $\beta$ -Ph-H(BENAC)), 7.28(s, 1H,  $\beta$ -Ph(BENAC)), 7.24(s, 1H,  $\beta$ -Ph(BENAC)), 6.60(d, <sup>3</sup>J<sub>H,H</sub> = 8 Hz, 4H,  $\beta$ -Ph(BENAC)), 5.35(d, <sup>3</sup>J<sub>H,H</sub> = 4 Hz, 2H,  $\beta$ -H), 5.04(d, <sup>3</sup>J<sub>H,H</sub> = 4 Hz, 2H, -CH). <sup>13</sup>C NMR (100 MHz, CDCl<sub>3</sub>)  $\delta$  (ppm): 188.5, 155.5, 155.0, 148.0, 142.2, 141.9, 134.7, 134.6, 129.1, 128.7, 128.4, 127.9, 121.9, 112.4, 47.65, 44.39. MALDI-TOF-MS



( $m/z$ ): found 1159.444  $[M+K]^+$ , calcd 1159.034; found 981.838  $[M]^+$  -BENAC, calcd 981.050; found 837.008  $[M]^+$ -2BENAC, calcd 837.997. Anal. Calcd for  $C_{62}H_{38}N_6O_2Br_2Zn$ : C, 66.24; H, 3.41; N, 7.48. Found: C, 66.39; H, 3.32; N, 7.24.

**2, 3-Di-(2'-indane-1',3'-dione)-5,10,15,20-tetraphenylchlorinato Zinc (II) ZnTPC(IND)<sub>2</sub> (10b):** Yield: 77% (25 mg, 0.026 mmol). UV/vis ( $CH_2Cl_2$ ):  $\lambda_{max}(nm)$  (log  $\epsilon$ ) 230(4.96), 420(5.39), 520(3.84), 590(4.11), 618(4.59).  $^1H$  NMR (400 MHz,  $CDCl_3$ )  $\delta$  (ppm): 8.49(d,  $^3J_{H,H} = 4$  Hz, 2H,  $\beta$ -H), 8.39(s, 2H,  $\beta$ -H), 8.20-8.18(m, 2H,  $\beta$ -H), 8.07(d,  $^3J_{H,H} = 8$  Hz, 2H, *meso*-*o*-Ph), 8.02(d,  $^3J_{H,H} = 8$  Hz, 4H, *meso*-*o*-Ph), 7.94(t,  $^3J_{H,H} = 8$  Hz, 2H, *meso*-*o*-Ph), 7.85(t,  $^3J_{H,H} = 8$  Hz, 2H, *meso*-*m,p*-Ph), 7.69-7.62(m, 10H, *meso*-*m,p*-Ph), 7.45-7.38(m, 4H,  $\beta$ -Ph(IND)), 7.38(d,  $^3J_{H,H} = 8$  Hz, 2H,  $\beta$ -Ph(IND)), 7.14(t,  $^3J_{H,H} = 8$  Hz, 2H,  $\beta$ -Ph(IND)), 4.70(d,  $^3J_{H,H} = 4$  Hz, 2H,  $\beta$ -H), 3.23(d,  $^3J_{H,H} = 4$  Hz, 2H, -CH). MALDI-TOF-MS ( $m/z$ ): found 968.457  $[M]^+$ , calcd 968.369; found 823.673  $[M+H]^+$ -IND, calcd 823.205; found 678.932  $[M+H]^+$ -2IND, calcd 678.176. Anal. Calcd for  $C_{62}H_{38}N_4O_4Zn$ : C, 76.90; H, 3.96; N, 5.79. Found: C, 77.12; H, 4.01; N, 5.82.

**2,3-Di-(2'-indane-1',3'-dione)-12,13-dibromo-5,10,15,20-tetraphenylchlorinato Zinc (II) ZnTPCBr<sub>2</sub>(IND)<sub>2</sub> (11b):** Yield: 87% (28 mg, 0.025 mmol). UV/vis ( $CH_2Cl_2$ ):  $\lambda_{max}(nm)$  (log  $\epsilon$ ) 230(4.92), 429(5.37), 531(3.86), 568(3.96), 617(4.42).  $^1H$  NMR (400 MHz,  $CDCl_3$ )  $\delta$  (ppm): 8.38(d,  $^3J_{H,H} = 4$  Hz, 2H,  $\beta$ -H), 8.06(d,  $^3J_{H,H} = 8$  Hz, 4H,  $\beta$ -H, *meso*-*o*-Ph), 7.96-7.92(m, 4H, *meso*-*o*-Ph), 7.85(t,  $^3J_{H,H} = 8$  Hz, 2H, *meso*-*o*-Ph), 7.80(d,  $^3J_{H,H} = 8$  Hz, 2H, *meso*-*m,p*-Ph), 7.67(t,  $^3J_{H,H} = 8$  Hz, 6H, *meso*-*m,p*-Ph), 7.58(d,  $^3J_{H,H} = 8$  Hz, 4H, *meso*-*m,p*-Ph), 7.44-7.37(m, 4H,  $\beta$ -Ph(IND)), 7.34(d,  $^3J_{H,H} = 8$  Hz, 2H,  $\beta$ -Ph(IND)), 7.16(t,  $^3J_{H,H} = 8$  Hz, 2H,  $\beta$ -Ph(IND)), 4.65(d,  $^3J_{H,H} = 4$  Hz, 2H,  $\beta$ -H), 3.18(d,  $^3J_{H,H} = 4$  Hz, 2H, -CH).  $^{13}C$  NMR (100 MHz,  $CDCl_3$ )  $\delta$  (ppm): 198.8, 196.7, 158.2, 155.0, 147.6, 143.1, 142.8, 142.2, 141.5, 139.9, 133.8, 127.5, 123.7, 112.2, 106.2, 56.1, 29.9. MALDI-TOF-MS ( $m/z$ ): found 1127.701  $[M+H]^+$ , calcd 1127.169; found 982.699  $[M+H]^+$ -IND, calcd 982.034. Anal. Calcd for  $C_{62}H_{36}N_4O_4Br_2Zn \cdot H_2O$ : C, 65.33; H, 3.48; N, 4.84; Found: C, 65.78; H, 3.62; N, 5.10.

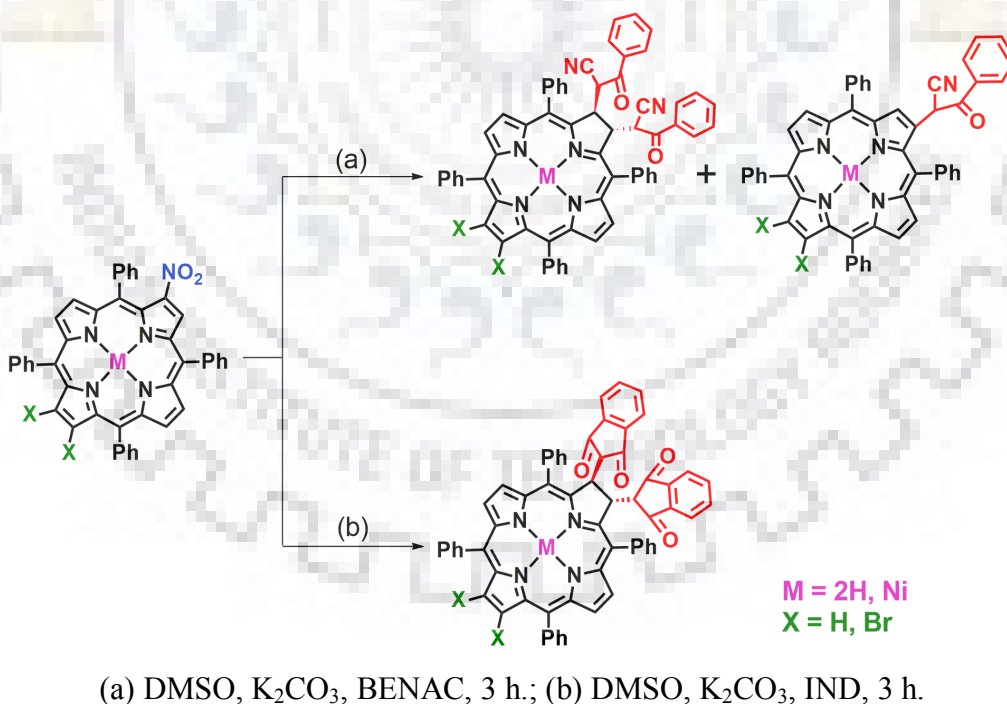
## 2.3 RESULTS AND DISCUSSION

### 2.3.1 Synthesis and Characterization

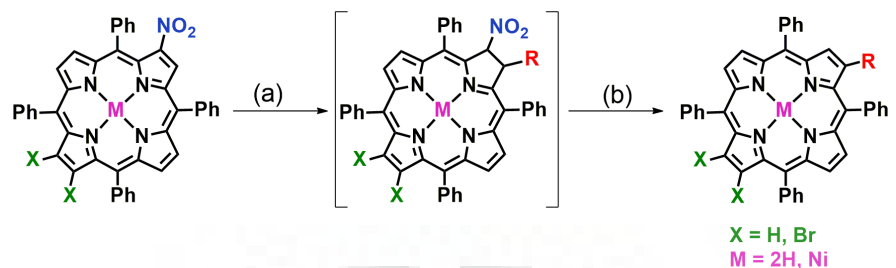


A wide variety of mixed  $\beta$ -substituted chlorins and porphyrins, *viz.*  $\beta$ -di/tetra substituted tetraphenylchlorins (MTPC(R)X<sub>2</sub>, X = H, Br and R = BENAC and IND) and  $\beta$ -mono/tri substituted tetraphenylporphyrins (MTPP(R)X<sub>2</sub>, X = H, Br and R = CHD and DMBA) were synthesized and characterized by various spectroscopic techniques. Nucleophilic substitution of NiTPP(NO<sub>2</sub>)X<sub>2</sub> where X = H and Br with different active methylene compounds including CHD, IND, DMBA, and BENAC has been carried out as shown in Schemes 2.1 and 2.2.

A methodology based on 1,4-addition of cyclic active methylene derivatives with MTPP(NO<sub>2</sub>) as a suitable route for the selective preparation of di/tetra- $\beta$ -substituted tetraphenylchlorin and mono/tri- $\beta$ -substituted tetraphenylporphyrin has been developed. Product distribution can be controlled by varying the size of cyclic carbanions, reaction time and/or temperature, as well as the absence or presence of metal ion in the H<sub>2</sub>TTPP(NO<sub>2</sub>) core. Higher temperature (~110-120 °C) combined with large size cyclic carbanion, favored the formation of the *trans*-chlorins, whereas lower temperature and small cyclic carbanion substituents afforded porphyrins. On the other hand, moderate carbanion with higher temperature and longer reaction time resulted in the formation of 2,3-disubstituted *trans*-chlorins and mono/tri substituted porphyrins in one pot.



**Scheme 2.1** Synthetic Routes for the Preparation of Di/tetra- $\beta$ -Substituted Tetraphenylchlorins.



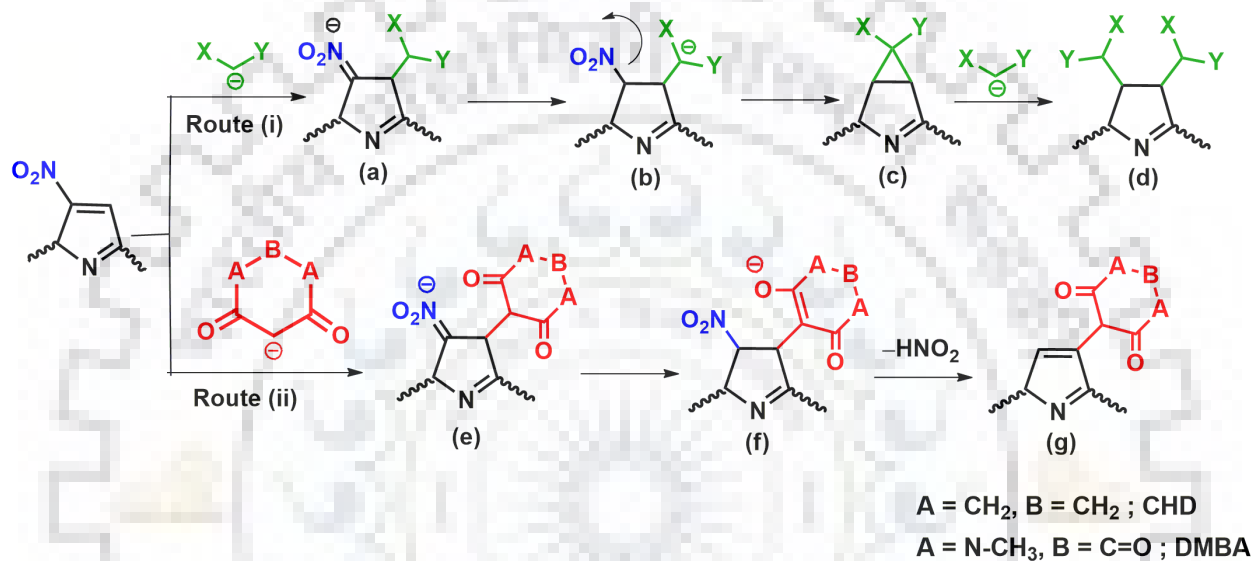
(a) DMSO,  $\text{K}_2\text{CO}_3$ , CHD/DMBA, 1.5 h.; (b)  $-\text{HNO}_2$ .

**Scheme 2.2** Synthetic Route for the Preparation of Mono/tri- $\beta$ -Substituted Tetraphenylporphyrins.

To extend this work, we have examined the reactivity of both Ni(II) and free base  $\beta$ -nitroporphyrin towards a wide variety of active methylene compounds. Interestingly, the reaction of free base nitroporphyrin with cyclic 1,3-diones and BENAC afforded only single product either porphyrin or chlorin. In principle, the addition of unsymmetrical active methylene compounds (benzoylacetonitrile) to  $\text{MTPP}(\text{NO}_2)\text{X}_2$  (where  $X = \text{H, Br}$ ) should yield diastereomers due to presence of chiral centres. However, BENAC reacts in a regioselective manner and produces single diastereomer in good yield. Evidence for regioselectivity was revealed by  $^1\text{H}$  NMR spectrum which has shown two doublets between 3.5 ppm to 5.0 ppm. In contrast, subjecting  $\text{NiTPP}(\text{NO}_2)/\text{NiTPP}(\text{NO}_2)\text{Br}_2$  to Michael addition with BENAC carbanion afforded both porphyrins and chlorins (Scheme 2.1).

In case of DMBA, we were able to isolate *nitro*-chlorins as a side product. However, we were unable to obtain *nitro*-chlorin while subjecting  $\text{H}_2\text{TPP}(\text{NO}_2)\text{Br}_2$  with DMBA due to *in situ* complete conversion of *nitro*-chlorin into porphyrin by eliminating  $\text{HNO}_2$ . While subjecting the  $\text{NiTPP}(\text{NO}_2)\text{X}_2$  (where  $X = \text{H}$  and  $\text{Br}$ ) to DMBA afforded only porphyrin as a single product due to complete *in situ* conversion of *nitro*-chlorin into  $\beta$ -functionalized porphyrin (Scheme 2.2). The reaction of CHD with  $\text{MTPP}(\text{NO}_2)$  ( $M = 2\text{H}$  and  $\text{Ni}(\text{II})$ ) led to the selective formation of porphyrin, whereas treatment of IND with  $\text{MTPP}(\text{NO}_2)$  ( $M = 2\text{H}$  and  $\text{Ni}$ ) resulted into the selective formation of 2,3-disubstituted *trans*-chlorins (Scheme 2.2).

Scheme 2.3 shows the plausible mechanism for product formation. In route (i) the nitronate adduct was formed as an intermediate (a) which resulted into the formation of cyclopropylchlorin due to intramolecular nucleophilic substitution (c). The chlorins (c) underwent further nucleophilic substitution to afford 2,3-disubstituted trans chlorins (d). In route (ii) the nitronate adduct (e) was converted into (f) instead of (b) which led to the formation of  $\beta$ -substituted porphyrin (g) via  $\text{HNO}_2$  elimination as shown in Scheme 2.3.



**Scheme 2.3** The Plausible Mechanism for the Synthesis of Porphyrins and Chlorins.

### 2.3.2 Crystal Structure Discussion

The single crystals of **2a** ( $\text{C}_{50}\text{H}_{32}\text{N}_4\text{O}_2\text{Br}_2\text{Ni}$ ), **8a** ( $\text{C}_{62}\text{H}_{40}\text{N}_6\text{O}_2\text{Ni}$ ), **9** ( $\text{C}_{62}\text{H}_{42}\text{N}_6\text{O}_2\text{Br}_2 \cdot 2\text{CHCl}_3$ ), and **11b** ( $\text{C}_{67}\text{H}_{41}\text{N}_5\text{O}_4\text{Br}_2\text{Zn}$ ) were grown at room temperature from toluene-methanol for **2a**,  $\text{CHCl}_3$ -hexane for **8a** and **9**, and  $\text{CHCl}_3$ -hexane with few drops of pyridine for **11b**. Nonhydrogen atoms were refined in anisotropic approximation except those for the disordered fragments. The crystallographic data of above mentioned chlorins and porphyrins are listed in Table A1 in the Appendix-I. The selected average bond distances and bond angles of these porphyrins and chlorins are given in Table A2 in the Appendix-I. ORTEP top and side views are shown in Figures 2.1 and A1 in Appendix-I.

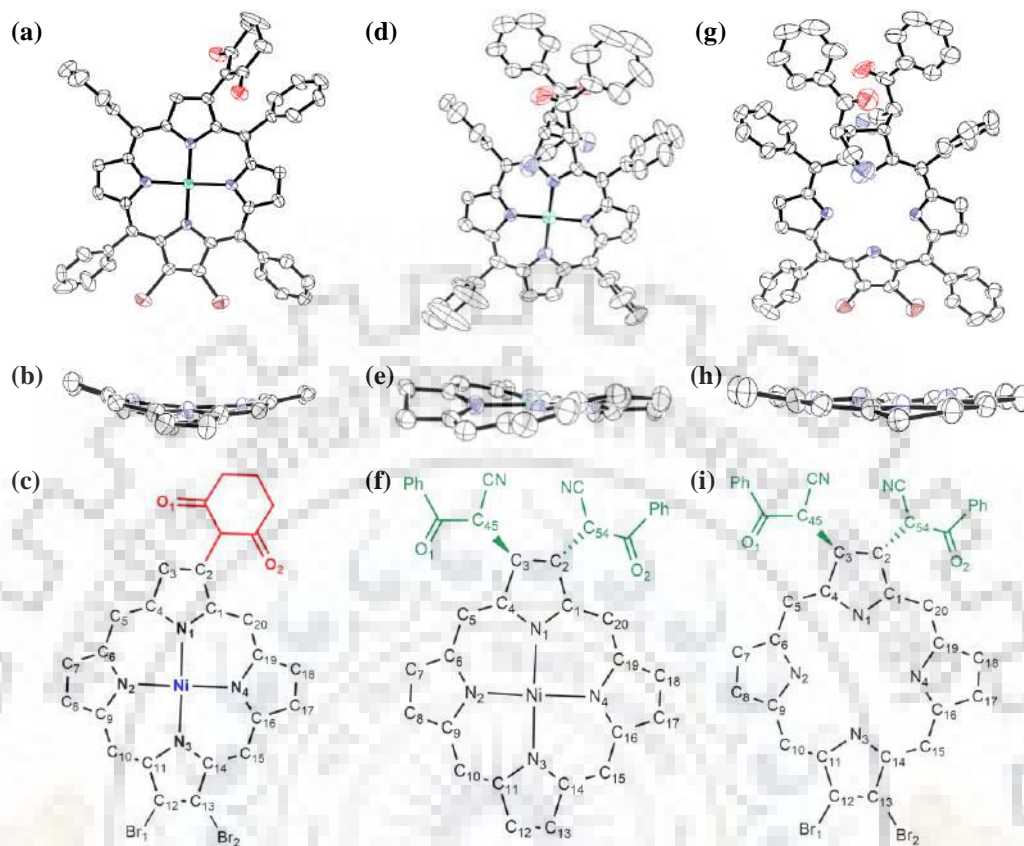


**Figure 2.1** ORTEP Diagrams Showing Top and Side Views of NiTPPBr<sub>2</sub>(CHD) (**2a**) (a and b) NiTPC(BENAC)<sub>2</sub> (**8a**) (d and e) and H<sub>2</sub>TPCBr<sub>2</sub>(BENAC)<sub>2</sub> (**9**) (g and h), Respectively. Solvates are Not Shown for Clarity, the  $\beta$ -Substituents and  $\beta$ -*meso*-Phenyls are Omitted for Clarity in Side View. (c), (f) and (i) Showing Numbering of Carbon Atoms in the Skeleton.

NiTPPBr<sub>2</sub>(CHD) (**2a**) crystallized in the triclinic crystal system with P $\bar{1}$  space group. The CHD moiety was present in the half chair conformation. The macrocycle exhibited saddle shape confirmation. Interestingly, tri- $\beta$ -substituted porphyrins have shown higher magnitude of the displacement of the  $\beta$ -pyrrole carbon ( $\Delta C_{\beta} = \pm 0.66 \text{ \AA}$ ) and 24 core atoms ( $\Delta 24 = \pm 0.430 \text{ \AA}$ ) as compared to  $\beta$ -tetrasubstituted chlorins. NiTPC(BENAC)<sub>2</sub> (**8a**) crystallized in the triclinic crystal system with P $\bar{1}$  space group in which one full molecule was present in the asymmetric unit. Both BENAC groups were *trans* to each other.  $\Delta 24$  value was found to be  $0.281 \text{ \AA}$ .

H<sub>2</sub>TPCBr<sub>2</sub>(BENAC)<sub>2</sub> (**9**) crystallized in the monoclinic crystal system with a C2/c space group. **9** showed two CHCl<sub>3</sub> as lattice solvate one of them was disordered. The X-ray structure revealed that both BENAC groups were *trans* to each other. The observed C3-C45 bond length ( $1.57 \text{ \AA}$ )

was close to C2-C54 bond length 1.59 Å. Both were slightly higher than C-C bond length present in  $sp^3$  hybridized carbons. C3 atom was more deviated (0.364 Å) from mean plane as compared to C2 atom (0.076 Å). The observed C2-C3 bond length (1.52 Å) was larger than other  $C_\beta$ - $C_\beta$  bond length (1.35 Å) which clearly indicates that the proposed structure was 2,3-disubstituted chlorin.  $\Delta C_\beta$  and  $\Delta 24$  were found to be  $\pm 0.262$  Å and  $\pm 0.132$  Å which revealed the slight the quasiplanar confirmation of the macrocycle. ZnTPCBr<sub>2</sub>(IND)<sub>2</sub>(py) crystallized in the triclinic crystal system with P $\bar{1}$  space group in which two molecules were present in the asymmetric unit. In both chlorins, each Zn atom was coordinated to one pyridine unit. Zn1 was 0.342 Å deviated from the mean plane, whereas Zn2 was 0.352 Å deviated from mean plane. Similar to H<sub>2</sub>TPCBr<sub>2</sub>(BENAC)<sub>2</sub> (**9**), both IND groups were *trans* to each other but in contrast to previous chlorin C2'-C54' and C3'-C45' were equal (1.56 Å). C3' atom was 0.251 Å deviated above the mean plane, while C2' was 0.233 Å deviated below the mean plane. In the case of second molecule in the same asymmetric unit, C3 was 0.397 Å deviated above the plane and C2 was 0.080 Å deviated below the plane. In both molecules, the reduced  $C_\beta$ - $C_\beta$  (C2'-C3' and C2-C3) bond lengths were equal to 1.53 Å but a remarkable difference was observed in the values of  $\Delta 24$  and  $\Delta C_\beta$  (Figure A2). Both the chlorin rings were moderately distorted having  $\Delta 24$  values  $\pm 0.174$  Å and  $\pm 0.099$  Å while  $\Delta C_\beta$  values were found to be  $\pm 0.327$  Å and  $\pm 0.146$  Å, respectively. The displacement of  $\beta$ -pyrrole carbons ( $\Delta C_\beta$ ) and 24 core atoms ( $\Delta 24$ ) from the porphyrin mean plane follows the order:

H<sub>2</sub>TPCBr<sub>2</sub>(BENAC)<sub>2</sub> (**9**) < ZnTPCBr<sub>2</sub>(IND)<sub>2</sub>(py) (**11b**) < NiTPC(BENAC)<sub>2</sub> (**8a**) < NiTPPBr<sub>2</sub>(CHD) (**2a**).

Notably, an oxygen-oxygen (O $\cdots$ O) interaction between the nearest CHD moiety of NiTPPBr<sub>2</sub>(CHD) (**2a**) was found at an O $\cdots$ O distance of 2.6 Å (Figure 2.2) which was comparable to O $\cdots$ O interaction found in ice [28]. These kinds of non-bonded interactions can be attractive candidates for the formation of supramolecular assemblies. These oxygen-oxygen (O $\cdots$ O) type interactions may be the result of local polarization effects, due to the electron-rich and electron-deficient regions in the O atoms which results the complementary electrostatic interactions [29]. These forces are responsible for the self-assembly of large molecules, crystal packing, and biological pattern recognition.



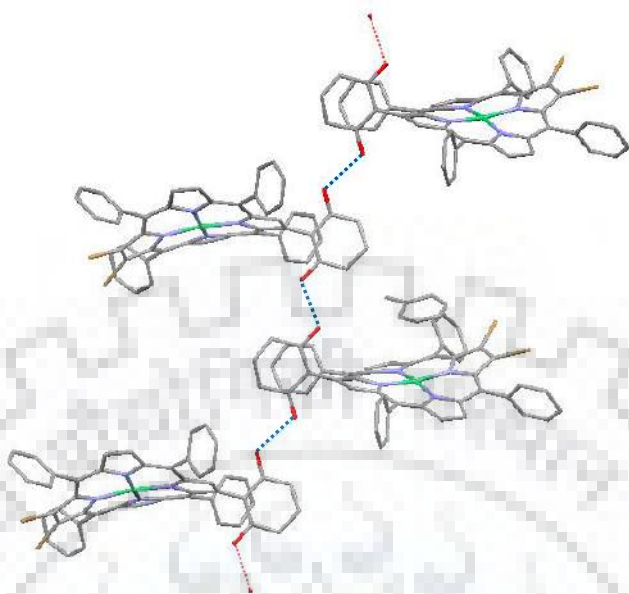


**Figure 2.2** Packing Diagram Showing O...O Interaction between the Nearest CHDs in NiTPPBr<sub>2</sub>(CHD) (**2a**).

### 2.3.3 DFT Studies

To gain insight into the trends in spectral and photophysical properties as a function of molecular characteristics, DFT calculations were performed. The ground state geometries of synthesized free base porphyrins/chlorins were optimized in the gas phase using B3LYP functional and 6-31G basis set. The structures obtained by DFT methods were in close agreement with those obtained by X-ray crystallography. The frontier molecular orbitals (FMOs) of H<sub>2</sub>TPP(CHD) (**1**) and other optimized free base compounds are shown in Figures 2.3 and A3-A9 in Appendix-I, respectively. According to Gouterman's four orbital model, the HOMO-LUMO and HOMO-1 to LUMO+1 configuration make roughly equal contribution to the S<sub>1</sub> wave function in case of porphyrin, whereas in chlorins HOMO-LUMO gap is greater. The HOMO of H<sub>2</sub>TPC(IND)<sub>2</sub> (**10**) have contributions mainly from the macrocycle, whereas the LUMOs of H<sub>2</sub>TPC(IND)<sub>2</sub> (**10**) contribute to the IND group, which indicates charge transfer from the conjugated ring to the  $\beta$ -substituents, However, this contribution is small as compared to the  $\pi$ - $\pi^*$  transition. DFT calculations of free base chlorins have shown the contribution from the tetrapyrrolic macrocycle and the  $\beta$ -substituents (IND and BENAC) to give linear-combination of orbitals, the HOMO-1, HOMO, LUMO, and LUMO+1 of which have mixed chlorins/ $\beta$ -substituents character.



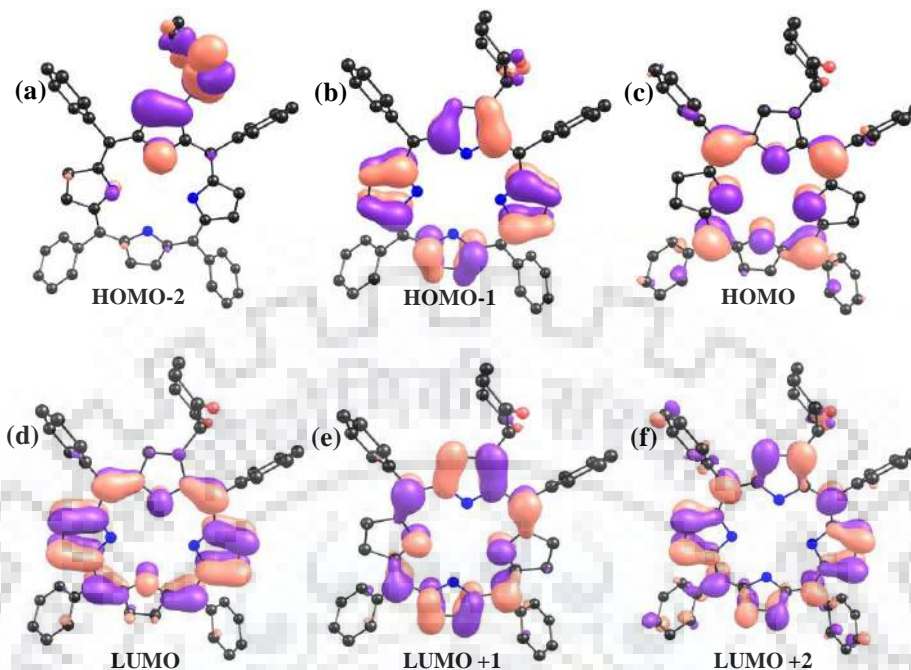


**Figure 2.3** Pictorial Representation of Frontier Molecular Orbitals (FMOs) of  $H_2TPP(CHD)$  (**1**).

### 2.3.4 Absorption Spectral Studies

The optical absorption spectra of each synthesized compound were recorded in  $CH_2Cl_2$  at 298 K. The electronics of the porphyrinic  $\pi$ -systems depend on their degree of saturation. The presence of core metal, type and position of substituents, degree of macrocyclic conjugation and the conformation of the macrocyclic core are also important factors that determine the electronic properties of macrocycle [30]. Figures 2.4 and A10 in Appendix-I represent the comparative UV-vis. spectra of synthesized porphyrins and chlorins in  $CH_2Cl_2$  at 298 K. Tables 2.1 and A3 in Appendix-I list the absorption spectral data of all synthesized chlorins and porphyrins. The red region band is a characteristic property that distinguishes chlorins from porphyrins. The presence of reduced pyrrole causes a relative increase in intensity of the last Q-band. On the other hand, the porphyrin exhibited a significant decrement in last Q-band intensity as compared to chlorins for e.g. Q/B ratio of  $H_2TPC(IND)_2$  (**10**) is  $\sim 9$  times higher as compared to  $H_2TPP(CHD)$  (**1**). In contrast to *meso*-substitution we observed that Q/B ratio altered upon substitution at  $\beta$ -position whereas position of last Q band remains same. Q/B ratio of **8** and **10** reduced to nearly half as compared to  $H_2TPC$ . Q/B ratio of  $H_2TPC$  was nearly four and six times higher as compared to **9** and **11**, respectively.

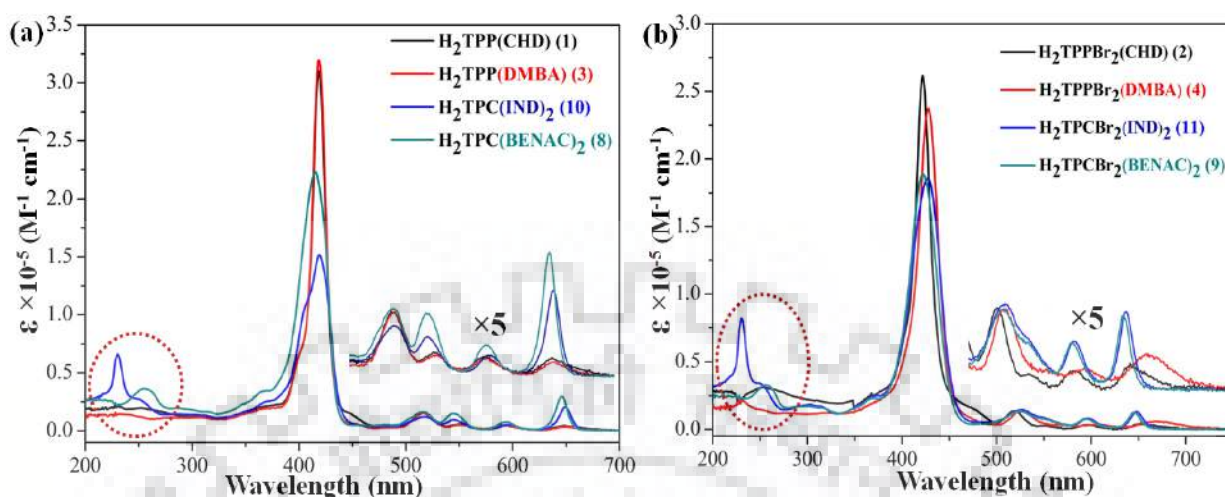


**Figure 2.4** Electronic Absorption Spectra of Synthesized Free Base Porphyrins/Chlorins in  $\text{CH}_2\text{Cl}_2$ . Circled Area Shows the Absorption due to BENAC and IND.

The last Q-band of synthesized free base chlorins were nearly 8-10 nm blue shifted as compared to  $\text{H}_2\text{TPC}$ . Blue shift was observed possibly due to stabilization of HOMO. All dibromo substituted compounds exhibited red shift in their B and/or Q-bands as compared to corresponding unbrominated ones. The Soret band of  $\text{NiTPPBr}_2(\text{CHD})$  (**2a**) was  $\sim 8$  nm red shifted as compared to  $\text{NiTPP}(\text{CHD})$  (**1a**), whereas the Soret band of  $\text{NiTPCBr}_2(\text{IND})_2$  (**11a**) was  $\sim 11$  nm red shifted as compared to  $\text{NiTPC}(\text{IND})_2$  (**10a**). The Soret (B) band is observed as a result of  $\text{S}_0\text{-S}_2$  transition; hence the red shift in the Soret band was possibly due to stabilization of LUMO+1. On the other hand, the position of the  $\text{Q}_{y(0,0)}$  band of dibromosubstituted chlorins was unaltered, yet the relative intensity was decreased as compared to unbrominated ones which may be due to reduced energy gap between LUMO and LUMO+1. Position of  $\text{Q}_{y(0,0)}$  band remained same, therefore HOMO-LUMO gap remains unaltered. The similar shifts were observed for other synthesized chlorins and porphyrins as listed in Table 2.2. Oscillator strength of above synthesized compounds ranges from 0.010 to 0.034. Experimental oscillator strengths were estimated by the following formula

$$f = 4.61 \times 10^{-9} \epsilon \delta$$

Here,  $\epsilon$  = molar absorption coefficient,  $\delta$  = full width at half maxima

### 2.3.5 Fluorescence Spectral Studies

Free base and Zn(II) complexes of the mono/tri-substituted porphyrins and di/tetra substituted chlorins were characterized by fluorescence spectroscopy in order to elucidate the role of substitution. Figures 2.5 and A11 in Appendix-I show the emission profile of synthesized free base and Zn(II) compounds, respectively. The fluorescence maxima of all synthesized chlorins were present within  $\sim 10$  nm of the corresponding  $Q_{y(0,0)}$  absorption maximum, reflecting a relatively small Stokes shift. Porphyrins exhibited higher Stokes shift as compared to chlorins. Among all synthesized compounds,  $H_2TPPBr_2$ (DMBA) (**4**) showed highest Stokes shift. Bromo substituted porphyrinoids exhibited lower quantum yields due to heavy atom effect of  $\beta$ -bromo substituents and nonplanar conformation of the macrocyclic core. We were unable to calculate the quantum yield for  $H_2TPPBr_2$ (DMBA) (**4**) due to very feeble fluorescence intensity. In case of bromochlorins, quantum yield profoundly decreased as compared to unbrominated chlorins due to heavy atom effect and low Q/B ratio. Table 2.2 represents the fluorescence yields ( $\phi_f$ ) and singlet excited-state lifetimes ( $\tau_s$ ) for the newly synthesized compounds. Quantum yields ( $\phi_f$ ) were calculated by using following formula

$$(\phi_f)_{\text{sample}} = (\phi_{f \text{ ref}} \times A_{\text{sample}} \times \epsilon_{\text{ref}}) / (A_{\text{ref}} \times \epsilon_{\text{sample}})$$

and follow the order:

$H_2TPCBr_2$ (BENAC)<sub>2</sub> (**9**) <  $H_2TPCBr_2$ (IND)<sub>2</sub> (**11**) <  $H_2TPPBr_2$ (CHD) (**2**) <  $H_2TPP$ (DMBA) (**3**) <  $H_2TPP$ (CHD) (**1**) <  $H_2TPC$ (NO<sub>2</sub>)(DMBA) (**7**) <  $H_2TPC$ (BENAC)<sub>2</sub> (**8**) <  $H_2TPC$ (IND)<sub>2</sub> (**10**)

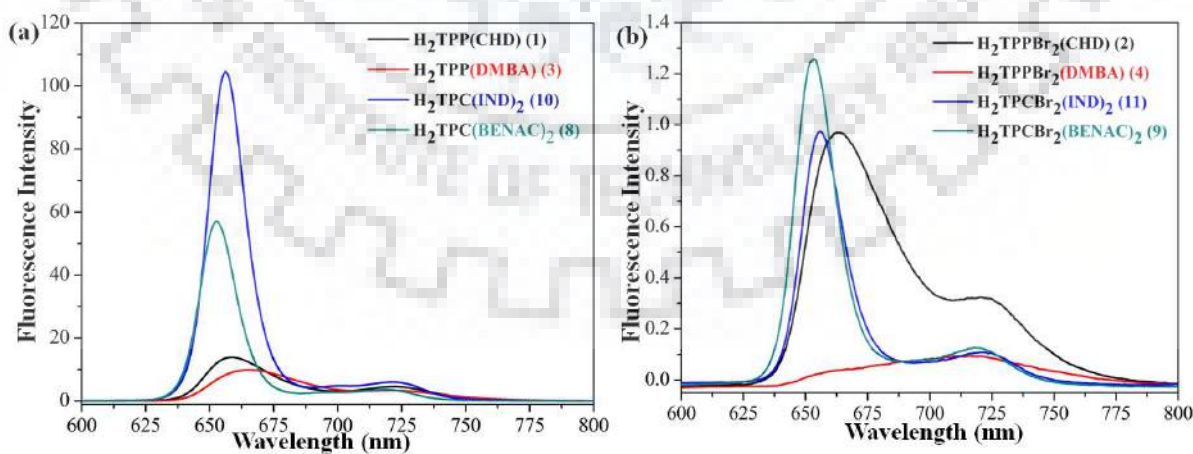


**Figure 2.5** Fluorescence Spectra of Synthesized Free Base Complexes.

**Table 2.1** Photophysical Properties<sup>a</sup> of Synthetic Chlorins and Porphyrins.

Porphyrin	$\lambda_{\text{abs}}$	$\lambda_{\text{em}}$	Q/B	$\Sigma Q/\Sigma B^b$	$f$
H <sub>2</sub> TPP(CHD) (1)	419(5.49), 518(4.18), 552(3.76), 591(3.68), 648(3.66)	657, 721	0.015	0.02	0.019
H <sub>2</sub> TPPBr <sub>2</sub> (CHD) (2)	422(5.41), 519(4.13), 550(3.43), 598(3.51), 655(3.61)	663, 720	0.016	0.02	0.023
H <sub>2</sub> TPP(DMBA) (3)	419(5.50), 515(4.18), 550(3.71), 595(3.65), 648(3.54)	666, 722	0.011	0.01	0.022
H <sub>2</sub> TPP Br <sub>2</sub> (DMBA) (4)	428(5.37), 525(4.12), 600(3.53), 670(3.79)	716	0.026	0.04	0.025
H <sub>2</sub> TPC(NO <sub>2</sub> )(DMBA) (7)	435(5.46), 537(4.03), 580(4.29), 618(3.64), 675(4.00)	683, 753	0.054	0.03	0.026
H <sub>2</sub> TPC(BENAC) <sub>2</sub> (8)	255(4.56), 416(5.34), 516(4.21), 544(4.18), 593(3.88), 646(4.47)	652, 718	0.133	0.06	0.031
H <sub>2</sub> TPCBr <sub>2</sub> (BENAC) <sub>2</sub> (9)	256(4.52), 423(5.27), 525(4.13), 595(3.97), 645(4.09)	653, 717	0.066	0.03	0.028
H <sub>2</sub> TPC(IND) <sub>2</sub> (10)	229(4.80), 419(5.18), 518(4.08), 545(3.97), 595(3.71), 649(4.31)	656, 721	0.136	0.12	0.023
H <sub>2</sub> TPCBr <sub>2</sub> (IND) <sub>2</sub> (11)	230(4.91), 427(5.27), 527(4.16), 596(3.90), 648(4.12)	655, 718	0.044	0.02	0.032

<sup>a</sup>The values in parentheses refer to log  $\epsilon$ , integrated ( $\Sigma Q/\Sigma B$ ) intensity ratios of the Q and Soret (B) absorption,  $f$  = Oscillator Strength

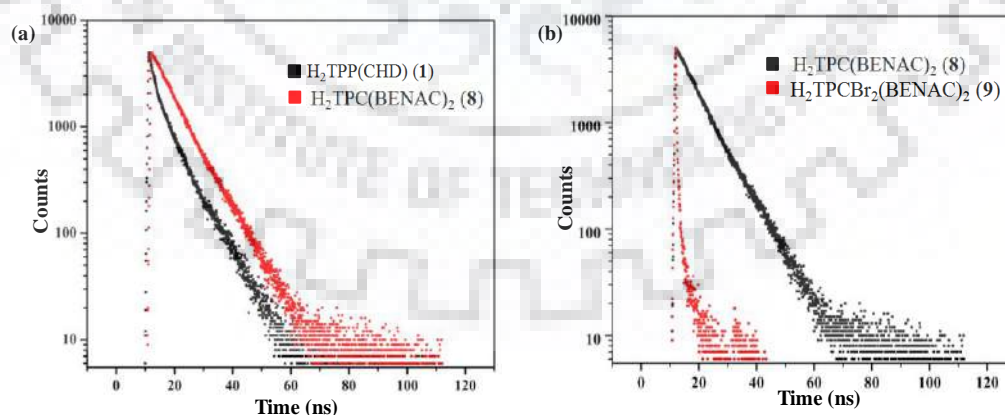


**Figure 2.6** Fluorescence Lifetime Decay Profiles of (a) H<sub>2</sub>TPP(CHD) (1) and H<sub>2</sub>TPC(BENAC)<sub>2</sub> (8) (b) H<sub>2</sub>TPC(BENAC)<sub>2</sub> (8) and H<sub>2</sub>TPCBr<sub>2</sub>(BENAC)<sub>2</sub> (9).

**Table 2.2** Photophysical Properties<sup>a</sup> of Synthetic Chlorins and Porphyrins.

<b>Porphyrin</b>	$\phi_r$	$\tau_s$ (ns)	$K_{nr}^{-1}$ (ns)	$K_r^{-1}$ (ns)
H <sub>2</sub> TPP(CHD) ( <b>1</b> )	0.097	5.23	5.85	54.49
H <sub>2</sub> TPP(CHD)Br <sub>2</sub> ( <b>2</b> )	0.008	0.42	0.42	52.50
H <sub>2</sub> TPP(DMBA) ( <b>3</b> )	0.095	0.056	0.06	0.60
H <sub>2</sub> TPC(NO <sub>2</sub> )(DMBA) ( <b>5</b> )	0.028	7.72	7.95	276.01
H <sub>2</sub> TPC(BENAC) <sub>2</sub> ( <b>8</b> )	0.402	7.63	12.76	18.96
H <sub>2</sub> TPC(BENAC) <sub>2</sub> Br <sub>2</sub> ( <b>9</b> )	0.004	1.00	1.00	250.00
H <sub>2</sub> TPC(IND) <sub>2</sub> ( <b>10</b> )	0.317	6.71	9.82	21.17
H <sub>2</sub> TPC(IND) <sub>2</sub> Br <sub>2</sub> ( <b>11</b> )	0.005	1.15	1.16	230.00
ZnTPP(CHD) ( <b>1b</b> )	0.038	1.56	1.63	41.16
ZnTPP(CHD)Br <sub>2</sub> ( <b>2b</b> )	0.004	0.44	0.45	110.83
ZnTPP(DMBA) ( <b>3b</b> )	0.041	5.71	5.96	139.34
ZnTPP(DMBA)Br <sub>2</sub> ( <b>4b</b> )	0.002	0.02	0.03	12.52
ZnTPC(BENAC) <sub>2</sub> ( <b>8b</b> )	0.154	1.51	1.79	9.83
ZnTPC(BENAC) <sub>2</sub> Br <sub>2</sub> ( <b>9b</b> )	0.010	0.506	0.51	50.62
ZnTPC(IND) <sub>2</sub> ( <b>10b</b> )	0.047	0.522	0.55	11.11
ZnTPC(IND) <sub>2</sub> Br <sub>2</sub> ( <b>11b</b> )	0.003	0.004	1.22	0.004

<sup>a</sup> values were calculated in CH<sub>2</sub>Cl<sub>2</sub> at 298 K.

The studies performed in the present work on  $\beta$ -substituted porphyrins and chlorins provide an opportunity to compare the quantum yields, lifetimes, and rate constants for the two S1 excited-state decay pathways across two classes of macrocycles having similar skeletons. The span of  $\tau_s$  values (0.004-7.72 ns) for chlorins were wider as compared to porphyrins (0.02-5.53 ns). Singlet state lifetime values of **8** and **10** were low as compared to H<sub>2</sub>TPC (13.1 ns) however lifetime values of **9** and **11** were lower than **8** and **10** respectively. In this way,  $\beta$ -substitution leads to dramatic shift in singlet state lifetime. Figure 2.6a shows the comparative lifetime plot of H<sub>2</sub>TPP(CHD) (**1**) and H<sub>2</sub>TPC(BENAC)<sub>2</sub> (**8**). The radiative ( $k_r$ ) and nonradiative ( $k_{nr}$ ) rate constants were calculated according to the method reported by Holten and coworkers [31].



$$k_r = \phi_f/\tau_S$$

$$k_{nr} = (1 - \phi_f)/\tau_S$$

$$k = 1/\tau_S$$

$$k_{nr} = k - k_r$$

These rate constants (Table 2.2) were cast as the associated time constants (in nanoseconds). The calculated  $k_r$  values were significantly lower than *meso*-tetraphenylporphyrin (120 ns<sup>-1</sup>). However, in case of bromo substituted chlorins and porphyrins radiative rate constants were invariably lower than those reported in literature for related systems (Table 2.2). The distinct differences in photophysical properties of mono/di- and tri/tetra- $\beta$ -substituted MTPPs/MTPCs differ strikingly from their parent molecules due to the nature of  $\beta$ -substituents, effect of substituents on molecular-orbital energy gaps, and excited-state configurational mixing and conformation of the macrocyclic core.

In summary, we can conclude that (a) the integrated intensity of S<sub>0</sub>-S<sub>1</sub> manifold decreased upon  $\beta$ -substitution which results into low  $\phi_f$  and  $k_r$  of synthesized free base and Zn(II) chlorins as compared to *meso*-tetraphenylchlorins (b) Reduced LUMO and LUMO+1 gap may be the another cause of low fluorescence intensity in synthesized  $\beta$ -substituted chlorins. (c) Finally, we can say that by means of mixed  $\beta$ -substitution photophysical properties of *meso*-tetraphenylchlorin can be tuned.

### 2.3.6 <sup>1</sup>H NMR and Mass Spectrometric Studies

All the synthesized porphyrins and chlorins exhibited characteristic chemical shifts arising from  $\beta$ -pyrrole protons,  $\beta$ -substituent protons, *meso*-phenyl, and imino protons for free base porphyrins and chlorins. Figures 2.7 and A12-A19 in Appendix-I represent the <sup>1</sup>H NMR spectra of all newly synthesized porphyrinoids. The presence of a sharp singlet with one proton intensity between 3.5 ppm to 5.0 ppm clearly indicates the formation of porphyrins (**1-6**, **1a-4a** and **1b-4b**) whereas the presence of two doublets of two proton intensity between 3.5 ppm to 5.0 ppm demonstrates the formation of 2,3-disubstituted trans chlorins (**7-11**, **8a-11a** and **8b-11b**). The  $\beta$ -pyrrole resonances of these synthesized free base TPCs were downfield shifted (~ 0.44 ppm) as compared to H<sub>2</sub>TPC (Figure 2.7). Inner core NH signals of **7**, **8** and **9** were upfield shifted (0.03-0.19 ppm) as compared to H<sub>2</sub>TPC, whereas no significant shift was observed for **10** and **11**. In



contrast to H<sub>2</sub>TPC, reduced  $\beta$ -pyrrolic protons of synthesized chlorins resonated at higher frequencies. Significantly, these protons were 0.66-1.44 ppm downfield shifted as compared to H<sub>2</sub>TPC. Downfield shift of  $\beta$ -protons and upfield shift of inner core NHs were observed due to electron withdrawing nature of  $\beta$ -substituents. Figure 2.8 shows the <sup>1</sup>H NMR spectra of the imino proton region of synthesized free base porphyrins and chlorins in CDCl<sub>3</sub> at 298 K.

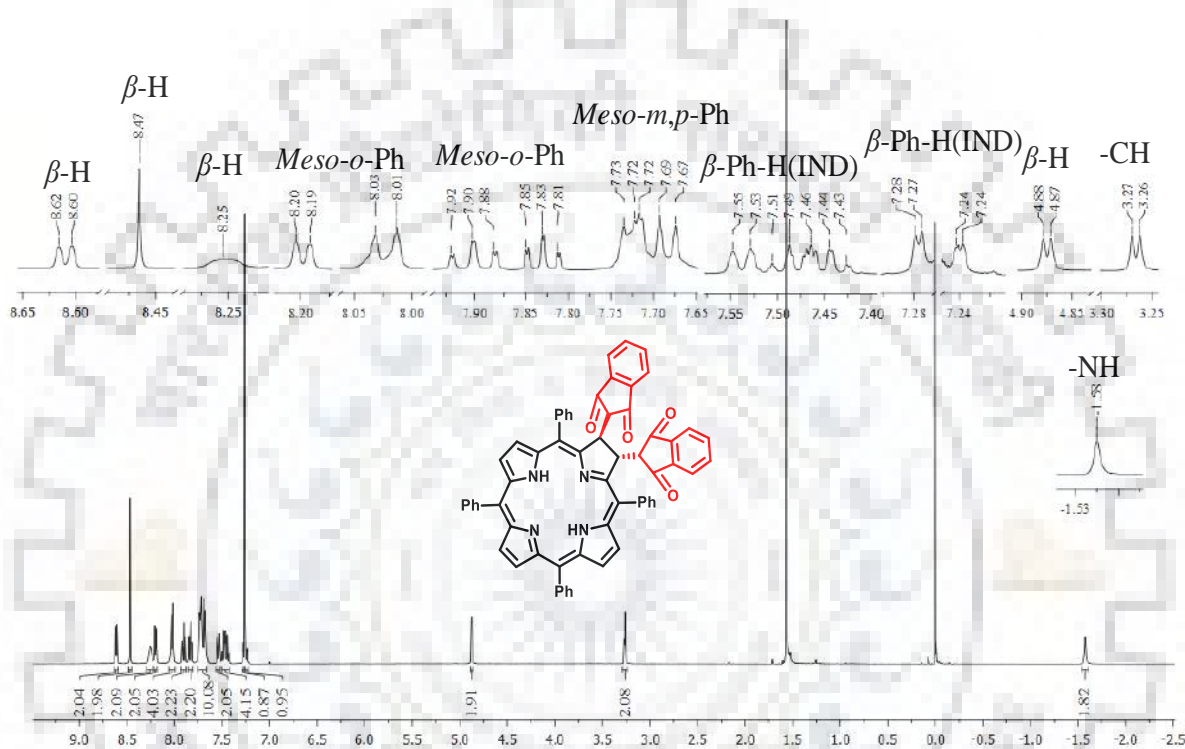


**Figure 2.7.** <sup>1</sup>H NMR Spectrum of H<sub>2</sub>TPC(IND)<sub>2</sub> (10) in CDCl<sub>3</sub> at 298K.

The  $\beta$ -pyrrole resonances of the synthesized free base TPPs were downfield shifted as compared to synthesized free base TPCs. The major differences for the position of core imino protons and  $\beta$ -pyrrole proton arise due to reduced ring current in chlorins. The number and positions of carbon signals were clearly in accordance with the proposed structures. However, we were unable to record <sup>13</sup>C NMR of **2b**, **4b**, **10**, and **10b** due to very poor solubility in CDCl<sub>3</sub> and DMSO-d<sub>6</sub>.

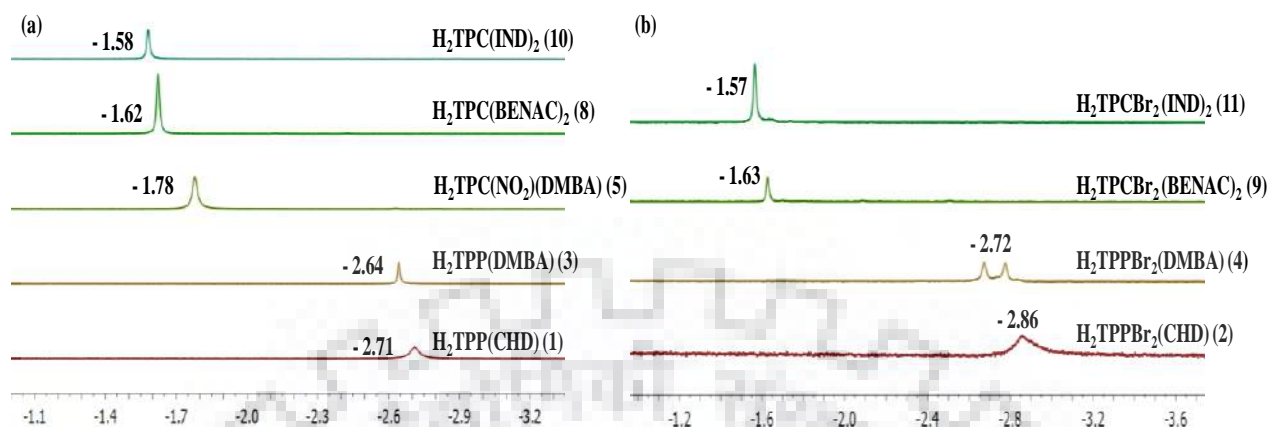


**Figure 2.8** Representative  $^1\text{H}$  NMR Spectra of Imino Proton Region of Synthesized Free Base Porphyrins and Chlorins.

The MALDI-TOF mass spectra of all the synthesized compounds have been recorded using HABA as matrix. The positive ion mode mass spectra of synthesized free base porphyrinoids are shown in Figures A20-A28 in the Appendix-I. BENAC and IND appended chlorins showed fragmentation pattern in the mass spectra due to removal of labile one and/or two  $\beta$ -substituents as shown in Figures A25-A28 in Appendix-I.

### 2.3.7 Protonation and Deprotonation Studies

To determine the acid-base properties of central coordination entity  $\text{H}_2\text{N}_4$  of macrocycles, we have carried out the protonation and deprotonation studies of synthesized free base porphyrins and chlorins using trifluoroacetic acid (TFA) and tetrabutylammonium hydroxide (TBAOH), respectively in toluene at 298 K. The acid-base properties of chlorins are largely unexplored. Figure 2.9 shows the UV-vis. spectral changes upon increasing the concentration of TFA ( $0.26 \times 10^{-5}$ - $3.84 \times 10^{-5}$  M) for porphyrin,  $\text{H}_2\text{TPPBr}_2(\text{DMBA})$  (**4**) and ( $0.34 \times 10^{-3}$ - $5.74 \times 10^{-3}$  M) for chlorin,  $\text{H}_2\text{TPCBr}_2(\text{IND})_2$  (**11**) in toluene at 298 K. Figure 2.9a represents the concomitant decrement in the absorbance of  $\text{H}_2\text{TPPBr}_2(\text{DMBA})$  (**4**) at 430 nm and rising of a new band at 456 nm upon increasing [TFA]. As protonation proceeded, the multiple Q bands disappeared and a new single broad band arose at 694 nm accompanied with the red-shift of 20 nm in  $\text{Q}_{x(0,0)}$  band. A similar behavior was observed for other free base porphyrins as shown in Figure A29 in Appendix-I.

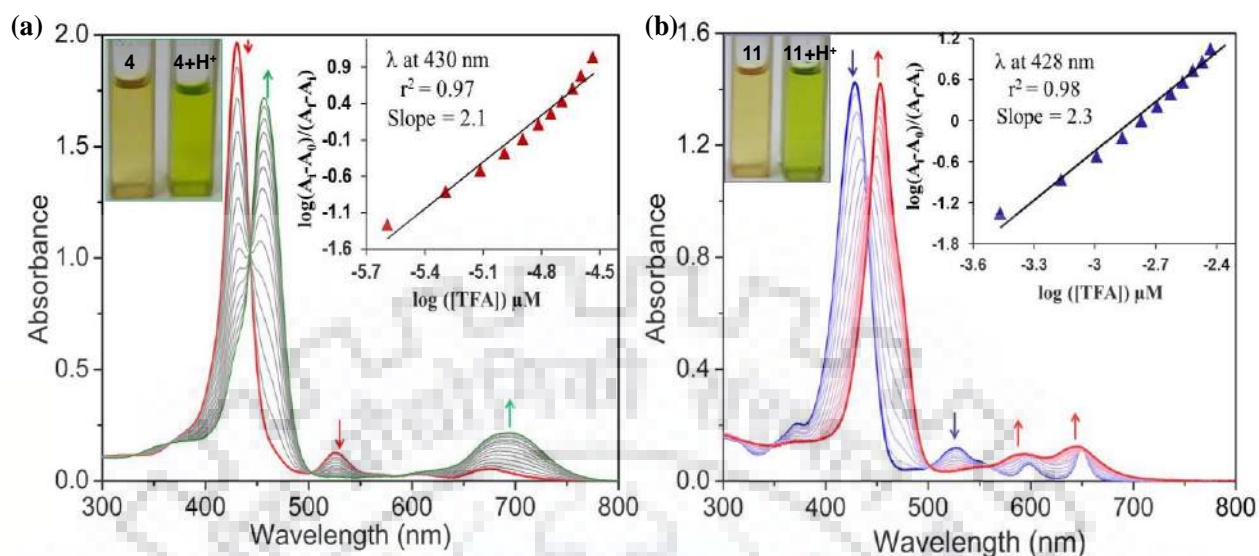


**Figure 2.9** UV-vis. Spectral Titration of (a)  $\text{H}_2\text{TPPBr}_2(\text{DMBA})$  (**4**) and; (b)  $\text{H}_2\text{TPCBr}_2(\text{IND})_2$  (**11**) With TFA in Toluene at 298 K; Insets Show the Corresponding Hill Plots.

**Table 2.3** Protonation and Deprotonation Constants ( $\log \beta_2$ )<sup>a</sup> of Free Base Mixed Substituted Chlorins and Porphyrins in Toluene at 298 K

Porphyrins/Chlorins	Protonation			Deprotonation		
	$\log \beta_2$	$n^b$	$r^2$	$\log \beta_2$	$n^b$	$r^2$
$\text{H}_2\text{TPP}(\text{CHD})$ ( <b>1</b> )	10.97	2.0	0.93			
$\text{H}_2\text{TPPBr}_2(\text{CHD})$ ( <b>2</b> )	11.36	2.1	0.96			
$\text{H}_2\text{TPP}(\text{DMBA})$ ( <b>3</b> )	10.29	2.1	0.97			
$\text{H}_2\text{TPPBr}_2(\text{DMBA})$ ( <b>4</b> )	10.50	2.1	0.97			
$\text{H}_2\text{TPC}(\text{BENAC})_2$ ( <b>8</b> )	5.94	2.2	0.99	10.03	1.9	0.97
$\text{H}_2\text{TPCBr}_2(\text{BENAC})_2$ ( <b>9</b> )	6.04	2.3	0.97	9.67	1.9	0.95
$\text{H}_2\text{TPC}(\text{IND})_2$ ( <b>10</b> )	5.41	1.9	0.98	14.12	2.5	0.95
$\text{H}_2\text{TPCBr}_2(\text{IND})_2$ ( <b>11</b> )	6.77	2.3	0.98	15.59	2.8	0.96

<sup>a</sup>Within the error range of  $\pm 0.05$  for  $\log \beta_2$ . <sup>b</sup> $n$  refers to stoichiometry.

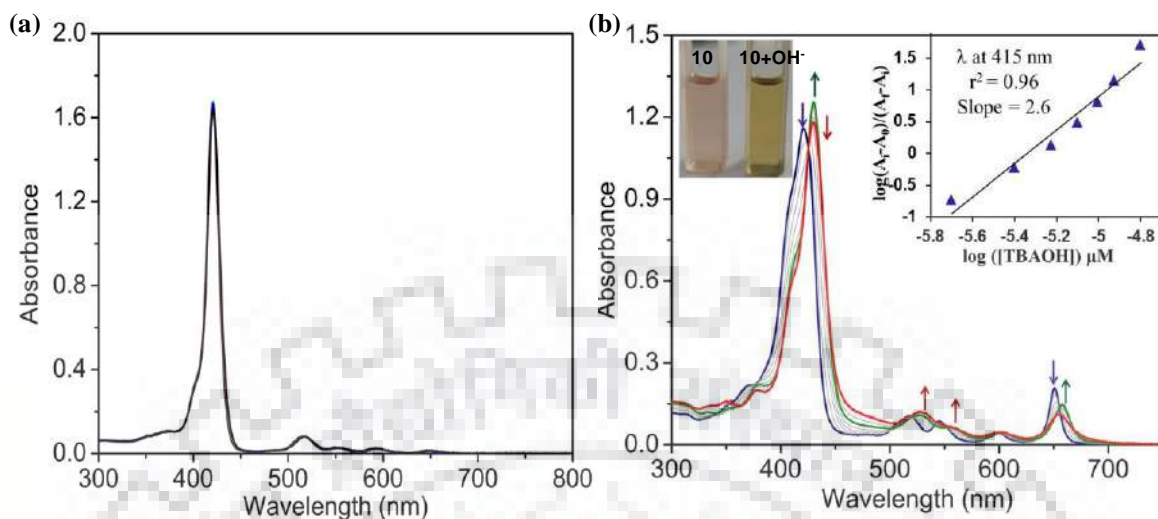


**Figure 2.10** UV-vis. Spectral Changes of (a) H<sub>2</sub>TPP(DMBA) (**3**) and; (b) H<sub>2</sub>TPC(IND)<sub>2</sub> (**10**) while Increasing [TBAOH] in Toluene at 298 K; Inset Shows the Corresponding Hill Plots.

In protonation studies, chlorins exhibited similar spectral changes in B band whereas different spectral changes were observed in Q bands as compared to porphyrins. Figure 2.9b shows the UV-vis. spectral titration of H<sub>2</sub>TPCBr<sub>2</sub>(IND)<sub>2</sub> (**11**) while increasing [TFA]. The absorbance concomitantly decreased at 428 nm with the emergence of a new B band at 453 nm accompanied by a minimal (5 nm) blue shift in the last Q<sub>y(0,0)</sub> band. Similar spectral changes were observed for remaining synthesized free base chlorins (Figure A30 in Appendix-I). The protonated porphyrins show enhanced Q<sub>x(0,0)</sub> band with 11-19 nm red shift, whereas in chlorins after protonation the intensity of last Q<sub>y(0,0)</sub> band was slightly decreased accompanied with 4-15 nm blue shift.

The protonation constants were calculated using Hill equation. Table 2.3 lists the protonation constants for various free base mixed substituted chlorins and porphyrins. In all cases, we obtained the diprotonated chlorin and porphyrin species which was further confirmed by Hill plot having a slope of  $\sim 2$  as shown in insets of Figures 2.9 and Figures A29, A30 in the Appendix-I. The bromo porphyrins exhibited higher  $\log\beta_2$  as compared to the porphyrins without bromo group due to moderate nonplanar conformation of the porphyrins. The diprotonated bromochlorins have shown minimal blue shift  $\sim 4$  nm in last Q<sub>y(0,0)</sub> band as compared to neutral bromochlorins whereas a prominent blue shift of  $\sim 15$  nm was observed after the protonation of unbrominated chlorins.

UV-vis. titration was carried out to determine the deprotonation constants of all the synthesized free base chlorins and porphyrins. All the synthesized free base porphyrins were unable to deprotonate even at a higher conc. of TBAOH, as expected.  $H_2TPP(R)$  (where  $R = CHD$  and  $DMBA$ ) did not show any spectral changes even after addition of excess of TBAOH (Figures 2.10a and A31a in the Appendix-I) which was possibly due to the electron-rich nature of the porphyrin core which prevents the formation of dianionic species. Moreover, in excess of TBAOH, the bromo containing porphyrins  $H_2TPPBr_2(R)$  ( $R = DMBA$  and  $CHD$ ) showed a small decrement in the B-band and emergence of a very less intense shoulder as shown in Figure A31b and A31c in the Appendix-I, this means that the reactant was in equilibrium with the anionic species and did not move forward to completion which indicated the slightly nonplanar conformation as compared to  $H_2TPP(R)$  ( $R = DMBA$  and  $CHD$ ). Interestingly, all the free base chlorins were easily deprotonated even at very low conc. of TBAOH. Table 2.3 lists the deprotonation constant data in toluene at 298 K. Figure 2.10b shows the concomitant decrement in absorbance of  $H_2TPC(IND)_2$  (**10**) at 418 nm and emergence of a new band at 429 nm with multiple isosbestic points while increasing the conc. of TBAOH ( $0.20 \times 10^{-5}$ - $1.00 \times 10^{-5}$  M). Simultaneously, the last  $Q_{y(0,0)}$  band of  $H_2TPC(IND)_2$  (**10**) concomitantly decreased at 650 nm and a new band rose at 658 nm. As we increase the concentration of TBAOH from  $1.00 \times 10^{-5}$  to  $2.18 \times 10^{-5}$  M, the newly generated B-band at 429 nm sequentially decreased at the same wavelength accompanied with 5 nm blue shift (658-653 nm) in the last  $Q_{x(0,0)}$  band as indicated by the red line spectrum in Figure 2.10b. These spectral changes may be attributed to the removal of indanedione protons attached to the  $\beta$ -pyrrole position of the chlorin. The Hill plot (Figure 2.10b inset) showed a straight line between  $\log[(TBAOH)]$  and  $\log(A_f - A_0 / A_f - A_i)$  having a slope value  $> 2$  which further confirmed the deprotonation of the outer proton (active methylene protons). Similar spectral changes were observed for other three free base chlorins (Figures A32 in the Appendix-I). All the chlorins exhibited very high deprotonation constants  $\log \beta_2$ . The bromochlorins  $H_2TPCBr_2(R)_2$  ( $R = IND$  and  $BENAC$ ) have shown slightly higher  $\log \beta_2$  values as compared to the  $H_2TPC(R)_2$  ( $R = IND$  and  $BENAC$ ) which may be due to the combined effect of electronic nature of  $\beta$ -substituents as well as outer proton abstraction. The deprotonation of inner core -NH and abstraction of outer CH proton has also been confirmed by  $^1H$  NMR spectroscopy in  $CDCl_3$  at 298 K.



Figure 2.11 shows the changes in proton signals after addition of TBAOH in  $\text{CDCl}_3$  at 298 K. The singlet of two protons intensity corresponding to inner core  $-\text{NH}$  at -1.56 ppm disappeared after addition of TBAOH as indicated by blue circle in Figure 2.11. Likewise the doublet of two protons at 3.23 ppm, which was corresponding to  $-\text{CH}$  of IND moiety attached to  $\beta$ -pyrrole position also nearly disappeared as shown by red circle in the Figure 2.11. The proton signals corresponding to other  $\beta$ -protons and phenyl rings were unaffected after TBAOH addition.  $^1\text{H}$  NMR studies also supported very high deprotonation constants  $\log \beta_2$  (9.67-15.59) of free base chlorins (Table 2.3).

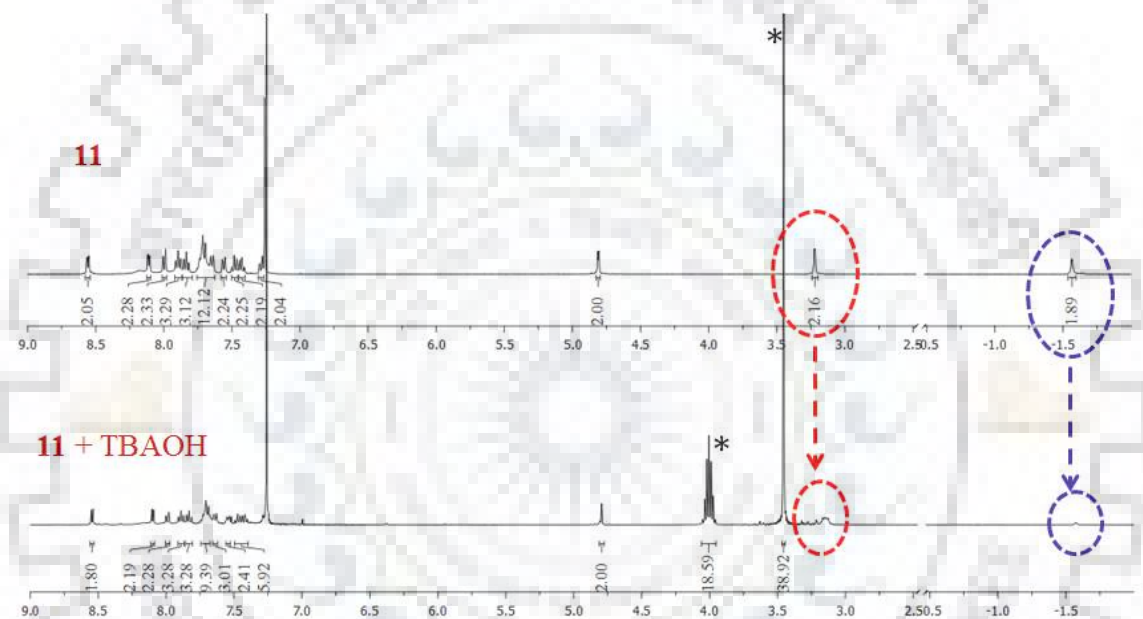


**Figure 2.11**  $^1\text{H}$  NMR Spectral Changes of  $\text{H}_2\text{TPCBr}_2(\text{IND})_2$  (**11**) Upon Addition of TBAOH in  $\text{CDCl}_3$  at 298 K. \*Corresponding to TBAOH Proton Signals.

### 2.3.8 Electrochemical Redox Properties

To determine the influence of macrocyclic conformation and the electronic nature of  $\beta$ -pyrrole substituents, cyclic voltammetric studies of synthesized porphyrinoids were carried out in  $\text{CH}_2\text{Cl}_2$  containing 0.1 M TBAPF<sub>6</sub>. Table 2.4 lists the redox potential data of the synthesized chlorins and porphyrins in  $\text{CH}_2\text{Cl}_2$  at 298 K. Figure 2.12 represents the comparative cyclic voltammograms (CVs) of Ni(II) and Zn(II) chlorins. The CVs of free base chlorins and porphyrins are shown in Figures A33 and A34, respectively in the Appendix-I. The synthesized porphyrins exhibited two, one-electron ring-centered oxidations and reductions. However,



DMBA substituted free base porphyrins (**3** and **4**) have shown third oxidation at 1.62 V. The first ring-centered reduction potentials of the MTPPBr<sub>2</sub>(R) (R = CHD and DMBA; M = 2H, Ni and Zn) exhibited anodic shift in the reduction potentials (0.09V-0.36V) indicating extensive stabilization of the LUMO. Whereas there were no observable shifts in oxidation potentials which was due to destabilization of HOMO induced by nonplanar conformation of macrocyclic core. The free base mono/tri- $\beta$ -substituted porphyrins exhibited the following trend in anodic shifts of their first ring-centered reduction potentials:

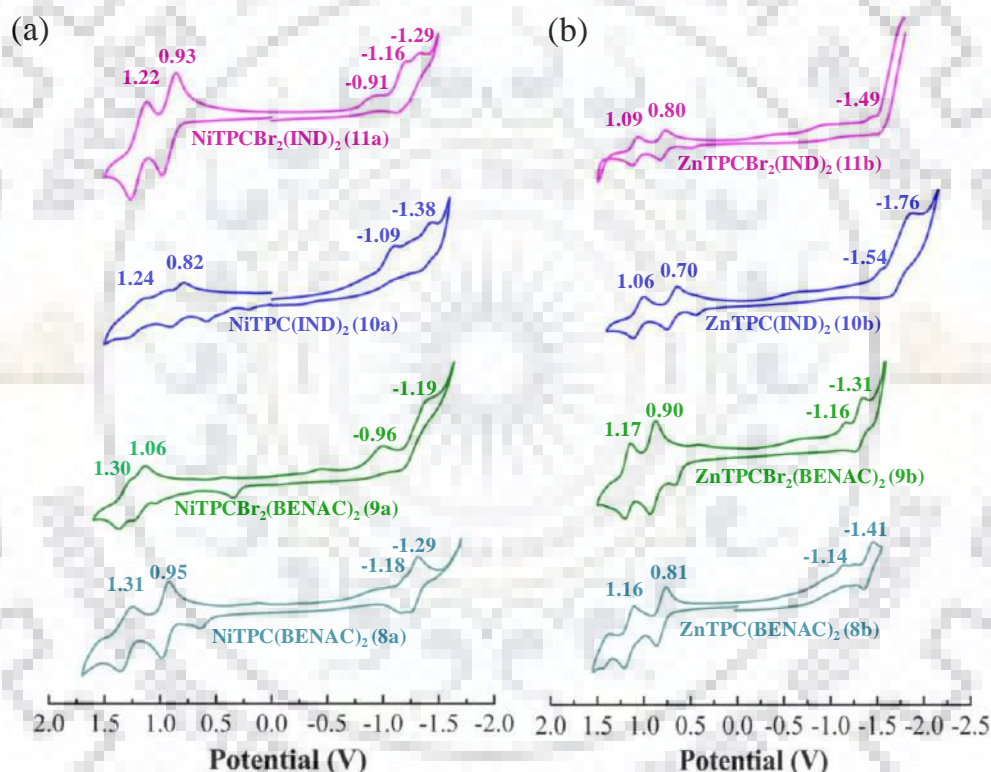


**Figure 2.12** Comparative Cyclic Voltammograms of (a) Ni(II) Chlorins and (b) Zn(II) Chlorins.

By introducing electron withdrawing groups such as indane-1,3-dione or benzoylacetonitrile, H<sub>2</sub>TPC(IND)<sub>2</sub> (**10**) and H<sub>2</sub>TPCBr<sub>2</sub>(IND)<sub>2</sub> (**11**) exhibited 60-130 mV anodic shift in oxidation potential with respect to H<sub>2</sub>TPC whereas H<sub>2</sub>TPC(BENAC)<sub>2</sub> (**8**) and H<sub>2</sub>TPCBr<sub>2</sub>(BENAC)<sub>2</sub> (**9**) exhibited 130-270 mV anodic shift in oxidation potentials due to the presence of electron withdrawing substituents at 2,3-position of the macrocyclic core.

**Table 2.4** Electrochemical Redox Data<sup>a</sup> of Porphyrinoids in CH<sub>2</sub>Cl<sub>2</sub> at 298 K.

Porphyrins/Chlorins	Oxidation(V)			$\Delta E_{1/2}$	Reduction(V)		
	I	II	III		I	II	III
H <sub>2</sub> TPP(CHD) ( <b>1</b> )	0.93 <sup>i</sup>	1.46		2.26	-1.33	-1.68	
H <sub>2</sub> TPPBr <sub>2</sub> (CHD) ( <b>2</b> )	0.98 <sup>i</sup>	1.40		2.22	-1.24	-1.40 <sup>i</sup>	
H <sub>2</sub> TPP(DMBA) ( <b>3</b> )	1.10 <sup>i</sup>	1.28 <sup>i</sup>	1.62	2.40	-1.30	-1.62	
H <sub>2</sub> TPPBr <sub>2</sub> (DMBA) ( <b>4</b> )	1.10 <sup>i</sup>	1.18 <sup>i</sup>	1.61	2.04	-0.94	-1.20	-1.40
H <sub>2</sub> TPC(NO <sub>2</sub> )(DMBA) ( <b>7</b> )	1.01	1.39		1.98	-0.97 <sup>i</sup>	-1.08	
H <sub>2</sub> TPC(BENAC) <sub>2</sub> ( <b>8</b> )	1.04	1.42		2.09	-1.05	-1.22 <sup>i</sup>	
H <sub>2</sub> TPCBr <sub>2</sub> (BENAC) <sub>2</sub> ( <b>9</b> )	1.18 <sup>i</sup>	1.40 <sup>i</sup>		2.22	-1.04	-1.22	
H <sub>2</sub> TPC(IND) <sub>2</sub> ( <b>10</b> )	0.41 <sup>i</sup>	0.97 <sup>i</sup>	1.30	1.78	-0.81 <sup>i</sup>	-1.51	
H <sub>2</sub> TPCBr <sub>2</sub> (IND) <sub>2</sub> ( <b>11</b> )	0.42 <sup>i</sup>	1.04 <sup>i</sup>	1.27	1.84	-0.80 <sup>d</sup>	-1.11 <sup>d</sup>	-1.34 <sup>d</sup>
NiTPP(CHD) ( <b>1a</b> )	1.08	1.49		2.07	-0.99 <sup>i</sup>	-1.31	
NiTPPBr <sub>2</sub> (CHD) ( <b>2a</b> )	1.09 <sup>i</sup>	1.515		2.08	-0.99 <sup>i</sup>	-1.30	
NiTPP(DMBA) ( <b>3a</b> )	1.06	1.45		2.25	-1.19 <sup>i</sup>	-1.45 <sup>d</sup>	
NiTPPBr <sub>2</sub> (DMBA) ( <b>4a</b> )	1.14	1.45		2.11	-0.97	-1.27	
NiTPP(BENAC) ( <b>5</b> )	1.09	1.30		2.07	-0.98 <sup>d</sup>	-1.35 <sup>d</sup>	
NiTPPBr <sub>2</sub> (BENAC) ( <b>6</b> )	1.18	1.32		2.17	-0.99 <sup>i</sup>	-1.27	
NiTPC(BENAC) <sub>2</sub> ( <b>8a</b> )	0.95	1.31		2.13	-1.18	-1.29	
NiTPCBr <sub>2</sub> (BENAC) <sub>2</sub> ( <b>9a</b> )	1.06	1.30		2.02	-0.96	-1.19	
NiTPC(IND) <sub>2</sub> ( <b>10a</b> )	0.58 <sup>i</sup>	0.82	1.24	1.91	-1.09 <sup>i</sup>	-1.38	
NiTPCBr <sub>2</sub> (IND) <sub>2</sub> ( <b>11a</b> )	0.93	1.22		1.84	0.91 <sup>i</sup>	-1.16	-1.29
ZnTPP(CHD) ( <b>1b</b> )	0.85 <sup>i</sup>	1.07	1.34 <sup>i</sup>	1.82	-0.97	-1.08 <sup>d</sup>	-1.67 <sup>d</sup>
ZnTPPBr <sub>2</sub> (CHD) ( <b>2b</b> )	0.94 <sup>i</sup>	1.42 <sup>i</sup>		1.95	-1.01 <sup>d</sup>	-1.27 <sup>d</sup>	-1.59 <sup>d</sup>
ZnTPP(DMBA) ( <b>4b</b> )	0.88	1.13		2.26	-1.38	-1.66 <sup>i</sup>	
ZnTPPBr <sub>2</sub> (DMBA) ( <b>4b</b> )	0.92	1.13		1.81	-0.89 <sup>i</sup>	-1.18 <sup>d</sup>	-1.51 <sup>i</sup>
ZnTPC(BENAC) <sub>2</sub> ( <b>8b</b> )	0.81	1.16		1.95	-1.14 <sup>i</sup>	-1.41	
ZnTPCBr <sub>2</sub> (BENAC) <sub>2</sub> ( <b>9b</b> )	0.90	1.17		2.06	-1.16	-1.31	
ZnTPC(IND) <sub>2</sub> ( <b>10b</b> )	0.44 <sup>i</sup>	0.70	1.06	2.24	-1.54	-1.76	
ZnTPCBr <sub>2</sub> (IND) <sub>2</sub> ( <b>11b</b> )	0.49 <sup>i</sup>	0.80	1.09	2.29	-1.49		

<sup>a</sup>Versus Ag/AgCl reference electrode. <sup>i</sup> Irreversible peaks. <sup>d</sup> Data obtained from DPV.

Zn(II) and Ni(II) complexes of synthesized chlorins exhibited a similar trend in redox potentials. In contrast to porphyrins,  $\text{MTPCBr}_2(\text{R})_2$  exhibited higher oxidation potentials as compared to  $\text{MTPC}(\text{R})_2$ . Indane-1,3-dione substituted chlorins exhibited an irreversible oxidation potential at 0.42 V which is due to oxidation of  $\beta$ -substituted indane-1,3-dione moiety. Observation of this peak is further proved by recording the CV of indane-1,3-dione under similar conditions. In general, HOMO-LUMO gap of chlorins were much lower as compared to synthesized porphyrins.  $\text{H}_2\text{TPC}(\text{IND})_2$ s exhibited lowest HOMO-LUMO gap among all synthesized free base porphyrins and chlorins.

## 2.4 CONCLUSIONS

A new synthetic strategy has been provided to access various  $\beta$ -substituted porphyrins and chlorins to expand the chemistry of porphyrinoids. The regioselectivity displayed in these reactions highlight the importance of method that facilitates the direct and predictable introduction of cyclic Michael donors at  $\beta$ -pyrrolic position. The orientation of  $\beta$ -substituents and conformation of macrocyclic core was revealed by single crystal X-ray analysis. A hypsochromic shift ( $\sim 8$ -10 nm) in the longest wavelength ( $\text{Q}_y$ ) absorption band was observed upon substitution of electron withdrawing groups (IND and BENAC) at 2,3-position of *meso*-tetraphenylchlorin. Notably, HOMO-LUMO gap altered upon substitution at 2,3 position of *meso*-tetraphenylchlorin whereas bromo-substitution at 12,13 position of 2,3-disubstituted *trans* chlorins reduced the gap between LUMO and LUMO+1. Electronic nature of synthesized macrocyclic skeletons was authenticated by protonation and deprotonation studies which revealed that the porphyrin core was more susceptible towards protonation, whereas deprotonation of chlorin macrocycle was more facile.

## 2.5 REFERENCES

1. *The Porphyrin Handbook*; Kadish, K. M., Smith, K. M., Guillard, R., Eds.; Academic Press: San Diego, 2000-2003; Vol. 1-20.
2. *Handbook of Porphyrin Science*; Kadish, K. M., Smith, K. M., Guillard, R., Eds.; World Scientific Publishing: Singapore, 2010-2014; Vol. 1-35.

3. Clave, G.; Chatelain, G.; Filoramo, A.; Gasparutto, D.; Saint-Pierre, C.; Cam, E. Le; Pietrement, O.; Guerineau, V.; Campidelli, S. Synthesis of a Multibranching Porphyrin-Oligonucleotide Scaffold for the Construction of DNA-based Nano-architectures. *Org. Biomol. Chem.* **2014**, *12*, 2778-2783.
4. Luo, J.; Chen, L-F.; Hu, P.; Chen, Z.-N. Tetranuclear Gadolinium(III) Porphyrin Complex as a Theranostic Agent for Multimodal Imaging and Photodynamic Therapy. *Inorg. Chem.* **2014**, *53*, 4184- 4191.
5. Suslick, K. S.; Rakow, N. A.; Kosal, M. E.; Chou, J. H. The Materials Chemistry of Porphyrins and Metalloporphyrins. *J. Porphyrins Phthalocyanines* **2000**, *4*, 407-413.
6. Springer, J. W.; Parkes-Loach, P. S.; Reddy, K. R.; Krayner, M.; Jiao, J.; Lee, G. M.; Niedzwiedzki, D. M.; Harris, M. A.; Kirmaier, C.; Bocian, D. F.; Lindsey, J. S.; Holten, D.; Loach, P. A. Biohybrid Photosynthetic Antenna Complexes for Enhanced Light-Harvesting. *J. Am. Chem. Soc.* **2012**, *134*, 4589-4599.
7. Jasinska, K. R.; Shan, W.; Zawada, K.; Kadish, K. M.; Gryko, D. Porphyrins as Photoredox Catalysts: Experimental and Theoretical Studies. *J. Am. Chem. Soc.* **2016**, *138*, 15451-15458.
8. Yella, A.; Lee, H.-W.; Tsao, H. N.; Yi, C.; Chandiran, A. K.; Nazeeruddin, Md. K.; Diau, E. W.-G.; Yeh, C.-Y.; Zakeeruddin, S. K.; Grätzel, M.; Porphyrin-Sensitized Solar Cells with Cobalt (II/III)-based Redox Electrolyte Exceed 12 Percent Efficiency. *Science* **2011**, *334*, 629-633.
9. Senge, M. O.; Fazekas, M.; Notaras, E. G. A.; Blau, W. J.; Zawadzka, M.; Locos, O. B.; Mhuircheartaigh, E. M. Ni. Nonlinear Optical Properties of Porphyrins. *Adv. Mater.* **2007**, *19*, 2737-2774.
10. Rodrigues, J. M. M.; Farinha, A. S. F.; Muteto, P. V.; Woranovicz-Barreira, S. M.; Paz, F. A. A.; Neves, M. G. P. M. S.; Cavaleiro, J. A. S.; Tome, A. C.; Gomes, M. T. S. R.; Sessler, J. L.; Tome, J. P. C. New Porphyrin Derivatives for Phosphate Anion Sensing in Both Organic and Aqueous Media. *Chem. Commun.* **2014**, *50*, 1359-1361.

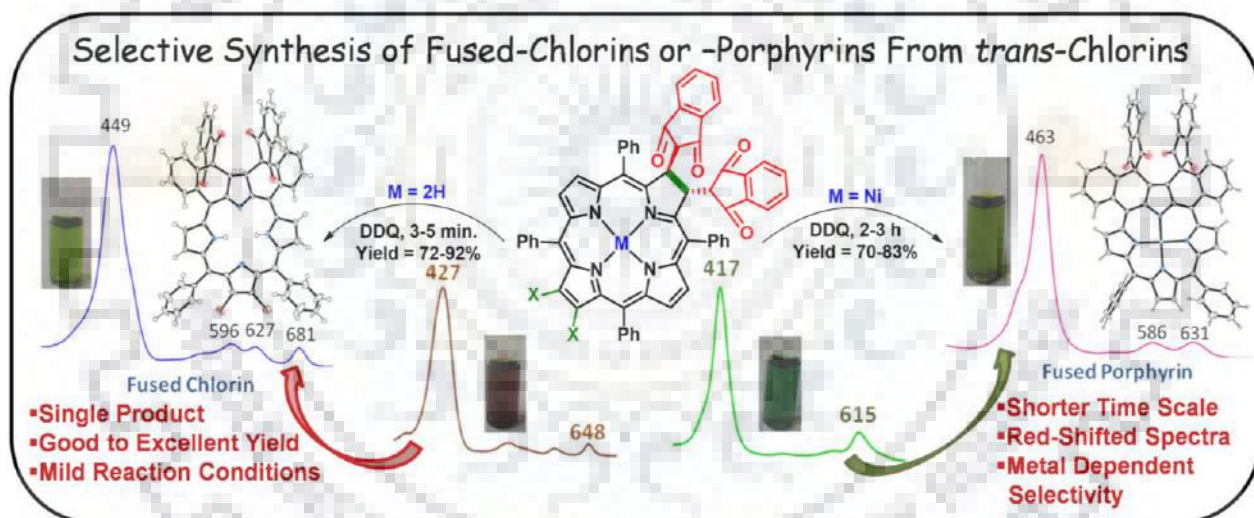
11. Bruckner, C. The Breaking and Mending of *meso*-Tetraarylporphyrins: Transmuting the Pyrrolic Building Blocks. *Acc. Chem. Res.* **2016**, *49*, 1080-1092.
12. Akhigbe, J.; Luciano, M.; Zeller, M.; Brückner, C. Mono- and Bisquinoline-Annulated Porphyrins from Porphyrin  $\beta,\beta'$ -Dione Oximes. *J. Org. Chem.* **2015**, *80*, 499-511.
13. Shea, K. M.; Jaquinod, L.; Smith, K. M. Dihydroporphyrin Synthesis: New Methodology. *J. Org. Chem.* **1998**, *63*, 7013-7021.
14. Jaquinod, L.; Gros, C.; Khoury, R. G.; Smith, K. M. A Convenient Synthesis of Functionalized Tetraphenylchlorins. *Chem. Commun.* **1996**, 2581-2582.
15. Shea, K. M.; Jaquinod, L.; Khoury, R. G.; Smith, K. M. Dodecasubstituted metallochlorins (metallo-dihydroporphyrins). *Chem. Commun.* **1998**, 759-760.
16. Shea, K. M.; Jaquinod, L.; Smith, K. M. Dihydroporphyrin Synthesis: New Methodology. *J. Org. Chem.* **1998**, *63*, 7013-7021.
17. Tamiaki, H.; Kunieda, M. *In Handbook of Porphyrin Science*; Kadish, K. M., Smith, K. M., Guillard, R., Eds.; World Scientific: Singapore, 2011; Vol. 11, pp 223-290.
18. Pandey, R. K.; Bellnier, D. A.; Smith, K. M.; Dougherty, T. J. Chlorin and Porphyrin Derivatives as Potential Photosensitizers in Photodynamic Therapy. *Photochem. Photobiol.* **1991**, *53*, 65-72.
19. Collins, H. A.; Khurana, M.; Moriyama, E. H.; Mariampillai, A.; Dahlstedt, E.; Balaz, M.; Kuimova, M. K.; Drobizhev, M.; Yang, V. X. D.; Phillips, D.; Aleksander, R.; Wilson, B. C.; Anderson, H. L. Blood-Vessel Closure Using Photosensitizers Engineered for Two-Photon Excitation. *Nat. Photonics* **2008**, *2*, 420-424.
20. Brückner, C.; Samankumara, L.; Ogikubo, J. *In Handbook of Porphyrin Science*; Kadish, K. M., Smith, K. M., Guillard, R., Eds.; World Scientific: River Edge, NY, 2012; Vol. 17, pp 1-112.
21. Sharma, M.; Banerjee, S.; Zeller, M.; Bruckner, C. Fusion and Desulfurization Reactions of Thiomorpholinochlorins. *J. Org. Chem.* **2016**, *81*, 12350-12356.

22. Brückner, C. The Breaking and Mending of *meso*-Tetraarylporphyrins: Transmuting the Pyrrolic Building Blocks. *Acc. Chem. Res.* **2016**, *49*, 1080-1092.
23. Saebang, Y.; Rukachaisirikul, V.; Kaeobamrung, J. Copper-catalysed Domino Reaction of 2-Bromobenzylidenemalonates and 1,3-Dicarbonyls for the Synthesis of Chromenes. *Tetrahedron Lett.* **2017**, *58*, 168-171.
24. Giraudeau, A.; Callot, H. J.; Jorden, J.; Ezhar, I.; Gross, M. Substituent Effects in the Electroreduction of Porphyrins and Metalloporphyrins. *J. Am. Chem. Soc.* **1979**, *101*, 3857-3862.
25. Jaquinod, L.; Khoury, R. G.; Shea, K. M.; Smith, K. M. Regioselective Syntheses and Structural Characterizations of 2,3-dibromo- and 2,3,7,8,12,13-hexabromo-5,10,15,20-tetraphenylporphyrins. *Tetrahedron* **1999**, *55*, 13151-13158.
26. Kumar, R.; Sankar, M. Synthesis, Spectral, and Electrochemical Studies of Electronically Tunable  $\beta$ -Substituted Porphyrins with Mixed Substituent Pattern. *Inorg. Chem.* **2014**, *53*, 12706-12719.
27. Spek, A. L. *PLATON, A Multipurpose Crystallographic Tool*, Utrecht University, Utrecht, The Netherlands, 2001.
28. Chen, S.; Xu, Z.; Li, J. The Observation of Oxygen-Oxygen Interactions in Ice. *New J. Phys.* **2016**, *18*, 1-7.
29. Remya, K.; Suresh, C. H. Intermolecular Carbon-Carbon, Nitrogen-Nitrogen and Oxygen-Oxygen Non-Covalent Bonding in Dipolar Molecules *Phys. Chem. Chem. Phys.* **2015**, *17*, 18380-18392.
30. Gouterman, M. J. Study of the Effects of Substitution on the Absorption Spectra of Porphine. *J. Chem. Phys.* **1959**, *30*, 1139-1161.



# CHAPTER 3

“Selective Conversion of Planar *trans*-Chlorins into Highly Twisted Doubly Fused-Porphyrins (DFPs) or -Chlorins (DFCs) *via* Oxidative Fusion”





## CHAPTER 3

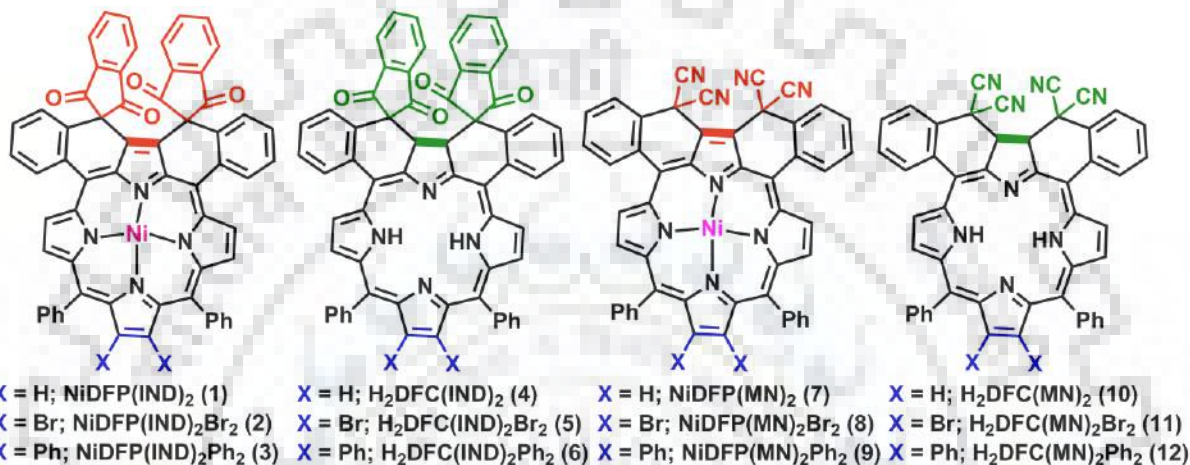
# SELECTIVE CONVERSION OF PLANAR TRANS CHLORINS INTO HIGHLY TWISTED DOUBLY FUSED-PORPHYRINS (DFPs) OR CHLORINS (DFCs) VIA OXIDATIVE FUSION

### 3.1 INTRODUCTION

The intramolecular fusion of porphyrin aromatic circuit has become an exciting subject of research over last decade due to the unique photophysical and electrochemical redox properties exhibited by the fused  $\pi$ -conjugated systems [1-3]. In particular, *meso*- $\beta$  fusion [4] exerts pronounce steric and electronic effects on the porphyrin  $\pi$ -system as compared to  $\beta$ - $\beta'$  fusion [5]. The unusual electronic properties of fused porphyrins depend upon the number of fused porphyrin units. Furthermore, the increment in fused units leads to the absorption in the near-infrared (NIR) region [6]. The remarkable optical and electronic properties of fused porphyrin systems make them appealing candidate for immense variety of applications including photoacoustic imaging [7], DSSCs [8], material [9], and two photon absorption (TPA) [10]. Ring-fusion breaks the degeneracy of frontier orbitals which further results into the relatively reduced HOMO-LUMO gap [11]. Osuka and coworkers are the pioneer researchers who have synthesized a variety of *meso-meso*, *meso*- $\beta$  and  $\beta$ - $\beta'$  fused porphyrin [1-2, 9-12]. Anderson and coworkers effectively utilized  $\text{FeCl}_3$  for the oxidative ring closure in order to obtain a variety of anthracene-fused porphyrins [13,14]. Kojima and coworkers have reported the synthesis of multiply-fused porphyrins through palladium catalyzed coupling reactions [15]. The synthesis of *meso*- $\beta$  fused porphyrins is well-documented in the literature [6-8, 13-15] whereas the chemistry of *meso*- $\beta$  fused chlorins is largely unexplored [16]. 1,3-dipolar cycloaddition reactions have been utilized for the synthesis of  $\beta$ - $\beta'$  fused chlorins [17]. However, Brückner *et al.* achieved the synthesis of few annulated chlorins through breaking and mending approach [18]. Plentiful reports by R. Ruppert and H. J. Callot are available in the literature which described the reaction of functional groups located on  $\beta$ -pyrrolic positions with the neighbouring phenyl groups and their interesting electronic and electrochemical redox properties [19,20]. Although the reported methods for ring fusion opened a door to synthesize a variety of

fused porphyrinoids, however the multistep syntheses, harsh reaction conditions, required proximity of substituent(s) and poor solubility of products hamper the bulk synthesis of fused porphyrins. In order to circumvent these problems, we present an elegant, cost effective and straightforward synthesis of highly soluble fused porphyrins and chlorins (Chart 1) and explored the fascinating chemistry of these porphyrinoids.

**Chart 3.1** Molecular Structures of Synthesized Doubly Fused Porphyrins and Chlorins.



Herein, we are reporting a facile and efficient conversion of planar *trans*-chlorins into highly twisted doubly fused chlorins or porphyrins in good to excellent yields (Chart 1). In all the cases, *ortho*-positions of two *meso*-phenyls were covalently linked to the  $\alpha$ -carbon of the  $\beta$ -substituents resulting into the formation of six membered rings.

## 3.2 EXPERIMENTAL SECTION

### 3.2.1 Chemicals

Pyrrole, 1,3-indanedione, and malononitrile were purchased from Alfa Aesar, UK and used as received. Benzaldehyde, N-bromosuccinimide,  $\text{K}_2\text{CO}_3$ , TBAPF<sub>6</sub>,  $\text{Ni}(\text{OAc})_2 \cdot 4\text{H}_2\text{O}$ , DDQ,  $\text{P}_2\text{O}_5$  and  $\text{CaH}_2$  were purchased from HiMedia, India and used without further purification. Silica gel (100-200 mesh) and DMSO purchased from Thomas Baker, India and used as received. Precoated thin layered silica gel chromatographic plates were purchased from E. Merck.

### 3.2.2 Instrumentation and Methods

All the characterization techniques were used same as for chapter 2. Absorption maxima ( $\lambda_{\text{max}}$ ) were reported in nm and molar extinction coefficients in  $\text{M}^{-1}\text{cm}^{-1}$ . The proton NMRs were

reported with chemical shifts as the  $\delta$  scale in ppm. The X-ray quality single crystals of NiDFP(IND)<sub>2</sub> (**1**), H<sub>2</sub>DFC(IND)<sub>2</sub>Br<sub>2</sub> (**5**) and NiDFP(MN)<sub>2</sub>Br<sub>2</sub> (**8**) were obtained by vapor diffusion of hexane into the CHCl<sub>3</sub> solution of these H<sub>2</sub>DFCs and NiDFPs whereas X-ray quality single crystals of NiDFC(MN)<sub>2</sub>Br<sub>2</sub> (**8a**) and H<sub>2</sub>TPC[CH(CN)<sub>2</sub>]<sub>2</sub> were obtained by vapor diffusion of hexane into the CH<sub>2</sub>Cl<sub>2</sub> solution of fused chlorins. The single-crystal X-ray diffraction data was collected on a Bruker Apex-II CCD diffractometer. In case of H<sub>2</sub>DFC(IND)<sub>2</sub>Br<sub>2</sub> (**5**), SQUEEZE procedure was applied in order to correct electron density contribution from disordered solvent molecules. The twisted angles were calculated as the dihedral angle between the plane defined by fused moiety and rest of the macrocyclic core. The geometry optimization of H<sub>2</sub>DFCs and NiDFPs in gas phase was carried out by DFT calculations using B3LYP functional with 6-31G basis set of C,H,N,O and LANL2DZ basis sets for Ni(II) respectively. H<sub>2</sub>TPP, H<sub>2</sub>TPP(NO<sub>2</sub>), H<sub>2</sub>TPP(NO<sub>2</sub>)Br<sub>2</sub>, H<sub>2</sub>TPP(NO<sub>2</sub>)Ph<sub>2</sub> and their Ni(II) complexes were synthesized according to the literature method [21]. All *trans*-chlorins were prepared by using similar procedures described in chapter 2.

### 3.2.3 General Procedure for the Synthesis of Ni(II) Doubly Fused Porphyrins (NiDFPs):

50 mg of NiTPC(R)<sub>2</sub>X<sub>2</sub> (R = 1,3-indanedione, malononitrile and X = H, Br and Ph) was dissolved in 25 ml of dry CHCl<sub>3</sub>. To this, 5 eq. of DDQ was added and the reaction mixture was refluxed for 2-3 hr. The resulting reaction mixture was washed thrice with water and organic layer passed over anhydrous sodium sulphate. Solvent was evaporated under reduced pressure. The crude solid was purified on silica gel column using CHCl<sub>3</sub>:hexane (6:4, v/v). The purified compound was recrystallized with CHCl<sub>3</sub>/MeOH (1:3 v/v) mixture.

**NiDFP(IND)<sub>2</sub> (1):** Yield: 78% (39 mg, 0.041 mmol). UV/vis (CH<sub>2</sub>Cl<sub>2</sub>):  $\lambda_{\max}$ (nm) (log  $\epsilon$ ): 463(5.33), 586(4.21), 631(4.22). <sup>1</sup>H NMR (400 MHz, CDCl<sub>3</sub>)  $\delta$  (ppm): 9.353(d, <sup>3</sup>J<sub>H,H</sub> = 5.6 Hz, 2H,  $\beta$ -H), 8.726(d, <sup>3</sup>J<sub>H,H</sub> = 4.8 Hz, 2H,  $\beta$ -H), 8.509(s, 2H,  $\beta$ -H), 7.977-7.871(m, 8H, *meso*-Ph-H), 7.677(s, 10H, *meso*-Ph-H), 7.423(t, <sup>3</sup>J<sub>H,H</sub> = 5.6 Hz, 3H, IND-Ph-H), 6.980(t, <sup>3</sup>J<sub>H,H</sub> = 6.8 Hz, 3H, IND-Ph-H), 6.784(d, <sup>3</sup>J<sub>H,H</sub> = 7.6 Hz, 2H, IND-Ph-H). MALDI-TOF-MS (*m/z*): found 956.012 [M+H]<sup>+</sup>, calcd 956.642. Anal. Calcd for C<sub>62</sub>H<sub>32</sub>N<sub>4</sub>NiO<sub>4</sub> C, 77.92; H, 3.38; N, 5.86. Found: C, 78.03; H, 3.26; N, 5.67.

**NiDFP(IND)<sub>2</sub>Br<sub>2</sub> (2):** Yield: 81% (40 mg, 0.036 mmol). UV/vis (CH<sub>2</sub>Cl<sub>2</sub>):  $\lambda_{\max}$ (nm) (log  $\epsilon$ ): 467(5.27), 592(4.20), 637(4.20). <sup>1</sup>H NMR (400 MHz, CDCl<sub>3</sub>)  $\delta$  (ppm): 9.244(d, <sup>3</sup>J<sub>H,H</sub> = 4.8 Hz,



2H,  $\beta$ -H), 8.725(d,  $^3J_{H,H} = 5.2$  Hz, 2H,  $\beta$ -H), 7.986-7.821(m, 10H, *meso*-Ph-H), 7.653(t,  $^3J_{H,H} = 7.6$  Hz, 8H, *meso*-Ph-H), 7.438(t,  $^3J_{H,H} = 7.6$  Hz, 3H, IND-Ph-H), 7.000(t,  $^3J_{H,H} = 8$  Hz, 3H, IND-Ph-H), 6.767(d,  $^3J_{H,H} = 8$  Hz, 2H, IND-Ph-H). MALDI-TOF-MS ( $m/z$ ): found 1113.241 [M]<sup>+</sup>, calcd 1113.427. Anal. Calcd for C<sub>62</sub>H<sub>30</sub>Br<sub>2</sub>N<sub>4</sub>NiO<sub>4</sub> C, 66.88; H, 2.72; N, 5.03. Found: C, 66.84; H, 2.89; N, 5.44.

**NiDFP(IND)<sub>2</sub>(Ph)<sub>2</sub> (3)**: Yield: 83% (41 mg, 0.037 mmol). UV/vis (CH<sub>2</sub>Cl<sub>2</sub>):  $\lambda_{\max}$ (nm) (log  $\epsilon$ ): 469(5.27), 591(4.26), 635(4.20). <sup>1</sup>H NMR (400 MHz, CDCl<sub>3</sub>)  $\delta$  (ppm): 9.189(d,  $^3J_{H,H} = 4.8$  Hz, 2H,  $\beta$ -H), 8.326(d,  $^3J_{H,H} = 4.8$  Hz, 2H,  $\beta$ -H), 7.946-7.859(m, 7H, *meso*-Ph-H), 7.411(t,  $^3J_{H,H} = 8$  Hz 3H, *meso*-Ph-H), 7.128(t,  $^3J_{H,H} = 7.2$  Hz 3H, *meso*-Ph-H), 7.058-6.981(m, 9H, *meso* and IND-Ph-H), 6.876-6.761(m, 14H, IND and  $\beta$ -Ph-H). MALDI-TOF-MS ( $m/z$ ): found 1107.672 [M+H]<sup>+</sup>, calcd 1107.247. Anal. Calcd for C<sub>74</sub>H<sub>40</sub>N<sub>4</sub>NiO<sub>4</sub> C, 80.23; H, 3.64; N, 5.06. Found: C, 80.57; H, 3.64; N, 5.12.

**NiDFP(MN)<sub>2</sub> (7)**: Yield: 72% (36 mg, 0.045 mmol). UV/vis (CH<sub>2</sub>Cl<sub>2</sub>):  $\lambda_{\max}$ (nm) (log  $\epsilon$ ): 465(5.20), 550(sh), 594(4.00), 645(4.27). <sup>1</sup>H NMR (400 MHz, CDCl<sub>3</sub>)  $\delta$  (ppm): 9.321(d,  $^3J_{H,H} = 5.2$  Hz, 2H,  $\beta$ -H), 8.717(d,  $^3J_{H,H} = 5.2$  Hz, 2H,  $\beta$ -H), 8.495(s, 2H,  $\beta$ -H), 8.477(s, 1H, *meso*-Ph-H), 7.992(d,  $^3J_{H,H} = 7.2$  Hz, 2H, *meso*-Ph-H), 7.781(t,  $^3J_{H,H} = 7.6$  Hz, 3H, *meso*-Ph-H), 7.730-7.670(m, 12H, *meso*-Ph-H). MALDI-TOF-MS ( $m/z$ ): found 769.883 [M+H]<sup>+</sup>, calcd 769.152. Anal. Calcd for C<sub>50</sub>H<sub>24</sub>N<sub>8</sub>Ni C, 75.49; H, 3.04; N, 14.09. Found: C, 75.75; H, 3.23; N, 14.27.

**NiDFP(MN)<sub>2</sub>Br<sub>2</sub> (8)**: Yield: 70% (35 mg, 0.036 mmol). UV/vis (CH<sub>2</sub>Cl<sub>2</sub>):  $\lambda_{\max}$ (nm) (log  $\epsilon$ ): 468(5.08), 553(sh), 597(3.94), 649(4.19). <sup>1</sup>H NMR (400 MHz, CDCl<sub>3</sub>)  $\delta$  (ppm): 9.208(d,  $^3J_{H,H} = 2.4$  Hz, 2H,  $\beta$ -H), 8.721(d,  $^3J_{H,H} = 5.2$  Hz, 2H,  $\beta$ -H), 8.459(d,  $^3J_{H,H} = 8$  Hz, 2H, *meso*-Ph-H), 7.659(d,  $^3J_{H,H} = 8$  Hz, 2H, *meso*-Ph-H), 7.809(t,  $^3J_{H,H} = 8$  Hz, 3H, *meso*-Ph-H), 7.694-7.651(m, 11H, *meso*-Ph-H). MALDI-TOF-MS ( $m/z$ ): found 928.795 [M]<sup>+</sup>-CN, calcd 928.255. Anal. Calcd for C<sub>50</sub>H<sub>22</sub>Br<sub>2</sub>N<sub>8</sub>Ni C, 63.00; H, 2.33; N, 11.75. Found: C, 63.12; H, 2.58; N, 12.02.

**NiDFC(MN)<sub>2</sub>Br<sub>2</sub> (8a)**: Yield: 6% (3 mg, 0.003 mmol). UV/vis (CH<sub>2</sub>Cl<sub>2</sub>):  $\lambda_{\max}$ (nm) (log  $\epsilon$ ): 438(5.20), 627(4.26). MALDI-TOF-MS ( $m/z$ ): found 955.235 [M]<sup>+</sup>, calcd. 955.281. Anal. Calcd for C<sub>50</sub>H<sub>24</sub>Br<sub>2</sub>N<sub>8</sub>Ni C, 62.86; H, 2.53; N, 11.73. Found: C, 62.42; H, 2.74; N, 11.74.

**NiDFP(MN)<sub>2</sub>(Ph)<sub>2</sub> (9)**: Yield: 70% (35 mg, 0.037 mmol). UV/vis (CH<sub>2</sub>Cl<sub>2</sub>):  $\lambda_{\max}$ (nm) (log  $\epsilon$ ): 468(5.09), 556(sh), 600(4.03), 648(4.22). <sup>1</sup>H NMR (400 MHz, CDCl<sub>3</sub>)  $\delta$  (ppm): 9.157(d,  $^3J_{H,H} = 5.2$  Hz, 2H,  $\beta$ -H), 8.472(d,  $^3J_{H,H} = 8$  Hz, 2H,  $\beta$ -H), 8.327(d,  $^3J_{H,H} = 4.8$  Hz, 2H, *meso*-Ph-H),



7.972(d,  $^3J_{\text{H,H}} = 7.6$  Hz, 2H, *meso*-Ph-H), 7.789(t,  $^3J_{\text{H,H}} = 6.8$  Hz, 2H, *meso*-Ph-H), 7.679(t,  $^3J_{\text{H,H}} = 7.6$  Hz, 2H, *meso*-Ph-H), 7.171(t,  $^3J_{\text{H,H}} = 8$  Hz, 3H, *meso*-Ph-H), 7.052(t,  $^3J_{\text{H,H}} = 8$  Hz, 5H, *meso*-Ph-H), 6.892-6.880(m, 2H, *meso*-Ph-H), 6.844(m, 10H,  $\beta$ -Ph). MALDI-TOF-MS ( $m/z$ ): found 921.320  $[\text{M}]^+\text{-CN}$ , calcd. 921.215. Anal. Calcd for  $\text{C}_{61}\text{H}_{35}\text{N}_7\text{Ni}$  C, 79.23; H, 3.82; N, 10.60. Found: C, 79.48; H, 3.97; N, 10.36.

### 3.2.4 General Synthetic Procedure for the Preparation of Free Base Doubly Fused Chlorins ( $\text{H}_2\text{DFCs}$ ):

A 100 mL RB flask was charged with 65 mg of  $\text{H}_2\text{TPC}(\text{R})_2\text{X}_2$  ( $\text{R} = 1,3\text{-indanedione}$ , malononitrile and  $\text{X} = \text{H}$ , Br and Ph) in 30 mL of distilled  $\text{CHCl}_3$ . To this, 5 equiv. of DDQ was added and heated to reflux for 3-5 min. The pink colour of free base *trans*-chlorins immediately turned to emerald green. The completeness of the reaction was monitored by TLC. The reaction mixture was washed thrice with distilled water and the organic layer was passed over anhydrous sodium sulphate and the solvent was evaporated to dryness. The residue was purified by column chromatography using  $\text{CHCl}_3$ :hexane (7:3, v/v) mixture and the purified products were recrystallized with  $\text{CHCl}_3$ /MeOH mixture (1:9, v/v).

**$\text{H}_2\text{DFC}(\text{IND})_2$  (4):** Yield: 72% (47 mg, 0.052 mmol). UV/vis ( $\text{CH}_2\text{Cl}_2$ ):  $\lambda_{\text{max}}(\text{nm})$  ( $\log \epsilon$ ): 434(5.21), 547(3.99), 589(4.43), 626(4.09), 682(4.39).  $^1\text{H}$  NMR (400 MHz,  $\text{CDCl}_3$ )  $\delta$  (ppm): 8.795(d,  $^3J_{\text{H,H}} = 4.8$  Hz, 2H,  $\beta$ -H), 8.536(d,  $^3J_{\text{H,H}} = 4.8$  Hz, 2H,  $\beta$ -H), 8.395(d,  $^3J_{\text{H,H}} = 8$  Hz, 2H,  $\beta$ -H), 8.282(s, 1H, *meso*-Ph-H), 8.117(t,  $^3J_{\text{H,H}} = 7.2$  Hz, 2H, *meso*-Ph-H), 7.973-7.897(m, 7H, *meso*-Ph-H), 7.715-7.647(m, 9H, *meso* and IND-Ph-H), 7.487(t,  $^3J_{\text{H,H}} = 7.6$  Hz, 3H, IND-Ph-H), 7.128(t,  $^3J_{\text{H,H}} = 7.2$  Hz, 2H, IND-Ph-H), 6.959(d,  $^3J_{\text{H,H}} = 7.6$  Hz, 2H, IND-Ph-H), 4.937(s, 2H,  $\beta$ -H), 0.342(s, 2H, -NH). MALDI-TOF-MS ( $m/z$ ): found 901.292  $[\text{M}+\text{H}]^+$ , calcd 901.281. Anal. Calcd for  $\text{C}_{62}\text{H}_{36}\text{N}_4\text{O}_4$  C, 82.65; H, 4.03; N, 6.22. Found: C, 85.88; H, 4.16; N, 6.47.

**$\text{H}_2\text{DFP}(\text{IND})_2$  (4a):** Yield: 5% (3 mg, 0.004 mmol). UV/vis ( $\text{CH}_2\text{Cl}_2$ ):  $\lambda_{\text{max}}(\text{nm})$  ( $\log \epsilon$ ): 463(5.24), 568(3.96), 611(4.31), 647(3.81), 708(4.02).  $^1\text{H}$  NMR (400 MHz,  $\text{CDCl}_3$ )  $\delta$  (ppm): 9.527(d,  $^3J_{\text{H,H}} = 4.8$  Hz, 2H,  $\beta$ -H), 8.779(d,  $^3J_{\text{H,H}} = 4.8$  Hz, 2H,  $\beta$ -H), 8.554(s, 2H,  $\beta$ -H), 8.170-8.125(m, 6H, *meso*-Ph-H), 8.008-7.976(m, 4H, *meso*-Ph-H), 7.935-7.889(m, 4H, *meso*-Ph-H), 7.755-7.730(m, 6H, *meso*-Ph and IND-Ph-H), 7.479(t,  $^3J_{\text{H,H}} = 7.2$  Hz, 2H, IND-Ph-H), 7.013(t,  $^3J_{\text{H,H}} = 7.6$  Hz, 2H, IND-Ph-H), 6.902(d,  $^3J_{\text{H,H}} = 7.6$  Hz, 2H, IND-Ph-H), -0.390(s, 2H, -NH).

MALDI-TOF-MS ( $m/z$ ): found 899.128  $[M+H]^+$ , calcd 899.265. Anal. Calcd for  $C_{62}H_{34}N_4O_4$  C, 82.84; H, 3.81; N, 6.23. Found: C, 82.56; H, 2.94; N, 6.62.

**H<sub>2</sub>DFC(IND)<sub>2</sub>Br<sub>2</sub> (5)**: Yield: 84% (54 mg, 0.051 mmol). UV/vis ( $CH_2Cl_2$ ):  $\lambda_{max}(nm)$  (log  $\epsilon$ ): 449(5.21), 555(3.98), 596(4.23), 627(4.17), 681(4.14). <sup>1</sup>H NMR (400 MHz,  $CDCl_3$ )  $\delta$  (ppm): 8.677(dd, <sup>3</sup> $J_{H,H} = 1.6$  Hz, 4.8 Hz, 2H,  $\beta$ -H), 8.29(dd, <sup>3</sup> $J_{H,H} = 4.6$  Hz, 4.8 Hz, 2H,  $\beta$ -H), 8.378(d, <sup>3</sup> $J_{H,H} = 8$  Hz, 2H, *meso*-Ph-H), 8.120(t, <sup>3</sup> $J_{H,H} = 7.6$  Hz, 3H, *meso*-Ph-H), 8.017-7.843(m, 9H, *meso*-Ph-H), 7.697(t, <sup>3</sup> $J_{H,H} = 6.8$  Hz, 4H, *meso*-Ph-H), 7.478(t, <sup>3</sup> $J_{H,H} = 7.6$  Hz, 3H, IND-Ph-H), 7.129(t, <sup>3</sup> $J_{H,H} = 8$  Hz, 3H, IND-Ph-H), 6.940(d, <sup>3</sup> $J_{H,H} = 8$  Hz, 2H, IND-Ph-H), 4.37(s, 2H,  $\beta$ -H), 0.441(s, 2H, -NH). MALDI-TOF-MS ( $m/z$ ): found 1059.264  $[M+H]^+$ , calcd 1059.774. Anal. Calcd for  $C_{62}H_{34}Br_2N_4O_4$  C, 70.33; H, 3.24; N, 5.29. Found: C, 70.48; H, 3.47; N, 5.12.

**H<sub>2</sub>DFC(IND)<sub>2</sub>(Ph)<sub>2</sub> (6)**: Yield: 81% (52 mg, 0.050 mmol). UV/vis ( $CH_2Cl_2$ ):  $\lambda_{max}(nm)$  (log  $\epsilon$ ): 443(5.20), 555(3.98), 592(4.33), 633(4.09), 689(4.32). <sup>1</sup>H NMR (400 MHz,  $CDCl_3$ )  $\delta$ : <sup>1</sup>H NMR (400 MHz,  $CDCl_3$ )  $\delta$  (ppm): 8.657(d, <sup>3</sup> $J_{H,H} = 4.8$  Hz, 2H,  $\beta$ -H), 8.378(d, <sup>3</sup> $J_{H,H} = 7.6$  Hz, 2H,  $\beta$ -H), 8.241(d, <sup>3</sup> $J_{H,H} = 4.8$  Hz, 2H, *meso*-Ph-H), 8.114(t, <sup>3</sup> $J_{H,H} = 8$  Hz, 2H, *meso*-Ph-H), 7.977-7.884(m, 7H, *meso*-Ph-H), 7.460(t, <sup>3</sup> $J_{H,H} = 7.6$  Hz, 3H *meso*-Ph-H), 7.172-7.052(m, 10H,  $\beta$ -Ph-H), 6.948-6.676(m, 12H, *meso*-Ph-H and IND-Ph-H), 4.894(s, 2H,  $\beta$ -H), 0.687(s, 2H, -NH). MALDI-TOF-MS ( $m/z$ ): found 1054.362  $[M+H]^+$ , calcd 1054.173. Anal. Calcd for  $C_{74}H_{44}N_4O_4$  C, 84.39; H, 4.21; N, 5.32. Found: C, 84.56; H, 4.35; N, 5.42.

**H<sub>2</sub>DFC(MN)<sub>2</sub> (10)**: Yield: 84% (54 mg, 0.073 mmol). UV/vis ( $CH_2Cl_2$ ):  $\lambda_{max}(nm)$  (log  $\epsilon$ ): 423(5.32), 539(3.99), 577(4.46), 614(4.18), 665(4.48). <sup>1</sup>H NMR (400 MHz,  $CDCl_3$ )  $\delta$  (ppm): 8.910(d, <sup>3</sup> $J_{H,H} = 4.8$  Hz, 2H,  $\beta$ -H), 8.663(d, <sup>3</sup> $J_{H,H} = 5.2$  Hz, 2H,  $\beta$ -H), 8.473(d, <sup>3</sup> $J_{H,H} = 6.8$  Hz, 2H,  $\beta$ -H), 8.375(d, <sup>3</sup> $J_{H,H} = 8$  Hz, 2H, *meso*-Ph-H), 8.344(s, 2H, *meso*-Ph-H), 8.234(d, <sup>3</sup> $J_{H,H} = 7.6$  Hz, 2H, *meso*-Ph-H), 7.937(t, <sup>3</sup> $J_{H,H} = 8$  Hz, 2H, *meso*-Ph-H), 7.824-7.734 (m, 6H, *meso*-Ph-H), 7.694(d, <sup>3</sup> $J_{H,H} = 6$  Hz, 2H, *meso*-Ph-H), 7.636(d, <sup>3</sup> $J_{H,H} = 6.4$  Hz, 2H, *meso*-Ph-H), 5.261(s, 2H,  $\beta$ -H), -0.177(s, 2H, -NH). MALDI-TOF-MS ( $m/z$ ): found 741.204  $[M+H]^+$ , calcd 741.251. Anal. Calcd for  $C_{50}H_{28}N_8$  C, 81.06; H, 3.81; N, 15.13. Found: C, 81.36; H, 4.02; N, 15.43.

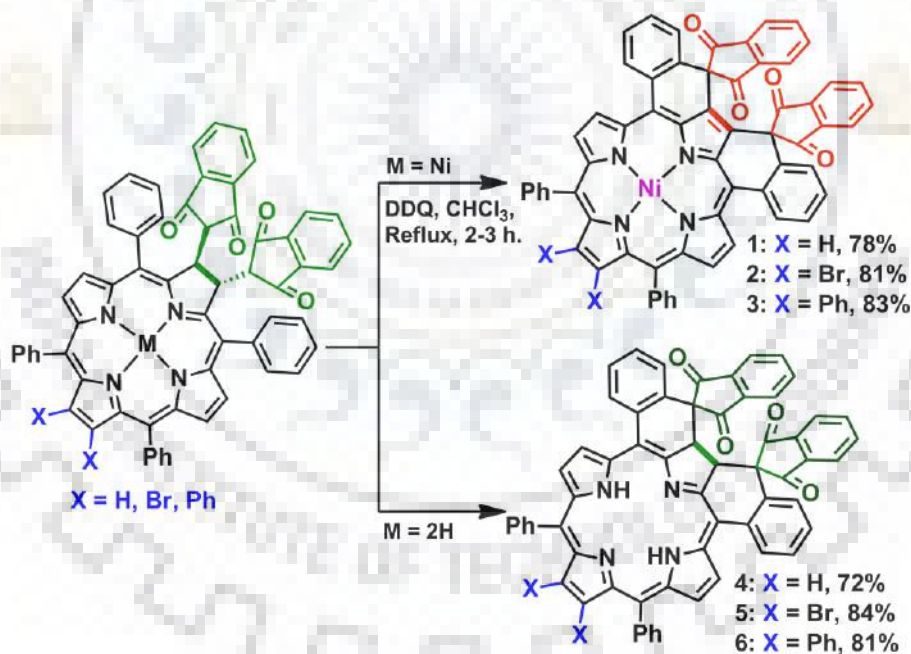
**H<sub>2</sub>DFC(MN)<sub>2</sub>Br<sub>2</sub> (11)**: Yield: 92% (60 mg, 0.066 mmol). UV/vis ( $CH_2Cl_2$ ):  $\lambda_{max}(nm)$  (log  $\epsilon$ ): 435(5.28), 548(3.98), 584(4.28), 614(4.19), 667(4.21). <sup>1</sup>H NMR (400 MHz,  $CDCl_3$ )  $\delta$  (ppm): 8.784(dd, <sup>3</sup> $J_{H,H} = 2$  Hz, 5.2 Hz, 2H,  $\beta$ -H), 8.563(dd, <sup>3</sup> $J_{H,H} = 1.6$  Hz, 4.8 Hz, 2H,  $\beta$ -H), 8.366(d, <sup>3</sup> $J_{H,H} = 7.6$  Hz, 3H *meso*-Ph-H), 8.119(d, <sup>3</sup> $J_{H,H} = 7.6$  Hz, 2H *meso*-Ph-H), 7.924(t, <sup>3</sup> $J_{H,H} = 7.6$

Hz, 3H *meso*-Ph-H), 7.790-7.748(m, 10H, *meso*-Ph-H), 5.180(s, 2H,  $\beta$ -H), -0.06(s, 2H, -NH). MALDI-TOF-MS ( $m/z$ ): found 898.084  $[M]^+$ , calcd 898.603. Anal. Calcd for  $C_{50}H_{26}Br_2N_8$  C, 66.83; H, 2.92; N, 12.47. Found: C, 66.95; H, 3.02; N, 12.64.

**H<sub>2</sub>DFC(MN)<sub>2</sub>(Ph)<sub>2</sub> (12):** Yield: 81% (52 mg, 0.060 mmol). UV/vis ( $CH_2Cl_2$ ):  $\lambda_{max}$ (nm) (log  $\epsilon$ ): 433(5.22), 545(3.93), 582(4.30), 620(4.09), 672(4.31). <sup>1</sup>H NMR (400 MHz,  $CDCl_3$ )  $\delta$  (ppm): 8.761(d, <sup>3</sup> $J_{H,H}$  = 8 Hz, 5.2H,  $\beta$ -H), 8.373(s, 2H,  $\beta$ -H), 8.357(d, <sup>3</sup> $J_{H,H}$  = 2.4Hz, 2H, *meso*-Ph-H), 8.170(d, <sup>3</sup> $J_{H,H}$  = 7.6 Hz, 2H, *meso*-Ph-H), 7.908(t, <sup>3</sup> $J_{H,H}$  = 7.6 Hz, 2H, *meso*-Ph-H), 7.747(t, <sup>3</sup> $J_{H,H}$  = 7.6 Hz, 3H, *meso*-Ph-H), 7.220(t, <sup>3</sup> $J_{H,H}$  = 7.2 Hz, 3H, *meso*-Ph-H), 7.160-7.145(m, 4H, *meso*-Ph-H), 6.989(d, <sup>3</sup> $J_{H,H}$  = 7.6 Hz, 2H, *meso*-Ph-H), 6.874-6.705(m, 10H,  $\beta$ -Ph-H), 5.215(s, 2H,  $\beta$ -H), 0.174(s, 2H, -NH). MALDI-TOF-MS ( $m/z$ ): found 894.205  $[M+H]^+$ , calcd 894.010. Anal. Calcd for  $C_{62}H_{36}N_8$  C, 83.39; H, 4.06; N, 12.55. Found: C, 83.48; H, 4.15; N, 12.72.

### 3.3 RESULTS AND DISCUSSION

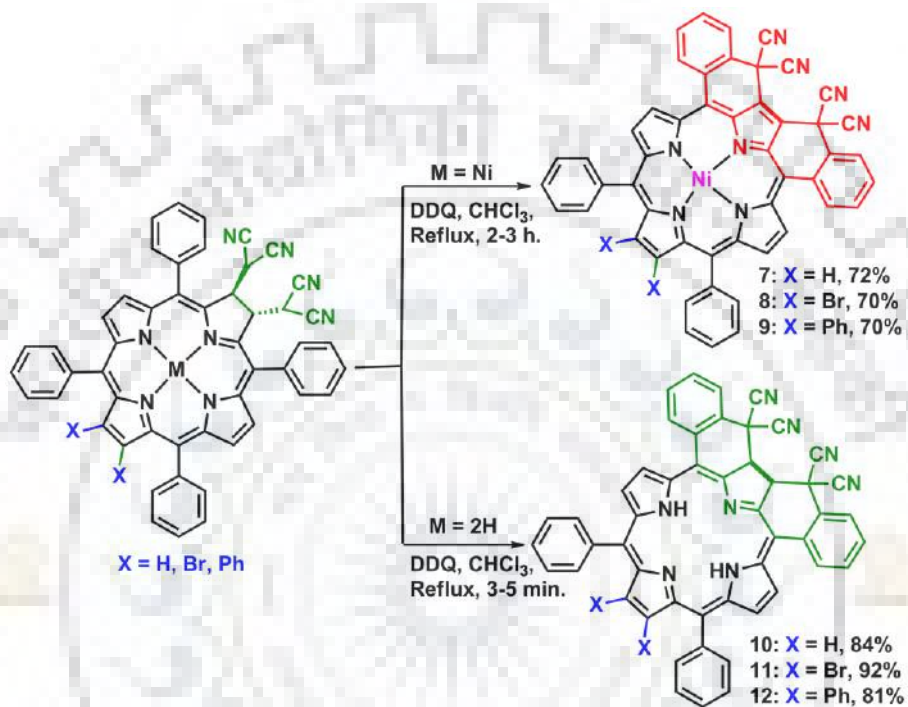
#### 3.3.1 Synthesis and Characterization



**Scheme 3.1** Synthetic Routes to NiDFP(IND)<sub>2</sub>X<sub>2</sub> and H<sub>2</sub>DFC(IND)<sub>2</sub>X<sub>2</sub> (Where X = H, Br, Ph).

*Trans*-chlorins (MTPCR<sub>2</sub>X<sub>2</sub> where M = Ni(II) and 2H; R = 1,3-indanedione and malononitrile; X = H, Br and Ph) were synthesized using similar synthetic procedure as described in Chapter 2. The oxidative fusion reactions were performed simply by refluxing a  $CHCl_3$  solution of free base

or Ni(II) complex of *trans*-chlorins with 5 eq. of 2,3-dichloro-5,6-dicyano-1,4-benzoquinone (DDQ) which afforded the formation of DFPs or DFCs in good to excellent yield (70-92%) as a single product as shown in Scheme 3.1 and 3.2. The ring fusion of free base *trans*-chlorins selectively yielded to doubly fused chlorins (DFCs), whereas the reaction of Ni(II) *trans*-chlorins with DDQ afforded the formation of doubly fused Ni(II) porphyrins (NiDFPs).



**Scheme 3.2** Synthetic Routes to NiDFP(MN)<sub>2</sub>X<sub>2</sub> and H<sub>2</sub>DFC(MN)<sub>2</sub>X<sub>2</sub> (where X = H, Br, Ph).

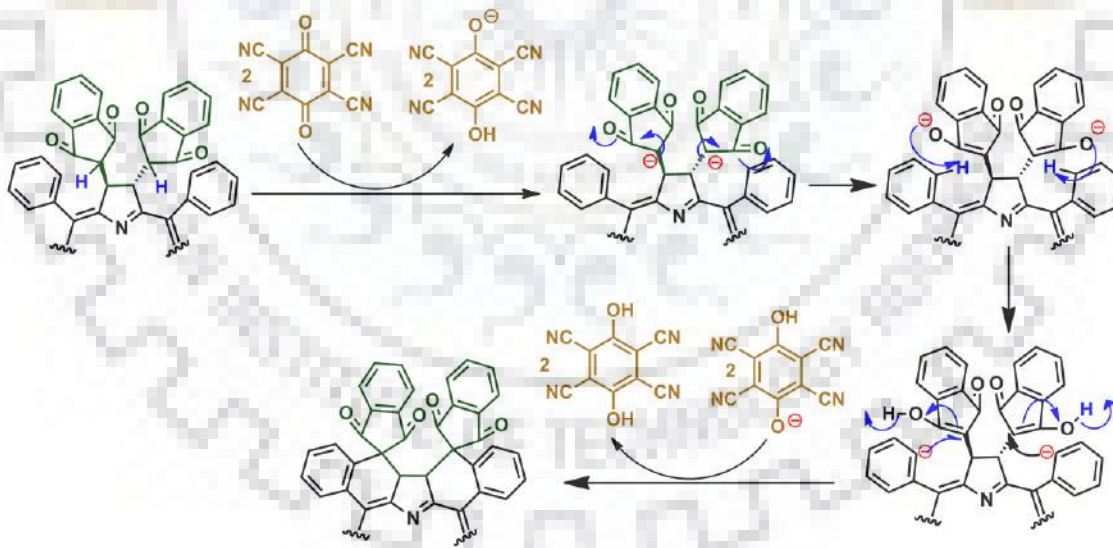
During reaction with free base chlorins, DDQ abstracted the most acidic indanedione protons which resulted into the generation of carbanion species. These resulting carbanions were stabilized by two carbonyl or cyano groups. Further, the carbanions facilitated the C-H activation of the neighboring *ortho*-phenyl positions and yielded difused chlorins (Scheme 3.3). In case of Ni(II) *trans*-chlorins, DDQ not only abstracted the acidic indanedione protons but also the adjacent  $\beta$ -pyrrolic protons which resulted the formation of doubly fused porphyrins. Since the first ring oxidation potential of NiTPC(R)<sub>2</sub> (R = IND, MN) is 150 mV cathodically shifted as compared to H<sub>2</sub>TPC(R)<sub>2</sub> (R = IND, MN) which facilitate the oxidation of reduced  $\beta$ - $\beta'$  bond along with ring fusion. Hence, the ring oxidation was observed due to the presence of electronegative Ni(II) ion in the macrocyclic core. Herein, the oxidative ring-closure reaction is performed *via* DDQ alone rather than common literature methods which includes the



combination of  $\text{Sc}(\text{OTf})_3/\text{DDQ}$  and  $\text{FeCl}_3/\text{DDQ}$  etc. The observed regioselectivity underscores the importance of method which allows introducing a six membered carbocyclic ring by  $\beta$ -*ortho*-phenyl fusion.

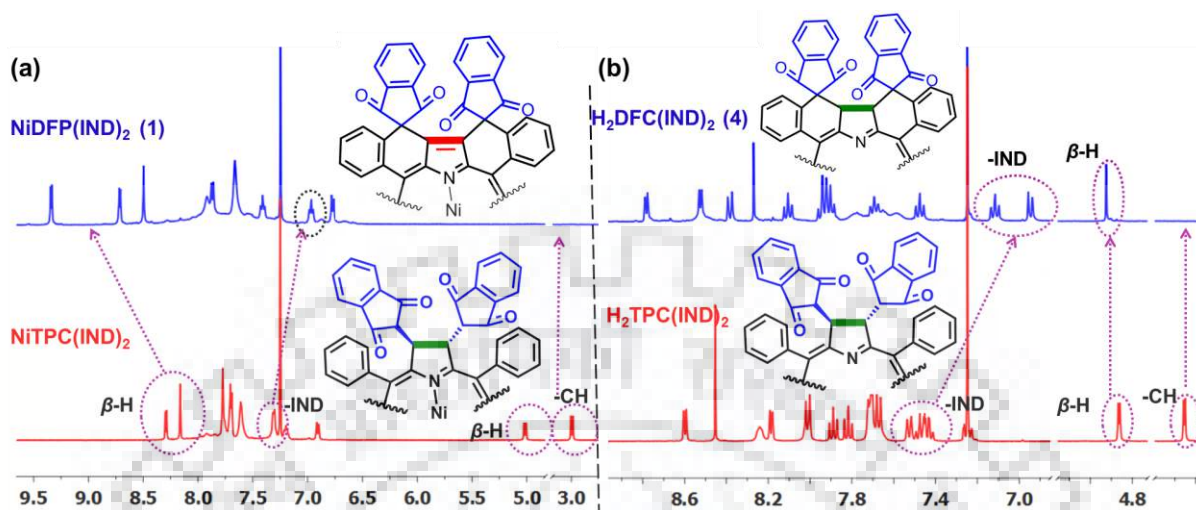
1,3-dipolar-cycloaddition reactions are widely used for the synthesis of fused chlorins as demonstrated in the literature [22]. However, some of the cyclized products were reversible, indicating that they were thermodynamically controlled, which resulted into low yields of the products [23].

Notably, the oxidative fusion reaction was carried out in shorter time scale (< 5 min.) and the products were thermodynamically stable. During the optimization of reaction conditions, we observed that the prolonged heating of  $\text{H}_2\text{TPC}(\text{IND})_2$  with 5 eq. of DDQ produced a small amount of porphyrin  $\text{H}_2\text{DFP}(\text{IND})_2$  (named as **4a**, 5%) also along with  $\text{H}_2\text{DFC}(\text{IND})_2$  (**4**, 72%). Particularly, the reaction of DDQ with  $\text{NiTPC}(\text{MN})_2\text{Br}_2$  yielded a small amount of  $\text{NiDFC}(\text{MN})_2\text{Br}_2$  (**8a**, 6%) along with the major product,  $\text{NiDFP}(\text{MN})_2\text{Br}_2$  (named as **8**, 70%). Hence, the present strategy provides a novel methodology towards the interconversion of porphyrinoids which expands the scope of fused porphyrin chemistry and sets an example for product selectivity.



**Scheme 3.3** The Proposed Mechanism for Ring Fusion.

The characterization of the ring-fused porphyrins/chlorins was performed using UV-Vis., Fluorescence,  $^1\text{H}$  NMR spectroscopic techniques, MALDI-TOF mass spectrometry, elemental analysis and single crystal X-ray analysis.

3.3.2  $^1\text{H}$  NMR and Mass Spectrometric Studies

**Figure 3.1** Comparative  $^1\text{H}$  NMR Spectra of (a) NiTPC(IND)<sub>2</sub> and NiDFP(IND)<sub>2</sub> (1); (b) H<sub>2</sub>TPC(IND)<sub>2</sub> and H<sub>2</sub>DFC(IND)<sub>2</sub> (4).

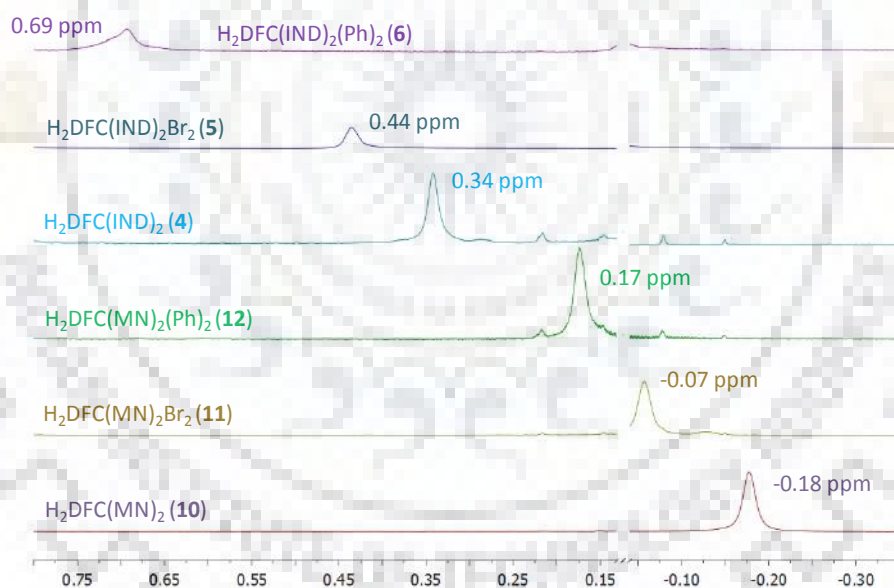


**Figure 3.2** Comparative Chemical Shifts of Core Imino Protons of Free Base Fused Chlorins.

The  $^1\text{H}$  NMR spectra of all synthesized porphyrinoids were recorded in CDCl<sub>3</sub>. Figures A1-A5 in Appendix-II are shown as  $^1\text{H}$  NMR spectra of H<sub>2</sub>DFC(R)<sub>2</sub>/NiDFP(R)<sub>2</sub> (where R = IND and MN). The  $^1\text{H}$  NMR spectra of fused porphyrins (1-3, 7-9, and 4a) did not display the proton signals corresponding to reduced pyrrole as well as for two *ortho*-phenyls as depicted in Figure



3.1a. Similarly the disappearance of two *ortho*-phenyl protons and the presence of one singlet of two proton intensity between 4.5 to 5.5 ppm confirmed the formation of fused chlorins (**4-6**, **10-12** and **8a**) as shown in Figure 3.1b. The  $\beta$ -protons of fused systems were significantly downfield shifted as compared to the corresponding precursors due to highly twisted conformation of the macrocyclic core. The synthesized chlorins exhibited interesting downfield shift in the inner core NH protons ranging from -0.18 to 0.69 ppm as shown in Figure 3.2. The observed downfield shift of inner core NHs follows the order:  $\text{H}_2\text{DFC}(\text{MN})_2$  (**10**) <  $\text{H}_2\text{DFC}(\text{MN})_2\text{Br}_2$  (**11**) <  $\text{H}_2\text{DFC}(\text{MN})_2(\text{Ph})_2$  (**12**) <  $\text{H}_2\text{DFC}(\text{IND})_2$  (**4**) <  $\text{H}_2\text{DFC}(\text{IND})_2\text{Br}_2$  (**5**) <  $\text{H}_2\text{DFC}(\text{IND})_2(\text{Ph})_2$  (**6**).

MALDI-TOF mass spectra of  $\text{H}_2\text{DFC}(\text{IND})_2$  (**4**) is given in Figure 3.3 whereas Figures A6-A9 in Appendix-II exhibit the MALDI-TOF mass spectra of  $\text{H}_2\text{DFP}(\text{R})_2$  and  $\text{NiDFP}(\text{R})_2$  (R = IND or MN). The observed molecular ion peak values were exactly matching with the calculated ones.

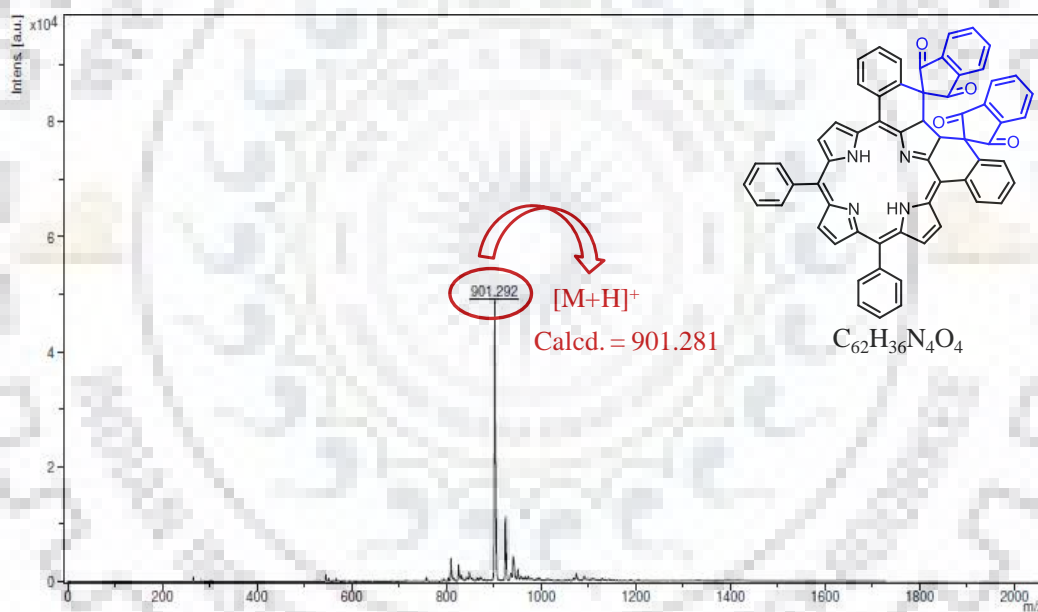
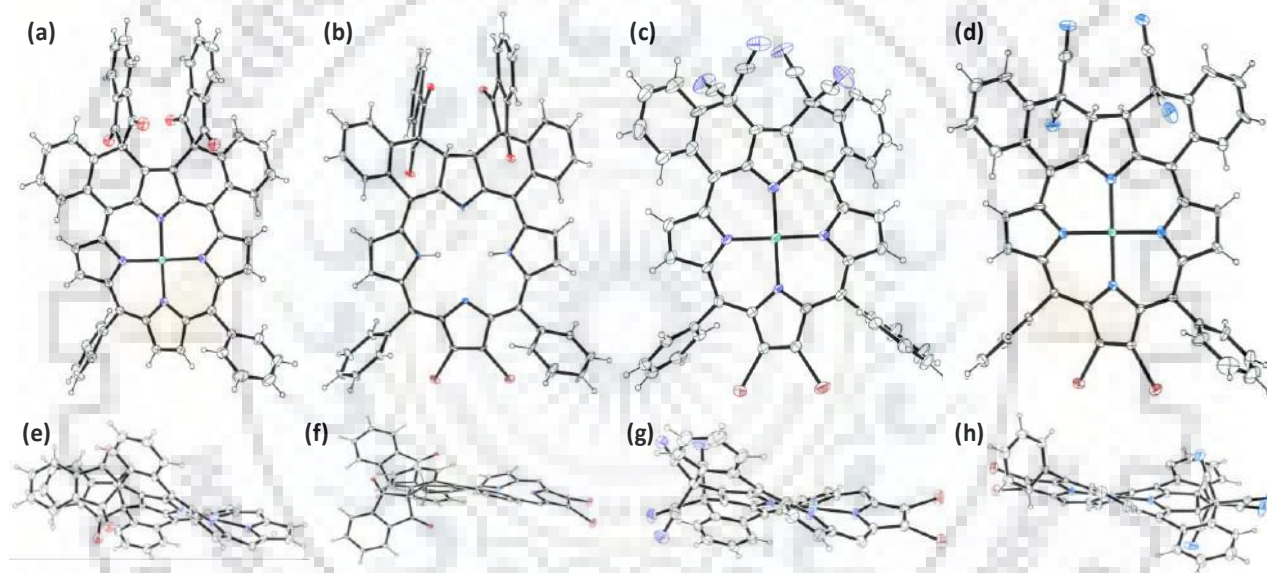


Figure 3.3 MALDI-TOF Mass Spectrum of  $\text{H}_2\text{DFC}(\text{IND})_2$  (**4**).

### 3.3.3 Crystal Structure Discussion

Synthesized fused porphyrins and chlorins were further characterized by single crystal X-ray analysis. The structure of  $\text{NiDFP}(\text{IND})_2$  (**1**),  $\text{H}_2\text{DFC}(\text{IND})_2\text{Br}_2$  (**5**),  $\text{NiDFP}(\text{MN})_2\text{Br}_2$  (**8**) and  $\text{NiDFC}(\text{MN})_2\text{Br}_2$  (**8a**) revealed that these compounds were doubly fused and exhibited highly twisted conformation of the macrocyclic core (Figure 3.4). Notably Ni(II) porphyrins were more twisted as compared to the corresponding chlorins as depicted by the deviation of core atoms

from the mean plane. In contrast to fused chlorins, *trans*-chlorins exhibited planar conformation of the macrocyclic core as revealed from single crystal X-ray analysis of  $\text{H}_2\text{TPC}[\text{CH}(\text{CN})_2]_2(\text{Ph})_2$  (Figure A10 in the Appendix-II). The crystallographic data are listed in Table 3.1 and Table A1 in Appendix-II. The selected average bond lengths and bond angles of crystallized porphyrinoids are listed in Table 3.2. The appraisal of bond angles led to the conclusion that  $sp^3$  hybridized carbon atom exhibited deformed tetrahedral geometry due to steric strain as shown in Figure 3.5. The numbering of C-atoms in the macrocyclic skeleton is given in Figure A11 in Appendix-II. In case of  $\text{H}_2\text{DFC}(\text{IND})_2\text{Br}_2$  (**5**) and  $\text{NiDFC}(\text{MN})_2\text{Br}_2$  (**8a**), the bond angles (C22-C46-C3 and C2-C45-C44) were found to be  $\sim 107\text{--}108^\circ$  which was deviated from the standard  $sp^3$  carbon ( $109.5^\circ$ ).

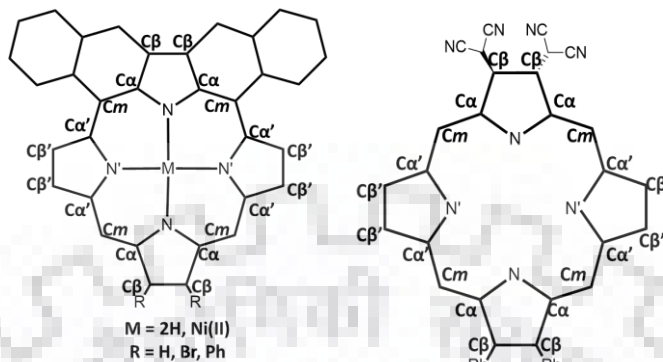


**Figure 3.4** ORTEP Showing Top and Side Views of (a and e)  $\text{NiDFP}(\text{IND})_2$  (**1**); (b and f)  $\text{H}_2\text{DFC}(\text{IND})_2\text{Br}_2$  (**5**); (c and g)  $\text{NiDFP}(\text{MN})_2\text{Br}_2$  (**8**) and  $\text{NiDFC}(\text{MN})_2\text{Br}_2$  (**8a**) (d and h).

In contrast to the chlorins, bond angles (C22-C46-C3 and C2-C45-C44) of fused porphyrins (**1**) and (**8**) were found to be  $\sim 112\text{--}113^\circ$  which was larger as compared to the standard  $sp^3$  carbon ( $109.5^\circ$ ). Ni-N bond lengths were shorter than corresponding unfused systems [24]. The observed C-C bond lengths (C22-C48, C48-C3, C2-C45 and C45-C44) in (**1**) and (**8a**) were found to be 1.50-1.52 Å which were slightly shorter than standard C-C bond length (1.54 Å).

**Table 3.1** Crystal Structure Data of NiDFP(IND) (**1**), H<sub>2</sub>DFC(IND)<sub>2</sub>Br<sub>2</sub> (**5**), H<sub>2</sub>TPC[CH(CN)<sub>2</sub>]<sub>2</sub>, NiDFP(MN)<sub>2</sub>Br<sub>2</sub> (**8**) and NiDFC(MN)<sub>2</sub>Br<sub>2</sub> (**8a**).

	<b>(1)</b>	<b>(5)</b>	<b>(8)</b>	<b>(8a)</b>
Empirical formula	C <sub>62</sub> H <sub>32</sub> N <sub>4</sub> NiO <sub>4</sub>	C <sub>62</sub> H <sub>34</sub> Br <sub>2</sub> N <sub>4</sub> O <sub>4</sub>	C <sub>50</sub> H <sub>22</sub> N <sub>8</sub> NiBr <sub>2</sub>	C <sub>50</sub> H <sub>24</sub> N <sub>8</sub> NiBr <sub>2</sub>
Formula wt.	1194.34	1058.73	1038.21	955.26
Crystal system	Monoclinic	Orthorhombic	Monoclinic	Triclinic
Space group	P 21/c	P n n c	P 21/n	P-1
<i>a</i> (Å)	17.71	19.07	9.44	14.23
<i>b</i> (Å)	21.75	30.66	28.85	16.15
<i>c</i> (Å)	13.91	17.69	17.68	21.07
$\alpha$ (°)	90	90	90	91.99
$\beta$ (°)	97.70	90	98.40	109.28
$\gamma$ (°)	90	90	90	105.91
Volume (Å <sup>3</sup> )	5317.4	10352.6	4766.3	4358.0
Z	4	8	4	4
D <sub>calcd.</sub> (mg/m <sup>3</sup> )	1.492	1.359	1.447	1.456
$\lambda$ (Å)	0.71073	0.71073	0.71073	0.71073
T (K)	293	293	293	293
No. of total reflns.	13664	12953	6757	21184
No. of indepnt. reflns.	5089	6392	4128	5198
R	7.4	12.31	6.64	7.68
Rw	18.9	26.52	18.30	21.77
GOOF	0.95	1.07	1.00	0.90
CCDC	<b>1570263</b>	<b>1570265</b>	<b>1570262</b>	<b>1570264</b>

**Table 3.2** Selected Average Bond Lengths and Bond Angles of NiDFP(IND) (**1**), H<sub>2</sub>DFC(IND)<sub>2</sub>Br<sub>2</sub> (**5**), H<sub>2</sub>TPC[CH(CN)<sub>2</sub>]<sub>2</sub>, NiDFP(MN)<sub>2</sub>Br<sub>2</sub> (**8**) and NiDFC(MN)<sub>2</sub>Br<sub>2</sub> (**8a**).

Bond Lengths (Å)	(1)	(5)	(8)	(8a)	H <sub>2</sub> TPC(MN) <sub>2</sub> Ph <sub>2</sub>
M-N	1.90(4)	--	1.91(6)	1.94(7)	--
M-N'	1.91(5)	--	1.89(6)	1.92(9)	--
N-C <sub>α</sub>	1.37(7)	1.35(8)	1.37(1)	1.38(1)	1.36(5)
N'-C <sub>α</sub>	1.38(7)	1.37(8)	1.38(8)	1.39(1)	1.37(6)
C <sub>α</sub> -C <sub>β</sub>	1.42(7)	1.48(8)	1.44(8)	1.49(1)	1.50(7)
C <sub>α</sub> -C <sub>β</sub>	1.42(8)	1.43(5)	1.45(1)	1.42(2)	1.42(6)
C <sub>β</sub> -C <sub>β</sub>	1.36(8)	1.44(8)	1.33(1)	1.44(2)	1.44(6)
C <sub>β</sub> -C <sub>β</sub>	1.34(8)	1.34(5)	1.34(1)	1.35(2)	1.35(7)
C <sub>α</sub> -C <sub>m</sub>	1.40(7)	1.40(8)	1.40(1)	1.40(2)	1.40(6)
C <sub>α</sub> -C <sub>m</sub>	1.41(8)	1.39(8)	1.39(1)	1.39(1)	1.40(7)
ΔC <sub>β</sub> <sup>a</sup>	<b>0.28</b>	<b>0.397</b>	<b>0.284</b>	<b>0.307</b>	<b>0.175</b>
Δ24 <sup>b</sup>	<b>0.364</b>	<b>0.329</b>	<b>0.37</b>	<b>0.36</b>	<b>0.148</b>
ΔM	<b>0.043</b>	--	<b>0.012</b>	<b>0.008</b>	--
<b>Bond Angles (°)</b>					
N-M-N	179.33(2)	--	179.25(2)	177.74(4)	--
N'-M-N'	178.60(2)	--	178.56(2)	178.75(4)	--
M-N-C <sub>α</sub>	127.34(3)	--	126.51(5)	125.78(7)	--
M-N'-C <sub>α</sub>	127.15(4)	--	126.82(5)	127.13(7)	--
N-C <sub>α</sub> -C <sub>m</sub>	124.52(5)	125.71(6)	125.24(6)	125.10(9)	125.30(4)
N'-C <sub>α</sub> -C <sub>m</sub>	123.49(5)	126.61(6)	124.71(7)	122.81(9)	127.44(4)
N-C <sub>α</sub> -C <sub>β</sub>	110.63(4)	110.57(5)	109.10(6)	109.40(8)	111.06(3)
N'-C <sub>α</sub> -C <sub>β</sub>	109.49(5)	105.20(5)	109.20(6)	110.87(9)	106.07(3)
C <sub>β</sub> -C <sub>α</sub> -C <sub>m</sub>	124.34(5)	123.46(6)	125.32(7)	124.91(9)	123.58(4)
C <sub>β</sub> -C <sub>α</sub> -C <sub>m</sub>	126.44(5)	127.97(6)	125.45(6)	125.82(1)	126.41(4)
C <sub>α</sub> -C <sub>β</sub> -C <sub>β</sub>	106.75(5)	104.36(5)	107.33(6)	15.46(9)	103.86(4)
C <sub>α</sub> -C <sub>β</sub> -C <sub>β</sub>	107.61(5)	108.79(6)	107.59(7)	107.05(1)	108.64(4)
C <sub>α</sub> -N-C <sub>α</sub>	105.12(4)	108.83(5)	106.97(6)	108.75(8)	107.38(3)
C <sub>α</sub> -N'-C <sub>α</sub>	105.59(4)	111.88(5)	106.23(6)	103.89(8)	110.49(3)
C <sub>α</sub> -C <sub>m</sub> -C <sub>α</sub>	120.79(5)	123.79(5)	119.85(7)	122.50(9)	125.58(4)

<sup>a</sup>ΔC<sub>β</sub> refers to the mean plane deviation of β-pyrrole carbons<sup>b</sup>Δ24 refers to the mean plane displacement of 24-atom core

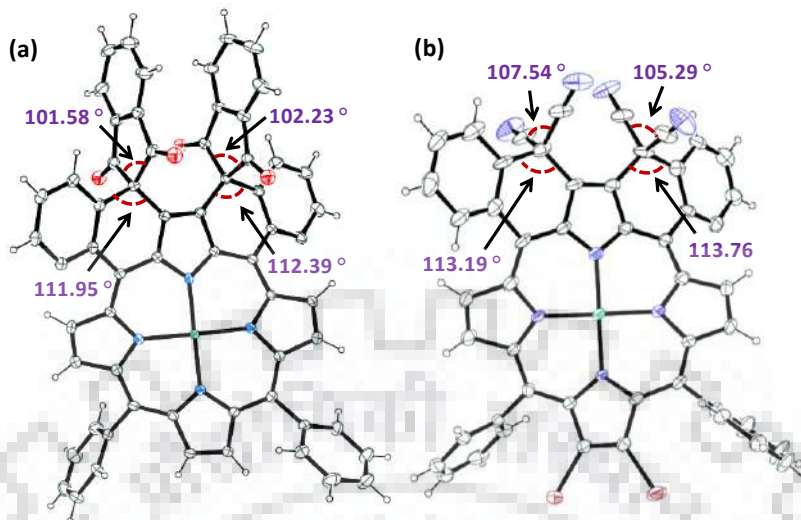


**Figure 3.5** ORTEP Diagrams (a) NiDFP(IND)<sub>2</sub> (**1**) and (b) NiDFP(MN)<sub>2</sub>Br<sub>2</sub> (**8**) Showing the Bond Angles for Fused Tetrahedral Carbon.

Interestingly, we were able to tune the twist angles of the fused rings from the mean plane of the macrocyclic core. It was observed that porphyrins NiDFP(IND)<sub>2</sub> (**1**) and NiDFP(MN)<sub>2</sub>Br<sub>2</sub> (**8**) were highly twisted (34.26° and 31.04°, respectively) as compared to chlorins H<sub>2</sub>DFC(IND)<sub>2</sub>Br<sub>2</sub> (**5**), and NiDFC(MN)<sub>2</sub>Br<sub>2</sub> (**8a**) (19.54° and 27.24°, respectively). The displacement of  $\beta$ -pyrrole carbons ( $\Delta C_{\beta}$ ) from the macrocyclic mean plane (Figure A12 in Appendix-II) follows the order:

H<sub>2</sub>DFC(IND)<sub>2</sub>Br<sub>2</sub> (**5**) > NiDFC(MN)<sub>2</sub>Br<sub>2</sub> (**8a**) > NiDFP(MN)<sub>2</sub>Br<sub>2</sub> (**8**) > NiDFP(IND)<sub>2</sub> (**1**) > H<sub>2</sub>TPC[CH(CN)<sub>2</sub>]<sub>2</sub>(Ph)<sub>2</sub>.

### 3.3.4 DFT Studies

DFT studies of synthesized fused porphyrins and chlorins were executed using B3LYP/6-31G for C,H,N,O and LANL2DZ basis sets were used for Ni(II) complexes. The frontier molecular orbitals of doubly fused chlorin H<sub>2</sub>DFC(MN)<sub>2</sub> (**10**) are shown in Figure 3.6 whereas the FMOs for porphyrinoids **1,4** and **7** are shown in Figures A13-A15 in the Appendix-II. The HOMO of these compounds has contributed mainly from the macrocyclic skeleton, whereas the LUMO+2 contributed to the fused groups. These data revealed that the electron withdrawing groups at the fused rings played a crucial role in the HOMO/LUMO segregation.



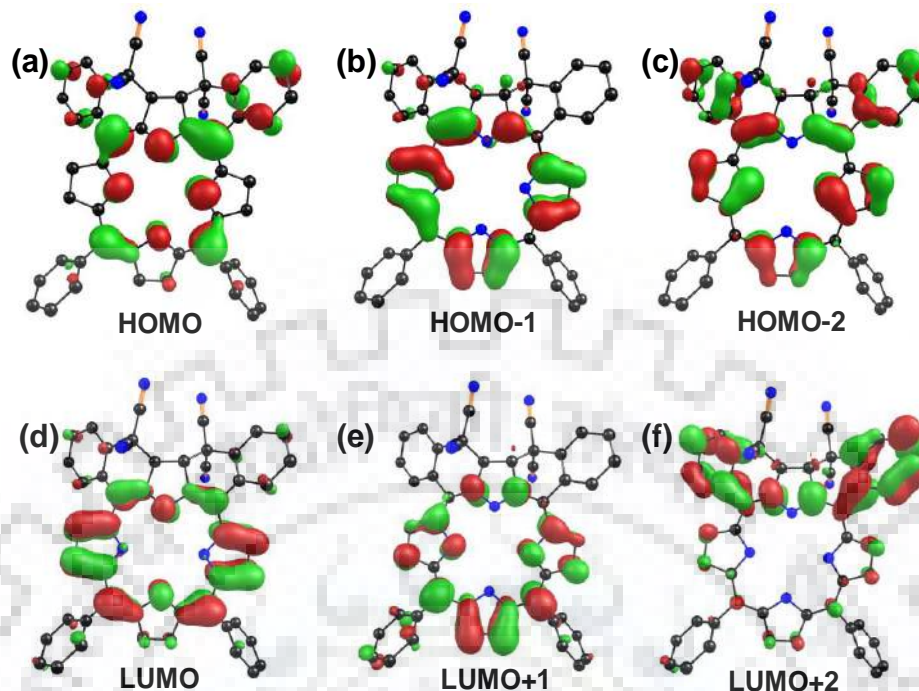


**Figure 3.6** Frontier Molecular Orbitals of  $H_2DFC(MN)_2$  (**10**).

### 3.3.5 Electronic Spectral Studies

The comparative absorption spectra of  $H_2DFCs/NiDFPs$  with their respective precursors are shown in Figures 3.7a, A16 and A17 in the Appendix-II. Table 3.3 and A2 in Appendix-II list the electronic spectral data.  $Ni(II)DFPs$  (**1-3**, **7-9**) exhibited large red-shift in their Soret band ( $\Delta\lambda_{max} = 38-53$  nm) as compared to the corresponding precursors,  $Ni(II)$  *trans*-chlorins. Similarly,  $H_2DFCs$  (**4-6**, **10-12**) exhibited significant red-shift in their Soret band ( $\Delta\lambda_{max} = 16-22$  nm) as compared to precursor free base *trans*-chlorins [24]. The significant red-shift in the Soret band was attributed to the twisted macrocyclic core and extended  $\pi$ -conjugation. Red-shifted  $Q_{y(0,0)}$  band in the  $H_2DFCs$  ascribed to the reduced HOMO-LUMO gap in these chlorins. In general,  $H_2DFC(IND)_2(X)_2$  ( $X = H, Br, Ph$ ) exhibited more red-shift in their Soret as well as in the longest wavelength bands as compared to  $H_2DFC(MN)_2X_2$  ( $X = H, Br, Ph$ ). The observed shift in the absorption spectra was due to more stabilization of HOMO and HOMO-1 in  $H_2DFC(MN)_2X_2$  ( $X = H, Br, Ph$ ).



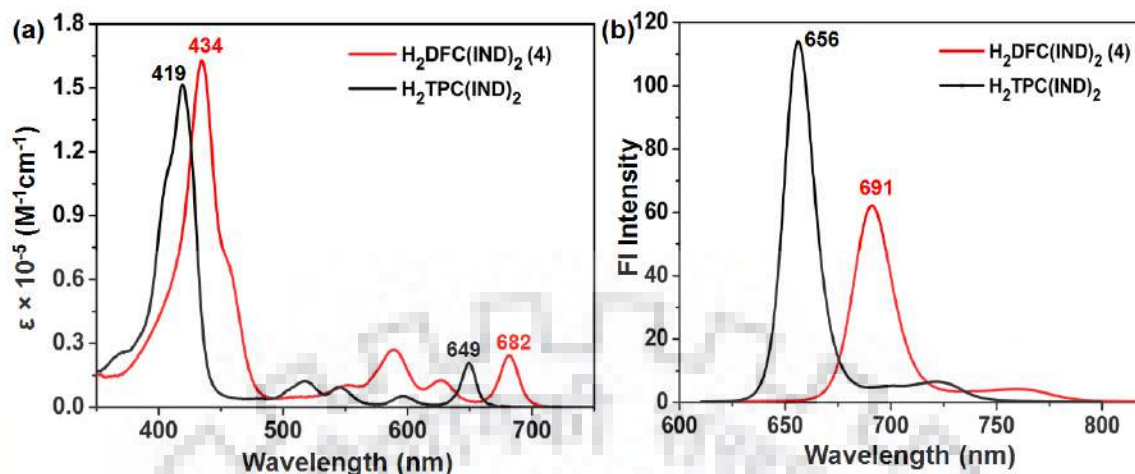


**Figure 3.7** (a) Comparative Absorption Spectra of  $\text{H}_2\text{DFC}(\text{IND})_2$  (**4**) and  $\text{H}_2\text{TPC}(\text{IND})_2$ . (b) Comparative Emission Spectra of  $\text{H}_2\text{DFC}(\text{IND})_2$  (**4**) and  $\text{H}_2\text{TPC}(\text{IND})_2$ .

The comparative emission spectra of  $\text{H}_2\text{DFCs}$  and their precursors in  $\text{CH}_2\text{Cl}_2$  are shown in Figures 3.7b and A16b in Appendix-II. These fused chlorins exhibited lower quantum yield and red shifted emission spectra as compared to their precursors (Table 3.3). Among all synthesized fused chlorins,  $\text{H}_2\text{DFC}(\text{Ph})_2$ s exhibited most red-shifted emission spectra, whereas  $\text{H}_2\text{DFCBr}_2$ s exhibited lowest quantum yield which was observed due to the nonplanar conformation of macrocyclic core as well as heavy atom effect of  $\beta$ -bromo substituents.

**Table 3.3** Absorption Spectral Data<sup>a</sup> of  $\text{H}_2\text{DFCs}$  in  $\text{CH}_2\text{Cl}_2$ .

$\text{H}_2\text{DFCs}$	$\lambda_{\text{abs}}$				$\lambda_{\text{em}}$	$\phi_f$
	B-Band		Q-bands			
$\text{H}_2\text{DFC}(\text{IND})_2$ ( <b>4</b> )	434(5.21)	547(3.99)	589(4.43), 626(4.09), 682(4.39)		691, 760	0.256
$\text{H}_2\text{DFP}(\text{IND})_2$ ( <b>4a</b> )	463(5.24)	568(3.96)	611(4.31), 647(3.81), 708(4.02)		717, 798	0.054
$\text{H}_2\text{DFC}(\text{IND})_2\text{Br}_2$ ( <b>5</b> )	449(5.21)	555(3.98)	596(4.23), 627(4.17), 681(4.14)		692, 765	0.011
$\text{H}_2\text{DFC}(\text{IND})_2(\text{Ph})_2$ ( <b>6</b> )	443(5.20)	555(3.98)	592(4.33), 633(4.09), 689(4.32)		699, 771	0.010
$\text{H}_2\text{DFC}(\text{MN})_2$ ( <b>10</b> )	423(5.32)	539(3.99)	577(4.46), 614(4.18), 665(4.48)		673, 742	0.565
$\text{H}_2\text{DFC}(\text{MN})_2\text{Br}_2$ ( <b>11</b> )	435(5.28)	548(3.98)	584(4.28), 614(4.19), 667(4.21)		675, 744	0.005
$\text{H}_2\text{DFC}(\text{MN})_2(\text{Ph})_2$ ( <b>12</b> )	433(5.22)	545(3.93)	582(4.30), 620(4.09), 672(4.31)		683, 756	0.012

<sup>a</sup>Values in parentheses refers to  $\log \epsilon$

## 3.3.6 Electrochemical Studies

To determine the combined influence of macrocyclic conformation and the electronic nature of fused substituents, the cyclic voltammetric studies of synthesized DFPs/DFCs were carried out in  $\text{CH}_2\text{Cl}_2$  containing 0.1 M  $\text{TBAPF}_6$  as supporting electrolyte. Table 3.4 lists the redox potential data of the synthesized chlorins and porphyrins. Figure 3.8 represents the comparative cyclic voltammograms (CVs) of  $\text{NiDFP}(\text{MN})_2\text{X}_2$  and  $\text{H}_2\text{DFC}(\text{MN})_2\text{X}_2$  ( $\text{X} = \text{H}, \text{Br}, \text{Ph}$ ). The CVs of  $\text{NiDFP}(\text{IND})_2\text{X}_2$  and  $\text{H}_2\text{DFC}(\text{IND})_2\text{X}_2$  ( $\text{X} = \text{H}, \text{Br}, \text{Ph}$ ) are shown in Figure A18 in the Appendix-II whereas the DPVs of all synthesized porphyrinoids are shown in Figure A19 in the Appendix-II.

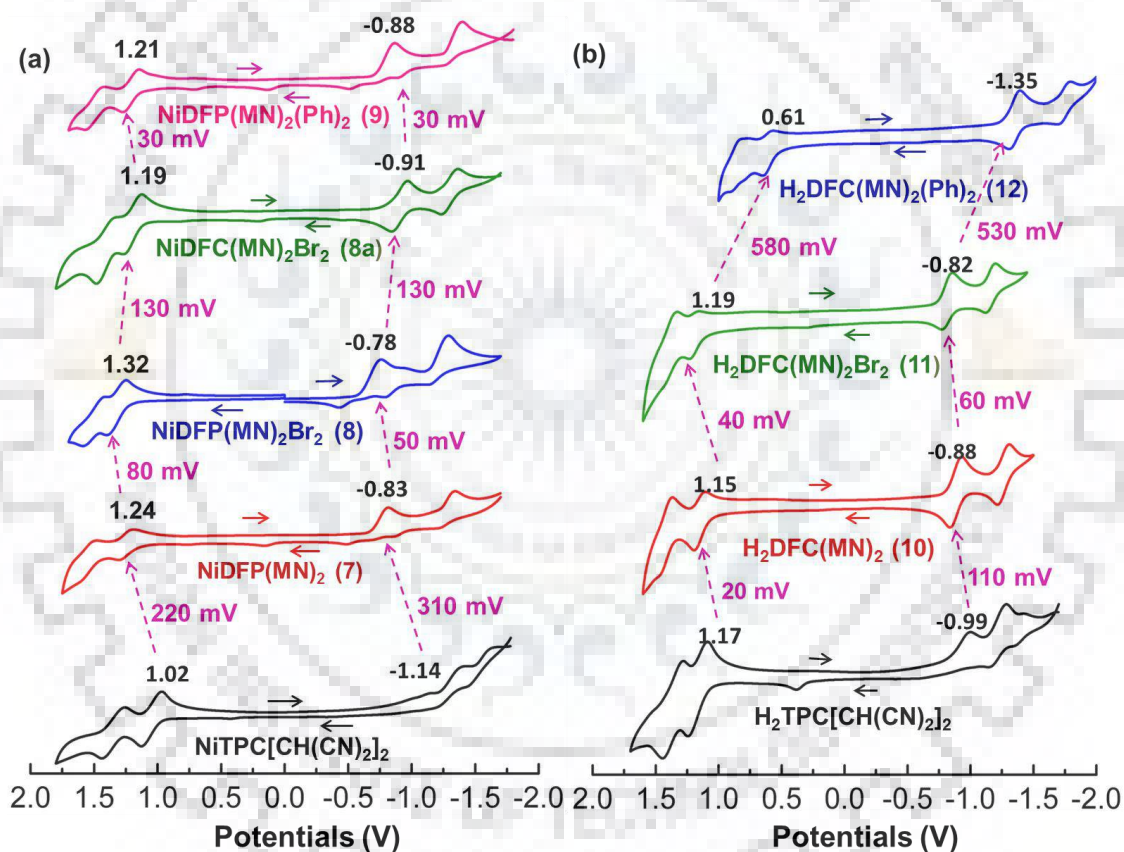


**Figure 3.8** Comparative CVs of (a)  $\text{NiDFP}(\text{MN})_2\text{X}_2$  (b)  $\text{H}_2\text{DFC}(\text{MN})_2\text{X}_2$  (where  $\text{X} = \text{H}, \text{Br}, \text{Ph}$ ) in  $\text{CH}_2\text{Cl}_2$ .

**Table 3.4** Redox Potentials<sup>a</sup> of Synthesized H<sub>2</sub>DFCs and NiDFPs in CH<sub>2</sub>Cl<sub>2</sub> at 298 K

Porphyrins/Chlorins	Oxidation (V)			$\Delta E^{1/2}$ (eV)	Reduction (V)		
	I	II	III		I	II	III
NiDFP(IND) <sub>2</sub> ( <b>1</b> )	0.94	1.39		2.07	-1.13	-1.37	-1.58
NiDFP(IND) <sub>2</sub> Br <sub>2</sub> ( <b>2</b> )	1.01	1.42		2.02	-1.01	-1.35	-1.58
NiDFP(IND) <sub>2</sub> (Ph) <sub>2</sub> ( <b>3</b> )	0.93	1.06 <sup>i</sup>	1.42	2.06	-1.13	-1.40	-1.61
H <sub>2</sub> DFC(IND) <sub>2</sub> ( <b>4</b> )	0.84	1.22		1.89	-1.05	-1.42	-1.65
H <sub>2</sub> DFP(IND) <sub>2</sub> ( <b>4a</b> )	1.19	1.36		2.01	-0.82	-1.16	
H <sub>2</sub> DFC(IND) <sub>2</sub> Br <sub>2</sub> ( <b>5</b> )	0.91	1.19		1.93	-1.02	-1.37	-1.68
H <sub>2</sub> DFC(IND) <sub>2</sub> (Ph) <sub>2</sub> ( <b>6</b> )	0.78	1.07		1.89	-1.11	-1.46	-1.64
NiDFP(MN) <sub>2</sub> ( <b>7</b> )	1.24	1.55		2.08	-0.83	-1.28	
NiDFP(MN) <sub>2</sub> Br <sub>2</sub> ( <b>8</b> )	1.32	1.50		2.10	-0.78	-1.29	
NiDFC(MN) <sub>2</sub> Br <sub>2</sub> ( <b>8a</b> )	1.19	1.42		2.10	-0.91	-1.31	
NiDFP(MN) <sub>2</sub> (Ph) <sub>2</sub> ( <b>9</b> )	1.21	1.50		2.09	-0.88	-1.34	
H <sub>2</sub> DFC(MN) <sub>2</sub> ( <b>10</b> )	1.15	1.42		2.03	-0.88	-1.26	
H <sub>2</sub> DFC(MN) <sub>2</sub> Br <sub>2</sub> ( <b>11</b> )	1.19	1.38		2.00	-0.82	-1.16	
H <sub>2</sub> DFC(MN) <sub>2</sub> (Ph) <sub>2</sub> ( <b>12</b> )	0.61	0.86		1.96	-1.35	-1.74	

<sup>a</sup>*V*<sub>s</sub> Ag/AgCl reference electrode; i = irreversible

Interestingly, NiDFP(IND)<sub>2</sub>Ph<sub>2</sub> (**3**) exhibited three oxidations, whereas H<sub>2</sub>DFC(IND)<sub>2</sub>X<sub>2</sub> and NiDFP(IND)<sub>2</sub>X<sub>2</sub> (X = H, Br, Ph) have shown three reversible reductions. The first oxidation and reduction potentials of indanedione fused porphyrinoids were cathodically shifted as compared to their corresponding precursors, MTPC(IND)<sub>2</sub> (M = 2H, Ni(II)). H<sub>2</sub>DFC(MN)<sub>2</sub> (**10**) exhibited 110 mV anodic shift in the first reduction potential as compared to its precursor, H<sub>2</sub>TPC[CH(CN)<sub>2</sub>]<sub>2</sub> which ascribed to the extensive stabilization of LUMO upon fusion. H<sub>2</sub>DFC(MN)<sub>2</sub>Ph<sub>2</sub> (**12**) exhibited a pronounced cathodic shift (540 mV) in the first oxidation potential with respect to H<sub>2</sub>DFC(MN)<sub>2</sub> (**10**) due to extensive destabilization of HOMO. The first oxidation and reduction potentials of NiDFP(MN)<sub>2</sub> (**7**) were 220 mV and 310 mV anodically shifted as compared to NiTPC[CH(CN)<sub>2</sub>]<sub>2</sub>.

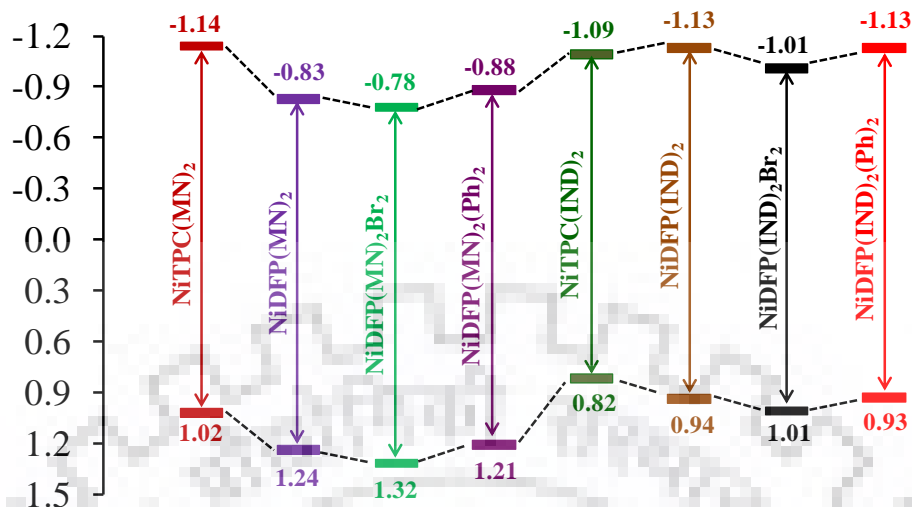


**Figure 3.9** Plot of HOMO-LUMO Trend in Ni(II)DFPs.

The redox behaviors of MN fused porphyrins and chlorins were quite distinguished from IND fused porphyrinoids. In general, NiDFP(IND)<sub>2</sub>X<sub>2</sub>/H<sub>2</sub>DFC(IND)<sub>2</sub>X<sub>2</sub> were easy to oxidize (170-310 mV) and harder to reduce (170-300 mV) as compared to NiDFP(MN)<sub>2</sub>X<sub>2</sub>/H<sub>2</sub>DFC(MN)<sub>2</sub>X<sub>2</sub>. We were able to achieve the redox tunability by appending mixed substituents at the antipodal position of fused rings which can be clearly seen from HOMO-LUMO levels in Figures 3.9 and A20 in Appendix-II. In general, Ni(II) *trans*-chlorins were easy to oxidize than the corresponding free base *trans*-chlorins that brought the product selectivity.

### 3.3.7 Protonation-Deprotonation Studies

The combined effect of  $\beta$ -*meso*-phenyl fusion,  $\beta$ -substitution and nonplanarity of macrocycles on the basicity of inner core was further probed by protonation and deprotonation studies of synthesized free base chlorins. Protonation and deprotonation titrations were carried out using trifluoroacetic acid (TFA) and tetrabutylammonium hydroxide (TBAOH), respectively in CH<sub>2</sub>Cl<sub>2</sub> at 298 K. The acid-base properties of porphyrins are well quoted in the literature [25] whereas there are only a few reports available on the protonation and deprotonation studies of chlorins [24]. Recently, Kojima and coworkers reported the stepwise protonation of the fused porphyrin [26]. To the best of our knowledge, this is the first report on protonation and deprotonation studies of difused chlorins. Figure 3.10a shows the UV-vis. spectral changes upon increasing the concentration of TFA ( $2.58 \times 10^{-3}$ - $26.9 \times 10^{-3}$  M) for H<sub>2</sub>DFC(MN)<sub>2</sub> (**10**). Table 3.5 summarizes the data of the protonation constants, stoichiometry, and correlation coefficients of H<sub>2</sub>DFCs.

Figure 3.10a represents the concomitant decrement in the absorbance of H<sub>2</sub>DFC(MN)<sub>2</sub> (**10**) at 425 nm and rising of a new band at 435 nm while increasing the concentration of TFA ( $2.58 \times 10^{-3}$ – $26.9 \times 10^{-3}$  M). As protonation proceeds, the first and last Q bands disappeared with the emergence of multiple Q-bands at 596 nm, 627 nm and 648 nm. Similar behavior was observed for rest of the chlorins as shown in Figures A21 and A22 in the Appendix-II. Upon protonation, the purple color of fused chlorins turned to green. Among all synthesized chlorins, H<sub>2</sub>DFC(MN)<sub>2</sub>X<sub>2</sub> (X = H, Br, Ph) exhibited lower protonation constants as compared to H<sub>2</sub>DFC(IND)<sub>2</sub>(X)<sub>2</sub> (X = H, Br, Ph) due to strong electron withdrawing nature of cyano groups as evidenced from electrochemical redox data (Table 3.4).

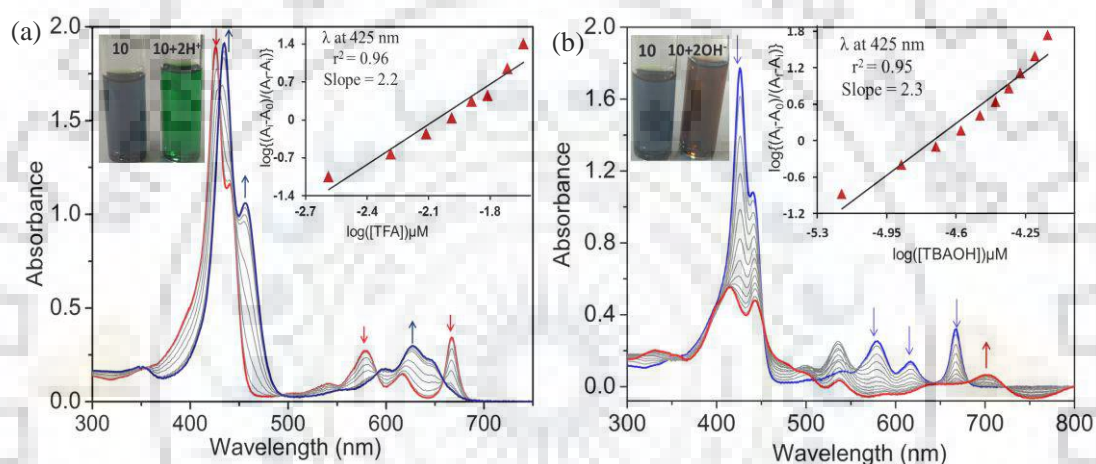


**Figure 3.10** UV-vis. Spectral Changes of H<sub>2</sub>DFC(MN)<sub>2</sub> (**10**) While Increasing the Conc. of (a) TFA (b) TBAOH in CH<sub>2</sub>Cl<sub>2</sub> at 298 K; Insets Show the Corresponding Hill Plots.

The UV-vis spectral titration was performed to calculate the deprotonation constants of the synthesized difused chlorins. Figure 3.10b represents the UV-vis. spectral changes upon sequential addition of TBAOH into H<sub>2</sub>DFC(MN)<sub>2</sub> (**10**). Upon increasing the conc. of TBAOH ( $0.66 \times 10^{-5}$ – $9.25 \times 10^{-5}$  M), the absorbance at 425 nm decreased with the appearance of new bands at 470 and 703 nm. Similar trend was observed for H<sub>2</sub>DFC(MN)<sub>2</sub>Br<sub>2</sub> (**11**) and H<sub>2</sub>DFC(MN)<sub>2</sub>Ph<sub>2</sub> (**12**) (Figure A23 in Appendix-II). As the deprotonation proceeded the purple and green color of fused chlorins turned to brownish red. However, we were unable to deprotonate H<sub>2</sub>DFC(IND)<sub>2</sub>X<sub>2</sub> (X = H, Br, Ph) even at higher conc. of TBAOH (Figure A24 in Appendix-II) due to their electron rich nature with respect to cyano substituted chlorins i.e. H<sub>2</sub>DFC(MN)<sub>2</sub>X<sub>2</sub> (X = H, Br, Ph). The electron rich nature of indanedione fused porphyrinoids was supported by



electrochemical studies as the first oxidation potentials of H<sub>2</sub>DFC(MN)<sub>2</sub>X<sub>2</sub> (X = H, Br, Ph) were much higher (anodically shifted) as compared to H<sub>2</sub>DFC(IND)<sub>2</sub>X<sub>2</sub> (X = H, Br, Ph) which resulted into the facile deprotonation of the core imino protons of H<sub>2</sub>DFC(MN)<sub>2</sub>X<sub>2</sub> (X = H, Br, Ph). The protonation/deprotonation constants and stoichiometry were calculated using Hill equation [27] and found to be ~2 in all the cases (Table 3.5).

**Table 3.5** Protonation and Deprotonation Constants ( $\log\beta_2$ )<sup>a</sup> of synthesized H<sub>2</sub>DFCs in CH<sub>2</sub>Cl<sub>2</sub> at 298 K.

H <sub>2</sub> DFCs	Protonation			Deprotonation		
	$\log\beta_2$	slope	r <sup>2</sup>	$\log\beta_2$	slope	r <sup>2</sup>
H <sub>2</sub> DFC(IND) <sub>2</sub> ( <b>4</b> )	6.05	2.2	0.98			
H <sub>2</sub> DFP(IND) <sub>2</sub> ( <b>4a</b> )	7.31	2.3	0.99			
H <sub>2</sub> DFC(IND) <sub>2</sub> Br <sub>2</sub> ( <b>5</b> )	6.14	2.5	0.98			
H <sub>2</sub> DFC(IND) <sub>2</sub> Ph <sub>2</sub> ( <b>6</b> )	8.29	2.1	0.96			
H <sub>2</sub> DFC(MN) <sub>2</sub> ( <b>10</b> )	4.51	2.2	0.96	11.55	2.3	0.95
H <sub>2</sub> DFC(MN) <sub>2</sub> Br <sub>2</sub> ( <b>11</b> )	4.62	2.1	0.94	12.22	2.5	0.98
H <sub>2</sub> DFC(MN) <sub>2</sub> Ph <sub>2</sub> ( <b>12</b> )	6.52	2.1	0.95	12.37	2.4	0.98

<sup>a</sup> Within the error range of  $\pm 0.075$  for  $\log\beta_2$ .

### 3.4 CONCLUSIONS

In summary, we developed a facile synthetic procedure to obtain  $\beta$ -to-ortho-phenyl doubly fused porphyrins or chlorins in good to excellent yields. This is the first report on core metal ion dependent regioselective oxidative fusion of *trans*-chlorins into doubly fused porphyrins or chlorins. The doubly fused porphyrins exhibited highly twisted macrocyclic conformation which results a dramatic red-shift in electronic absorption spectral features as compared to doubly fused chlorins. Inner core protons of fused chlorins exhibited tremendous downfield shift ( $\Delta\delta = 1.71$ - $2.02$  ppm) as compared to their precursors, *trans*-chlorins due to fused macrocyclic core.  $\beta$ -Phenyl substituted chlorin (H<sub>2</sub>DFC(MN)<sub>2</sub>Ph<sub>2</sub> (**12**)) exhibited a large cathodic shift in first oxidation ( $\Delta E_{\text{oxdn}} = 0.54$  V) and first reduction ( $\Delta E_{\text{redn}} = 0.47$  V) potentials due to pushing effect of  $\beta$ -phenyl substituents. Malononitrile fused porphyrinoids were harder to oxidize and easier to reduce as compared to indane fused systems due to strong electron withdrawing nature of cyano



substituents which supported the facile deprotonation of H<sub>2</sub>DFC(MN)<sub>2</sub>X<sub>2</sub>. On the contrary, indane fused chlorins exhibited 40-60 folds higher protonation constants as compared to malononitrile fused chlorins. Overall, the present methodology provides a new standpoint to develop a wide variety of highly twisted  $\beta$ -*meso* doubly fused chlorins and porphyrins.

### 3.5 REFERENCES

1. Tsuda, A.; Osuka, A. Fully Conjugated Porphyrin Tapes with Electronic Absorption Bands That Reach into Infrared. *Science*, **2001**, *293*, 79-82.
2. Nakamura, Y.; Aratani, N.; Shinokubo, H.; Takagi, A.; Kawai, T.; Matsumoto, T.; Yoon, Z. S.; Kim, D. Y.; Ahn, T. K.; Kim, D.; Muranaka, A.; Kobayashi, N.; Osuka, A. A Directly Fused Tetrameric Porphyrin Sheet and Its Anomalous Electronic Properties that Arise from the Planar Cyclooctatetraene Core. *J. Am. Chem. Soc.* **2006**, *128*, 4119-4127.
3. Diev, V. V.; Schlenker, C. W.; Hanson, K.; Zhong, Q.; Zimmerman, J. D.; Forrest, S. R.; Thompson, M. E. Porphyrins Fused with Unactivated Polycyclic Aromatic Hydrocarbons. *J. Org. Chem.* **2012**, *77*, 143-159.
4. Diev, V. V.; Hanson, K.; Zimmerman, J. D.; Forrest, S. R.; Thompson, M. E. Fused Pyrene-Diporphyrins: Shifting Near-Infrared Absorption to 1.5  $\mu$ m and Beyond *Angew. Chem. Int. Ed.* **2010**, *49*, 5523-5526.
5. Lo, M.; Lefebvre, J.-F.; Leclercq, D.; van der Lee, A.; Richeter, S. Stepwise Fusion of Porphyrin  $\beta, \beta'$ -Pyrrolic Positions to Imidazole Rings. *Org. Lett.* **2011**, *13*, 3110-3113.
6. Diev, V. V.; Femia, D.; Zhong, Q.; Djurovich, P. I.; Haiges, R.; Thompson, M. E. A Quinoidal Bis-Phenalenyl-Fused Porphyrin with Supramolecular Organization and Broad Near-Infrared Absorption. *Chem. Commun.* **2016**, *52*, 1949-1952.
7. Banala, S.; Fokong, S.; Brand, C.; Andreou, C.; Krautler, B.; Rueping, M.; Kiessling, F. Quinone-Fused Porphyrins as Contrast Agents for Photoacoustic Imaging. *Chem. Sci.* **2017**, *8*, 6176-6181.
8. Jiao, C.; Zu, N.; Huang, K.-W.; Wang, P.; Wu, J. Perylene Anhydride Fused Porphyrins as Near-Infrared Sensitizers for Dye-Sensitized Solar Cells. *Org. Lett.* **2011**, *13*, 3652-3655.

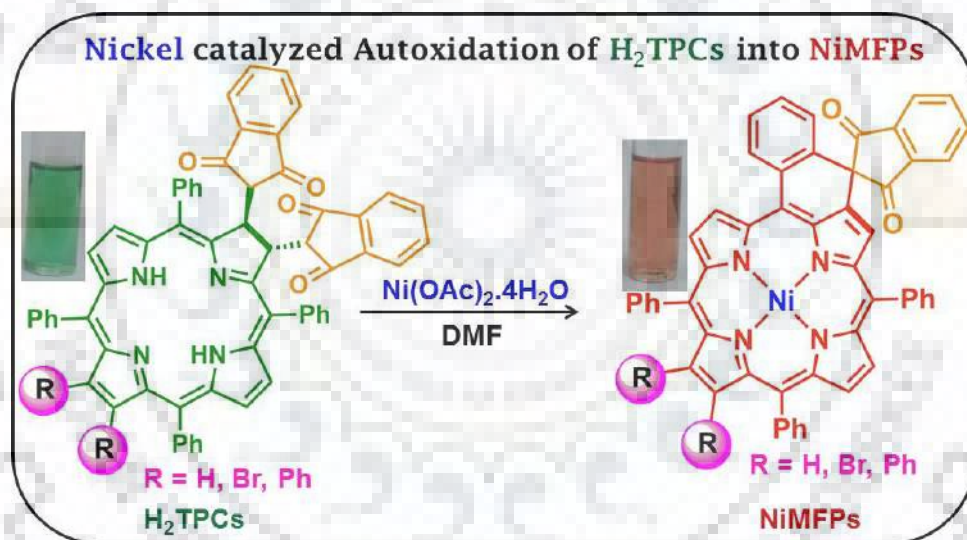
9. Tanaka, T.; Osuka, A. Conjugated Porphyrin Arrays: Synthesis, Properties and Applications for Functional Materials. *Chem. Soc. Rev.* **2015**, *44*, 943-969.
10. Aratani, N.; Kim, D.; Osuka, A.  $\pi$ -Conjugation Enlargement Toward the Creation of Multi-Porphyrinic Systems with Large Two-Photon Absorption Properties. *Chem. Asian J.* **2009**, *4*, 1172-1182.
11. Kato, K.; Kim, J. O.; Yorimitsu, H.; Kim, D.; Osuka, A. Triphenylsilane-fused Porphyrins *Chem. Asian J.* **2016**, *11*, 1738-1746.
12. Fukui, N.; Cha, W.; Shimizu, D.; Oh, J.; Furukawa, K.; Yorimitsu, H.; Kim, D.; Osuka, A. Highly Planar Diarylamine-Fused Porphyrins and Their Remarkably Stable Radical Cations *Chem. Sci.* **2017**, *8*, 189-199.
13. Davis, N. K. S.; Thompson, A. L.; Anderson, H. L. A Porphyrin Fused to Four Anthracenes. *J. Am. Chem. Soc.* **2011**, *133*, 30-31.
14. Davis, N. K. S.; Thompson, A. L.; Anderson, H. L. Bis-Anthracene Fused Porphyrins: Synthesis, Crystal Structure, and Near-IR Absorption. *Org. Lett.* **2010**, *12*, 2124-2127.
15. Ishizuka, T.; Saegusa, Y.; Shiota, Y.; Ohtake, K.; Yoshizawa, K.; Kojima, T. Multiply-Fused Porphyrins-Effects of Extended  $\pi$ -Conjugation on the Optical and Electrochemical Properties. *Chem. Commun.* **2013**, *49*, 5939-5941.
16. Aguiar, A.; Leite, A.; Silva, A. M. N.; Tome, A. C.; Cunha-Silva, L.; de Castro, B.; Rangel, M.; Silva, A. M. G. Isoxazolidine-Fused *meso*-Tetraarylchlorins as Key Tools for the Synthesis of Mono- and Bis-annulated Chlorins. *Org. Biomol. Chem.* **2015**, *13*, 7131-7135.
17. Silva, A. M. G.; Tomé, A. C.; Neves, M. G. P. M. S.; Cavaleiro, J. A. S. Novel Barrelene-Fused Chlorins by Diels-Alder Reactions. *Tetrahedron Lett.* **2000**, *41*, 3065.
18. Akhigbe, J.; Zeller, M.; Brückner, C. Quinoline-Annulated Porphyrins. *Org. Lett.* **2011**, *13*, 1322.
19. Richeter, S.; Jeandon, C.; Gisselbrecht, J.-P.; Ruppert, R.; Callot, H. J. Syntheses and Optical and Electrochemical Properties of Porphyrin Dimers Linked by Metal Ions. *J. Am. Chem. Soc.* **2002**, *124*, 6168-6179.

20. Richeter, S.; Jeandon, C.; Gisselbrecht, J.-P.; Ruppert, R.; Callot, H. J. Synthesis, Structural Characterization, and Electrochemical Studies of Nickel Porphyrins Bearing Two Peripheral Conjugated Chelating Groups. *Inorg. Chem.* **2007**, *46*, 10241-10251.
21. Kumar, R.; Sankar, M. Synthesis, Spectral, and Electrochemical Studies of Electronically Tunable  $\beta$ -Substituted Porphyrins with Mixed Substituent Pattern. *Inorg. Chem.* **2014**, *53*, 12706-12719.
22. Almeida, J.; Aguiar, A.; Leite, A.; Silva, A. M. N.; Cunha-Silva, L.; de Castro, B.; Rangel, M.; Barone, G.; Tome, A. C.; Silva, A. M. N. G. 1,3-Dipolar Cycloadditions with *meso*-Tetraarylchlorins-Site Selectivity and Mixed Bisadducts. *Org. Chem. Front.* **2017**, *4*, 534-544.
23. Jiménez-Osés, G.; García, J. I.; Silva, A. M. G.; Santos, A. R. N.; Tomé, A. C.; Neves, M. G. P. M. S.; Cavaleiro, J. A. S. Mechanistic Insights on the Site Selectivity in Successive 1,3-Dipolar Cycloadditions to *meso*-Tetraarylporphyrins. *Tetrahedron* **2008**, *64*, 7937-7943.
24. Chaudhri, N.; Grover, N.; Sankar, M. Versatile Synthetic Route for  $\beta$ -Functionalized Chlorins and Porphyrins by Varying the Size of Michael Donors: Syntheses, Photophysical, and Electrochemical Redox Properties. *Inorg. Chem.* **2017**, *56*, 11532-11545.
25. Honda, T.; Nakanishi, T.; Ohkubo, K.; Kojima, T.; Fukuzumi, S. Structure and Photoinduced Electron Transfer Dynamics of a Series of Hydrogen-Bonded Supramolecular Complexes Composed of Electron Donors and a Saddle-Distorted Diprotonated Porphyrin. *J. Am. Chem. Soc.* **2010**, *132*, 10155-10163.
26. Saegusa, Y.; Ishizuka, T.; Shiota, Y.; Yoshizawa, K.; Kojima, T. Acid-Base Properties of a Freebase Form of a Quadruply Ring-Fused Porphyrin-Stepwise Protonation Induced by Rigid Ring-Fused Structure. *J. Org. Chem.* **2017**, *82*, 322-330.
27. Hill, A. V. The Possible Effects of the Aggregation of The Molecules of Haemoglobin on its Dissociation Curves. *J. Physiol.* **1910**, *40*, IV-VII.



## CHAPTER 4

### “One-Pot Synthesis of Ni(II) Monofused Porphyrins (NiMFPs) *via* Nickel Acetate Catalyzed Oxidation of Free Base *trans*-Chlorins”







## CHAPTER 4

### ONE-POT SYNTHESIS OF Ni(II) MONOFUSED PORPHYRINS (NiMFPs) VIA NICKEL ACETATE CATALYZED OXIDATION OF FREE BASE TRANS CHLORINS

#### 4.1 INTRODUCTION

Chlorophyll consists of chlorins and associated pigments, which are responsible for light harvesting on earth [1]. As a photosensitizer in photodynamic therapy, chlorins are often chosen since they exhibit intense long wavelength absorption  $\geq 600$  nm [2]. The recent advancement in synthetic methodologies over the past few years brought classical methods to bring functionalized chlorins [3]. Several methods are available in the literature for the synthesis of tetraphenylchlorins (TPC) from *meso*-tetraphenylporphyrins (TPP) [4]. However, only a few reports in literature described the smooth conversion of chlorins into porphyrins [5]. The interconversion of chlorins into porphyrinoids is of great interest since it opens a new synthetic route to access a wide variety of nonviable  $\beta$ -functionalized porphyrinoids which exhibit distinguish photophysical and electrochemical redox properties [6].

$\beta$ -Functionalization *via* aromatic electrophilic substitutions including nitration, formylation, arylation, acylation and bromination etc. is a facile and important synthetic tool to obtain  $\beta$ -substituted macrocycles [7-9]. The above mentioned  $\beta$ -substituted porphyrins have also been used by synthetic chemists as starting compounds to build up extended porphyrins with enhanced optoelectronic properties [8,10]. Ruppert, Callot and others have effectively utilized *meso*-tetraarylporphyrins for the extension of  $\pi$ -conjugation by fusing *meso-ortho*-aryl groups with neighboring  $\beta$ -pyrroles by ketone functionalities, thus leading to oxo-naphthoporphyrins [10,11]. As chlorins have a reduced  $\beta$ -pyrrolic bond, hence chlorins based  $\pi$ -expansion or fusion is largely unexplored.

The ring fusion onto the porphyrin macrocyclic skeleton leads to the red-shifted absorption spectra extending to near infrared region (NIR) [12]. The fused porphyrinoids are attractive candidates for a variety of important biological and material applications due to their noteworthy optical and electronic properties [13,14]. In context to this, several pioneer research groups have shown their continuous interest to envision the fusion of *meso*-aryl group with peripheral  $\beta$ -

substituent, keeping in mind that the expected fused porphyrinoids products would be interesting to modulate the structural and photophysical properties of macrocycles [15,16]. Although  $\text{FeCl}_3$  and  $\text{Sc}(\text{OTf})_3$  have been frequently used for the oxidative ring fusion reactions whereas metal acetate catalyzed ring fusion is not reported in the literature. Nickel-mediated oxidation has attracted significant attention in organic synthesis [17]. Since nickel is more nucleophilic than palladium therefore favors the oxidative addition of a variety of electrophiles such as phenol derivatives and aryl halides [18]. Moreover, nickel shows multiple oxidation states where Ni(0) and Ni(II) species allow the fascinating transformations to access Ni(I), Ni(III), and sometimes even in Ni(IV) oxidation states [19] which renders feasible radical reaction pathways. However, the use of nickel metal for the oxidative ring fusion of chlorins to build up  $\pi$ -extending chromophores is completely unexplored.

**Chart 4.1** Molecular Structures of Synthesized Fused Porphyrins.

R	M	Name	Code	Yield%
	2H	$\text{H}_2\text{MFP}(\text{IND})$	<b>1</b>	83
	Co(II)	CoMFP(IND)	<b>1a</b>	82
H	Ni(II)	NiMFP(IND)	<b>1b</b>	61
	Cu(II)	CuMFP(IND)	<b>1c</b>	80
	Zn(II)	ZnMFP(IND)	<b>1d</b>	89
	2H	$\text{H}_2\text{MFP}(\text{IND})\text{Br}_2$	<b>2</b>	81
	Co(II)	CoMFP(IND) $\text{Br}_2$	<b>2a</b>	85
Br	Ni(II)	NiMFP(IND) $\text{Br}_2$	<b>2b</b>	59
	Cu(II)	CuMFP(IND) $\text{Br}_2$	<b>2c</b>	83
	Zn(II)	ZnMFP(IND) $\text{Br}_2$	<b>2d</b>	90
	2H	$\text{H}_2\text{MFP}(\text{IND})(\text{Ph})_2$	<b>3</b>	84
	Co(II)	CoMFP(IND)( $\text{Ph})_2$	<b>3a</b>	79
Ph	Ni(II)	NiMFP(IND)( $\text{Ph})_2$	<b>3b</b>	68
	Cu(II)	CuMFP(IND)( $\text{Ph})_2$	<b>3c</b>	86
	Zn(II)	ZnMFP(IND)( $\text{Ph})_2$	<b>3d</b>	84

Indane-1,3-dione derivatives have often been studied as important building blocks in organic synthesis due to their marvelous biological activities such as Pim-1 kinase inhibition, anti-

allergic activity, cytotoxicity, CDK inhibition, and EGFR inhibition [20]. Since indane-1,3-dione is a benzene-fused cyclopentane having two keto groups at 1,3 positions, its incorporation into porphyrinoids *via* carbon-carbon double bond exhibits interesting anion sensing abilities [21]. Despite the potential usefulness of such indanedione-based porphyrinoids in many fields, only a few examples have been reported till date [22]. We recently reported the synthesis of the indanedione-based *trans*-chlorins [6], which exhibited distinct UV-vis. and electrochemical properties. Herein, we are presenting the selective synthesis of indanedione monofused porphyrins *via* autoxidation of free base *trans*-chlorins using nickel acetate (Chart 1).

## 4.2 EXPERIMENTAL SECTION

### 4.2.1 Materials.

Pyrrrole and 1,3-indanedione were purchased from Alfa Aesar, UK and used as received. Phenylboronic acid was received from Sigma Aldrich. Benzaldehyde, N-bromosuccinimide,  $K_2CO_3$ , DDQ,  $TBAPF_6$ ,  $M(OAc)_2 \cdot nH_2O$ ,  $P_2O_5$  and  $CaH_2$  were purchased from HiMedia, India and used without further purification. Silica gel (100-200 mesh), dimethylformamide and dimethylsulphoxide purchased from Thomas Baker, India and used as received.  $CH_2Cl_2$  for CV analysis was distilled twice with  $P_2O_5$  and third time with  $CaH_2$ . NBS was recrystallized with hot water and  $TBAPF_6$  for CV analysis was recrystallized with hot ethanol and dried before use.

### 4.2.2 Instrumentation and Methods

Characterization techniques and instrumentation have been used same as described in Chapter 2. The single crystals of NiMFP(IND) (**1b**) and ZnMFP(IND)Ph<sub>2</sub> (**3d**) for XRD analysis were grown by vapor diffusion of methanol onto the conc.  $CHCl_3$  solutions of respective porphyrins, whereas the X-ray quality single crystals of pyridine coordinated ZnMFP(IND) (**1d**•Py) were obtained by vapor diffusion of methanol into the toluene solution of porphyrin with few drops of pyridine and single crystals of NiMFP(IND)Ph<sub>2</sub> (**3b**) were grown by vapor diffusion of hexane onto the concentrated solution of porphyrin in toluene.

### 4.2.3 General Procedure for the Synthesis of Ni(II) Monofused Porphyrins (NiMFPs)

200 mg of  $H_2TPC(IND)_2X_2$  ( $X = H, Br, \text{ and } Ph$ ) was dissolved in 45 ml of DMF. To this, 10 eq. of nickel(II) acetate tetrahydrate was added and the resulting reaction mixture was refluxed for 3-4 h. As the starting material was consumed (reaction monitored by UV-vis. and naked-eye), the

reaction mixture cooled to room temperature and ice cold water was added into it. The precipitate was filtered off through G<sub>4</sub> and the residue was dried in vacuum. The resulting crude porphyrin was purified by column chromatography using CHCl<sub>3</sub>/Hexane (6:4 v/v) to provide a red colored compound. The pure porphyrin was recrystallized by CHCl<sub>3</sub>/MeOH mixture.

**NiMFP(IND) (1b)**: Yield: 61% (110 mg, 0.13 mmol). UV/vis (CH<sub>2</sub>Cl<sub>2</sub>):  $\lambda_{\max}$ (nm) (log  $\epsilon$ ): 230(4.80), 435(5.30), 553(4.17), 592(3.97). <sup>1</sup>H NMR (400 MHz, CDCl<sub>3</sub>)  $\delta$  (ppm): 9.56(d, <sup>3</sup>J<sub>H,H</sub> = 4 Hz, 1H,  $\beta$ -H), 8.87(d, <sup>3</sup>J<sub>H,H</sub> = 4Hz, 1H,  $\beta$ -H), 8.65(d, <sup>3</sup>J<sub>H,H</sub> = 4Hz, 1H,  $\beta$ -H), 8.61-8.59(m, 2H,  $\beta$ -H), 8.50(d, <sup>3</sup>J<sub>H,H</sub> = 8Hz, 1H,  $\beta$ -H), 8.32-8.29(m, 2H,  $\beta$ -H & *meso*-Ph-H), 8.16(d, <sup>3</sup>J<sub>H,H</sub> = 8Hz, 2H, *meso*-Ph-H), 8.08-8.05(m, 2H,  $\beta$ -H & *meso*-Ph-H), 8.01(d, <sup>3</sup>J<sub>H,H</sub> = 4 Hz, 2H, *meso*-Ph-H), 7.97(d, <sup>3</sup>J<sub>H,H</sub> = 4 Hz 2H, *meso*-Ph-H), 7.87(d, <sup>3</sup>J<sub>H,H</sub> = 4 Hz, 2H, *meso*-Ph-H), 7.71-7.61(m, 8H, *meso*-Ph-H), 7.57(d, <sup>3</sup>J<sub>H,H</sub> = 4 Hz, 2H, IND-H), 7.30(t, <sup>3</sup>J<sub>H,H</sub> = 8 Hz, 1H, IND-H). 7.25(d, <sup>3</sup>J<sub>H,H</sub> = 8 Hz, 1H, IND-H). MALDI-TOF-MS (*m/z*): found 813.037 [M+H]<sup>+</sup>, calcd 813.180. Anal. Calcd for C<sub>53</sub>H<sub>30</sub>N<sub>4</sub>O<sub>2</sub>Ni C, 78.25; H, 3.72; N, 6.89. Found: C, 78.36; H, 3.69; N, 6.90.

**NiMFP(IND)Br<sub>2</sub> (2b)**: Yield: 59% (108 mg, 0.11 mmol). UV/vis (CH<sub>2</sub>Cl<sub>2</sub>):  $\lambda_{\max}$ (nm) (log  $\epsilon$ ): 229(4.74), 441(5.18), 563(4.05), 602(3.90). <sup>1</sup>H NMR (400 MHz, CDCl<sub>3</sub>)  $\delta$  (ppm): 9.41(d, <sup>3</sup>J<sub>H,H</sub> = 4 Hz, 1H,  $\beta$ -H), 8.91(d, <sup>3</sup>J<sub>H,H</sub> = 4Hz, 1H,  $\beta$ -H), 8.53(d, <sup>3</sup>J<sub>H,H</sub> = 4Hz, 1H,  $\beta$ -H), 8.40(d, <sup>3</sup>J<sub>H,H</sub> = 4Hz, 1H,  $\beta$ -H), 8.31-8.29(m, 2H,  $\beta$ -H & *meso*-Ph-H), 8.15(d, <sup>3</sup>J<sub>H,H</sub> = 8 Hz, 1H, *meso*-Ph-H), 8.12(s, 1H, *meso*-Ph-H), 8.08-8.06(m, 2H, *meso*-Ph-H), 7.82-7.76(m, 5H, *meso*-Ph-H), 7.65-7.56(m, 10H, *meso*-Ph-H & IND-H), 7.38-7.30(m, 2H, IND-H), 7.21(d, <sup>3</sup>J<sub>H,H</sub> = 8 Hz, 2H, IND-H). MALDI-TOF-MS (*m/z*): found 971.284 [M+H]<sup>+</sup>, calcd 971.316. Anal. Calcd for C<sub>53</sub>H<sub>28</sub>Br<sub>2</sub>N<sub>4</sub>O<sub>2</sub>Ni•0.5CH<sub>3</sub>OH C, 65.08; H, 3.06; N, 5.67. Found: C, 64.98; H, 3.08; N, 5.69.

**NiMFP(IND)Ph<sub>2</sub> (3b)**: Yield: 68% (125 mg, 0.129 mmol). UV/vis (CH<sub>2</sub>Cl<sub>2</sub>):  $\lambda_{\max}$ (nm) (log  $\epsilon$ ): 229(4.81), 443(5.26), 562(4.17), 604(3.97). <sup>1</sup>H NMR (400 MHz, CDCl<sub>3</sub>)  $\delta$  (ppm): 9.36(d, <sup>3</sup>J<sub>H,H</sub> = 4 Hz, 1H,  $\beta$ -H), 8.50(d, <sup>3</sup>J<sub>H,H</sub> = 4Hz, 1H,  $\beta$ -H), 8.36-8.31(m, 3H,  $\beta$ -H), 8.19-8.14(m, 2H, *meso*-Ph-H), 8.12(s, 1H, *meso*-Ph-H), 8.08-8.06(m, 2H, *meso*-Ph-H), 7.84(d, <sup>3</sup>J<sub>H,H</sub> = 8 Hz, 2H, *meso*-Ph-H), 7.61(t, <sup>3</sup>J<sub>H,H</sub> = 8 Hz, 1H, *meso*-Ph-H), 7.55(d, <sup>3</sup>J<sub>H,H</sub> = 4 Hz, 3H, *meso*-Ph-H), 7.42(dd, <sup>3</sup>J<sub>H,H</sub> = 8 Hz, 20 Hz, 4H, *meso*-Ph-H), 7.29(t, <sup>3</sup>J<sub>H,H</sub> = 8 Hz, 1H, *meso*-Ph-H), 7.20(dd, <sup>3</sup>J<sub>H,H</sub> = 8 Hz, 12 Hz, 2H, *meso*-Ph-H), 7.12-7.00(m, 5H, *meso*-Ph-H & IND-H), 6.93-6.79(m, 10H,  $\beta$ -Ph-H). MALDI-TOF-MS (*m/z*): found 965.181 [M+H]<sup>+</sup>, calcd 965.242. Anal. Calcd for C<sub>65</sub>H<sub>38</sub>N<sub>4</sub>O<sub>2</sub>Ni C, 80.84; H, 3.97; N, 5.80. Found: C, 80.36; H, 4.00; N, 5.79.

#### 4.2.4 Synthesis of Free Base Monofused Porphyrins (H<sub>2</sub>MFPs)

110 mg of NiMFP(IND)X<sub>2</sub> (X =H, Br, and Ph) was dissolved in minimum amount of CHCl<sub>3</sub>. To this, 0.6 ml of conc. H<sub>2</sub>SO<sub>4</sub> was added dropwise and stirred for 15 minutes at 0 °C. Once the Ni(II) porphyrin got demetallated, it settled down to the bottom of RB flask. The excess of acid was quenched by adding 20% NH<sub>4</sub>OH solution (15 ml) and the organic layer was washed twice with water. The organic layer was separated with CHCl<sub>3</sub>, dried over anhydrous Na<sub>2</sub>SO<sub>4</sub> and evaporated to dryness by rotary evaporation. The crude product was purified by column chromatography using CHCl<sub>3</sub> as eluent. The pure product was recrystallized with CHCl<sub>3</sub>/MeOH mixture.

**H<sub>2</sub>MFP(IND) (1):** Yield: 83% (85 mg, 0.11 mmol). UV/vis (CH<sub>2</sub>Cl<sub>2</sub>): λ<sub>max</sub>(nm) (log ε): 228(4.69), 435(5.49), 503(3.70), 537(4.05), 579(4.33), 615(3.69), 672(3.98). <sup>1</sup>H NMR (400 MHz, CDCl<sub>3</sub>) δ (ppm): 9.76(d, <sup>3</sup>J<sub>H,H</sub> = 4 Hz, 1H, β-H), 8.94(d, <sup>3</sup>J<sub>H,H</sub> = 4 Hz, 1H, β-H), 8.75(d, <sup>3</sup>J<sub>H,H</sub> = 4 Hz, 1H, β-H), 8.67(t, <sup>3</sup>J<sub>H,H</sub> = 4 Hz, 3H, β-H), 8.60(d, <sup>3</sup>J<sub>H,H</sub> = 8 Hz, 1H, β-H), 8.24-8.15(m, 7H, meso-Ph-H), 8.07-8.00(m, 4H, meso-Ph-H), 7.78-7.69(m, 8H, meso-Ph-H), 7.65(d, <sup>3</sup>J<sub>H,H</sub> = 4 Hz, 2H, IND-H), 7.38(d, <sup>3</sup>J<sub>H,H</sub> = 4 Hz, 2H, IND-H). MALDI-TOF-MS (*m/z*): found 757.259 [M+H]<sup>+</sup>, calcd 757.260. Anal. Calcd for C<sub>53</sub>H<sub>32</sub>N<sub>4</sub>O<sub>2</sub> C, 84.11; H, 4.26; N, 7.40. Found: C, 84.76; H, 4.09; N, 7.39.

**H<sub>2</sub>MFP(IND)Br<sub>2</sub> (2):** Yield: 81% (84 mg, 0.09 mmol). UV/vis (CH<sub>2</sub>Cl<sub>2</sub>): λ<sub>max</sub>(nm) (log ε): 229(4.73), 444(5.43), 542(4.12), 585(4.13), 622(3.66), 682(4.02). <sup>1</sup>H NMR (400 MHz, CDCl<sub>3</sub>) δ (ppm): 9.68(d, <sup>3</sup>J<sub>H,H</sub> = 4 Hz, 1H, β-H), 8.92(d, <sup>3</sup>J<sub>H,H</sub> = 8 Hz, 1H, β-H), 8.68-8.59(m, 3H, β-H), 8.29-8.25(m, 2H, meso-Ph-H), 8.14-8.00(m, 9H, meso-Ph-H), 7.80-7.61(m, 10H, meso-Ph-H & IND-H), 7.42-7.35(m, 2H, IND-H), 1.85(d, 2H, -NH). MALDI-TOF-MS (*m/z*): found 914.550 [M]<sup>+</sup>, calcd 914.639. Anal. Calcd for C<sub>53</sub>H<sub>30</sub>N<sub>4</sub>O<sub>2</sub>Br<sub>2</sub>.CHCl<sub>3</sub> C, 62.72; H, 3.02; N, 5.42. Found: C, 62.80; H, 3.98; N, 5.50.

**H<sub>2</sub>MFP(IND)Ph<sub>2</sub> (3):** Yield: 84% (87 mg, 0.10 mmol). UV/vis (CH<sub>2</sub>Cl<sub>2</sub>): λ<sub>max</sub>(nm) (log ε): 229(4.77), 444(5.40), 542(4.12), 583(4.18), 618(3.77), 682(3.93). <sup>1</sup>H NMR (400 MHz, CDCl<sub>3</sub>) δ (ppm): 9.57(d, <sup>3</sup>J<sub>H,H</sub> = 4 Hz, 1H, β-H), 8.63(d, <sup>3</sup>J<sub>H,H</sub> = 8 Hz, 2H, β-H), 8.53(d, <sup>3</sup>J<sub>H,H</sub> = 4 Hz, 1H, β-H), 8.44(d, <sup>3</sup>J<sub>H,H</sub> = 4 Hz, 1H, β-H), 8.30(dd, <sup>3</sup>J<sub>H,H</sub> = 4 Hz, 8 Hz, 2H, meso-Ph-H), 8.16(s, 1H, meso-Ph-H), 8.08-8.02(m, 4H, meso-Ph-H), 8.78-8.62(m, 8H, meso-Ph-H), 7.40-7.29(m, 3H, meso-Ph-H), 7.23-7.14(m, 5H, meso-Ph-H & IND-H), 6.96-6.77(m, 10H, β-Ph-H), -1.54(s, 2H, -



NH). MALDI-TOF-MS ( $m/z$ ): found 910.364  $[M+H]^+$ , calcd 910.046. Anal. Calcd for  $C_{65}H_{40}N_4O_2$  C, 85.88; H, 4.44; N, 6.16. Found: C, 85.02; H, 4.01; N, 6.14.

#### 4.2.5 General Procedure for the Synthesis of Metal Complexes of Monofused Porphyrins [(M(II)MFPs) (M = Co(II), Cu(II), and Zn(II))]

25 mg of  $H_2MFP(IND)X_2$  (X = H, Br, and Ph) was dissolved in 15 ml of  $CHCl_3$ . To this, 10 equivalents of  $M(OAc)_2 \cdot nH_2O$  in 2 ml of  $CH_3OH$  was added and the reaction mixture was refluxed for 25-40 min. The resulting reaction mixture was washed with water to remove excess of metal acetate and the organic layer was separated, dried over anhydrous  $Na_2SO_4$  and evaporated to dryness. The crude porphyrin was purified by column chromatography using  $CHCl_3$  as eluent. The purified compound was recrystallized with  $CHCl_3/MeOH$  mixture.

**CoMFP(IND) (1a)**: Yield: 82% (22 mg, 0.027 mmol). UV/vis ( $CH_2Cl_2$ ):  $\lambda_{max}(nm)$  ( $\log \epsilon$ ): 229(4.69), 429(5.18), 556(3.99), 596(3.84). MALDI-TOF-MS ( $m/z$ ): found 814.284  $[M+H]^+$ , calcd 814.177, found 890.499  $[M]^+ + THF + 0.5H_2O$ , calcd 890.202. Anal. Calcd for  $C_{53}H_{30}N_4O_2Co$  C, 78.23; H, 3.72; N, 6.88. Found: C, 78.31; H, 3.71; N, 6.58. **CuMFP(IND) (1c)**: Yield: 80% (21 mg, 0.025 mmol). UV/vis ( $CH_2Cl_2$ ):  $\lambda_{max}(nm)$  ( $\log \epsilon$ ): 230(4.83), 434(5.52), 563(4.23), 605(4.16). MALDI-TOF-MS ( $m/z$ ): found 818.233  $[M+H]^+$ , calcd 818.174. Anal. Calcd for  $C_{53}H_{30}N_4O_2Cu$  C, 77.78; H, 3.69; N, 6.85. Found: C, 77.81; H, 3.72; N, 6.82. **ZnMFP(IND) (1d)**: Yield: 89% (24 mg, 0.029 mmol). UV/vis ( $CH_2Cl_2$ ):  $\lambda_{max}(nm)$  ( $\log \epsilon$ ): 228(4.72), 437(5.68), 570(4.22), 616(4.24).  $^1H$  NMR (400 MHz,  $CDCl_3$ )  $\delta$  (ppm): 9.79(d,  $^3J_{H,H} = 4$  Hz, 1H,  $\beta$ -H), 8.98(d,  $^3J_{H,H} = 8$  Hz, 1H,  $\beta$ -H), 8.85(s, 2H,  $\beta$ -H), 8.79(d,  $^3J_{H,H} = 8$  Hz, 1H,  $\beta$ -H), 8.73(d,  $^3J_{H,H} = 8$  Hz, 1H,  $\beta$ -H), 8.67(d,  $^3J_{H,H} = 8$  Hz, 1H,  $\beta$ -H), 8.37(s, 1H, *meso*-Ph-H), 8.29(dd,  $^3J_{H,H} = 4$  Hz, 8 Hz, 2H, *meso*-Ph-H), 8.24(dd,  $^3J_{H,H} = 4$  Hz, 8 Hz, 2H, *meso*-Ph-H), 8.18(d,  $^3J_{H,H} = 8$  Hz, 2H, *meso*-Ph-H), 8.09-8.05(m, 4H, *meso*-Ph-H), 7.80-7.72(m, 8H, *meso*-Ph-H), 7.70-7.64(m, 2H, IND-H), 7.37(d,  $^3J_{H,H} = 4$  Hz, 2H, IND-H). MALDI-TOF-MS ( $m/z$ ): found 821.048  $[M+H]^+$ , calcd 821.218. Anal. Calcd for  $C_{53}H_{30}N_4O_2Zn$  C, 77.61; H, 3.69; N, 6.83. Found: C, 77.07; H, 3.72; N, 6.90.

**CoMFP(IND)Br<sub>2</sub> (2a)**: Yield: 85% (23 mg, 0.023 mmol). UV/vis ( $CH_2Cl_2$ ):  $\lambda_{max}(nm)$  ( $\log \epsilon$ ): 229(4.79), 434(5.20), 566(4.05), 606(3.93). MALDI-TOF-MS ( $m/z$ ): found 971.056  $[M]^+$ , calcd 971.556, found 1048.159  $[M]^+ + THF + 0.5H_2O$ , calcd 1048.638. Anal. Calcd for  $C_{53}H_{28}N_4O_2Br_2Co \cdot 0.5CHCl_3$  C, 62.31; H, 2.79; N, 5.43. Found: C, 62.30; H, 2.60; N, 5.50.



**CuMFP(IND)Br<sub>2</sub> (2c)**: Yield: 83% (22 mg, 0.023 mmol). UV/vis (CH<sub>2</sub>Cl<sub>2</sub>):  $\lambda_{\max}$ (nm) (log  $\epsilon$ ): 229(4.83), 440(5.46), 570(4.16), 612(4.08). MALDI-TOF-MS ( $m/z$ ): found 973.796 [M+H]<sup>+</sup>, calcd 973.995. Anal. Calcd for C<sub>53</sub>H<sub>28</sub>N<sub>4</sub>O<sub>2</sub>Br<sub>2</sub>Cu C, 65.21; H, 2.89; N, 5.74. Found: C, 65.46; H, 2.84; N, 5.70. **ZnMFP(IND)Br<sub>2</sub> (2d)**: Yield: 90% (24 mg, 0.024 mmol). UV/vis (CH<sub>2</sub>Cl<sub>2</sub>):  $\lambda_{\max}$ (nm) (log  $\epsilon$ ): 228(4.78), 443(5.57), 575(4.23), 622(4.21). <sup>1</sup>H NMR (400 MHz, CDCl<sub>3</sub>)  $\delta$  (ppm): 9.67(d, <sup>3</sup>J<sub>H,H</sub> = 4 Hz, 1H,  $\beta$ -H), 8.87(d, <sup>3</sup>J<sub>H,H</sub> = 4 Hz, 1H,  $\beta$ -H), 8.65-8.60(m, 3H,  $\beta$ -H), 8.31-8.27(m, 3H, *meso*-Ph-H), 8.09-8.00(m, 8H, *meso*-Ph-H), 7.79-7.61(m, 10H, *meso*-Ph-H & IND-H), 7.39-7.33(m, 2H, IND-H). MALDI-TOF-MS ( $m/z$ ): found 978.598 [M]<sup>+</sup>, calcd 978.003. Anal. Calcd for C<sub>53</sub>H<sub>28</sub>N<sub>4</sub>O<sub>2</sub>Br<sub>2</sub>Zn•0.5 CH<sub>3</sub>OH C, 64.64; H, 3.04; N, 5.64. Found: C, 64.32; H, 3.20; N, 5.79.

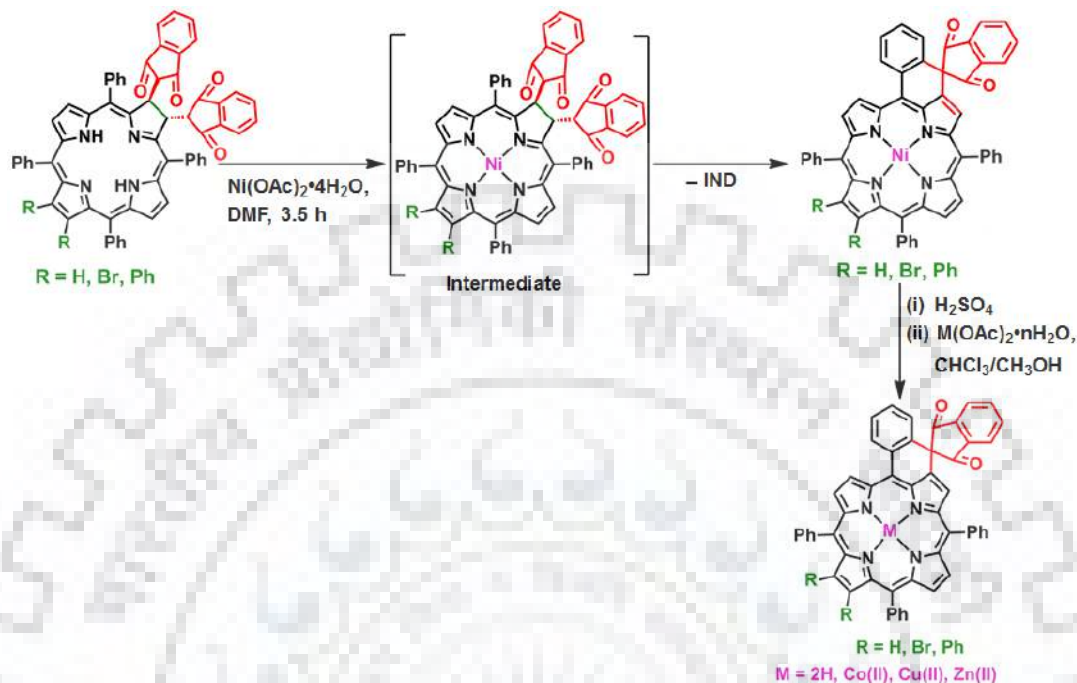
**CoMFP(IND)Ph<sub>2</sub> (3a)**: Yield: 79% (21 mg, 0.022 mmol). UV/vis (CH<sub>2</sub>Cl<sub>2</sub>):  $\lambda_{\max}$ (nm) (log  $\epsilon$ ): 229(4.72), 435(5.11), 567(3.97), 610(3.79). MALDI-TOF-MS ( $m/z$ ): found 966.238 [M+H]<sup>+</sup>, calcd 966.20. Anal. Calcd for C<sub>65</sub>H<sub>38</sub>N<sub>4</sub>O<sub>2</sub>Co C, 80.82; H, 3.97; N, 5.80. Found: C, 81.00; H, 4.01; N, 5.76. **CuMFP(IND)Ph<sub>2</sub> (3c)**: Yield: 86% (23 mg, 0.024 mmol). UV/vis (CH<sub>2</sub>Cl<sub>2</sub>):  $\lambda_{\max}$ (nm) (log  $\epsilon$ ): 229(4.85), 441(5.45), 570(4.22), 611(4.07). MALDI-TOF-MS ( $m/z$ ): found 970.375 [M+H]<sup>+</sup>, calcd 970.236. Anal. Calcd for C<sub>65</sub>H<sub>38</sub>N<sub>4</sub>O<sub>2</sub>Cu•CH<sub>3</sub>OH C, 79.74; H, 4.09; N, 5.68. Found: C, 79.70; H, 4.13; N, 5.64. **ZnMFP(IND)Ph<sub>2</sub> (3d)**: Yield: 84% (22 mg, 0.023 mmol). UV/vis (CH<sub>2</sub>Cl<sub>2</sub>):  $\lambda_{\max}$ (nm) (log  $\epsilon$ ): 229(4.72), 444(5.40), 578(4.10), 621(4.07). <sup>1</sup>H NMR (400 MHz, CDCl<sub>3</sub>)  $\delta$  (ppm): 9.68(d, <sup>3</sup>J<sub>H,H</sub> = 4 Hz, 1H,  $\beta$ -H), 8.66-8.61(m, 3H,  $\beta$ -H), 8.47(d, <sup>3</sup>J<sub>H,H</sub> = 8 Hz, 1H,  $\beta$ -H), 8.34-8.30(m, 3H, *meso*-Ph-H), 8.09-8.05(m, 4H, *meso*-Ph-H), 7.74(d, <sup>3</sup>J<sub>H,H</sub> = 8 Hz, 5H, *meso*-Ph-H), 7.67-7.61(m, 3H, *meso*-Ph-H), 7.36(d, <sup>3</sup>J<sub>H,H</sub> = 8 Hz, 2H, *meso*-Ph-H), 7.19-7.12(m, 6H, (d, <sup>3</sup>J<sub>H,H</sub> = 8 Hz, 5H, *meso*-Ph-H & IND-H), 7.02-6.97(m, 4H,  $\beta$ -Ph-H), 6.90-6.84(m, 6H,  $\beta$ -Ph-H). MALDI-TOF-MS ( $m/z$ ): found 971.309 [M+H]<sup>+</sup>, calcd 971.236. Anal. Calcd for C<sub>65</sub>H<sub>38</sub>N<sub>4</sub>O<sub>2</sub>Zn C, 80.29; H, 3.94; N, 5.76. Found: C, 80.31; H, 3.91; N, 5.80.

## 4.3 RESULTS AND DISCUSSION

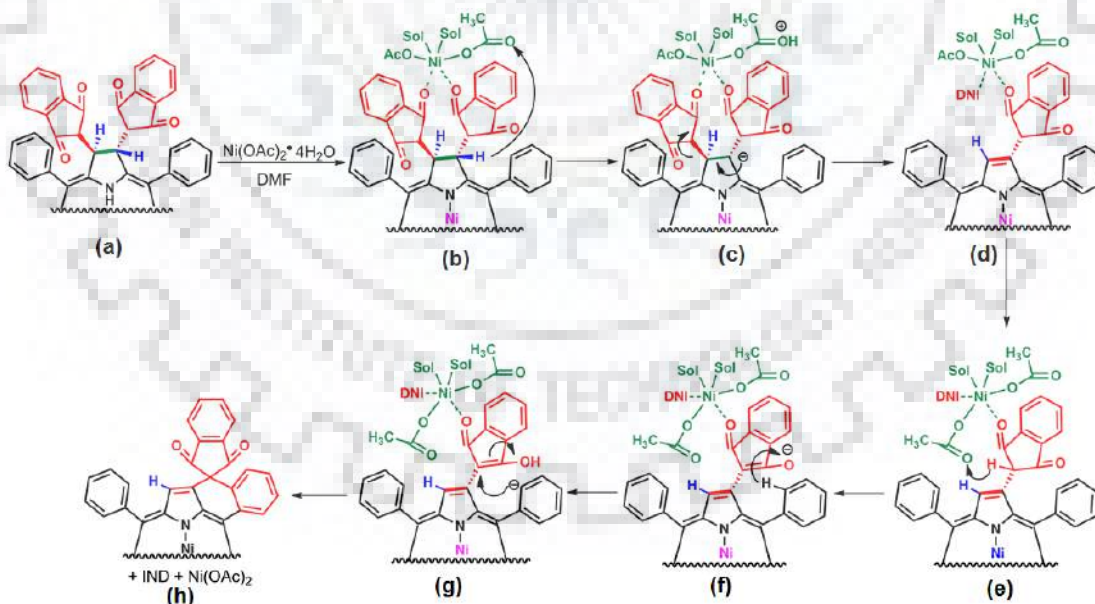
### 4.3.1 Synthesis and Characterization

The precursors free base *trans*-chlorins H<sub>2</sub>TPC(R)<sub>2</sub> (where R = H, Br, and Ph) were synthesized in good yields by Michal addition reaction of indane-1,3-dione with H<sub>2</sub>TPP(NO<sub>2</sub>) using same procedure as described in Chapter-2. Treatment of free base *trans*-chlorins with 10 eq. of nickel acetate in dimethylformamide at refluxing temperature for 15-20 minutes led to the conversion

of pink-colored starting material  $\text{H}_2\text{TPC}(\text{IND})_2\text{R}_2$  ( $\text{R} = \text{H}, \text{Br}, \text{and Ph}$ ) into dark green nickel metallated *trans*-chlorins  $\text{NiTPC}(\text{IND})_2\text{R}_2$  (where  $\text{R} = \text{H}, \text{Br}, \text{and Ph}$ ).



**Scheme 4.1** Synthetic Route to  $\text{M(II)MFP(IND)R}_2$  (where  $\text{M(II)} = 2\text{H}, \text{Co(II)}, \text{Ni(II)}, \text{Cu(II)}, \text{Zn(II)}$  and  $\text{X} = \text{H}, \text{Br}, \text{and Ph}$ ).



**Scheme 4.2** The plausible Mechanistic Pathway for Monofused Porphyrins.

The prolonged heating (3-4 h) of resulting reaction mixture converted the dark green colored Ni-*trans*-chlorins into monofused porphyrins (Scheme 4.1). *In situ* formation of intermediate

Ni(II)-*trans*-chlorins was also confirmed by TLC as well as UV-vis. spectroscopy which showed a typical metallochlorin type spectrum with one Soret and one enhanced Q band. The reaction has been performed for three free base *trans*-chlorins which proved that a number of  $\beta$ -substituted chlorins can be used to access various  $\beta$ -substituted monofused porphyrins. Ni(II)-monofused porphyrins were demetallated and remetallated with different metals such as Co(II), Ni(II), Cu(II), and Zn(II) in order to obtain different metal derivatives.

A reasonable mechanistic model for oxidative fusion of planar free base *trans*-chlorins into monofused Ni(II) porphyrins is shown in Scheme 4.2. Sol represents a solvent molecule. One equivalent of added nickel acetate to (a) was used for core metallation to form Ni(II) *trans*-chlorin (b) as an intermediate, while the remaining amount coordinated outside with keto groups of two indanedione moiety at the periphery of macrocycle. Nickel insertion to the macrocyclic core made the reduced  $\beta$ -pyrrolic hydrogens more acidic. Now, it is of course possible that the acetate attached to nickel atom can abstract the acidic  $\beta$ -pyrrolic proton as shown in (c) which further facilitate the oxidation of reduced  $\beta$ -pyrrolic position and promote the dissociation of one indanedione group from the porphyrin periphery (d). On the other hand, formulation of process as IND dissociation would imply that (d) is a complex of Ni(II) porphyrin having one another acidic proton i.e.  $\alpha$ -proton of indanedione moiety. Now, the second acetate molecule attached to nickel metal again abstracted the notified proton as shown in (e) which resulted into the formation of enolate anion (f). This enolate anion promotes the CH activation of the neighboring *ortho*-phenyl position (g) which resulted into the formation of a six membered fused ring (h). At the end, after fusion of  $\beta$ -pyrrolic position with *ortho*-phenyl group through indanedione functionalities, the nickel metal which was chelating with one indanedione group and periphery of the fused Ni(II)-porphyrin has cleaved out. After completion of the reaction, the fused porphyrin was precipitated by adding distilled water to the reaction mixture and the dissociation of one indanedione group was further monitored by color of filtrate which was yellowish brown in color. Overall, the transformation of the macrocyclic core highlights again the enormous influence which central nickel ion possess on the conformation of these porphyrinoids.

All the synthesized mono ring-fused porphyrins have been characterized *via* UV-vis, fluorescence,  $^1\text{H}$  NMR spectroscopic techniques, MALDI-TOF mass spectrometry, elemental analysis and single crystal X-ray analysis.

### 4.3.2 $^1\text{H}$ NMR and Mass Spectrometric Studies

$^1\text{H}$  NMR spectra of fused porphyrins  $\text{M}^{\text{II}}\text{MFP}(\text{IND})\text{R}_2$  (where  $\text{M}^{\text{II}} = 2\text{H}, \text{Ni}, \text{Zn}$  and  $\text{R} = \text{H}, \text{Br}$  and  $\text{Ph}$ ) were recorded in  $\text{CDCl}_3$ . Figures 4.1 and A1-A5 in Appendix-III have shown the  $^1\text{H}$  NMR spectra of synthesized free base and Ni(II) complexes of fused porphyrins. The fused porphyrins shown readily distinguish proton NMR spectra as compared to their precursors (Figure 4.2).  $^1\text{H}$  NMR spectrum of NiMFP(IND) clearly showed that the proton corresponding to reduced  $\beta$ -pyrrolic position as well as  $-\text{CH}$  of indanedione moiety were disappeared upon fusion. The diagnostic shifts and pattern for the presence of a  $\beta$ -to-*ortho*-phenyl linkage became evident as the presence of one singlet for one proton intensity beyond 9.5 ppm corresponding to  $\beta$ -proton neighboring to fused unit was observed. The inner core  $-\text{NH}$ s of  $\beta$ -to-*ortho*-phenyl fused systems usually resonate at very downfield region sometimes even in positive region also but the inner core  $-\text{NH}$ s of the synthesized free base monofused porphyrins, although they behaved like fused systems since they have shown much downfield shifted  $-\text{NH}$  as compared to the mono-substituted unfused porphyrins whereas upfield shifted as compared to their precursors (free base *trans*-chlorins). The inner core  $\text{NH}$ s of the synthesized free base MFPs were highly upfield shifted as compared to the corresponding free base difused porphyrins (DFPs) indicated the less twisted nature of the fused unit. The effect of antipodal  $\beta$ -substituent to the fused unit was also clearly evidenced by inner core  $\text{NH}$ s as well as  $\beta$ -substituted proton signals.

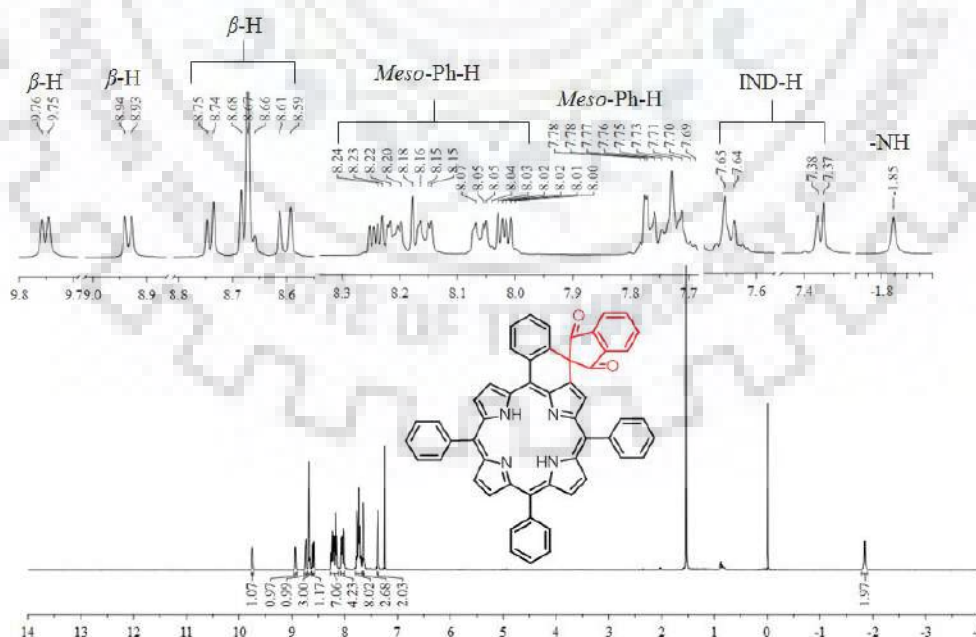


**Figure 4.1**  $^1\text{H}$  NMR Spectrum of  $\text{H}_2\text{MFP}(\text{IND})$  (**1**) in  $\text{CDCl}_3$ .



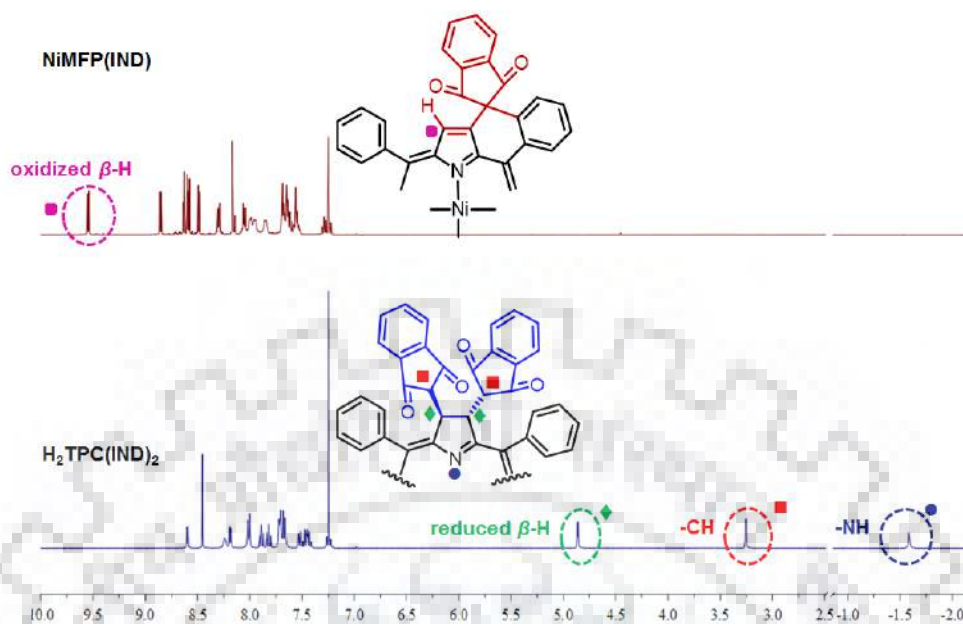


**Figure 4.2** Comparative  $^1\text{H}$  NMR Spectra of Precursor  $\text{H}_2\text{TPC(IND)}_2$  and Ni(II) Monofused Porphyrin Ni(II)MFP(IND).

The MALDI-TOF-Mass spectra of all synthesized porphyrins have been recorded in positive ion mode. Figures 4.3 and A6-A10 in the Appendix-III show the MALDI-TOF-MS spectra synthesized free base fused porphyrins and their corresponding Ni(II) complexes. The observed mass values were exactly matching with the calculated mass values of proposed structures.

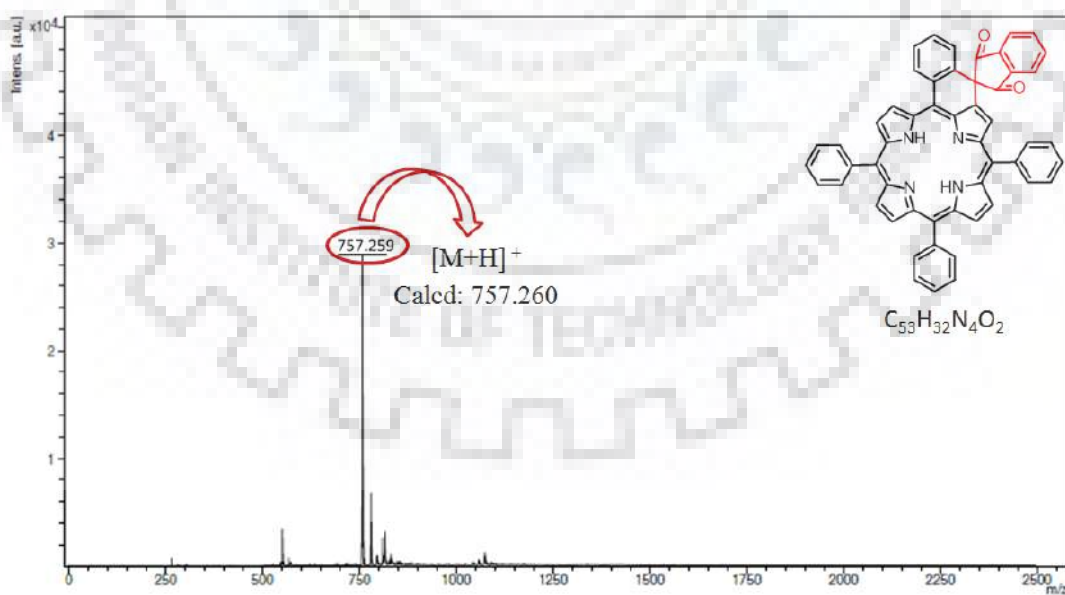


**Figure 4.3** MALDI-TOF-MS Spectrum of  $\text{H}_2\text{MFP(IND)}$  (1) in  $\text{CH}_2\text{Cl}_2$ .

### 4.3.3 X-Ray Crystal Structure Discussion

We were able to grow the crystals of Ni(II) and Zn(II) complex of monofused porphyrins suitable for X-ray diffraction analysis. The crystal structure of NiMFP(IND) (**1b**), ZnMFP(IND)•Py (**1d**•Py), NiMFP(IND)Ph<sub>2</sub> (**3b**) and ZnMFP(IND)Ph<sub>2</sub> (**3d**) have been analyzed which revealed that these compounds were monofused and slightly twisted at the fused side from the macrocyclic core. The twist angles were found to be in the range from 20.97- 27.97° in all crystallized compounds which were found to be lower as compared to the difused systems (Chapter 3). The twist angles were calculated as the dihedral angle between the plane defined by fused moiety and rest of the macrocyclic core, keeping core 24 atoms in one plane and fused pyrrole and phenyl ring in another plane. Table 4.1 lists the crystallographic data for all crystallized compounds whereas Table 4.2 summarizes the selected average bond lengths and bond angles of crystallized compounds.

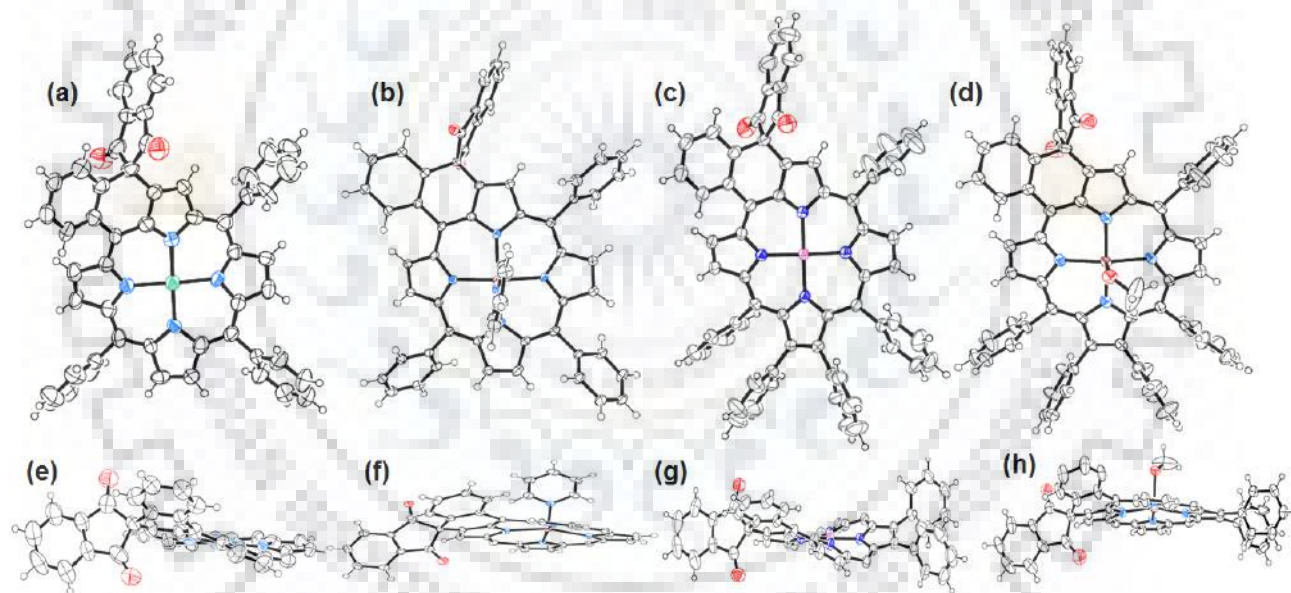


**Figure 4.4** ORTEP Showing Top and Side Views of (a and e) NiMFP(IND) (**1b**); (b and f) ZnMFP(IND)•Py (**1d**•Py); (c and g) NiMFP(IND)Ph<sub>2</sub> (**3b**), and (d and h) ZnMFP(IND)Ph<sub>2</sub>•OCH<sub>3</sub> (**3d**•OCH<sub>3</sub>). Phenyl Rings in the Side Views are Omitted for Clarity.

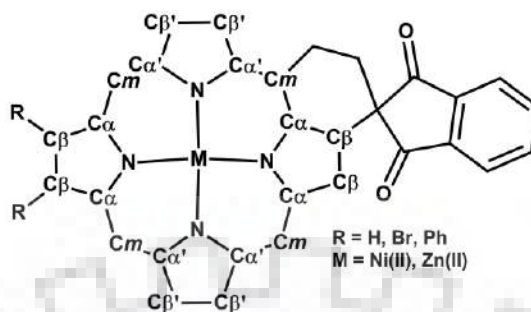
The NiMFP(IND)R<sub>2</sub> (where R = H and Ph) were best described as typically *ruffled* as the Ni(II) ion and four nitrogens of pyrrole units were coplanar whereas two opposite *meso*-positions were present above the mean plane and rest of the two opposite *meso*-positions were placed down to the mean plane. The four Ni-N distances were almost equal ~1.95Å and ~1.90Å in NiMFP(IND)



and NiMFP(IND)Ph<sub>2</sub>, respectively and found to be shorter as compared to Zn-N bond distances in ZnMFPs.

**Table 4.1** Crystal Structure Data of NiMFP(IND) (**1b**), ZnMFP(IND) (**1d**), NiMFP(IND)Ph<sub>2</sub> (**3b**), and ZnMFP(IND)Ph<sub>2</sub> (**3d**).

	NiMFP(IND) ( <b>1b</b> )	ZnMFP(IND) ( <b>1d</b> )	ZnMFP(IND)Ph <sub>2</sub> ( <b>3d</b> )	NiMFP(IND)Ph <sub>2</sub> ( <b>3b</b> )
Empirical formula	C <sub>53</sub> H <sub>30</sub> N <sub>4</sub> NiO <sub>2</sub>	C <sub>58</sub> H <sub>35</sub> N <sub>5</sub> O <sub>2</sub> Zn •C <sub>5</sub> H <sub>5</sub> N	C <sub>65</sub> H <sub>38</sub> N <sub>4</sub> O <sub>2</sub> Zn •OCH <sub>3</sub>	C <sub>66</sub> H <sub>46</sub> N <sub>6</sub> O <sub>6</sub> Ni
Formula wt.	813.50	899.30	1031.43	1077.80
Crystal system	Triclinic	Triclinic	Triclinic	Triclinic
Space group	p-1	p-1	p-1	p-1
<i>a</i> (Å)	11.0202(9)	11.065(5)	11.8710(6)	12.0880(17)
<i>b</i> (Å)	18.4611(16)	14.753(5)	19.5636(10)	13.6580(19)
<i>c</i> (Å)	19.1532(17)	15.304(5)	24.3010(13)	19.910(3)
<i>α</i> (°)	74.227(6)	70.142(5)	113.431(1)	109.874(5)
<i>β</i> (°)	90	81.754(5)	90.042(1)	102.908(5)
<i>γ</i> (°)	90	72.187(5)	90.074(2)	92.300(6)
Volume (Å <sup>3</sup> )	3749.9(6)	2234.9(15)	5178.3(5)	2989.0(7)
Z	2	2	4	2
D <sub>calcd.</sub> (mg/m <sup>3</sup> )	1.441	1.336	1.323	1.198
<i>λ</i> (Å)	0.71073	0.71073	0.71073	0.71073
T (K)	293 K	293 K	293 K	293 K
No. of total reflns.	18141	11048	25565	12275
No. of indepnt. reflns.	4439	7223	12966	8125
R	0.0848	0.0867	0.0983	0.0615
Rw	0.3355	0.3073	0.3213	0.1707
GOOF	0.893	1.069	1.033	0.956
CCDC	<b>1830106</b>	<b>1830108</b>	<b>1830109</b>	<b>1830107</b>

**Table 4.2** Selected Average Bond Lengths and Bond Angles.

	ZnMFP(IND)	NiMFP(IND)	ZnMFP(IND)Ph <sub>2</sub>	NiMFP(IND)Ph <sub>2</sub>
M -N	2.07(4)	1.93(8)	2.08(6)	1.91(2)
M -N'	2.09(5)	1.96(7)	2.04(4)	1.90(2)
N -C <sub>α</sub>	1.37(8)	1.39(1)	1.37(8)	1.38(4)
N' -C <sub>α</sub>	1.37(7)	1.39(1)	1.38(8)	1.38(4)
C <sub>α</sub> -C <sub>β</sub>	1.44(8)	1.43(1)	1.45(7)	1.44(3)
C <sub>α</sub> ' -C <sub>β</sub> '	1.45(9)	1.44(1)	1.44(7)	1.44(5)
C <sub>β</sub> ' -C <sub>β</sub>	1.36(8)	1.34(1)	1.35(8)	1.36(4)
C <sub>β</sub> ' -C <sub>β</sub> '	1.36(8)	1.34(2)	1.34(1)	1.34(4)
C <sub>α</sub> -C <sub>m</sub>	1.41(9)	1.40(1)	1.41(8)	1.40(4)
C <sub>α</sub> ' -C <sub>m</sub> '	1.40(9)	1.38(2)	1.40(8)	1.39(3)
$\Delta C_{\beta}$ <sup>a</sup>	<b>0.260</b>	<b>0.258</b>	<b>0.106</b>	<b>0.280</b>
$\Delta 24$ <sup>b</sup>	<b>0.127</b>	<b>0.230</b>	<b>0.083</b>	<b>0.362</b>
$\Delta M$	<b>0.486</b>	<b>0.017</b>	<b>0.401</b>	<b>0.036</b>
<b>Bond Angles (°)</b>				
N - M -N	160.80(2)	178.07(3)	163.05(2)	179.80(1)
N' -M -N'	158.82(2)	176.82(3)	163.73(2)	178.60(1)
M -N -C <sub>α</sub>	126.47(4)	127.79(5)	126.54(4)	127.00(2)
M -N' -C <sub>α</sub> '	125.63(4)	127.08(5)	126.66(4)	126.75(2)
N -C <sub>α</sub> -C <sub>m</sub>	125.85(5)	125.12(8)	125.32(6)	123.95(2)
N' -C <sub>α</sub> ' -C <sub>m</sub> '	125.86(5)	125.55(9)	126.23(5)	124.80(2)
N -C <sub>α</sub> -C <sub>β</sub>	109.80(5)	110.50(8)	109.74(5)	110.18(2)
N' -C <sub>α</sub> ' -C <sub>β</sub> '	109.19(5)	109.34(9)	109.34(5)	109.33(2)
C <sub>β</sub> -C <sub>α</sub> -C <sub>m</sub>	124.29(6)	124.12(9)	124.93(6)	125.18(2)
C <sub>β</sub> ' -C <sub>α</sub> ' -C <sub>m</sub> '	124.60(6)	124.90(9)	124.40(6)	125.37(3)
C <sub>α</sub> -C <sub>β</sub> -C <sub>β</sub>	107.00(6)	107.39(9)	106.87(6)	110.18(2)
C <sub>α</sub> ' -C <sub>β</sub> ' -C <sub>β</sub> '	107.01(5)	107.66(9)	107.45(6)	107.53(3)
C <sub>α</sub> -N -C <sub>α</sub>	106.44(5)	104.18(7)	106.75(5)	105.85(2)
C <sub>α</sub> ' -N' -C <sub>α</sub> '	107.09(5)	105.73(8)	106.41(5)	106.25(2)
C <sub>α</sub> -C <sub>m</sub> -C <sub>α</sub>	124.57(5)	121.89(9)	124.69(6)	120.90(3)

<sup>a</sup> $\Delta C_{\beta}$  = mean plane deviation of  $\beta$ -pyrrole carbons<sup>b</sup> $\Delta 24$  = the mean plane deviation of 24-atom core

Additionally the NiMFPs were showing higher twist angles (25.07 and 27.97 for NiMFP(IND) and NiMFP(IND)Ph<sub>2</sub>, respectively) as compared to ZnMFPs (20.97 and 23.02 for ZnMFP(IND) and ZnMFP(IND)Ph<sub>2</sub>, respectively) which again demonstrated highly ruffled nature of Ni(II) fused porphyrins. In case of ZnMFP(IND)R<sub>2</sub>, Zn(II) metal was found (~0.40-0.47 Å) to be placed above the mean plane. ZnMFPs were also adopting slightly *ruffled* conformation. The four Zn-N distances were almost identical (2.07-2.09 Å) and (2.05-2.07 Å) in ZnMFP(IND) (**1d**) and ZnMFP(IND)Ph<sub>2</sub> (**3d**), respectively (Table 4.2). The mean plane deviation ( $\Delta_{24}$ ) and deviation of eight  $\beta$ -pyrrolic carbons from the mean plane ( $\Delta C_{\beta}$ ) were found to be higher in case of NiMFP(IND)Ph<sub>2</sub> as compared to NiMFP(IND) (Figure A11 in Appendix-III and Table 4.2) which clearly reflect the induced nonplanarity provided by  $\beta$ -phenyl substituents whereas in case of Zn(II) complexes, ZnMFP(IND) had higher values of  $\Delta C_{\beta}$  and  $\Delta_{24}$  as compared to the  $\beta$ -phenyl substituted fused Zn(II) porphyrin (ZnMFP(IND)Ph<sub>2</sub>) possibly due to the induced nonplanarity caused by axial coordination of pyridine to Zn(II) ion.

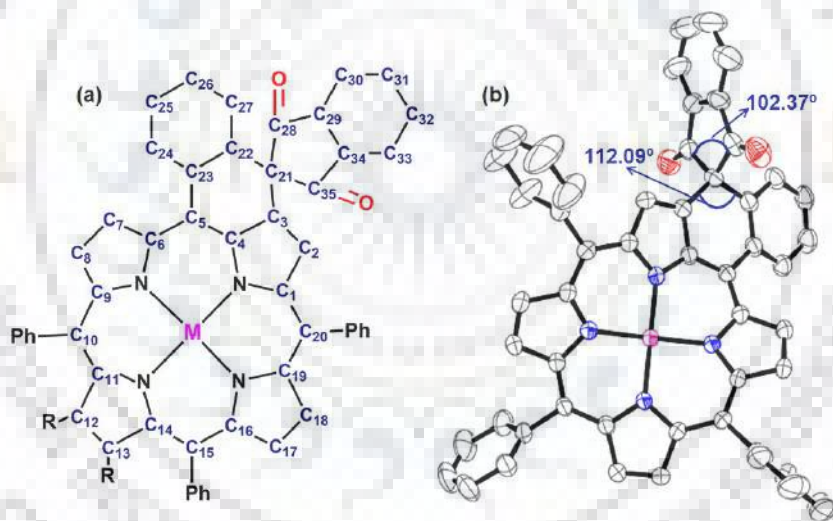


**Figure 4.5** (a) Numbering of Carbon Atoms in the Macrocyclic Skeleton; (b) ORTEP Showing the  $sp^3$  Hybridized Carbon with Deformed Tetrahedral Geometry.

In addition to specific features, the six-membered rings formed by fusion of indanedione moiety with *ortho-meso*-phenyls in all cases were almost planar. The major effect of this ring is to bring coplanar with porphyrin plane, the *meso*-phenyl to which it is fused became more deviated above the mean plane as compared to the other three unfused phenyls. A useful consequence of this deviation was a strong deshielding effect on the neighboring  $\beta$ -pyrrolic hydrogen of the fused unit (Figure 4.2).  $sp^3$  Hybridized carbon in the fused six membered ring exhibited deformed

tetrahedral geometry due to the steric strain. The bond angle C3-C21-C22 was found to be  $112.09^\circ$  slightly larger as compared to bond angle for perfect tetrahedral carbon ( $109.47^\circ$ ) whereas the C28-C21-C35 bond angle ( $102.37^\circ$ ) was significantly smaller as compared to perfect tetrahedral carbon due to steric strain caused by indanedione ring (Figure 4.5).

#### 4.3.4 DFT Calculation

The effects on the energy levels by oxidation of one  $\beta$ - $\beta'$  single bond and fusion of  $\beta$ -substituents with *meso*-phenyl to form fused porphyrin from chlorin was rationalized by optimizing the geometries of synthesized free base MFPs (Figure A12 in Appendix-III). The geometry optimization has been performed using B3LYP functional and 6-31G basis set in gas phase. Figures 4.6, A13 and A14 in Appendix-III represent the frontier molecular orbitals (FMOs) of  $H_2MFP(IND)(R)_2$  (where R = H, Br, and Ph). The oxidation of the reduced C-C bond stabilized the HOMO ( $b_2$ ) and LUMO+1 ( $C_1$ ) of the free base *trans*-chlorin, as a result, the electron density appeared over the  $\beta$ -pyrrolic positions and HOMO of the fused porphyrin become  $a_{2u}$ .

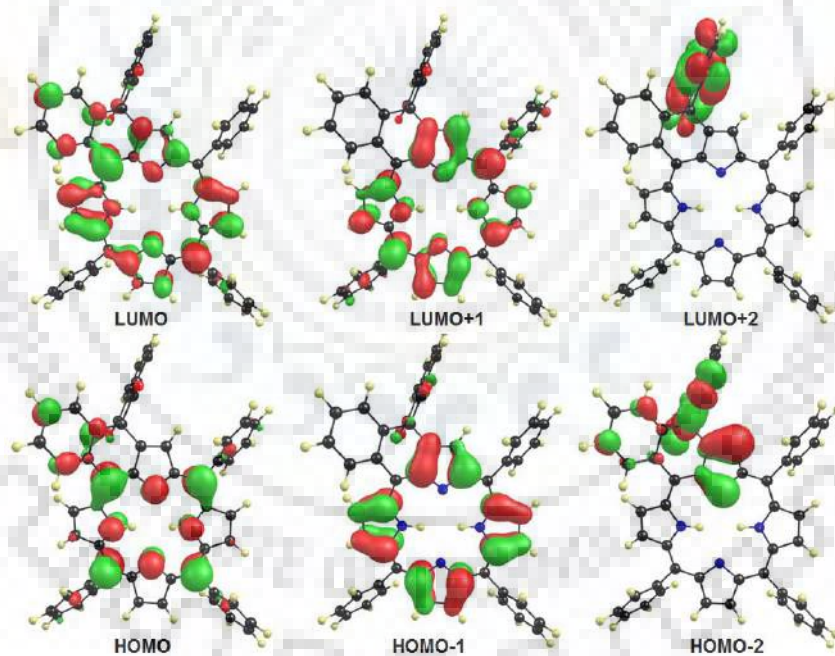


**Figure 4.6** Frontier Molecular Orbitals of  $H_2MFP(IND)$  (1) Using B3LYP/6-31G Basis Sets.

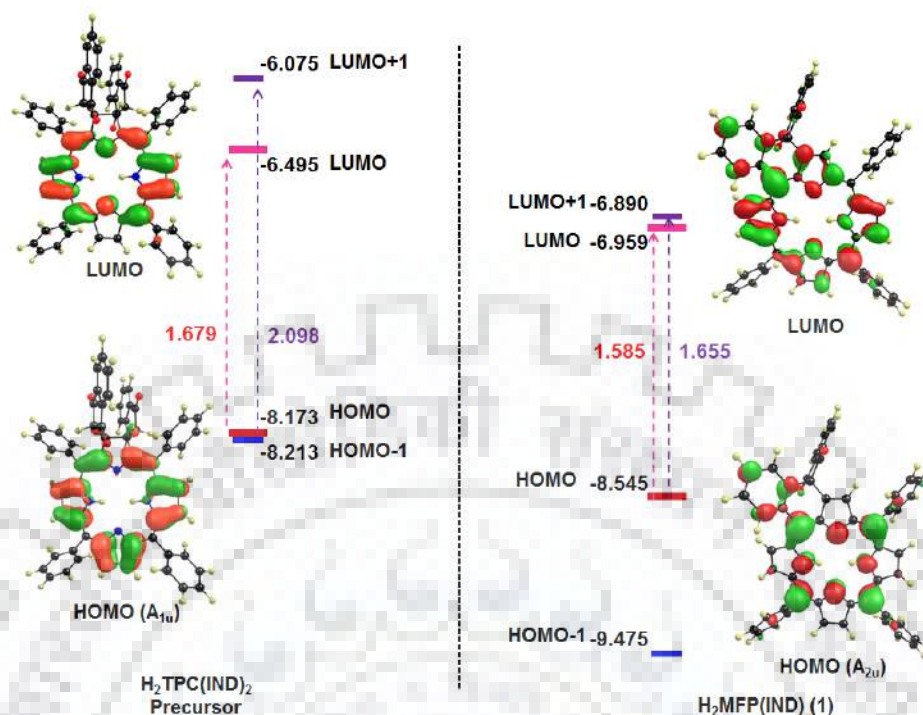


**Figure 4.7** Frontier Molecular Orbitals of the Two Highest Energy Filled (HOMOs) and Two Lowest Energy Unfilled (LUMOs) Orbitals of Precursor  $\text{H}_2\text{TPC}(\text{IND})_2$  and Product  $\text{H}_2\text{MFP}(\text{IND})$  (**1**). The Orbitals were Generated Based on a Density Functional Calculation (B3LYP) Using a 6-31G Basis Set. The Energies are given in eV Units.

Ring-fusion removed the degeneracy of frontier molecular orbitals which further resulted into the relatively reduced HOMO-LUMO gap (Figure 4.7). The HOMO of the fused porphyrin systems contributed mainly from the macrocyclic core whereas LUMO+2 contributed from the indanedione moiety. Upon oxidation of the C-C bond and ring fusion, the degeneracy of LUMOs retained and HOMOs became more splitted thus the gap between HOMO and LUMO+1 was found to be reduced in the resulting fused porphyrins as shown in Figure 4.7. These fusions affect the symmetry and electronic distribution of the parent molecule, yet the electronic consequences of these fused porphyrins compared to the precursor chlorins have not been fully explored.

#### 4.3.5 Electronic Spectral Studies

The absorption spectra of synthesized fused porphyrins (MFPs) were recorded in  $\text{CH}_2\text{Cl}_2$ . Table 4.3 and Table A1 in the Appendix-III summarize the electronic absorption data of  $\text{H}_2\text{MFPs}$ ,  $\text{ZnMFPs}$  and  $\text{M}(\text{II})\text{MFPs}$  (where  $\text{M} = \text{Co}, \text{Ni}$  and  $\text{Cu}$ ), respectively. Figure 4.8 shows the



comparative absorption spectra of synthesized free base porphyrins whereas Figure A15 in the Appendix-III represents the electronic absorption spectra of synthesized M(II)MFPs (M = Co, Ni, Cu, and Zn). All of the synthesized mono fused porphyrins were red shifted as compared to their precursors [23] whereas hypsochromically shifted with respect to their difused porphyrin systems. Synthesized Ni(II) complexes of monofused porphyrins NiMFP(IND)(R)<sub>2</sub> (R = H, Br, and Ph) exhibited 26-28 nm blue shifts in their Soret band as compared to the corresponding difused porphyrins NiDFP(IND)<sub>2</sub>(R)<sub>2</sub> (R= H, Br, and Ph) which may be due to comparatively less electron withdrawing nature and lower nonplanar conformation of monofused porphyrins with respected to their difused systems (Chapter-3). The Soret band of M<sup>II</sup>MFP(IND)<sub>s</sub> (M<sup>II</sup> = 2H, Co, Ni, Cu, and Zn) were 8-12 nm red-shifted as compared to the electron deficient MTPP(NO<sub>2</sub>) (M = 2H, Co, Ni, Cu, and Zn) this ascribed to the conformational effect of macrocycles upon fusion. All the fused porphyrin chromophores have shown the absorption band at 228 or 229 nm corresponding to the indanedione unit which shows the possibility of charge transfer from porphyrin  $\pi$ -system to indanedione units. The Q<sub>y(0,0)</sub> band in all the free base porphyrins were highly intense whereas the Q<sub>x(1,0)</sub> were found very weak. The bromo and phenyl substituted porphyrins were red shifted as compared to the unbrominated porphyrins which clearly reflected the impact of  $\beta$ -substituents on the electronic properties of the porphyrin systems. The M<sup>II</sup>MFP(IND)Ph<sub>2</sub> have shown least molar extinction coefficients for the Soret band among all the synthesized fused porphyrins.

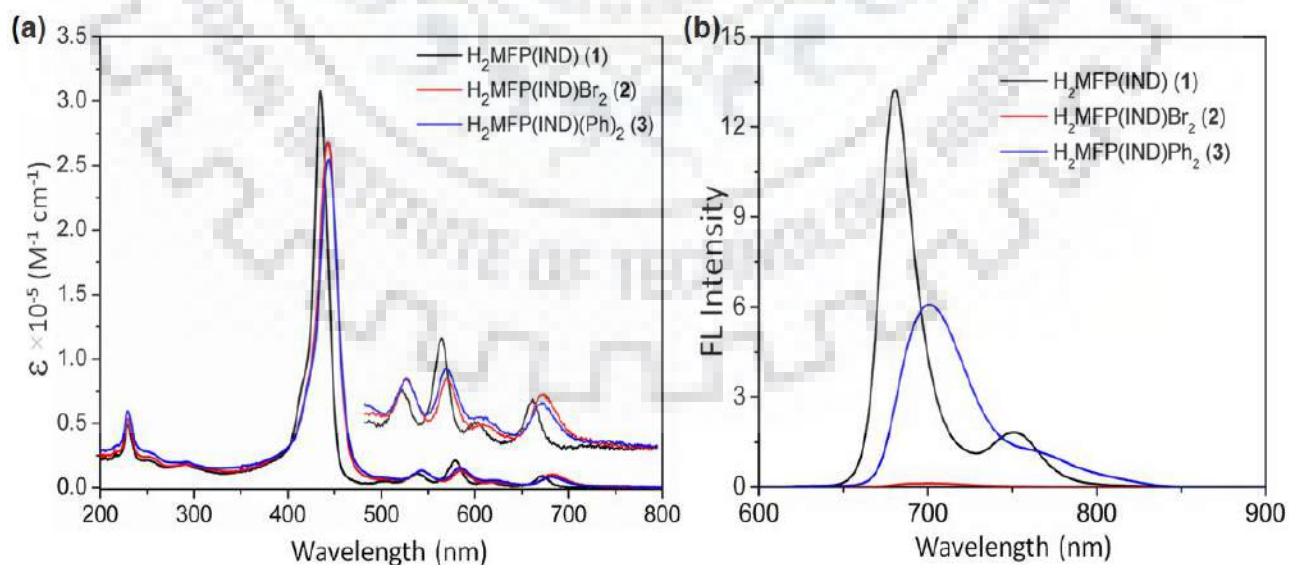


**Figure 4.8** Comparative Absorption Spectra (a), Comparative Emission Spectra (b) of Synthesized Free Base Monofused Porphyrins in CH<sub>2</sub>Cl<sub>2</sub>.



**Table 4.3** Photophysical Data<sup>a</sup> of Synthesized Free base Monofused Porphyrins and Their Corresponding Zn(II) complexes in CH<sub>2</sub>Cl<sub>2</sub>.

Porphyrin	<sup>a</sup> $\lambda_{\text{abs}}$		$\lambda_{\text{em}}$	$\phi_f$
	B band(s), nm	Q band(s), nm		
H <sub>2</sub> TPP(NO <sub>2</sub> )	426(5.34)	526(4.21), 604(3.62), 664(3.95)		
H <sub>2</sub> MFP(IND) ( <b>1</b> )	228(4.69), 435(5.49)	537(4.05), 579(4.33), 615(3.69), 672(3.98)	680, 751	0.019
H <sub>2</sub> MFP(IND)Br <sub>2</sub> ( <b>2</b> )	229(4.73), 444(5.43)	542(4.12), 585(4.13), 622(3.66), 682(4.02)	701	0.001
H <sub>2</sub> MFP(IND)Ph <sub>2</sub> ( <b>3</b> )	229(4.77), 444(5.40)	542(4.12), 583(4.18), 618(3.77), 682(3.93)	699, 701(sh)	0.010
ZnTPP(NO <sub>2</sub> )	426(5.23)	556(4.07), 599(3.90)		
ZnMFP(IND) ( <b>1d</b> )	228(4.72), 437(5.68)	570(4.22), 616(4.24)	628, 683	0.006
ZnMFP(IND)Br <sub>2</sub> ( <b>2d</b> )	228(4.78), 443(5.57)	575(4.23), 622(4.21),	640, 691(sh)	0.0004
ZnMFP(IND)Ph <sub>2</sub> ( <b>3d</b> )	229(4.72), 444(5.40)	578(4.10), 621(4.07)	639, 694(sh)	0.003

<sup>a</sup>Values in parentheses refer to log  $\epsilon$ . sh = shoulder

The emission spectra of synthesized free base and Zn(II) complexes of monofused porphyrins have been recorded in CH<sub>2</sub>Cl<sub>2</sub>. The comparative emission spectra for free base porphyrins are shown in Figure 4.8b whereas for Zn(II) complexes is given in Figure A16 in Appendix-III. MFPs showed the less intense fluorescence spectra as compared to the precursors but comparatively more intense as compared to the corresponding difused systems. MFPs have shown the red shifted emission spectra as compared to the corresponding precursors i.e. *trans*-chlorins (Table 4.3). M<sup>II</sup>MFP(IND)Br<sub>2</sub> have shown a negligible fluorescence as well as least quantum yield due to heavy atom effect of bromo groups.

#### 4.3.6 Electrochemical Redox Studies

The cyclic voltammetric studies of the synthesized fused derivatives have been investigated in CH<sub>2</sub>Cl<sub>2</sub> at 298 K using 0.1 M TBAPF<sub>6</sub> as the supporting electrolyte. Figure 4.9 represent the comparative cyclic voltammograms of NiMFP(IND)R<sub>2</sub> and CuMFP(IND)R<sub>2</sub> in CH<sub>2</sub>Cl<sub>2</sub>. Figure A17 in Appendix-III shows the comparative CVs of M<sup>II</sup>MFP(IND)R<sub>2</sub> (where M<sup>II</sup> = Co, Ni, Zn and R = H, Br, Ph).

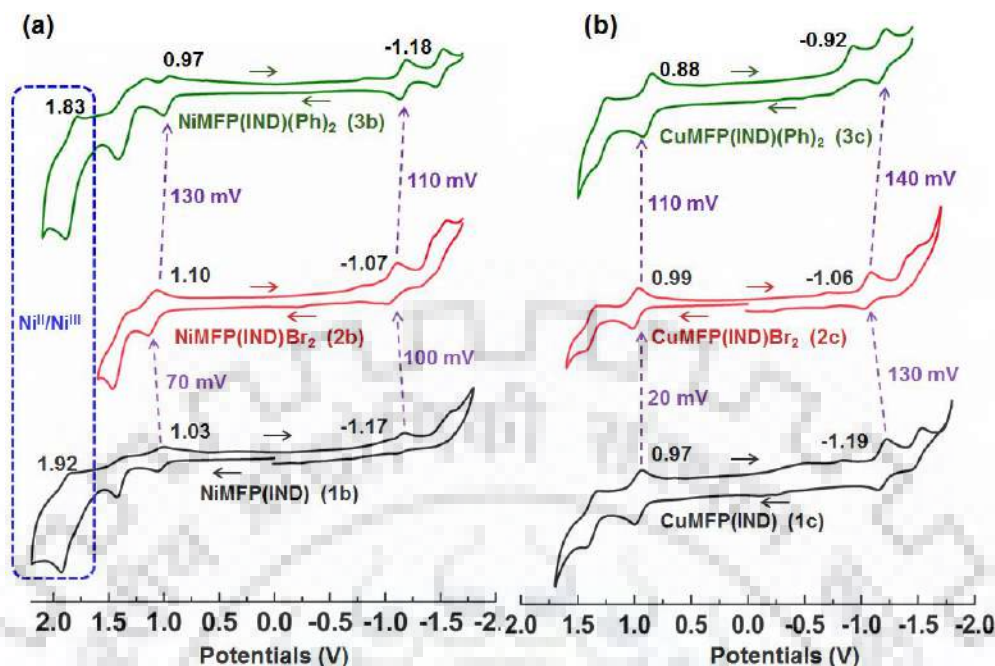


**Figure 4.9** Comparative Cyclic Voltammograms of (a) NiMFP(IND) $R_2$  (b) CuMFP(IND) $R_2$  (Where R = H, Br, and Ph) in  $CH_2Cl_2$  Using 0.1 M TBAPF<sub>6</sub> as Supporting Electrolyte.

The assignment of a Ni(II)/Ni(III) reaction after formation of a porphyrin dication was first projected in 1993 by the groups of Kadish, Vogel and Smith [24]. Later, few more reaction examples have been reported from the last two decades [25]. Interestingly, the electron rich NiMFP(IND) $R_2$  (R = H and Ph) have shown three one electron oxidations. The third oxidation was possibly due to metal center oxidation after electrogeneration of the dication of NiMFP(IND) $R_2$ . The metal-centered Ni<sup>II</sup>/Ni<sup>III</sup> oxidation usually depends upon the nature of the  $\beta$ -substituents. For e.g. NiMFP(IND)Ph<sub>2</sub> is 90 mV cathodically shifted as compared to the NiMFP(IND). In opposite, M(II)MFP(IND)Br<sub>2</sub> (M = Ni and Cu) have shown three reversible reduction due to electron withdrawing nature of bromo groups. In case of Cu(II) complexes, Cu(II)/Cu(I) reduction was observed possibly due to removal of metal centered  $dx^2-y^2$  [26]. Free base and zinc complexes of synthesized fused porphyrins have shown two reversible oxidations and two reversible reductions for macrocyclic systems whereas cobalt complexes have shown an additional oxidation due to Co(II)/Co(III) species. Co(II) porphyrins exhibited first metal centered redox reactions followed by ring centered redox reactions. Co(II)/Co(I) and Co(II)/Co(III) electrochemical reactions are well documented in the literature [27]. Bromo substituted fused porphyrins were easy to reduce as compared to the unbrominated fused

porphyrins. The first ring reduction potential of MFP(IND)Br<sub>2</sub>s were 80-140 mV anodically shifted as compared to MFP(IND)s whereas a minimal anodic shift of 20-70 mV has been observed in the first oxidation potentials of bromo-substituted fused porphyrins with respect to porphyrins without bromo groups. NiMFP(IND)(R)<sub>2</sub> (Where R = H, Br, and Ph) are harder to oxidize and harder to reduce as compared to the corresponding difused porphyrins NiDFP(IND)<sub>2</sub>(R)<sub>2</sub> (Where R = H, Br, and Ph) (values taken from Chapter-3) which resulted into the higher HOMO-LUMO gap (80-150 mV) in monofused porphyrins as compared to the difused porphyrins.

**Table 4.4** Electrochemical Redox Data<sup>a</sup> of Monofused Porphyrins in CH<sub>2</sub>Cl<sub>2</sub> at 298 K

Porphyrins	Oxidation(V)			$\Delta E_{1/2}$	Reduction(V)		
	I	II	III		I	II	III
H <sub>2</sub> MFP(IND) ( <b>1</b> )	1.00	1.38		2.07	-1.07	-1.43	
H <sub>2</sub> MFP(IND)Br <sub>2</sub> ( <b>2</b> )	1.03	1.28		1.96	-0.93	-1.11	
H <sub>2</sub> MFP(IND)Ph <sub>2</sub> ( <b>3</b> )	0.94	1.15		2.01	-1.07	-1.33	
CoMFP(IND) ( <b>1a</b> )	0.89	1.08		1.70	-0.81	-1.24	
CoMFP(IND)Br <sub>2</sub> ( <b>2a</b> )	0.94	1.15	1.51	1.67	-0.73	-1.53 <sup>d</sup>	
CoMFP(IND)Ph <sub>2</sub> ( <b>3a</b> )	0.85	1.03	1.31	1.69	-1.28 <sup>i</sup>	-1.26	
NiMFP(IND) ( <b>1b</b> )	1.03	1.29	1.92	2.20	-1.17	-1.51	
NiMFP(IND)Br <sub>2</sub> ( <b>2b</b> )	1.10	1.40		2.17	-1.07	-1.38	-1.50
NiMFP(IND)Ph <sub>2</sub> ( <b>3b</b> )	0.97	1.29	1.83	2.14	-1.18	-1.50	
CuMFP(IND) ( <b>1c</b> )	0.97	1.37		2.16	-1.19	-1.50	
CuMFP(IND)Br <sub>2</sub> ( <b>2c</b> )	0.99	1.38		2.05	-1.06	-1.37	-1.47
CuMFP(IND)Ph <sub>2</sub> ( <b>3c</b> )	0.88	1.28		1.80	-0.92 <sup>i</sup>	-1.18	
ZnMFP(IND) ( <b>1d</b> )	0.81	1.14		2.06	-1.26 <sup>i</sup>	-1.45	
ZnMFP(IND)Br <sub>2</sub> ( <b>2d</b> )	0.87	1.15		2.08	-1.12	-1.47	
ZnMFP(IND)Ph <sub>2</sub> ( <b>3d</b> )	0.77	1.03		2.05	-1.28 <sup>i</sup>	-1.46	-1.60

<sup>a</sup>Versus Ag/AgCl reference electrode, <sup>i</sup>Irreversible peaks, <sup>d</sup>Data obtained from DPV.

## 4.4 CONCLUSIONS

A novel one pot synthesis of  $\beta$ -to *ortho*-phenyl monofused porphyrins with indanedione functionalities has been described *via* metal mediated oxidative fusion of free base planar *trans*-chlorins. Extended  $\pi$ -conjugation of porphyrins aromatic circuit was accomplished by connecting  $\beta$ -pyrrolic indanedione groups with *meso-ortho*-phenyls. As compared to the unfused precursors, these monofused porphyrins have shown a spectacular bathochromic shift of the Soret as well as the longest wavelength bands in absorption spectra. The NiMFP(IND)R<sub>2</sub> (where R = H and Ph) were best described as typically *ruffled* conformation due to their high  $\Delta\epsilon$  and  $\Delta C_{\beta}$  as compared to the Zinc(II) complexes. Notably, Ni(II) complexes of **1** and **3** NiMFP(IND)R<sub>2</sub> (R = H and Ph) exhibited metal centered oxidation (Ni<sup>II</sup>/Ni<sup>III</sup>) due to extended conjugation and electronic nature of  $\beta$ -substituents. Monofused Ni(II) complexes (Ni(II)MFP(IND)s) exhibited higher HOMO-LUMO gap (80-150 mV) as compared to the corresponding difused porphyrins (Ni<sup>II</sup>DFP(IND)<sub>2</sub>s).

## 4.5 REFERENCES

1. Lindsey, J. S. De Novo Synthesis of Gem-Dialkyl Chlorophyll Analogues for Probing and Emulating Our Green World. *Chem. Rev.* **2015**, *115*, 6534-6620.
2. Asano, R.; Nagami, A.; Fukumoto, Y.; Yazama, F.; Ito, H.; Sakata, I.; Tai, A. Synthesis and Biological Evaluation of New Chlorin Derivatives as Potential Photosensitizers for Photodynamic Therapy. *Bioorganic Med. Chem.* **2013**, *21*, 2298-2304.
3. Taniguchi, M.; Lindsey, J. S. Synthetic Chlorins, Possible Surrogates for Chlorophylls, Prepared by Derivatization of Porphyrins. *Chem. Rev.* **2017**, *117*, 344-535.
4. Whitlock, H. W. Jr.; Hanauer, R.; Oester, M. Y.; Bower, B. K. Diimide Reduction of Porphyrins. *J. Am. Chem. Soc.* **1969**, *91*, 7485-7489.
5. Crossley, M. J.; King, L. G. Reaction of Metallo-2-nitro-5,10,15,20-tetraphenylporphyrins with Oxyanions. Temperature-Dependent Competition between Nucleophilic Addition and Single-Electron Transfer Processes. *J. Chem. Soc., Perkin Trans. 1* **1996**, 1251-1260.

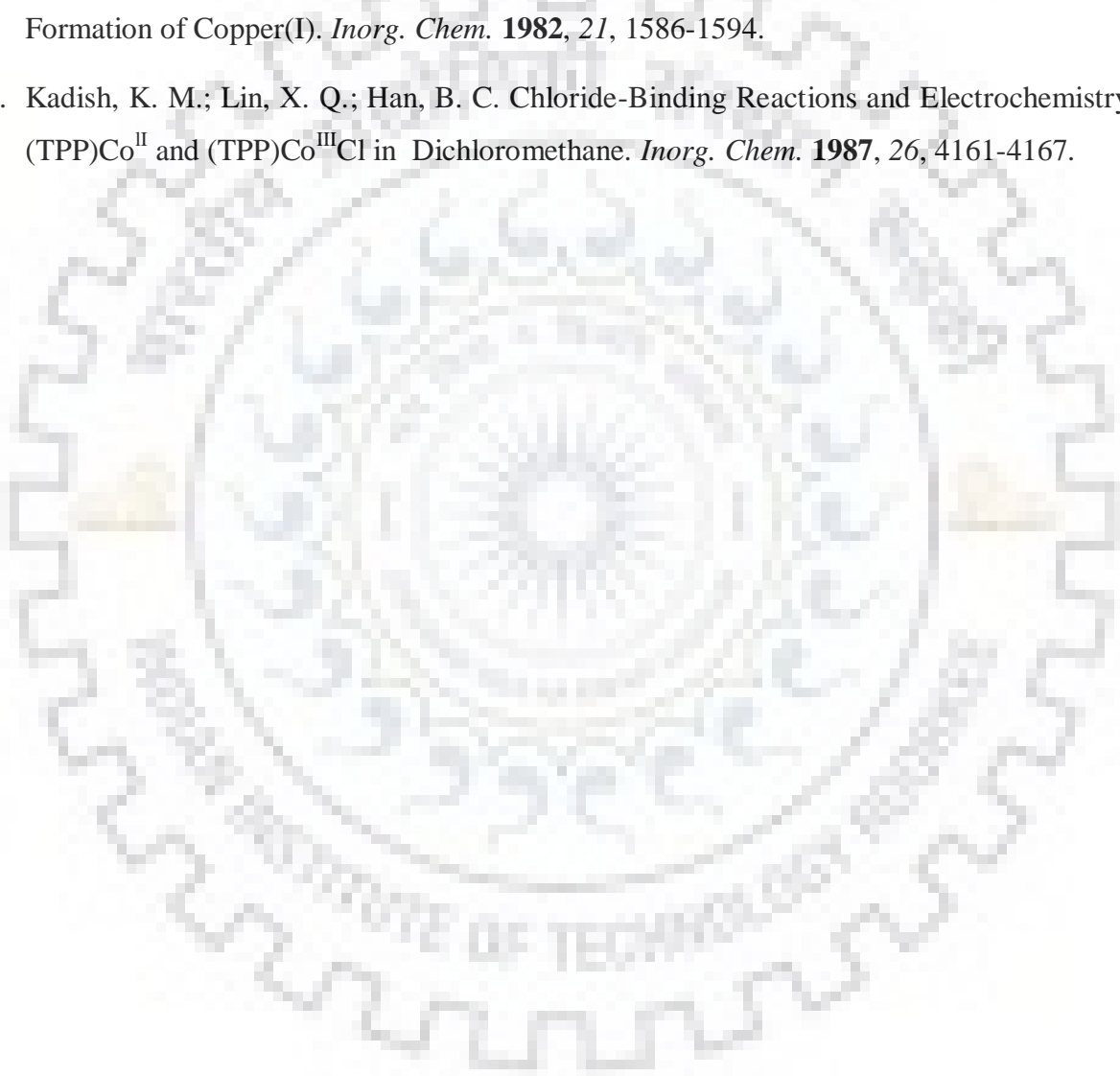
- Grover, N.; Chaudhri, N.; Sankar, M. Facile Conversion of Ni(II) Cyclopropylchlorins into Novel  $\beta$ -Substituted Porphyrins through Acid-Catalyzed Ring-Opening Reaction. *Inorg. Chem.* **2017**, *56*, 424-437.
- Giraudeau, A.; Callot, H. J.; Jordan, J.; Ezhar, I.; Gross, M. Substituent Effects in the Electroreduction of Porphyrins and Metalloporphyrins. *J. Am. Chem. Soc.* **1979**, *101*, 3857-3862.
- Bonfantini, E. E.; Burrell, A. K.; Campbell, W. M.; Crossley, M. J.; Gosper, J. J.; Harding, M. M.; Officer, D. L.; Reid, D. C. W. J. Efficient Synthesis of Free-Base 2-Formyl-5, 10, 15, 20-Tetraarylporphyrins, their Reduction and Conversion to [(Porphyrin-2-yl) Methyl] Phosphonium Salts. *Porphyrins Phthalocyanines* **2002**, *6*, 708-719.
- Jaquinod, L.; Khoury, R. G.; Shea, K. M.; Smith, K. M. Regioselective Syntheses and Structural Characterizations of 2,3-Dibromo- and 2,3,7,8,12,13-Hexabromo-5,10,15,20-Tetraphenyl porphyrins. *Tetrahedron* **1999**, *55*, 13151-13158.
- Jeandon, C.; Ruppert, R.; Richeter, S.; Callot, H. J. Colorful Friedel-Crafts Chemistry of *meso*-Tetraarylporphyrins. An Unexpected Route to Porphyrinic Spiro Dimers. *Org. Lett.* **2003**, *5*, 1487-1489.
- Richeter, S.; Jeandon, C.; Ruppert, R.; Callot, H. J. Reactivity of Oxonaphthoporphyrins. Efficient  $\beta$ -Functionalization of the Porphyrin Ring on Reaction with Nitrogen or Carbon Nucleophiles. *Tetrahedron Lett.* **2001**, *42*, 2103-2106.
- Diev, V.V.; Hanson, K.; Zimmerman, J. D.; Forrest, S. R.; Thompson, M. E. Fused Pyrene-Diporphyrins: Shifting Near-Infrared Absorption to 1.5  $\mu$ m and Beyond. *Angew. Chem.* **2010**, *122*, 5655-5658.
- Hayashi, S.; Tanaka, M.; Hayashi, H.; Eu, S.; Umeyama, T.; Matano, Y.; Araki, Y.; Imahori, H. Naphthyl-Fused  $\pi$ -Elongated Porphyrins for Dye-Sensitized TiO<sub>2</sub> Cells. *J. Phys. Chem. C* **2008**, *112*, 15576-15585.
- Tanaka, T.; Osuka, A. Conjugated Porphyrin Arrays: Synthesis, Properties and Applications for Functional Materials. *Chem. Soc. Rev.* **2015**, *44*, 943-969.



15. Fukui, N.; Cha, W.-Y.; Lee, S.; Tokuji, S.; Kim, D.; Yorimitsu, H.; Osuka, A. Oxidative Fusion Reactions of *Meso*-(diarylamino)porphyrins. *Angew. Chem. Int. Ed.* **2013**, *52*, 9728-9732.
16. Saegusa, Y.; Ishizuka, T.; Komamura, K.; Shimizu, S.; Kotani, H.; Kobayashi, N.; Kojima, T. Ring-Fused Porphyrins: Extension of  $\pi$ -Conjugation Significantly Affects the Aromaticity and Optical Properties of The Porphyrin  $\pi$ -Systems and the Lewis acidity of The Central Metal Ions. *Phys. Chem. Chem. Phys.* **2015**, *17*, 15001-15011.
17. Hammond, G. S.; Wu, C.-H. S. Nickel Acetate Catalyzed Autoxidation of Benzoin. *J. Am. Chem. Soc.* **1973**, *95*, 8215-8222.
18. Tobisu, M.; Xu, T.; Shimasaki, T.; Chatani, N. Nickel-Catalyzed Suzuki-Miyaura Reaction of Aryl Fluorides. *J. Am. Chem. Soc.* **2011**, *133*, 19505-19511.
19. Camasso, N. M.; Sanford, M. S. Design, Synthesis, and Carbon-Heteroatom Coupling Reactions of Organometallic Nickel(IV) Complexes. *Science* **2015**, *347*, 1218-1220.
20. Usui, T.; Ban, H. S.; Kawada, J.; Hirokawa, T.; Nakamura, H. Discovery Of Indenopyrazoles as EGFR and VEGFR-2 Tyrosine Kinase Inhibitors by in Silico High-Throughput Screening. *Bioorg. Med. Chem. Lett.* **2008**, *18*, 285-288.
21. Kim, S.-H.; Hong, S.-J.; Yoo, J.; Kim, S. K.; Sessler, J. L.; Lee, C.-H. Strapped Calix[4]pyrroles Bearing a 1,3-Indanedione at  $\beta$ -Pyrrolic Position: Chemodosimeters for the Cyanide Anion. *Org. Lett.* **2009**, *11*, 3626-3629.
22. Götz, D. C. G.; Gehrold, A. C.; Dorazio, S. J.; Daddario, P.; Samankumara, L.; Bringmann, G.; Brückner, C. Torsten Bruhn Indaphyrins and Indachlorins: Optical and Chiroptical Properties of a Family of Helimeric Porphyrinoids. *Eur. J. Org. Chem.* **2015**, 3913-3922.
23. Chaudhri, N.; Grover, N.; Sankar, M. Versatile Synthetic Route for  $\beta$ -Functionalized Chlorins and Porphyrins by Varying the Size of Michael Donors: Syntheses, Photophysical, and Electrochemical Redox Properties. *Inorg. Chem.* **2017**, *56*, 11532-11545.
24. Kadish, K. M.; Van Caemelbecke, E.; Bolas, P.; D'Souza, F.; Vogel, E.; Kisters, M; Medforth, C. J.; Smith, K. M. First Reversible Electrogeneration of Triply Oxidized Nickel Porphyrins and Porphycenes. Formation of Nickel(III)  $\pi$ -Dications. *Inorg. Chem.* **1993**, *32*, 4177-4178.



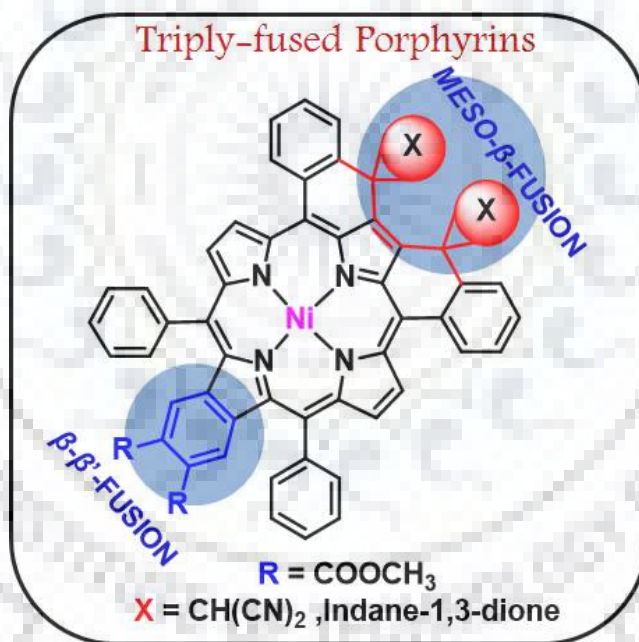
25. Fang, Y.; Senge, M. O.; Van Caemelbecke, E.; Smith, K. M.; Medforth, C. J.; Zhang, M.; Kadish, K. M. Impact of Substituents and Nonplanarity on Nickel and Copper Porphyrin Electrochemistry: First Observation of a  $\text{Cu}^{\text{II}}/\text{Cu}^{\text{III}}$  Reaction in Nonaqueous Media. *Inorg. Chem.* **2014**, *53*, 10772-10778.
26. Giraudeau, A.; Louati, A.; Gross, M.; Callot, H. J.; Hanson, L. K.; Rhodes, R. K.; Kadish, K. M. Reduction of Copper Tetracyanotetraphenylporphyrin in Nonaqueous Media. Formation of Copper(I). *Inorg. Chem.* **1982**, *21*, 1586-1594.
27. Kadish, K. M.; Lin, X. Q.; Han, B. C. Chloride-Binding Reactions and Electrochemistry of  $(\text{TPP})\text{Co}^{\text{II}}$  and  $(\text{TPP})\text{Co}^{\text{III}}\text{Cl}$  in Dichloromethane. *Inorg. Chem.* **1987**, *26*, 4161-4167.





## CHAPTER 5

### “Triply Fused Porphyrins: Synthesis, Spectral, Electrochemical Redox and Anion Sensing Properties”





## CHAPTER 5

### TRIPLY FUSED PORPHYRINS: SYNTHESIS, SPECTRAL, ELECTROCHEMICAL REDOX AND ANION SENSING PROPERTIES

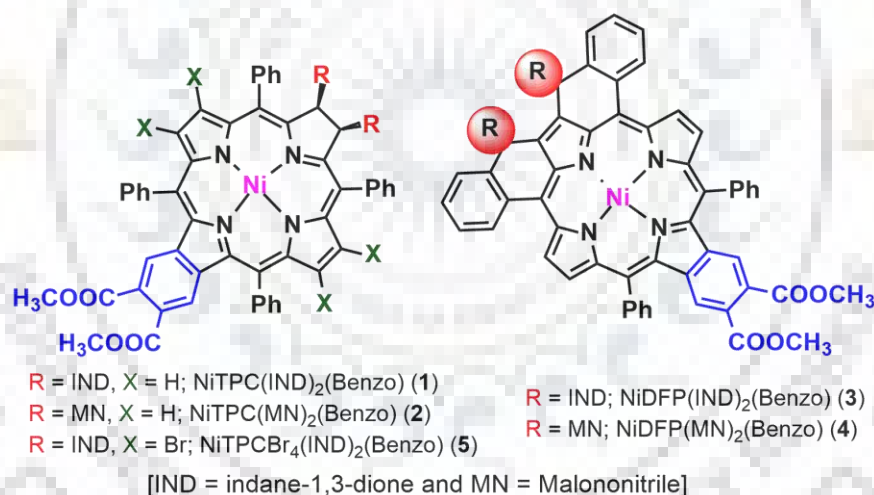
#### 5.1 INTRODUCTION

$\beta$ -Modified porphyrins have received much attention in the research community in recent years due to their unique structural, intriguing photophysical and electrochemical redox properties [1, 2]. The extension of  $\pi$ -conjugation *via* fusion of *meso*- $\beta$ -positions or through incorporation of a fused benzene ring typically causes significant red shifts in the absorption spectra and increases the basicity of the macrocyclic ring [3,4] which make them an appealing candidate for photodynamic therapy and optoelectronic applications [5,6]. In general, fusion alters the redox potentials leading to reduced HOMO-LUMO gap which is relevant for application as light harvesting agents in DSSC [7]. Notably, the benzoporphyrin derivatives were used as photosensitizers to optimize their phototherapeutic activity [8]. In 2002, Kelley and coworkers found the light dose of benzoporphyrin derivative Monoacid Ring A, BPD-MA which effectively ablated canine esophageal mucosa after 30 min. of delivery time [9].

The naturally occurring tetrapyrrole containing nickel in macrocyclic core is present as cofactor F430 of the MCR enzyme which catalyzes methane formation from methyl-coenzyme M [10]. In enzyme cofactor F430, Ni(I) is usually found as axially coordinated in all protein-bound forms. The structural, spectroscopic studies and chemical behavior of Nickel tetrapyrrolic macrocycles have been widely investigated using a range of experimental and theoretical techniques [11]. The low spin Ni(II) porphyrins are known as one of the extensively studied nickel tetrapyrroles; In absence of axial ligation, Ni(II) has  $d^8$  electronic configuration filled through  $dz^2$  orbital and referred to  $Ni(dz^2)^2$  which favors comparatively short Ni-N bond lengths and supports the macrocycle to adopt a nonplanar conformation [12] while high-spin nickel(II) porphyrins can be obtained by axial ligation which exhibits  $(dz^2)-(dx^2-y^2)$  electronic configuration due to the presence of one electron in antibonding  $dx^2-y^2$  orbital and leads to elongation of Ni-N bond distances [13]. The previous studies on Ni(II) porphyrinoids showed that there is an additional conformational change in macrocyclic core upon axial binding which exhibits many catalytic application, where reduced Ni(I) is found as the active form of the enzyme [11-14]. Only a few

reports in literature determined the relationship between Ni(II) tetrapyrrole's nonplanarity and axial ligand affinity [13-16]. In this context, we decided to systematically investigate the relationship between Ni(II) macrocyclic conformation and axial ligation affinity of basic anions using few electron deficient nickel porphyrinoids having enhanced nonplanar macrocycles generated by fused  $\beta$ -benzene ring and *meso*- $\beta$ -fused bulky substituents. Herges and coworkers have investigated the spin state switching of Ni(II) electron deficient chlorins through axial coordination of the bases [17]. The most important reason for investigating the present molecules was to analyze the possible changes in the macrocyclic conformation, photophysical and electrochemical redox properties caused by  $\beta$ - $\beta'$  fusion over *meso*- $\beta$  fusion. Herein, we have synthesized highly nonplanar electron deficient benzochlorins with extended  $\pi$ -conjugation and oxidized into *meso*- $\beta$ -fused benzoporphyrins (Chart 1) and utilized them for selective rapid visual detection of cyanide ion.

**Chart 5.1** Molecular Structures of Synthesized Porphyrinoids.



## 5.2 EXPERIMENTAL SECTION

### 5.2.1 Materials

Methyl acrylate, triphenylphosphine, and pyrrole were purchased from Alfa Aesar and used as received. Palladium acetate, indane-1,3-dione, and liquid bromine were purchased from Sigma Aldrich and directly used without further purification. Benzaldehyde,  $\text{Ni}(\text{OAc})_2 \cdot 4\text{H}_2\text{O}$ , DDQ,  $\text{K}_2\text{CO}_3$ , malononitrile were purchased from Hi-Media, India. All the solvents employed in the present work have been distilled or dried before use.



## 5.2.2 Instrumentation and Methods

Characterization techniques and instrumentation has been used same as described in Chapter 2. DFT studies were performed using B3LYP/LANL2DZ basis sets. Dichloromethane for electronic spectral studies, CV analysis, and anion sensing studies was distilled twice or thrice as per need.

## 5.2.3 General Procedure for the Synthesis of *trans*-Benzochlorins NiTPC(IND)<sub>2</sub>(Benzo) (1) and NiTPC(MN)<sub>2</sub>(Benzo) (2)

200 mg (0.227 mmol) of NiTPP(NO<sub>2</sub>)(Benzo) was dissolved in 7 ml of DMSO. To this, 10 eq. of K<sub>2</sub>CO<sub>3</sub> and 10 eq. of active methylene compound (malononitrile or indane-1,3-dione) were added and the reaction mixture was purged with argon for 10-15 min. The reaction mixture was stirred at 85 °C for 2.5-3.0 h. The completion of the reaction was monitored by thin layer chromatography and UV-visible spectroscopy. After completion, the reaction mixture was cooled to room temperature and diluted with 25 ml CHCl<sub>3</sub>. The diluted reaction mixture was washed twice with brine solution and the organic layer was separated and passed through anhydrous sodium sulphate. The solvent was removed by rotatory evaporation and crude porphyrin mixture was purified by silica gel column chromatography. Trace of unreacted precursor was removed using CHCl<sub>3</sub> as an eluent and the desired compound was eluted using CHCl<sub>3</sub> to CHCl<sub>3</sub>:acetone (95:5, v/v) mixture. The pure products were obtained by recrystallization with CHCl<sub>3</sub>/CH<sub>3</sub>OH mixture.

**NiTPC(IND)<sub>2</sub>(Benzo) (1):** Yield: 76% (194 mg, 0.172 mmol). UV/vis (CH<sub>2</sub>Cl<sub>2</sub>):  $\lambda_{\max}$ (nm) (log  $\epsilon$ ): 230(5.04), 448(5.17), 527(3.96), 612(sh), 659(4.48). <sup>1</sup>H NMR (400 MHz, CDCl<sub>3</sub>)  $\delta$  (ppm): 8.49(d, <sup>3</sup>J<sub>H,H</sub> = 4 Hz, 2H,  $\beta$ -H), 8.31(d, <sup>3</sup>J<sub>H,H</sub> = 4 Hz, 2H,  $\beta$ -H), 7.87-7.74(m, 14H, *meso*-Ph-H), 7.68(d, <sup>3</sup>J<sub>H,H</sub> = 8 Hz, 2H, *meso*-Ph-H), 7.58(t, <sup>3</sup>J<sub>H,H</sub> = 8 Hz, 2H, *meso*-Ph-H), 7.41(d, <sup>3</sup>J<sub>H,H</sub> = 8 Hz, 2H, *meso*-Ph-H), 7.35-7.35(m, 4H, IND-H), 7.22-7.19(m, 4H, IND-H), 6.88(d, <sup>3</sup>J<sub>H,H</sub> = 8 Hz, 2H,  $\beta$ -fused-H), 5.07(d, <sup>3</sup>J<sub>H,H</sub> = 4 Hz, 2H,  $\beta$ -H), 3.84(s, 6H, -CH<sub>3</sub>), 3.00(d, <sup>3</sup>J<sub>H,H</sub> = 4 Hz, 2H, -CH(IND)). MALDI-TOF-MS (*m/z*): found 1127.627 [M+H]<sup>+</sup>, calcd 1127.259, found 1216.322 [M]<sup>+</sup>+THF+H<sub>2</sub>O, calcd 1216.319. Anal. Calcd for C<sub>70</sub>H<sub>44</sub>N<sub>4</sub>O<sub>8</sub>Ni C, 74.55; H, 3.93; N, 4.97. Found C, 74.49; H, 3.90; N, 4.98.

**NiTPC(MN)<sub>2</sub>(Benzo) (2):** Yield: 70% (154 mg, 0.159 mmol). UV/vis (CH<sub>2</sub>Cl<sub>2</sub>):  $\lambda_{\max}$ (nm) (log  $\epsilon$ ): 267(4.36), 442(5.00), 552(3.42), 662(sh), 651(4.32). <sup>1</sup>H NMR (400 MHz, CDCl<sub>3</sub>)  $\delta$  (ppm):

8.45(d,  $^3J_{\text{H,H}} = 4$  Hz, 4H,  $\beta$ -H), 8.27(s, 2H, *meso*-Ph-H), 7.91-7.86 (m, 5H, *meso*-Ph-H), 7.78(t,  $^3J_{\text{H,H}} = 8$  Hz, 3H, *meso*-Ph-H), 7.71(t,  $^3J_{\text{H,H}} = 8$  Hz, 2H, *meso*-Ph-H), 7.58(s, 2H, *meso*-Ph-H), 7.51(t,  $^3J_{\text{H,H}} = 8$  Hz, 2H, *meso*-Ph-H), 7.35(s, 2H, *meso*-Ph-H), 7.18(s, 2H, *meso*-Ph-H), 7.06(d,  $^3J_{\text{H,H}} = 8$  Hz, 2H,  $\beta$ -fused-H), 5.04(d,  $^3J_{\text{H,H}} = 4$  Hz, 2H,  $\beta$ -H), 3.86-3.83(m, 8H, -CH(MN) & -CH<sub>3</sub>). MALDI-TOF-MS ( $m/z$ ): found 966.218 [M]<sup>+</sup>, calcd 966.221, found 938.187 [M]<sup>+</sup>-2MN, calcd 938.209. Anal. Calcd for C<sub>58</sub>H<sub>36</sub>N<sub>8</sub>O<sub>4</sub>Ni C, 71.99; H, 3.75; N, 11.58. Found: C, 72.01; H, 3.76; N, 11.39.

#### 5.2.4 Synthetic Procedure for Oxidative Fusion of *trans*-Benzochlorins into Difused Benzoporphyrins NiDFP(IND)<sub>2</sub>(Benzo) and NiDFP(MN)<sub>2</sub>(Benzo) (3 and 4)

70 mg of *trans*-Benzochlorins **1** or **2** was treated with 6 eq. of DDQ in 20 ml of distilled CHCl<sub>3</sub>. The reaction mixture was allowed to reflux for 2-3 h. as the starting material was totally consumed. After completion of the reaction, the reaction mixture was washed thrice with distilled water to remove excess of DDQ. The organic layer was passed through anhydrous sodium sulphate and dried under reduced pressure. The crude porphyrins were purified on silica gel column using CHCl<sub>3</sub> followed by 5-7% acetone in CHCl<sub>3</sub> as the eluent. The final solid product was washed with methanol to get pure product.

**NiDFP(IND)<sub>2</sub>(Benzo) (3):** Yield: 69% (48 mg, 0.043 mmol). UV/vis (CH<sub>2</sub>Cl<sub>2</sub>):  $\lambda_{\text{max}}$ (nm) (log  $\epsilon$ ): 229(4.90), 480(5.26), 596(4.28), 664(3.76). <sup>1</sup>H NMR (400 MHz, CDCl<sub>3</sub>)  $\delta$  (ppm): 9.31(d,  $^3J_{\text{H,H}} = 4$  Hz, 2H,  $\beta$ -H), 8.72(d,  $^3J_{\text{H,H}} = 4$  Hz, 2H,  $\beta$ -H), 8.27(s, 2H, *meso*-Ph-H), 8.04-7.57(m, 16H, *meso*-Ph-H), 7.44(t,  $^3J_{\text{H,H}} = 4$  Hz, 3H, IND-H), 7.31(s, 2H, IND-H), 7.01(t,  $^3J_{\text{H,H}} = 8$  Hz, 3H, IND-H), 6.78(d,  $^3J_{\text{H,H}} = 8$  Hz, 2H, fused-H), 3.87(s, 6H, -CH<sub>3</sub>). MALDI-TOF-MS ( $m/z$ ): found 1122.432 [M]<sup>+</sup>, calcd 1122.774. Anal. Calcd for C<sub>70</sub>H<sub>38</sub>N<sub>4</sub>O<sub>8</sub>Ni C, 74.95; H, 3.41; N, 4.99. Found: C, 75.00; H, 3.42; N, 4.97.

**NiDFP(MN)<sub>2</sub>(Benzo) (4):** Yield: 65% (45 mg, 0.047 mmol). UV/vis (CH<sub>2</sub>Cl<sub>2</sub>):  $\lambda_{\text{max}}$ (nm) (log  $\epsilon$ ): 277(4.40), 478(5.10), 599(4.07), 647(4.09). <sup>1</sup>H NMR (400 MHz, CDCl<sub>3</sub>)  $\delta$  (ppm): 9.26(d,  $^3J_{\text{H,H}} = 4$  Hz, 2H,  $\beta$ -H), 8.69(d,  $^3J_{\text{H,H}} = 8$  Hz, 2H,  $\beta$ -H), 8.48(d,  $^3J_{\text{H,H}} = 8$  Hz, 2H, *meso*-Ph-H), 8.00(d,  $^3J_{\text{H,H}} = 8$  Hz, 2H, *meso*-Ph-H), 7.87-7.70(m, 14H, *meso*-Ph-H), 7.22(s, 2H, fused-H), 3.87(s, 6H, -CH<sub>3</sub>). MALDI-TOF-MS ( $m/z$ ): found 935.401 [M]<sup>+</sup>-CN<sup>-</sup> calcd 935.179. Anal. Calcd for C<sub>58</sub>H<sub>30</sub>N<sub>8</sub>O<sub>4</sub>Ni•0.5CH<sub>3</sub>OH C, 71.87; H, 3.30; N, 11.46. Found: C, 71.90; H, 3.33; N, 11.39.

#### 5.2.5 Synthetic Procedure for NiTPCBr<sub>4</sub>(IND)<sub>2</sub>(Benzo) (5)

120 mg (0.106 mmol) of NiTPC(IND)<sub>2</sub>(Benzo) (**1**) was dissolved in 25 ml distilled chloroform. To this, 16 q. of liq. Br<sub>2</sub> (87  $\mu$ L, 1.7 mmol) dissolved in 10 ml of distilled CHCl<sub>3</sub> was added slowly. The resulted reaction mixture was stirred for 3-5 min at room temperature. The completeness of reaction was monitored by UV-Vis. spectroscopy with expected red shifts in the Soret and Q bands. After completion of reaction, the reaction mixture was washed twice with 20% sodium metabisulphite solution and organic layer was separated and dried over anhydrous sodium sulphate. Solvent was removed to dryness and the crude porphyrin was purified on silica gel column chromatography using chloroform as eluent.

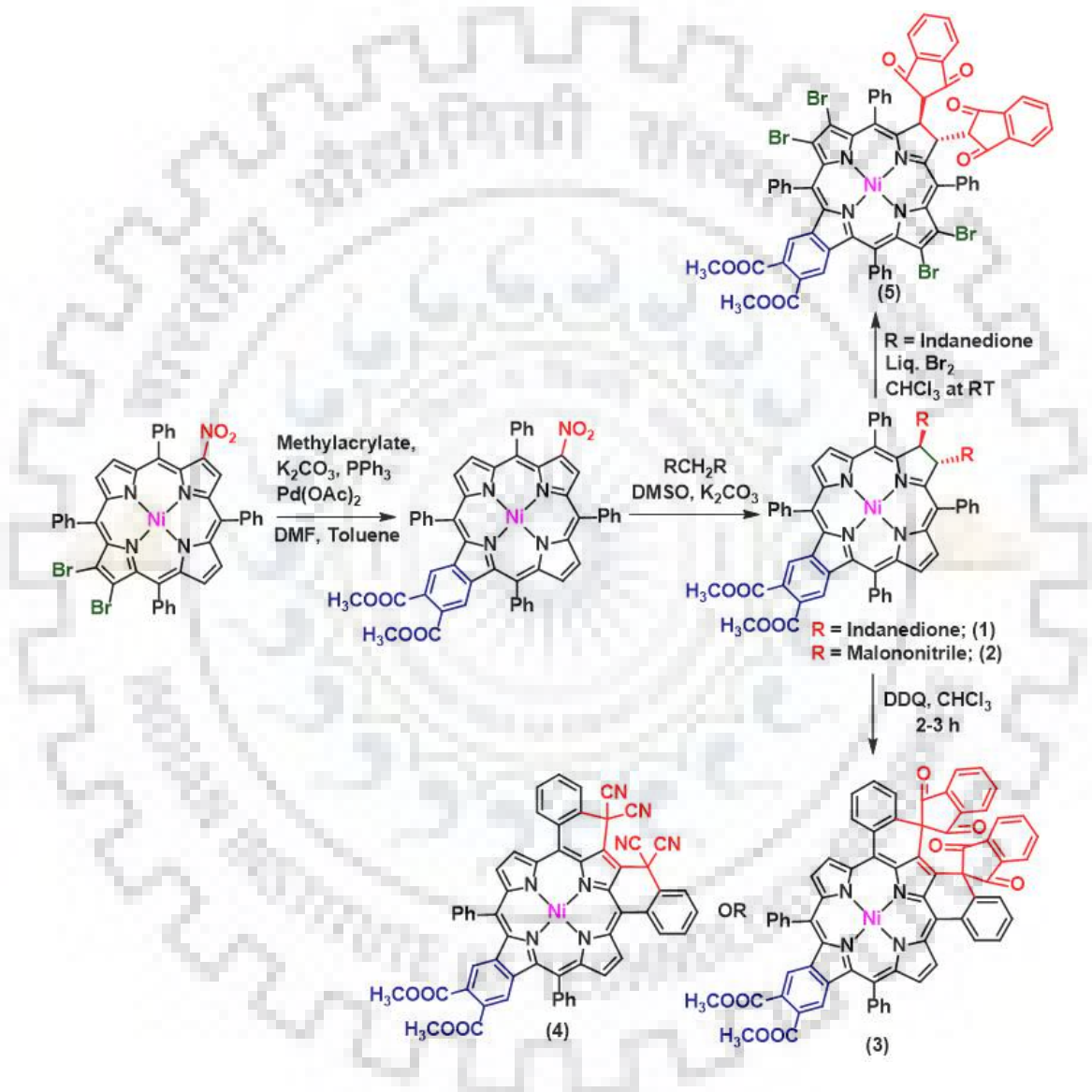
**NiTPCBr<sub>4</sub>(IND)<sub>2</sub>(Benzo) (5):** Yield: 80% (122 mg, 0.08 mmol). UV/vis (CH<sub>2</sub>Cl<sub>2</sub>):  $\lambda_{\max}$ (nm) (log  $\epsilon$ ): 230(5.05), 466(5.02), 549(3.85), 597(3.67), 650(sh), 706(4.60). <sup>1</sup>H NMR (400 MHz, CDCl<sub>3</sub>)  $\delta$ : 7.81-7.64(m, 13H, *meso*-Ph-H), 7.58-7.46(m, 5H, *meso*-Ph-H), 7.29-7.25(m, 3H, IND-H), 7.17-7.08(m, 3H, IND-H), 6.91(s, 2H, fused-H), 6.50(d, <sup>3</sup>J<sub>H, H</sub> = 8 Hz, 2H, IND-H), 5.29(d, <sup>3</sup>J<sub>H, H</sub> = 8 Hz, 2H,  $\beta$ -H), 3.84(d, <sup>3</sup>J<sub>H, H</sub> = 4 Hz, 6H, -CH<sub>3</sub>), 2.72(d, <sup>3</sup>J<sub>H, H</sub> = 8 Hz, 2H, -CH(IND)). MALDI-TOF-MS (*m/z*): found 1443.598 [M]<sup>+</sup> calcd 1443.398, found 1299.282 [M]<sup>+</sup>-IND calcd 1299.271. Anal. Calcd for C<sub>70</sub>H<sub>40</sub>Br<sub>4</sub>N<sub>4</sub>O<sub>8</sub>Ni C, 58.28; H, 2.79; N, 3.88. Found: C, 58.25; H, 2.80; N, 3.90.

## 5.3 RESULTS AND DISCUSSION

### 5.3.1 Synthesis and Characterization

2-Nitro-12,13-dibromo-tetraphenylporphyrinato nickel(II) (NiTPP(NO<sub>2</sub>)Br<sub>2</sub>) was synthesized according to the method developed in our laboratory [18]. Further, NiTPP(NO<sub>2</sub>)Br<sub>2</sub> was subjected to Heck coupling in order to get 2-nitro-12,13-benzo-tetraphenylporphyrin (NiTPP(NO<sub>2</sub>)(Benzo)) [19]. Chlorins can be easily prepared by reducing one  $\beta$ -pyrrolic bond thus to obtain corresponding *trans*-chlorins ((**1**) and (**2**) in Scheme 1), NiTPP(NO<sub>2</sub>)(Benzo) was treated with 10 eq. of active methylene compounds including malononitrile and indane-1,3-dione. These *trans*-chlorins upon refluxing with 6 eq. of DDQ in CHCl<sub>3</sub> resulted into the formation of corresponding  $\beta$ -*ortho*-phenyl doubly fused benzoporphyrins (**3**) and (**4**) (Scheme 1). In order to obtain the highly nonplanar and electron deficient chlorins, we performed the tetrabromination of synthesized *trans*-chlorins (**1**) and (**2**) using liquid bromine. NiTPC(IND)<sub>2</sub>(Benzo) (**1**) yielded to fully  $\beta$ -substituted NiTPCBr<sub>4</sub>(IND)<sub>2</sub>(Benzo) (**5**) upon bromination whereas the bromination of malononitrile appended *trans*-chlorin i.e.

NiTPC(MN)<sub>2</sub>(Benzo) (**2**) yielded the mixture of products which were not separable. NiTPCBr<sub>4</sub>(IND)<sub>2</sub>(Benzo) (**5**) was further subjected to oxidative fusion using 6 eq. of DDQ but this was also leading to inseparable mixture of products. All the newly synthesized porphyrinoids were characterized by <sup>1</sup>H NMR, UV-Visible spectroscopy, MALDI-TOF mass spectrometry and elemental analysis.



**Scheme 5.1** Synthetic Route to Benzochlorins and Difused Benzoporphyrins.

### 5.3.2 <sup>1</sup>H NMR and Mass Spectrometric Studies

The <sup>1</sup>H NMR spectra of synthesized Ni(II) benzochlorins and fused porphyrinoids were recorded in CDCl<sub>3</sub> at 298 K. Figures 5.1, A1 and A3 in Appendix-IV represent the <sup>1</sup>H NMR spectra of

synthesized *trans*-benzochlorins. Further, the  $^1\text{H}$  NMR spectra of triply fused porphyrins, (2) and (4), are shown in Figures 5.2 and A2 in Appendix-IV. Figures 5.1, A1 and A3 in Appendix-IV exhibited two doublets of two proton intensity at  $\sim 5$  and  $\sim 3$  ppm which correspond to the reduced  $\beta$ -pyrroles and  $-\text{CH}$  of  $\beta$ -substituents (IND or MN), respectively, whereas after fusion these both doublet have disappeared along with disappearance of two *ortho*-phenyl protons (Figures 5.2 and A2 in the Appendix-IV). No considerable shift in the proton signals of fused benzene ring was observed. In case of  $\text{NiTPCBr}_4(\text{IND})_2(\text{Benzo})$  (5), we have not observed any  $\beta$ -pyrrolic proton which clearly indicated the formation of fully  $\beta$ -substituted benzochlorin.

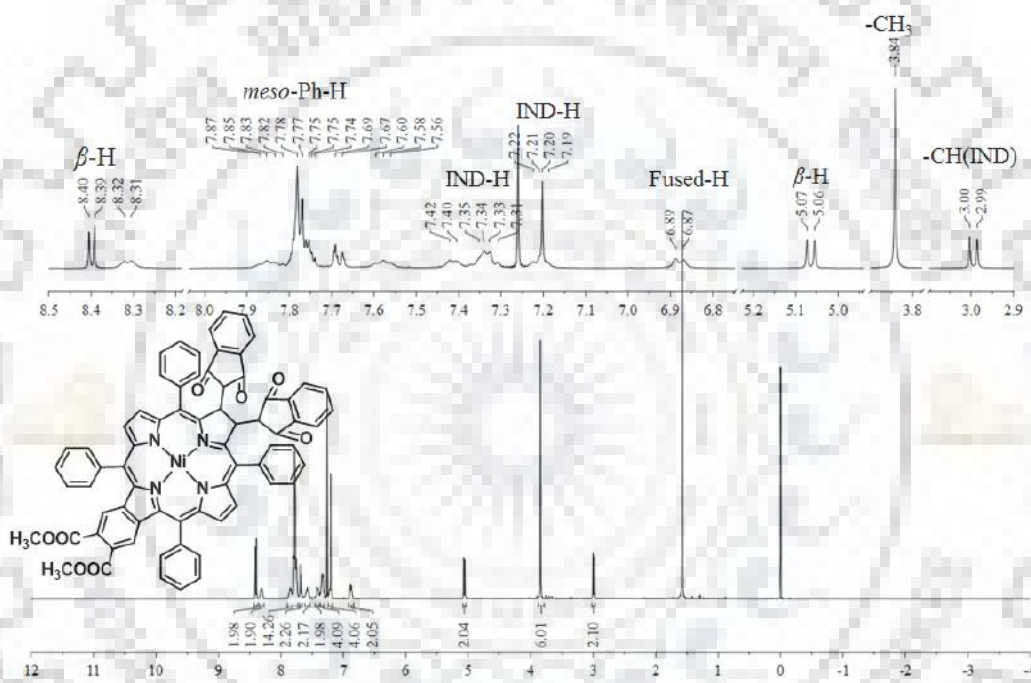


**Figure 5.1**  $^1\text{H}$  NMR Spectrum of  $\text{NiTPC}(\text{IND})_2(\text{Benzo})$  (1) in  $\text{CDCl}_3$  at 298 K.

The MALDI-TOF mass spectra of all synthesized Ni(II) porphyrinoids were recorded in positive ion mode using HABA as matrix. Figures 5.3 and A4-A7 in Appendix-IV have shown the MALDI-TOF mass spectra of synthesized compounds. The observed mass values were exactly matching with the proposed structures. Due to the presence of labile substituents, we observed the fragmentation in some of the recorded mass spectra for e.g. in case of malononitrile appended porphyrinoids (Figures A5 and A6 in Appendix-IV) sideways some extra peaks have been observed which were corresponding to removal of one or more cyano groups.



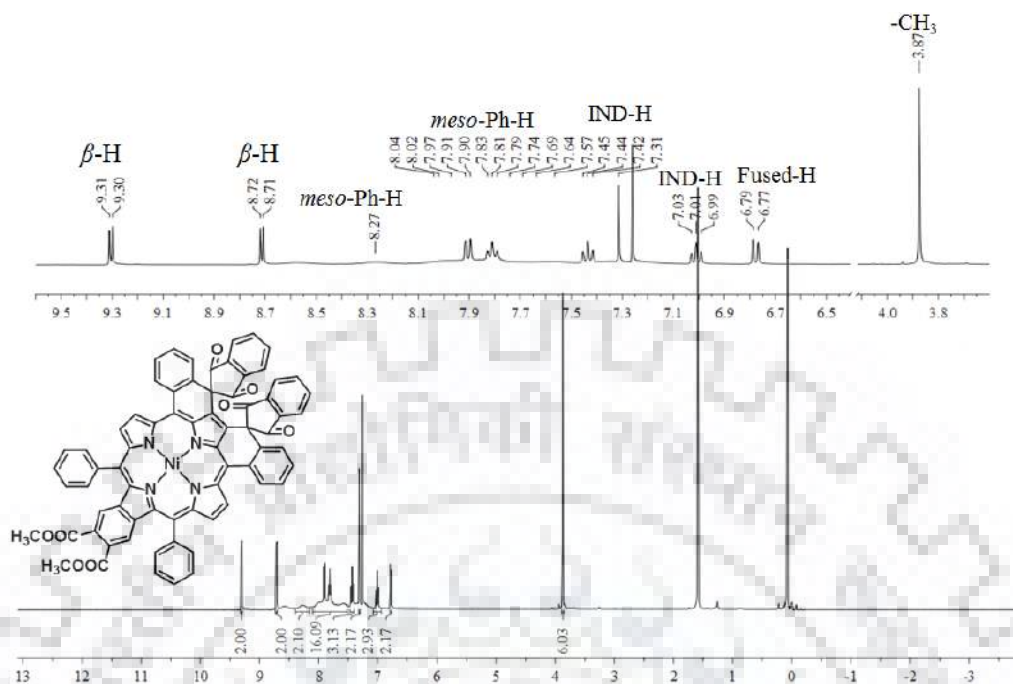


**Figure 5.2**  $^1\text{H}$  NMR Spectrum of NiDFP(IND) $_2$ (Benzo) (**3**) in  $\text{CDCl}_3$  at 298 K.

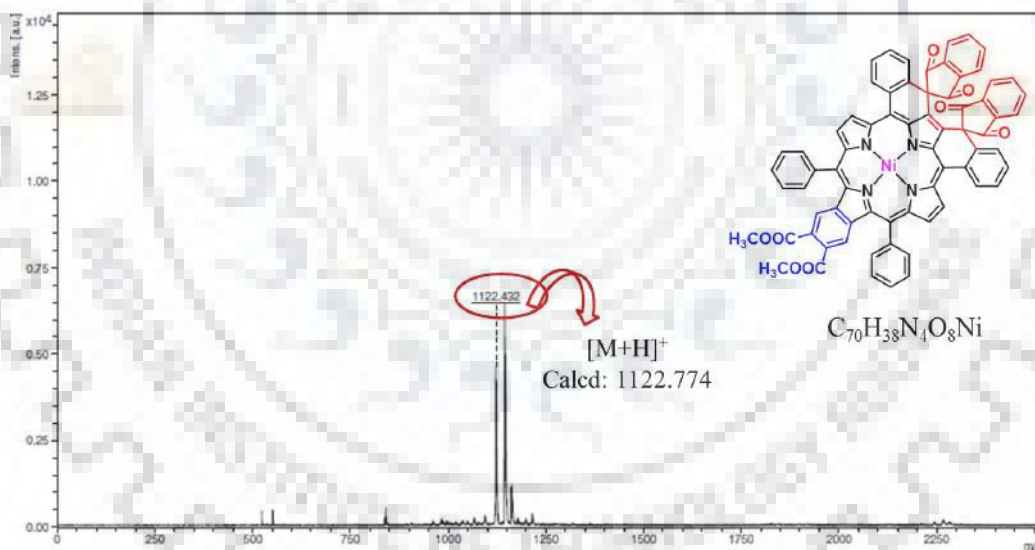


**Figure 5.3** MALDI-TOF-Mass Spectrum of NiDFP(IND) $_2$ (Benzo) (**3**) in Positive Ion Mode.

### 5.3.3 DFT Calculation

The gas phase geometry optimization of synthesized porphyrinoids **1-4** was performed using B3LYP functional with LANL2DZ basis sets. The optimized structures of **1-4** are shown in Figures 5.4 and A8-A10 in Appendix-IV. The highest occupied molecular orbitals (HOMO) and HOMO-1 in NiTPC(IND) $_2$ (benzo) (**1**) have contributed mainly from indanedione moiety and  $d_{xy}$



metal orbitals, respectively which shows the comparatively electron rich nature of indanedione moiety and charge transfer from metal to macrocyclic ring. In opposite, *trans*-chlorin NiTPC(MN)<sub>2</sub>(benzo) (**2**) has shown a<sub>1u</sub> as HOMO and a<sub>2u</sub> as HOMO-1 as for the symmetrically substituted chlorins. However upon fusion, the difused benzoporphyrins **3** and **4** both have shown a<sub>2u</sub> as HOMO and a<sub>1u</sub> as LUMO as similar for electron deficient porphyrins.

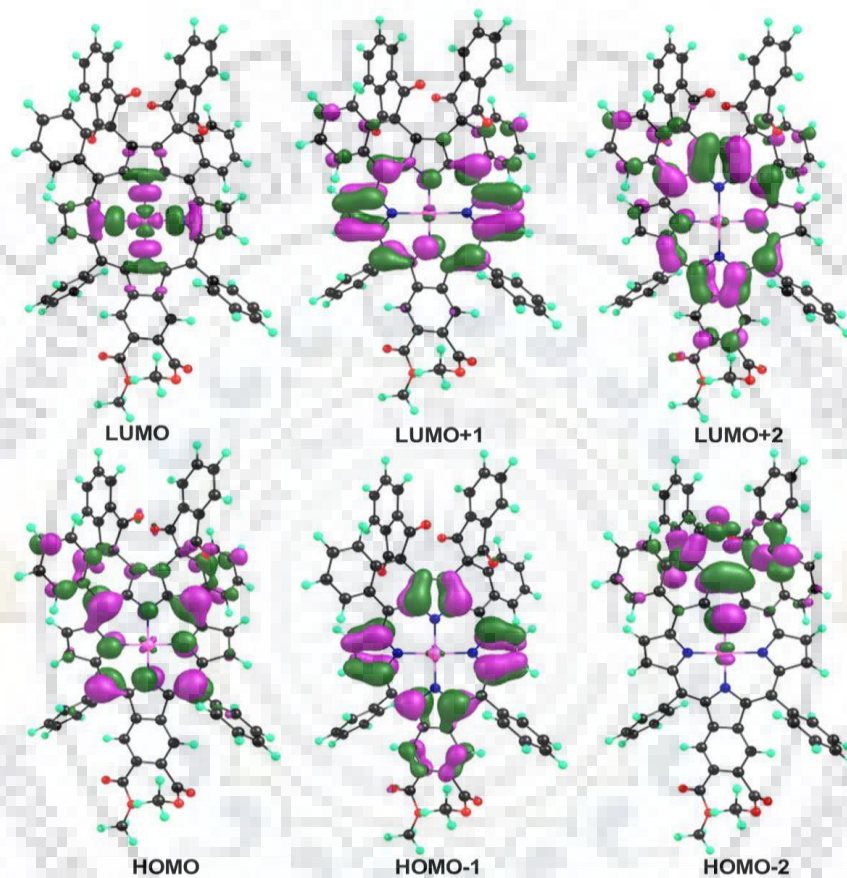


**Figure 5.4** Frontier Molecular Orbitals of NiDFP(IND)<sub>2</sub>(Benzo) (**3**).

### 5.3.4 Absorption Studies

The electronic absorption spectra of synthesized porphyrinoids were recorded in CH<sub>2</sub>Cl<sub>2</sub> at 298 K. The comparative absorption spectra of synthesized benzochlorins are shown in Figure 5.5a whereas the absorption spectra of synthesized difused benzoporphyrins are given in Figure 5.5b. Table 5.1 lists the electronic spectral data of synthesized porphyrinoids in CH<sub>2</sub>Cl<sub>2</sub>. The *meso*- $\beta$  and  $\beta$ - $\beta'$  fusion strongly affected the conformation of macrocycle which resulted into the highly red shifted spectral features of synthesized chlorins and porphyrins. The synthesized *trans*-benzochlorins **1** and **2** were highly red shifted as compared to the *trans*-chlorins reported in

literature [20,21]. On one hand,  $\beta$ -substitution with highly electron withdrawing bromo groups in NiTPCBr<sub>4</sub>(IND)<sub>2</sub>(Benzo) (**5**) brought the longest wavelength Q<sub>y(0,0)</sub> band beyond 700 nm which is possibly due to electron withdrawing bromo groups, extended  $\pi$ -conjugation and highly nonplanar conformation of the macrocyclic core. On the other hand,  $\beta$ -bromination caused a relative increase in intensity of the last Q-band which resulted into the higher Q/B ratio of **5**. The triply fused porphyrin NiDFP(IND)<sub>2</sub>(Benzo) (**3**) exhibited 17 nm and 45 nm red shifts in the Soret band as compared to corresponding difused porphyrin NiDFP(IND)<sub>2</sub> ( $\lambda_B = 463$  nm) (Chapter 3) and monofused porphyrin NiMFP(IND) ( $\lambda_B = 435$  nm) porphyrins (Chapter 4), respectively which may be due to enhanced nonplanarity and extended  $\pi$ -conjugation provided by fused benzene ring at the  $\beta$ -pyrrolic position. Difused benzoporphyrins **3** and **4** have shown 33-35 nm red shift in the Soret band as compared to starting material NiTPP(NO<sub>2</sub>)(Benzo) which ascribed to the *meso*- $\beta$ -fusion.

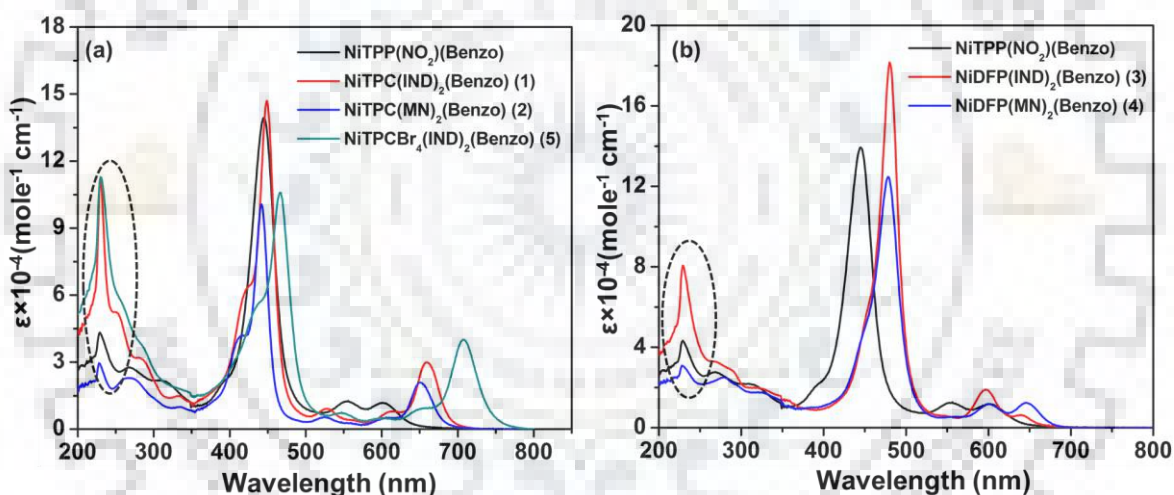


**Figure 5.5** (a) Comparative Absorption Spectra of Synthesized *trans*-Benzochlorins; (b) Synthesized Difused Benzoporphyrins in CH<sub>2</sub>Cl<sub>2</sub> at 298 K. Circled Areas show the Absorption due to  $\beta$ -Substituents.

Notably *trans*-chlorins NiTPC(IND)<sub>2</sub>(Benzo) (**1**) and NiTPC(MN)<sub>2</sub>(Benzo) (**2**) have shown lower FWHM and oscillator strength as compared to precursor NiTPP(NO<sub>2</sub>)(Benzo) due to the sharpening of Soret band which is the characteristic feature of chlorins. However, *trans*-chlorin (**5**) has shown the highest FWHM and oscillator strength due to the broadening of Soret band because of the bulkier bromo groups. The calculated oscillator strengths for synthesized compounds ranges from 0.011-0.024 which were estimated by the following formula

$$f = 4.61 \times 10^{-9} \epsilon \delta$$

Where,  $\epsilon$  = molar absorption coefficient of Soret band and  $\delta$  = full width at half maxima

Porphyrinoids **3** and **4** have shown slightly higher FWHM and oscillator strength with low values of Q/B ratio as compared to the precursor *trans*-chlorins, **1** and **2**, which is the clear indication for the porphyrin formation upon fusion.

**Table 5.1** Electronic Spectral Data<sup>a</sup> of Synthesized Porphyrinoids in CH<sub>2</sub>Cl<sub>2</sub> at 298 K.

Porphyrinoids	$\lambda_{\text{abs}}$	FWHM	Q/B	$\Sigma Q/\Sigma B$	$f$
NiTPP(NO <sub>2</sub> )(Benzo)	268(4.44), 445(5.14), 554(4.09), 602(4.07)	37	0.088	0.080	0.024
NiTPC(IND) <sub>2</sub> (Benzo) ( <b>1</b> )	230(5.04), 448(5.17), 527(3.96), 612(sh), 659(4.48)	26	0.207	0.217	0.018
NiTPC(MN) <sub>2</sub> (Benzo) ( <b>2</b> )	267(4.36), 442(5.00), 552(3.42), 602(sh), 651(4.32)	23	0.213	0.256	0.011
NiDFP(IND) <sub>2</sub> (Benzo) ( <b>3</b> )	229(4.90), 480(5.26), 596(4.28), 664(3.76)	27	0.037	0.023	0.023
NiDFP(MN) <sub>2</sub> (Benzo) ( <b>4</b> )	277(4.40), 478(5.10), 599(4.07), 647(4.09)	34	0.081	0.082	0.020
NiTPCBr <sub>4</sub> (IND) <sub>2</sub> (Benzo) ( <b>5</b> )	230(5.05), 466(5.02), 549(3.85), 597(3.67), 650(sh), 706(4.60)	49	0.385	0.338	0.024

<sup>a</sup>The values in parentheses refer to log  $\epsilon$ , integrated ( $\Sigma Q/\Sigma B$ ) intensity ratios of the Q and Soret (B) absorption,  $f$  = oscillator strength.

### 5.3.5 Electrochemical Studies

The electrochemical redox properties of all synthesized porphyrinoids were investigated in CH<sub>2</sub>Cl<sub>2</sub> using 0.1M TBAPF<sub>6</sub> as supporting electrolyte at 298 K. The comparative cyclic voltammograms of synthesized porphyrinoids are given in Figure 5.6. Figure A11 in Appendix-IV represents the comparative differential pulse voltammograms (DPVs) of all synthesized compounds. Table 5.2 lists the redox potential data of synthesized Ni(II) complexes in CH<sub>2</sub>Cl<sub>2</sub> at 298K. *Trans*-benzochlorins **1**, **2** and **5** were very easier to oxidize and harder to reduce as compared to the precursor NiTPP(NO<sub>2</sub>)(Benzo). In general, malononitrile appended *trans*-benzochlorin i.e. NiTPC(MN)<sub>2</sub>(Benzo) (**2**) and difused benzoporphyrin NiDFP(MN)<sub>2</sub>(Benzo) (**4**)

were difficult to oxidize and easy to reduce as compared to the corresponding indanedione appended porphyrinoids which clearly reflected the electron withdrawing nature of malononitrile group. The first oxidation and reduction potentials of NiTPC(MN)<sub>2</sub>(Benzo) (**2**) were 230 mV and 130 mV anodically shifted, respectively as compared to NiTPC(IND)<sub>2</sub>(Benzo) (**1**). Likewise, NiDFP(MN)<sub>2</sub>(Benzo) (**4**) has shown a significant anodic shift (250 mV) in first reduction potential and 30 mV anodic shift in first ring oxidation potentials as compared to NiDFP(IND)<sub>2</sub>(Benzo) (**3**). Substitution effect of bromo groups was strongly observed in the redox potentials of NiTPCBr<sub>4</sub>(IND)<sub>2</sub>(Benzo) (**5**) as the first ring oxidation and reduction potentials of **5** were profoundly anodically shifted (220 mV and 320 mV, respectively) as compared to the unbrominated NiTPC(IND)<sub>2</sub>(Benzo) (**1**). Fusion onto the macrocyclic skeleton also strongly affected the redox potentials. The difused benzoporphyrins (**3**) and (**4**) were 200-270 mV cathodically shifted in their first ring oxidation potentials and 110-230 mV anodically shifted in their first ring redox potentials as compared to the precursor *trans*-chlorins (**1**) and (**2**). Notably, all newly synthesized porphyrinoids have shown an additional reduction due to the presence of  $\beta$ -substituents.

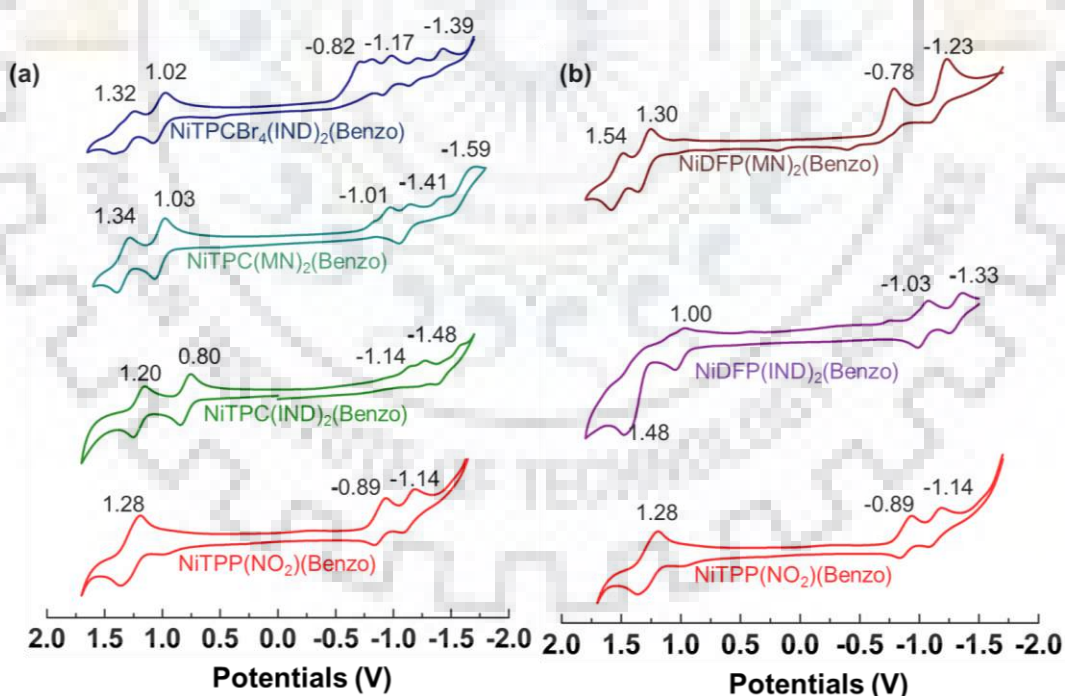


**Figure 5.6** Comparative Cyclic Voltammograms of Synthesized Porphyrinoids in CH<sub>2</sub>Cl<sub>2</sub> at 298 K using 0.1M TBAPF<sub>6</sub>.

Among all, the starting material NiTPP(NO<sub>2</sub>)(benzo) have highest HOMO-LUMO gap whereas reduction of  $\beta$ - $\beta'$  bond as well as fusion led to the decrement in HOMO-LUMO gap (Figure 5.7). Noticeably, NiTPCBr<sub>4</sub>(IND)<sub>2</sub>(Benzo) (**5**) has shown the lowest HOMO-LUMO gap due to the presence of four electron withdrawing bromo groups. Thus, we were able to tune the redox potentials and HOMO-LUMO gap by means of appending electron withdrawing substituents and fusing the  $\beta$ -pyrrolic positions.

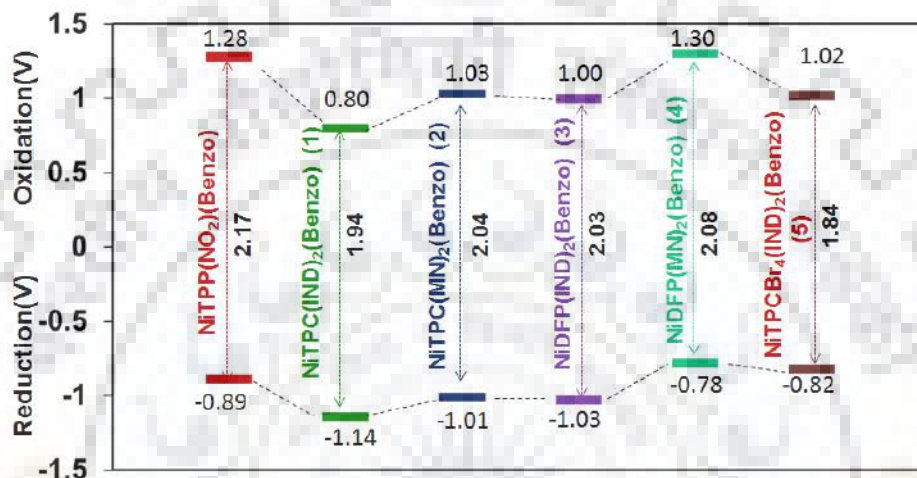


Figure 5.7 Variations in HOMO-LUMO Gap of Porphyrinoids.

Table 5.2 Comparative Electrochemical Redox Data<sup>a</sup> of Synthesized Porphyrinoids in CH<sub>2</sub>Cl<sub>2</sub> at 298 K.

Porphyrinoids	Oxidation (V)			Reduction (V)			$\Delta E_{1/2}$
	I	II	III	I	II	III	
NiTPP(NO <sub>2</sub> )(Benzo)	1.28			-0.89	-1.14		2.17
NiTPC(IND) <sub>2</sub> (Benzo) ( <b>1</b> )	0.80	1.20		-1.14 <sup>i</sup>	-1.25	-1.48	1.94
NiTPC(MN) <sub>2</sub> (Benzo) ( <b>2</b> )	1.03	1.34		-1.01	-1.41 <sup>i</sup>	-1.59	2.04
NiDFP(IND) <sub>2</sub> (Benzo) ( <b>3</b> )	1.00	1.48 <sup>i</sup>	1.66 <sup>d</sup>	-1.03	-1.33	-1.71 <sup>d</sup>	2.03
NiDFP(MN) <sub>2</sub> (Benzo) ( <b>4</b> )	1.30	1.54		-0.78 <sup>i</sup>	-1.23 <sup>i</sup>	-1.89 <sup>d</sup>	2.08
NiTPCBr <sub>4</sub> (IND) <sub>2</sub> (Benzo) ( <b>5</b> )	1.02	1.32		-0.82 <sup>i</sup>	-0.94	-1.17	1.84

<sup>a</sup>vs Ag/AgCl reference electrode, i = irreversible, d = data obtained from differential pulse voltammetry (DPV)



### 5.3.6 Anion Sensing Properties

To gain insight into the electronic nature and macrocyclic conformation on the ligation behavior of inner core nickel metal, we have carried out the anion sensing studies of synthesized Ni(II) porphyrinoids in  $\text{CH}_2\text{Cl}_2$  using different basic anions in the form of their tetrabutylammonium salts. All the synthesized *trans*-benzochlorins **1**, **2** and **5** have shown the quick colorimetric response with spectral changes towards some of the basic anions. Figure 5.8 represents the spectral changes of NiTPC(IND)<sub>2</sub>(Benzo) (**1**) with cyanide ion whereas Figure A12 in Appendix-IV shows the spectral changes of **2** and **5** with cyanide ion. The sequential addition of basic anions to **1** led to the 9 nm and 18 nm red shifts in the Soret and Q bands, respectively with broadening of Soret as well as Q bands which were possibly due to the abstraction of acidic proton present on the indanedione substituent at reduced  $\beta$ -pyrrolic side (Scheme 5.2). *Trans*-chlorin **2** has also shown the similar spectral changes with relatively less broadening of Soret band as compared to IND substituted chlorin **1**. Similarly, all the *trans*-benzochlorins have shown the colorimetric and spectral changes with other basic anions due to their higher pKa values.

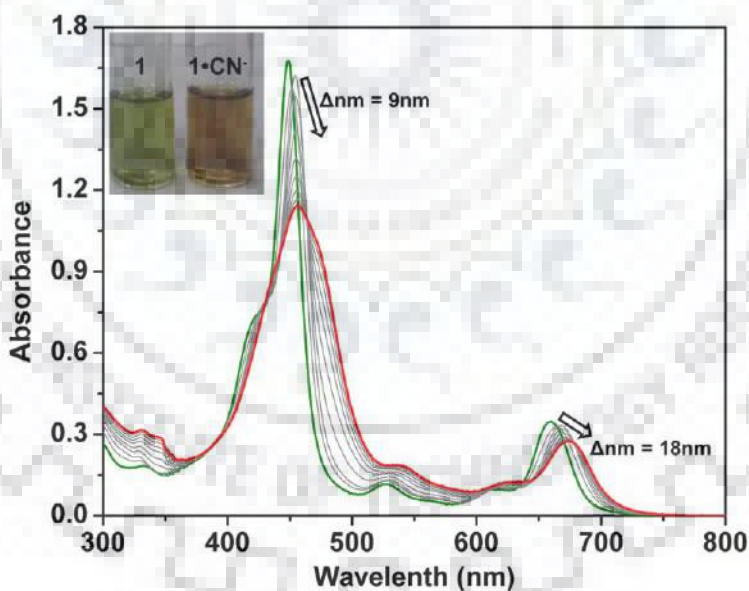
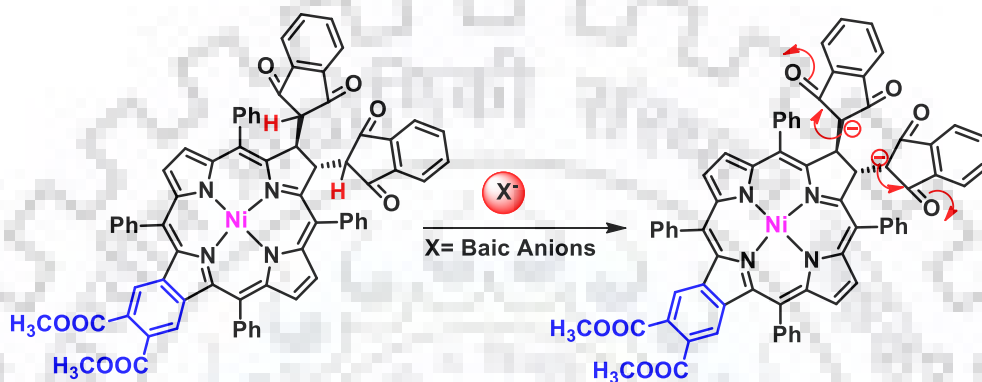


**Figure 5.8** UV-Visible Spectral Changes of NiTPC(IND)<sub>2</sub>(Benzo) (**1**) Upon Sequential Addition of Cyanide Ion in  $\text{CH}_2\text{Cl}_2$  at 298 K.

These results can be explained in such a way that the abstraction of acidic proton resulted into the generation of carbanion which effectively stabilized *via* either two carbonyl or cyano groups. In the case of difused benzoporphyrins, no acidic proton was left to interact with basic anion,



thus, NiDFP(IND)<sub>2</sub>(Benzo) (**3**) has not shown any spectral change upon addition of even excess of highly basic anion such as CN<sup>-</sup> (Figure A13 in Appendix-IV). Interestingly, malononitrile appended difused benzoporphyrin NiDFP(MN)<sub>2</sub>(Benzo) (**4**), selectively detected the cyanide ion among all other anions. That ascribed to the axial coordination of cyanide ion to the highly electron deficient porphyrin which can also be seen from the electrochemical redox data (*vide supra*)



**Scheme 5.2** Plausible Mechanism for the Detection of Basic Anions through *trans*-Chlorins.

### 5.3.7 Selective Detection of Cyanide Ion by NiDFP(MN)<sub>2</sub>(Benzo) (**4**)

The selective anion recognition properties of NiDFP(MN)<sub>2</sub>(Benzo) (**4**) were studied in CH<sub>2</sub>Cl<sub>2</sub> using various anions in the form of their TBA salts. Interestingly, a specific feature of this sensor was determined as its ability to specifically recognize cyanide ion in a mixture of other anions. It exhibited a specific red shift in the Soret and last Q band with instant color change from green to yellow with cyanide ion as shown in Figure 5.9a whereas no observable color change and spectral shifts were observed with other tested anions as shown in Figure 5.9b. Figure 5.9c shows the UV-visible spectral changes upon sequential addition of cyanide ion. As we increased the conc. of cyanide ion ( $1.20 \times 10^{-5}$ – $11.90 \times 10^{-5}$  M), the absorbance of **4** at 478 nm decreased with the emergence of new B bands along with some charge transfer bands also. At the same time, both the Q bands had disappeared with the appearance of multiple isosbestic points. Binding constants and stoichiometry were evaluated using Hill equation [22]. The inset of Figure 5.9c representing the Hill plot between  $\log(A_i - A_0)/(A_f - A_i)$  vs  $\log[\text{CN}^-]$  which shows a straight line with  $\eta$  value more the 2 which indicated that two cyanide ions were axially coordinated to Ni(II) metal center. The observed very high binding constant ( $\beta = 2.75 \times 10^{11}$ ) for NiDFP(MN)<sub>2</sub>(Benzo) (**4**) and high magnitude of Hill coefficient  $\eta$  (2.6) was clearly reflecting the presence of positive cooperativity

between the binding events as shown in Figure 5.10b which showed a sigmoidal curve for  $\Delta A$  vs  $[\text{CN}^-] M$ .

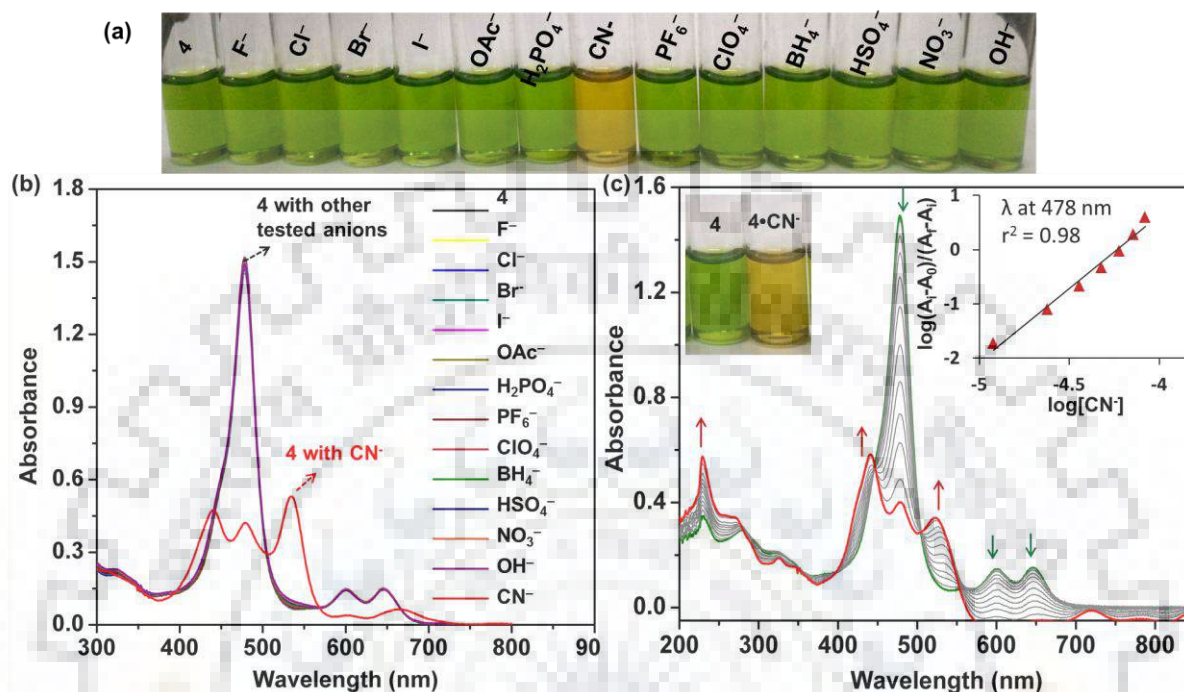


**Figure 5.9** (a) Colorimetric Response of **4** with Tested Anions in  $\text{CH}_2\text{Cl}_2$ ; (b) UV-Vis Spectral Changes of **4** ( $1.08 \times 10^{-5} M$ ) upon Addition of Excess of Tested Anions in the Form of TBA Salts in  $\text{CH}_2\text{Cl}_2$  298 K; (c) UV-visible Spectral Titrations of **4** ( $10 \mu\text{M}$ ) upon Sequential Addition of TBACN ( $0.018 M$ ) in  $\text{CH}_2\text{Cl}_2$ , Inset Shows Corresponding Hill Plot.

For the real-world application of this potential sensor, the test kits were prepared by dipping Whatman filter papers in a bit concentrated solution of **4** ( $5 \text{ mM}$ ) in  $\text{CH}_2\text{Cl}_2$ . The prepared test kits were dried in air. These dried test strips were exposed to different anion solutions ( $1 \times 10^{-4} M$ ) in dichloromethane for few seconds. Interestingly, the green color of test strip was turned to yellow only with  $\text{CN}^-$  ion in  $\text{CH}_2\text{Cl}_2$  (Figure 5.10a) whereas no color change was observed for other tested anions. Hence this potential sensor **4** was found very selective towards cyanide ion. Interestingly, other basic anions such as fluoride, acetate and dihydrogen phosphate which usually known as most common interfering anions did not show any response towards this sensor. To ascertain the competitive behavior, ratiometric experiment was performed using two equivalents of cyanide ions with 10 equivalents of interfering anions in  $\text{CH}_2\text{Cl}_2$ . Figure 5.10c shows the representative bar graph observed for NiDFP(MN)<sub>2</sub>(Benzo) (**4**) in presence of

interfering anion which clearly demonstrated the tolerance of **4** against these potential interfering anions to detect the cyanide ion.

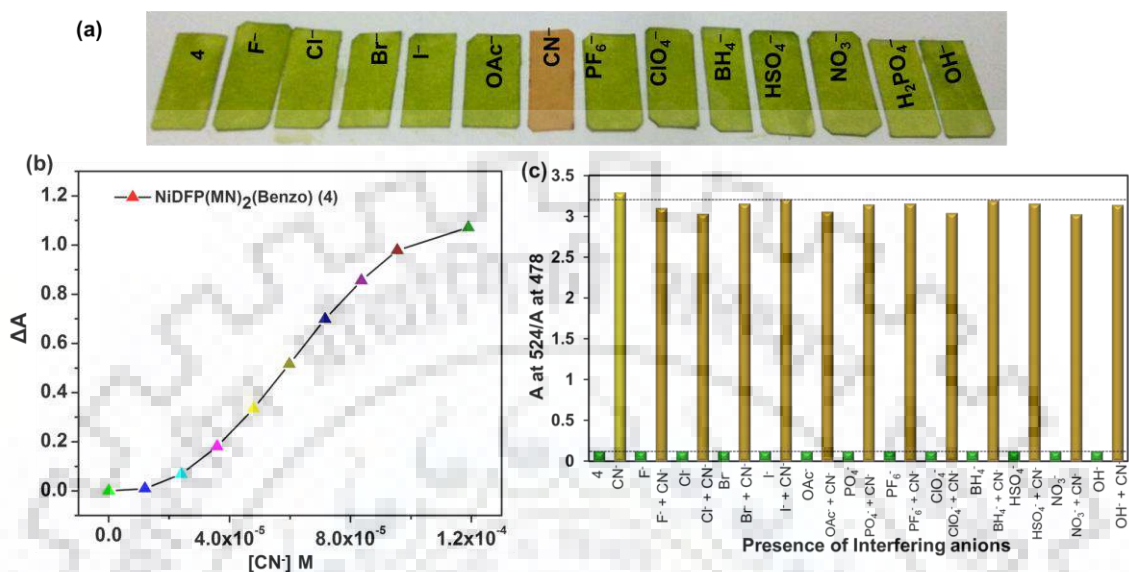


**Figure 5.10** (a) Picture of Test Strips of **4** (5 mM) for Detection of Cyanide ion in  $CH_2Cl_2$ . (b) Sigmoidal Curve for **4** Representing Graph between  $[CN^-]$  vs  $\Delta A$  Indicating Positive Cooperative Behavior. (c) Ratiometric Absorbance Ratio ( $A_{524}/A_{478}$ ) of **4** (10  $\mu$ M) upon Addition of 2 eq. of  $CN^-$  and 10 eq. of Other Interfering Anions.

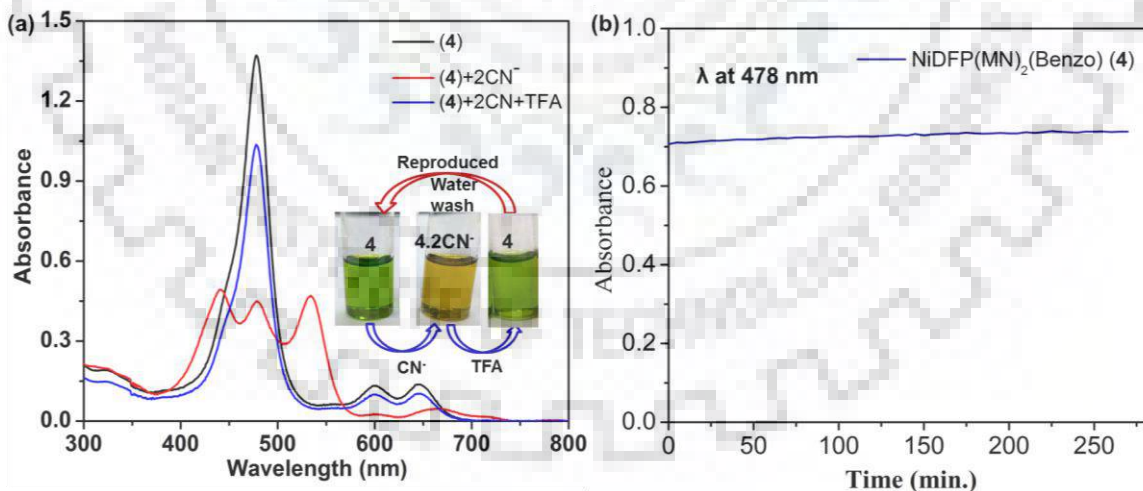
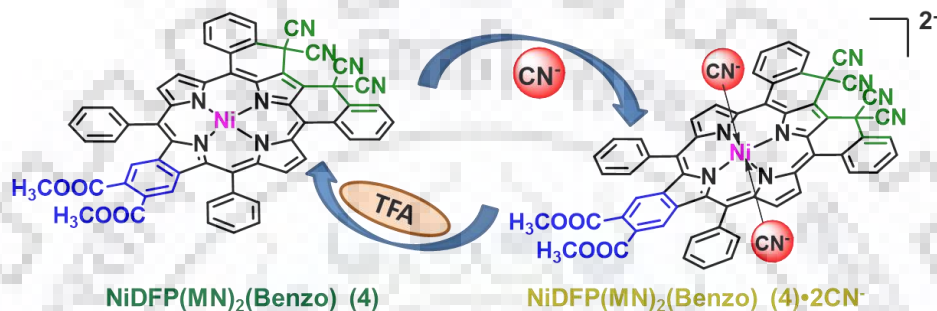


**Figure 5.11** (a) The Colorimetric and UV-Visible Spectral Changes of **4** for Reversibility Test; (b) The Stability Test of **4.2CN<sup>-</sup>** Adduct Observed for 300 min.

To gain further insights into the range of applicability, the reversibility test has been applied. The sensor **4** was treated with 2 eq. of cyanide ion which resulted into the generation of **4.2CN<sup>-</sup>** that

can be visualized with spectral changes as well as color changes.  $4.2\text{CN}^-$  adduct was treated with trace of TFA solution to switch the cyanide ion binding as shown in Figure 5.11a. Addition of TFA immediately restored the probe **4** (Scheme 5.3). To remove TFA the solution was washed with water and reused again for sensing of cyanide ion. The stability of adduct  $4.2\text{CN}^-$  was also monitored by UV-visible spectroscopy which clearly indicates that the axially ligated  $\text{CN}^-$  to **4** is very stable for a longer period of time as shown in Figure 5.11b.



**Scheme 5.3** The Schematic Representation of Binding of  $\text{CN}^-$  Ion to **4** and Its Reversibility in Presence of Trifluoroacetic Acid.

## 5.4 CONCLUSIONS

In summary, we have synthesized highly nonplanar and electron deficient *trans*-benzochlorins and converted them into  $\beta$ -*ortho*-meso-phenyl doubly fused benzoporphyrins. The synthesized porphyrinoids exhibited highly red shifted spectral features as compared to known *trans*-chlorins and other structurally related compounds. Interestingly, **5** has shown very high Q/B ratio with very high FWHM and oscillator strength which ascribed to highest nonplanar nature among all synthesized porphyrinoids. Malonitrile appended porphyrinoids **2** and **4** were difficult to oxidize and easy to reduce as compared to corresponding indanedione appended porphyrinoids (**1** and **3**) which strongly supported the higher electron deficient nature of these compounds. *Trans*-chlorins recognize the basic ion through outer proton abstraction whereas highly electron deficient and nonplanar difused benzoporphyrin  $\text{NiDFP(MN)}_2(\text{Benzo})$  (**4**) exhibited “Naked Eye” selective detection of cyanide ion with very high binding constant. The reversibility study demonstrated that the sensor **4** is recoverable and can be reused for selective cyanide ion detection without losing its sensing ability for numerous times.

## 5.5 REFERENCES

1. Sharma, M.; Ticho, A. L.; Samankumara, L.; Zeller, M.; Brückner, C. Conformational Landscapes of Metal(II) Porphyrinato, Chlorinato, and Morpholinochlorinato Complexes. *Inorg. Chem.* **2017**, *56*, 11490-11502.
2. Costa, L. D.; Costa, J. I. T.; Tomé, A. C. Porphyrin Macrocycle Modification: Pyrrole Ring-Contracted or -Expanded Porphyrinoids. *Molecules* **2016**, *21*, 320 (1-30).
3. Lebedev, A. Y.; Filatov, M. A.; Cheprakov, A. V.; Vinogradov, S. A. Effects of Structural Deformations on Optical Properties of Tetrabenzoporphyrins: Free-Bases and Pd Complexes. *J. Phys. Chem. A* **2008**, *112*, 7723-7733.
4. Cho, H. S.; Jeong, D. H.; Cho, S.; Kim, D.; Matsuzaki, Y.; Tanaka, K.; Tsuda, A.; Osuka, A. Photophysical Properties of Porphyrin Tapes. *J. Am. Chem. Soc.* **2002**, *124*, 14642-14654.
5. Gottumukkala, V.; Ongayi, O.; Baker, D. G.; Lomax, L. G.; Vicente, M. G. H. Synthesis, Cellular Uptake and Animal Toxicity of a Tetra(carboranylphenyl)-tetrabenzoporphyrin. *Bioorg. Med. Chem. Lett.* **2006**, *14*, 1871-1879.
6. Osaki, T.; Takagi, S.; Hoshino, Y.; Okumura, M.; Kadosawa, T.; Fujinaga, T. Efficacy of Antivascular Photodynamic Therapy using Benzoporphyrin Derivative Monoacid Ring A (BPD-MA) in 14 Dogs with Oral and Nasal Tumors. *J. Vet. Med. Sci.* **2009**, *71*, 125-32.
7. Deshpande, R.; Wang, B.; Dai, L.; Jiang, L.; Hartley, C. S.; Zou, S. Wang, H. Kerr, L. Opp-Dibenzoporphyrins as a Light-Harvester for Dye-Sensitized Solar Cells. *Chem. Asian J.* **2012**, *7*, 2662-2669.
8. Aveline, B.; Hasan, T.; Redmond, R. W. Photophysical and Photosensitizing Properties of Benzoporphyrin Derivative Monoacid Ring A (BPD-MA). *Photochem Photobiol.* **1994**, *59*, 328-335.
9. Panjehpour, M.; DeNovo, R. C.; Petersen, M. G.; Overholt, B. F.; Bower, R.; Rubinchik, V.; B. Kelly, Photodynamic Therapy using Verteporfin (Benzoporphyrin Derivative Monoacid Ring A, BPD-MA) and 630 nm Laser Light in Canine Esophagus. *Lasers Surg. Med.* **2002**, *30*, 26-30.



10. Taylor, C. D.; Wolfe, R. S. Structure and Methylation of Coenzyme M (HSCH<sub>2</sub>CH<sub>2</sub>SO<sub>3</sub>) *J. Biol. Chem.* **1974**, *249*, 4879-4885.
11. Tang, Q.; Carrington, P. E.; Horng, Y.-C.; Maroney, M. J.; Ragsdale, S. W.; Bocian, D. F. X-Ray Absorption and Resonance Raman Studies of Methyl-Coenzyme M Reductase Indicating that Ligand Exchange and Macrocycle Reduction Accompany Reductive Activation. *J. Am. Chem. Soc.* **2002**, *124*, 13242-13256.
12. Shelnut, J. A. *In The Porphyrin Handbook*; Kadish, K. M., Smith, K. M.; Guillard, R. Eds.; Academic Press: New York, 2000; Vol. 7, pp 167-223.
13. Kruglik, S. G.; Ermolenkov, V. V.; Orlovich, V. A.; Turpin, P.-Y. Axial Ligand Binding and Release Processes in Nickel(II)-tetraphenylporphyrin Revisited: a Resonance Raman Study *Chem. Phys.* **2003**, *286*, 97-108.
14. Song, Y.; Haddad, R. E.; Jia, S.-L.; Hok, S.; Olmstead, M. M.; Nurco, D. J.; Schore, N. E.; Zhang, J.; Ma, J.-G.; Smith, K. M.; Gazeau, S.; Pecaut, J.; Marchon, J.-C.; Medforth, C. J.; Shelnut J. A. Energetics and Structural Consequences of Axial Ligand Coordination in Nonplanar Nickel Porphyrins. *J. Am. Chem. Soc.* **2005**, *127*, 1179-1192.
15. Kumar, R.; Chaudhri, N.; Sankar, M. Ratiometric and Colorimetric “Naked Eye” Selective Detection of CN<sup>-</sup> Ions by Electron Deficient Ni(II) Porphyrins and Their Reversibility Studies. *Dalton Trans.* **2015**, *44*, 9149-9157.
16. Retsek, J. L.; Drain, C. M.; Kirmaier, C.; Nurco, D. J.; Medforth, C. J.; Smith, K. M.; Sazanovich, I. V.; Chirvony, V. S.; Fajer, J.; Holten, D. Photoinduced Axial Ligation and Deligation Dynamics of Nonplanar Nickel Dodecaarylporphyrins. *J. Am. Chem. Soc.* **2003**, *125*, 9787-9800.
17. Dommaschk, M.; Thoms, V.; Schütt, C.; Nather, C.; Puttreddy, R.; Rissanen, K.; Herges, R. Coordination-Induced Spin-State Switching with Nickel Chlorin and Nickel Isobacteriochlorin. *Inorg. Chem.* **2015**, *54*, 9390-9392.
18. Kumar, R.; Sankar, M. Synthesis, Spectral, and Electrochemical Studies of Electronically Tunable  $\beta$ -Substituted Porphyrins with Mixed Substituent Pattern. *Inorg. Chem.* **2014**, *53*, 12706-12719.



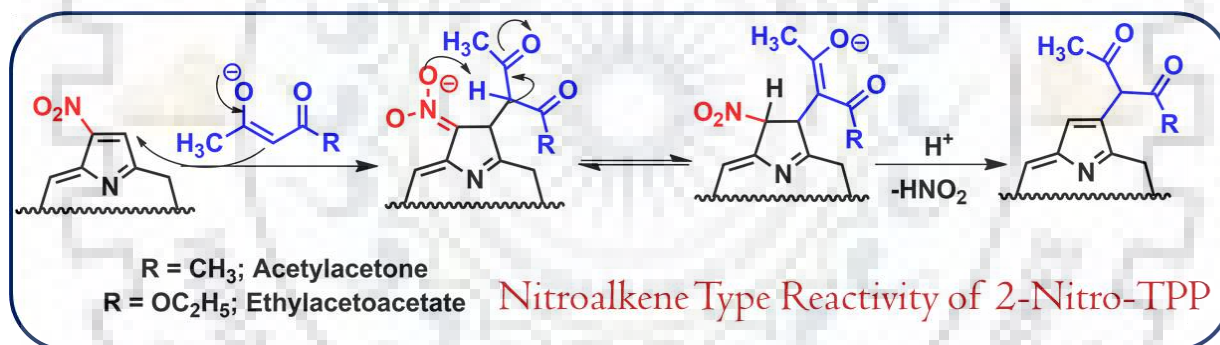
19. Jinadasa, R. G. W.; Fang, Y.; Deng, Y.; Deshpande, R.; Jiang, X.; Kadish, K. M.; Wang, H. Unsymmetrically Functionalized Benzoporphyrins. *RSC Adv.* **2015**, *5*, 51489-51492.
20. Hyland, M. A.; Morton, M. D.; Brückner, C. *meso*-Tetrakis(pentafluorophenyl)porphyrin-Derived Chromene Annulated Chlorins. *J. Org. Chem.* **2012**, *77*, 3038-3048.
21. Xiong, R.; Bornhof, A.-B.; Arkhypchuk, A. I.; Orthaber, A.; Borbas, K. E. Furan- and Thiophene-Based Auxochromes Red-shift Chlorin Absorptions and Enable Oxidative Chlorin Polymerizations. *Chem. Eur. J.* **2017**, *23*, 4089-4095.
22. Hill, A. V. The Possible Effects of the Aggregation of The Molecules of Haemoglobin on Its Dissociation Curves. *J. Physiol.* **1910**, *40*, IV-VII.





## CHAPTER 6

# “Synthesis, Structural, Photophysical and Electrochemical Redox Studies of $\beta$ -Trisubstituted Porphyrins”





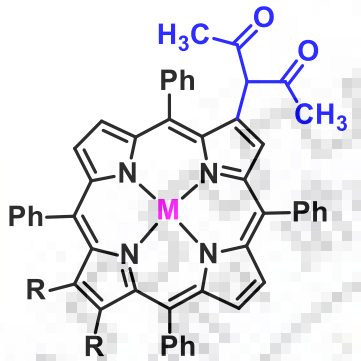
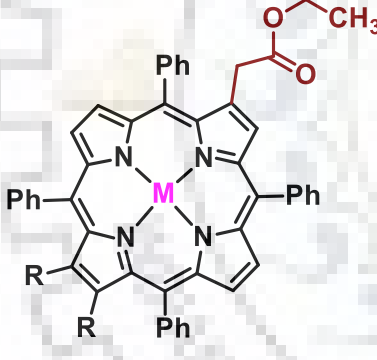
## CHAPTER 6

### SYNTHESIS, STRUCTURAL, PHOTOPHYSICAL AND ELECTROCHEMICAL REDOX STUDIES OF $\beta$ -TRISUBSTITUTED PORPHYRINS DERIVED

#### 6.1 INTRODUCTION

The chemical modification at  $\beta$ -pyrrolic position of porphyrin macrocycles has become an exciting research area as it opens an easy access to reach a wide variety of  $\beta$ -functionalized porphyrinoids for various biological and material applications [1-3]. The aromatic electrophilic substitution of tetraarylporphyrins has involved the reaction like nitration, formylation, acylation and bromination which has been proved a powerful synthetic methodology to effectively expand the chemistry of  $\beta$ -functionalized porphyrins [4,5].  $\beta$ -Nitration *via* Menke reaction has been considered as an important tool to introduce nitro group at the  $\beta$ -pyrrolic position [6] and particularly useful in post modification of the porphyrin skeleton [7,8].  $\beta$ -Nitro tetraarylporphyrins are versatile starting materials due to their ease of synthesis in high yields and nitroalkene type reactivity where they undergo Michael addition reaction with a wide range of nucleophiles to afford corresponding 2-substituted and 2-nitro-3-substituted porphyrins [7-9]. Moreover, it is easily convertible into several other functional groups [10]. The Menke nitration in porphyrins is usually carried out using Ni(II) or Cu(II) complexes because other metal complexes such as Co(II), Zn(II), Mg(II) and even free base porphyrin do not tolerate the acidic Menke reaction conditions and leads to either demetallated or protonated porphyrins [7]. However Ostrowski and coworkers have reported the selective electrophilic nitration of *meso*-tetraphenylporphyrin complexes using HNO<sub>3</sub> with different metal derivatives [11]. Initially Smith and coworkers have reported the reactivity of MTPP(NO<sub>2</sub>) with active methylene compounds including malonates and malononitriles leading to the preparation of either cyclopropylchlorin or *trans*-chlorins [12,13]. Later in 2005, Cavaleiro and coworkers described the different reactivity of 2-nitroporphyrin with 1,3-dicarbonyls to afford the corresponding porphyrins rather than chlorins [14].

**Chart 6.1** Molecular Structures of Synthesized  $\beta$ -Trisubstituted Porphyrins MTPP[CH(COCH<sub>3</sub>)<sub>2</sub>]R<sub>2</sub> and MTPP[CH<sub>2</sub>COOC<sub>2</sub>H<sub>5</sub>]R<sub>2</sub> (where R = Br and Ph).

Molecular Structure	R	M	Name	code	Yield%
	Br	2H	H <sub>2</sub> TPP[CH(COCH <sub>3</sub> ) <sub>2</sub> ]Br <sub>2</sub>	<b>1</b>	69
	Br	Co(II)	CoTPP[CH(COCH <sub>3</sub> ) <sub>2</sub> ]Br <sub>2</sub>	<b>1a</b>	86
	Br	Ni(II)	NiTPP[CH(COCH <sub>3</sub> ) <sub>2</sub> ]Br <sub>2</sub>	<b>1b</b>	73
	Br	Cu(II)	CuTPP[CH(COCH <sub>3</sub> ) <sub>2</sub> ]Br <sub>2</sub>	<b>1c</b>	83
	Br	Zn(II)	ZnTPP[CH(COCH <sub>3</sub> ) <sub>2</sub> ]Br <sub>2</sub>	<b>1d</b>	78
	Ph	2H	H <sub>2</sub> TPP[CH(COCH <sub>3</sub> ) <sub>2</sub> ]Ph <sub>2</sub>	<b>2</b>	77
	Ph	Co(II)	CoTPP[CH(COCH <sub>3</sub> ) <sub>2</sub> ]Ph <sub>2</sub>	<b>2a</b>	81
	Ph	Ni(II)	NiTPP[CH(COCH <sub>3</sub> ) <sub>2</sub> ]Ph <sub>2</sub>	<b>2b</b>	76
	Ph	Cu(II)	CuTPP[CH(COCH <sub>3</sub> ) <sub>2</sub> ]Ph <sub>2</sub>	<b>2c</b>	85
	Ph	Zn(II)	ZnTPP[CH(COCH <sub>3</sub> ) <sub>2</sub> ]Ph <sub>2</sub>	<b>2d</b>	80
	Br	2H	H <sub>2</sub> TPP[CH <sub>2</sub> COOC <sub>2</sub> H <sub>5</sub> ]Br <sub>2</sub>	<b>3</b>	79
	Br	Co(II)	CoTPP[CH <sub>2</sub> COOC <sub>2</sub> H <sub>5</sub> ]Br <sub>2</sub>	<b>3a</b>	74
	Br	Ni(II)	NiTPP[CH <sub>2</sub> COOC <sub>2</sub> H <sub>5</sub> ]Br <sub>2</sub>	<b>3b</b>	74
	Br	Cu(II)	CuTPP[CH <sub>2</sub> COOC <sub>2</sub> H <sub>5</sub> ]Br <sub>2</sub>	<b>3c</b>	76
	Br	Zn(II)	ZnTPP[CH <sub>2</sub> COOC <sub>2</sub> H <sub>5</sub> ]Br <sub>2</sub>	<b>3d</b>	81
	Ph	2H	H <sub>2</sub> TPP[CH <sub>2</sub> COOC <sub>2</sub> H <sub>5</sub> ]Ph <sub>2</sub>	<b>4</b>	81
	Ph	Co(II)	CoTPP[CH <sub>2</sub> COOC <sub>2</sub> H <sub>5</sub> ]Ph <sub>2</sub>	<b>4a</b>	83
	Ph	Ni(II)	NiTPP[CH <sub>2</sub> COOC <sub>2</sub> H <sub>5</sub> ]Ph <sub>2</sub>	<b>4b</b>	71
	Ph	Cu(II)	CuTPP[CH <sub>2</sub> COOC <sub>2</sub> H <sub>5</sub> ]Ph <sub>2</sub>	<b>4c</b>	87
	Ph	Zn(II)	ZnTPP[CH <sub>2</sub> COOC <sub>2</sub> H <sub>5</sub> ]Ph <sub>2</sub>	<b>4d</b>	79

Previous reported methods for the generation of C-C bond to afford functionalized porphyrins involve Pd coupling reactions [15]. However, the coupling reactions do suffer one or more problems such as insertion of palladium to the macrocyclic core, formation of debrominated/hydrogenated product along with desired product, lengthy synthetic procedures and most important low yield of the products which limit the large scale synthesis. Thus, from a synthetic point of view the construction of C-C bond at  $\beta$ -pyrrolic position by a facile route in good yield without use of Pd cross coupling reaction is of significant importance [9,14,16]. In addition, the incorporation of 1,3-dicarbonyls onto the periphery of porphyrin macrocycles make



them attractive candidates with rich synthetic potentiality due to their participation in various important chemical reactions such as complexation with metal ions to form dimers, multicomponent reactions such as Hantzsch or Biginelli reactions and condensation reaction to build heterocycles [17-19].

In an effort to elucidate the role of unsymmetrical substitution on the photophysical and electrochemical redox properties of the macrocycles, a new class of dibromo and diphenyl-TPPs bearing active methylene moiety at the  $\beta$ -pyrrolic position has been synthesized by nucleophilic substitution of nitro group (Chart 1) and characterized by various spectroscopic techniques.

## 6.2 EXPERIMENTAL SECTION

### 6.2.1 Materials

Ethyl acetoacetate, acetylacetone,  $K_2CO_3$ ,  $M(OAc)_2 \cdot nH_2O$ ,  $P_2O_5$  and  $CaH_2$  were purchased from HiMedia, India and used as received. DMSO and DMF were purchased from Thomas Baker and used without further purification. The solvents employed in the present work were distilled or dried before use.

### 6.2.2 Instrumentation and Methods

Characterization techniques and instrumentation were described in Chapter 2 in detail. Dichloromethane for electronic spectral studies and CV analysis was distilled and dried before use. The X-ray quality single crystals of  $NiTPP[CH(COCH_3)_2]Br_2$  (**1b**) were grown by vapor diffusion of methanol onto the **1b** solution in distilled  $CHCl_3$ . X-ray quality single crystals for  $H_2TPP[CH_2COOC_2H_5]Br_2$  (**3**) were obtained by vapor diffusion of methanol onto the toluene solution of porphyrin.  $ZnTPP[CH_2COOC_2H_5]Br_2$  (**4d**) crystals were obtained by vapor diffusion of hexane into the toluene solution containing a few drops of pyridine.

### 6.2.3 Synthetic Procedures

#### 6.2.3.1 General Synthetic Procedure for the Preparation of 2-(1-Acetyl-2'-oxopropyl)-12,13-dibromo/diphenyl-5,10,15,20-tetraphenyl Porphyrinato Nickel(II); $NiTPP[CH(COCH_3)_2]R_2$ (where R = Br or Ph)

200 mg of  $NiTPP(NO_2)_2$  (R = Br or Ph), 10 eq. of  $K_2CO_3$  and 5-6 ml of DMSO were taken in 100 ml degassed two necked RB flask. The reaction mixture was purged with argon for 10-15 minutes and then 10 eq. of acetylacetone was added into the resulting mixture. Further, the

reaction mixture was purged with argon gas for 10-15 minutes and stirred for 3-4 hours at 80 °C under inert atmosphere. After completion of the reaction, the reaction mixture was cooled to room temperature and diluted with  $\text{CHCl}_3$  and washed twice with saturated NaCl solution. The organic layer was dried over anhydrous sodium sulphate and evaporated to dryness. The crude porphyrin was purified by column chromatography using  $\text{CHCl}_3$ /hexane (7:3, v/v) mixture.

**NiTPP[CH(COCH<sub>3</sub>)<sub>2</sub>]Br<sub>2</sub> (1b):** (yield = 73%, 154 mg, 0.167 mmol). Mp > 300 °C. UV-vis in  $\text{CH}_2\text{Cl}_2$ :  $\lambda_{\text{max}}$  (nm) (log  $\epsilon$ ): 423(5.33), 539(4.19), 578(3.75). <sup>1</sup>H NMR (400 MHz,  $\text{CDCl}_3$ )  $\delta$  (ppm): 16.36 (s, 1H, enolic OH), 8.81-8.49 (m, 5H,  $\beta$ -H), 7.95 (d, <sup>3</sup> $J_{\text{H,H}}$  = 8Hz, 3H, *meso-o*-Ph-H), 7.84 (d, <sup>3</sup> $J_{\text{H,H}}$  = 4Hz, 3H, *meso-o*-Ph-H), 7.73-7.48 (m, 14H, *meso-o*, *m* & *p*-Ph-H), 2.17 (s, 1H, -CH), 1.82 (s, 6H, -CH<sub>3</sub>). MALDI-TOF-MS ( $m/z$ ): found 927.881 [M]<sup>+</sup>, calcd 927.305, found 848.809 [M]<sup>+</sup>-Br<sup>-</sup>, calcd 848.409, Found 768.204 [M]<sup>+</sup>-2Br<sup>-</sup>, calcd 768.940, Anal. Calcd for C<sub>49</sub>H<sub>32</sub>N<sub>4</sub>O<sub>2</sub>Br<sub>2</sub>Ni: C, 63.47; H, 3.48; N, 6.04. Found C, 63.48; H, 3.43; N, 6.08.

**NiTPP[CH(COCH<sub>3</sub>)<sub>2</sub>]Ph<sub>2</sub> (2b):** (Yield = 76%, 161mg, 0.174 mmol). Mp > 310 °C. UV-vis ( $\text{CH}_2\text{Cl}_2$ )  $\lambda_{\text{max}}$  (nm) (log  $\epsilon$ ): 425(5.33), 542(4.22), 580(sh). <sup>1</sup>H NMR (400 MHz,  $\text{CDCl}_3$ )  $\delta$  (ppm): 16.38 (s, 1H, enolic-OH), 8.55 (d, <sup>3</sup> $J_{\text{H,H}}$  = 4 Hz, 1H,  $\beta$ -H), 8.50 (s, 1H,  $\beta$ -H), 8.46 (d, <sup>3</sup> $J_{\text{H,H}}$  = 8 Hz, 1H,  $\beta$ -H), 8.38 (d, <sup>3</sup> $J_{\text{H,H}}$  = 4 Hz, 1H,  $\beta$ -H), 8.29 (d, <sup>3</sup> $J_{\text{H,H}}$  = 8 Hz, 1H,  $\beta$ -H), 7.98-7.96 (m, 2H, *meso-o*-Ph-H), 7.69-7.66 (m, 4H, *meso-o*-Ph-H), 7.55-7.45 (m, 7H, *meso-o*- & *m*, *p*-Ph-H), 7.19-7.15 (m, 3H, *meso-m*, *p*-Ph-H), 7.08-7.04 (m, 4H, *meso-m*, *p*-Ph-H), 6.89-6.86 (m, 10H,  $\beta$ -Ph-H), 2.36 (s, 1H, -CH), 1.85 (s, 6H, -CH<sub>3</sub>). MALDI-TOF-MS ( $m/z$ ): found 921.302 [M+H]<sup>+</sup>, calcd 921.273, found 878.203 [M]<sup>+</sup>-COCH<sub>3</sub>, calcd 878.256. Anal. Calcd for C<sub>61</sub>H<sub>42</sub>N<sub>4</sub>O<sub>2</sub>Ni: C, 79.49; H, 4.59; N, 6.08. Found C, 79.46; H, 4.60; N, 6.11.

### 6.2.3.2 General Synthetic Procedures for the Preparation of 2-(1-Acetyl-1-ethoxycarbonylmethyl)-12,13-dibromo/diphenyl-5,10,15,20-tetraphenyl Porphyrinato Nickel(II); NiTPP[CH<sub>2</sub>COOC<sub>2</sub>H<sub>5</sub>]R<sub>2</sub> (Where R = Br or Ph)

To verify the unusual reactivity of NiTPP(NO<sub>2</sub>)R<sub>2</sub> (where R = Br or Ph) with ethyl acetoacetate in order to attain ester appended porphyrins, we have utilized two different reaction pathways. The following two reaction pathways resulted into the same final product.

**Path A:** A 100 ml two necked RB flask was charged with 100 mg NiTPP(NO<sub>2</sub>)R<sub>2</sub> (where R = Br or Ph), 10 eq. of K<sub>2</sub>CO<sub>3</sub> and 5 ml of DMSO. The reaction mixture was degassed with argon for 10-15 minutes and then 10 eq. of ethyl acetoacetate was added under argon atmosphere and the

resulting mixture was purged with argon for additional 10-15 minutes. The reaction mixture was stirred for 2.5-3.0 h. at 90 °C under the inert atmosphere. After completion of the reaction, reaction mixture was cooled to room temperature and diluted with  $\text{CHCl}_3$  and washed twice with brine solution. The organic layer was separated and dried over anhydrous sodium sulphate and evaporated to dryness. The crude product was purified on the silica gel column eluted with toluene/hexane mixture (6:4, v/v). The product was recrystallized using  $\text{CHCl}_3/\text{CH}_3\text{OH}$  mixture (1:3, v/v).

**Path B:** 100 mg (0.114 mmol) of  $\text{NiTPP}(\text{NO}_2)\text{Br}_2$ , 10 eq. of  $\text{K}_2\text{CO}_3$  (157 mg, 1.14 mmol) and 10 eq. (146  $\mu\text{L}$ , 1.14 mmol) of ethyl acetoacetate were taken in a two necked RB flask. To this, 5 ml of DMF was added and reaction mixture was purged with argon gas for 15-20 minutes and the resulting reaction mixture was stirred at 100 °C for 3-4 hr. The reaction mixture was cooled to room temperature. 30 ml of distilled water was added to precipitate out the product. The precipitate was filtered through G4 crucible and crude porphyrin was dried under vacuum heating. The solid crude porphyrin was purified on column chromatography with toluene/hexane mixture (6:4, v/v). The product was recrystallized using  $\text{CHCl}_3$ /methanol mixture (1:3, v/v).

**NiTPP[CH<sub>2</sub>COOC<sub>2</sub>H<sub>5</sub>]Br<sub>2</sub> (3b).** (Yield = 74%, 77mg, 0.085 mmol). Mp > 310 °C. UV-vis ( $\text{CH}_2\text{Cl}_2$ )  $\lambda_{\text{max}}$  (nm) (log  $\epsilon$ ): 423(5.32), 539(4.19), 578(3.75). <sup>1</sup>H NMR (400 MHz,  $\text{CDCl}_3$ )  $\delta$  (ppm): 8.71 (d, <sup>3</sup> $J_{\text{H,H}}$  = 4 Hz, 1H,  $\beta$ -H), 8.61 (d, <sup>3</sup> $J_{\text{H,H}}$  = 4Hz, 1H,  $\beta$ -H), 8.56 (d, <sup>3</sup> $J_{\text{H,H}}$  = 8 Hz, 1H,  $\beta$ -H), 8.53 (d, <sup>3</sup> $J_{\text{H,H}}$  = 4 Hz, 2H,  $\beta$ -H), 7.96-7.94 (m, 2H, *meso-o*-Ph-H), 7.84-7.82 (m, 6H, *meso-o*-Ph-H), 7.71-7.60 (m, 12H, *meso-m, p*-Ph-H), 4.04 (q, <sup>3</sup> $J_{\text{H,H}}$  = 8 Hz, 16 Hz, 2H, -OCH<sub>2</sub>), 3.75(s, 2H, -CH<sub>2</sub>), 1.18 (t, 3H, -CH<sub>3</sub>). MALDI-TOF-MS ( $m/z$ ): found 927.881 [ $\text{M}$ ]<sup>+</sup>, calcd 927.305, found 848.809 [ $\text{M}$ ]<sup>+</sup>-1Br<sup>-</sup>, calcd 848.409, found 768.940 [ $\text{M}$ ]<sup>+</sup>-2Br<sup>-</sup>, calcd 768.204. Anal. Calcd for  $\text{C}_{49}\text{H}_{32}\text{N}_4\text{O}_2\text{Br}_2\text{Ni}$ : C, 63.47; H, 3.48; N, 6.04. Found C, 63.50; H, 3.46, N, 6.55.

**NiTPP[CH<sub>2</sub>COOC<sub>2</sub>H<sub>5</sub>]Ph<sub>2</sub> (4b).** (Yield = 71%, 74mg, 0.082 mmol). Mp > 300 °C. UV-vis ( $\text{CH}_2\text{Cl}_2$ )  $\lambda_{\text{max}}$  (nm) (log  $\epsilon$ ): 423(5.36), 540(4.25), 579(sh). <sup>1</sup>H NMR (400 MHz,  $\text{CDCl}_3$ )  $\delta$  (ppm): 8.54 (s, 1H,  $\beta$ -H), 8.51 (dd, <sup>3</sup> $J_{\text{H,H}}$  = 4 Hz, 8 Hz, 2H,  $\beta$ -H), 8.35 (d, <sup>3</sup> $J_{\text{H,H}}$  = 4 Hz, 1H,  $\beta$ -H), 8.27 (d, <sup>3</sup> $J_{\text{H,H}}$  = 8 Hz, 1H,  $\beta$ -H), 7.98-7.95 (m, 2H, *meso-o*-Ph-H), 7.84 (d, <sup>3</sup> $J_{\text{H,H}}$  = 4 Hz, 2H, *meso-o*-Ph-H), 7.65- 7.65 (m, 6H, *meso-o*- & *m, p*-Ph-H), 7.44 (t, <sup>3</sup> $J_{\text{H,H}}$  = 8 Hz, 4H, *meso-m, p*-Ph-H), 7.18-7.14 (m, 2H, *meso-m, p*-Ph-H), 7.05 (t, <sup>3</sup> $J_{\text{H,H}}$  = 8 Hz, 4H, *meso-m, p*-Ph-H), 6.90-6.78 (m, 10H,  $\beta$ -Ph-H), 4.07 (q, <sup>3</sup> $J_{\text{H,H}}$  = 8 Hz, 12 Hz, 2H, -OCH<sub>2</sub>), 3.79 (s, 2H, -CH<sub>2</sub>), 1.20 (t, <sup>3</sup> $J_{\text{H,H}}$  = 8 Hz, 3H, -

CH<sub>3</sub>). MALDI-TOF-MS ( $m/z$ ): found 913.987 [M]<sup>+</sup>, calcd 913.032. Anal. Calcd for C<sub>60</sub>H<sub>42</sub>N<sub>4</sub>O<sub>2</sub>Ni.0.5 CHCl<sub>3</sub>: C, 74.96; H, 4.42; N, 5.78. Found C, 75.00; H, 4.41; N, 5.78.

### 6.2.3.3 Synthesis of H<sub>2</sub>TPP[CH(COCH<sub>3</sub>)<sub>2</sub>]R<sub>2</sub> (1 and 2), H<sub>2</sub>TPP[CH<sub>2</sub>COOC<sub>2</sub>H<sub>5</sub>]R<sub>2</sub> (3 and 4) (where R = Br or Ph) and Their Metal Complexes (1a-1d and 2a-2d)

120 mg of nickel complex of synthesized free base complexes were dissolved in minimum amount of CHCl<sub>3</sub>. To this, 0.8 mL of conc. H<sub>2</sub>SO<sub>4</sub> was added drop wise and stirred for 15 min at 0 °C. To this, 30 mL of distilled water was added slowly with constant stirring. The organic layer was washed once with water (100 ml), twice with 20% aq. ammonia solution (2×30 mL), and finally with distilled water (100 ml) to remove excess ammonia. The washed organic layer was passed over anhydrous Na<sub>2</sub>SO<sub>4</sub> and dried with rotatory evaporator. The crude porphyrin was purified on a silica gel column using CHCl<sub>3</sub> as eluent.

**H<sub>2</sub>TPP[CH(COCH<sub>3</sub>)<sub>2</sub>]Br<sub>2</sub> (1):** (Yield = 69%, 76mg, 0.088 mmol). Mp > 310 °C. UV-vis (CH<sub>2</sub>Cl<sub>2</sub>)  $\lambda_{\max}$  (nm) (log  $\epsilon$ ): 423(5.45), (4.28), 599(3.64), 660(3.70). <sup>1</sup>H NMR (400 MHz, CDCl<sub>3</sub>)  $\delta$  (ppm): 16.37(s, 1H, enolic-OH), 8.89-8.44(m, 5H,  $\beta$ -H), 8.22-8.08(m, 6H, *meso-o*-Ph-H), 7.95(d, <sup>3</sup>J<sub>H,H</sub> = 4Hz, 2H, *meso-o*-Ph-H), 7.78-7.62(m, 12H, *meso-m,p*-Ph-H), 2.18(s, 1H, -CH), 1.88(s, 6H, -CH<sub>3</sub>), -2.81(d, <sup>3</sup>J<sub>H,H</sub> = 24 Hz, 2H,-NH). MALDI-TOF-MS ( $m/z$ ): found 870.042 [M]<sup>+</sup>, calcd 870.628, found 791.718 [M]<sup>+</sup>-Br<sup>-</sup>, calcd 791.732. Anal. Calcd for C<sub>49</sub>H<sub>34</sub>N<sub>4</sub>O<sub>2</sub>Br<sub>2</sub>: C, 67.60; H, 3.94; N, 6.44. Found C, 67.64; H, 3.95; N, 6.43.

**H<sub>2</sub>TPP[CH(COCH<sub>3</sub>)<sub>2</sub>]Ph<sub>2</sub> (2):** (Yield = 77%, 87mg, 0.100 mmol). Mp ~295-300 °C. UV-vis (CH<sub>2</sub>Cl<sub>2</sub>)  $\lambda_{\max}$  (nm) (log  $\epsilon$ ): 425(5.41), 521(4.19), 557(3.73), 598(3.69), 663(3.44). <sup>1</sup>H NMR (400 MHz, CDCl<sub>3</sub>)  $\delta$  (ppm): 16.42 (s, 1H, enolic-OH), 8.68 (d, <sup>3</sup>J<sub>H,H</sub> = 4 Hz, 1H,  $\beta$ -H), 8.57-8.45(m, 4H,  $\beta$ -H), 8.23-8.21(m, 2H, *meso-o*-Ph-H), 7.95 (d, <sup>3</sup>J<sub>H,H</sub> = 8 Hz, 2H, *meso-o*-Ph-H), 7.81-7.73 (m, 7H, *meso-o* & *m, p*-Ph-H), 7.65-7.59 (m, 3H, *meso-m, p*-Ph-H), 7.30-7.25 (m, 2H, *meso-m, p*-Ph-H), 7.19 (q, <sup>3</sup>J<sub>H,H</sub> = 8 Hz, 16 Hz, 4H, *meso-m, p*-Ph-H), 6.93-6.83 (m, 10H,  $\beta$ -Ph-H), 1.87 (s, 6H, -CH<sub>3</sub>), -2.33 (s, 2H, -NH). MALDI-TOF-MS ( $m/z$ ): found 866.342 [M+H]<sup>+</sup>, calcd 866.035. Anal. Calcd for C<sub>61</sub>H<sub>44</sub>N<sub>4</sub>O<sub>2</sub>: C, 84.70; H, 5.13; N, 6.48. Found C, 84.67; H, 5.15; N, 6.49.

**H<sub>2</sub>TPP[CH<sub>2</sub>COOC<sub>2</sub>H<sub>5</sub>]Br<sub>2</sub> (3):** (Yield = 79%, 89mg, 0.103 mmol). Mp > 310 °C. UV-vis (CH<sub>2</sub>Cl<sub>2</sub>)  $\lambda_{\max}$  (nm) (log  $\epsilon$ ): 426(5.40), 523(4.22), 600(3.65), 665(3.76). <sup>1</sup>H NMR (400 MHz, CDCl<sub>3</sub>)  $\delta$  (ppm): 8.84 (d, <sup>3</sup>J<sub>H,H</sub> = 4 Hz, 1H,  $\beta$ -H), 8.78-8.75 (m, 2H,  $\beta$ -H), 8.57 (d, <sup>3</sup>J<sub>H,H</sub> = 4 Hz,  $\beta$ -H), 8.46 (s, 1H,  $\beta$ -H), 8.21-8.13 (m, 6H, *meso-o*-Ph-H), 8.09 (d, <sup>3</sup>J<sub>H,H</sub> = 4 Hz, 2H, *meso-o*-Ph-

H), 7.81-7.70 (m, *meso-m*, *p*-Ph-H), 4.05 (q,  $^3J_{\text{H,H}} = 4$  Hz, 12 Hz, 2H, -OCH<sub>2</sub>), 3.78 (s, 2H, -CH<sub>2</sub>), 1.16 (t,  $^3J_{\text{H,H}} = 8$  Hz, 3H, -CH<sub>3</sub>). MALDI-TOF-MS ( $m/z$ ): found 857.992 [M+H]<sup>+</sup>, calcd 857.112. Anal. Calcd for C<sub>48</sub>H<sub>34</sub>N<sub>4</sub>O<sub>2</sub>Br<sub>2</sub>: C, 67.14; H, 3.99; N, 6.53. Found C, 67.13; H, 4.00; N, 6.49.

**H<sub>2</sub>TPP[CH<sub>2</sub>COOC<sub>2</sub>H<sub>5</sub>]Ph<sub>2</sub> (4)**: (Yield = 81%, 91mg, 0.107 mmol). Mp > 310 °C. UV-vis (CH<sub>2</sub>Cl<sub>2</sub>)  $\lambda_{\text{max}}$  (nm) (log  $\epsilon$ ): 423(5.47), 520(4.25), 557(3.72), 596(3.67), 659(3.35). <sup>1</sup>H NMR (400 MHz, CDCl<sub>3</sub>)  $\delta$  (ppm): 8.64 (t,  $^3J_{\text{H,H}} = 4$  Hz, 2H,  $\beta$ -H), 8.51 (d,  $^3J_{\text{H,H}} = 4$  Hz, 1H,  $\beta$ -H), 8.45 (d,  $^3J_{\text{H,H}} = 4$  Hz, 2H,  $\beta$ -H), 8.22-8.20 (m, 2H, *meso-o*-Ph-H), 8.08 (d,  $^3J_{\text{H,H}} = 8$  Hz, *meso-o*-Ph-H), 7.80-7.68 (m, 10H, *meso-o*-&*m,p*-Ph-H), 7.25-7.23 (m, 2H, *meso-m*, *p*-Ph-H), 7.20-7.15 (m, 4H, *meso-m*, *p*-Ph-H), 6.95-6.83 (m, 10H,  $\beta$ -Ph-H), 4.09 (q,  $^3J_{\text{H,H}} = 8$  Hz, 12 Hz, 2H, -OCH<sub>2</sub>), 3.92 (s, 2H, -CH<sub>2</sub>), 1.18 (t,  $^3J_{\text{H,H}} = 8$  Hz, 3H, -CH<sub>3</sub>), -2.43 (s, 2H, -NH). MALDI-TOF-MS ( $m/z$ ): found 853.347 [M+H]<sup>+</sup>, calcd 853.354. Anal. Calcd for C<sub>60</sub>H<sub>44</sub>N<sub>4</sub>O<sub>2</sub>.0.5 CH<sub>3</sub>OH: C, 79.61; H, 4.91; N, 6.41. Found C, 79.62; H, 4.89; N, 6.43.

30 mg of free base porphyrins were dissolved in 15 ml of CHCl<sub>3</sub>. To this, 10 eq. of M(OAc)<sub>2</sub>.nH<sub>2</sub>O dissolved in 2-3 ml CH<sub>3</sub>OH was added and the resulting reaction mixture was refluxed for 25-45 minutes. After completion of the reaction, the reaction mixture was washed twice with water to remove excess of metal salt and the organic layer dried over anhydrous sodium sulphate and the solvent was removed with rotatory evaporator. The crude porphyrin was purified by column chromatography with CHCl<sub>3</sub> as eluent. The pure product was obtained by recrystallization from CHCl<sub>3</sub>/CH<sub>3</sub>OH mixture.

**CoTPP[CH(COCH<sub>3</sub>)<sub>2</sub>]Br<sub>2</sub> (1a)**. (Yield = 86%, 27mg, 0.030 mmol). Mp > 310 °C. UV-vis (CH<sub>2</sub>Cl<sub>2</sub>)  $\lambda_{\text{max}}$  (nm) (log  $\epsilon$ ): 417(5.25), 540(4.09). MALDI-TOF-MS ( $m/z$ ): found 926.080 [M+H]<sup>+</sup>, calcd 926.030, found 1004.067 [M]<sup>+</sup>+THF+0.5H<sub>2</sub>O, Calcd 1004.627. Anal. Calcd for C<sub>49</sub>H<sub>32</sub>N<sub>4</sub>O<sub>2</sub>Br<sub>2</sub>Co: C, 63.45; H, 3.48; N, 6.04. Found C, 63.52; H, 3.42; N, 6.10.

**CuTPP[CH(COCH<sub>3</sub>)<sub>2</sub>]Br<sub>2</sub> (1c)**. (Yield = 83%, 27mg, 0.029 mmol). Mp > 300 °C. UV-vis (CH<sub>2</sub>Cl<sub>2</sub>)  $\lambda_{\text{max}}$  (nm) (log  $\epsilon$ ): 420(5.54), 543(4.26), 583sh. MALDI-TOF-MS ( $m/z$ ): found 932.874 [M+H]<sup>+</sup>, calcd 932.158, found 953.939 [M]<sup>+</sup>-1Br<sup>-</sup>, calcd 953.262, found 973.366 [M]<sup>+</sup>-2Br<sup>-</sup>, calcd 773.198. Anal. Calcd for C<sub>49</sub>H<sub>32</sub>N<sub>4</sub>O<sub>2</sub>Br<sub>2</sub>Co: C, 63.14; H, 3.46; N, 6.01. Found C, 63.04; H, 3.52; N, 5.98. **ZnTPP[CH(COCH<sub>3</sub>)<sub>2</sub>]Br<sub>2</sub> (1d)**. (Yield = 78%, 25mg, 0.027 mmol). Mp > 310 °C. UV-vis (CH<sub>2</sub>Cl<sub>2</sub>)  $\lambda_{\text{max}}$  (nm) (log  $\epsilon$ ): 424(5.67), 553(4.41), 592(3.75). <sup>1</sup>H NMR (400 MHz, CDCl<sub>3</sub>)  $\delta$  (ppm): 16.18 (s, 1H, enolic-OH), 8.88-8.83 (m, 2H,  $\beta$ -H), 8.77(d,  $^3J_{\text{H,H}} = 4$  Hz, 1H,  $\beta$ -



H), 8.70-8.65 (m, 2H,  $\beta$ -H), 8.18 (d,  $^3J_{\text{H,H}} = 4$  Hz, 2H, *meso-o*-Ph-H), 8.04 (t,  $^3J_{\text{H,H}} = 8$  Hz, 3H, *meso-o*-Ph-H), 7.87 (d,  $^3J_{\text{H,H}} = 8$  Hz, 2H, *meso-o*-Ph-H), 7.78-7.68 (m, 10H, *meso-o*- & *m*, *p*-Ph-H), 7.61-7.53 (m, 3H, *meso-m*, *p*-Ph-H), 1.77 (s, 6H, -CH<sub>3</sub>). MALDI-TOF-MS ( $m/z$ ): found 933.840 [M]<sup>+</sup>, calcd 933.992, found 852.098 [M]<sup>+</sup>-Br<sup>-</sup>, calcd 852.108, found 774.907 [M]<sup>+</sup>-2Br, calcd 774.197. Anal. Calcd for C<sub>49</sub>H<sub>32</sub>N<sub>4</sub>O<sub>2</sub>Br<sub>2</sub>Co: C, 63.01; H, 3.45; N, 6.00. Found C, 62.98; H, 3.49, N, 6.04.

**CoTPP[CH(COCH<sub>3</sub>)<sub>2</sub>]Ph<sub>2</sub> (2a)**. (Yield = 81%, 26mg, 0.028 mmol). Mp > 310 °C. UV-vis (CH<sub>2</sub>Cl<sub>2</sub>)  $\lambda_{\text{max}}$  (nm) (log  $\epsilon$ ): 418(5.26), 540(4.13). MALDI-TOF-MS ( $m/z$ ): found 921.671 [M]<sup>+</sup>, calcd 921.264, found 897.80 [M]<sup>+</sup>-COCH<sub>3</sub>, calcd 897.253. Anal. Calcd for C<sub>61</sub>H<sub>42</sub>N<sub>4</sub>O<sub>2</sub>Co: C, 79.47; H, 4.59; N, 6.08. Found C, 79.50; H, 4.56; N, 6.10. **CuTPP[CH(COCH<sub>3</sub>)<sub>2</sub>]Ph<sub>2</sub> (2c)**. (Yield = 85%, 27mg, 0.029 mmol). Mp > 310 °C. UV-vis (CH<sub>2</sub>Cl<sub>2</sub>)  $\lambda_{\text{max}}$  (nm) (log  $\epsilon$ ): 422(5.24), 547(3.98). MALDI-TOF-MS ( $m/z$ ): found 926.203 [M+H]<sup>+</sup>, calcd 926.268. Anal. Calcd for C<sub>61</sub>H<sub>42</sub>N<sub>4</sub>O<sub>2</sub>Cu.CH<sub>2</sub>Cl<sub>2</sub>: C, 73.62; H, 4.38; N, 5.54. Found C, 73.60; H, 4.37; N, 5.60. **ZnTPP[CH(COCH<sub>3</sub>)<sub>2</sub>]Ph<sub>2</sub> (2d)**. (Yield = 80%, 26mg, 0.028 mmol). Mp > 310 °C. UV-vis (CH<sub>2</sub>Cl<sub>2</sub>)  $\lambda_{\text{max}}$  (nm) (log  $\epsilon$ ): 425(5.58), 554(4.31), 599(sh). MALDI-TOF-MS ( $m/z$ ): found 927.338 [M+H]<sup>+</sup>, calcd 927.267. Anal. Calcd for C<sub>61</sub>H<sub>42</sub>N<sub>4</sub>O<sub>2</sub>Zn.0.5 CH<sub>3</sub>OH: C, 78.21; H, 4.70; N, 5.93. Found C, 78.30; H, 4.67; N, 5.99.

**CoTPP[CH<sub>2</sub>COOC<sub>2</sub>H<sub>5</sub>]Br<sub>2</sub> (3a)**. (Yield = 74%, 24mg, 0.026 mmol). Mp > 310 °C. UV-vis (CH<sub>2</sub>Cl<sub>2</sub>)  $\lambda_{\text{max}}$  (nm) (log  $\epsilon$ ): 418(5.29), 541(4.12). MALDI-TOF-MS ( $m/z$ ): Found 913.178 [M]<sup>+</sup>, Calcd 913.022. Anal. Calcd for C<sub>48</sub>H<sub>32</sub>N<sub>4</sub>O<sub>2</sub>Br<sub>2</sub>Co: C, 62.97; H, 3.52; N, 6.12. Found C, 62.93, H, 3.59, N, 6.07. **CuTPP[CH<sub>2</sub>COOC<sub>2</sub>H<sub>5</sub>]Br<sub>2</sub> (3c)**. (Yield = 76%, 24mg, 0.027 mmol). Mp > 310 °C. UV-vis (CH<sub>2</sub>Cl<sub>2</sub>)  $\lambda_{\text{max}}$  (nm) (log  $\epsilon$ ): 421(5.57), 545(4.29), 585(sh). MALDI-TOF-MS ( $m/z$ ): Found 917.052 [M]<sup>+</sup>, Calcd 917.019. Anal. Calcd for C<sub>48</sub>H<sub>32</sub>N<sub>4</sub>O<sub>2</sub>Br<sub>2</sub>Cu: C, 62.65; H, 3.51; N, 6.09. Found C, 62.69; H, 3.50, N, 6.12. **ZnTPP[CH<sub>2</sub>COOC<sub>2</sub>H<sub>5</sub>]Br<sub>2</sub> (3d)**. (Yield = 81%, 26mg, 0.028 mmol). Mp > 310 °C. UV-vis (CH<sub>2</sub>Cl<sub>2</sub>)  $\lambda_{\text{max}}$  (nm) (log  $\epsilon$ ): 423(5.54), 553(4.22), 591(3.61). <sup>1</sup>H NMR (400 MHz, CDCl<sub>3</sub>)  $\delta$  (ppm): 8.85-8.82 (m, 2H,  $\beta$ -H), 8.77-8.71 (m, 2H,  $\beta$ -H), 8.65-8.60 (m, 1H,  $\beta$ -H), 8.23-8.15 (m, 2H, *meso-o*-Ph-H), 8.06-7.94 (m, 6H, *meso-o*-Ph-H), 7.77-7.68 (m, 12H, *meso-m*, *p*-Ph-H), 4.09 (q,  $^3J_{\text{H,H}} = 8$  Hz, 16 Hz, 2H, -OCH<sub>2</sub>), 3.92 (s, 2H, -CH<sub>2</sub>), 1.22 (t,  $^3J_{\text{H,H}} = 8$  Hz, 3H, -CH<sub>3</sub>). MALDI-TOF-MS ( $m/z$ ): found 919.189 [M]<sup>+</sup>, calcd 919.026. Anal. Calcd for C<sub>48</sub>H<sub>32</sub>N<sub>4</sub>O<sub>2</sub>Br<sub>2</sub>Zn.0.5 CH<sub>3</sub>OH: C, 62.10, H, 3.65; N, 5.97. Found C, 62.07; H, 3.69; N, 5.95.



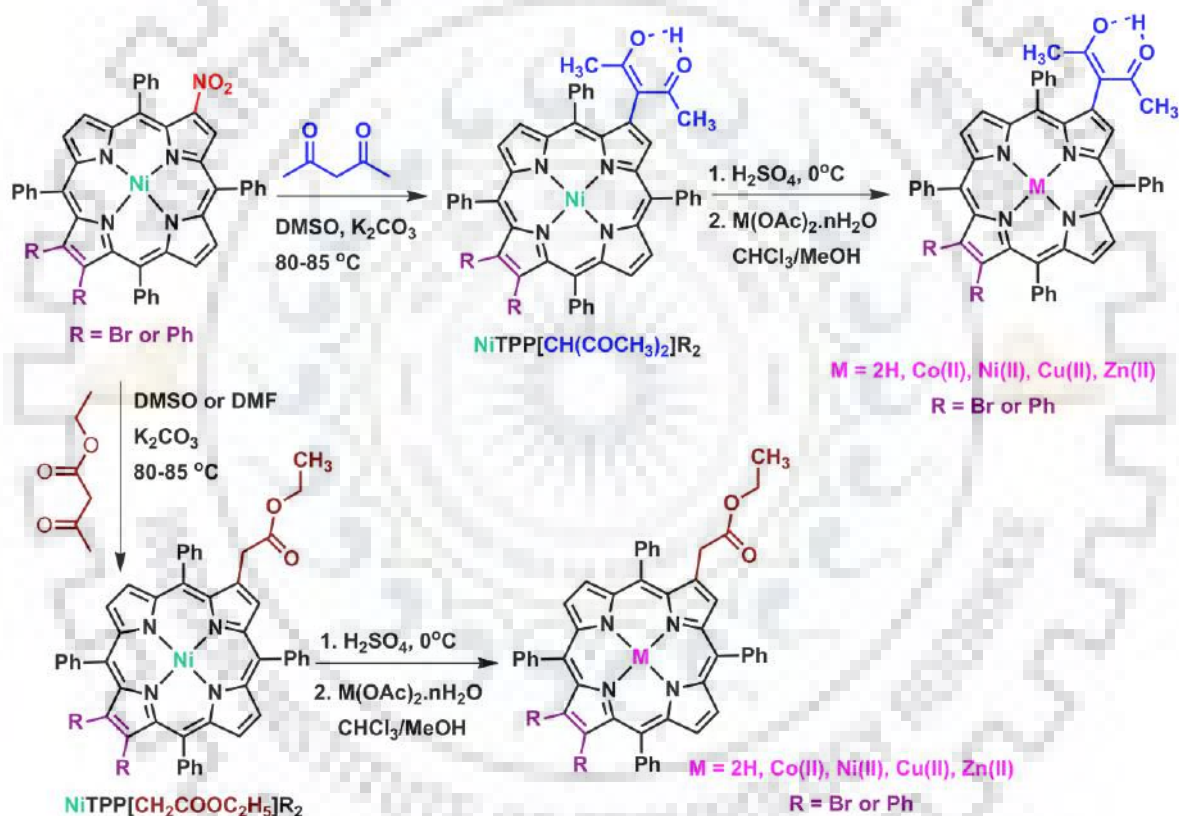
**CoTPP[CH<sub>2</sub>COOC<sub>2</sub>H<sub>5</sub>]Ph<sub>2</sub> (4a).** (Yield 83%, 26mg, 0.029 mmol). Mp > 310 °C. UV-vis (CH<sub>2</sub>Cl<sub>2</sub>)  $\lambda_{\max}$  (nm) (log  $\epsilon$ ): 416(5.27), 539(4.13). MALDI-TOF-MS ( $m/z$ ): Found 910.193 [M+H]<sup>+</sup>, Calcd 910.271. Anal. Calcd for C<sub>60</sub>H<sub>42</sub>N<sub>4</sub>O<sub>2</sub>Co: C, 79.20; H, 4.65; N, 6.16. Found C, 79.17; H, 4.66; N, 6.20. **CuTPP[CH<sub>2</sub>COOC<sub>2</sub>H<sub>5</sub>]Ph<sub>2</sub> (4c).** (Yield = 87%, 28mg, 0.031 mmol). Mp > 310 °C. UV-vis (CH<sub>2</sub>Cl<sub>2</sub>)  $\lambda_{\max}$  (nm) (log  $\epsilon$ ): 420(5.55), 545(4.29). MALDI-TOF-MS ( $m/z$ ): Found 914.291 [M+H]<sup>+</sup>, Calcd 914.268. Anal. Calcd for C<sub>60</sub>H<sub>42</sub>N<sub>4</sub>O<sub>2</sub>Cu: C, 78.80; H, 4.63; N, 6.13. Found C, 78.89; H, 4.63; N, 6.11. **ZnTPP[CH<sub>2</sub>COOC<sub>2</sub>H<sub>5</sub>]Ph<sub>2</sub> (4d).** (Yield = 79%, 25mg, 0.028 mmol). Mp > 310 °C. UV-vis (CH<sub>2</sub>Cl<sub>2</sub>)  $\lambda_{\max}$  (nm) (log  $\epsilon$ ): 423(5.62), 551(4.33). <sup>1</sup>H NMR (400 MHz, CDCl<sub>3</sub>)  $\delta$  (ppm): 8.81 (d, <sup>3</sup>J<sub>H,H</sub> = 4 Hz, 1H,  $\beta$ -H), 8.75 (s, 1H,  $\beta$ -H), 8.63 (d, <sup>3</sup>J<sub>H,H</sub> = 4 Hz, 1H,  $\beta$ -H), 8.57 (dd, <sup>3</sup>J<sub>H,H</sub> = 4 Hz, 12 Hz, 2H,  $\beta$ -H), 8.20 (d, <sup>3</sup>J<sub>H,H</sub> = 8 Hz, 2H, *meso-o*-Ph-H), 8.07 (d, <sup>3</sup>J<sub>H,H</sub> = 4 Hz, 2H, *meso-o*-Ph-H), 7.79-7.76 (m, 10H, *meso-o*-& *m, p*-Ph-H), 7.23-7.20 (m, 2H, *meso-m, p*-Ph-H), 7.16-7.11 (m, 4H, *meso-m, p*-Ph-H), 6.99-6.96 (m, 4H,  $\beta$ -Ph-H), 6.88-6.85 (m, 6H,  $\beta$ -Ph-H), 4.12 (q, <sup>3</sup>J<sub>H,H</sub> = 8 Hz, 16 Hz, 2H, -OCH<sub>2</sub>), 3.96 (s, 2H, -CH<sub>2</sub>), 1.23 (t, <sup>3</sup>J<sub>H,H</sub> = 8 Hz, 3H, -CH<sub>3</sub>). MALDI-TOF-MS ( $m/z$ ): found 915.335 [M+H]<sup>+</sup>, calcd 915.267. Anal. Calcd for C<sub>60</sub>H<sub>42</sub>N<sub>4</sub>O<sub>2</sub>Zn: C, 78.64; H, 4.61; N, 6.11. Found C, 78.63; H, 4.64; N, 6.09.

## 6.3 RESULTS AND DISCUSSION

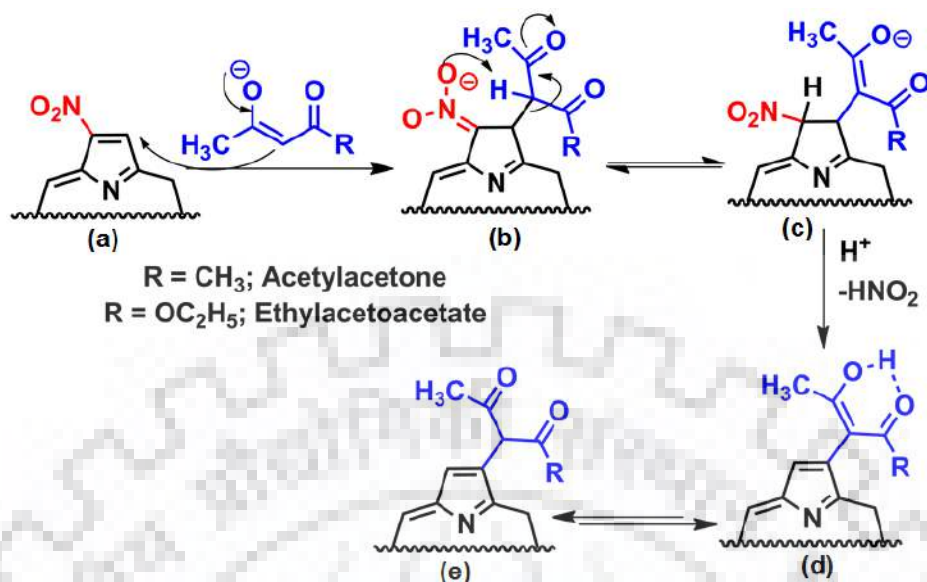
### 6.3.1 Synthesis and Characterization

The synthetic route involved the reaction of 2-nitro-5,10,15,20-tetraphenylporphyrins. NiTPP(NO<sub>2</sub>)R<sub>2</sub> (Where R = Br and Ph) with 1,3-diketones (acetylacetone and ethyl acetoacetate) in presence of 10 eq. of K<sub>2</sub>CO<sub>3</sub> in DMSO to obtained corresponding di-carbonyl appended derivatives in good yields using modified literature method which has been described for MTPP(NO<sub>2</sub>) (Scheme 6.1). Michael addition reaction of the used active methylene compounds led to the formation of single product only. The isolation of intermediate nitro chlorin was not possible in any of the case. Acetylacetone appended porphyrins existed in tautomeric mixture as shown in Scheme 1 which was further confirmed by <sup>1</sup>H NMR Spectroscopy. Whereas an interesting aspect has been observed in case of ethyl acetoacetate, the desired porphyrins underwent a rapid cleavage of C-C bond due to the high temperature of reaction mixture which resulted into the dissociation of acetyl group and yielded to ester appended porphyrins only which was further confirmed by <sup>1</sup>H NMR spectroscopy and single crystal X-ray diffraction analysis.

We just wanted to check whether the reaction solvent had any impact on the reactivity of the starting materials NiTPP(NO<sub>2</sub>)R<sub>2</sub> (where R = Br or Ph) with ethyl acetoacetate and/or over the product formation. We have also used DMF as a solvent under similar reaction conditions as described for DMSO. Again we observed the C-C bond cleavage but this time the purity and yield of the product was found better as compared to DMSO. However, Cavaleiro and coworkers reported that DMF led to the extensive decomposition of the starting material i.e. MTPPNO<sub>2</sub>. Change of central metal did not much affect the reactivity of nitroporphyrin as well as the yield of the products. A plausible mechanistic pathway for Michael addition reaction of used active methylene with NiTPP(NO<sub>2</sub>)R<sub>2</sub> (R= Br or Ph) is given in Scheme 6.2.



**Scheme 6.1** Michael Addition of 1,3-Diketone and 3-ketoester with  $\beta$ -Nitroporphyrins.



**Scheme 6.2** Plausible Mechanism for the Synthesis of Asymmetrically Substituted Porphyrins.

In 1998, Smith and coworkers explained that the reaction of 2-nitroporphyrin with active methylene compounds led to the formation of dihydroporphyrins (either cyclopropylchlorins or 2,3-*trans*-chlorins) only due to the intramolecular cyclization of nitronate adduct. Later in 2005, Cavalerio and coworkers have shown the different reactivity of 1,3-diketone and 3-ketoesters with 2-nitroporphyrin where intermediate nitronate adduct was in equilibrium with enolate ion rather than intramolecular cyclization as also shown in Scheme 6.2. The nitrous acid elimination from (c) led to the formation of product (d) which exhibited keto enol tautomerism. The free base complexes have been prepared by using few drops of conc.  $\text{H}_2\text{SO}_4$  in  $\text{CHCl}_3$  at  $0^\circ\text{C}$  and again remetalated with different metal ions in order to get the corresponding metal complexes. All the synthesised compound have been characterized by  $^1\text{H}$  NMR, MALDI-TOF mass spectrometry, Elemental analysis, UV-Vis. spectroscopy, cyclic voltammetry and single crystal X-ray diffraction analysis.

### 6.3.2 $^1\text{H}$ NMR and Mass Spectrometric Studies

$^1\text{H}$  NMR spectra of synthesised  $\text{MTPP}(\text{X})\text{R}_2$  (Where  $\text{M} = 2\text{H}$ ,  $\text{Ni}(\text{II})$ , and  $\text{Zn}(\text{II})$ ;  $\text{X} = \text{CH}(\text{COCH}_3)_2$  and  $\text{CH}_2\text{COOC}_2\text{H}_5$ ;  $\text{R} = \text{Br}$  and  $\text{Ph}$ ) have been recorded in  $\text{CDCl}_3$ . Figure 6.1 shows the  $^1\text{H}$  NMR spectrum of  $\text{H}_2\text{TPP}[\text{CH}(\text{COCH}_3)_2]\text{Ph}_2$  (**2**) whereas Figures A1-A3 in the Appendix-V are shown as  $^1\text{H}$  NMR spectra of synthesized free base porphyrins. The synthesized porphyrins exhibited proton signals arising from  $\beta$ -substituent,  $\beta$ -protons, *meso*-phenyls and

inner core nitrogens in case of free base porphyrins. The  $\beta$ -resonances in MTPP(X)R<sub>2</sub> (Where M = 2H, Ni(II), and Zn(II); X = CH(COCH<sub>3</sub>)<sub>2</sub> and CH<sub>2</sub>COOC<sub>2</sub>H<sub>5</sub>; R = Br and Ph) were marginally upfield shifted as compared to the precursors MTPP(NO<sub>2</sub>)(R)<sub>2</sub> (Where R = Br and Ph) due to comparatively less electron withdrawing nature of diketone and ketoester as compared to nitro group. <sup>1</sup>H NMR spectra of acetylacetonate appended porphyrins exhibited proton signals beyond 16 ppm corresponding to -OH along with one proton signal at ~2.17 ppm corresponding to -CH which means that these compounds were exhibiting keto-enol tautomerism. Whereas in each spectrum of synthesised ethyl acetoacetate appended porphyrins the proton signal corresponding to -CH<sub>3</sub> of acetyl group was missing which strongly supported the C-C bond cleavage during reaction.

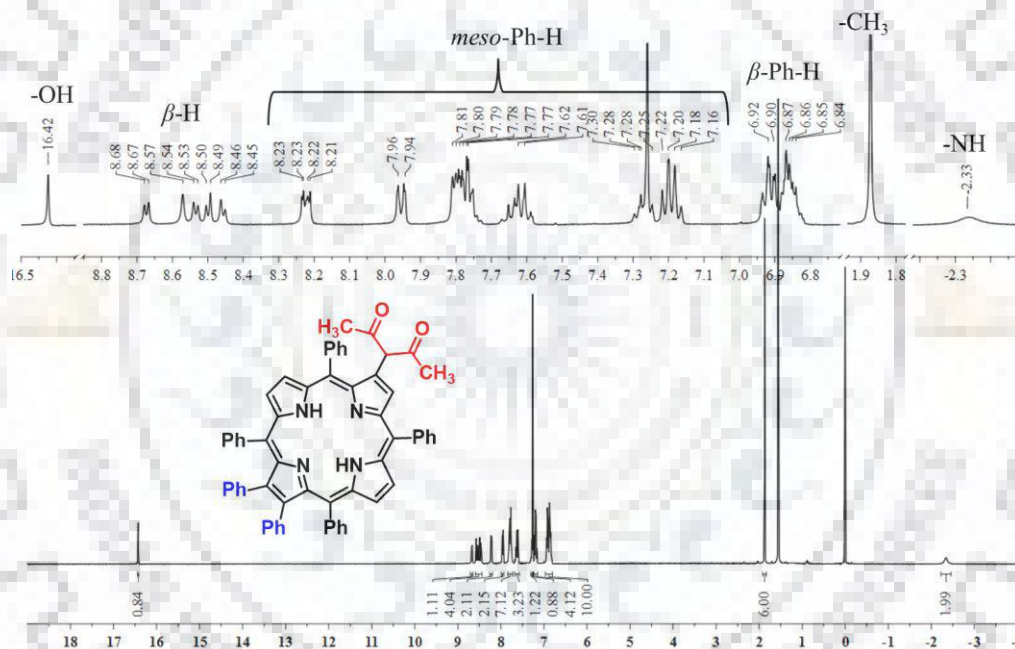


**Figure 6.1** <sup>1</sup>H NMR Spectrum of H<sub>2</sub>TPP[CH(COCH<sub>3</sub>)<sub>2</sub>]Ph<sub>2</sub> (**2**) in CDCl<sub>3</sub>.

Interestingly, the <sup>1</sup>H NMR signals of the inner core NH protons for H<sub>2</sub>TPP[CH(COCH<sub>3</sub>)<sub>2</sub>]Br<sub>2</sub> (**1**) and H<sub>2</sub>TPP[CH<sub>2</sub>COOC<sub>2</sub>H<sub>5</sub>]Br<sub>2</sub> (**3**) were observed as splitted signal which demonstrated that the proton exchange process of the two inner core NHs (NH tautomerism) is slow enough even at room temperature be distinguished these two protons in the NMR time scale (Figures A1 and A2 in Appendix-V). Whereas the phenyl substituted porphyrins **2** and **4** have shown a broad singlet for inner core protons which indicated that the exchange process of the two protons involved in NH tautomerism was fast in these cases.

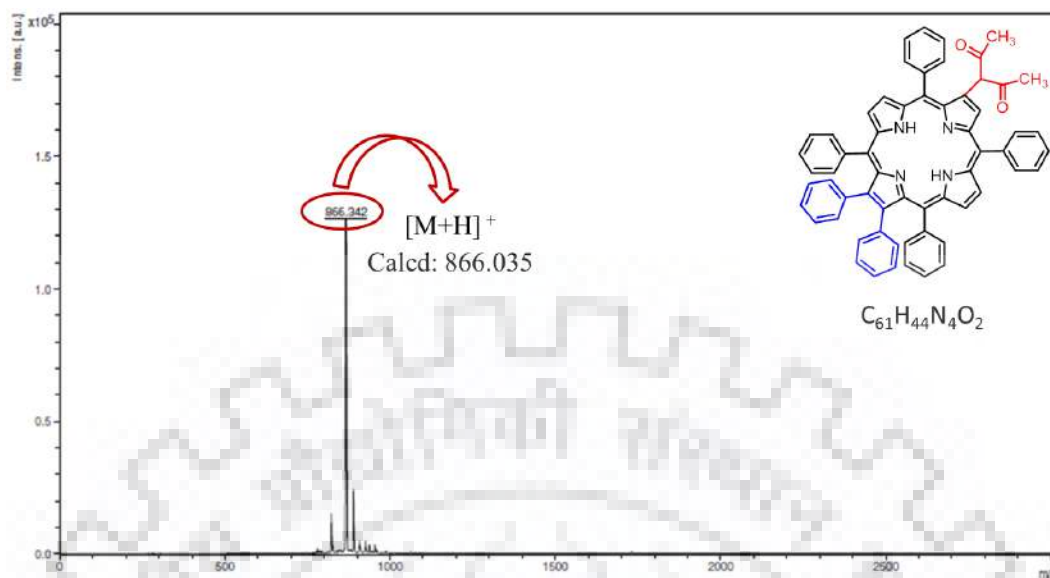


**Figure 6.2** MALDI-TOF Mass Spectrum of  $H_2TPP[CH(COCH_3)_2]Ph_2$  (**2**) in Positive Ion Mode.

The MALDI-TOF Mass spectra of all synthesized compounds have been recorded in positive ion mode using HABA as matrix. Figures 6.2 and A4-A6 in Appendix-V have shown the MALDI-TOF mass spectra of synthesized free base porphyrins. The observed mass values were exactly matching with proposed structures. The observed mass values for  $H_2TPP[CH_2COOC_2H_5]Br_2$  (**3**),  $H_2TPP[CH_2COOC_2H_5]Ph_2$  (**4**) and their metal complexes are also supporting the removal of acetyl group from ethyl acetoacetate (Figures A5 and A6 in Appendix-V).

### 6.3.3 Single Crystal X-ray Structures

The structural identification of porphyrins, viz.  $NiTPP[CH(COCH_3)_2]Br_2$  (**1b**),  $H_2TPP[CH_2COOC_2H_5]Br_2$  (**3**) and  $ZnTPP[CH_2COOC_2H_5]Ph_2 \cdot Py$  (**4d**•Py) has been carried out using single crystal X-ray analysis. Figure 6.3 shows the ORTEP diagrams of top and side views of crystallized compounds. The two acetyl groups in **1b** were *trans* oriented to each other and were located at the antipodal  $\beta$ -dibromo functionality. Table A1 in Appendix-V lists the crystallographic data whereas the selected average bond length and bond angles are listed in Table 6.1. Porphyrins **1b** and **4d** were crystallized in triclinic P-1 system whereas **3** was crystallized in triclinic system with P1 space group. Notably in case of porphyrin **3**, two molecules were present in a unit cell. Ketoester appended porphyrins **3** and **4d** have shown quasi planar conformation with low magnitude of  $\Delta_{24}$  and  $\Delta C_\beta$  values and the bond lengths and bond angles of these porphyrins were fairly matching to those reported in literature [20]. Whereas



acetylacetonate appended porphyrin **1b** has nonplanar (saddle shaped) conformation of the macrocyclic core which is clearly reflecting from the higher  $\Delta C_{\beta}$  and  $\Delta 24$  values for **1b**.

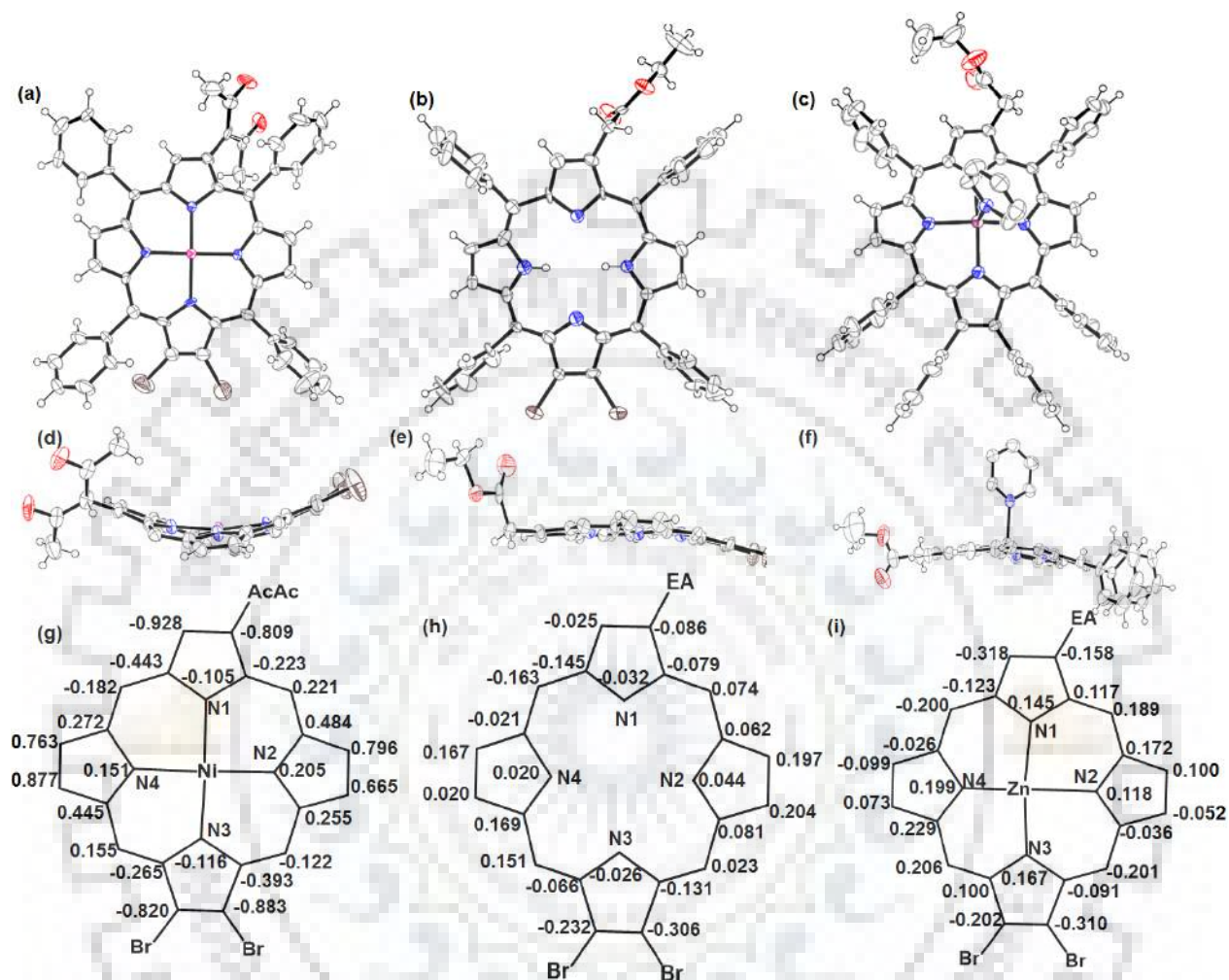


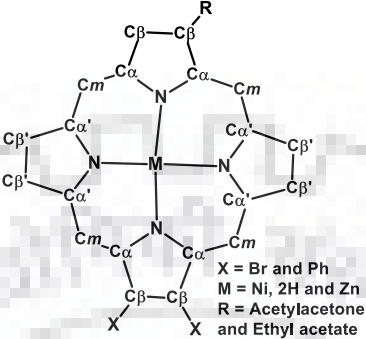
**Figure 6.3** ORTEP Diagrams Showing Top and Side Views of (a and d) NiTPP[CH(COCH<sub>3</sub>)<sub>2</sub>]Br<sub>2</sub> (**1b**); (b and e) H<sub>2</sub>TPP[CH<sub>2</sub>COOC<sub>2</sub>H<sub>5</sub>]Br<sub>2</sub> (**3**) and (c and f) ZnTPP[CH<sub>2</sub>COOC<sub>2</sub>H<sub>5</sub>]Ph<sub>2</sub>•Py (**4d•Py**). (g-i) Displacement of Porphyrin 24-Core Atoms (in Å) from the Mean Plane.

The structural chemistry of **1b** is totally different from the reported mixed  $\beta$ -trisubstituted porphyrins [21] as it was having high magnitude displacement of 24-core atoms and eight  $\beta$ -pyrrole carbons ( $\Delta 24 = 0.44$  Å,  $\Delta C_{\beta} = 0.82$  Å) from the mean plane. This is highly nonplanar mixed  $\beta$ -trisubstituted MTPP reported till date. The nickel atom was displayed by  $0.057$  Å deviated from the mean plane which is found very low as compared to the previously reported  $\beta$ -tri-substituted porphyrins ( $\Delta M = 0.237$ - $0.307$ Å). It is remarkable that the deviation of Zn(II) ion



in ZnTPP[CH(COOC<sub>2</sub>H<sub>5</sub>)Ph]<sub>2</sub> was 0.51 Å above the mean plane, which is profoundly higher than that of similar type trisubstituted porphyrin ZnTPP(NO<sub>2</sub>)Br<sub>2</sub>•(CH<sub>3</sub>OH) complex (0.237Å) [22].

**Table 6.1** Selected Bond Lengths (Å) and Bond Angles (°) of Crystallized Compounds



	NiTPP[CH(COCH <sub>3</sub> ) <sub>2</sub> ]Br <sub>2</sub>	H <sub>2</sub> TPP[CH <sub>2</sub> COOC <sub>2</sub> H <sub>5</sub> ]Br <sub>2</sub>	ZnTPP[CH <sub>2</sub> COOC <sub>2</sub> H <sub>5</sub> ]Ph <sub>2</sub>
M - N	1.938(7)	--	2.122(3)
M - N'	1.909(8)	--	2.037(3)
N - C <sub>α</sub>	1.380(1)	1.380(3)	1.370(4)
N' - C <sub>α</sub>	1.383(1)	1.355(2)	1.367(4)
C <sub>α</sub> - C <sub>β</sub>	1.433(2)	1.471(2)	1.447(5)
C <sub>α</sub> - C <sub>β</sub>	1.420(2)	1.414(3)	1.434(6)
C <sub>β</sub> - C <sub>β</sub>	1.330(2)	1.317(3)	1.353(6)
C <sub>β</sub> - C <sub>β</sub>	1.315(2)	1.356(3)	1.332(5)
C <sub>α</sub> - C <sub>m</sub>	1.388(2)	1.367(3)	1.404(5)
C <sub>α</sub> - C <sub>m</sub>	1.395(2)	1.430(3)	1.401(5)
$\Delta C_{\beta}$ <sup>a</sup>	<b>0.818</b>	<b>0.213</b>	<b>0.164</b>
$\Delta 24$ <sup>b</sup>	<b>0.441</b>	<b>0.124</b>	<b>0.151</b>
$\Delta M$	<b>0.057</b>	--	<b>0.510</b>
Bond Angles (°)			
N - M - N	170.08(4)	--	160.78(1)
N' - M - N'	172.72(4)	--	160.10(1)
M - N - C <sub>α</sub>	126.65(8)	--	126.33(2)
M - N' - C <sub>α</sub>	127.35(8)	--	126.63(2)
N - C <sub>α</sub> - C <sub>m</sub>	123.66(1)	125.65(2)	124.53(3)
N' - C <sub>α</sub> - C <sub>m</sub>	123.71(1)	127.12(2)	126.63(3)
N - C <sub>α</sub> - C <sub>β</sub>	109.47(1)	107.05(2)	109.13(3)
N' - C <sub>α</sub> - C <sub>β</sub>	110.03(1)	107.25(2)	109.43(3)
C <sub>β</sub> - C <sub>α</sub> - C <sub>m</sub>	126.67(1)	126.75(2)	126.18(3)
C <sub>β</sub> - C <sub>α</sub> - C <sub>m</sub>	125.66(1)	125.50(2)	123.70(3)
C <sub>α</sub> - C <sub>β</sub> - C <sub>β</sub>	107.85(1)	108.50(2)	107.20(3)
C <sub>α</sub> - C <sub>β</sub> - C <sub>β</sub>	107.77(1)	107.50(2)	107.38(4)
C <sub>α</sub> - N - C <sub>α</sub>	105.25(9)	108.60(2)	107.30(3)
C <sub>α</sub> - N - C <sub>α</sub>	104.09(9)	110.07(2)	106.35(3)
C <sub>α</sub> - C <sub>m</sub> - C <sub>α</sub>	121.74(1)	125.73(2)	125.60(3)

<sup>a</sup> $\Delta C_{\beta}$  = mean plane deviation of  $\beta$ -pyrrole carbons

<sup>b</sup> $\Delta 24$  = the mean plane deviation of 24-atom core

Moreover, the N-M-N and N'-M-N' (M = Ni(II) and Zn(II)) angles ( $160$ - $170^\circ$ ) were deviated from the accurate  $180^\circ$  which clearly indicated the nonplanar conformation of the M-4N core which may be due to induced nonplanarity provided by bulkier  $\beta$ -substituents. In all cases, the C-C bond length ( $C_\beta$ - $C_{AM}$ ; AM = Active Methylene) was found shorted ( $\sim 1.51$  Å) as compared to the standard C-C single bond ( $1.54$  Å). The inner core imino protons (NH) of **3** exhibited hydrogen bonding with adjacent pyrrolic nitrogens which were further evidenced by shortest N-N distance of  $\sim 2.9$  Å. The longer M-N distances as compared to M-N' in both **1b** and **4d** (Table 6.1) was possibly due to electron deficient nature of the  $\beta$ -substituents.

The saddle shape conformation of NiTPP[CH(COCH<sub>3</sub>)<sub>2</sub>]Br<sub>2</sub> (**1b**) was further supported by decrement in the N-C $\alpha$ -C $m$  ( $\sim 123^\circ$ ) which was lower among all crystallized compounds. The acetylacetonate group of **1b** exhibited an intramolecular O $\cdots$ O interaction (van der Waals interaction) with a distance of  $2.44$  Å.

#### 6.3.4 DFT Studies

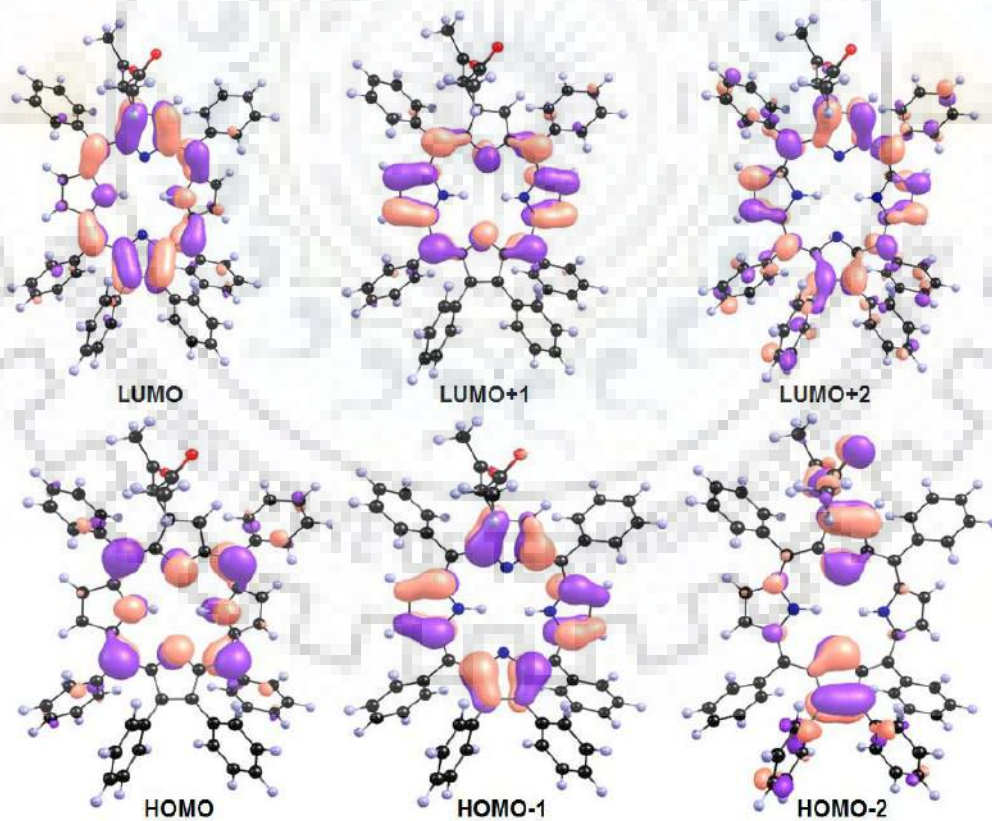


**Figure 6.4** Frontier Molecular Orbitals of H<sub>2</sub>TPP[CH(COCH<sub>3</sub>)<sub>2</sub>]Ph<sub>2</sub> (**2**).

DFT calculations were performed using Gaussian 09 at the B3LYP/6-31G level on a model of synthesized free base porphyrins to elucidate the effect of appended  $\beta$ -substituent over the delocalization pathway of the frontier molecular orbitals (FMOs). The fully optimized geometries of free base porphyrins are shown in Figure A7 in the Appendix-V which were fairly matching with the structures obtained from single crystals. Diketone appended porphyrins (**1** and **2**) were found more nonplanar as compared to the ketoester appended porphyrins (**3** and **4**) due to the repulsive interaction between two carbonyl groups of bulkier  $\beta$ -substituent. The frontier molecular orbitals of  $H_2TPP[CH(COCH_3)_2]Ph_2$  (**2**) are shown in Figure 6.4 whereas for rest of the optimized porphyrins are given in Figures A8-A10 in the Appendix-V. In case of phenyl substituted porphyrins **2** and **4** the HOMOs were found as  $a_{2u}$  and both the HOMO and LUMO were contributed mainly from the macrocyclic core as for the electron deficient porphyrins. Whereas LUMO+2 was showing contribution from *meso*-phenyl rings also alongwith with macrocyclic core.

### 6.3.5 Photophysical Studies

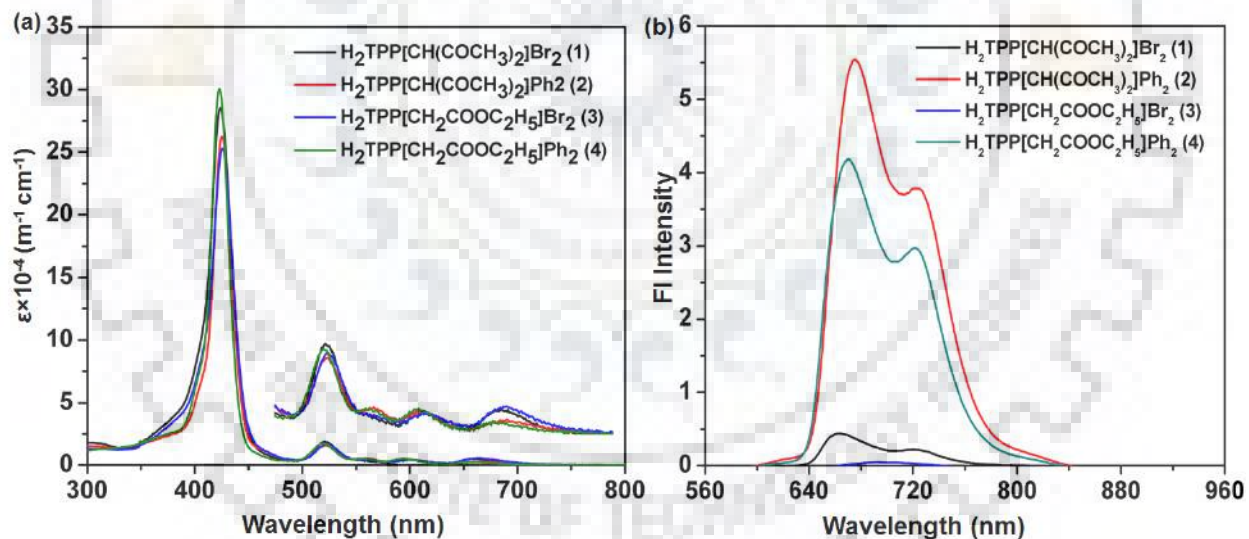


**Figure 6.5** (a) Comparative UV-Visible Spectra of Synthesized Free Base Porphyrins in  $CH_2Cl_2$  at 298 K. (b) Comparative Emission Spectra of Free Base Complexes in  $CH_2Cl_2$  at 298 K.

The electronic absorption spectra of porphyrins usually depends upon the  $\beta$ -substituents and core metal ion. The absorption spectra of each of synthesised porphyrin have been recored in  $CH_2Cl_2$  at 298 K.

**Table 6.2** Spectroscopic Data<sup>a</sup> of **1-4** and Corresponding Zn(II) Complexes (**1d-4d**) in CH<sub>2</sub>Cl<sub>2</sub>.

Porphyrin	B-band	Q-band(s)	$\lambda_{em.}$	$\phi_f$
H <sub>2</sub> TPP(NO <sub>2</sub> )Br <sub>2</sub>	436(5.23)	536(4.08), 623(3.43), 683(3.91)		
H <sub>2</sub> TPP[CH(COCH <sub>3</sub> ) <sub>2</sub> ]Br <sub>2</sub> ( <b>1</b> )	423(5.45)	521(4.28), 599(3.64), 659(3.70)	664, 723	0.0037
H <sub>2</sub> TPP[CH <sub>2</sub> COOC <sub>2</sub> H <sub>5</sub> ]Br <sub>2</sub> ( <b>3</b> )	426(5.40)	523(4.22), 600(3.65), 665(3.76)	698	0.0011
H <sub>2</sub> TPP(NO <sub>2</sub> )Ph <sub>2</sub>	439(5.09)	536(4.01), 686(3.80)	756	0.0167
H <sub>2</sub> TPP[CH(COCH <sub>3</sub> ) <sub>2</sub> ]Ph <sub>2</sub> ( <b>2</b> )	425(5.41)	521(4.19), 557(3.73), 598(3.69), 663(3.44)	675, 724	0.0295
H <sub>2</sub> TPP[CH <sub>2</sub> COOC <sub>2</sub> H <sub>5</sub> ]Ph <sub>2</sub> ( <b>4</b> )	423(5.47)	520(4.25), 557(3.72), 596(3.67), 659(3.35)	669, 722	0.0349
ZnTPP(NO <sub>2</sub> )Br <sub>2</sub>	433(5.36)	562(4.12), 606(4.10)		
ZnTPP[CH(COCH <sub>3</sub> ) <sub>2</sub> ]Br <sub>2</sub> ( <b>1d</b> )	424(5.67)	553(4.41), 592(3.75)	610, 651	0.0023
ZnTPP[CH <sub>2</sub> COOC <sub>2</sub> H <sub>5</sub> ]Br <sub>2</sub> ( <b>3d</b> )	423(5.54)	553(4.22), 591(3.61)	623, 652	0.0005
ZnTPP(NO <sub>2</sub> )Ph <sub>2</sub>	435(5.27)	561(4.12), 607(4.00)	709	0.0110
ZnTPP[CH(COCH <sub>3</sub> ) <sub>2</sub> ]Ph <sub>2</sub> ( <b>2d</b> )	425(5.58)	554(4.31), 599sh	643	0.0069
ZnTPP[CH <sub>2</sub> COOC <sub>2</sub> H <sub>5</sub> ]Ph <sub>2</sub> ( <b>4d</b> )	423(5.62)	551(4.33)	650	0.0072

<sup>a</sup>Values in parentheses refers to log  $\epsilon$ , sh = shoulder

**Table 6.3** Photophysical Data of Synthesized Free base and Their Zn(II) Complexes.

Por.	FWHM (nm)	$f$	Stokes Shift (cm <sup>-1</sup> )	Life time $\tau_f$ (ns)	$k_r$ (s <sup>-1</sup> )	$k_{nr}$ (s <sup>-1</sup> )
<b>1</b>	29	0.038	114	2.19	$1.69 \times 10^6$	$4.55 \times 10^8$
<b>3</b>	28	0.032	711	0.011	$1.05 \times 10^8$	$9.51 \times 10^{10}$
<b>2</b>	24	0.028	268	5.17	$5.71 \times 10^6$	$1.88 \times 10^8$
<b>4</b>	22	0.030	226	3.28	$1.06 \times 10^7$	$2.94 \times 10^8$
<b>1d</b>	16	0.035	498	0.185	$1.24 \times 10^7$	$5.39 \times 10^9$
<b>3d</b>	15	0.024	869	0.0713	$7.01 \times 10^6$	$1.40 \times 10^{10}$
<b>2d</b>	17	0.030	2498	0.548	$1.26 \times 10^7$	$1.81 \times 10^9$
<b>4d</b>	16	0.031	2764	0.202	$3.56 \times 10^7$	$4.91 \times 10^9$

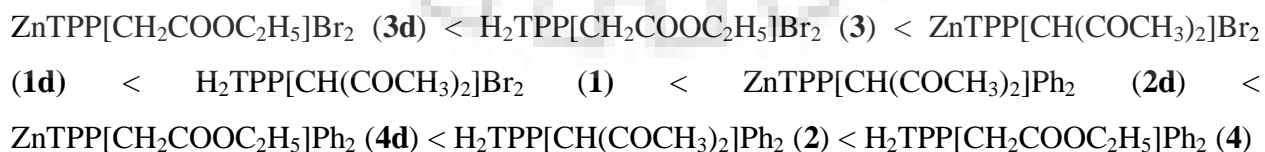
Figures 6.5(a) and A11(a) in Appendix-V represents the absorption spectra of synthesised free base and Zn(II) complexes whereas the electronic absorption spectra of MTPP(X)(R)<sub>2</sub> (where X = acetylacetone and methylketoester; R = Br and Ph; M = Co, Ni, and Cu) are given in Figure A12 in appendix-V. MTPPBr<sub>2</sub>(X) (X = CH(COCH<sub>3</sub>)<sub>2</sub> and CH<sub>2</sub>COOC<sub>2</sub>H<sub>5</sub>) exhibited remarkable red-shift (10-15 nm) in B and Q bands as compared to corresponding MTPP whereas these porphyrins were ~10-14 nm blue shifted as compared to their precursors i.e. MTPPBr<sub>2</sub>(NO<sub>2</sub>) which is probably due to less electron withdrawing nature of acetylacetone and ethyl acetate as compared to nitro group. On the other hand, in comparison to MTPP(X)Br<sub>2</sub>, MTPP(X)Ph<sub>2</sub> (X = CH(COCH<sub>3</sub>)<sub>2</sub> and CH<sub>2</sub>COOC<sub>2</sub>H<sub>5</sub>) have shown more red shifted spectra (10-18 nm) with respect to their precursors MTPP(NO<sub>2</sub>)Ph<sub>2</sub> which may be due to the combined effect of electron rich nature of phenyl groups and induced nonplanarity as compared to bromo groups. Electronic spectral data of free base and Zn(II) complexes is given in Table 6.2 whereas for other synthesised metal complexes is given in Table A2 in Appendix-V.

Fluorescence spectra of free bases and zinc complexes were recorded in CH<sub>2</sub>Cl<sub>2</sub> at 298 K. Figures 6.5(b) and A11(b) in Appendix-V exhibit the comparative emission spectra of synthesized free base and Zn(II) complexes in CH<sub>2</sub>Cl<sub>2</sub>. The emission data is given in Table 6.2. Bromoporphyrins have shown very feeble fluorescence and low quantum yield due to heavy atom effect of bromo groups. MTPP[CH<sub>2</sub>COOC<sub>2</sub>H<sub>5</sub>]Br<sub>2</sub> (where M = 2H and Zn) were showing least fluorescence and quantum yield which is ascribed to the combined effect of heavy atoms of bromo groups and nonplanarity. On the other hand, H<sub>2</sub>TPP[CH<sub>2</sub>COOC<sub>2</sub>H<sub>5</sub>]Ph<sub>2</sub> (**4**) has shown highest fluorescence intensity with maximum quantum yield. The quantum yields ( $\phi$ ) were calculated by using the following formula:

$$\phi_{\text{sample}} = (\phi_{\text{ref}} \times A_{\text{sample}} \times \epsilon_{\text{ref}}) / (A_{\text{ref}} \times \epsilon_{\text{sample}}) \quad \text{Eq.1}$$

Here A = area calculated from emission spectra and  $\epsilon$  = absorption

The quantum yield followed the order:



Among bromo substituted porphyrins, MTPP[CH<sub>2</sub>COOC<sub>2</sub>H<sub>5</sub>]Br<sub>2</sub> (M = 2H and Zn) have shown highest Stokes shifts values as compared to the MTPP[CH(COCH<sub>3</sub>)<sub>2</sub>]Br<sub>2</sub> (M = 2H and Zn) The



calculated oscillator strengths range from 0.014-0.038 which is clearly describing the effect of  $\beta$ -substituents and estimated by the following formula

$$f = 4.61 \times 10^{-9} \epsilon \delta \quad \text{Eq.2}$$

Here,  $\epsilon$  = molar absorption coefficient of Soret band,  $\delta$  = full width at half maxima.

The synthesized compounds exhibited lower singlet state lifetime as compared to the H<sub>2</sub>TPP (11 ns) which is due to the fast intersystem crossing or rapid interconversion of the excited states. Similarly, Zn(II) complexes exhibited lower singlet state lifetime as compared to the ZnTPP.

The radiative ( $k_r$ ) and nonradiative ( $k_{nr}$ ) rate constants were calculated using the following equations [23]

$$k_r = \phi_f / \tau_f \quad \text{Eq.3}$$

$$k_{nr} = (1 - \phi_f) / \tau_f \quad \text{Eq.4}$$

Notably, the calculated radiative rate constants ( $k_r$ ) of synthesized free base are lower as compared to the H<sub>2</sub>TPP, whereas the non-radiative rate constants ( $k_{nr}$ ) are higher than H<sub>2</sub>TPP. The higher non-radiative rate constants attributed to effect of electron withdrawing -CH(COCH<sub>3</sub>) and -CH<sub>2</sub>COOC<sub>2</sub>H<sub>5</sub>. The lower radiative rate constants ( $k_r$ ) are attributed to the quasi-planar conformation of the macrocyclic core. Bromo-substituted porphyrins exhibited lower singlet state lifetime, lower radiative rate constants and higher non-radiative constants as compared to the phenyl substituted porphyrins which are due to combine effect of nonplanar conformation and heavy atom effect of bromo group.

### 6.3.6 Electrochemical Redox Studies

To determine the electronic effect of  $\beta$ -substituents on the macrocyclic skeleton, the electrochemical redox properties of synthesized mixed substituted porphyrins were investigated by cyclic voltammetry in CH<sub>2</sub>Cl<sub>2</sub> containing 0.1 M TBAPF<sub>6</sub> supporting electrolyte. Table 6.4 lists the measured redox potentials of MTPP(X)Br<sub>2</sub> and MTPP(X)Ph<sub>2</sub> (Where X = CH(COCH<sub>3</sub>)<sub>2</sub> or CH<sub>2</sub>COOC<sub>2</sub>H<sub>5</sub>) in CH<sub>2</sub>Cl<sub>2</sub> at 298 K. Figures 6.6 and A13 in Appendix-V represent the comparative cyclic voltammograms of synthesized free bases porphyrins and their metal complexes (Co(II), Ni(II), Cu(II) and Zn(II)). Analysis of electrochemical data revealed that the electron withdrawing/donating substituents at the TPP skeleton affect the magnitude of the HOMO-LUMO gap.



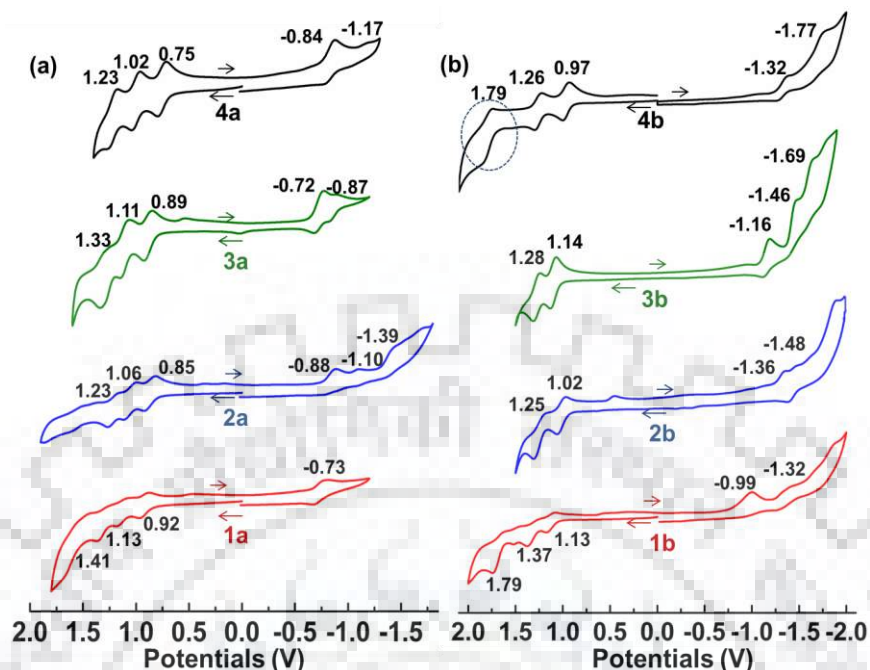


**Figure 6.6** Comparative Cyclic Voltammograms of Synthesized (a) Co(II) complexes, and (b) Ni(II) Complexes in  $\text{CH}_2\text{Cl}_2$  at 298K.

Interestingly, most of the acetylacetonone appended porphyrins  $\text{MTPP}[\text{CH}(\text{COCH}_3)_2](\text{R})_2$  (where  $\text{R} = \text{Br}$  and  $\text{Ph}$ ) have shown multiple oxidations which is due to presence of keto-enol tautomer of acetylacetonone appended porphyrins. On contrary, ester appended porphyrins exhibited only two ring centered oxidations and reductions except  $\text{NiTPP}[\text{CH}_2\text{COOC}_2\text{H}_5]\text{Ph}_2$  (**4b**) and Co(II) complexes. Notably, the enol form causes extension of  $\pi$ -conjugation at  $\beta$ -pyrrolic position which induces the interaction of porphyrin skeleton and MO of acetylacetonone. This interaction and extended  $\pi$ -conjugation resulted into the multiple ring centered oxidations. The synthesized  $\beta$ -substituted Co(II) tetraphenylporphyrins exhibited facile  $\text{Co}^{\text{III/II}}$  and  $\text{Co}^{\text{II/I}}$  in addition to two ring centered oxidations which is common phenomenon and well quoted in the literature [24-26]. Interestingly, the electron rich  $\text{NiTPP}[\text{CH}_2\text{COOC}_2\text{H}_5]\text{Ph}_2$  (**4b**) have shown three oxidations. The first two oxidations were ascribed to ring centered oxidation whereas the third oxidation was observed due to the electrogeneration of the  $\text{Ni}^{\text{II}}/\text{Ni}^{\text{III}}$ . In the free base and fully filled  $d^{10}$  system, Zn(II) complexes, while moving from electron withdrawing  $\beta$ -substituents such as bromo to electron donating  $\beta$ -substituents such as phenyl a considerable increment in the HOMO-LUMO gap was observed. For example,  $\text{ZnTPP}[\text{CH}_2\text{COOC}_2\text{H}_5]\text{Ph}_2$  (**4d**) has 0.31 V higher HOMO-LUMO gap as compared to corresponding  $\text{ZnTPP}[\text{CH}_2\text{COOC}_2\text{H}_5]\text{Br}_2$  (**3d**). Significant cathodic

shifts in the first oxidation potentials (70-170 mV) and first reduction potentials (50-390 mV) were observed in  $\beta$ -phenyl substituted porphyrins as compared to corresponding  $\beta$ -bromo substituted porphyrins which clearly indicated the electron rich nature of  $\beta$ -phenyl rings.

**Table 6.4** Electrochemical Redox Data<sup>a</sup> in CH<sub>2</sub>Cl<sub>2</sub> at 298K using TBAPF<sub>6</sub> as Supporting Electrolyte

Porphyrin	Oxidation (V)			$\Delta E_{1/2}$	Reduction (V)		
	I	II	III		I	II	III
<b>1</b>	1.13 <sup>i</sup>	1.66		2.21	-1.08	-1.23	
<b>2</b>	0.99 <sup>i</sup>	1.49	1.69 <sup>i</sup>	2.23	-1.24	-1.35	
<b>3</b>	1.06 <sup>i</sup>	1.25 <sup>i</sup>		2.09	-1.03	-1.18	
<b>4</b>	0.93	1.06		2.14	-1.21	-1.41	
<b>1a</b>	0.92	1.13	1.41	1.65	-0.73	-0.83 <sup>d</sup>	1.34 <sup>d</sup>
<b>2a</b>	0.85	1.06	1.23	1.73	-0.88	-1.10	
<b>3a</b>	0.89	1.11	1.33	1.61	-0.72	-0.87	
<b>4a</b>	0.75	1.02	1.23	1.59	-0.84	-1.17	
<b>1b</b>	1.13	1.37 <sup>i</sup>	1.79	2.12	-0.99 <sup>i</sup>	-1.32	-1.81
<b>2b</b>	1.02	1.25		2.38	-1.36	-1.48	
<b>3b</b>	1.14	1.28		2.30	-1.16	-1.46	-1.69
<b>4b</b>	0.97	1.26	1.79	2.29	-1.32	-1.77	
<b>1c</b>	1.01	1.35	1.61	2.29	-1.28 <sup>i</sup>	-1.40	-1.61
<b>2c</b>	0.89	1.27		2.27	-1.38	-1.48	
<b>3c</b>	0.98	1.39		2.22	-1.24 <sup>i</sup>	-1.50	-1.73
<b>4c</b>	0.85	1.25		2.14	-1.29	-1.69	
<b>1d</b>	0.92	1.12	1.44	2.16	-1.24	-1.47	
<b>2d</b>	0.83	1.00	1.28	2.21	-1.38	-1.68	
<b>3d</b>	0.89	1.11		1.86	-0.97	-1.20	
<b>4d</b>	0.81	0.98		2.17	-1.36	-1.75	-1.87

<sup>a</sup>vs Ag/AgCl electrode, i = irreversible peaks, d = data obtained from differential pulse voltammetry

Some of the bromo-substituted porphyrins have shown three reductions which may be due to the electron withdrawing nature of bromo groups.

## 6.4 CONCLUSIONS

In summary, we have synthesized a new series of asymmetrically  $\beta$ -trisubstituted porphyrins through nucleophilic substitution of  $\beta$ -NO<sub>2</sub> group of 5,10,15,20-tetraphenylporphyrin by 1,3-diketone and ester functionalities. Interestingly, NiTPP[CH(COCH<sub>3</sub>)<sub>2</sub>]Br<sub>2</sub> (**1b**) exhibited very high magnitude displacement of 24-core atoms and  $\beta$ -pyrrole carbons ( $\Delta_{24} = 0.44 \text{ \AA}$ ,  $\Delta C_{\beta} = 0.82 \text{ \AA}$ ) from the mean plane which is the highly nonplanar mixed  $\beta$ -trisubstituted MTPP reported till date. The nature of the diketone or ester have shown very little influence on the absorption and fluorescence profiles inducing small bathochromic shifts and slight decrement in the fluorescence intensity with low quantum yield as compared to the precursor 2-nitroporphyrin whereas a noticeable effect of acetylacetone group on the redox properties have been observed. Diketone appended porphyrins MTPP[CH(COCH<sub>3</sub>)<sub>2</sub>](R)<sub>2</sub> (where R = Br and Ph) have shown multiple oxidations and reductions due to the presence of keto-enol tautomeric form of acetylacetone group as well the impact of the antipodal  $\beta$ -substituent on the redox behavior of the macrocyclic skeleton.

## 6.5 REFERENCES

1. Jaquinod, L. *In The Porphyrin Handbook*; Kadish, K. M.; Smith, K. M.; Guillard, R., Eds.; Academic: New York, 2000; Vol. 1, pp 215-218.
2. Suslick, K. S.; Rakow, N. A.; Kosal, M. E.; Chou, J. H. The Materials Chemistry of Porphyrins and Metalloporphyrins. *J. Porphyrins Phthalocyanines* **2000**, *4*, 407-413.
3. Luo, J.; Chen, L.-F.; Hu, P.; Chen, Z.-N. Tetranuclear Gadolinium(III) Porphyrin Complex as a Theranostic Agent for Multimodal Imaging and Photodynamic Therapy. *Inorg. Chem.* **2014**, *53*, 4184-4191.
4. Moura, N. M. M.; Faustino, M. A. F.; Neves, M. G. P. M. S.; Duarte, A. C.; Cavaleiro, J. A. S. Vilsmeier-Haack Formylation of Cu(II) and Ni(II) Porphyrin Complexes under Microwaves Irradiation. *J. Porphyrins Phthalocyanines* **2011**, *15*, 653-658.

5. Bhyrappa, P.; Sankar, M.; Varghese, B. Mixed Substituted Porphyrins: Structural and Electrochemical Redox Properties. *Inorg. Chem.* **2006**, *45*, 4136-4149.
6. Giraudeau, A.; Callot, H. J.; Jordan, J.; Ezhar, I.; Gross, M. Substituent Effects in the Electroreduction of Porphyrins and Metalloporphyrins. *J. Am. Chem. Soc.* **1979**, *101*, 3857-3862.
7. Jaquinod, L.; Gros, C.; Khoury, R. G.; Smith, K. M. A Convenient Synthesis of Functionalized Tetraphenylchlorins. *Chem. Commun.* **1996**, 2851-2852.
8. Crossley, M. J.; King, L. G. Reaction of Metallo-2-nitro-5,10,15,20-tetraphenylporphyrins with Oxyanions. Temperature-dependent Competition between Nucleophilic Addition and Single-electron Transfer Processes. *J. Chem. Soc., Perkin Trans. I* **1996**, 1251-1260.
9. Grover, N.; Chaudhri, N.; Sankar, M. Facile Conversion of Ni(II) Cyclopropylchlorins into Novel  $\beta$ -Substituted Porphyrins through Acid-Catalyzed Ring-Opening Reaction. *Inorg. Chem.* **2017**, *56*, 424-437.
10. Serra, V. I. V.; Pires, S. M. G.; Alonso, C. M. A.; Neves, M. G. P. M. S.; Tome, A. C.; Cavaleiro J. A. S. *Meso*-Tetraarylporphyrins Bearing Nitro or Amino Groups: Synthetic Strategies and Reactivity Profiles. *Top. Heterocycl. Chem.* **2014**, *33*, 35-78.
11. Wyrębka, P.; Ostrowski, S. Synthesis of Some  $\beta$ -Nitro-*meso*-tetraphenylporphyrin Derivatives. *J. Porphyrins Phthalocyanines* **2007**, *11*, 822-828.
12. Shea, K. M.; Jaquinod, L.; Smith, K. M. Dihydroporphyrin Synthesis: New Methodology. *J. Org. Chem.* **1998**, *63*, 7013-7021.
13. Shea, K. M.; Jaquinod, L.; Khoury, R. G.; Smith, K. M. Functionalization of 2,3-Disubstituted-2,3-dihydro-5,10,15,20-tetraphenylporphyrins *Tetrahedron*, **2000**, *56*, 3139-3144.
14. Guintini, F.; Faustion, M. A. F.; Neves, M. G. P. M. S.; Tome, A. C.; Silva, A. M. S., Cavaleiro, J. A. S. Synthesis and Reactivity of 2-(Porphyrin-2yl)-1,3-dicarbonyl Compounds. *Tetrahedron*, **2005**, *61*, 10454-10461.
15. Hiroto, S.; Miyake, Y.; Shinokubo, H. Synthesis and Functionalization of Porphyrins through Organometallic Methodologies. *Chem. Rev.* **2017**, *117*, 2910-3043.

16. Chaudhri, N.; Grover, N.; Sankar, M. Versatile Synthetic Route for  $\beta$ -Functionalized Chlorins and Porphyrins by Varying the Size of Michael Donors: Syntheses, Photophysical, and Electrochemical Redox Properties. *Inorg. Chem.* **2017**, *56*, 11532-11545.
17. Richeter, S.; Jeandon, C.; Gisselbrecht, J.-P.; Graff, R.; Ruppert, R.; Callot, H. J. Synthesis of New Porphyrins with Peripheral Conjugated Chelates and Their Use for the Preparation of Porphyrin Dimers Linked by Metal Ions. *Inorg. Chem.* **2004**, *43*, 251-263.
18. Otway, D. J.; Rees, W. S., Jr. Group 2 Element  $\beta$ -Diketonate Complexes: Synthetic and Structural Investigations. *Coord. Chem. Rev.* **2000**, *210*, 279-328.
19. Simon, C.; Constantieux, T.; Rodriguez, J. Utilisation of 1,3-Dicarbonyl Derivatives in Multicomponent Reactions. *Eur. J. Org. Chem.* **2004**, *2004*, 4957-4980.
20. Chahal, M. K.; Sankar, M.; Butcher, R. J. An Insight into the Communication between  $\beta$ -Olefin/Phenyl Olefin-mediated Acceptors and Porphyrin  $\pi$ -System: a Way to Establish Porphyrin based Chemodosimeters and Chemosensors. *Phys. Chem. Chem. Phys.* **2017**, *19*, 4530-4540.
21. Yadav, P.; Kumar, R.; Saxena, A.; Butcher, R. J.; Sankar, M.  $\beta$ -Trisubstituted "Push-Pull" Porphyrins-Synthesis and Structural, Photophysical, and Electrochemical Redox Properties. *Eur. J. Inorg. Chem.* **2017**, 3269-3274.
22. Kumar, R.; Sankar, M. Synthesis, Spectral, and Electrochemical Studies of Electronically Tunable  $\beta$ -Substituted Porphyrins with Mixed Substituent Pattern. *Inorg. Chem.* **2014**, *53*, 12706-12719.
23. Gentemann, S.; Medforth, C. J.; Forsyth, T. P.; Nurco, D. J.; Smith, K. M.; Fajer, J.; Holten, D. Photophysical Properties of Conformationally Distorted Metal-Free Porphyrins. Investigation into the Deactivation Mechanisms of the Lowest Excited Singlet State *J. Am. Chem. Soc.* **1994**, *116*, 7363-7368.
24. Truxillo, L. A.; Davis, D. G. Electrochemistry of Cobalt Tetraphenylporphyrin in Aprotic Media. *Anal. Chem.* **1975**, *47*, 2260-2267.
25. D'Souza, F.; Villard, A.; Van Caemelbecke, E.; Franzen, M.; Boschi, T.; Tagliatesta, P.; Kadish, K. M. Electrochemical and Spectroelectrochemical Behavior of Cobalt(III),

Cobalt(II), and Cobalt(I) Complexes of *meso*-Tetraphenylporphyrinate Bearing Bromides on the  $\beta$ -Pyrrole Positions. *Inorg. Chem.* **1993**, 32, 4042–4048.

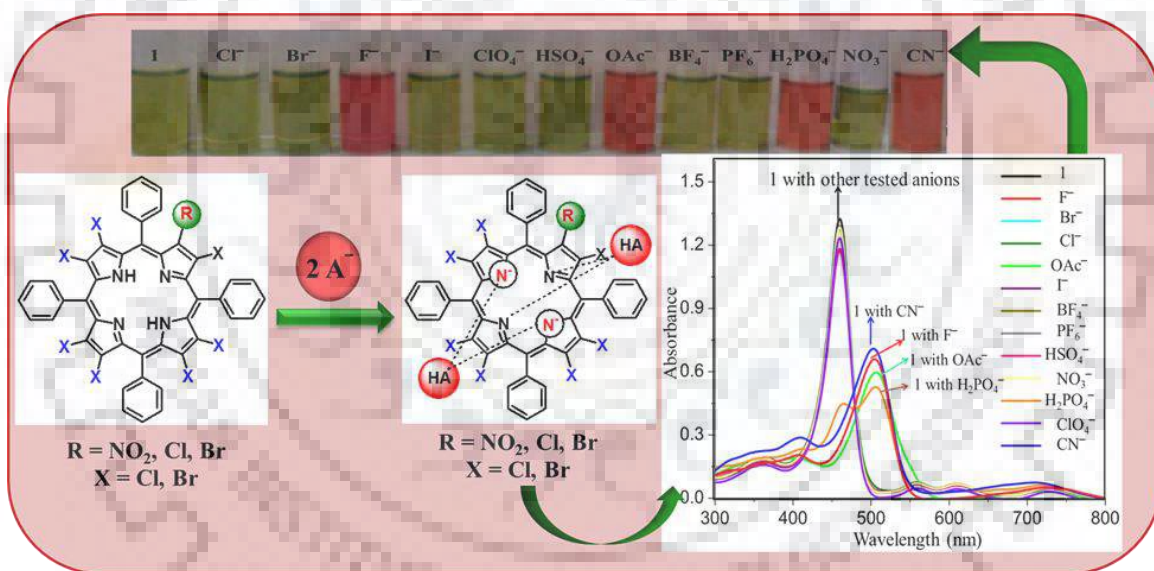
26. Mu, X. H.; Kadish, K. M. Oxidative Electrochemistry of Cobalt Tetraphenylporphyrin under a CO Atmosphere. Interaction between Carbon Monoxide and Electrogenenerated [(TPP)Co]<sup>+</sup> in Nonbonding Media. *Inorg. Chem.* **1989**, 28, 3743-3747.





# CHAPTER 7

## “Perhaloporphyrins: Synthesis, Structural, Electrochemical Redox and Anion Sensing Properties”





## CHAPTER 7

### PERHALOPORPHYRINS: SYNTHESIS, STRUCTURAL, ELECTROCHEMICAL REDOX AND ANION SENSING PROPERTIES

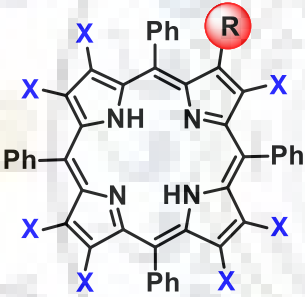
#### 7.1 INTRODUCTION

Porphyrins with exhaustive substitution are of considerable interest due to their critical role in modulating physicochemical properties [1], nonplanar conformation [2] and acid-base properties of central coordination entity  $H_2N_4$  of the macrocycle [3]. Introduction of bulky groups at the  $\beta$ -pyrrolic positions distorts the macrocyclic ring and this effect is more when more than four halogens or electron withdrawing groups are present at the  $\beta$ -pyrrolic positions [4]. In particular, substitution with halogens at  $\beta$ -positions of porphyrins seems to confer some unusual optical properties [5], enhanced electrochemical redox stability [6] and increased catalytic efficiency to the metal complexes [7,8]. The ligand binding and dissociation dynamics can vary according to the electronic structure and radius of the metal centre as well as substitution at porphyrin macrocycle. The degree of nonplanarity is totally built upon the nature of substituents. The fully  $\beta$ -substituted (dodecasubstituted) porphyrins exhibit saddle-shaped distortion with  $\Delta C_\beta$  in the range of 1.0-1.2 Å from the mean plane [9]. Dodecasubstituted porphyrins fall into two classes namely symmetrically and asymmetrically  $\beta$ -substituted porphyrins. The symmetrically  $\beta$ -octasubstituted porphyrins have been widely explored due to their ease of synthesis and interesting electronic, electrochemical and crystallographic studies [10]. Contrary to the well-studied symmetrically  $\beta$ -substituted octaalkyl [11] and octahaloporphyrins [12] due to their rich spin state and catalytic studies, only a little chemistry of the unsymmetrically dodecasubstituted porphyrins is known in the literature [13].

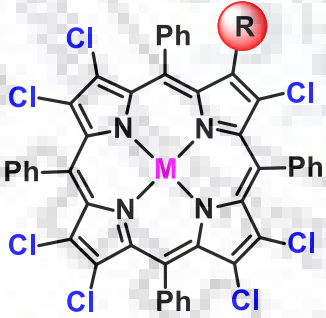
Inspired by nature's fundamental biological processes involving enzyme-substrate or host-guest interactions which are regulated by light, ions and small molecule concentrations, the design of effective anion receptors containing responsive functional groups as an integral part of a host macrocyclic framework has been an active area of research [14]. In order to achieve an enhanced selectivity and sensitivity towards a particular anion, a fine tuning of binding sites is required which is often difficult because of their wide range of geometries, larger size, high solvation

energies and accessibility in a very narrow pH range as compared to their cationic counterparts [15]. Cyanide is extremely toxic to living organisms; it completely stops oxygen transport in the blood and mitochondrial electron-transport chain, thus inhibiting cellular respiration [16]. The selective recognition of fluoride ions is of great importance for monitoring  $F^-$  ion metabolism in nature, the analysis of drinking water and in the treatment of osteoporosis [17]. Phosphate ions are playing a vital role in biological processes like signalling, energy transduction, information storage and expression [18]. The acetate ions are the most common building blocks in biosynthesis and a critical component of numerous metabolic processes. The rate of  $OAc^-$  production and oxidation has been frequently used as an indicator of organic decomposition in marine sediments [19]. Thus to design an anion receptor with high selectivity has become the area of intensive research.

**Chart 7.1** Molecular Structures of Synthesized Porphyrins.

	<b>R</b>	<b>X</b>	<b>Name</b>	<b>Code</b>
	NO <sub>2</sub>	Cl	H <sub>2</sub> TPP(NO <sub>2</sub> )Cl <sub>7</sub>	<b>1</b>
	Cl	Cl	H <sub>2</sub> TPPCL <sub>8</sub>	<b>2</b>
	NO <sub>2</sub>	Br	H <sub>2</sub> TPP(NO <sub>2</sub> )Br <sub>7</sub>	<b>3</b>
Br	Br	H <sub>2</sub> TPPBr <sub>8</sub>	<b>4</b>	

	<b>R</b>	<b>M</b>	<b>Name</b>	<b>Code</b>
	NO <sub>2</sub>	Co(II)	CoTPP(NO <sub>2</sub> )Cl <sub>7</sub>	<b>1a</b>
	NO <sub>2</sub>	Ni(II)	NiTPP(NO <sub>2</sub> )Cl <sub>7</sub>	<b>1b</b>
	NO <sub>2</sub>	Cu(II)	CuTPP(NO <sub>2</sub> )Cl <sub>7</sub>	<b>1c</b>
	NO <sub>2</sub>	Zn(II)	ZnTPP(NO <sub>2</sub> )Cl <sub>7</sub>	<b>1d</b>
	Cl	Co(II)	CoTPPCL <sub>8</sub>	<b>2a</b>
	Cl	Ni(II)	NiTPPCL <sub>8</sub>	<b>2b</b>
	Cl	Cu(II)	CuTPPCL <sub>8</sub>	<b>2c</b>
	Cl	Zn(II)	ZnTPPCL <sub>8</sub>	<b>2d</b>

Calixpyrroles, phlorins, corroles, sapphyrins, N-confused porphyrins, oxoporphyrinogens and porphyrins are excellent multifunctional candidates for a great variety of anion sensor applications *via* NH groups of the pyrrole units [20-22]. Many transformation and modifications have been carried out on porphyrin macrocycles for selective ion recognition [23].

Metalloporphyrins have been utilized for the detection of  $\text{CN}^-$  ions due to intrinsic affinity of cyanide for many metals such as zinc, rhodium, and copper coordinated to porphyrins [24,25]. In general, the detection of basic anions through anion induced deprotonation mechanism is quite common in organic hosts whereas it is very difficult to deprotonate imino protons of planar porphyrins under ambient conditions. Herein, we attempted to make highly nonplanar electron deficient perhaloporphyrins (Chart 1) which can be utilized as anion sensors through pyrrolic NH deprotonation as a detection mechanism. On the other hand, visual detection of cyanide ion by Co(II) or Zn(II) complexes of organic ligands is known in literature whereas this is the first report on selective naked-eye detection of cyanide ions by Co(II)-porphyrin with low detection limit ( $>1.5 \mu\text{M}$ ).

## 7.2 EXPERIMENTAL SECTION

### 7.2.1 Chemicals

Pyrrole,  $\text{C}_6\text{H}_5\text{CHO}$ , N-chlorosuccinimide,  $\text{M}(\text{OAc})_2 \cdot n\text{H}_2\text{O}$  ( $\text{M} = \text{Co}, \text{Ni}, \text{Cu}, \text{and Zn}$ ),  $\text{Na}_2\text{S}_2\text{O}_4$ , TFA, TBAOH and  $\text{NaHCO}_3$  were purchased from HiMedia, India and used as received. 1,1,2,2-tetrachloroethane was purchased from Rankem and dried over molecular sieves ( $4\text{\AA}$ ) before use. The tetrabutylammonium salts (TBAX,  $\text{X} = \text{CN}^-, \text{F}^-, \text{Cl}^-, \text{Br}^-, \text{I}^-, \text{HSO}_4^-, \text{BF}_4^-, \text{OAc}^-, \text{H}_2\text{PO}_4^-, \text{ClO}_4^-, \text{PF}_6^-$  and  $\text{NO}_3^-$ ) were purchased from Alfa Aesar and used as received. Dry toluene for UV-Visible spectral studies was dried and distilled from sodium-benzophenone mixture.

### 7.2.2 Instrumentation and Methods

UV-vis,  $^1\text{H}$  NMR, electrochemical measurements and elemental analysis were performed using same characterization techniques as described in Chapter 2. ESI mass spectra were recorded on Bruker Daltonics microTOF mass spectrometer in negative ion mode using  $\text{CH}_3\text{CN}$  as solvent. The X-ray quality single crystals of **2** were obtained by vapor diffusion of  $\text{CH}_3\text{CN}$  into the toluene solution of **2**. The X-ray quality single crystals of **1a**, **1d**, and **2d** were obtained by vapor diffusion of methanol onto a  $\text{CHCl}_3$  solution of respective porphyrins. **1d** was also crystallized with vapor diffusion of hexane onto the  $\text{CHCl}_3$  solution of **1d** with few drops of pyridine, and the single crystals of **2b** were obtained by vapor diffusion of methanol onto the toluene solution of **2b**. Protonation, deprotonation and anion detection studies were carried out in distilled toluene at 298 K and the concentration of **1-4** were kept  $\sim 10\text{-}13 \mu\text{M}$  throughout the experiments whereas

the stock solution of anions were maintained in between 0.003 to 0.05 M as per their need. The protonation, deprotonation constants ( $\beta_2$ ) and stoichiometry for anion binding with **1-4** were calculated using Hill equation [26]. We have calculated the limit of detection (LOD) and limit of quantification (LOQ) for anions in toluene by **1-4** using the formulae  $LOD = 3.3(SD/S)$ ,  $LOQ = 10(SD/S)$  where SD stands for standard deviation of blank and S stands for slope of regression line. Ligation studies of Zn(II) complexes (**1d** and **2d**) with nitrogenous bases and basic anions and selective cyanide ion sensing by Co(II) complexes (**1a** and **2a**) were carried out in toluene and association constants were calculated using Benesi-Hildebrand method.

### 7.2.3 Synthetic Procedures

NiTTP(NO<sub>2</sub>) was prepared by nitration of NiTTP using copper nitrate in acetic anhydride as reported in literature [27].

#### 7.2.3.1 Synthetic Procedures for NiTTP(NO<sub>2</sub>)Cl<sub>7</sub>

NiTTP(NO<sub>2</sub>) (0.2 gm, 0.28 mmol) was dissolved in 70 ml of 1,1,2,2-tetrachloroethane (TCE) in a 100 mL RB flask. To this, 15 eq. of N-chlorosuccinimide (0.56 gm, 4.19 mmol) was added and then refluxed for 2.5 hours under argon atmosphere. The solvent was removed under vacuum and the crude porphyrin was purified by silica gel column chromatography using CHCl<sub>3</sub>/hexane mixture (1:1, v/v) as eluent. The desired product was eluted as second fraction and the yield was found to be 23% (0.062 gm, 0.064 mmol). NiTTPCl<sub>8</sub> was collected as first fraction and the yield was found to be 19% (0.050 gm, 0.053 mmol). The spectroscopic data of NiTTPCl<sub>8</sub> was in accordance in with reported literature [28].

**NiTTP(NO<sub>2</sub>)Cl<sub>7</sub>**: UV/Vis (CH<sub>2</sub>Cl<sub>2</sub>):  $\lambda_{max}$  in nm (log $\epsilon$ ) 448 (5.12), 562(4.04), 604(3.80). <sup>1</sup>H NMR in CDCl<sub>3</sub> (500 MHz)  $\delta$  (ppm): 7.93-7.87(m, 8H, *meso-o*-phenyl-H), 7.73-7.60 (m, 12H, *meso-m,p*-phenyl-H). ESI-MS (*m/z*): found 987.82 [M•OCH<sub>3</sub>]<sup>+</sup>, calcd 987.56. Anal. Calcd for C<sub>44</sub>H<sub>20</sub>N<sub>5</sub>O<sub>2</sub>Cl<sub>7</sub>Ni: C, 55.19; H, 2.11; N, 7.31. Found C, 55.45; H, 2.44; N, 7.57.

#### 7.2.3.2 Synthesis of H<sub>2</sub>TTP(NO<sub>2</sub>)Cl<sub>7</sub> (**1**)

NiTTP(NO<sub>2</sub>)Cl<sub>7</sub> (0.1 g, 0.10 mmol) was dissolved in 70 ml of distilled CHCl<sub>3</sub> in a 250 ml RB flask. To this, 8 ml of conc. H<sub>2</sub>SO<sub>4</sub> was added drop wise and allowed to stir for 3 h. at 0 °C. Then 100 ml of water was added and the compound was extracted into CHCl<sub>3</sub>. The organic layer was



washed with water (2×100 ml) and then neutralized with 100 ml of aq. NH<sub>3</sub> solution (10%). The excess ammonia was removed by washing with water and then dried over Na<sub>2</sub>SO<sub>4</sub>. The crude porphyrin was purified by silica gel column chromatography using CHCl<sub>3</sub> as eluent. The yield of **1** was found to be 79% (0.074 gm, 0.082 mmol) respectively.

**H<sub>2</sub>TPP(NO<sub>2</sub>)Cl<sub>7</sub>**: UV/Vis (CH<sub>2</sub>Cl<sub>2</sub>): λ<sub>max</sub> in nm (log ε): 461 (5.18), 562(3.88), 615(3.85), 732(3.78). <sup>1</sup>H NMR in CDCl<sub>3</sub> (500 MHz): δ (ppm) 8.23-8.15 (m, 8H, *meso-o*-phenyl-H), 7.82-7.72 (m, 12H, *meso-m, p*-phenyl-H). ESI-MS (*m/z*): found 900.58 [M]<sup>-</sup> calcd. 900.86). Anal. Calcd for C<sub>44</sub>H<sub>22</sub>N<sub>5</sub>O<sub>2</sub>Cl<sub>7</sub>: C, 58.66; H, 2.46; N, 7.77. Found C, 58.37; H, 2.62; N, 7.56.

The demetallation of NiTPPCL<sub>8</sub> yielded to H<sub>2</sub>TPPCL<sub>8</sub> and the spectroscopic data was in accordance with the proposed structure of **2** and clearly matching with literature [28].

### 7.2.3.3 General Procedure for the Synthesis of MTPP(NO<sub>2</sub>)Cl<sub>7</sub> and MTPPCL<sub>8</sub> (where M = Co<sup>II</sup>, Cu<sup>II</sup> and Zn<sup>II</sup>):

Free base porphyrins H<sub>2</sub>TPP(NO<sub>2</sub>)Cl<sub>7</sub> and H<sub>2</sub>TPPCL<sub>8</sub> (25-30 mg) were dissolved in 20-25 ml of distilled CHCl<sub>3</sub>. To this, 10 eq. of M(OAc)<sub>2</sub>•nH<sub>2</sub>O (where M = Co<sup>II</sup>, Cu<sup>II</sup>, Zn<sup>II</sup>) in 2 ml of methanol were added and refluxed for 20-35 minute at 75 °C on water bath. After completion of reaction, solvent was removed by rotary evaporation and crude porphyrin was washed with water to remove excess of metal salt. Then compounds were purified by silica-gel column chromatography except **2c** and **2d** due to their poor solubility in CHCl<sub>3</sub>. these were purified by water wash only and dried in vacuum oven overnight at 75-80 °C. Yield of the metal derivatives were found to be almost quantitative (80-90%).

**CoTPP(NO<sub>2</sub>)Cl<sub>7</sub>**: UV/Vis (CH<sub>2</sub>Cl<sub>2</sub>): λ<sub>max</sub> (nm) (ε × 10<sup>-3</sup> L mol<sup>-1</sup> cm<sup>-1</sup>) 447(186.2), 562(16.59), 605(9.77). ESI-MS (*m/z*): found 992.821 [M+K]<sup>+</sup>, calcd 992.840. Anal. Calcd for C<sub>44</sub>H<sub>20</sub>N<sub>5</sub>O<sub>2</sub>Cl<sub>7</sub>Co: C, 55.18; H, 2.10; N, 7.31. Found C, 54.98; H, 2.12; N, 7.40.

**NiTPP(NO<sub>2</sub>)Cl<sub>7</sub>**: UV/Vis (CH<sub>2</sub>Cl<sub>2</sub>): λ<sub>max</sub> (nm) (ε × 10<sup>-3</sup> L mol<sup>-1</sup> cm<sup>-1</sup>) 448(128.8), 562(10.96), 604(6.31). <sup>1</sup>H NMR in CDCl<sub>3</sub> (500 MHz): δ (ppm), 7.94-7.87 (m, 8H, *meso-o*-Ph-H), 7.73-7.60(m, 12H, *meso-m,p*-Ph-H). ESI-MS (*m/z*): found 991.80 [M+K]<sup>+</sup>, calcd 991.84. Anal. Calcd for C<sub>44</sub>H<sub>20</sub>N<sub>5</sub>O<sub>2</sub>Cl<sub>7</sub>Ni•(0.5CH<sub>2</sub>Cl<sub>2</sub>): C, 53.45; H, 2.12; N, 7.00, Found: C, 53.19; H, 2.09; N, 7.34.

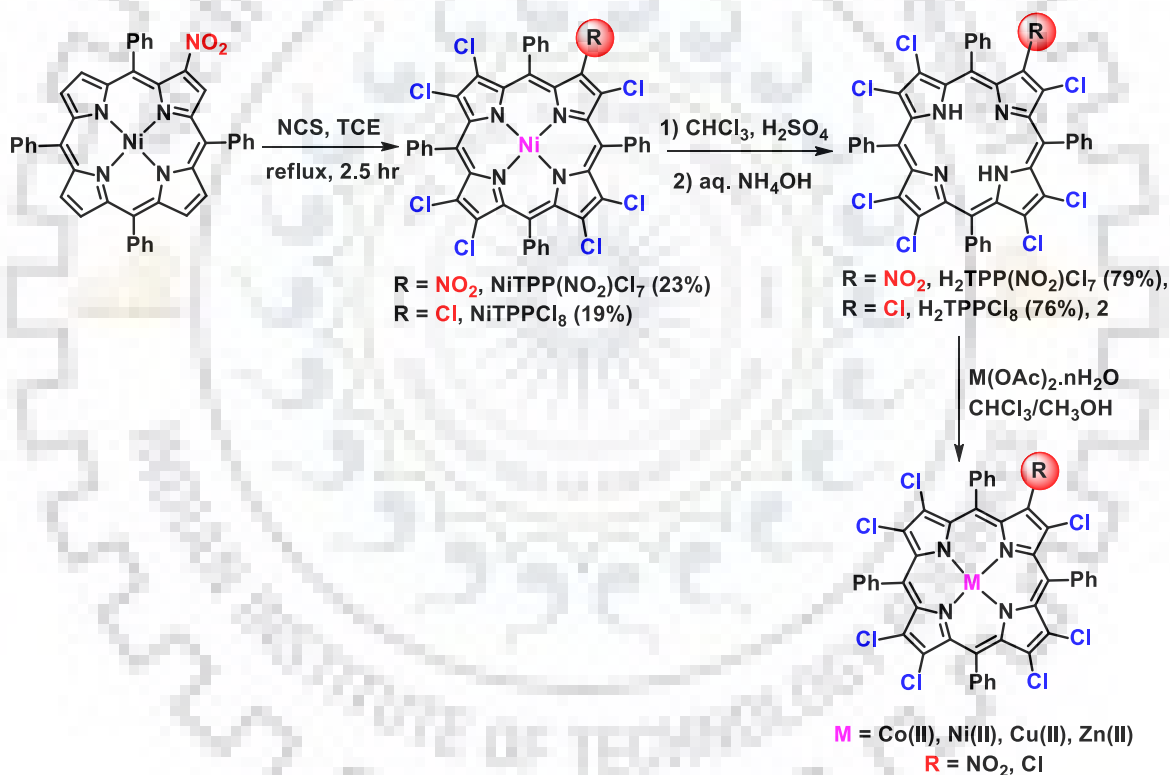
**CuTPP(NO<sub>2</sub>)Cl<sub>7</sub>**: UV/Vis (CH<sub>2</sub>Cl<sub>2</sub>): λ<sub>max</sub> (nm) (ε × 10<sup>-3</sup> L mol<sup>-1</sup> cm<sup>-1</sup>) 449(117.5), 575(12.88), 605(6.46). ESI-MS (*m/z*): found 996.90 [M+K]<sup>+</sup>, calcd 996.84. Anal. Calcd for

$C_{44}H_{20}N_5O_2Cl_7Cu$ : C, 54.91; H, 2.09; N, 7.28. Found: C, 54.48; H, 2.10; N, 7.50.  
**ZnTPP(NO<sub>2</sub>)Cl<sub>7</sub>**: UV/Vis (CH<sub>2</sub>Cl<sub>2</sub>):  $\lambda_{max}$  (nm) ( $\epsilon \times 10^{-3} \text{ L mol}^{-1} \text{ cm}^{-1}$ ) 457(158.5), 590(9.12), 647(8.31). <sup>1</sup>H NMR in CDCl<sub>3</sub> (500 MHz):  $\delta$  (ppm) 7.51-7.47 (m, 8H, *meso*-*o*-Ph-H), 7.20-7.13 (m 10H, *meso*-*m,p*-Ph-H), 7.04-7.01 (t, <sup>3</sup>J<sub>H,H</sub> = 8 Hz, 2H, *meso*-*m,p*-Ph-H). ESI-MS (*m/z*): found 997.190 [M+K]<sup>+</sup>, calcd 997.836. Anal. Calcd for C<sub>44</sub>H<sub>21</sub>N<sub>5</sub>O<sub>2.5</sub>Cl<sub>7</sub>Zn•(0.5CH<sub>3</sub>OH): C, 54.53; H, 2.26; N, 7.14, Found C, 54.30; H, 2.48; N, 7.00.

The spectroscopic data of MTPPCl<sub>8</sub> were exactly matching with the reported literature [28].

## 7.3 RESULTS AND DISCUSSION

### 7.3.1 Synthesis and Characterization



**Scheme 7.1** Facile Synthetic Route to Mixed  $\beta$ -substituted Perchlorometalloporphyrins.

Herein, we used a straightforward synthetic route to prepare synthetically nonviable mixed dodecasubstituted porphyrin through direct functionalization instead of taking  $\beta$ -substituted pyrrole (Scheme 1). NiTPP(NO<sub>2</sub>)Cl<sub>7</sub> (**1b**) was synthesized by direct chlorination of NiTPP(NO<sub>2</sub>) using 15 eq. of N-chlorosuccinimide in tetrachloroethane. Along with desired product we also

obtained NiTPPCl<sub>8</sub> (**2b**) as the side product, this was possibly due to replacement of nitro group by chloro group at higher temperature. **1b** and **2b** were demetallated to obtained corresponding free base porphyrins **1** and **2**. **3** and **4** having idiosyncratic nature have also been synthesized using modified literature methods [29,30]. MTPP(NO<sub>2</sub>)Cl<sub>7</sub> and MTPPCl<sub>8</sub> (Where M = Co<sup>II</sup>, Cu<sup>II</sup>, and Zn<sup>II</sup>) were prepared by simple metallation of **1** and **2** with different metal acetate in CHCl<sub>3</sub>/MeOH in good yields.

All the synthesized porphyrins were characterized by various spectroscopic techniques including UV-Visible, fluorescence, <sup>1</sup>H NMR, ESI-MS and cyclic voltammetric studies and elemental analyses. The structural aspects were justified by X-ray single crystal analysis and DFT calculations.

### 7.3.2 Crystal Structures Discussion

To determine the correct stereochemical features and the extend of strics offered by NO<sub>2</sub> substituent as compared to chloro at β-positions, we have examined the crystal structures of MTPP(NO<sub>2</sub>)Cl<sub>7</sub> (M = Co(II) and Zn(II)), H<sub>2</sub>TPPCl<sub>8</sub> (**2**), and MTPPCl<sub>8</sub> (M = Ni(II) and Zn(II)). The crystallographic data of H<sub>2</sub>TPPCl<sub>8</sub> (**2**), NiTPPCl<sub>8</sub> (**2b**), CoTPP(NO<sub>2</sub>)Cl<sub>7</sub>(CH<sub>3</sub>OH) (**1a**•CH<sub>3</sub>OH), ZnTPP(NO<sub>2</sub>)Cl<sub>7</sub>(CH<sub>3</sub>OH)(**1d**•CH<sub>3</sub>OH), ZnTPP(NO<sub>2</sub>)Cl<sub>7</sub>(Py) (**1d**•Py) and ZnTPPCl<sub>8</sub>(CH<sub>3</sub>OH) (**2d**•CH<sub>3</sub>OH) are listed in Tables A1 and A2 in Appendix-VI. The top ORTEP views and displacement of macrocyclic core from mean plane for ZnTPP(NO<sub>2</sub>)Cl<sub>7</sub>•CH<sub>3</sub>OH (**1d**•CH<sub>3</sub>OH) and ZnTPPCl<sub>8</sub>•CH<sub>3</sub>OH (**2d**•CH<sub>3</sub>OH) are shown in Figure 7.1. The top ORTEP views for MTPP(NO<sub>2</sub>)Cl<sub>7</sub> (M = Co(II) and Zn(II)), H<sub>2</sub>TPPCl<sub>8</sub> (**2**), and NiTPPCl<sub>8</sub> (**1b**) are shown in Figures A1 and A2 in Appendix-VI.

The nonplanarity of the porphyrin macrocycle is induced by the steric repulsion among the peripheral substituents, which enforces the relief of the strain through bond lengths and bond angles. Selected average bond lengths and bond angles of all crystallized porphyrins are listed in Tables A2 and A3 in the Appendix-VI. All the crystallized porphyrins have shown saddle shape conformation of macrocyclic core with very high ΔC<sub>β</sub> (±0.642 to ±1.210) and displacement of 24 atoms core (Δ24 = 0.313 to 0.571 Å) from the mean plane of porphyrin which clearly describing severe nonplanar nature of porphyrins cores. Induced nonplanarity was further supported by the increment in C<sub>β</sub>-C<sub>α</sub>-C<sub>m</sub> angle (~127°-129°) with simultaneous decrement in the N-C<sub>α</sub>-C<sub>m</sub> angle

( $\sim 124^\circ$ ) accompanied with larger  $C_\beta-C_\beta$  bond length ( $\sim 1.345^\circ\text{A}$ ) as compared to reported planar porphyrins.

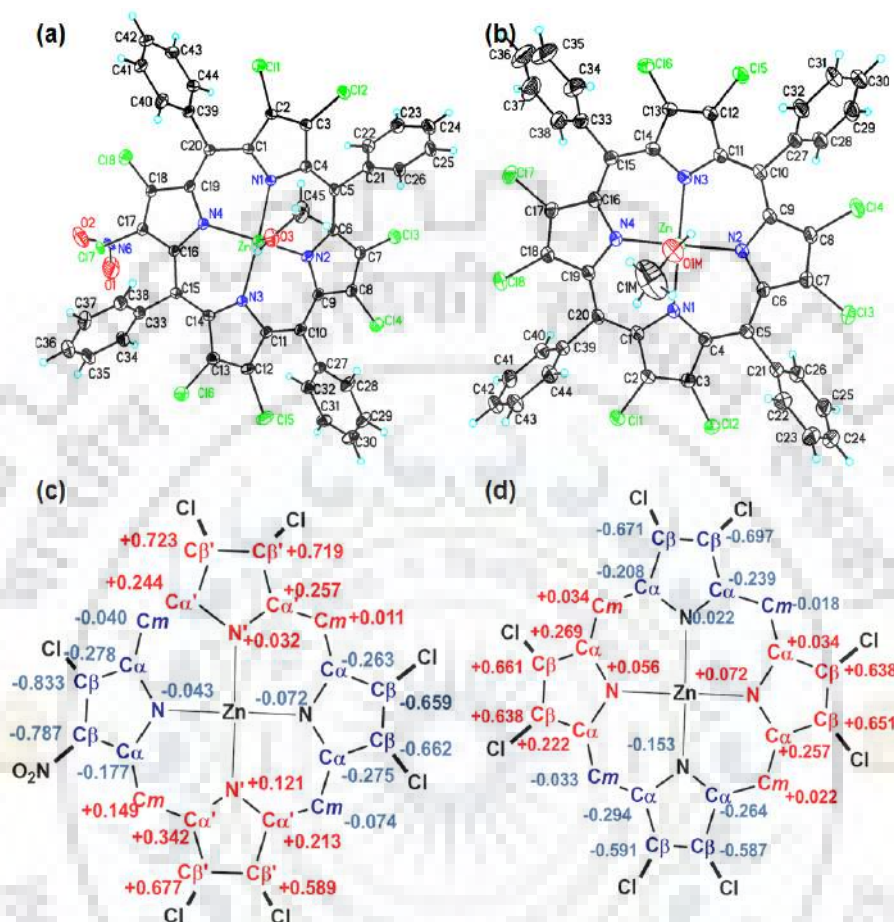


**Figure 7.1** ORTEP Diagrams Showing Top Views of (a) ZnTPP(NO<sub>2</sub>)Cl<sub>7</sub> (**1d**) and; (b) ZnTPP(Cl)<sub>8</sub> (**2d**). (c,d) Displacement of Porphyrin Core Atoms (Å) from the Mean Plane for **1d** and **2d**.

We have observed higher  $\Delta C_\beta$  for **2** than expected due to the strong hydrogen bonding interaction between solvate water molecules and the porphyrin core NH with a distance of 2.831 Å. It is known that **4** has greater extend of nonplanarity (saddle-shape conformation) in comparison to **2** as evidenced by single crystal X-ray structures. The decreased N-M-N values ( $171^\circ$ - $162^\circ$ ) also indicating the saddle shape conformation of the macrocyclic core. The higher  $\Delta C_\beta$  for **1d** as compared to **2d** reflecting the impact of NO<sub>2</sub> group over Cl group. The packing diagram of **1a** is showing that the NO<sub>2</sub> group of one porphyrin unit is interacting with the hydrogen of another

unit (Figure 7.2). Figure A3 in Appendix-VI shows the packing diagram of ZnTPP(NO<sub>2</sub>)Cl<sub>7</sub> (**1d**) and ZnTPPCl<sub>8</sub> (**2d**), respectively. Both the porphyrins have shown two molecules in a unit cell.

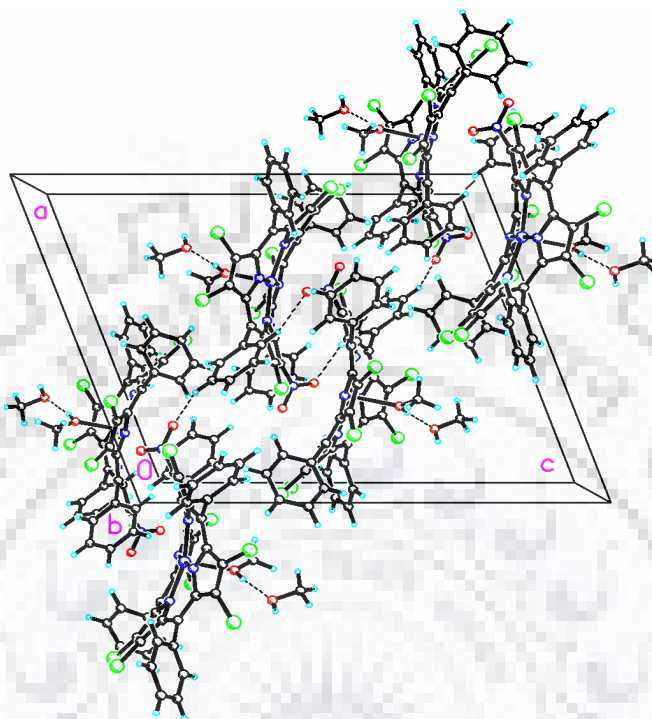


Figure 7.2 Packing Diagram of CoTPP(NO<sub>2</sub>)Cl<sub>7</sub> (**1a**) in a Unit Cell.

### 7.3.3 <sup>1</sup>H NMR and Mass Spectrometric Studies

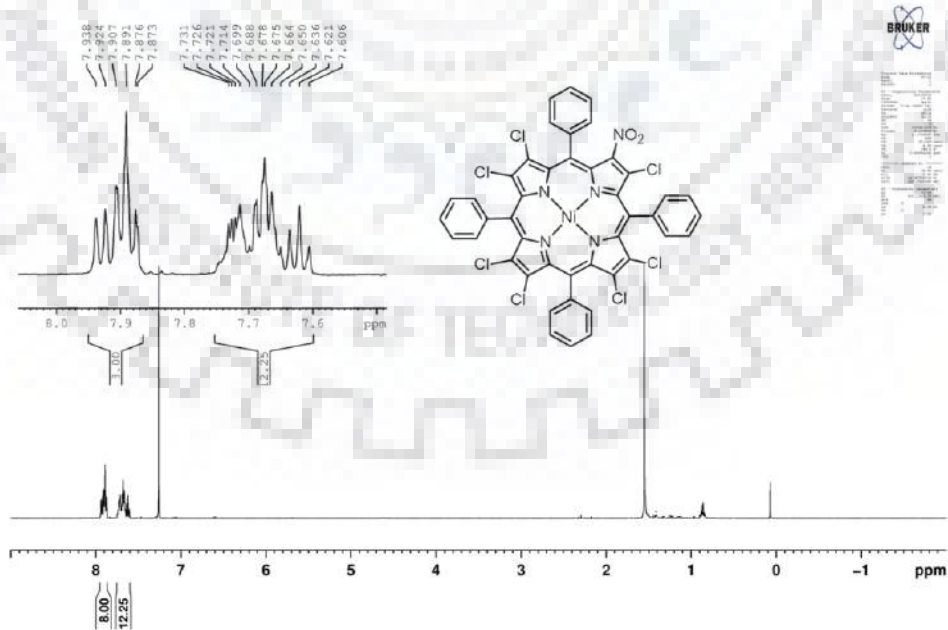
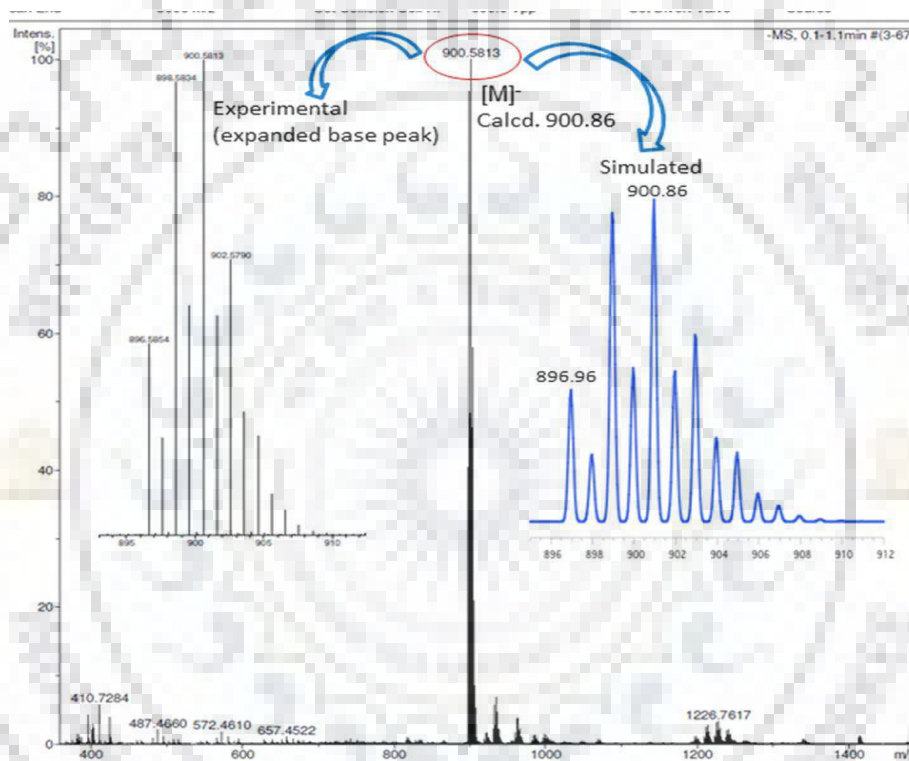


Figure 7.3 <sup>1</sup>H NMR Spectrum of NiTPP(NO<sub>2</sub>)Cl<sub>7</sub> (**2b**) in CDCl<sub>3</sub> at 298 K.



The  $^1\text{H}$  NMR spectra of  $\text{MTPP}(\text{R})\text{Cl}_7$  (Where  $\text{M} = 2\text{H}$ ,  $\text{Ni}(\text{II})$ ,  $\text{Zn}(\text{II})$ , and  $\text{R} = \text{Cl}$ ,  $\text{NO}_2$ ) and **3** and **4** were recorded in  $\text{CDCl}_3$  at 298 K. Figure 7.3 and A5 in Appendix-VI show the  $^1\text{H}$  NMR spectra of  $\text{Ni}(\text{II})$  complexes **1b** and **2b**, respectively. The spectral data for **3**, **4** and  $\text{MTPPCl}_8$  were exactly matching with the reported literature. The integrated intensities of the protons were in accordance with the proposed structures.  $\text{MTPP}(\text{NO}_2)\text{Cl}_7$  have shown an asymmetric multiplet for *ortho*-phenyl protons relative to their corresponding homosubstituted  $\text{MTPPCl}_8$  (Figure A5 in Appendix-VI) which has indicated the reduced symmetry provided by mixed substitution.



**Figure 7.4** Negative Ion Mode ESI Mass Spectrum of  $\text{H}_2\text{TPPNO}_2\text{Cl}_7$  (**1**) in  $\text{CH}_3\text{CN}$ .

Figure A6 in Appendix-VI have shown the  $^1\text{H}$  NMR spectra of imino proton region of **1-4** in  $\text{CDCl}_3$  at 298 K. Interestingly, the downfield shift of  $\text{NH}$  or the acidity of imino-protons of **1-4** has shown the following order: **3** > **4** > **1** > **2** which readily reflects the extend of nonplanarity of the porphyrin core and electron withdrawing effect of nitro substituent.

The negative ion ESI mass spectra of  $\text{MTPP}(\text{NO}_2)\text{Cl}_7$  were recorded in  $\text{CH}_3\text{CN}$  and the observed mass values were fairly matching with the calculated values for proposed structures (Figures 7.4 and A7-A10 in Appendix-VI).



## 7.3.4 Electronic Spectral Studies

To determine the effect of mixed substitution on the electronics of macrocyclic core, we have recorded the UV-Visible absorption spectra of **1-4** in toluene. Figure 7.5a shows the comparative electronic absorption spectra of **1** and **3**. Table 7.1 lists the electronic absorption spectral data of **1-4** in toluene. **1** exhibited similar spectral features to **2** and showed red-shifted absorption in Soret (6 nm) and in  $Q_{x(0,0)}$  band (12 nm) relative to **2** possibly due to the electron withdrawing nature of nitro group and increased nonplanarity by mixed substitution. Interestingly, **3** has shown red-shifted absorption in B (12 nm) and  $Q_{x(0,0)}$  band (17 nm) relative to **1** possibly due to increased nonplanarity produced by larger sized bromo substituents. The B and  $Q_{x(0,0)}$  bands of **1-4** have shown an interesting trend in red-shift and aligned in the following order:  $2 < 1 < 4 < 3$ .

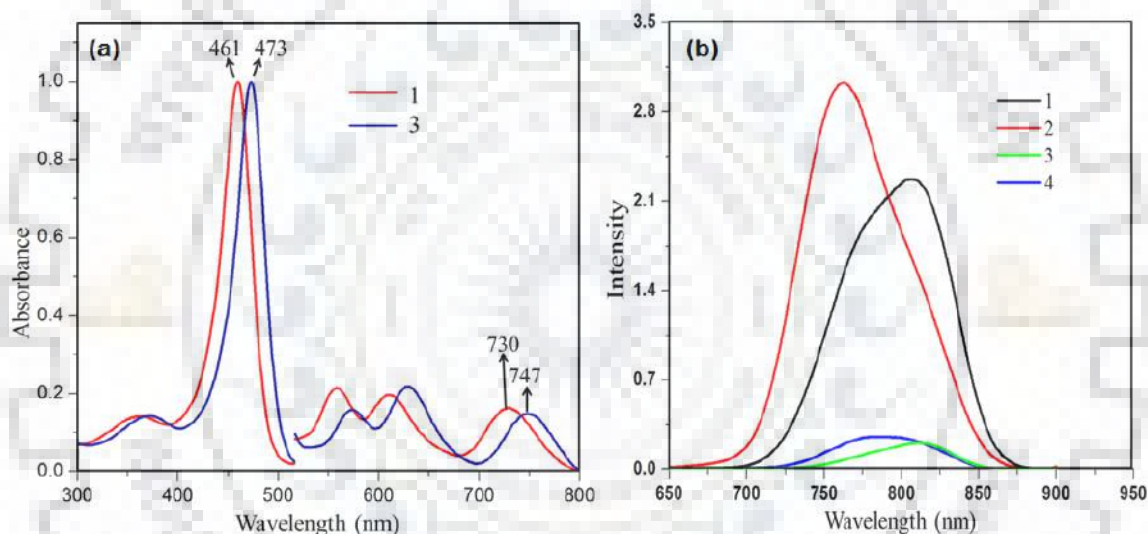


**Figure 7.5** (a) UV-Vis. Absorption Spectra of **1** and **3** and (b) Fluorescence Spectra of **1-4** in Toluene at 298 K.

**Table 7.1** UV-Visible and Fluorescence Spectral Data<sup>a</sup> of **1-4** in Toluene at 298 K.

Porphyrin	B (Bands)	Q (Bands)	$\lambda_{em}$ , nm
H <sub>2</sub> TPP(NO <sub>2</sub> )Cl <sub>7</sub> ( <b>1</b> )	363(26.91), 461(190.5)	559(10.23), 612(9.54), 730(7.58)	809
H <sub>2</sub> TPPCl <sub>8</sub> ( <b>2</b> )	356(24.54), 455(204.1)	552(11.48), 601(11.75), 718(6.17)	762
H <sub>2</sub> TPP(NO <sub>2</sub> )Br <sub>7</sub> ( <b>3</b> )	371(33.85), 473(239.9)	574(9.55), 628(13.49), 747(9.12)	816
H <sub>2</sub> TPPB <sub>8</sub> ( <b>4</b> )	364(31.62), 469(257.0)	570(11.48), 623(16.98), 739(8.70)	789

<sup>a</sup>The values in parentheses refer to  $\epsilon \times 10^{-3} \text{ L mol}^{-1} \text{ cm}^{-1}$

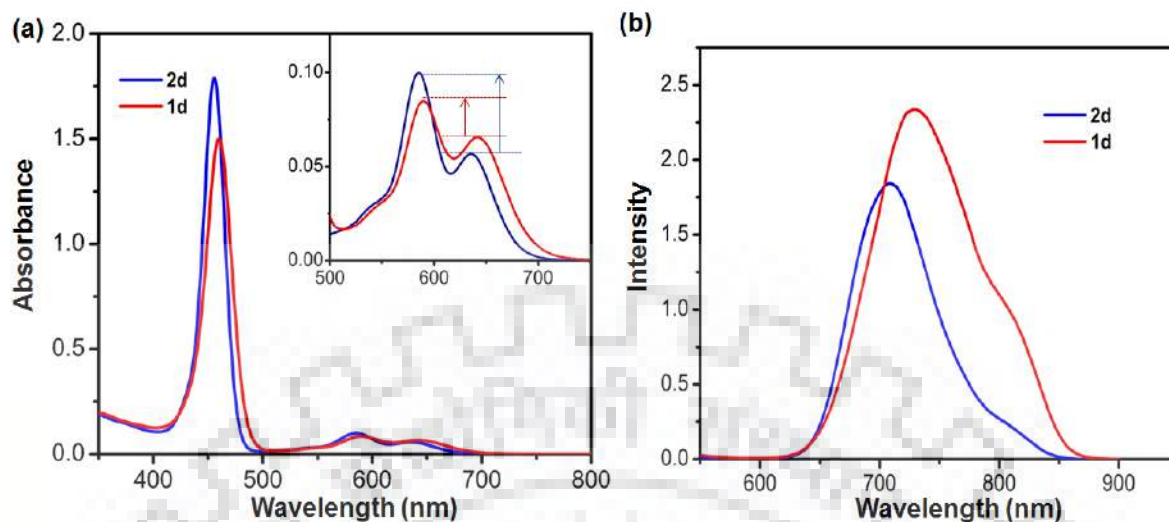


**Figure 7.6** (a) Electronic Absorption Spectra of **1d** and **2d** in  $\text{CH}_2\text{Cl}_2$ , Inset Shows Expanded Region for Q bands. (b) Electronic Emission Spectra of **1d** and **2d** in  $\text{CH}_2\text{Cl}_2$  at 298 K.

**Table 7.2** Optical Absorption and Emission Spectral Data<sup>a</sup> of  $\text{MTPP}(\text{NO}_2)\text{Cl}_7$  and  $\text{MTPPCl}_8$ .

Porphyrin	B (Band)	Q (Bands)	$\lambda_{\text{em}}$ , nm	$\phi_f$
$\text{CoTPP}(\text{NO}_2)\text{Cl}_7$ ( <b>1a</b> )	447(186.2)	562(16.59), 605(9.77)		
$\text{CoTPPCl}_8$ ( <b>2a</b> )	437(147.9)	556(12.30)		
$\text{NiTPP}(\text{NO}_2)\text{Cl}_7$ ( <b>1b</b> )	448(128.8)	562(10.96), 604(6.31)		
$\text{NiTPPCl}_8$ ( <b>2b</b> )	439(190.5)	554(15.13)		
$\text{CuTPP}(\text{NO}_2)\text{Cl}_7$ ( <b>1c</b> )	449(117.5)	576(12.88), 624(6.46)		
$\text{CoTPPCl}_8$ ( <b>2c</b> )	437(158.4)	571(17.78), 610(6.16)		
$\text{ZnTPP}(\text{NO}_2)\text{Cl}_7$ ( <b>1d</b> )	459(158.5)	593(9.12), 647(8.31)	729	0.0009
$\text{CoTPPCl}_8$ ( <b>2d</b> )	455(204.1)	592(10.2), 646(9.55)	708	0.0019

<sup>a</sup>The values in parentheses refer to  $\epsilon \times 10^{-3} \text{L mol}^{-1} \text{cm}^{-1}$

The UV Visible spectra of synthesized metal derivatives were recorded in  $\text{CH}_2\text{Cl}_2$  at 298 K. Table 7.2 lists the electronic spectral data in  $\text{CH}_2\text{Cl}_2$  at 298 K.  $\text{MTPP}(\text{NO}_2)\text{Cl}_7$  also exhibited similar spectral features to  $\text{MTPPCl}_8$  and showed red shift in Soret band (4 - 12 nm) as well as in  $\text{Q}_{x(0,0)}$  band (8-14 nm) relative to  $\text{MTPPCl}_8$  (Figure A11 in Appendix-VI), this attributes to the induced nonplanarity due to more electrostatic repulsion between mixed  $\beta$ -substituents. The comparative optical absorption spectra of **1d** and **2d** complexes are shown in Figure 7.6.

HOMOs of normal porphyrins are usually situated at the  $\beta$ -pyrrolic positions and substitution at these positions with electron withdrawing substituents will further lift the degeneracy of  $a_{1u}$  and  $a_{2u}$  orbitals by stabilization of  $a_{1u}$  relative to  $a_{2u}$  which resulted into the depletion of intensity gap ratio between  $Q_{x(0,0)}$  and  $Q_{x(1,0)}$  for **1d** as compared to **2d** as shown in inset of Figure 7.6a. Figure 7.6b represents the comparative emission spectra of **1d** and **2d** complexes in  $\text{CH}_2\text{Cl}_2$  at 298 K. Due to heavy atom effect, these perchlorinated-2-nitrotetraphenyl porphyrins also exhibited very feeble emission intensity with very low quantum yields like bromo derivatives [30]. Porphyrin **1d** has shown relatively more intense and red shifted emission spectra relative to **2d**.

### 7.3.5 Electrochemical Studies

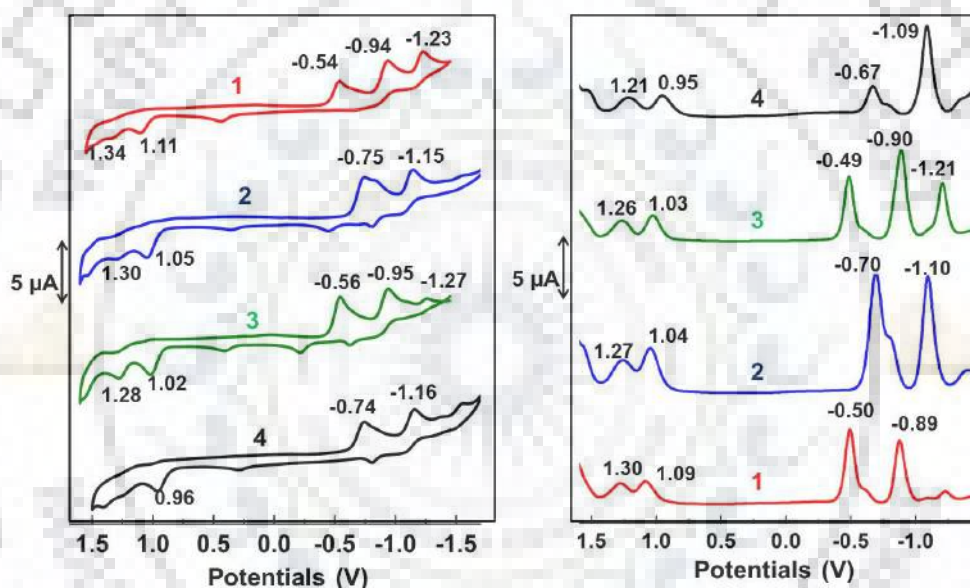


**Figure 7.7** CVs and DPVs of **1-4** in  $\text{CH}_2\text{Cl}_2$  Containing 0.1 M  $\text{TBAPF}_6$  at 298 K.

A wide variety of perhaloporphyrins have been examined in non-aqueous media [31]. To analyse the influence of mixed substitution on the redox potentials of porphyrin core, the electrochemical redox properties of all synthesized porphyrins were examined by cyclic voltammetric studies in distilled  $\text{CH}_2\text{Cl}_2$  at 298 K under argon using 0.1M  $\text{TBAPF}_6$  as the supporting electrolyte. Cyclic voltammograms and DPVs of **1-4** in  $\text{CH}_2\text{Cl}_2$  containing  $\text{TBAPF}_6$  as supporting electrolyte are shown in Figure 7.7 and the redox data is listed in Table 7.3. Interestingly, the mixed substituted porphyrins (**1** and **3**) exhibited  $\sim 200$  mV anodic shift in the reduction potentials as compared to homo substituted porphyrins (**2** and **4**) whereas in oxidation potentials only 60 mV anodic shift was observed. This can be attributed to the strong electron withdrawing nature of the nitro

substituent. Notably, the bromoporphyrins (**3** and **4**) exhibited 90 mV cathodic shift in the oxidation potentials relative to their corresponding chloroporphyrins (**1** and **2**) is ascribed to enhanced nonplanarity provided by bulkier bromo groups.

**Table 7.3** Electrochemical Redox Data<sup>a</sup> of Synthesised Porphyrins in CH<sub>2</sub>Cl<sub>2</sub> at 298 K.

Porphyrins	Oxidation				Reduction			$\Delta E$
	I	II	M(II/III)	M(II/I)	I	II	III	
H <sub>2</sub> TPP(NO <sub>2</sub> )Cl <sub>7</sub> ( <b>1</b> )	1.11	1.34			-0.54	-0.94	-1.23	1.65
H <sub>2</sub> TPPCl <sub>8</sub> ( <b>2</b> )	1.05	1.30			-0.75	-1.15		1.80
H <sub>2</sub> TPP(NO <sub>2</sub> )Br <sub>7</sub> ( <b>3</b> )	1.02	1.28			-0.56	-0.95	-1.27	1.58
H <sub>2</sub> TPPBr <sub>8</sub> ( <b>4</b> )	0.96	1.21 <sup>d</sup>			-0.74	-1.16		1.70
CoTPP(NO <sub>2</sub> )Cl <sub>7</sub> ( <b>1a</b> )	1.34	1.51	1.00	-0.27	-1.12	-1.60 <sup>d</sup>		2.46
CoTPPCl <sub>8</sub> ( <b>2a</b> )	1.13	1.25	0.91	-0.37	-1.44	-		2.57
NiTPP(NO <sub>2</sub> )Cl <sub>7</sub> ( <b>1b</b> )	1.27	-	-	-	-0.64	-0.89		1.91
NiTPPCl <sub>8</sub> ( <b>2b</b> )	1.22	-	-	-	-0.85	-1.16		2.07
CuTPP(NO <sub>2</sub> )Cl <sub>7</sub> ( <b>1c</b> )	1.13	1.63	-	-	-0.66	-0.89		1.79
CuTPPCl <sub>8</sub> ( <b>2c</b> )	1.04	-	-	-	-0.85	-1.11		1.89
ZnTPP(NO <sub>2</sub> )Cl <sub>7</sub> ( <b>1d</b> )	0.99	1.23	-	-	-0.92	-1.18		1.91
ZnTPPCl <sub>8</sub> ( <b>2d</b> ) <sup>c</sup>	0.98	1.22	-	-	-1.12	-1.47 <sup>d</sup>		2.10

<sup>a</sup> In V, vs Ag/AgCl electrode, <sup>d</sup>data obtained from differential pulse voltammetry, <sup>c</sup> in 5% THF in CH<sub>2</sub>Cl<sub>2</sub>

Comparative cyclic voltammograms of **1a-1c** and **2a-2c** are shown in Figure A12 in Appendix-VI. The observed behaviors of metal complexes of **1** are quite similar to **2** containing two reversible reduction and one to three reversible oxidations but there is a remarkable shift in redox potentials. Table 7.3 lists the electrochemical redox data of metal complexes of MTPP(NO<sub>2</sub>)Cl<sub>7</sub> and MTPPCl<sub>8</sub> in CH<sub>2</sub>Cl<sub>2</sub>. The  $\beta$ -nitro substituted porphyrins are easier to reduce and harder to oxidize as compared to homosubstituted porphyrins. Interestingly, nitro bearing porphyrins exhibited a significant anodic shift (190-325 mV) in the first ring reduction potentials as compared to homosubstituted porphyrins (MTPPCl<sub>8</sub>), whereas a minimal anodic shift (12-86 mV) was observed in the oxidation potentials which ascribed to the impact of strong electron

withdrawing nature of nitro group on the porphyrin  $\pi$ -system. MTPP(NO<sub>2</sub>)Cl<sub>7</sub> have shown the reduced HOMO-LUMO gap as compared to MTPP(Cl)<sub>8</sub> (Table 7.3).

### 7.3.6 Protonation and Deprotonation Studies of 1-4

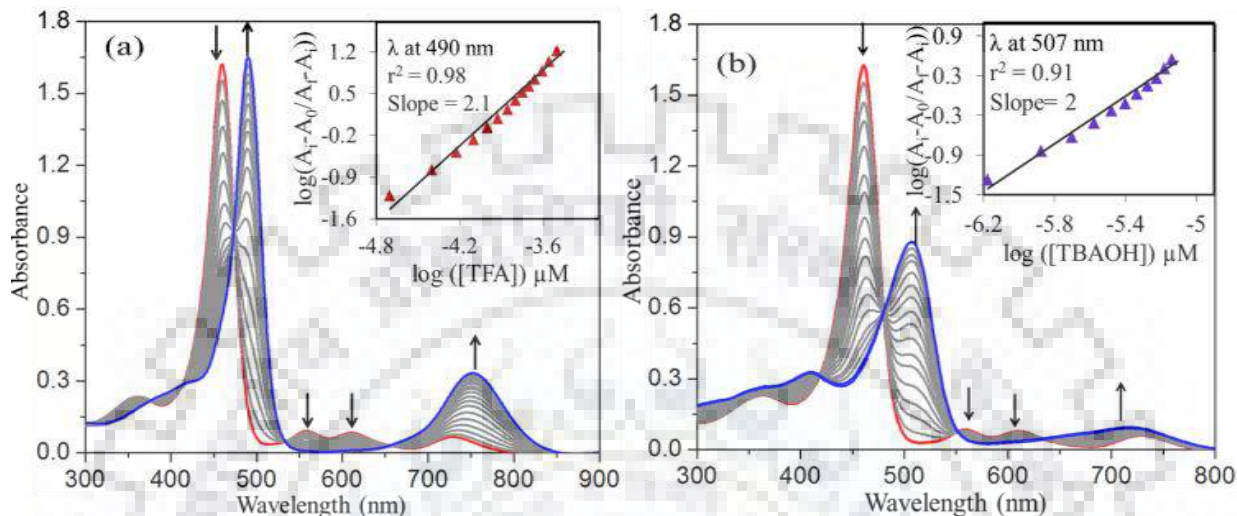


**Figure 7.8** UV-Visible Spectral Titrations of **1** with TFA (a) and TBAOH (b) in Toluene at 298 K. Insets Show the Corresponding Hill Plots.

**Table 7.4** Protonation and Deprotonation Constants ( $\beta_2$  and  $\log \beta_2$ )<sup>a</sup> of **1-4** in Toluene.

Porphyrins	Protonation			Deprotonation		
	$\log \beta_2$	$\beta_2$	$n^b$	$\log \beta_2$	$\beta_2$	$n^b$
H <sub>2</sub> TPP(NO <sub>2</sub> )Cl <sub>7</sub> ( <b>1</b> )	8.51	$3.30 \times 10^8$	2.1	10.77	$5.91 \times 10^{10}$	2.0
H <sub>2</sub> TPP(Cl) <sub>8</sub> ( <b>2</b> )	9.21	$1.90 \times 10^9$	2.0	10.21	$1.65 \times 10^{10}$	1.9
H <sub>2</sub> TPP(NO <sub>2</sub> )Br <sub>7</sub> ( <b>3</b> )	9.70	$5.07 \times 10^9$	2.1	11.60	$4.06 \times 10^{11}$	2.1
H <sub>2</sub> TPPBr <sub>8</sub> ( <b>4</b> )	10.53	$3.43 \times 10^{10}$	2.1	10.40	$2.53 \times 10^{10}$	2.0

<sup>a</sup>Within the error of  $\pm 0.07$  for  $\log \beta_2$  and  $\pm 10\%$  for  $\beta_2$ ; <sup>b</sup> $n$  refers stoichiometry

To examine the effect of mixed substitution on nonplanarity, we have carried out protonation and deprotonation studies of **1-4** in toluene using trifluoroacetic acid (TFA) and tetrabutylammonium hydroxide (TBAOH), respectively. Figure 7.8 shows the UV-Visible spectral changes of **1** while increasing the conc. of TFA (20 - 60  $\mu$ M) and TBAOH (0.07 - 11  $\mu$ M), respectively. The protonation and deprotonation constants of **1-4** are calculated using Hill equation [26] (Table



7.4). Figure 7.8a represents the concomitant decrement in absorbance of **1** at 461 nm and rising of a new band at 490 nm upon increasing [TFA]. As protonation proceeded, the multiple Q bands disappeared with the rising of single broad band at 752 nm accompanied with the red-shift of 22 nm in  $Q_{x(0,0)}$  band. In all cases, we have obtained diprotonated porphyrin species which is further confirmed by Hill plot having the slope value of  $\sim 2$  as shown in figures 7.8a inset and A13 in Appendix-VI. **4** has shown highest protonation constant ( $\log\beta_2$ ) as compared to all other porphyrins. **3** and **4** have shown 15-18 times higher  $\log\beta_2$  values as compared to **1** and **2**. The protonation constants of **1-4** have shown the following order:  $\mathbf{4} > \mathbf{3} > \mathbf{2} > \mathbf{1}$  which reveals the extent of basicity of inner core nitrogens.

The deprotonation of free base porphyrin is influenced by the electronic nature of the substituents, the extent of nonplanarity of the porphyrin core and the basicity of the base employed. Figure 7.8b shows the concomitant decrement in the absorbance of **1** at 461 nm while increasing [TBAOH] and the new band rises at 507 nm. During deprotonation, a new band has grown at 721 nm with the disappearance of multiple Q bands of **1**. The insets of Figures 7.8b and A14 in Appendix-VI show the Hill plot with the slope value of 2 indicating the formation of dianionic species in all cases. **3** have shown highest deprotonation constant ( $\log\beta_2 = 11.6$ ) which was 7 folds greater than **1** and ascribed to the increased nonplanarity of the porphyrin macrocycle. The  $\log\beta_2$  values of **1-4** have shown the following order:  $\mathbf{3} > \mathbf{4} > \mathbf{1} > \mathbf{2}$  which suggests that porphyrins bearing mixed substitution with bulky bromo groups favour the high degree of deprotonation.

### 7.3.7 Detection of Basic Anions by **1-4** through Anion Induced Deprotonation

The anion recognition properties of **1-4** were studied in toluene with different anions such as  $\text{CN}^-$ ,  $\text{F}^-$ ,  $\text{Cl}^-$ ,  $\text{Br}^-$ ,  $\text{I}^-$ ,  $\text{NO}_3^-$ ,  $\text{HSO}_4^-$ ,  $\text{PF}_6^-$ ,  $\text{ClO}_4^-$ ,  $\text{BF}_4^-$ ,  $\text{CH}_3\text{COO}^-$  and  $\text{H}_2\text{PO}_4^-$  ions using UV-Visible spectroscopy with the addition of the aliquot anion in the form of TBA salt. Among all,  $\text{CN}^-$ ,  $\text{F}^-$ ,  $\text{CH}_3\text{COO}^-$  and  $\text{H}_2\text{PO}_4^-$  were selectively interacts with **1-4** and showing considerable red-shift (43-48 nm) in the UV- Visible spectra as shown in Figures 7.9b and A15 in Appendix-VI whereas there were no shifts observed for other tested anions. Interestingly, the green colour solution of **1** was turned to dark pink upon addition of aliquots of  $\text{CN}^-$ ,  $\text{F}^-$ ,  $\text{OAc}^-$  and  $\text{H}_2\text{PO}_4^-$  solution which enabled the naked eye detection of these anions in solution (Figure 7.9a). The UV-Visible spectra obtained for **1** with  $\text{CN}^-$ ,  $\text{F}^-$ ,  $\text{OAc}^-$  and  $\text{H}_2\text{PO}_4^-$  resemble the optical absorption spectrum



of  $\mathbf{1}^{2-}$  obtained by the addition of TBAOH indicating the possibility of dianion formation during the addition of anions (Table A4 in Appendix-VI).

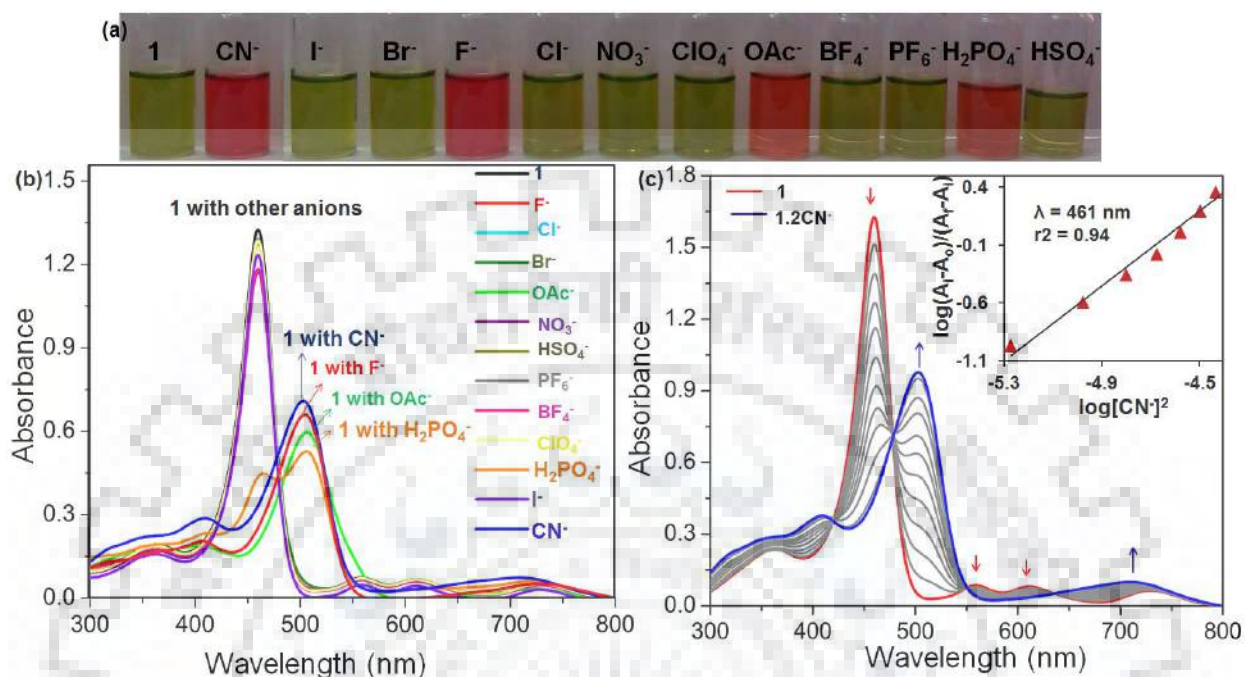


**Figure 7.9** (a) Colorimetric Response of **1** with Tested Anions; (b) Optical Absorption Spectra of **1** with Tested Anions and; (c) UV-Visible Spectral Titration of **1** with  $\text{CN}^-$  Ions in Toluene.

The UV-Visible spectrophotometric titration of **1** with  $\text{CN}^-$  ions is shown in Figure 7.9b. As we increased the concentration of  $\text{CN}^-$  ions, the decrement in the absorbance of **1** was observed at 461 nm, 559 nm and 612 nm and at the same time concomitant increment at 503 and 711 nm with multiple isosbestic points was observed. The Hill plot (Figure 7.9b inset) shows a straight line between  $\log[\text{CN}^-]$  and  $\log(A_1 - A_0/A_f - A_1)$  having slope value  $\sim 2$  which indicates 1:2 (porphyrin-to-anion) stoichiometry. Also the similar behaviour was observed for **2-4** with  $\text{CN}^-$  ions as shown in Figure A16 in Appendix-VI. Further, we have performed the UV-Visible spectral titrations for **1-4** with  $\text{F}^-$ ,  $\text{OAc}^-$  and  $\text{H}_2\text{PO}_4^-$  anions and found to have almost similar spectral features with variation in the association constants. Table 7.5 lists the association constants obtained for  $\text{CN}^-$ ,  $\text{F}^-$ ,  $\text{OAc}^-$  and  $\text{H}_2\text{PO}_4^-$  ions with **1-4** in toluene at 298 K. Each of the system studied displays higher  $\beta_2$  values which are  $>10^8 \text{ M}^{-2}$ , establishing that these porphyrins (**1-4**) are capable of strongly interacting with 2 eq. of  $\text{CN}^-$ ,  $\text{F}^-$ ,  $\text{OAc}^-$  and  $\text{H}_2\text{PO}_4^-$  ions. Interestingly, **1-4** exhibited much higher association constants ( $\log\beta_2$  values ranges from 8.7 to

11.4) with anions such as  $\text{CN}^-$ ,  $\text{F}^-$ ,  $\text{OAc}^-$  and  $\text{H}_2\text{PO}_4^-$  ions as compared to other porphyrins known in the literature [21-24].

**Table 7.5** Association Constants<sup>a</sup> of **1-4** with Various Anions in Toluene.

Porphyrin	$\text{CN}^-$		$\text{F}^-$		$\text{OAc}^-$		$\text{H}_2\text{PO}_4^-$	
	$\log\beta_2$	$n^b$	$\log\beta_2$	$n^b$	$\log\beta_2$	$n^b$	$\log\beta_2$	$n^b$
$\text{H}_2\text{TPP}(\text{NO}_2)\text{Cl}_7$ ( <b>1</b> )	10.57	2.2	10.53	2.7	9.59	2	9.39	2
$\text{H}_2\text{TPP}\text{Cl}_8$ ( <b>2</b> )	9.56	2.0	9.33	2.3	8.77	2	8.68	2
$\text{H}_2\text{TPP}(\text{NO}_2)\text{Br}_7$ ( <b>3</b> )	11.36	2.4	11.12	2.8	10.21	2	9.86	2
$\text{H}_2\text{TPP}\text{Br}_8$ ( <b>4</b> )	10.23	2.1	8.76	2.3	8.95	2	8.72	2

<sup>a</sup>Within the error of  $\pm 0.06$ ; <sup>b</sup> $n$  refers to stoichiometry.

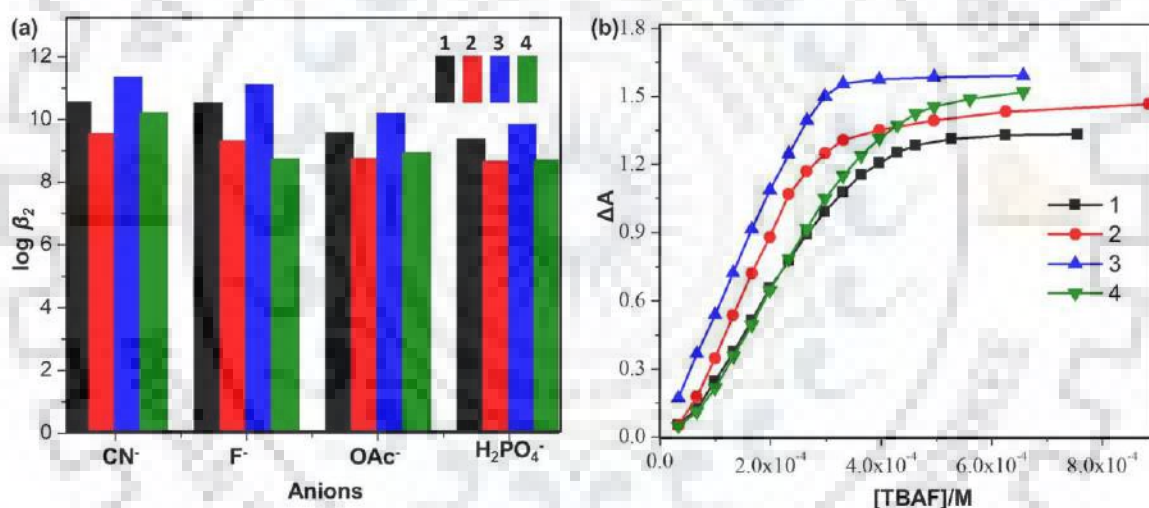


**Figure 7.10** (a) Bar graph constructed  $\log \beta_2$  vs. [Anions] for **1-4** in Toluene at 298 K. (b) Sigmoidal Curve for **1-4**,  $\Delta A$  vs. [TBAF] Indicating Positive Cooperative Behavior.

Notably, the  $\beta_2$  values for **1** and **3** were  $\sim 220$  times higher than **2** and **4** for  $\text{F}^-$  ions which ascribed to strong electron withdrawing nature of nitro substituent and the effect of mixed substitution. With  $\text{CN}^-$  ions, **3** and **4** showed two-to-six fold higher  $\beta_2$  values as compared to **1** and **2**. This is ascribed to enhanced nonplanarity of the macrocycle due to bulkier bromo groups relative to their chloro substituents. The general trend in  $\beta_2$  values for free base porphyrins with anions is found to be  $3 > 1 > 4 > 2$  (Table 7.5). Among the anions, the general trend in  $\beta_2$  values was found to be  $\text{CN}^- > \text{F}^- > \text{OAc}^- > \text{H}_2\text{PO}_4^-$  which was slightly different from the expected trend

( $\text{CN}^- > \text{OAc}^- > \text{F}^- > \text{H}_2\text{PO}_4^-$ ) according to their  $\text{pK}_a$  values. The higher  $\log \beta_2$  values of  $\text{F}^-$  ions are possibly due to smaller ionic size (1.3 Å) and high electronegativity (4.1) of  $\text{F}^-$  ions.

**Table 7.6** The Detection Limits (LOD) and Quantification Limits (LOQ) of Anions by **1-4** in Toluene at 298 K.

Por.	$\text{CN}^-$		$\text{F}^-$		$\text{CH}_3\text{COO}^-$		$\text{H}_2\text{PO}_4^-$	
	LOD	LOQ	LOD	LOQ	LOD	LOQ	LOD	LOQ
	nM (ppb)	nM (ppb)	nM (ppb)	nM (ppb)	nM (ppb)	nM (ppb)	nM (ppb)	nM (ppb)
<b>1</b>	7.3(0.19)	22.3(0.87)	6.0(0.11)	18.2(0.34)	8.2(0.48)	24.7(1.45)	7.7(0.75)	23.4(2.26)
<b>2</b>	9.5(0.24)	28.7(0.75)	8.4(0.16)	25.4(0.48)	9.7(0.57)	29.4(1.73)	9.6(0.93)	29.2(2.83)
<b>3</b>	8.6(0.22)	26.1(0.68)	7.4(0.14)	22.3(0.42)	10.0(0.59)	30.3(1.78)	10.3(1.00)	31.3(3.04)
<b>4</b>	8.3(0.21)	25.3(0.66)	8.4(0.16)	25.3(0.48)	8.7(0.51)	26.2(1.55)	8.6(0.83)	26.0(2.52)

nM and ppb represent nanomolar and parts per billion respectively

The detection limit (LOD) and quantification limit (LOQ) for  $\text{CN}^-$ ,  $\text{F}^-$ ,  $\text{OAc}^-$  and  $\text{H}_2\text{PO}_4^-$  ions were calculated in presence of **1-4** in toluene and summarized in Table 7.6. In all cases, the observed LOD (6 - 10 nM) and LOQ (18 - 31 nM) were found to be extremely low which were in nanomolar scale. Hence, these porphyrins **1-4** were highly sensitive for basic anions such as  $\text{CN}^-$ ,  $\text{F}^-$ ,  $\text{OAc}^-$  and  $\text{H}_2\text{PO}_4^-$  ions. **1-4** have shown positive cooperative binding as evidenced from the plot (Figures 7.10b and A17 in Appendix-VI) which indicates the interaction of first anion with  $\text{N}_4$  core distorts the macrocycle ring intern that favours second anion binding. The anions detection was further supported by the fluorescence quenching of **1-4** with increasing  $[\text{F}^-]$  in toluene (Figure A18 in Appendix-VI). We have carried out the  $^1\text{H}$  NMR studies of **1-4** in presence of  $\text{F}^-$  ions and observed the disappearance of NH peak while increasing  $[\text{F}^-]$  which further confirmed the formation of dianionic species.

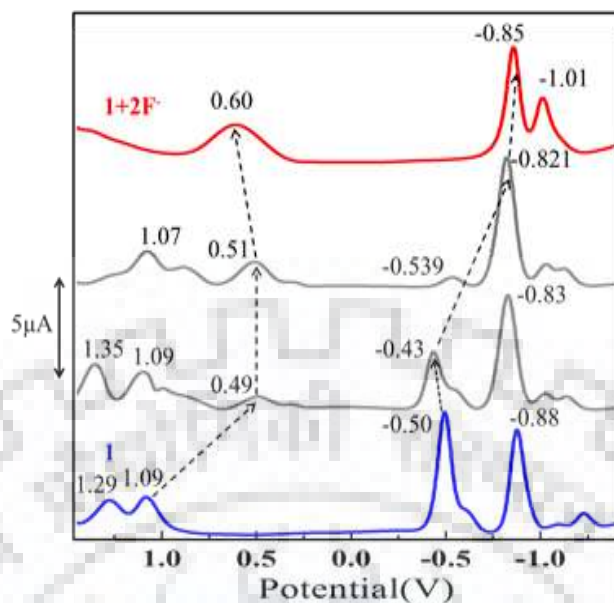
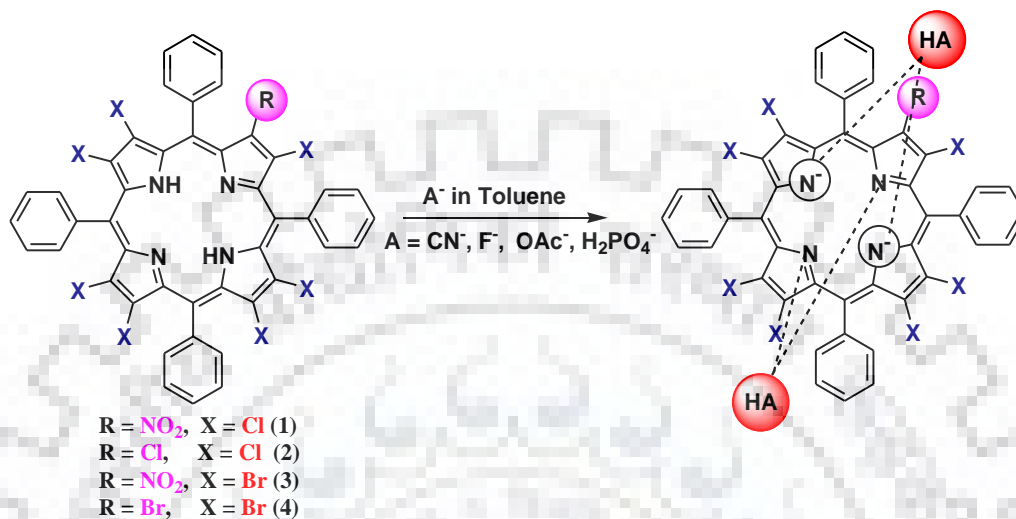


**Figure 7.11** DPV Traces of **1** While Increasing Concentration of  $F^-$  Ion in  $CH_2Cl_2$  Containing 0.1 M TBAPF<sub>6</sub> at 298 K.

To probe further, we have carried out the differential pulse voltammetric (DPV) studies of **1-4** with excess addition of fluoride ions as shown in Figures 7.11 and A19 in Appendix-VI. The observed cathodic shift in oxidation (450 - 530 mV) and in reduction (230 - 360 mV) potentials after addition of aliquots of  $F^-$  also supports the formation of dianionic species [31] whereas the opposite trend (anodic shift) was observed for the protonation of free base dodecaphenylporphyrins [32]. The cation radicals of **1-4** formed after electrochemical oxidation are unstable and undergo disproportionation hence the peak currents for the anodic and cathodic processes are different. Also, we have carried out UV-vis. spectral titrations for some planar porphyrins ( $H_2TPP$  and  $H_2TPP(Ph)_4$ ) and nonplanar porphyrins ( $H_2TPPBr_4$  and  $H_2TPP(Ph)_8$ ) with  $F^-$  ions (Figure A20 in Appendix-VI) and found no spectral changes were observed even at high conc. of anions which clearly suggested the highly nonplanar conformation with electron withdrawing substituents is necessary for anion recognition.

It is known that the perhaloporphyrins, **2** and **4** hydrogen bonds with various polar solvents including Lewis bases and forms 1:1 host-guest complex with very low binding constants ( $0.2 - 16 M^{-1}$ ). In general, **1-4** with anions didn't display 1:1 host-guest complexation neither in the UV-Visible spectral features (Figure A21, Appendix-VI) nor in binding constant values (very high  $\log \beta_2$  values ranges from 8.7 to 11.4) except **3** which interacted with  $Cl^-$  ions through

hydrogen bonding (Figure A21, Appendix-VI) with very low binding constant ( $\log\beta_2 = 3.82$ ) in 1:1 stoichiometry. On our experimental evidences, we are representing the plausible mechanism of anion recognition by **1-4** as shown in Scheme 7.2.



**Scheme 7.2** Plausible Mechanism for the Detection of Anions by **1-4**.

Reversibility studies were carried out on these porphyrin-anion host-guest systems to acknowledge the range of their applicability. First, **1**• $2CN^-$  complex was prepared by adding 2 eq. of cyanide ions to the solution of **1** in toluene which led to the colour change from green to pink (Figure 7.12a). Then it was treated with aliquots of 1 mM solution of TFA in toluene. This led to a complete regeneration of **1** which can be visualized by colorimetric change from pink to green accompanied by UV-Visible spectral changes as shown in Figure 7.12b. On this basis, we conclude that the formation and dissociation of **1**• $2CN^-$  is a reversible process. To confirm the regeneration, the resulting mixture was washed with water and dried over anhydrous  $Na_2SO_4$ . Then the recovered **1** was treated with 2 eq. of  $CN^-$  ions (Figure S23b, in Appendix-VI) which exhibited similar binding constant as fresh solution of **1** with cyanide ions. The similar results were obtained for the receptors **2-4** with  $CN^-$  ions and TFA solution. Notably, the receptors **1-4** exhibited similar results with other anions such as  $F^-$ ,  $CH_3COO^-$  and  $H_2PO_4^-$  ions. These results clearly demonstrated that the receptors **1-4** can be recoverable and reusable for basic anions detection.



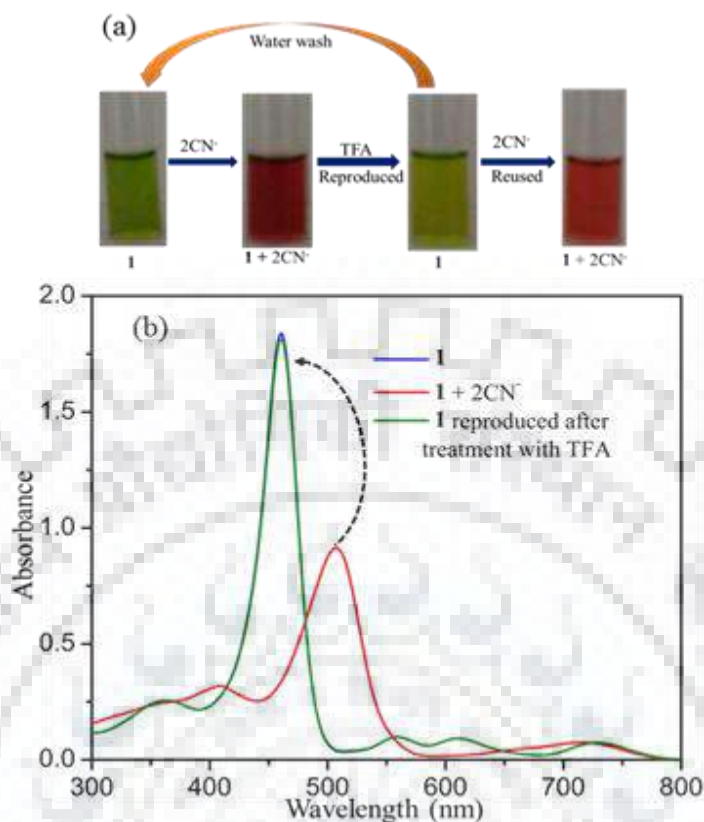


**Figure 7.12** (a) Colorimetric Response of **1** for Reversibility and Reusability Test with  $\text{CN}^-$  (b) Reversibility test: Treatment of The Complex  $1 \cdot 2\text{CN}^-$  with a Solution of TFA.

### 7.3.8 Axial Ligation Studies of Zn(II) Complexes

To demonstrate the effect of basicity of axial ligands and effect of electron withdrawing substituents (chloro, nitro) on the acidity of Zn(II) center of the porphyrin ring, we have examined the axial ligation studies of  $\text{ZnTPP}(\text{NO}_2)\text{Cl}_7$  (**1d**) and  $\text{ZnTPPCl}_8$  (**2d**) with different  $\sigma$ -donor nitrogenous bases (pyridine, N-Methylimidazole, 4-Dimethylaminopyridine and piperidine) and highly basic anions such as  $\text{CN}^-$ ,  $\text{OAc}^-$ ,  $\text{F}^-$  and  $\text{H}_2\text{PO}_4^-$  in the form of their respective tetrabutylammonium salts in toluene at 298 K. Figure 7.13a represents the concomitant decrement in the absorbance of **1d** ( $8.29 \times 10^{-6}$  M) at 460 nm with emergence of a new B-Band at 465 nm accompanied by 5 nm red shift upon sequential addition of pyridine (4-150  $\mu\text{M}$ ). As axial ligation proceed, the decrement in the  $Q_{(1,0)}$  band with 16 nm red shift with simultaneous increment in  $Q_{(0,0)}$  band accompanied with 29 nm red shift was observed. A plot of  $[\text{base}]$  vs  $[\text{base}]/(\Delta A)$  bring forth a straight line which indicating 1:1 complexation of porphyrin:base as shown in inset of Figure 7.13a.



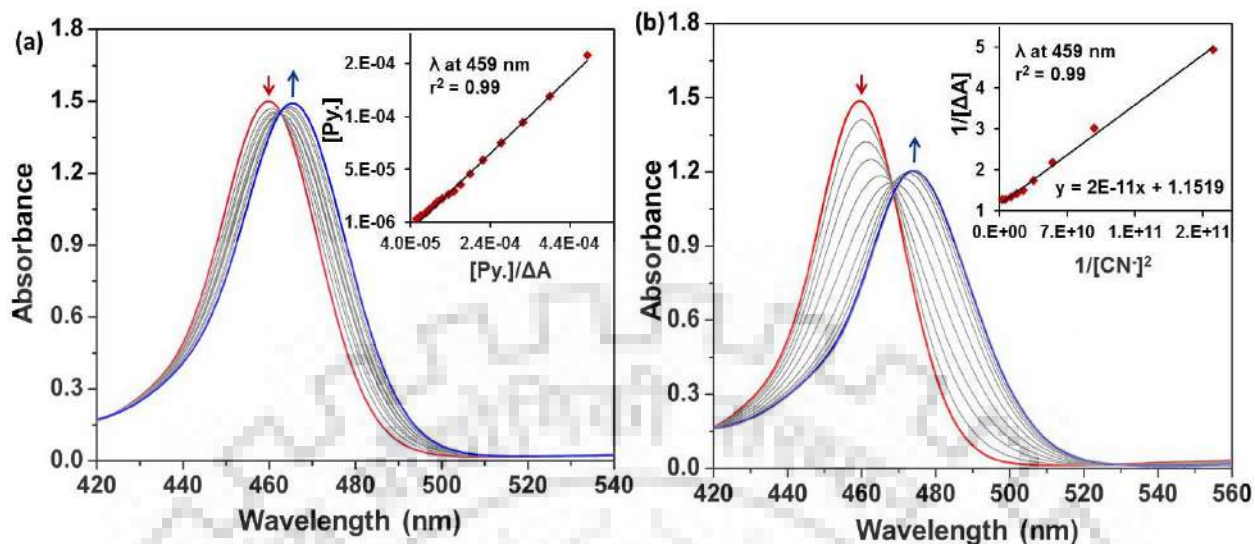


**Figure 7.13** (a) Axial Ligation of Pyridine to **1d** ( $8.29 \times 10^{-6}$  M) in Toluene at 298 K. (b) Axial Ligation of  $\text{CN}^-$  Ion to **1d** ( $8.29 \times 10^{-6}$  M) in Toluene. Main Plots Show the Spectral Changes in Soret Region and Insets Show Plot [Pyridine] vs [Pyridine]/ $\Delta A$ .

The equilibrium constants ( $K_{\text{eq}}$ ) were calculated using following equation:

$$1/K_{\text{eq}} = [\text{base}] / \{ [\text{por.}] L (\epsilon_p - \epsilon^{\text{pa}}) / (A_0 - A_n) - 1 \} \quad \text{Eq.1}$$

Where  $\epsilon_p$  and  $\epsilon_{\text{pa}}$  are molar extinction coefficient for Zn(II) complexes and porphyrin:anion/base complex, respectively.  $A_0$  is the initial absorbance and  $A_n$  is the absorbance in presence of added base or anion at a particular wavelength.  $L$  is the path length of the cell.

Similar UV-Vis spectral changes have been perceived for  $\text{ZnTPPCl}_8$  (**2d**) with pyridine (Figure A24 in Appendix-VI), which also shown 1:1 stoichiometry (porphyrin:pyridine) indicated by slope of regression line. The axial ligation of other bases also performed with **1d** and **2d** and found to be axially ligated with porphyrins in 1:1 stoichiometric ratio. Table 7.7 lists the equilibrium constant data, which clearly reveals that **1d** having higher equilibrium constant values as compared to **2d**, which again attributing to enhanced nonplanarity provided by mixed substitution and increased acidic nature of Zn(II) metal center of porphyrin due to the presence of electron withdrawing  $\text{NO}_2$  group.

**Table 7.7** Equilibrium Constants<sup>a</sup> ( $K_{eq}$ ) for The Ligation of Nitrogenous Bases With Zn(II) Complexes of Perchloroporphyrins in Toluene at 298 K.

Base	1d		2d		pK <sub>a</sub>
	K	B:P	K	P:B	
Piperidine	2076.97	1:1	1710.31	1:1	11.22
4-DMAP	212.12	1:1	163.00	1:1	9.70
N-Methylimidazole	219.68	1:1	159.37	1:1	7.33
Pyridine	57.01	1:1	46.85	1:1	5.23

<sup>a</sup>The  $K_{eq}$  values refers to ( $\times 10^3 K_{eq}/M^{-1}$ ) within the error range of  $\pm 6\%$ , P refers to porphyrin and B refers to base.

To gain insight into the electronic effect of chloro vs. bromo on the ligation properties, we have compared the data obtained for perchlorinated porphyrins with perbrominated porphyrins reported in literature [30]. Data listed in Table 7.7 revealing high binding constant for chloro complexes as compared to bromo derivatives is straightforward indication of higher electron deficient nature of porphyrin. The plot constructed for **1d** and **2d** between  $\log K_{eq}$  and the pK<sub>a</sub> values of utilized bases is shown in Figure 7.14 which displayed a linear relation with  $K_{eq}$ . **1d** showing comparative impartial straight line as compared to ZnTPP(NO<sub>2</sub>)Br<sub>7</sub> with higher correlation coefficient. Among all used bases, the trend in  $K_{eq}$  values was found to be in accordance with their pK<sub>a</sub> values, higher the pK<sub>a</sub> value greater is the equilibrium constant.

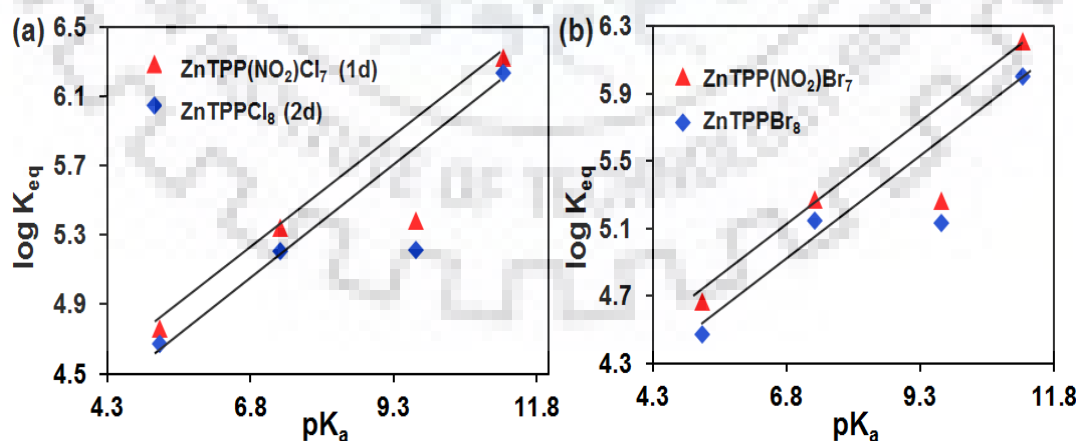


**Figure 7.14** (a) Comparative Plot of  $\log K_{eq}$  vs pK<sub>a</sub> is given for **1d** and **2d**. (b) Comparative Plot of  $\log K_{eq}$  vs pK<sub>a</sub> is given for ZnTPP(NO<sub>2</sub>)Br<sub>7</sub> and ZnTPPBr<sub>8</sub>; (Values are Taken from Ref<sup>30</sup>).

**Table 7.8** The Overall Binding Constants ( $\beta_2$ )<sup>a</sup> for the Ligation of Basic Anions with Zn<sup>(II)</sup> Complexes of Perchloroporphyrins in Toluene at 298 K.

Anions	ZnTPP(NO <sub>2</sub> )Cl <sub>7</sub> ( <b>1d</b> )			ZnTPPCL <sub>8</sub> ( <b>2d</b> )		
	$\beta_2$	log $\beta_2$	P:A	$\beta_2$	log $\beta_2$	A:P
CN <sup>-</sup>	5.75×10 <sup>10</sup>	10.75	1:2	3.53×10 <sup>10</sup>	10.54	2:1
OAc <sup>-</sup>	2.45×10 <sup>10</sup>	10.38	1:2	2.01×10 <sup>10</sup>	10.30	2:1
H <sub>2</sub> PO <sub>4</sub> <sup>-</sup>	2.33×10 <sup>10</sup>	10.36	1:2	1.12×10 <sup>10</sup>	10.04	2:1
F <sup>-</sup>	9.22×10 <sup>8</sup>	8.96	1:2	7.78×10 <sup>8</sup>	8.89	2:1

<sup>a</sup>Within the error range of ±5% for  $\beta_2$ , P refers to porphyrin and A refers to anion.

The effect of electron withdrawing groups on the acidity of Zn<sup>II</sup> core of the porphyrin  $\pi$ -system further proved by performing again axial ligation studies with highly basic anions such as CN<sup>-</sup>, OAc<sup>-</sup>, F<sup>-</sup> and H<sub>2</sub>PO<sub>4</sub><sup>-</sup> in toluene at 298 K. Figure 7.13b represents the changes in Soret Band region upon successive addition of CN<sup>-</sup> (1-18  $\mu$ M) to **1d** in toluene at 298 K. The UV-vis. spectral features of anion binding are almost similar to base binding. After increasing the concentration of cyanide ion to **1d** ( $8.29 \times 10^{-6}$  M), the decrement in absorbance at 459, 589, 644 nm and the concomitant increments in the absorbance at 475 and 690 nm was observed with multiple isosbestic points. Overall binding constants and stoichiometry were analyzed by Benesi-Hildebrand method. **1d** and **2d** both were found to be axially ligated with basic anions in 1:2 (Porphyrin:Anions) stoichiometric ratio (Figure A25 in Appendix-VI). Similar spectral changes were observed during titration of **2d** ( $8.38 \times 10^{-6}$  M) with CN<sup>-</sup>. The standard Benesi-Hildebrand plots were also constructed in 1:1 stoichiometric ratio from the titration data of **1d** and **2d** with cyanide ion as shown in Figure A26 in Appendix-VI. The cyanide binding was not accurately modeled by these plots clearly indicating that the binding of anions with **1d** and **2d** cannot be fit in 1:1 stoichiometric fashion. Other anions were also tested with both Zn(II) complexes and the data for equilibrium constant is listed in Table 7.8. Data revealed that as the basicity of anions increases the equilibrium constant also increases.

## 7.3.9 Selective Cyanide Sensing by Cobalt (II) Complexes

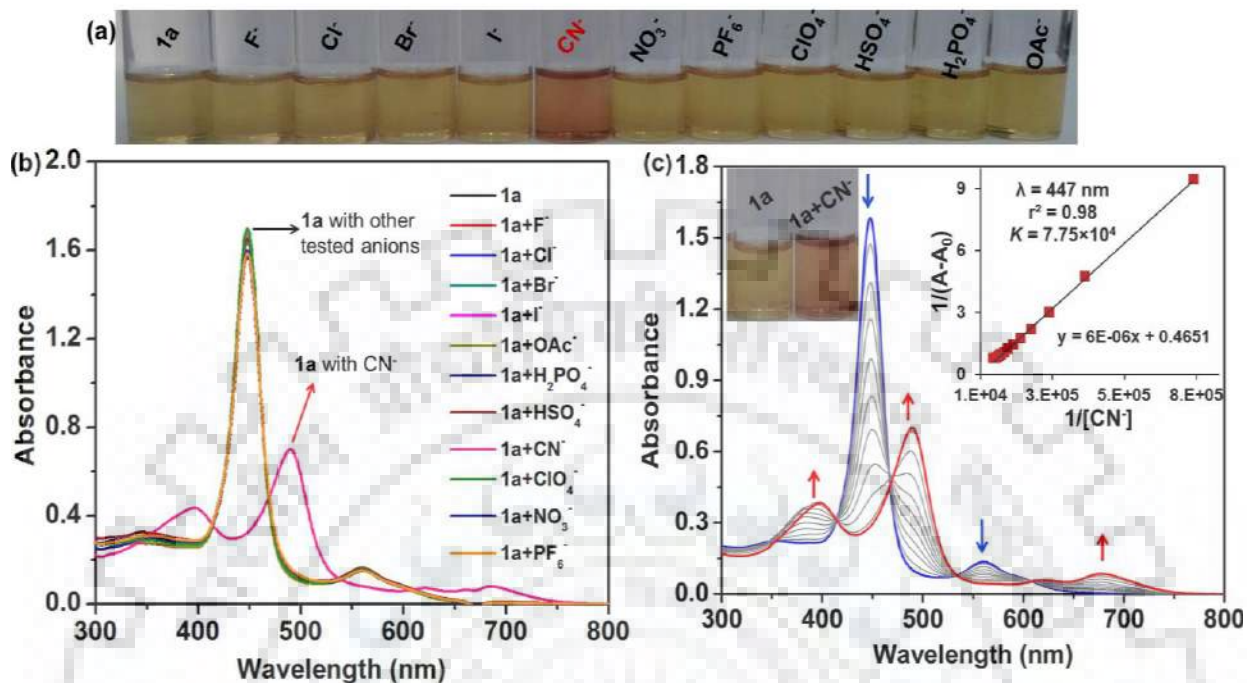


**Figure 7.15** (a) Colorimetric Changes of **1a** with Tested Anions in Toluene. (b) UV-vis. Spectral Changes of **1a** upon Addition of Excess of Anions in Toluene. (c) UV-visible Spectral Changes of **1a** ( $1.04 \times 10^{-5}$  M) upon Sequential Addition of CN<sup>-</sup> ion. Insight Shows a Plot between  $[\text{CN}^-]^2$  and  $[\text{CN}^-]^2/\Delta A$ .

The use of *3d* transition metal complexes of porphyrins for anion sensing is cost effective and environment friendly. The use of Ni(II) complexes of perchloroporphyrins for selective detection of cyanide ions through axial coordination of CN<sup>-</sup> ion are already reported by our research group [33]. The anion recognition properties of Co(II) complexes of these porphyrin were studied in toluene with various anions by UV-Visible spectroscopy with the sequential addition of their TBA salts. Interestingly, their remarkable feature was identified to specially recognize cyanide ion among all used various anions. **1a** and **2a** showed remarkable red shifted absorption spectra with cyanide ion with distinct color change whereas no observable shift was found with other tested anion as shown in Figures 7.15a and A27 in the Appendix-VI.

The UV-Visible spectral titration of **1a** ( $1.04 \times 10^{-5}$  M) with cyanide ion is shown in Figure 7.15b. As we increase the concentration of cyanide ion ( $0.13 \times 10^{-5}$ - $1.58 \times 10^{-5}$  M), the decrement in the absorbance of **1a** was observed at 447 and 561nm with the concomitant

increment at 397, 489 and 682nm with multiple isosbestic points. The same behavior was observed by **2a** ( $1.05 \times 10^{-5}$  M) with sequential addition of  $\text{CN}^-$  ion as shown in Figure S17 in the ESI. Both the Soret (43-45nm) and Q bands (113-120 nm) were red shifted upon addition of aliquots of  $\text{CN}^-$  ions to **1a** and **2a**. The stoichiometry and binding constant were calculated by Benesi-Hildebrand method by plotting a graph between  $1/[\Delta A]$  and  $1/[\text{CN}^-]$  which shows a straight line with  $r^2 = 0.99$ . The representative plot of  $K_{\text{eq}}$  for cyanide ion sensing is shown as insets of Figures 7.15c and A27b in Appendix-VI. The  $K$  values were found to be 4.89 and 4.59 with 1:1 (Porphyrin: Cyanide) stoichiometry for **1a** and **2a**, respectively. The higher binding constant for **1a** is clearly reflecting the highly electron deficient nature of nitro group.

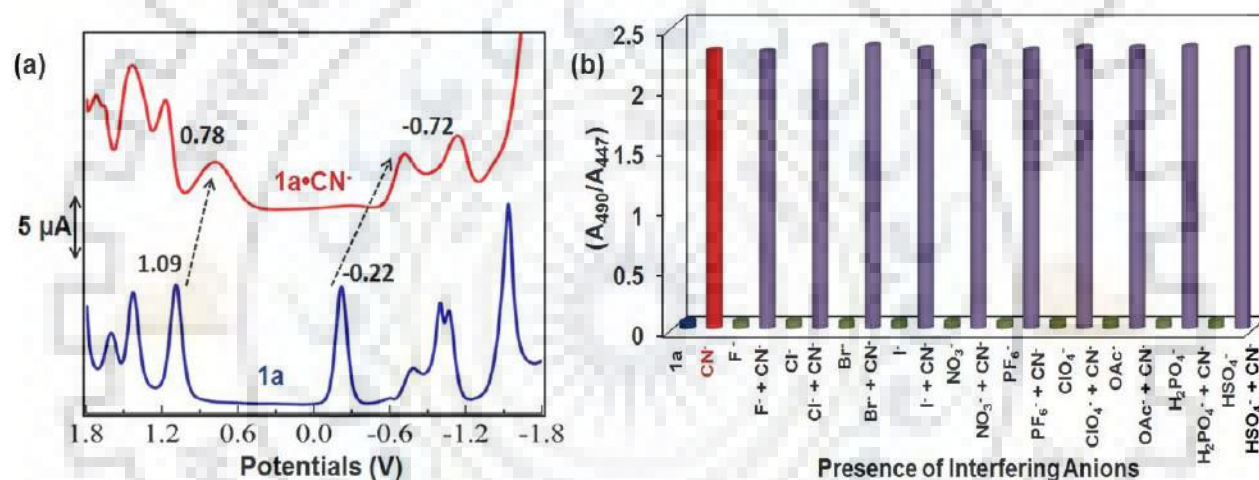


**Figure 7.16** (a) DPV (in V vs Ag/ AgCl) Traces Recorded for **1a** and **1a·2CN<sup>-</sup>** in  $\text{CH}_2\text{Cl}_2$  with a scan rate of  $0.1 \text{ Vs}^{-1}$  at 298 K. (b) Ratiometric Absorbance Changes ( $A_{490}/A_{447}$ ) of **1a** ( $1.04 \times 10^{-5}$  M) on Addition of 1-2 Equiv. of  $\text{CN}^-$  and 10 eq. of Other Anions.

The cyanide detection behavior of these porphyrins (**1a** and **2a**) was also revealed by differential pulse voltammetric (DPV) studies. The DPV changes of **1a** and **2a** upon addition of cyanide ion were carried out in  $\text{CH}_2\text{Cl}_2$  at 298 K using 0.1M TBAPF<sub>6</sub> as supporting electrolytes. Interestingly, the successive addition of cyanide ions into **1a** results in a cathodic shift of 310 mV in the first oxidation potential (Figure 7.16a) and a dramatic cathodic shift of 700 mV in the first reduction potential which may be expected upon going from Co(II) to Co(III) porphyrin or due to upon going neutral species to the charged porphyrin adduct (**1a·CN<sup>-</sup>**). This cathodic shift in the first redox potentials for **2a** is also pronounced (Figure A28a, Appendix-VI).



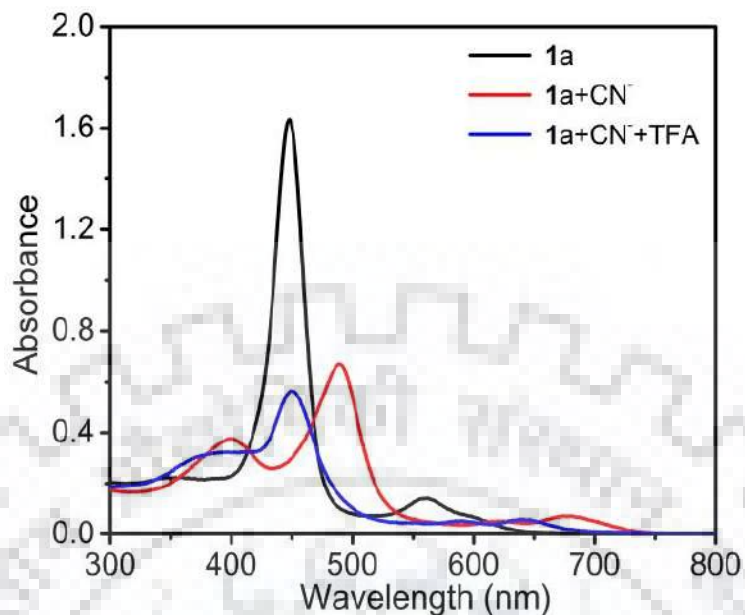
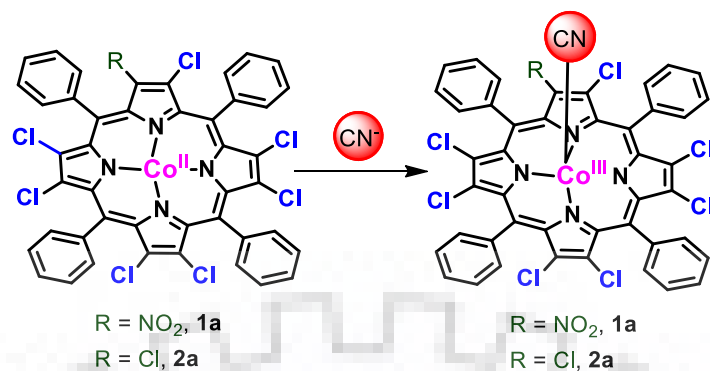


**Figure 7.17** Reversible Studies of **1a** Using 1mM Solution of TFA in Toluene at 298 K.

Interestingly, the most common interfering anions especially basic anions such as fluoride, acetate and dihydrogen phosphate were inactive towards these sensors. The ratiometric experiments were performed to ascertain the selectivity of synthesized Co(II) porphyrins using 10 eq. of interfering anions followed by two eq. of cyanide ions in toluene. The representative bar graph observed for **1a** is shown in Figure 7.16b which clearly demonstrates the tolerance of **1a** towards these potentially interfering anions and thus can be used quantitatively and selectively to detect cyanide ions. Similar results were observed for **2a** as shown in Figure A28b in Appendix-VI.

To recognize the range of applicability of **1a** and **2a** the reversibility test has been performed in toluene. **1a** was treated with 2 eq. of cyanide ion resulted in a red shift of 43 nm in Soret band (447-490 nm) which correspond to Co(II) to Co(III) due to cyanide ion binding (Scheme 7.3). Again the switching of cyanide ion binding was carried out using TFA as shown in Figure 7.17. The addition of TFA to **1a.CN<sup>-</sup>** adduct does not restore the **1a** which clearly indicate that the behavior of cyanide ion binding is irreversible as indicated by the different spectral behavior of **1a.CN<sup>-</sup>** with TFA and without TFA.





**Scheme 7.3** The plausible Mechanism for Cyanide Ion Sensing.

### 7.3.10 DFT Studies

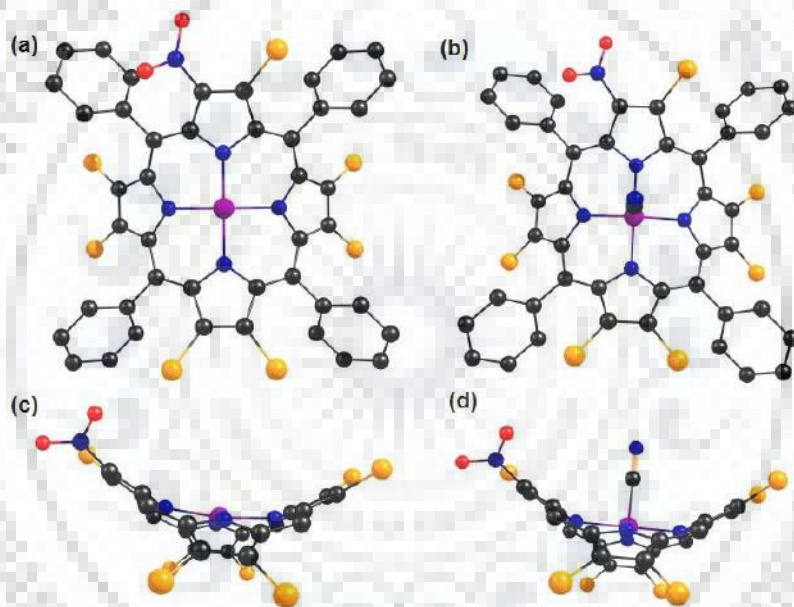


**Figure 7.18** Fully Optimized Geometries of (a and c) Top and Side Views of  $\text{CoTPP}(\text{NO}_2)\text{Cl}_7$  (**1a**), (b and d) Top and Side Views of  $\text{CoTPP}(\text{NO}_2)\text{Cl}_7 \cdot \text{CN}^-$  (**1a·CN<sup>-</sup>**). H Atoms in Top Views and Phenyl Rings in Side Views are Omitted for Clarity.

The geometry optimization of Zn(II) and Co(II) complexes has been performed on Gaussian 09 using B3LYP functional with LANL2DZ basis set in gas phase. To get insight into the electronic modulation of porphyrin core after cyanide binding and their impact onto the molecular orbitals, further we performed the geometry optimization of Co(II) complexes (low spin;  $S = \frac{1}{2}$ ) with cyanide ion i.e. Co(III) complex, as well as TD-DFT has also been evaluated to obtain the electronic spectra. Figure 7.18 shows the fully optimized geometries of  $\text{CoTPP}(\text{NO}_2)\text{Cl}_7$  (**1a**)

and  $\text{CoTPP}(\text{NO}_2)\text{Cl}_7\cdot\text{CN}^-$  (**1a.CN**<sup>-</sup>). The repulsive interaction between  $\beta$ -substituents leads to the saddle shape conformation of the porphyrins core. As expected from Gouterman's four-orbital model the Soret transitions of these metalloperhaloporphyrins were found to involve substantial  $a_{1u}$  to  $e_g$  character. The frontier molecular orbitals of Zn(II) complexes **1d** and **2d** were exactly matching with FMOs for  $\text{ZnBr}_8$  and  $\text{ZnI}_8$  complexes given by Ghosh and coworkers [34]. The HOMO were found as  $b_2$  ( $a_{2u}$  type) and HOMO-1 as  $b_1$  ( $a_{1u}$  type).

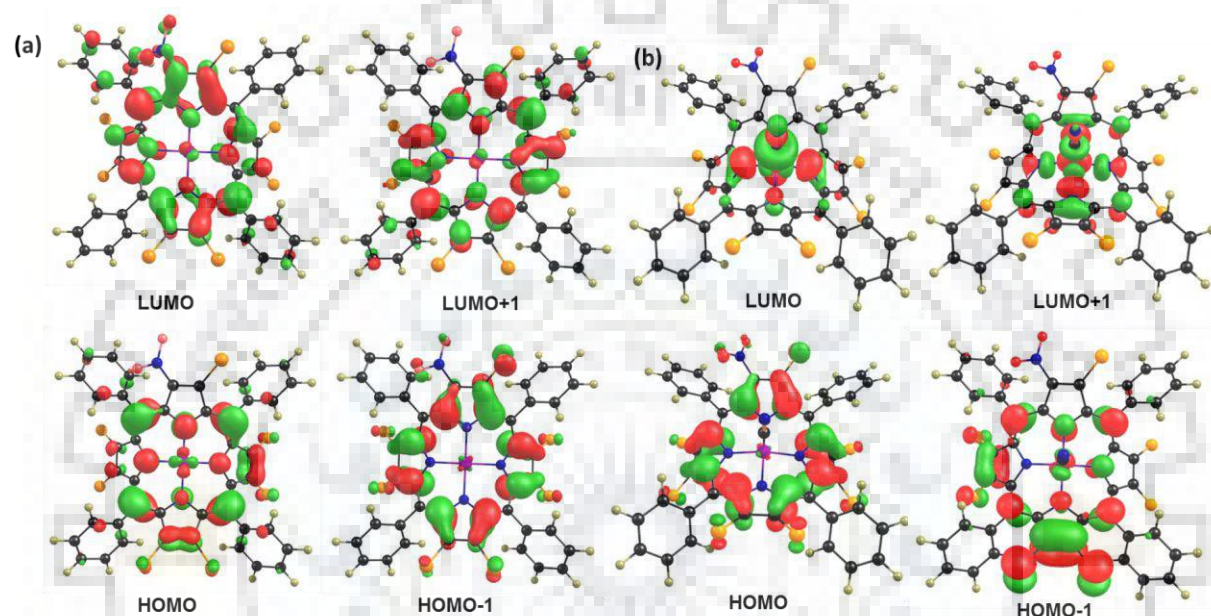


**Figure 7.19** The Pictorial Representation of Frontier Molecular Orbitals of (a)  $\text{CoTPP}(\text{NO}_2)\text{Cl}_7$  (b)  $\text{CoTPP}(\text{NO}_2)\text{Cl}_7$  (**1a.CN**<sup>-</sup>).

In 2002, Scheiner and Liao have explained that for a simple  $\text{CoTPP}$ , the porphyrin MOs ( $a_{2u}$  and  $a_{1u}$ ) lie in between  $^1e_g$  ( $d\pi$ ) and  $^a1_g$  ( $dz^2$ ) of the metal due to the stabilization of MOs of porphyrin by metal (Co) and Porphyrin orbital interaction [35]. However, the introduction of electron withdrawing substituents at porphyrin periphery switches the HOMO from metal  $^1e_g$  to  $a_{2u}$  type. The open shell molecular orbitals and spin density profile of  $\text{CoTPP}(\text{NO}_2)\text{Cl}_7$  is clearly indicating the significant orbital interaction of the metal ( $dx^2-y^2$ ) and porphyrin ( $a_{2u}$ ) (Figure 7.19a). The  $a_{2u}$  type highest occupied molecular orbitals  $b_2$  and SUMO  $b_1$  for electron deficient saddle shaped optimized porphyrins are in good agreement with the reported in literature [33]. The axial coordination of the cyanide ion changed the spin and multiplicity of system which again perturbed the FMOs (Figures 7.19b and A29 in Appendix-VI). Figure A30 in Appendix-VI

represents the theoretical UV-Vis spectra of **1a** and **2a** obtained by TD-DFT in gas phase which are fairly matching with the experimental UV-vis. spectra. The broader absorption for **1a** as compared to **2a** due to the presence of nitro group is again conformed by TD spectra. The obtained UV-Vis spectra of **1a** and **2a** with cyanide ion are given in Figures 7.20b and A31b in Appendix-VI, respectively. The spectral features and absorption values are also matching with experimental UV-Visible spectra. Red shift in the Soret band of cobalt complexes and charge transfer band upon axial coordination of cyanide ion were also observed by TD-DFT spectra.

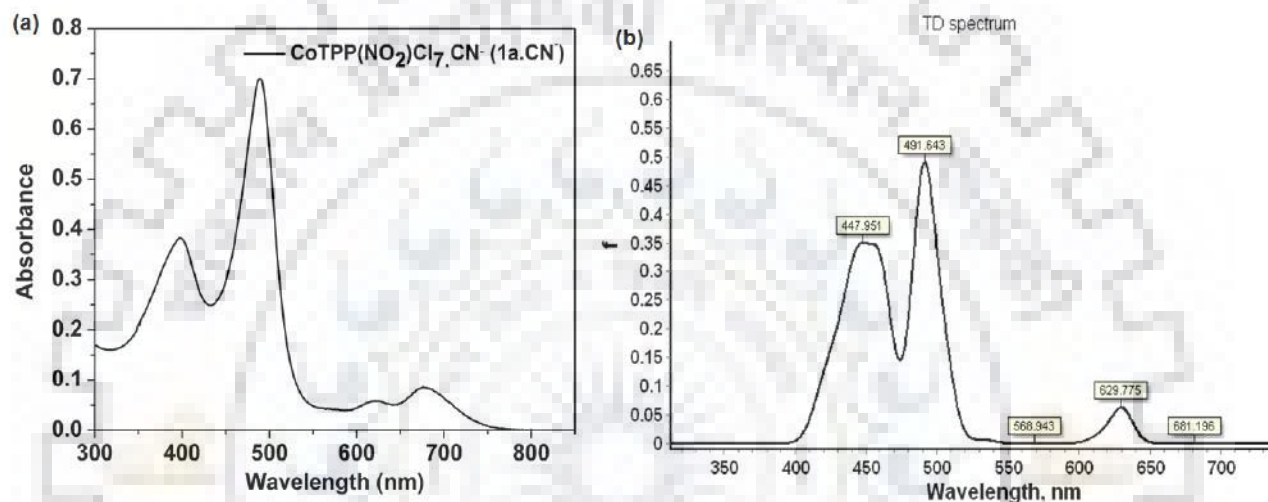


**Figure 7.20** (a) Experimental UV-Vis. Spectrum and (b) Theoretical UV-Vis. Spectrum of CoTPP(NO<sub>2</sub>)Cl<sub>7</sub>.CN<sup>-</sup> (**1a.CN<sup>-</sup>**).

## 7.4 CONCLUSIONS

We reported the facile synthesis of perchlorinated-2-nitro-*meso*-tetraphenylporphyrin and metal complexes and the data was compared with homosubstituted MTPPCl<sub>8</sub> to highlight the effect of nitro group over their conformation as well as their spectral properties. Nitro bearing porphyrins exhibited 10-15 nm red-shifts in the electronic spectra and dramatic anodic shift in the reduction potentials. The lower C<sub>β</sub>'-C<sub>α</sub>'-C<sub>m</sub> and higher Δ24 values for **1d** as compared to **2d** indicates the effect of mixed β-substitution and induced nonplanarity by the nitro group. Perhaloporphyrins (**1-4**) exhibited colorimetric responses toward basic anions such as CN<sup>-</sup>, F<sup>-</sup>, CH<sub>3</sub>COO<sup>-</sup> and H<sub>2</sub>PO<sub>4</sub><sup>-</sup> ions and being able to detect these anions in nM concentration. The red-shifted electronic spectral features, the higher β<sub>2</sub> values for deprotonation and anion recognition of **1-4** were interpreted in terms of enhanced nonplanarity and electron withdrawing effect of NO<sub>2</sub> and/or

halo substituents. The large anodic shift in voltammetric studies and disappearance of  $^1\text{H}$  NMR signals for imino protons strongly supports the anion induced deprotonation. The spectroscopic studies and voltammetric titrations reveal that the formation of dianionic porphyrin species which intern hydrogen bonded with protonated anions (HA). The electron deficient Co(II) porphyrins (**1a** and **2a**) were utilized as sensors for the selective rapid visual detection of cyanide ions for the first time in porphyrin chemistry.

These results reported herein will provide a new standpoint to develop recyclable electron deficient nonplanar porphyrin-based anion sensors.

## 7.5 REFERENCES

1. Senge, M. O. *In The Porphyrin Handbook*; Kadish, K. M.; Smith, K. M.; Guillard, R., Eds.; Academic Press: San Diego, 2000; Vol. 1, pp. 239-347 and references cited therein.
2. Senge, M. O. Exercises in Molecular Gymnastics-Bending, Stretching and Twisting Porphyrins. *Chem. Commun.* **2006**, 243-256.
3. Honda, T.; Kojima, T.; Fukuzumi, S. Crystal Structures and Properties of a Monoprotonated Porphyrin. *Chem. Commun.* **2009**, 4994-4996.
4. Lai, S. W.; Hou, Y. J.; Che, C. M.; Pang, H. L.; Wong, K. Y.; Chang, C. K.; Zhu, N. Electronic Spectroscopy, Photophysical Properties, and Emission Quenching Studies of an Oxidatively Robust Perfluorinated Platinum Porphyrin. *Inorg. Chem.* **2004**, *43*, 3724-3732.
5. Mandon, D.; Ochsenein, P.; Fischer, J.; Weiss, R.; Jayaraj, K.; Austin, R. N.; Gold, A.; White, P. S.; Brigaud, O.; Battioni, P.; Mansuy, D.  $\beta$ -Halogenated-Pyrrole Porphyrins. Molecular Structures of 2,3,7,8,12,13,17,18-Octabromo-5,10,15,20-tetramesitylporphyrin, Nickel(II)2,3,7,8,12,13,17,18-Octabromo-5,10,15,20-tetramesitylporphyrin, and Nickel(II)2,3,7,8,12,13,17,18-Octabromo-5,10,15,20-tetrakis(pentafluorophenyl)porphyrin. *Inorg. Chem.* **1992**, *31*, 2044-2049.
6. Kadish, K. M.; Li, J.; Caemelbecke, E. V.; Ou, Z.; Guo, N.; Autret, M.; D'Souza, F.; Tagliatesta, P. Electrooxidation of Cobalt(II)  $\beta$ -Brominated-Pyrrole Tetraphenylporphyrins in  $\text{CH}_2\text{Cl}_2$  under an  $\text{N}_2$  or a CO Atmosphere. *Inorg. Chem.* **1997**, *36*, 6292-6298.

7. Dolphin, D.; Traylor, T. G.; Xie, L. Y. Polyhaloporphyrins: Unusual Ligands for Metals and Metal-Catalyzed Oxidations. *Acc. Chem. Res.* **1997**, *30*, 251-259.
8. Kumar, R.; Chaudhary, N.; Sankar M.; Maurya, M. R. Electron Deficient Nonplanar  $\beta$ -Octachlorovanadylporphyrin as a Highly Efficient and Selective Epoxidation Catalyst for Olefins. *Dalton Trans.* **2015**, *44*, 17720- 17729.
9. Senge, M. O.; Kalisch, W. W. Synthesis and Structural Characterization of Nonplanar Tetraphenylporphyrins and Their Metal Complexes with Graded Degrees of  $\beta$ -Ethyl Substitution. *Inorg. Chem.* **1997**, *36*, 6103-6116.
10. Fang, Y.; Senge, M. O.; Caemelbecke, E. V.; Smith, K. M.; Medforth, C. J.; Zhang, M.; Kadish, K. M. Impact of Substituents and Nonplanarity on Nickel and Copper Porphyrin Electrochemistry: First Observation of a  $\text{Cu}^{\text{II}}/\text{Cu}^{\text{III}}$  Reaction in Nonaqueous Media. *Inorg. Chem.* **2014**, *53*, 10772-10778.
11. Singh, A. K.; Khan, F. S. T.; Rath, S. P. Silver(III)···Silver(III) Interactions that Stabilize the syn Form in a Porphyrin Dimer Upon Oxidation. *Angew. Chem. Int. Ed.* **2017**, *56*, 8849-8854.
12. Spyroulias, G. A.; Despotopoulos, A. P.; Raptopoulou, C. P.; Terzis, A.; de Montauzon, D.; Poilblanc, R.; Coutsolelos, A. G. Comparative Study of Structure-Properties Relationship for Novel  $\beta$ -Halogenated Lanthanide Porphyrins and Their Nickel and Free Bases Precursors, as a Function of Number and Nature of Halogens Atoms. *Inorg. Chem.* **2002**, *41*, 2648-2659.
13. Bhyrappa, P.; Sankar, M.; Varghese, B. Mixed Substituted Porphyrins: Structural and Electrochemical Redox Properties. *Inorg. Chem.* **2006**, *45*, 4136-4149.
14. Kim, D. S.; Sessler, J. L. Calix[4]pyrroles: Versatile Molecular Containers With Ion Transport, Recognition, and Molecular Switching functions *Chem. Soc. Rev.* **2014**, DOI: 10.1039/c4cs00157e.
15. Gale, P. A.; Caltagirone, C. Anion Sensing by Small Molecules and Molecular Ensembles. *Chem. Soc. Rev.* **2015**, *44*, 4212-4227.



16. Vennesland, B.; Comm, E. E.; Knowles, C. J.; Westly, J.; Wissing, F. *Cyanide in Biology*, Academic press, London, 1981.
17. Briancon, D. Fluoride and Osteoporosis: an overview. *Rev. Rheum.* **1997**, *64*, 78-81.
18. Adams, R. L. P.; Knowler, J. T.; Leader, D. P. *The Biochemistry of the Nucleic Acids, Ed.*, Chapman and Hall, New York, 11<sup>th</sup> ed., 1992.
19. Shang, X. F.; Xu, X. F. The Anion Recognition Properties of Hydrazone Derivatives Containing Anthracene. *BioSystems* **2009**, *96*, 165-171.
20. Kim S. K.; Sessler, J. L. Calix [4] Pyrrole-based Ion Pair Receptors. *Acc. Chem. Res.* **2014**, *47*, 2525.
21. Pistner, A. J.; Lutterman, D. A.; Ghidui, M. J.; Ma, Y.-Z.; Rosenthal, J. Synthesis, Electrochemistry, and Photophysics of a Family of Phlorin Macrocycles that Display Cooperative Fluoride Binding. *J. Am. Chem. Soc.* **2013**, *135*, 6601-6607.
22. Sessler, J. L.; Davis, J. M. Sapphyrins: Versatile Anion Binding Agents. *Acc. Chem. Res.* **2001**, *34*, 989-997.
23. Rodrigues, J. M. M.; Farinha, A. S.; Muteto, P. V.; Woranovicz-Barreira, S. M.; Paz, F. A. A.; Neves, M. G.; Cavaleiro, J. A. S.; Tome, A. C.; Gomes, M. T.; Sessler, J. L.; Tome, J. P. C. New Porphyrin Derivatives for Phosphate Anion Sensing in Both Organic and Aqueous Media. *Chem. Commun.* **2014**, *50*, 1359-1361.
24. Yoon, H.; Lee, C.-H.; Jeong, Y.-H.; Gee, H.-C.; Jang, W.-D. A Zinc Porphyrin-based Molecular Probe for the Determination of Contamination in Commercial Acetonitrile *Chem. Commun.* **2012**, *48*, 5109-5111.
25. Worlinsky, J. L.; Halepas S.; Brukner, C. PEGylated *meso*-Arylporpholactone Metal Complexes as Optical Cyanide Sensors in Water. *Org. Biomol. Chem.* **2014**, *12*, 3991-4001.
26. Hill, A. V. The Possible Effects of the Aggregation of the Molecules of Haemoglobin on Its Dissociation Curves *J. Physiol. (London)*, **1910**, *40*, IV-VII.
27. Giraudeau, A.; Callot, H. J.; Gross, M. Effects of Electron-Withdrawing Substituents on the Electrochemical Oxidation of Porphyrins. *Inorg. Chem.* **1979**, *18*, 201-206.

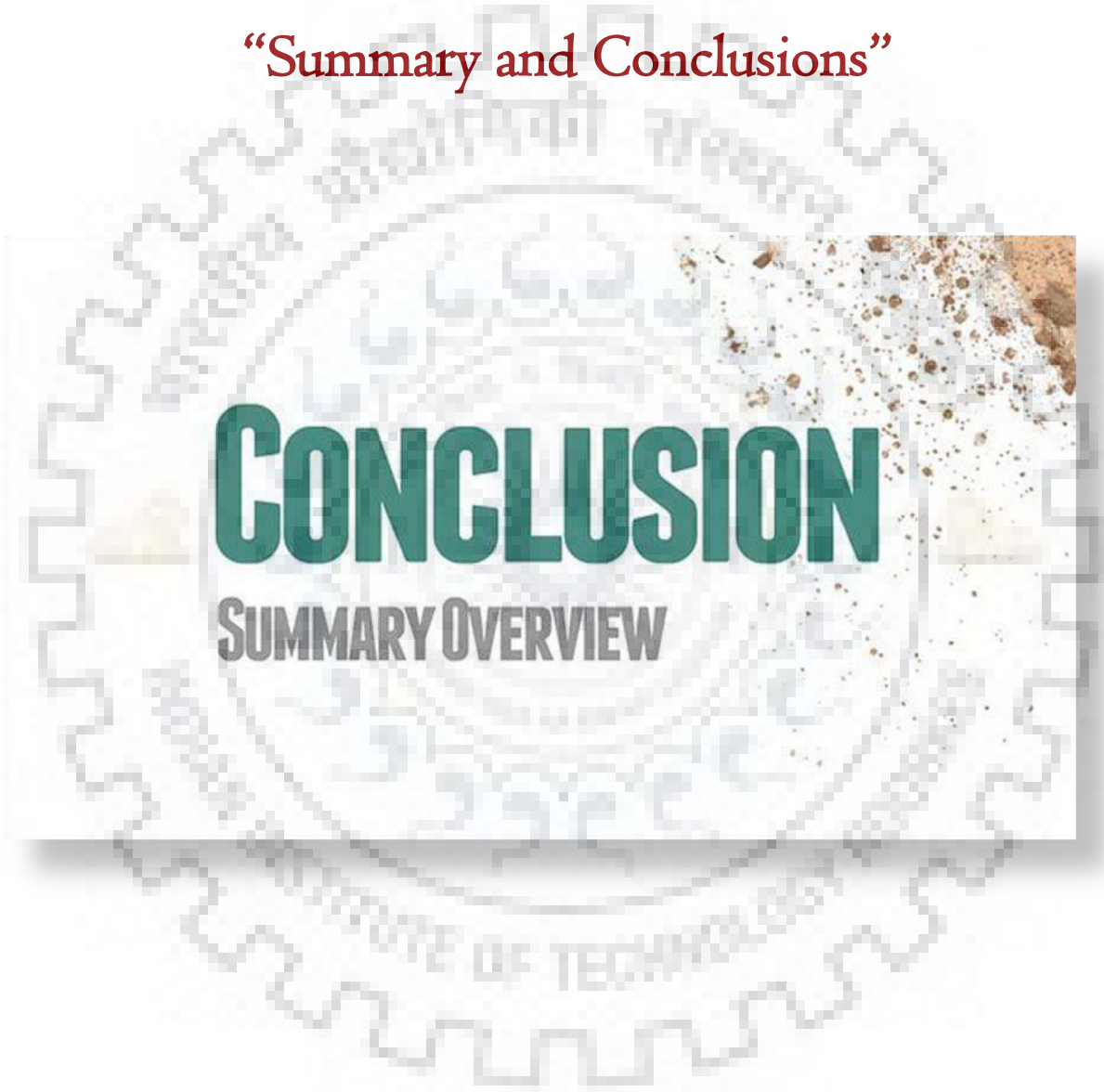


28. Spyroulias, G. A.; Despotopoulos, A. P.; Raptopoulou, C. P.; Terzis, A.; de Montauzon, D.; Poilblanc, R.; Coutsolelos, A. G. Comparative Study of Structure-Properties Relationship for Novel  $\beta$ -Halogenated Lanthanide Porphyrins and Their Nickel and Free Bases Precursors, as a Function of Number and Nature of Halogens Atoms. *Inorg. Chem.* **2002**, *41*, 2648-2659.
29. Bhyrappa, P.; Krishnan, V. Octabromotetraphenylporphyrin and Its Metal Derivatives: Electronic Structure and Electrochemical Properties. *Inorg. Chem.* **1991**, *30*, 239-245.
30. Bhyrappa, P.; Bhavana, P.; Perbrominated 2-Nitrotetraphenylporphyrins: Electrochemical and Axial Ligation Properties *J. Chem. Soc. Perkin Trans. 2*, **2001**, *0*, 238-242.
31. Fang, Y.; Bhyrappa, P.; Ou, Z.; Kadish, K. M. Planar and Nonplanar Free-Base Tetraarylporphyrins:  $\beta$ -Pyrrole Substituents and Geometric Effects on Electrochemistry, Spectroelectrochemistry, and Protonation/Deprotonation Reactions in Nonaqueous Media. *Chem. Eur. J.* **2014**, *20*, 524-532.
32. Harada R.; Kojima, T. A Porphyrin Nanochannel: Formation of Cationic Channels by a Protonated Saddle-Distorted Porphyrin and Its Inclusion Behaviour. *Chem. Commun.* **2005**, *0*, 716-718.
33. Kumar, R.; Chaudhri, N.; Sankar, M. Ratiometric and Colorimetric "Naked Eye" Selective Detection of  $\text{CN}^-$  ions by Electron Deficient Ni(II) Porphyrins and Their Reversibility. *Dalton Trans.* **2015**, *44*, 9149-9157.
34. Thomassen, I. K.; Vazquez-Lima, H.; Gagnon, K. J.; Ghosh, A. Octaiodoporphyrin. *Inorg. Chem.* **2015**, *54*, 11493-11497.
35. Liao, M.-S.; Scheiner, S. Electronic Structure and Bonding in Metal Porphyrins, Metal=Fe, Co, Ni, Cu, Zn. *J. Chem. Phys.* **2002**, *117*, 205-219.



## CHAPTER 8

### “Summary and Conclusions”





## CHAPTER 8

### SUMMARY AND CONCLUSIONS

The mixed  $\beta$ -substituted porphyrins are of great importance due to their intriguing photophysical and electrochemical studies. Due to their varying degree of nonplanar conformation they have been proved to be potential candidates for variety of material and medicinal applications including dye sensitized solar cells (DSSC), nonlinear optics (NLO), photodynamic therapy (PDT), chemosensing, catalysis and biomimetic model compounds in many biological applications. In chapter 1, we briefly discussed the general introduction of naturally occurring tetrapyrroles and their synthetic analogues. Further, the applications of porphyrinoids in DSSC, Catalysis, NLO, PDT and ion sensing have been discussed in detail. Chapter 1 also elucidates the information regarding the  $\beta$ -functionalization of the macrocycles. 2-Nitroporphyrins has been proved to be an outstanding precursor for further functionalization of porphyrin due to its ease of synthesis and tendency to convert into different functional groups. The increase in the number of bulky  $\beta$ -substituents leads to the tunable physicochemical and electrochemical redox properties. Apart from porphyrins, a concise overview of some fused porphyrinoids and oxidized and reduced macrocycles (chlorins) is also provided in chapter 1.

In chapter 2, one-pot facile synthesis and characterization of novel  $\beta$ -substituted *meso*-tetraphenylporphyrins and/or chlorins were described. The high regioselective reactivity of active methylene compounds in Michael addition reaction was reported to access  $\beta$ -substituted *trans*-chlorins. Size dependent approach was applied for the fine-tuning of product formation from porphyrins to chlorins. Notably, we were able to isolate mono/trisubstituted porphyrin and/or di/tetra-substituted chlorin from one-pot synthesis for the first time in porphyrin chemistry. The orientation of  $\beta$ -substituents and conformation of macrocyclic core was revealed by Single crystal X-ray analysis. Single-crystal X-ray diffraction analysis revealed the quasi-planar to moderate nonplanar conformation of chlorins due to *trans*-orientation of  $\beta$ -substituents, whereas porphyrins exhibited higher mean plane deviation from 24-atom core ( $\Delta 24$ ) as compared to chlorins. A hypsochromic shift ( $\sim 8$ -10 nm) in the longest wavelength ( $Q_y$ ) absorption band was observed upon substitution of electron withdrawing groups (IND and BENAC) at 2,3-position of *meso*-tetraphenylchlorin. Notably, HOMO-LUMO gap altered upon substitution at 2,3 position of *meso*-tetraphenylchlorin whereas bromo-substitution at 12,13

position of 2,3-disubstituted *trans*-chlorins reduced the gap between LUMO and LUMO+1. Electronic nature of synthesized macrocyclic skeletons was authenticated by protonation and deprotonation studies. The  $\beta$ -functionalized chlorins exhibited lower protonation constants and much higher deprotonation constants as compared to porphyrins which revealed the combined effect of macrocyclic conformation and the electronic nature of  $\beta$ -substituents. Facile synthesis of porphyrins and/or chlorins based on the size of Michael donor employed and in turn resulted in tunable photophysical and electrochemical redox properties are the significant features of the present work.

In chapter 3, highly twisted  $\beta$ -to-*ortho*-phenyl doubly fused-porphyrins (DFPs) or doubly fused-chlorins (DFCs) were regioselectively synthesized by facile oxidative fusion of planar *trans*-chlorins using DDQ in good to excellent yields (70-92%) under mild reaction conditions with high atom economy. The regioselectivity in product formation either difused porphyrins or chlorins was controlled by the presence or absence of Ni(II) ion in the macrocyclic core. Ni(II) *trans*-chlorins selectively yielded difused porphyrins (DFPs) whereas free base *trans*-chlorins afforded only difused chlorins (DFCs). This is the first report on core metal ion dependent regioselective oxidative fusion of *trans*-chlorins into doubly fused porphyrins or chlorins. The synthesized fused porphyrinoids exhibited significantly red-shifted spectral features ( $\Delta\lambda_{\text{max}} = 16-53$  nm) of Soret Band due to extended  $\pi$ -conjugation and highly twisted macrocyclic conformation (twist angle  $\sim 20-34^\circ$ ). The difused porphyrins have shown higher twist angles as compared to the difused chlorins. A tremendous downfield shift ( $\Delta\delta = 1.71-2.02$  ppm) has been observed for core NHs of these fused chlorins as compared to their precursors (*trans*-chlorins) due to the fused macrocyclic core.  $\beta$ -Phenyl substituted chlorin  $\text{H}_2\text{DFC}(\text{MN})_2\text{Ph}_2$  exhibited a large cathodic shift in first oxidation ( $\Delta E_{\text{oxdn}} = 0.54$  V) and first reduction ( $\Delta E_{\text{redn}} = 0.47$  V) potentials due to pushing effect of  $\beta$ -phenyl substituents. Malononitrile fused porphyrinoids were harder to oxidize and easy to reduce as compared to indane fused systems which supported the facile deprotonation of  $\text{H}_2\text{DFC}(\text{MN})_2\text{X}_2$ . On the contrary, indane fused chlorins exhibited 40-60 folds higher protonation constants as compared to malononitrile fused chlorins. Overall, the present methodology provides a new standpoint to develop a wide variety of highly twisted  $\beta$ -*meso* doubly fused chlorins and porphyrins.



In chapter 4, we synthesized several *ruffled*  $\beta$ -to-*ortho*-phenyl monofused porphyrins (MFPs). A novel one pot synthesis of  $\beta$ -to *ortho*-phenyl monofused Ni(II) porphyrins with indanedione functionalities have been reported *via* nickel acetate mediated oxidative fusion of planar free base *trans*-chlorins. Further these Ni(II) monofused porphyrins were demetallated and remetallated with different metals to obtain the corresponding metalloporphyrins. Extended  $\pi$ -conjugation of porphyrins aromatic circuit was accomplished by connecting  $\beta$ -pyrrolic indanedione groups with *meso-ortho*-phenyls. As compared to the unfused precursors (*trans*-chlorins), these monofused derivatives have shown a spectacular bathochromic shift of the Soret as well as the longest wavelength bands in their absorption spectra. The synthesized monofused derivatives were blue shifted in their absorption spectra as compared to their correspond difused system which described in chapter 3 this may be due to less twisted nature of macrocyclic core as compared to difused systems. NiMFP(IND)R<sub>2</sub> (where R = H and Ph) were best described as typically *ruffled* due to their high  $\Delta_{24}$  and  $\Delta C_{\beta}$  as compared to the Zinc(II) complexes. Notably, Ni(II) complexes NiMFP(IND) and NiMFP(IND)Ph<sub>2</sub> exhibited metal centered oxidation (Ni<sup>II</sup>/Ni<sup>III</sup>) due to extended conjugation and electronic rich nature of the  $\beta$ -substituent. Monofused Ni(II) complexes (Ni(II)MFP(IND)s) have shown slightly higher HOMO-LUMO gap (80-150 mV) as compared to corresponding difused porphyrins (Ni(II)DFP(IND)<sub>2</sub>s).

In chapter 5, highly nonplanar and electron deficient *trans*-benzochlorins have been synthesized. In order to examine the effect of  $\beta$ - $\beta'$  fusion over *meso*- $\beta$ -fusion, these *trans*-benzochlorins were oxidized into  $\beta$ -*ortho-meso*-phenyl doubly fused benzoporphyrins which are novel class of triply fused porphyrins. The synthesized *trans*-benzochlorins exhibited highly red shifted spectral features as compared to previously reported *trans*-chlorins and other structurally related compounds. Likewise these triply fused-porphyrins were highly red shifted as compared to mono-fused and difused systems due to higher nonplanar and extended  $\pi$ -conjugation. On the other hand, the  $\beta$ -bromination of *trans*-benzochlorin exerted pronounced effect on the electronic properties. Interestingly, NiTPCBr<sub>4</sub>(IND)<sub>2</sub>(Benzo) **5** has shown very high Q/B ratio with very high FWHM and oscillator strength which ascribed to highest nonplanar nature among all synthesized porphyrinoids. Malononitrile appended porphyrinoids such as NiTPC(MN)<sub>2</sub>(Benzo) (**2**) and NiDFP(MN)<sub>2</sub>(Benzo) (**4**) were difficult to oxidize and easy to reduce as compared to corresponding indanedione appended porphyrinoids NiTPC(IND)<sub>2</sub>(Benzo) (**1**) and NiDFP(IND)<sub>2</sub>(Benzo) (**3**) that strongly supported the highly electron deficient nature of

malononitrile appended porphyrinoids. *Trans*-chlorins are capable of sensing basic anions through outer proton abstraction whereas highly electron deficient and nonplanar difused benzoporphyrin NiDFP(MN)<sub>2</sub>(Benzo) **4** exhibited “Naked Eye” selective detection of cyanide ion with very high binding constant. The reversibility study demonstrated that the sensor NiDFP(MN)<sub>2</sub>(Benzo) **4** was recoverable and can be reused for selective cyanide ion detection without losing its sensing ability for numerous times.

Chapter 6 described the synthesis of 12,13-dibromo/diphenyl-tetraphenylporphyrins functionalized with 1,3-diketone and ester (ethyl acetate) functionalities at the antipodal  $\beta$ -position. The nucleophilic substitution of 2-nitroporphyrins *via* acetylacetone and ethyl acetoacetate has been performed in order to obtain corresponding mixed  $\beta$ -trisubstituted porphyrins. The single crystal X-ray diffraction analysis revealed that NiTPP[CH(COCH<sub>3</sub>)<sub>2</sub>]Br<sub>2</sub> (**1b**) exhibited very high magnitude displacement of 24-core atoms and eight  $\beta$ -pyrrole carbons ( $\Delta Z = 0.44 \text{ \AA}$ ,  $\Delta C_{\beta} = 0.82 \text{ \AA}$ ) from the mean plane which is highly nonplanar mixed  $\beta$ -trisubstituted MTPP reported till date. The synthesized mixed  $\beta$ -substituted porphyrins have shown very least influence on the absorption and fluorescence profiles inducing small blue shifts in the Soret as well as Q bands and marginal decrement in the fluorescence intensity with low quantum yield as compared to the precursor 2-nitroporphyrins. Notably, the acetylacetone group has shown a distinguish impact on the redox properties of corresponding porphyrins. The diketone appended porphyrins MTPP[CH(COCH<sub>3</sub>)<sub>2</sub>](R)<sub>2</sub> (where R = Br and Ph) have shown multiple oxidation and reduction due to the presence of keto-enol tautomeric form of acetylacetone moiety. The overall impact of the antipodal  $\beta$ -substituents on the redox behavior of the macrocyclic skeleton has also been clearly demonstrated.

In Chapter 7, highly nonplanar electron deficient perhalogenated-2-nitro-*meso*-tetraphenylporphyrins have been synthesized and the spectroscopic data was compared with homosubstituted perhaloporphyrins. Nitro bearing porphyrins, MTPP(NO<sub>2</sub>)X<sub>7</sub> (X = Cl and Br) exhibited 10-15 nm red shift in the electronic spectra and dramatic anodic shift in the reduction potentials as compared to the homosubstituted porphyrins, MTPPX<sub>8</sub> (where X = Cl, and Br). Free base perhaloporphyrins (**1-4**) exhibited colorimetric responses toward basic anions such as CN<sup>-</sup>, F<sup>-</sup>, CH<sub>3</sub>COO<sup>-</sup> and H<sub>2</sub>PO<sub>4</sub><sup>-</sup> ions and being able to detect these anions in nanomolar concentration. The red-shifted electronic spectral features, the higher  $\beta_2$  values for deprotonation

and anion recognition properties were interpreted in terms of enhanced nonplanarity and electron withdrawing effect of NO<sub>2</sub> and/or halo substituents. The large anodic shift in voltammetric studies and disappearance of <sup>1</sup>H NMR signals for imino protons strongly supports the anion induced deprotonation in free base porphyrins. Further, electron deficient Co(II) porphyrins CoTPP(NO<sub>2</sub>)Cl<sub>7</sub> (**1a**) and CoTPPCL<sub>8</sub> (**2a**) were utilized as sensors for the selective rapid visual detection of cyanide ions for the first time in porphyrin chemistry. The presented results will provide a new standpoint to develop recyclable electron deficient nonplanar porphyrin-based anion sensors.

Herein, we developed novel synthetic methodologies for  $\beta$ -functionalized chlorins and porphyrins, mono/doubly/triply fused porphyrinoids as well as tri/octa mixed  $\beta$ -substituted porphyrins. All the synthesized porphyrinoids were derived from a single precursor i.e 2-nitroporphyrin.  $\beta$ -Modified porphyrinoids exhibited tunable photophysical and intriguing electrochemical properties and some of them exhibited interesting anion sensing properties. This thesis represents a new outlook for  $\beta$ -functionalized porphyrinoids. The utilization of these porphyrinoids in DSSC, NLO, Catalysis and PDT is under progress.





# APPENDIX





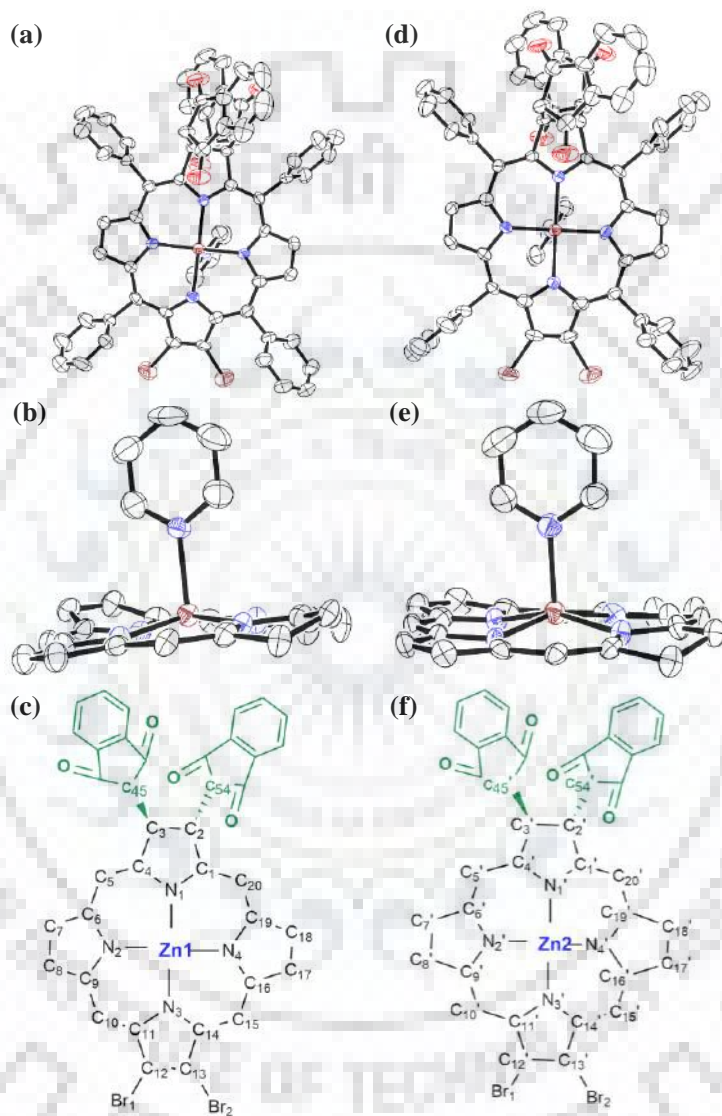
## APPENDIX-I

**Versatile Synthetic Route for  $\beta$ -Functionalized Chlorins and Porphyrins by Varying the Size of Michael Donors: Syntheses, Photophysical and Electrochemical Redox Properties**

<b>Table of Contents</b>	<b>Page No.</b>
<b>Figure A1.</b> ORTEP Diagrams Showing Top and Side Views of ZnTPCBr <sub>2</sub> (IND) <sub>2</sub> ( <b>11b</b> ). (c) and (f) are showing numbering of carbon atom in the skeleton.	235
<b>Figure A2.</b> Displacement of The Mean Plane of The Porphyrin Core from The Mean Plane for (a) NiTPPBr <sub>2</sub> (CHD) (b) NiTPC(BENAC) <sub>2</sub> (c) H <sub>2</sub> TPCBr <sub>2</sub> (BENAC) <sub>2</sub> (d) Zn <sub>2</sub> TPCBr <sub>2</sub> (IND) <sub>2</sub> (e) Zn <sub>1</sub> TPCBr <sub>2</sub> (IND) <sub>2</sub>	238
<b>Figure A3-A9.</b> Pictorial Representation of Frontier Molecular Orbitals of Synthesized Free Base Complexes.	238- 241
<b>Figure A10.</b> Electronic Absorption Spectra of Synthesized Ni(II) and Zn(II) Complexes. Circled Area Shows The Absorption due to Benzoylacetonitrile and Indane-1,3-dione.	242
<b>Figure A11.</b> Fluorescence Spectra of Synthesized Zn(II) Porphyrins and Chlorins.	242
<b>Figure A12-A19.</b> <sup>1</sup> H NMR Spectra of All Newly Synthesized Free Base Complexes in CDCl <sub>3</sub> at 298K.	244- 247
<b>Figure A20-A28.</b> MALDI-TOF Mass Spectrum of Synthesized Free Base Complexes in Positive Ion Mode	248- 252
<b>Figure A29.</b> UV-vis. Spectral Titrations of Synthesized Free Base Porphyrins (a) H <sub>2</sub> TPP(CHD) ( <b>1</b> ), (b) H <sub>2</sub> TPPBr <sub>2</sub> (CHD) ( <b>2</b> ), and (c) H <sub>2</sub> TPP(DMBA) ( <b>3</b> ) with TFA in Toluene at 298 K.	252
<b>Figure A30.</b> UV-vis. Spectral Titrations of Synthesized Free Base Chlorins (a) H <sub>2</sub> TPC(BENAC) <sub>2</sub> ( <b>8</b> ), (b) H <sub>2</sub> TPCBr <sub>2</sub> (BENAC) <sub>2</sub> ( <b>9</b> ), and (c) H <sub>2</sub> TPC(IND) <sub>2</sub> ( <b>10</b> ) with TFA in toluene at 298 K.	253

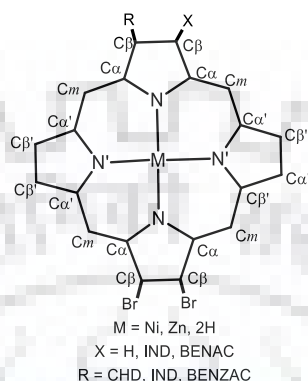
<b>Figure A31.</b> UV-vis. Spectral Titrations of Synthesized Free Base Porphyrins (a) $H_2TPP(CHD)$ (1), (b) $H_2TPPBr_2(CHD)$ (2), and (c) $H_2TPPBr_2(DMBA)$ (3) with TBAOH in Toluene at 298 K.	254
<b>Figure A32.</b> UV-vis. Spectral Titrations of Synthesized Free Base Chlorins $H_2TPC(BENAC)_2$ (8), (b) $H_2TPCBr_2(BENAC)_2$ (9), and (c) $H_2TPCBr_2(IND)_2$ (11) with TBAOH in Toluene at 298 K.	255
<b>Figure A33.</b> Comparative Cyclic Voltammograms of Synthesized Free Base Chlorins.	256
<b>Figure A34.</b> Comparative Cyclic Voltammograms of (a) Zn(II) Porphyrins (b) Free Base Porphyrins.	256
<b>Table A1.</b> Crystal Structure Data of $NiTPPBr_2(CHD)$ , $ZnTPPBr_2(IND)_2$ , and $H_2TPCBr_2(BENAC)_2$ $NiTPC(BENAC)_2$	236
<b>Table A2.</b> Selected Average Bond Lengths and Bond Angles of $NiTPPBr_2(CHD)$ , $ZnTPCBr_2(IND)_2$ and $H_2TPCBr_2(BENAC)_2$	237
<b>Table A3.</b> Photophysical Properties of Synthetic Chlorins and porphyrins.	243

**Figure A1.** ORTEP Diagrams Showing Top (a, d) and Side (b, e) Views of  $\text{ZnTPCBr}_2(\text{IND})_2$  (**11b**). Solvates are Not Shown for Clarity, The  $\beta$ -Substituents and  $\beta$ -/*meso*-phenyls are Omitted for Clarity in Side View. (c) and (f) are Showing Numbering of Carbon atom in The Skeleton.



**Table A1.** Crystal Structure Data of NiTPPBr<sub>2</sub>(CHD), ZnTPPBr<sub>2</sub>(IND)<sub>2</sub>, and H<sub>2</sub>TPCBr<sub>2</sub>(BENAC)<sub>2</sub> NiTPC(BENAC)<sub>2</sub>

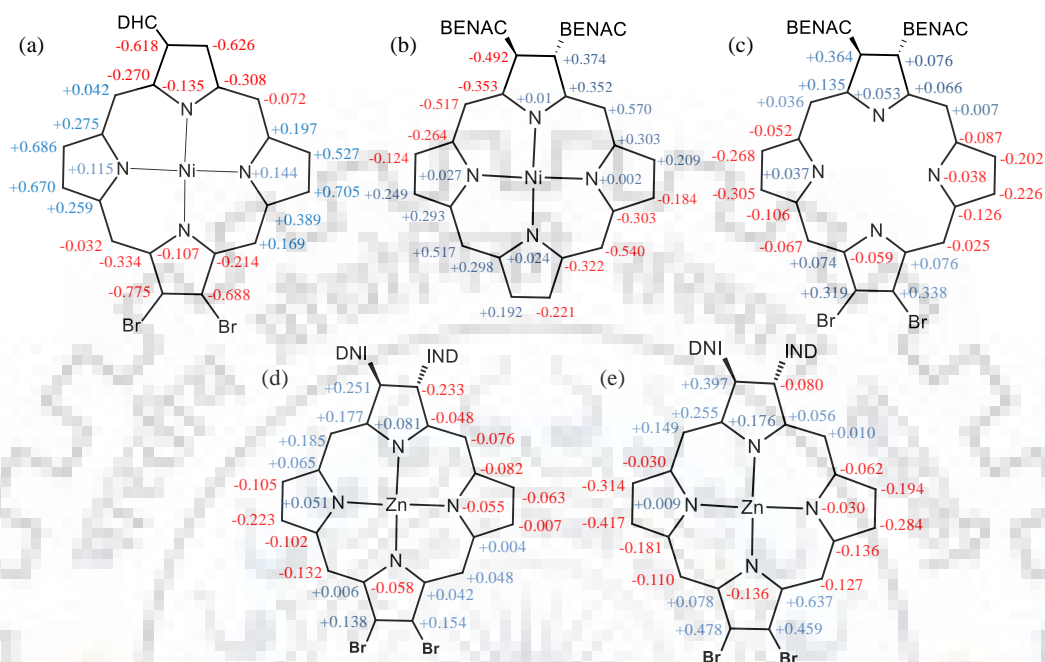
	NiTPPBr <sub>2</sub> (CHD)	ZnTPPBr <sub>2</sub> (IND) <sub>2</sub>	H <sub>2</sub> TPCBr <sub>2</sub> (BENAC) <sub>2</sub>	NiTPC(BENAC) <sub>2</sub>
Empirical formula	C <sub>50</sub> H <sub>31</sub> Br <sub>2</sub> N <sub>4</sub> NiO <sub>2</sub>	C <sub>67</sub> H <sub>41</sub> Br <sub>2</sub> N <sub>5</sub> O <sub>4</sub> Zn	C <sub>62</sub> H <sub>39</sub> Br <sub>2</sub> N <sub>6</sub> O <sub>2</sub>	C <sub>62</sub> H <sub>40</sub> N <sub>6</sub> NiO <sub>2</sub>
Formula wt.	938.28	1205.24	1238.34	959.69
Crystal system	orthorhombic	triclinic	monoclinic	triclinic
Space group	C12/c1	P -1	C2/c	P -1
<i>a</i> (Å)	13.7029(9)	17.7539(7)	36.070(5)	10.4599(5)
<i>b</i> (Å)	25.8207(17)	18.7437(8)	18.601(5)	16.2033(7)
<i>c</i> (Å)	27.0861(19)	19.2057(8)	18.210(5)	16.3222(8)
$\alpha$ (°)	90	82.924(2)	90.000(5)	108.860(3)
$\beta$ (°)	90	62.508(1)	113.647(5)	107.624(2)
$\gamma$ (°)	90	81.082(1)	90.000(5)	97.271(2)
Volume (Å <sup>3</sup> )	9583.6(11)	5591.2(4)	11192(5)	2416.5(2)
Z	8	4	4	2
D <sub>calc</sub> (mg/m <sup>3</sup> )	1.301	1.432	1.470	1.319
$\lambda$ (Å)	0.71073	0.71073	0.71073	0.71073
T (K)	296(2)	296(2)	293(2)	293(2)
No. of total reflns.	11086	14177	13899	8418
No. of indepnt. reflns.	4198	8079	5529	3315
R	0.0737	0.0572	0.0760	0.0628
R <sub>w</sub>	0.1661	0.1486	0.3127	0.2493
GOOF	0.975	0.992	0.962	0.966
CCDC	<b>1533453</b>	<b>1547059</b>	<b>1532468</b>	<b>1534972</b>

**Table A2.** Selected Average Bond Lengths and Bond Angles of NiTPPBr<sub>2</sub> (CHD), ZnTPCBr<sub>2</sub>(IND)<sub>2</sub> and H<sub>2</sub>TPCBr<sub>2</sub>(BENAC)<sub>2</sub>

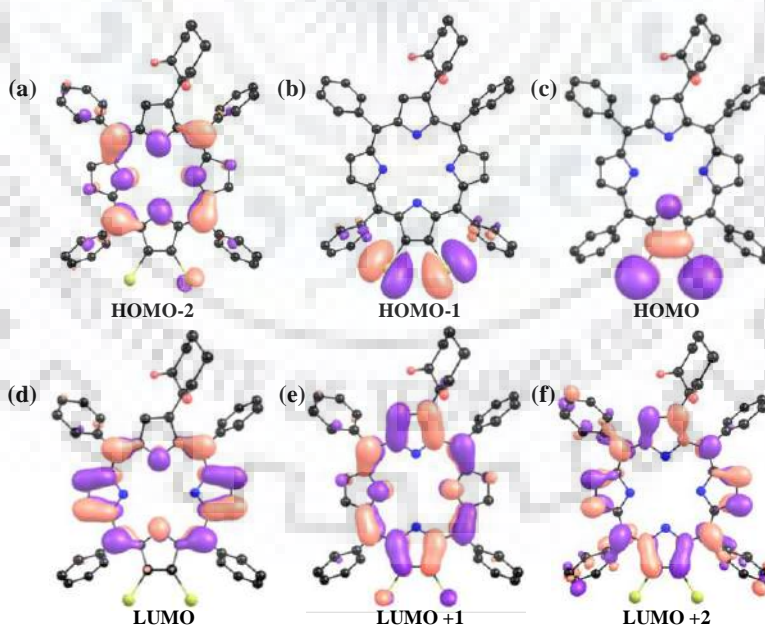
	NiTPPBr <sub>2</sub> (CHD)	Zn1TPPBr <sub>2</sub> (IND) <sub>2</sub>	Zn2TPPBr <sub>2</sub> (IND) <sub>2</sub>	H <sub>2</sub> TPCBr <sub>2</sub> (BENAC) <sub>2</sub>	NiTPC(BENAC) <sub>2</sub>
<b>Bond Lengths (Å)</b>					
M-N	1.959(5)	2.136(6)	2.144(6)	--	1.939(4)
M-N'	1.916(5)	2.041(5)	2.038(5)	--	1.925(6)
N-C <sub>α</sub>	1.391(7)	1.369(9)	1.371(9)	1.372(8)	1.382(8)
N'-C <sub>α</sub>	1.386(7)	1.369(8)	1.367(8)	1.375(8)	1.386(8)
C <sub>α</sub> -C <sub>β</sub>	1.449(1)	1.466(9)	1.472(7)	1.487(8)	1.466(8)
C <sub>α</sub> -C <sub>β'</sub>	1.429(1)	1.436(9)	1.434(7)	1.423(1)	1.423(1)
C <sub>β</sub> -C <sub>β'</sub>	1.326(1)	1.433(9)	1.449(8)	1.440(1)	1.440(1)
C <sub>β</sub> -C <sub>β'</sub>	1.371(1)	1.325(9)	1.332(1)	1.352(8)	1.342(8)
C <sub>α</sub> -C <sub>m</sub>	1.381(7)	1.397(9)	1.386(9)	1.391(1)	1.372(1)
C <sub>α</sub> -C <sub>m'</sub>	1.378(7)	1.416(9)	1.411(9)	1.402(8)	1.389(8)
$\Delta C_{\beta}$ <sup>a</sup>	<b>0.662</b>	<b>0.327</b>	<b>0.146</b>	<b>0.262</b>	<b>0.256</b>
$\Delta 24$ <sup>b</sup>	<b>0.344</b>	<b>0.174</b>	<b>0.099</b>	<b>0.132</b>	<b>0.281</b>
$\Delta M$	<b>0.027</b>	<b>0.342</b>	<b>0.351</b>	--	0.008
<b>Bond Angles (°)</b>					
N-M-N	171.31(2)	161.63(2)	162.58(2)	--	179.72(2)
N'-M-N'	173.80(2)	159.85(2)	160.01(2)	--	179.53(3)
M-N-C <sub>α</sub>	127.06(4)	124.14(4)	123.59(5)	--	126.89(4)
M-N'-C <sub>α</sub>	127.27(4)	126.48(4)	126.74(5)	--	127.35(5)
N-C <sub>α</sub> -C <sub>m</sub>	123.69(5)	125.28(6)	124.73(7)	124.76(5)	125.47(6)
N'-C <sub>α</sub> -C <sub>m</sub>	125.52(5)	126.32(6)	126.35(6)	128.39(5)	125.18(7)
N-C <sub>α</sub> -C <sub>β</sub>	109.34(5)	108.89(6)	109.60(6)	110.16(5)	110.84(6)
N'-C <sub>α</sub> -C <sub>β</sub>	109.61(6)	109.71(6)	109.31(6)	105.84(5)	109.82(6)
C <sub>β</sub> -C <sub>α</sub> -C <sub>m</sub>	126.66(6)	125.71(6)	125.65(6)	125.04(5)	124.16(6)
C <sub>β</sub> -C <sub>α</sub> -C <sub>m'</sub>	123.64(6)	123.96(6)	124.33(6)	125.73(5)	124.82(7)
C <sub>α</sub> -C <sub>β</sub> -C <sub>β'</sub>	107.82(7)	105.25(6)	105.17(6)	105.11(5)	104.45(6)
C <sub>α</sub> -C <sub>β</sub> -C <sub>β'</sub>	106.73(7)	107.30(6)	107.50(7)	108.72(6)	107.57(6)
C <sub>α</sub> -N-C <sub>α</sub>	105.28(5)	109.80(6)	108.47(6)	108.39(5)	106.20(5)
C <sub>α</sub> -N'-C <sub>α</sub>	104.78(5)	106.00(5)	106.29(6)	110.88(5)	105.20(6)
C <sub>α</sub> -C <sub>m</sub> -C <sub>α</sub>	122.35(6)	125.87(6)	125.22(6)	125.94(5)	121.89(7)

<sup>a</sup> $\Delta C_{\beta}$  refers to the mean plane deviation of  $\beta$ -pyrrole carbons<sup>b</sup> $\Delta 24$  refers to the mean plane displacement of 24-atom core

**Figure A2.** Displacement of The Mean Plane of The Porphyrin Core from The Mean Plane for (a) NiTPPBr<sub>2</sub>(CHD) (b) NiTPC(BENAC)<sub>2</sub> (c) H<sub>2</sub>TPCBr<sub>2</sub>(BENAC)<sub>2</sub> (d) Zn<sub>2</sub>TPCBr<sub>2</sub>(IND)<sub>2</sub> (e) Zn<sub>1</sub>TPCBr<sub>2</sub>(IND)<sub>2</sub>

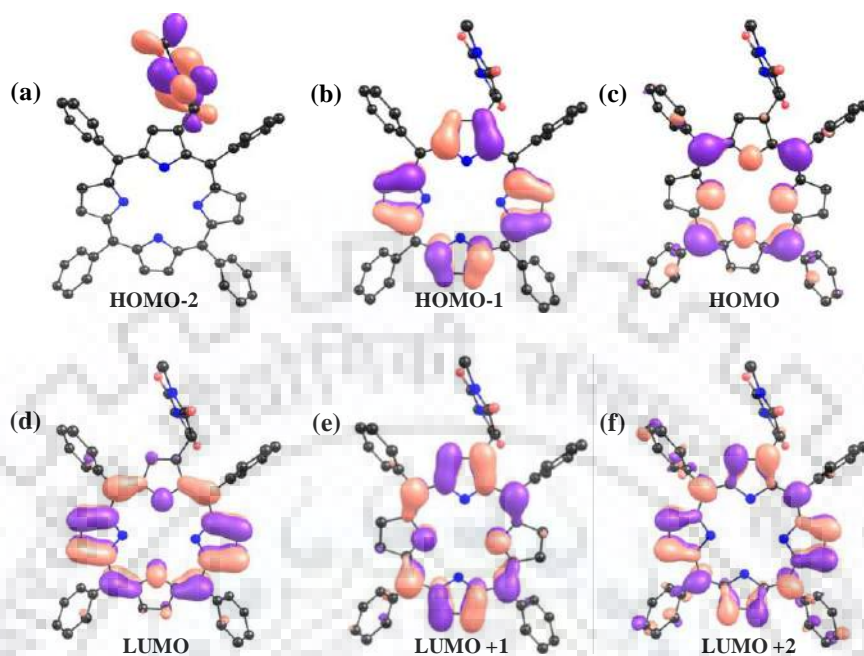


**Figure A3.** Pictorial Representation of Frontier Molecular Orbitals of H<sub>2</sub>TPPBr<sub>2</sub>(CHD) (2).

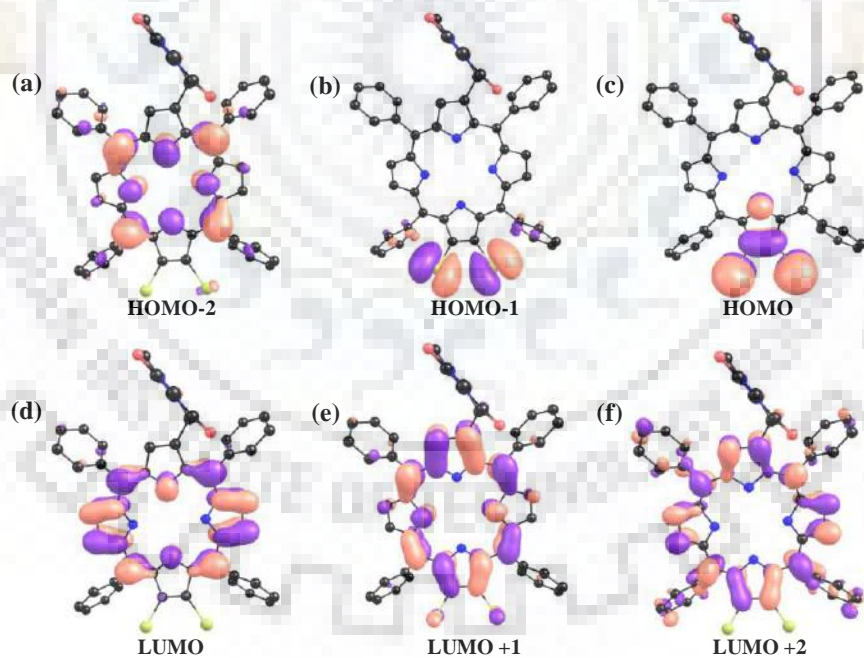




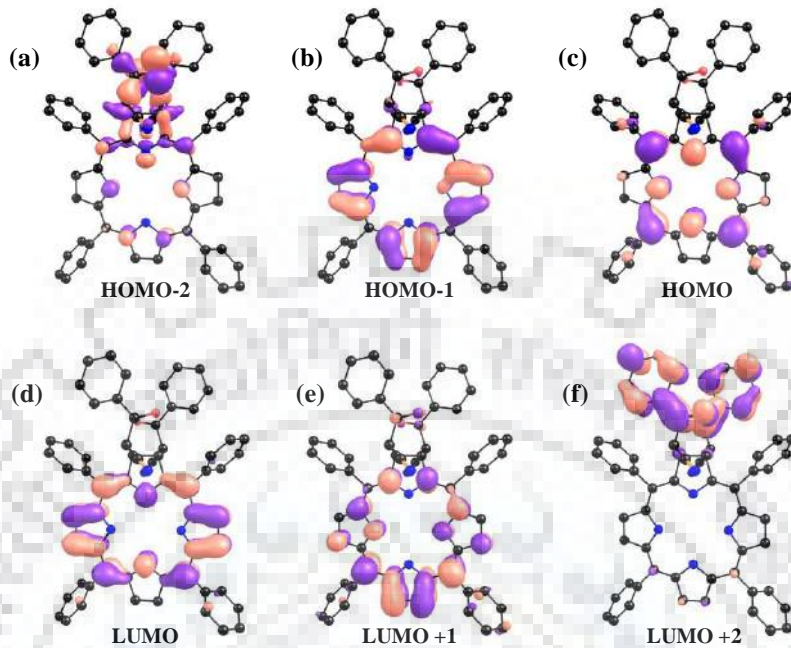
**Figure A4.** Pictorial Representation of Frontier Molecular Orbitals of  $H_2TPP(DMBA)$  (3).



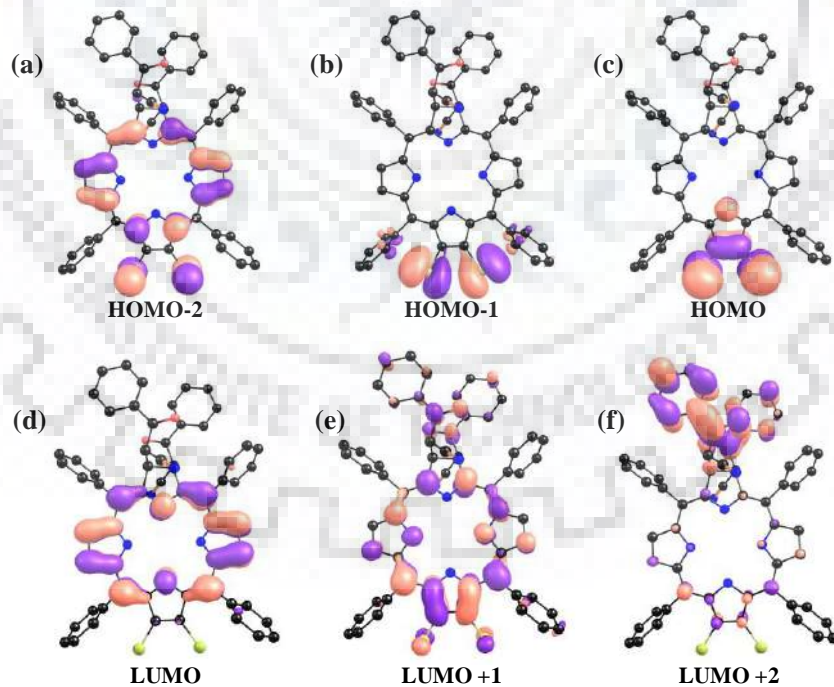
**Figure A5.** Pictorial Representation of Frontier Molecular Orbitals of  $H_2TPPBr_2(DMBA)$  (4).



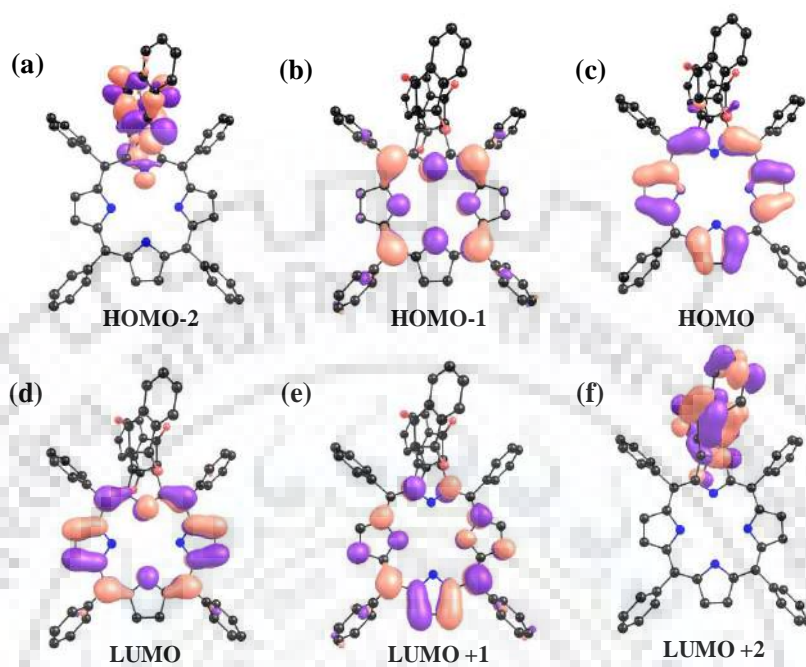
**Figure A6.** Pictorial Representation of Frontier Molecular Orbitals of  $H_2TPC(BENAC)_2$  (**8**).



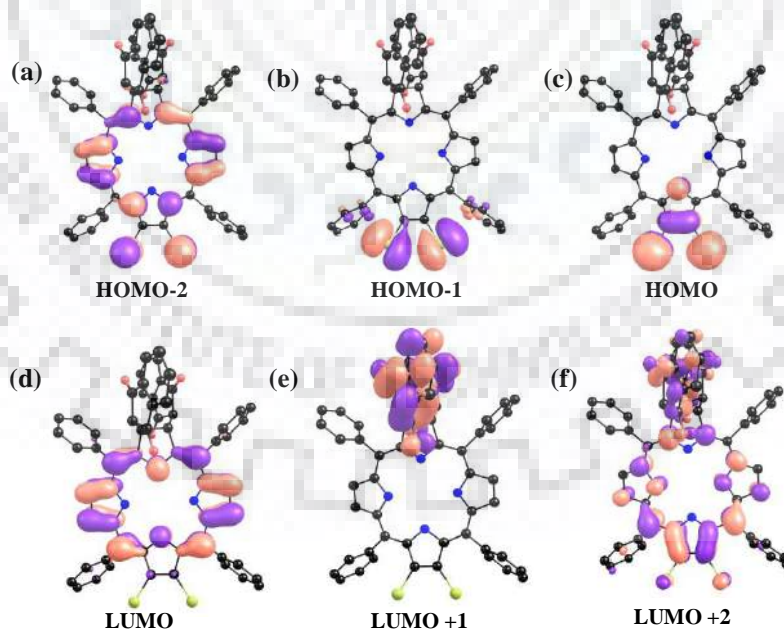
**Figure A7.** Pictorial Representation of Frontier Molecular Orbitals of  $H_2TPCBr_2(BENAC)_2$  (**9**).



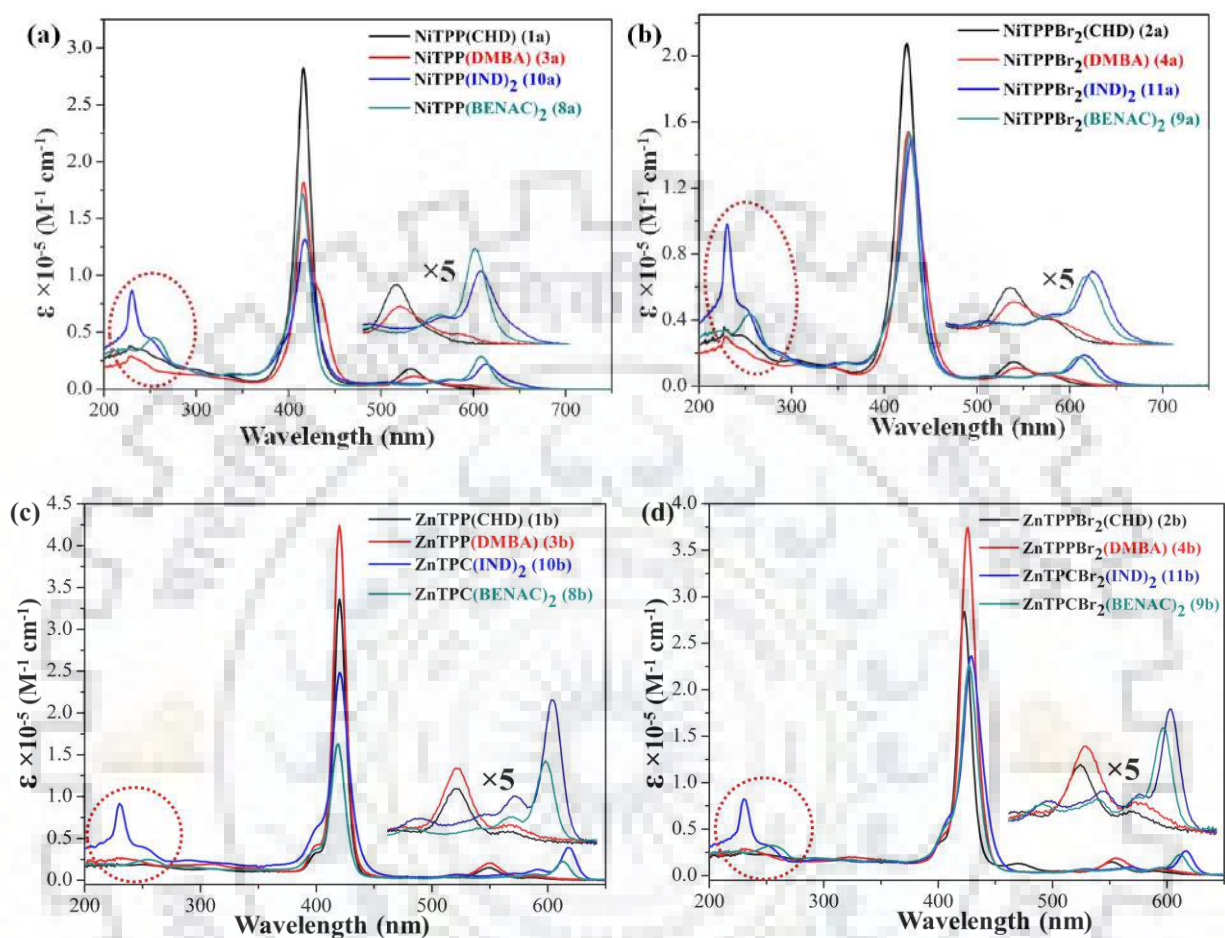
**Figure A8.** Pictorial Representation of Frontier Molecular Orbitals of  $H_2TPC(IND)_2$  (**10**).



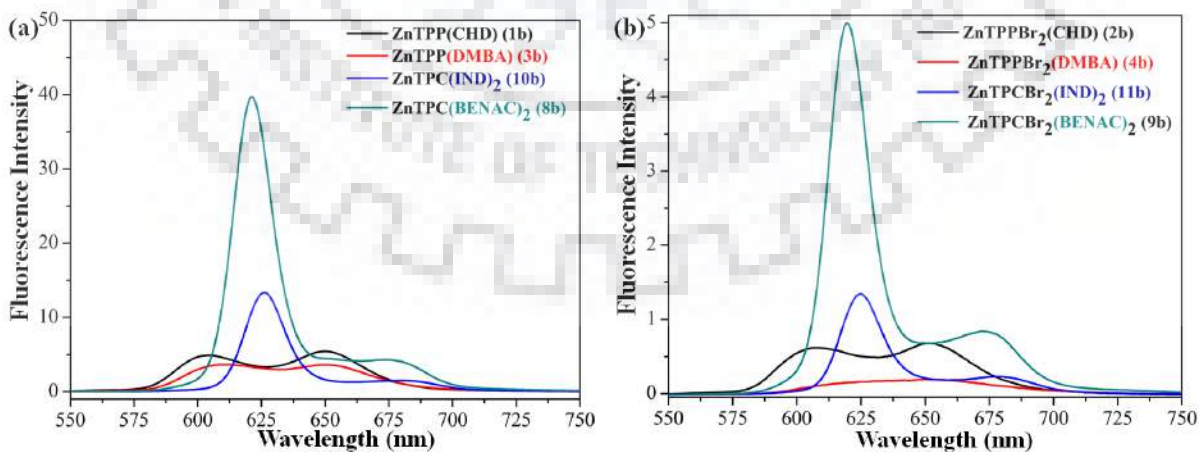
**Figure SA9** Pictorial Representation of Frontier Molecular Orbitals of  $H_2TPCBr_2(IND)_2$  (**11**).



**Figure A10.** Electronic Absorption Spectra of Synthesized Ni(II) and Zn(II) Complexes. Circled Area Shows The Absorption due to Benzoylacetonitrile and Indane-1,3-dione.



**Figure A11.** Fluorescence Spectra of Synthesized Zn(II) Porphyrins and Chlorins.

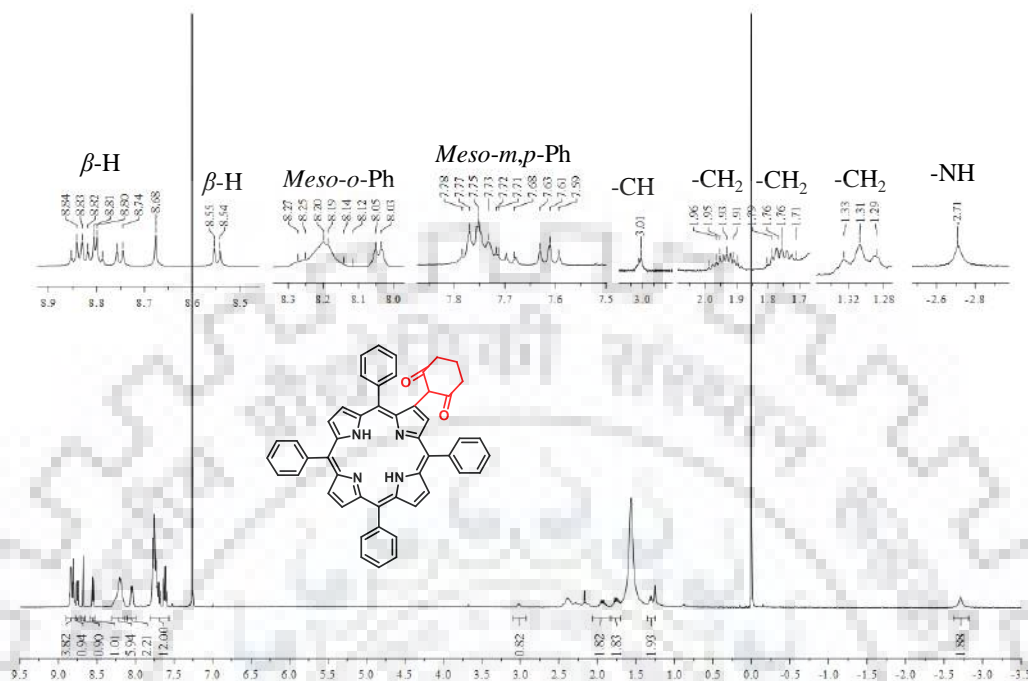
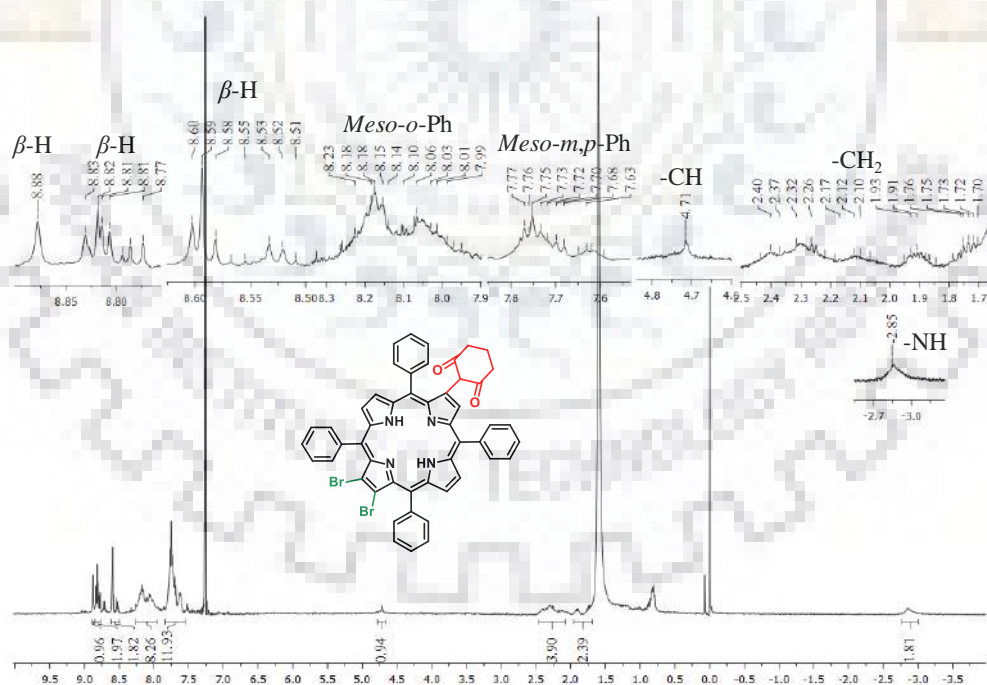




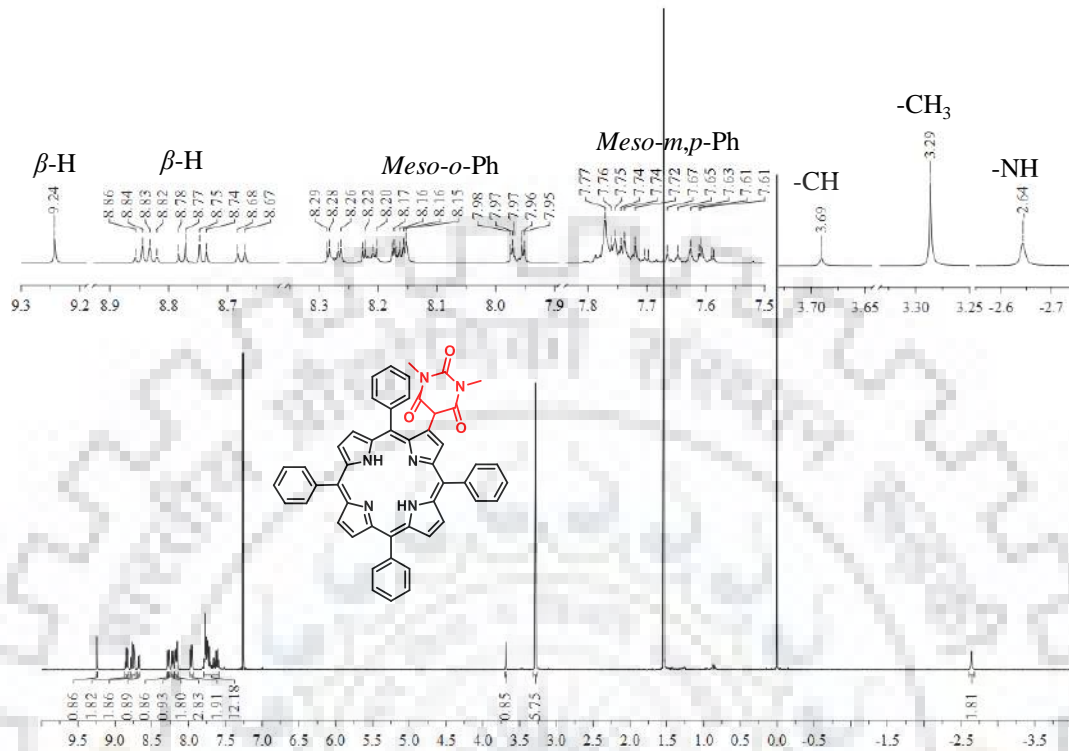
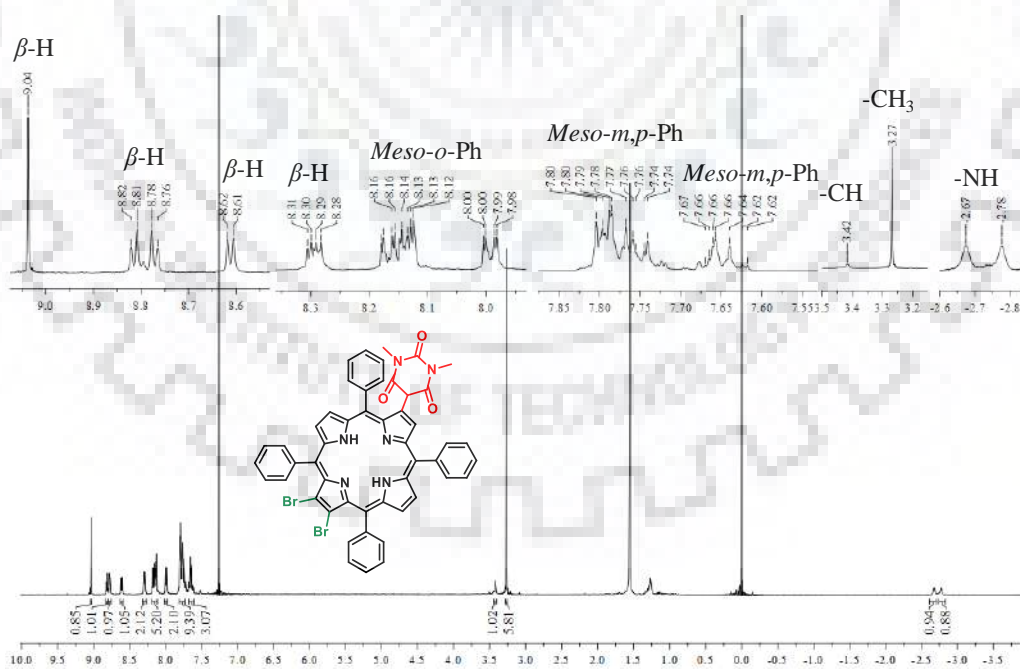
**Table A3.** Photophysical Properties of Synthetic Chlorins and porphyrins.<sup>a</sup>

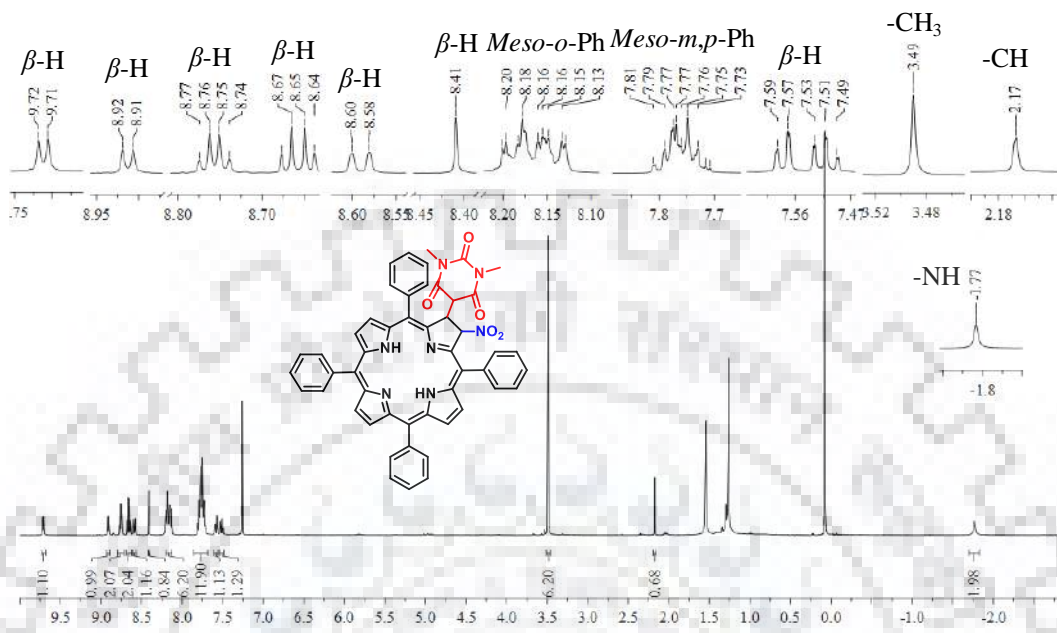
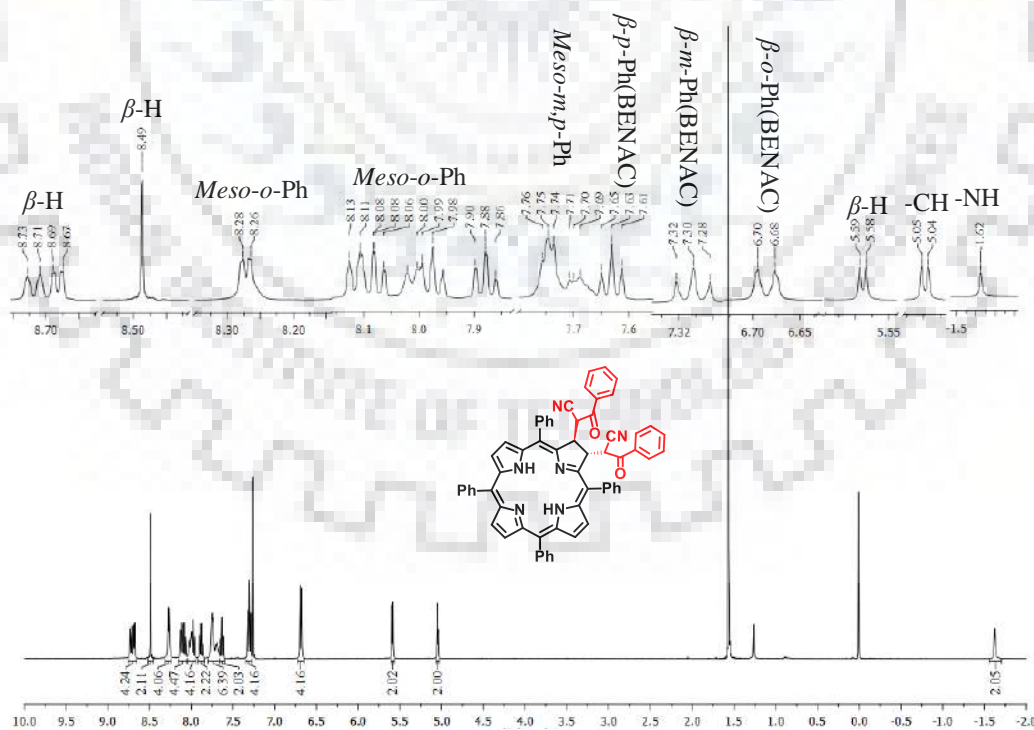
<b>Porphyrin</b>	$\lambda_{\text{abs}}$	$\lambda_{\text{em}}$	<b>Q/B</b>	$\frac{\Sigma Q}{\Sigma B^b}$	<b><i>f</i></b>
NiTPP(CHD) ( <b>1a</b> )	416(5.45), 533(4.25)		0.064	0.11	0.025
NiTPP Br <sub>2</sub> (CHD) ( <b>2a</b> )	424(5.31), 540(4.16), 578(3.81)		0.071	0.11	0.023
NiTPP(DMBA) ( <b>3a</b> )	416(5.25), 536(4.06), 592(3.52)		0.063	0.10	0.019
NiTPP Br <sub>2</sub> (DMBA) ( <b>4a</b> )	426(5.33), 540(4.17), 582(3.88)		0.067	0.12	0.021
NiTPC(BENAC) <sub>2</sub> ( <b>8a</b> )	253(4.65), 415(5.23), 506(3.71), 570(3.94), 608(4.46)		0.170	0.17	0.016
NiTPCBr <sub>2</sub> (BENAC) <sub>2</sub> ( <b>9a</b> )	255(4.64), 427(5.19), 520(3.76), 572(3.85), 610(4.24)		0.110	0.17	0.017
NiTPC(IND) <sub>2</sub> ( <b>10a</b> )	230(4.94), 417(5.12), 505(3.78), 577(3.91), 615(4.34)		0.170	0.21	0.016
NiTPCBr <sub>2</sub> (IND) <sub>2</sub> ( <b>11a</b> )	230(4.99), 429(5.17), 515(3.79), 573(3.88), 617(4.27)		0.130	0.18	0.019
NiTPP(BENAC) ( <b>5</b> )	418(5.34), 534(4.12)		0.061	0.09	0.019
NiTPPBr <sub>2</sub> (BENAC) ( <b>6</b> )	247(4.51), 426(5.33), 540(4.16), 581(3.88)		0.067	0.07	0.023
ZnTPP(CHD) ( <b>1b</b> )	420(5.53), 549(4.17), 586(3.54)	602, 650	0.010	0.08	0.018
ZnTPP Br <sub>2</sub> (CHD) ( <b>2b</b> )	423(5.45), 552(4.17), 590(3.71)	607, 651	0.052	0.08	0.021
ZnTPP(DMBA) ( <b>3b</b> )	420(5.63), 549(4.31), 587(3.71)	609, 650	0.048	0.09	0.024
ZnTPP Br <sub>2</sub> (DMBA) ( <b>4b</b> )	426(5.57), 556(4.27), 592(3.85)	652	0.050	0.08	0.027
ZnTPC(IND) <sub>2</sub> ( <b>10b</b> )	230(4.96), 420(5.39), 520(3.84), 590(4.11), 618(4.59)	626, 678	0.157	0.10	0.019
ZnTPC Br <sub>2</sub> (IND) <sub>2</sub> ( <b>11b</b> )	230(4.92), 429(5.37), 531(3.86), 568(3.96), 617(4.42)	625, 678	0.112	0.10	0.022
ZnTPC(BENAC) <sub>2</sub> ( <b>8b</b> )	255(4.39), 419(5.21), 515(3.62), 588(3.86), 613(4.35)	621, 671	0.138	0.11	0.011
ZnTPC Br <sub>2</sub> (BENAC) <sub>2</sub> ( <b>9b</b> )	254(4.51), 427(5.36), 524(3.82), 563(3.88), 611(4.35)	619, 678	0.099	0.08	0.017

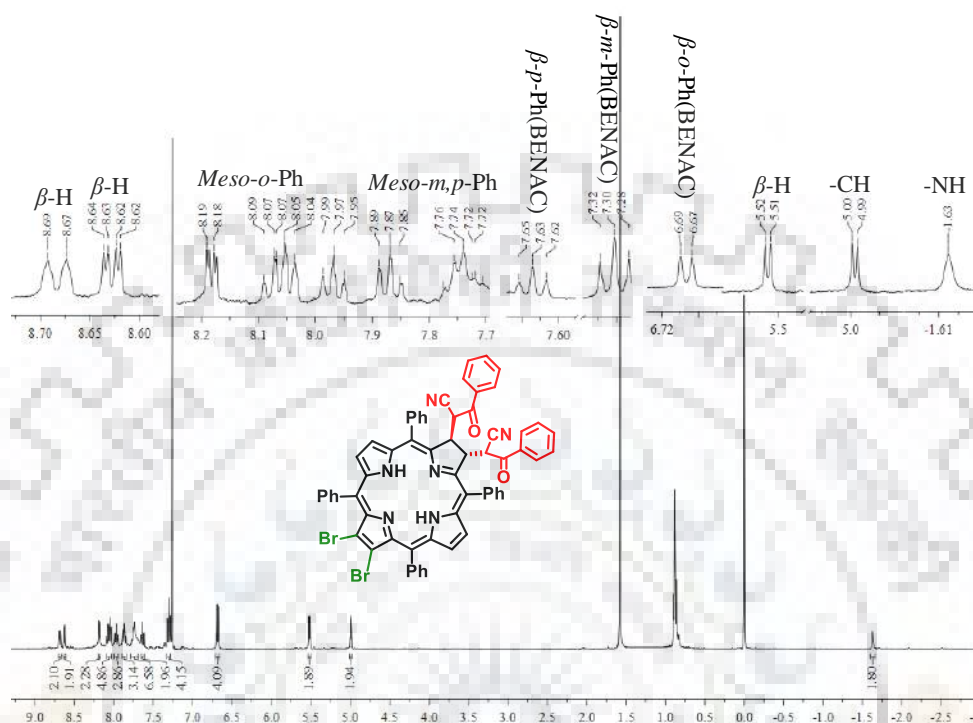
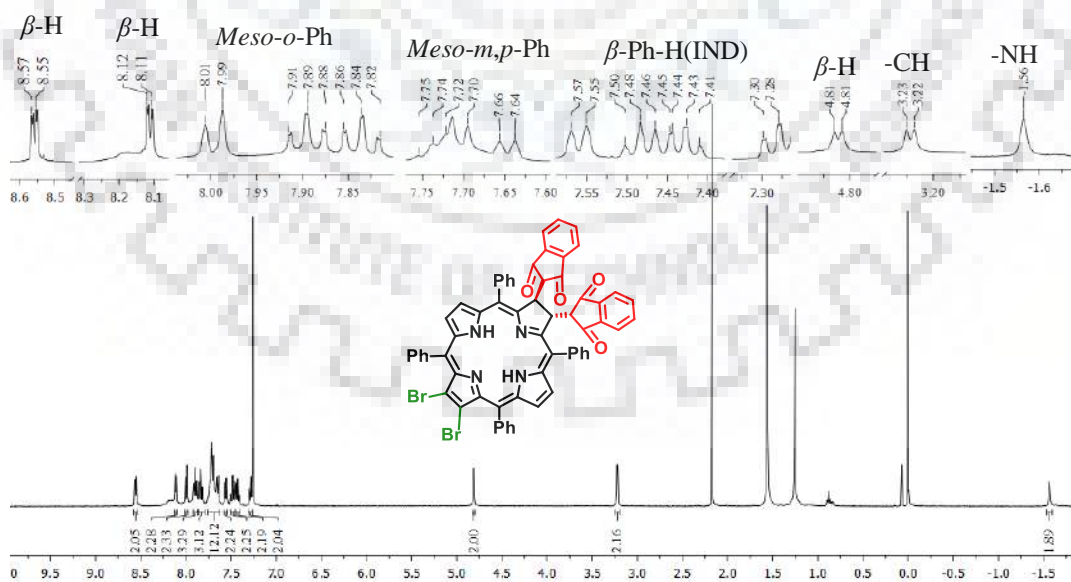
<sup>a</sup>The values in parentheses refer to log $\epsilon$ , integrated ( $\Sigma B/\Sigma Q$ ) intensity ratios of the Q and Soret (B) absorption,  $f$  = Oscillator Strength

**Figure A12.**  $^1\text{H}$  NMR Spectrum of  $\text{H}_2\text{TPP}(\text{CHD})$  (**1**) in  $\text{CDCl}_3$  at 298 K.**Figure A13.**  $^1\text{H}$  NMR Spectrum of  $\text{H}_2\text{TPPBr}_2(\text{CHD})$  (**2**) in  $\text{CDCl}_3$  at 298 K.

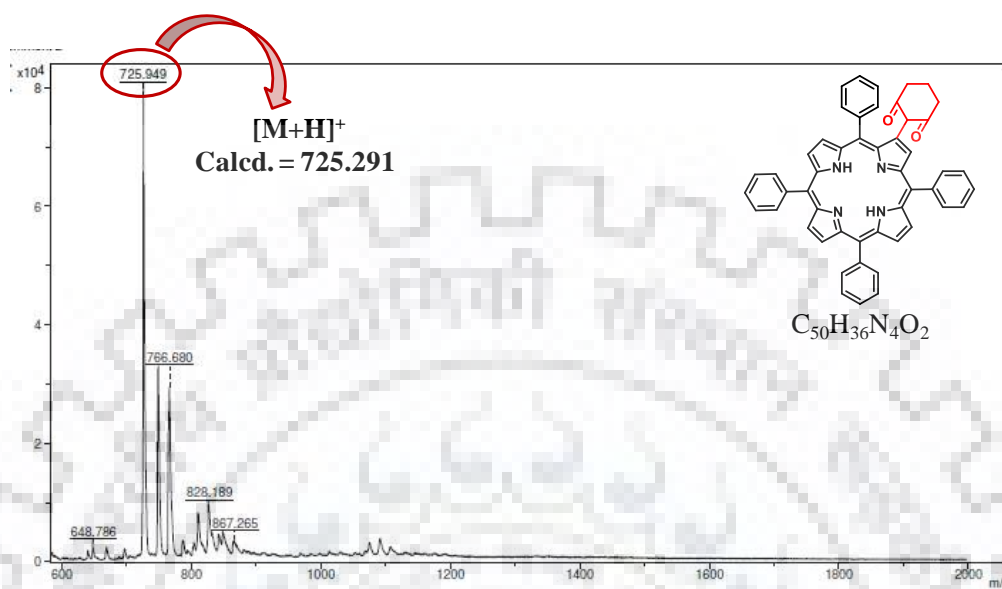


**Figure A14.**  $^1\text{H}$  NMR Spectrum of  $\text{H}_2\text{TPP}(\text{DMBA})$  (**3**) in  $\text{CDCl}_3$  at 298 K.**Figure A15.**  $^1\text{H}$  NMR Spectrum of  $\text{H}_2\text{TPPBr}_2(\text{DMBA})$  (**4**) in  $\text{CDCl}_3$  at 298 K.

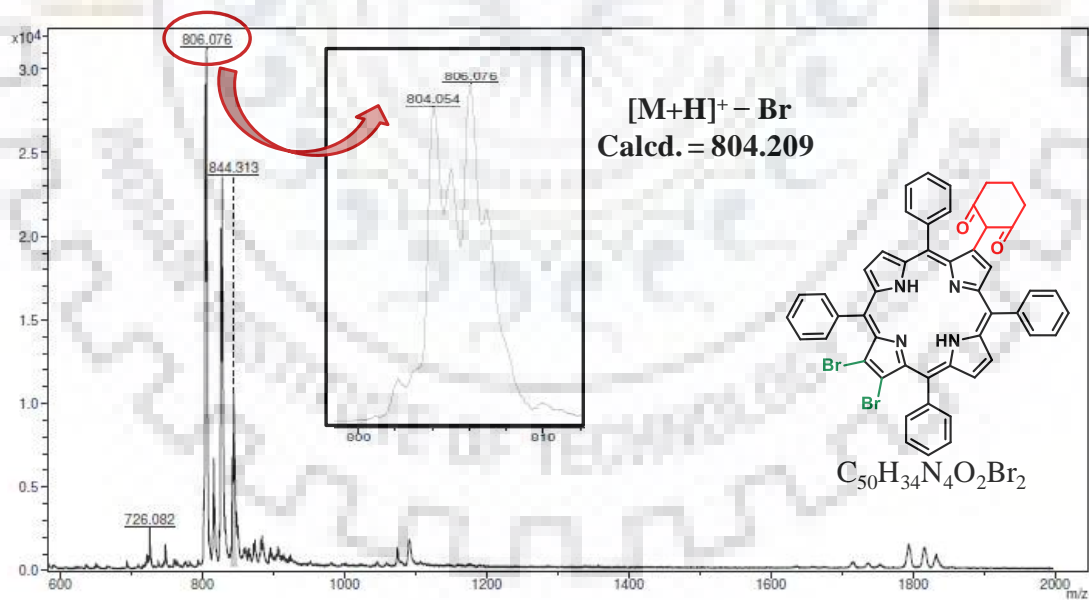
**Figure A16.**  $^1\text{H}$  NMR Spectrum of  $\text{H}_2\text{TPP}(\text{NO}_2)(\text{DMBA})$  (**7**) in  $\text{CDCl}_3$  at 298 K.**Figure A17.**  $^1\text{H}$  NMR Spectrum of  $\text{H}_2\text{TPC}(\text{BENAC})_2$  (**8**) in  $\text{CDCl}_3$  at 298 K.

**Figure A18.**  $^1\text{H}$  NMR Spectrum of  $\text{H}_2\text{TPCBr}_2(\text{BENAC})_2$  (**9**) in  $\text{CDCl}_3$  at 298 K.**Figure A19.**  $^1\text{H}$  NMR Spectrum of  $\text{H}_2\text{TPCBr}_2(\text{IND})_2$  (**11**) in  $\text{CDCl}_3$  at 298 K.

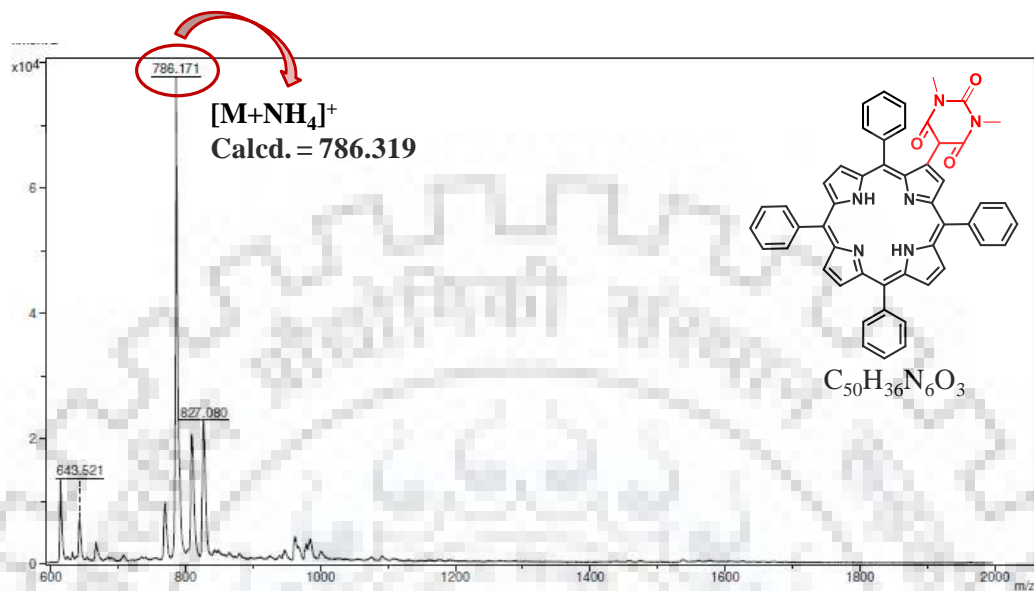
**Figure A20.** MALDI-TOF Mass Spectrum of  $H_2TPP(CHD)$  (**1**) in  $CH_2Cl_2$  at 298 K.



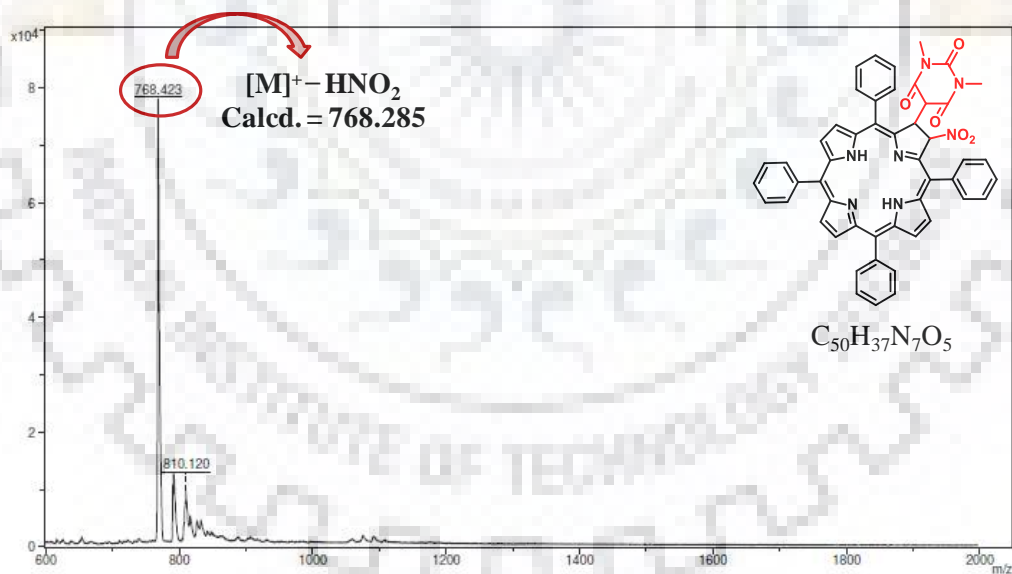
**Figure A21.** MALDI-TOF Mass Spectrum of  $H_2TPPBr_2(CHD)$  (**2**) in  $CH_2Cl_2$  at 298 K.



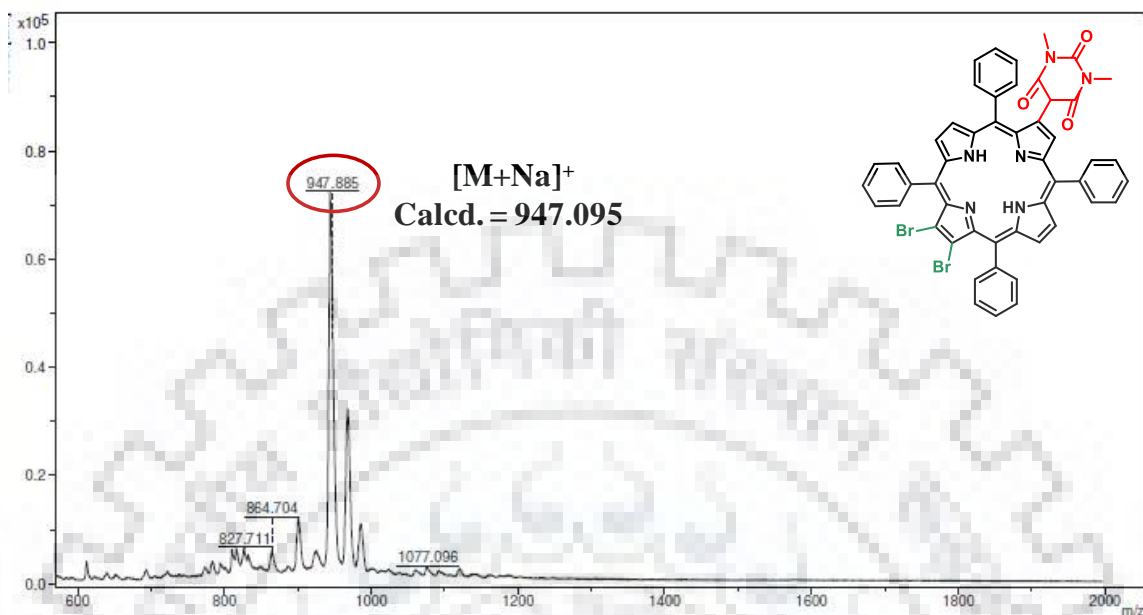
**Figure A22.** MALDI-TOF Mass Spectrum of H<sub>2</sub>TPP(DMBA) (**3**) in CH<sub>2</sub>Cl<sub>2</sub> at 298 K.



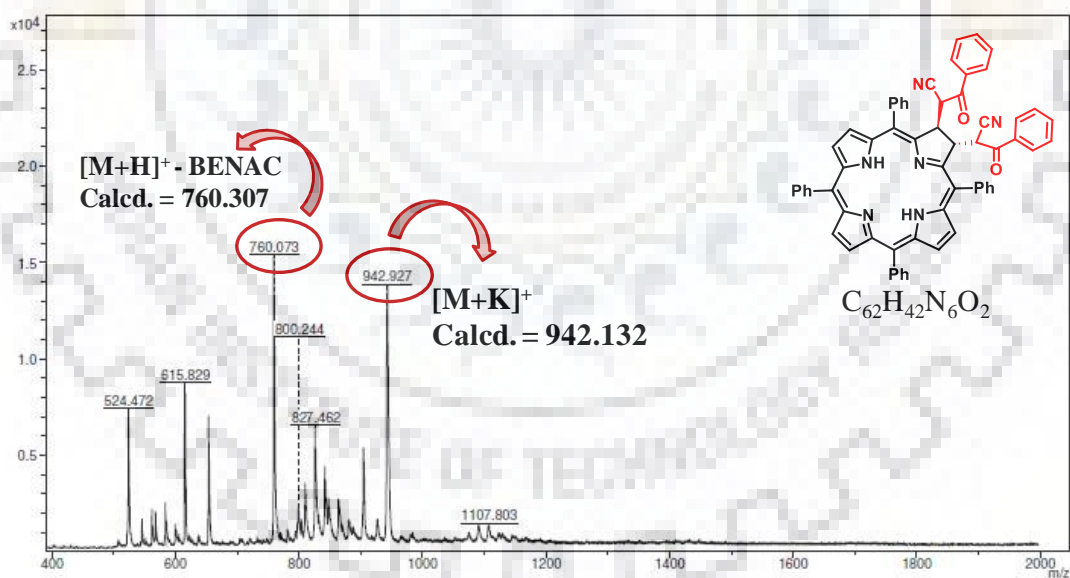
**Figure A23.** MALDI-TOF Mass Spectrum of H<sub>2</sub>TPP(NO<sub>2</sub>)(DMBA) (**7**) in CH<sub>2</sub>Cl<sub>2</sub> at 298 K.



**Figure A24.** MALDI-TOF Mass Spectrum of  $H_2TPPBr_2(DMBA)$  (**4**) in  $CH_2Cl_2$  at 298 K.

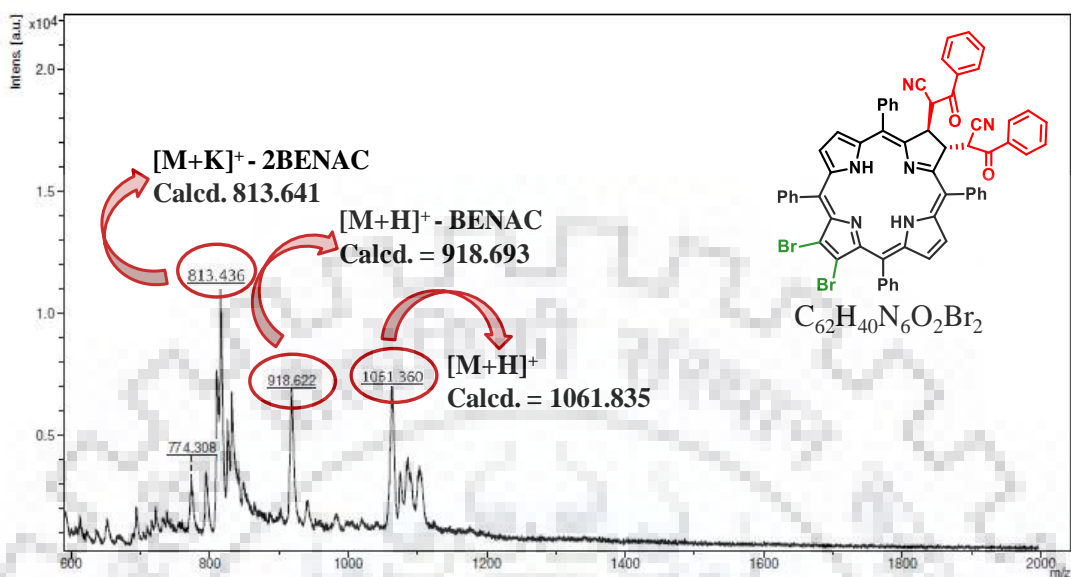


**Figure A25.** MALDI-TOF Mass Spectrum of  $H_2TPC(BENAC)_2$  (**8**) in  $CH_2Cl_2$  at 298 K.

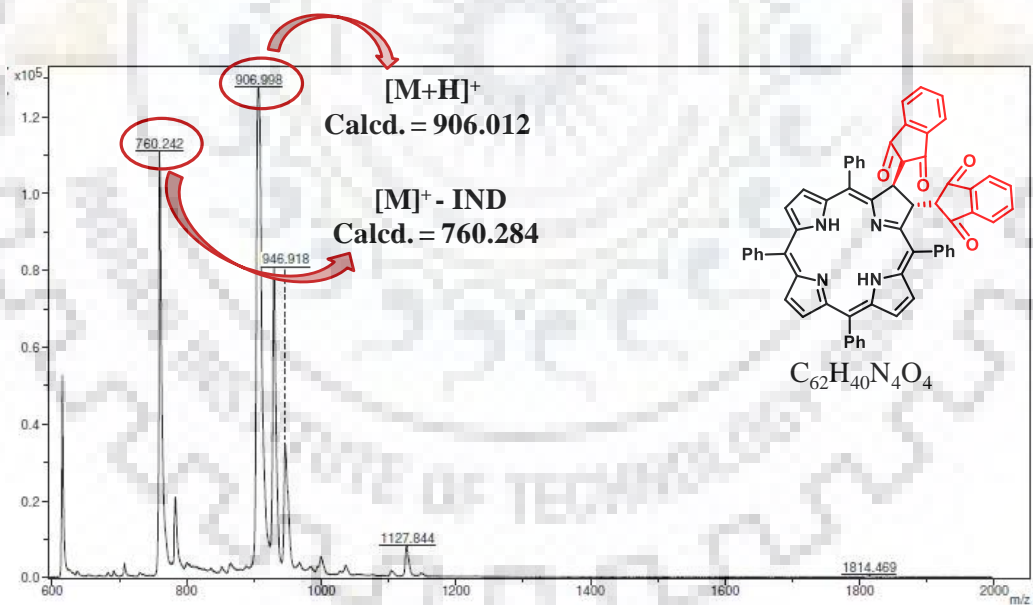


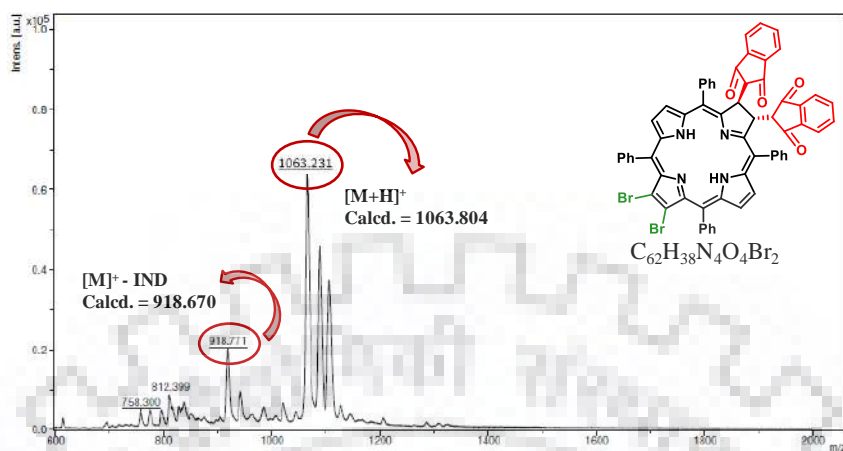
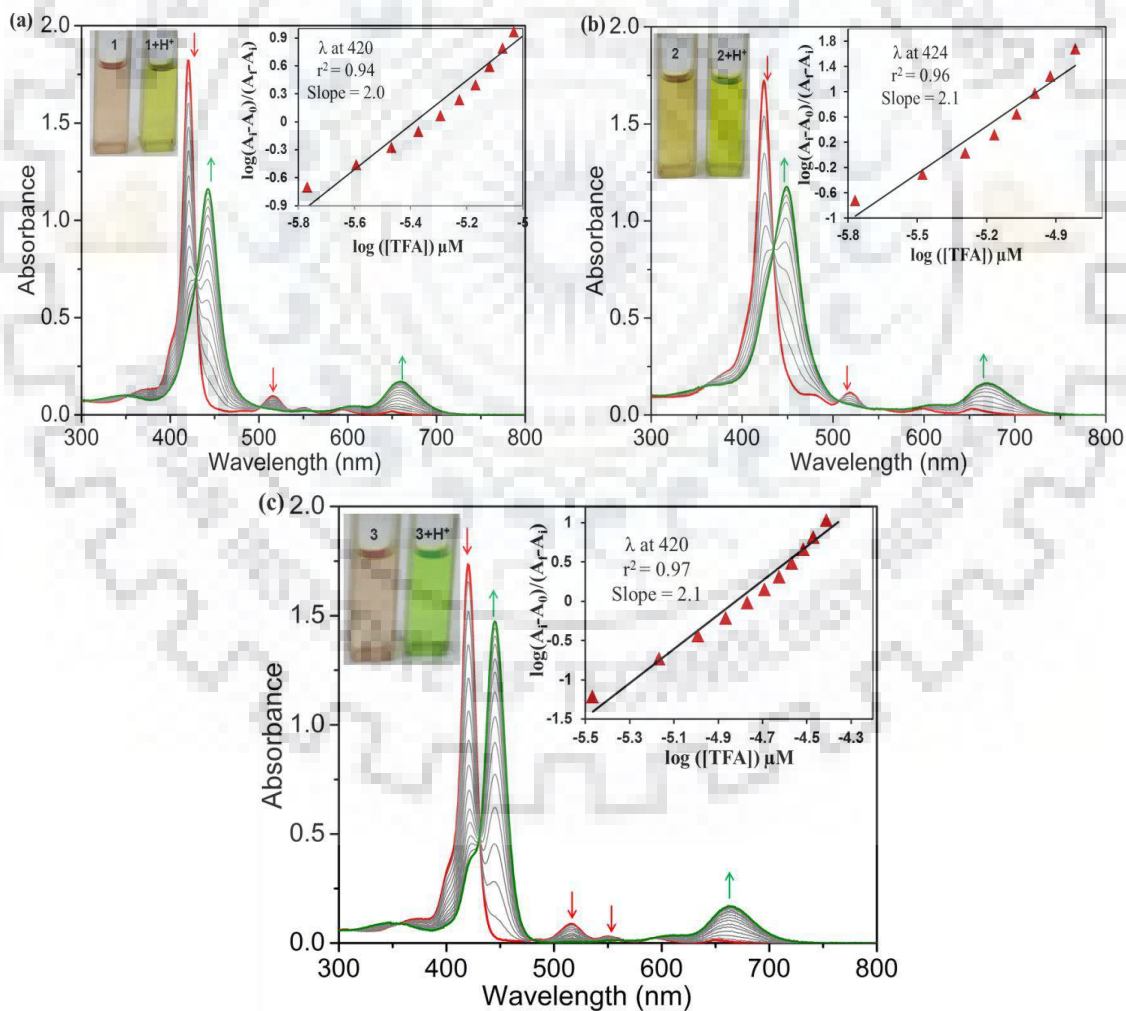


**Figure A26.** MALDI-TOF Mass Spectrum of  $H_2TPCBr_2(BENAC)_2$  (**9**) in  $CH_2Cl_2$  at 298 K.



**Figure A27.** MALDI-TOF Mass Spectrum of  $H_2TPC(IND)_2$  (**10**) in  $CH_2Cl_2$  at 298 K.



**Figure A28.** MALDI-TOF Mass Spectrum of  $\text{H}_2\text{TTPCBr}_2(\text{IND})_2$  (**11**) in  $\text{CH}_2\text{Cl}_2$  at 298 K.**Figure A29.** UV-vis. Spectral Titrations of Synthesized Free Base Porphyrins (a)  $\text{H}_2\text{TPP}(\text{CHD})$  (**1**), (b)  $\text{H}_2\text{TPPBr}_2(\text{CHD})$  (**2**), and (c)  $\text{H}_2\text{TPP}(\text{DMBA})$  (**3**) with TFA in Toluene at 298 K.

**Figure A30.** UV-vis. Spectral Titrations of Synthesized Free Base Chlorins (a)  $\text{H}_2\text{TPC}(\text{BENAC})_2$  (**8**), (b)  $\text{H}_2\text{TPCBr}_2(\text{BENAC})_2$  (**9**), and (c)  $\text{H}_2\text{TPC}(\text{IND})_2$  (**10**) with TFA in toluene at 298 K.

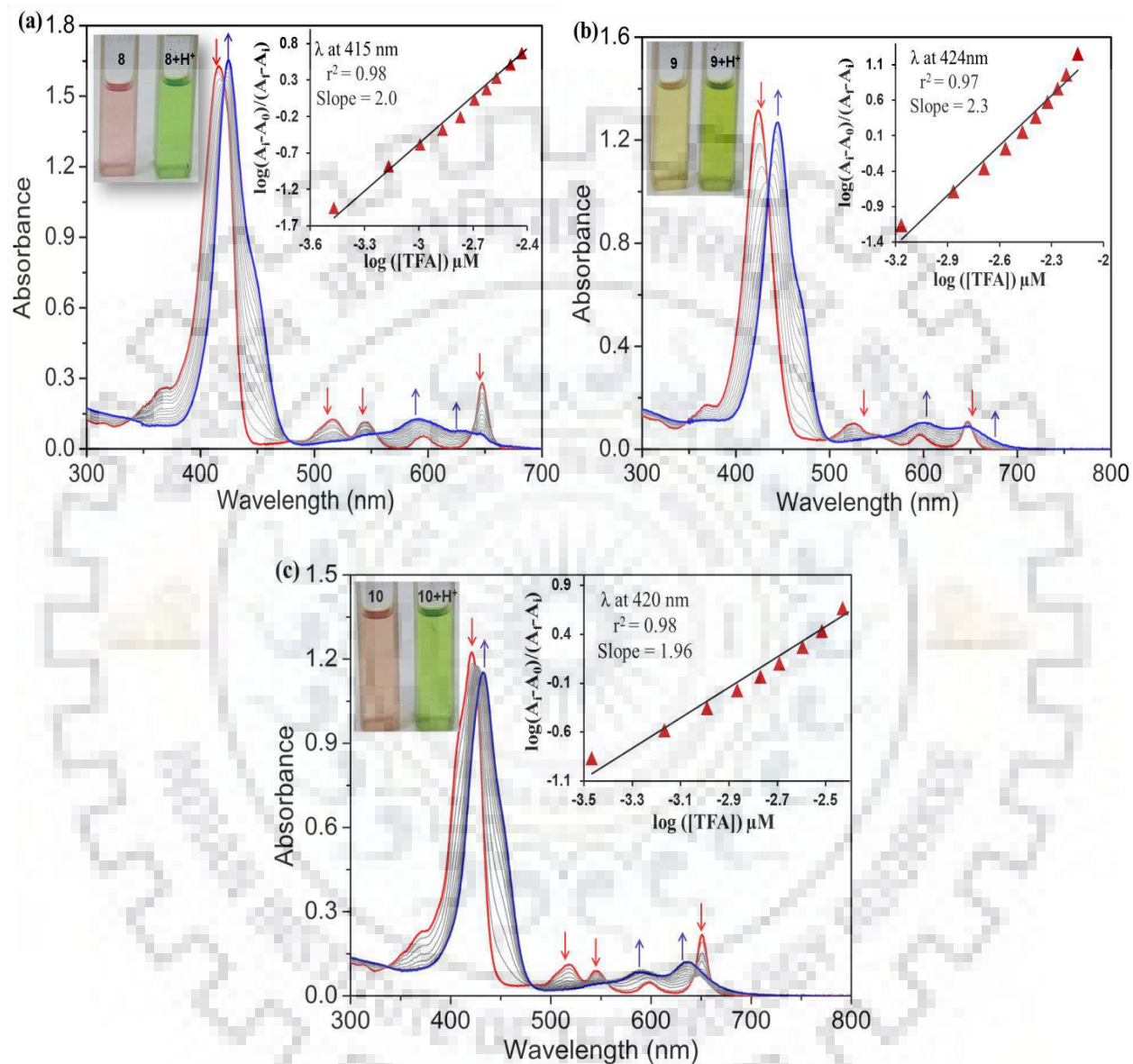


**Figure A31.** UV-vis. Spectral Titrations of Synthesized Free Base Porphyrins (a)  $H_2TPP(CHD)$  (1), (b)  $H_2TPPBr_2(CHD)$  (2), and (c)  $H_2TPPBr_2(DMBA)$  (3) with TBAOH in Toluene at 298 K.

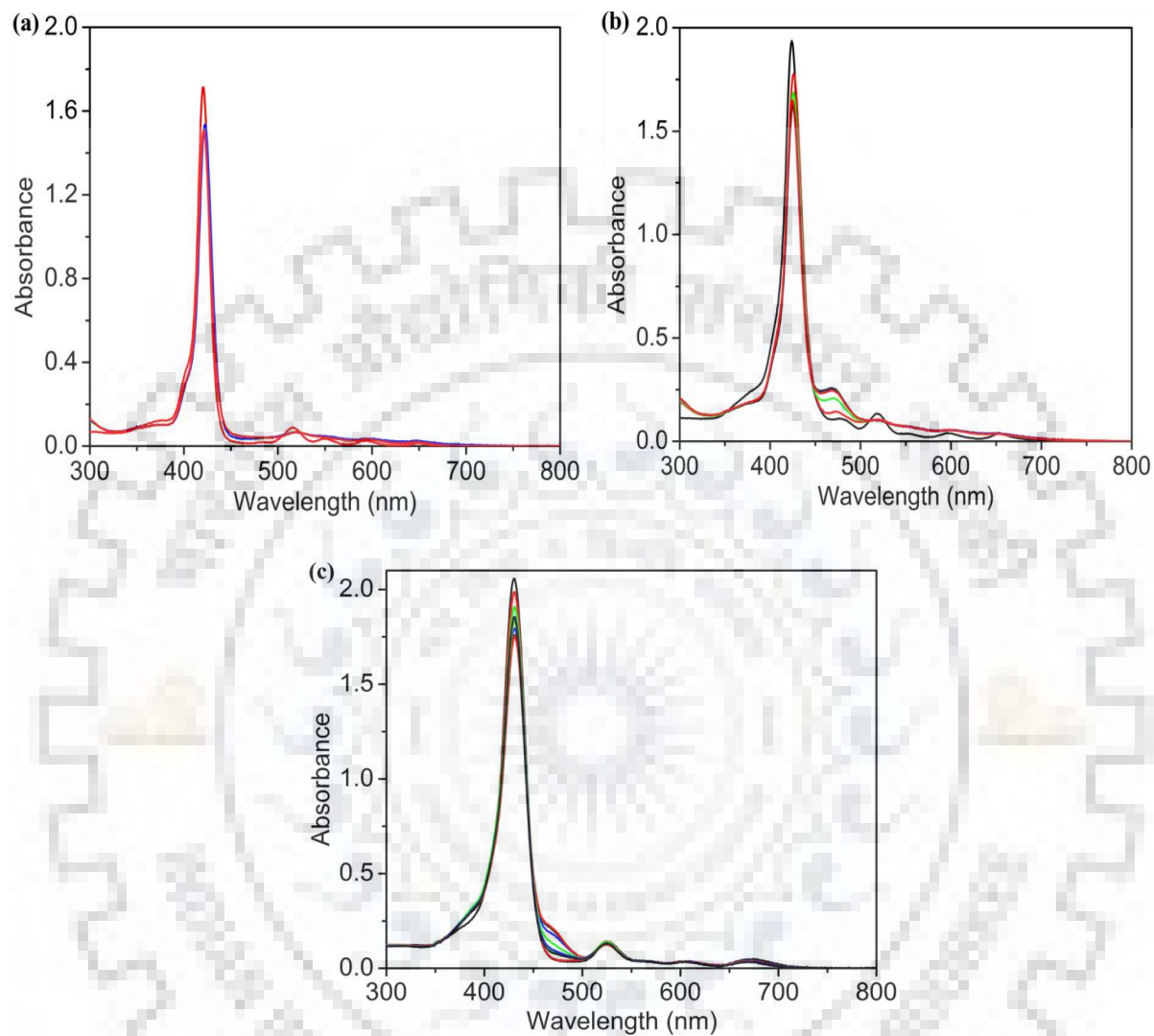


**Figure A32.** UV-vis. Spectral Titrations of Synthesized Free Base Chlorins H<sub>2</sub>TPC(BENAC)<sub>2</sub> (**8**), (b) H<sub>2</sub>TPCBr<sub>2</sub>(BENAC)<sub>2</sub> (**9**), and (c) H<sub>2</sub>TPCBr<sub>2</sub>(IND)<sub>2</sub> (**11**) with TBAOH in Toluene at 298 K.

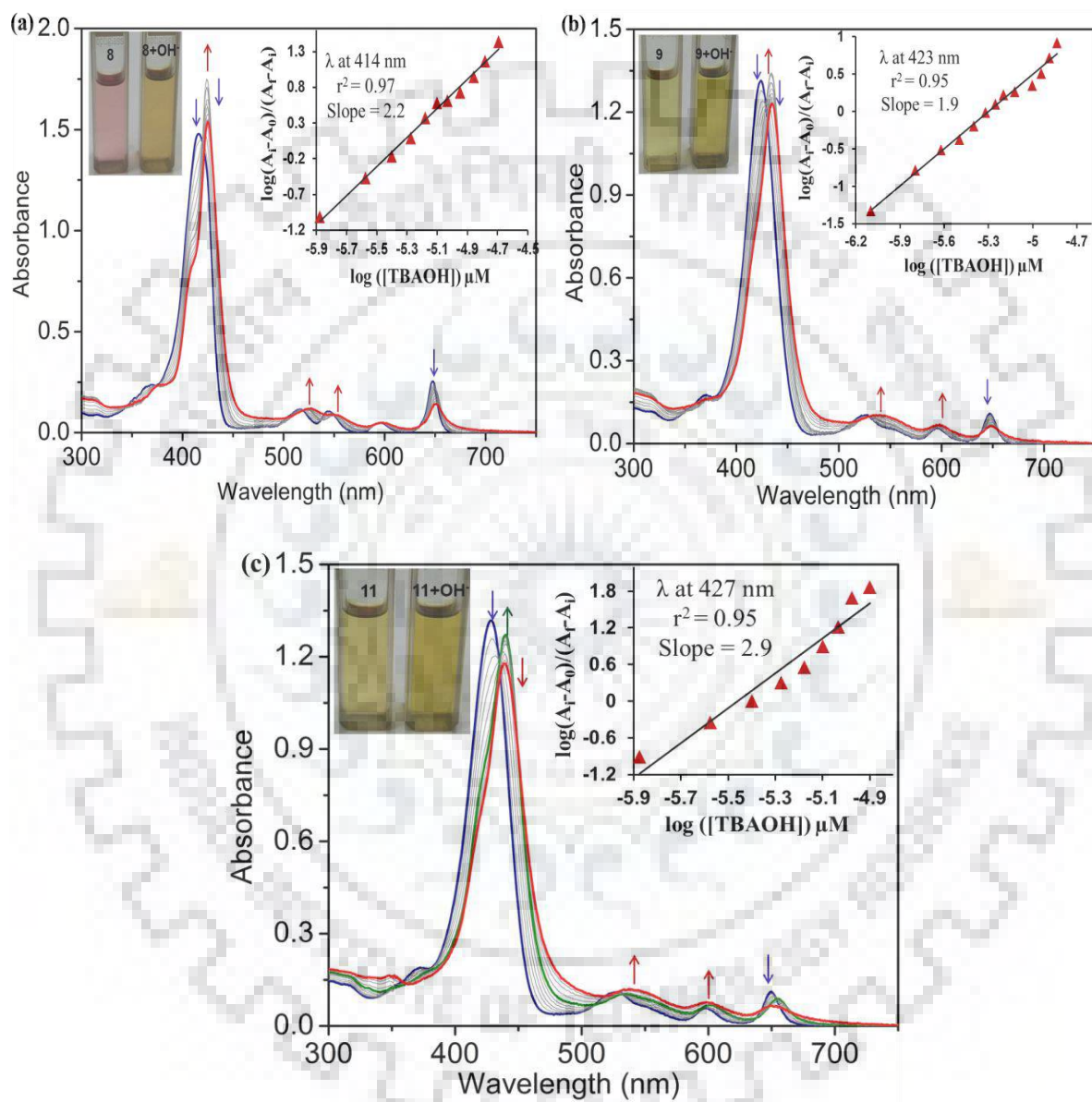


**Figure A33.** Comparative Cyclic Voltammograms of Synthesized Free Base Chlorins.

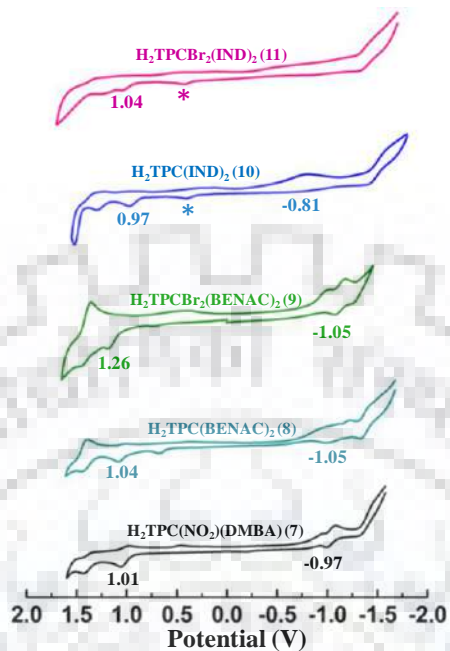
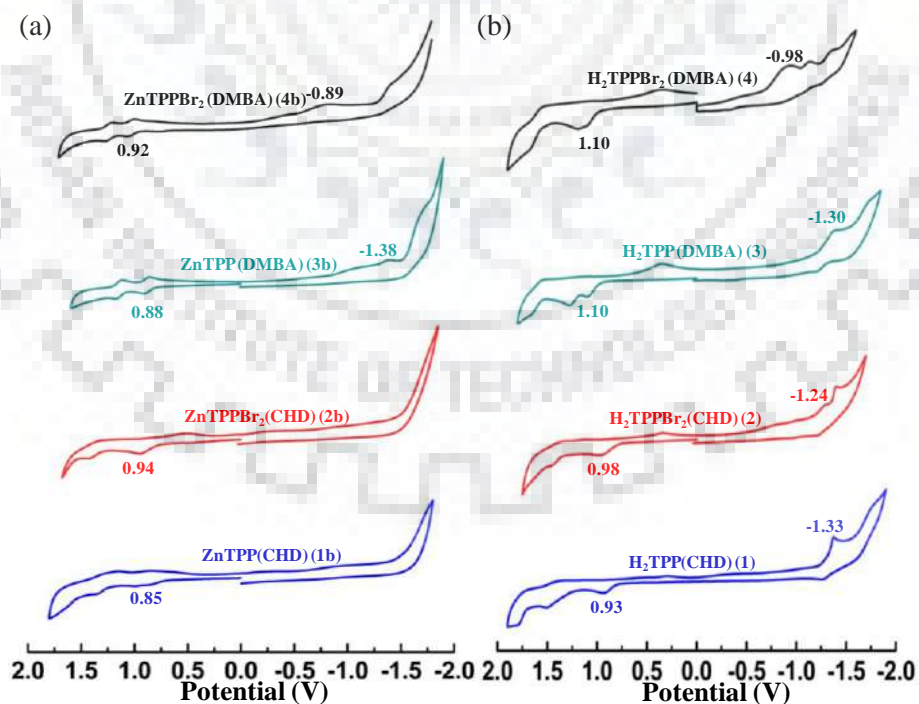


**Figure A34.** Comparative Cyclic Voltammograms of (a) Zn(II) Porphyrins (b) Free Base Porphyrins.





## APPENDIX-II

**Regioselective Conversion of Planar *trans*-Chlorins into Highly Twisted Doubly Fused-Porphyrins (DFPs) or -Chlorins (DFCs) via Oxidative Fusion**

Table of Contents	Page No.
<b>Figure A1.</b> <sup>1</sup> H NMR Spectrum of NiDFP(IND) <sub>2</sub> ( <b>1</b> ) in CDCl <sub>3</sub> at 298 K.	259
<b>Figure A2.</b> <sup>1</sup> H NMR Spectrum of H <sub>2</sub> DFC(IND) <sub>2</sub> ( <b>4</b> ) in CDCl <sub>3</sub> at 298 K.	259
<b>Figure A3.</b> <sup>1</sup> H NMR Spectrum of H <sub>2</sub> DFP(IND) <sub>2</sub> ( <b>4a</b> ) in CDCl <sub>3</sub> at 298 K.	260
<b>Figure A4.</b> <sup>1</sup> H NMR Spectrum of NiDFP(MN) <sub>2</sub> ( <b>7</b> ) in CDCl <sub>3</sub> at 298 K.	260
<b>Figure A5.</b> <sup>1</sup> H NMR Spectrum of H <sub>2</sub> DFC(MN) <sub>2</sub> ( <b>10</b> ) in CDCl <sub>3</sub> at 298 K.	261
<b>Figure A6.</b> MALDI-TOF Mass Spectrum of NiDFP(IND) <sub>2</sub> ( <b>1</b> ).	261
<b>Figure A7.</b> MALDI-TOF Mass Spectrum of H <sub>2</sub> DFP(IND) <sub>2</sub> ( <b>4a</b> ).	262
<b>Figure A8.</b> MALDI-TOF Mass Spectrum of NiDFP(MN) <sub>2</sub> ( <b>7</b> ).	262
<b>Figure A9.</b> MALDI-TOF Mass Spectrum of H <sub>2</sub> DFC(MN) <sub>2</sub> ( <b>10</b> ).	263
<b>Figure A10.</b> ORTEP Showing Top and Side Views of H <sub>2</sub> TPC(MN) <sub>2</sub> (Ph) <sub>2</sub> .	263
<b>Figure A11.</b> Numbering of Carbon Atoms in the Macrocyclic Skeleton of (a) NiDFP(IND) <sub>2</sub> ( <b>1</b> ) (b) H <sub>2</sub> DFC(IND) <sub>2</sub> Br <sub>2</sub> ( <b>5</b> ) (c) H <sub>2</sub> TPC[CH(CN) <sub>2</sub> ] <sub>2</sub> (d) NiDFP(MN) <sub>2</sub> Br <sub>2</sub> ( <b>8</b> ) (e) NiDFC(MN) <sub>2</sub> Br <sub>2</sub> ( <b>8a</b> ).	264
<b>Figure A12.</b> Displacement of Atoms From the Mean Plane of (a) H <sub>2</sub> DFC(IND) <sub>2</sub> Br <sub>2</sub> ( <b>5</b> ) (b) NiDFP(IND) <sub>2</sub> ( <b>1</b> ) (c) NiDFC(MN) <sub>2</sub> Br <sub>2</sub> ( <b>8a</b> ) (d) H <sub>2</sub> TPC[CH(CN) <sub>2</sub> ] <sub>2</sub> (e) NiDFP(MN) <sub>2</sub> Br <sub>2</sub> ( <b>8</b> ).	265
<b>Figure A13.</b> Frontier molecular orbitals of NiDFP(IND) <sub>2</sub> ( <b>1</b> ).	265
<b>Figure A14.</b> Frontier Molecular Orbitals of H <sub>2</sub> DFC(IND) <sub>2</sub> ( <b>4</b> ).	266
<b>Figure A15.</b> Frontier Molecular Orbitals of NiDFP(MN) <sub>2</sub> ( <b>7</b> ).	266
<b>Figure A16.</b> (a) Comparative UV-Vis Absorption Spectra and (b) Emission Spectra of	267

H<sub>2</sub>DFC(MN)<sub>2</sub> (**10**) and Precursor H<sub>2</sub>TPC(MN)<sub>2</sub> in CH<sub>2</sub>Cl<sub>2</sub> at 298K.

**Figure A17.** Comparative Absorption Spectra of (a) NiTPC(IND)<sub>2</sub> and NiDFP(IND)<sub>2</sub> (**1**) (b) 267  
NiTPC[CH(CN)<sub>2</sub>]<sub>2</sub> and NiDFP(MN)<sub>2</sub> (**7**).

**Figure A18.** Comparative Cyclic Voltammograms of (a) NiDFP(IND)<sub>2</sub>X<sub>2</sub> (b) 268  
H<sub>2</sub>DFP(IND)<sub>2</sub>X<sub>2</sub> (Where X = Br, Ph).

**Figure A19.** Differential Pulse Voltammograms (DPVs) of Synthesized Fused Porphyrinoids 269  
in CH<sub>2</sub>Cl<sub>2</sub>.

**Figure A20.** Plot of HOMO-LUMO Trend in H<sub>2</sub>DFCs. 269

**Figure A21** UV-vis. Spectral Titrations of Synthesized H<sub>2</sub>DFCs (a) H<sub>2</sub>DFC(IND)<sub>2</sub> (**4**), (b) 270  
H<sub>2</sub>DFP(IND)<sub>2</sub> (**4a**), (c) H<sub>2</sub>DFC(IND)<sub>2</sub>Br<sub>2</sub> (**5**) and (d) H<sub>2</sub>DFC(IND)<sub>2</sub>Ph<sub>2</sub> (**6**) with TFA in  
CH<sub>2</sub>Cl<sub>2</sub>.

**Figure A22.** UV-vis. Spectral Titrations of Synthesized H<sub>2</sub>DFCs (a) H<sub>2</sub>DFC(MN)<sub>2</sub>Br<sub>2</sub> (**11**) 270  
and (b) H<sub>2</sub>DFC(MN)<sub>2</sub>Ph<sub>2</sub> (**12**) with TFA in CH<sub>2</sub>Cl<sub>2</sub> .

**Figure A23.** UV-vis. Spectral Titrations of Synthesized H<sub>2</sub>DFCs (a) H<sub>2</sub>DFC(MN)<sub>2</sub>Br<sub>2</sub> (**11**), 271  
(b) H<sub>2</sub>DFC(MN)<sub>2</sub>Ph<sub>2</sub> (**12**) with TBAOH in CH<sub>2</sub>Cl<sub>2</sub>.

**Figure A24.** UV-vis. Spectral Titrations of Synthesized H<sub>2</sub>DFCs (a) H<sub>2</sub>DFC(IND)<sub>2</sub> (**4**), (b) 271  
H<sub>2</sub>DFP(IND)<sub>2</sub> (**4a**), (C) H<sub>2</sub>DFC(IND)<sub>2</sub>Br<sub>2</sub> (**5**) and (d) H<sub>2</sub>DFC(IND)<sub>2</sub>Ph<sub>2</sub> (**6**) with TBAOH in  
CH<sub>2</sub>Cl<sub>2</sub>.

**Table A1.** Crystal Structure Data of H<sub>2</sub>TPC[CH(CN)<sub>2</sub>]<sub>2</sub>. 264

**Table A2.** Absorption Spectral Data of NiDFPs in CH<sub>2</sub>Cl<sub>2</sub>. 268

**Figure A1**  $^1\text{H}$  NMR Spectrum of NiDFP(IND) $_2$  (**1**) in  $\text{CDCl}_3$  at 298 K.

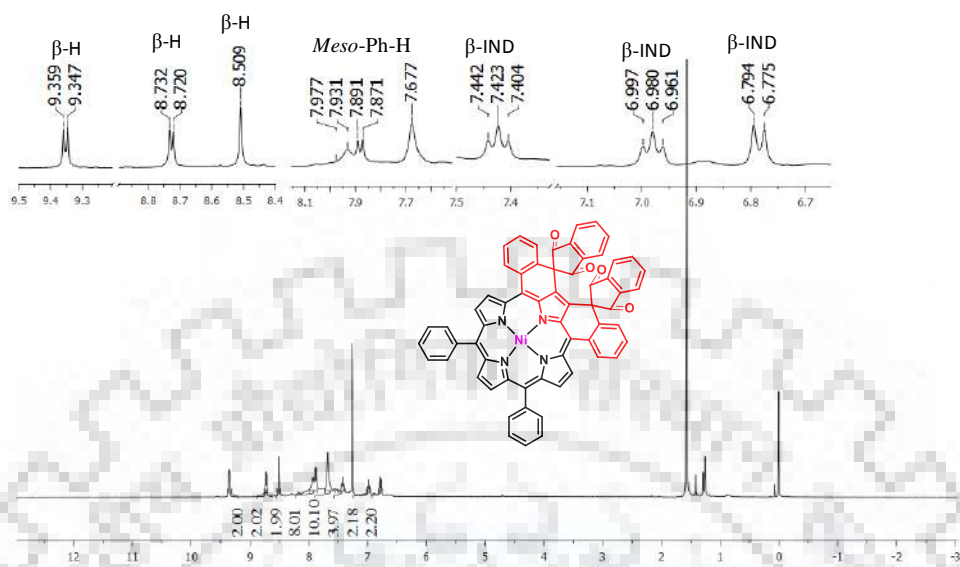


**Figure A2.**  $^1\text{H}$  NMR Spectrum of  $\text{H}_2\text{DFC}(\text{IND})_2$  (**4**) in  $\text{CDCl}_3$  at 298 K.

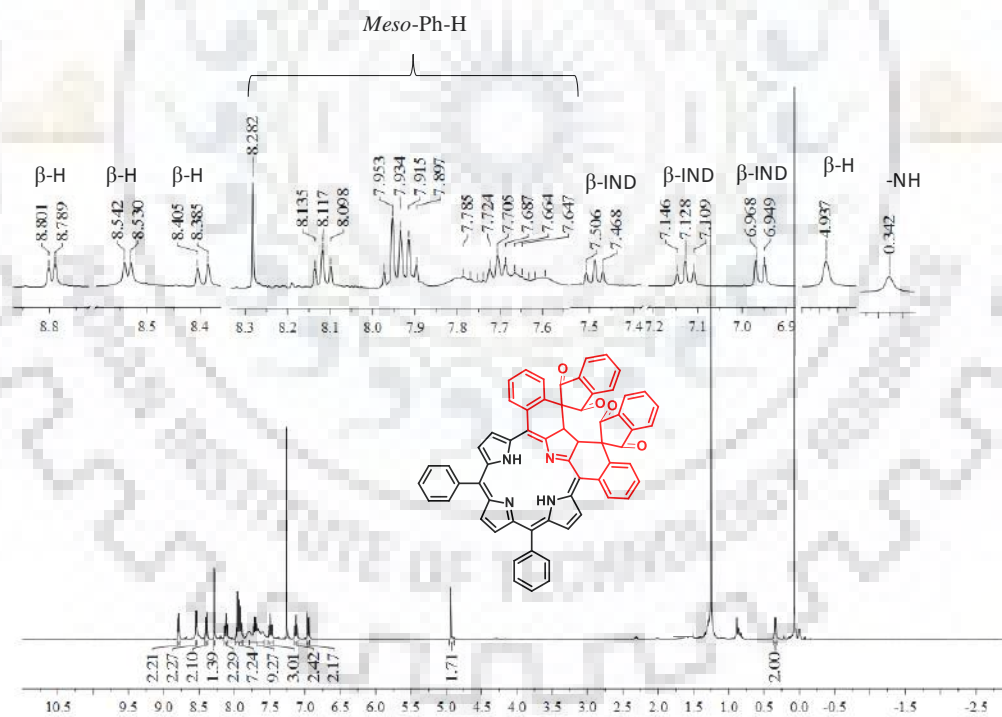


Figure A3.  $^1\text{H}$  NMR Spectrum of  $\text{H}_2\text{DFP}(\text{IND})_2$  (**4a**) in  $\text{CDCl}_3$  at 298 K.

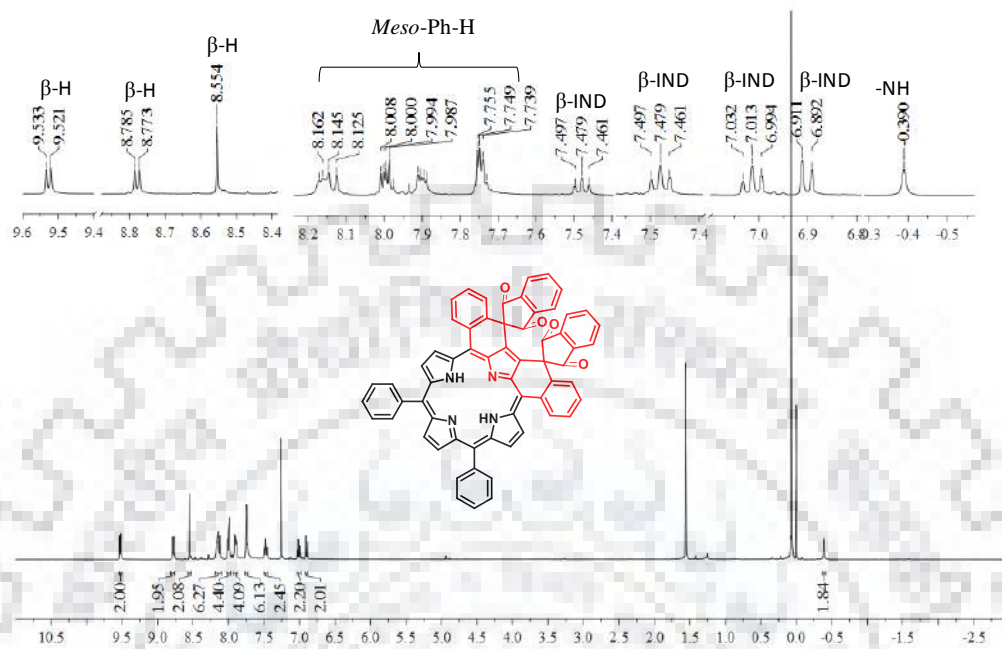
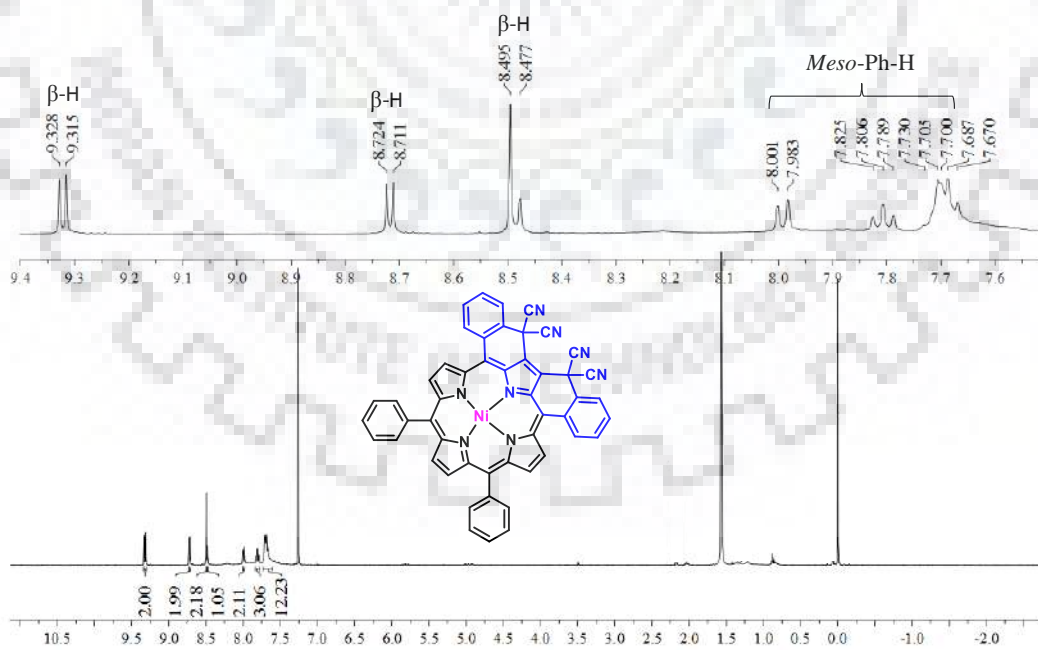
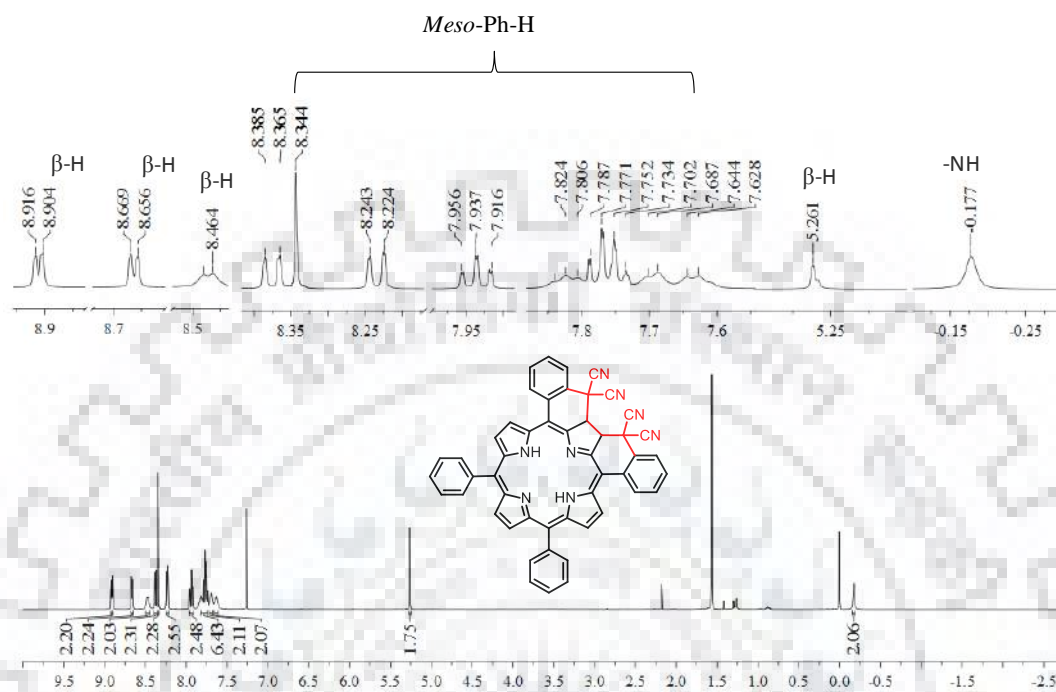


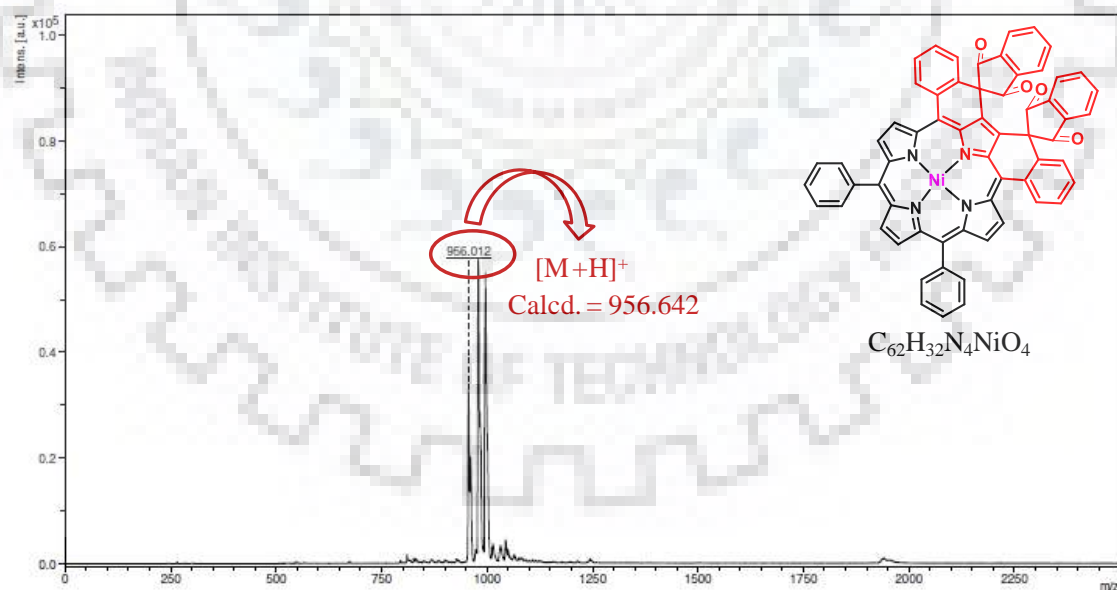
Figure A4.  $^1\text{H}$  NMR Spectrum of  $\text{NiDFP}(\text{MN})_2$  (**7**) in  $\text{CDCl}_3$  at 298 K.



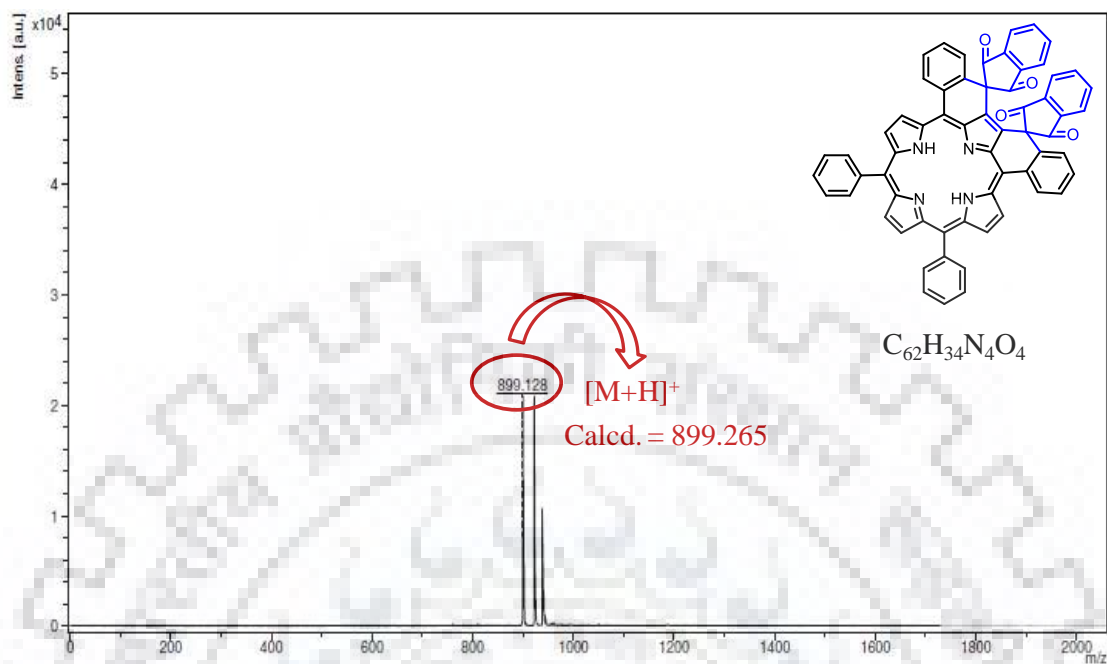
**Figure A5.**  $^1\text{H}$  NMR Spectrum of  $\text{H}_2\text{DFC}(\text{MN})_2$  (**10**) in  $\text{CDCl}_3$  at 298 K.



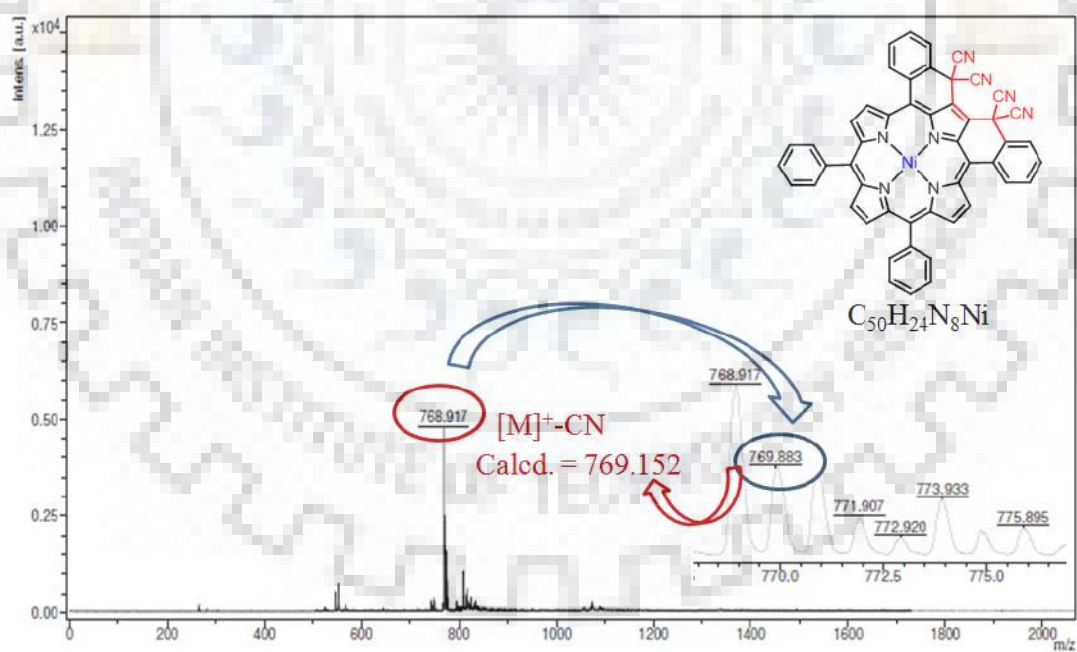
**Figure A6.** MALDI-TOF Mass Spectrum of  $\text{NiDFP}(\text{IND})_2$  (**1**).



**Figure A7.** MALDI-TOF Mass Spectrum of H<sub>2</sub>DFP(IND)<sub>2</sub> (**4a**).

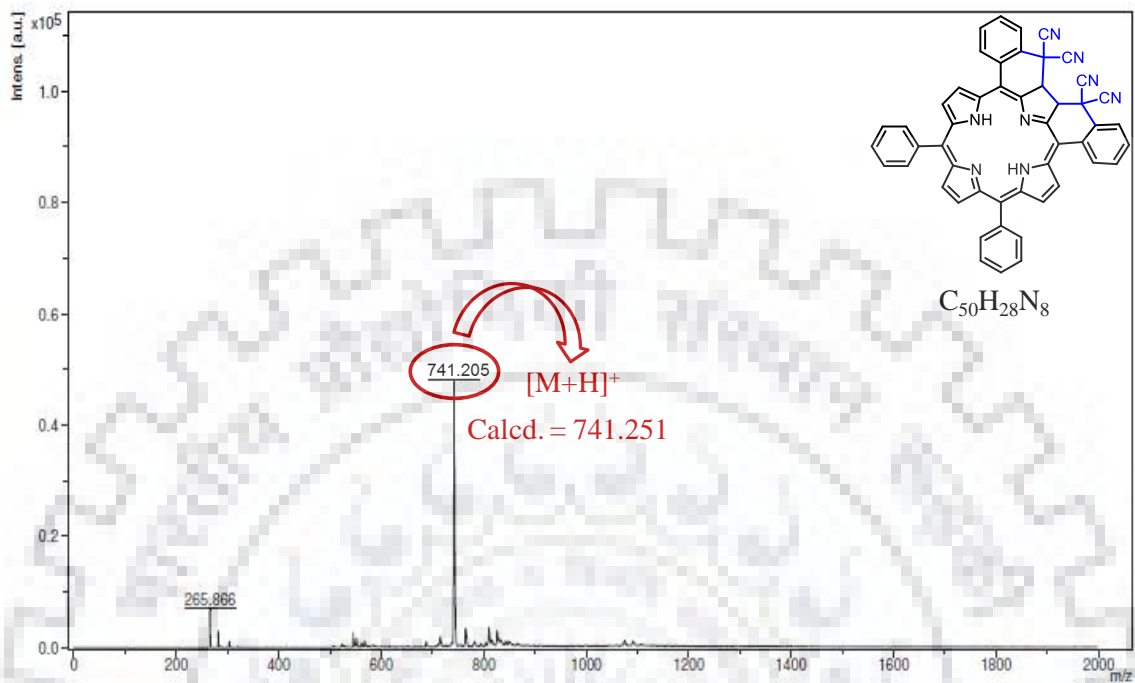


**Figure A8.** MALDI-TOF Mass Spectrum of NiDFP(MN)<sub>2</sub> (**7**).

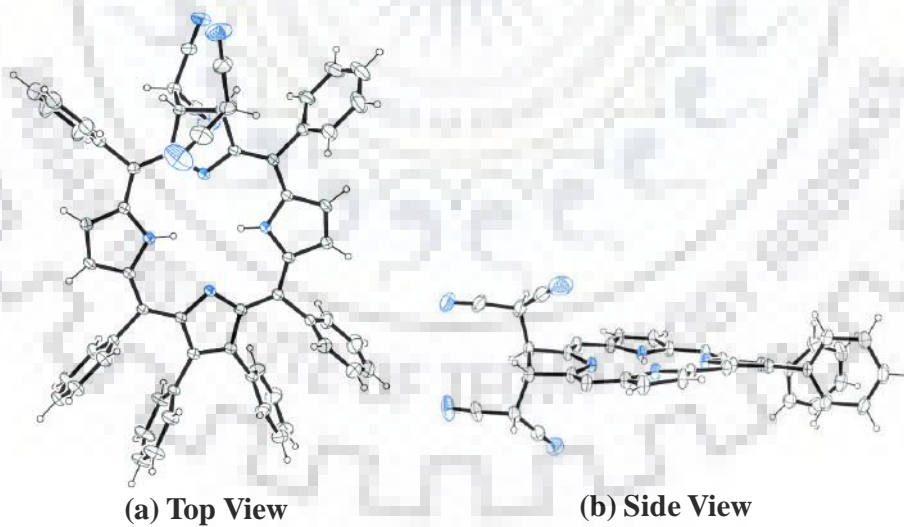




**Figure A9.** MALDI-TOF Mass Spectrum of H<sub>2</sub>DFC(MN)<sub>2</sub> (10).

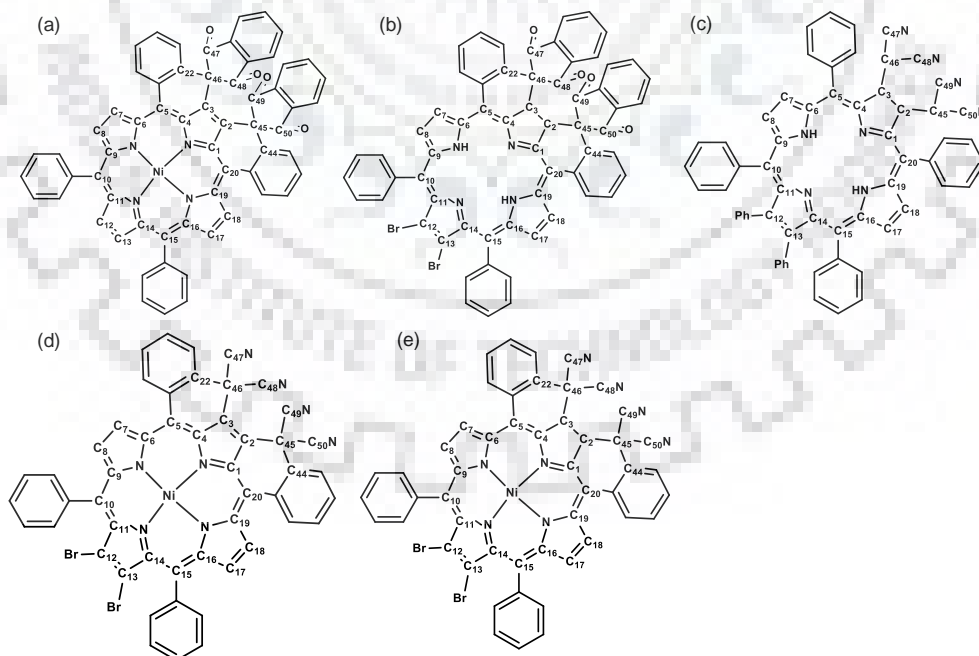


**Figure A10.** ORTEP Showing Top and Side Views of H<sub>2</sub>TPC(MN)<sub>2</sub>(Ph)<sub>2</sub>.



**Table A1.** Crystal Structure Data of H<sub>2</sub>TPC[CH(CN)<sub>2</sub>]<sub>2</sub>.

H <sub>2</sub> TPC[CH(CN) <sub>2</sub> ]Ph <sub>2</sub>		H <sub>2</sub> TPC[CH(CN) <sub>2</sub> ]Ph <sub>2</sub>	
Empirical formula	C <sub>62</sub> H <sub>40</sub> N <sub>8</sub>	Z	2
Formula wt.	897.02	D <sub>calcd.</sub> (mg/m <sup>3</sup> )	1.241
Crystal system	Triclinic	λ (Å)	0.71073
Space group	P-1	T (K)	293
a (Å)	12.92	No. of total reflns.	12130
b (Å)	13.42	No. of indepnt. reflns.	3610
c (Å)	15.42	R	7.36
α (°)	65.83	Rw	18.23
β (°)	79.52	GOOF	0.91
γ (°)	87.06	<b>CCDC</b>	<b>1570261</b>
Volume (Å <sup>3</sup> )	2399.9		

**Figure A11.** Numbering of Carbon Atoms in the Macrocyclic Skeleton of (a) NiDFP(IND)<sub>2</sub> (**1**) (b) H<sub>2</sub>DFC(IND)<sub>2</sub>Br<sub>2</sub> (**5**) (c) H<sub>2</sub>TPC[CH(CN)<sub>2</sub>]<sub>2</sub> (d) NiDFP(MN)<sub>2</sub>Br<sub>2</sub> (**8**) (e) NiDFC(MN)<sub>2</sub>Br<sub>2</sub> (**8a**).

**Figure A12.** Displacement of Carbon Atoms From the Mean Plane of (a) H<sub>2</sub>DFC(IND)<sub>2</sub>Br<sub>2</sub> (**5**) (b) NiDFP(IND)<sub>2</sub> (**1**) (c) NiDFC(MN)<sub>2</sub>Br<sub>2</sub> (**8a**) (d) H<sub>2</sub>TPC[CH(CN)<sub>2</sub>]<sub>2</sub> (e) NiDFP(MN)<sub>2</sub>Br<sub>2</sub> (**8**).

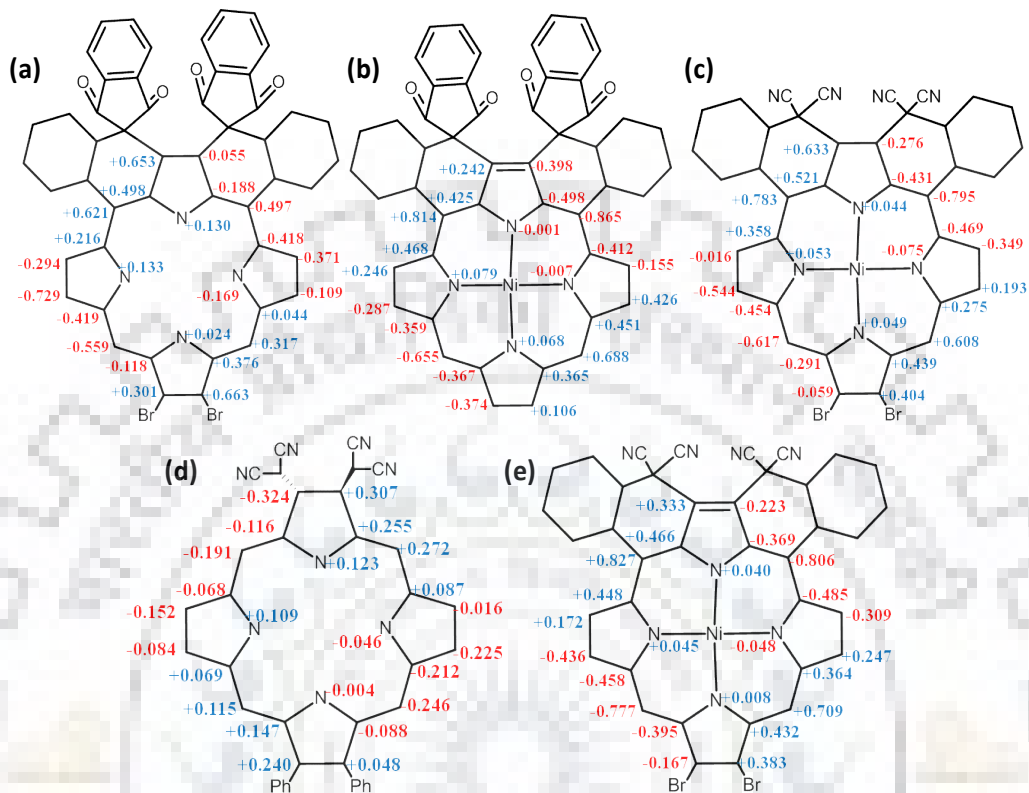


**Figure A13.** Frontier Molecular Orbitals of NiDFP(IND)<sub>2</sub> (**1**).

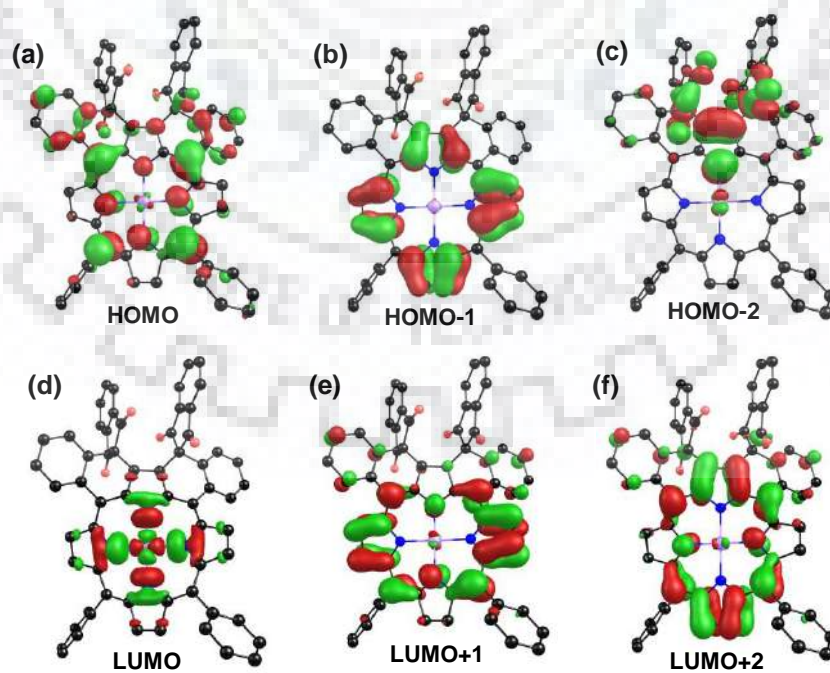


Figure A14. Frontier Molecular Orbitals of  $H_2DFC(IND)_2$  (4).

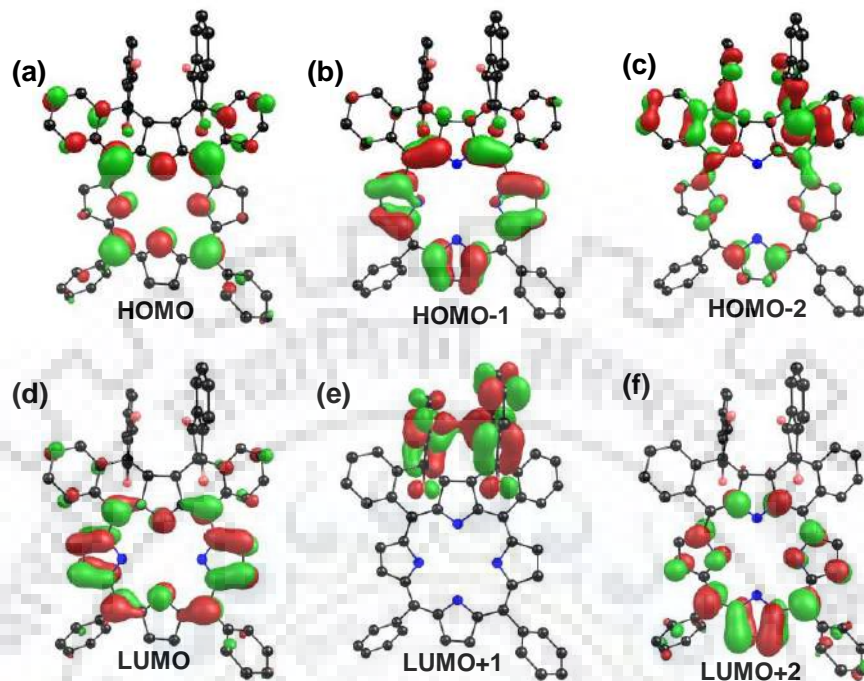
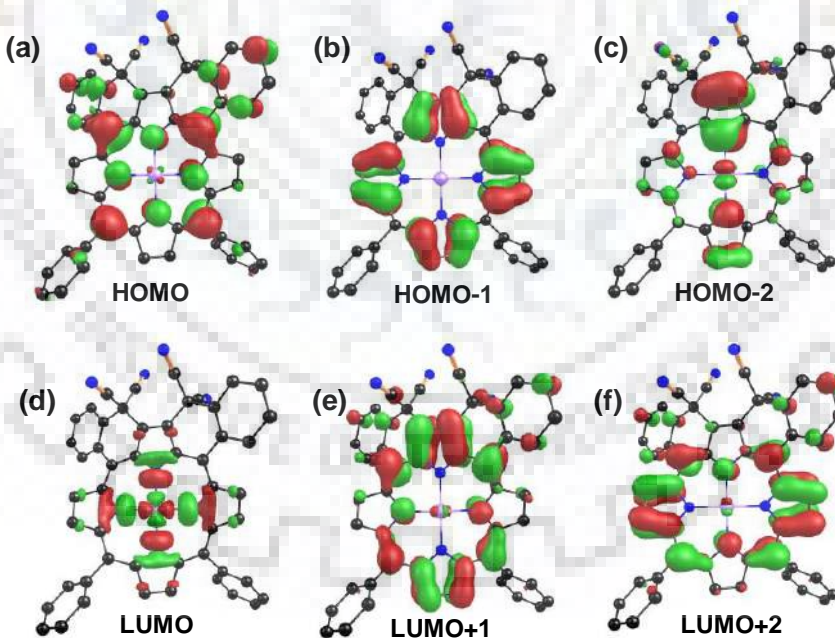
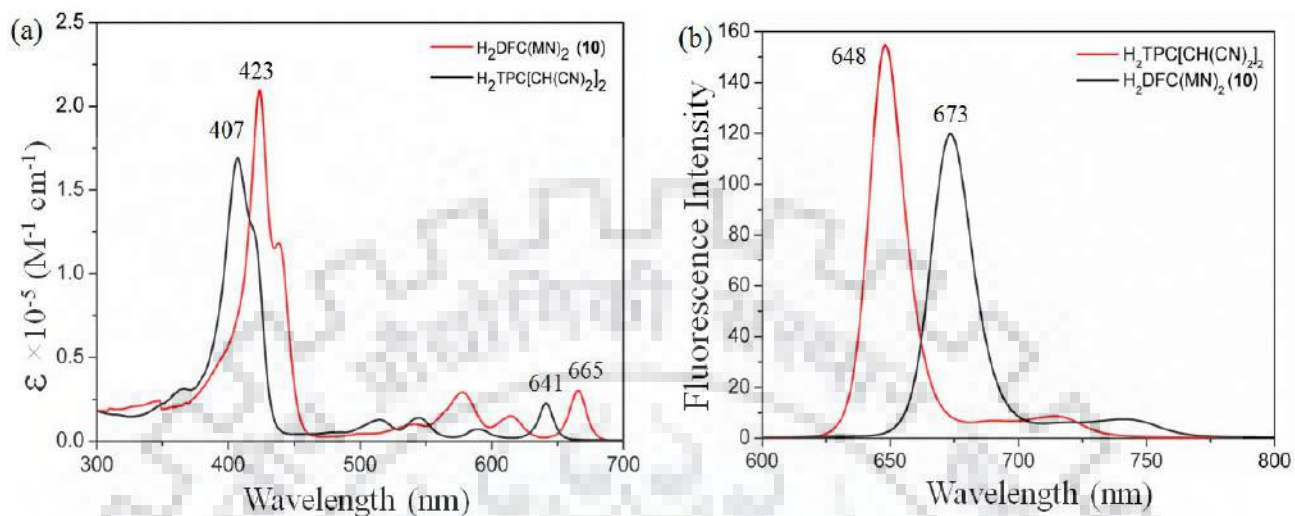


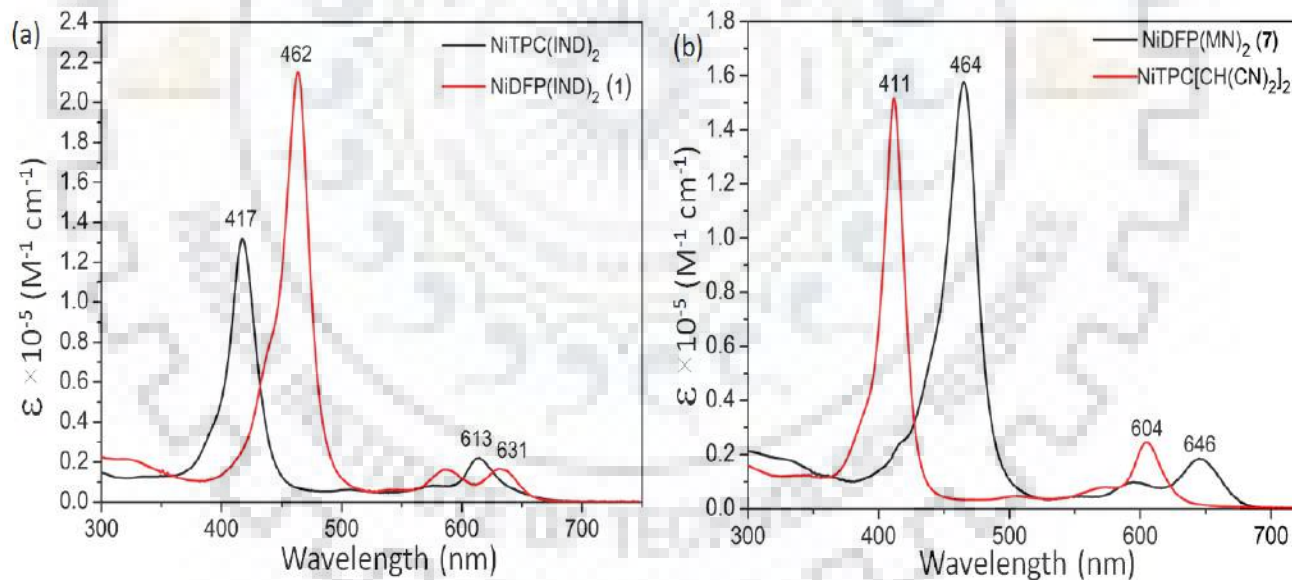
Figure A15. Frontier Molecular Orbitals of  $NiDFP(MN)_2$  (7).



**Figure A16.** (a) Comparative UV-Vis Absorption Spectra and (b) Emission Spectra of  $\text{H}_2\text{DFC}(\text{MN})_2$  (**10**) and Precursor  $\text{H}_2\text{TPC}(\text{MN})_2$  in  $\text{CH}_2\text{Cl}_2$  at 298K.



**Figure A17.** Comparative Absorption Spectra of (a)  $\text{NiTPC}(\text{IND})_2$  and  $\text{NiDFP}(\text{IND})_2$  (**1**) (b)  $\text{NiTPC}[\text{CH}(\text{CN})_2]_2$  and  $\text{NiDFP}(\text{MN})_2$  (**7**).

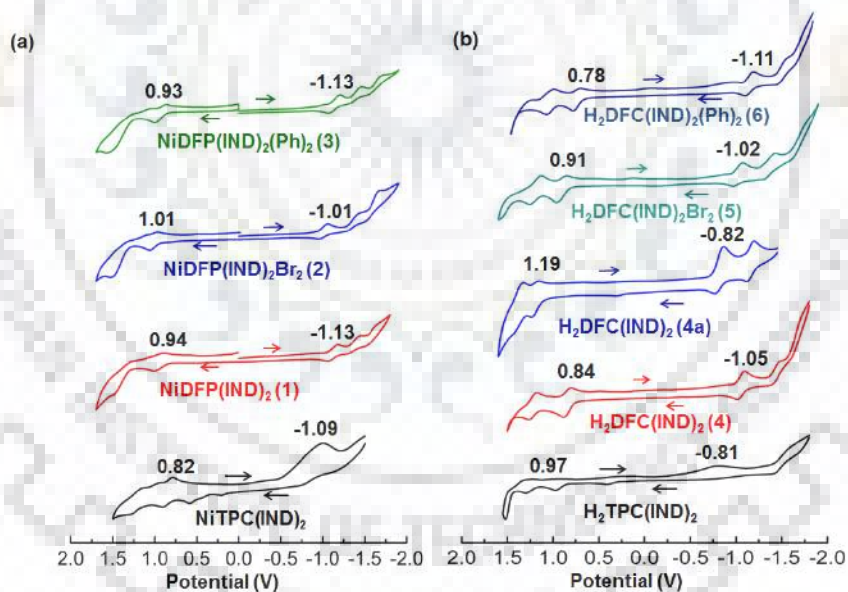




**Table A2.** Absorption Spectral Data<sup>a</sup> of NiDFPs in CH<sub>2</sub>Cl<sub>2</sub>.

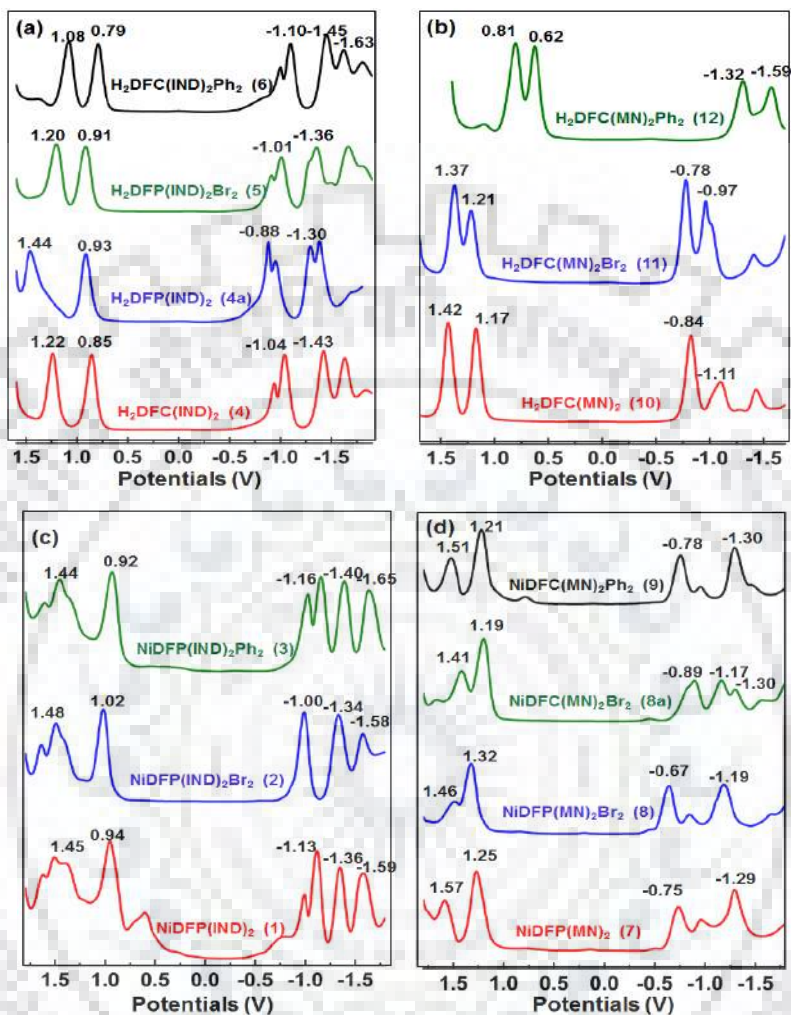
NiDFPs	$\lambda_{\text{abs}}$	
	B Band	Q Band(s)
NiDFP(MN) <sub>2</sub>	465(5.20)	550(sh), 594(4.00), 645(4.27)
NiDFP(MN) <sub>2</sub> Br <sub>2</sub>	468(5.08)	553(sh), 597(3.94), 649(4.19)
NiDFC(MN) <sub>2</sub> Br <sub>2</sub>	438(5.20)	627(4.26)
NiDFP(MN) <sub>2</sub> Ph <sub>2</sub>	468(5.09)	556(sh), 600(4.03), 648(4.22)
NiDFP(IND) <sub>2</sub>	463(5.33)	586(4.21), 631(4.22)
NiDFP(IND) <sub>2</sub> Br <sub>2</sub>	467(5.27)	592(4.20), 637(4.20)
NiDFP(IND) <sub>2</sub> Ph <sub>2</sub>	469(5.27)	591(4.26), 635(4.20)

<sup>a</sup>Values in parentheses refers to log  $\epsilon$

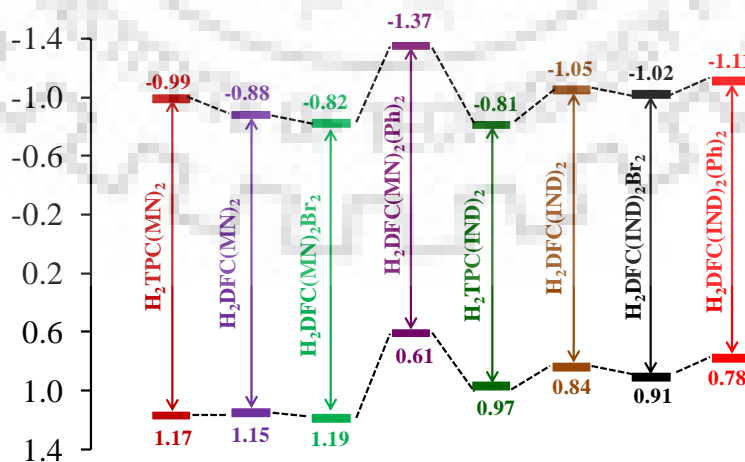
**Figure A18.** Comparative Cyclic Voltammograms of (a) NiDFP(IND)<sub>2</sub>X<sub>2</sub> (b) H<sub>2</sub>DFP(IND)<sub>2</sub>X<sub>2</sub> (Where X = Br, Ph).



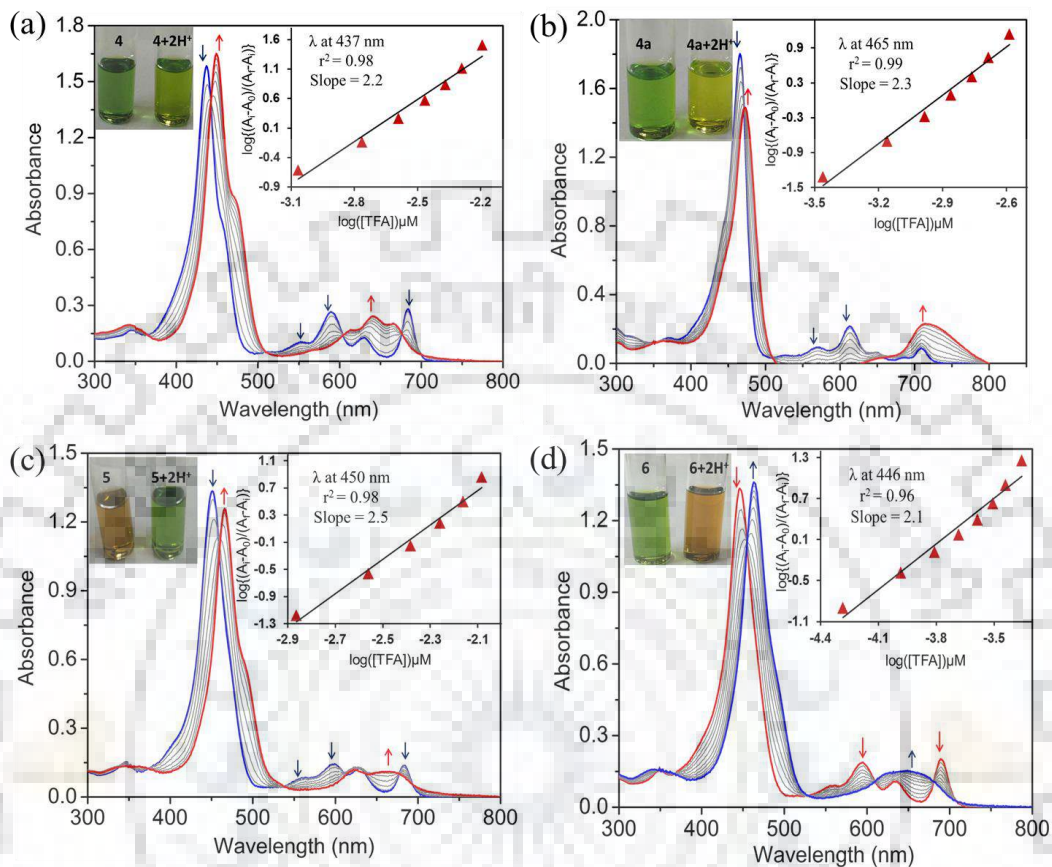
**Figure A19.** Differential Pulse Voltammograms (DPVs) of Synthesized Fused Porphyrinoids in  $\text{CH}_2\text{Cl}_2$ .



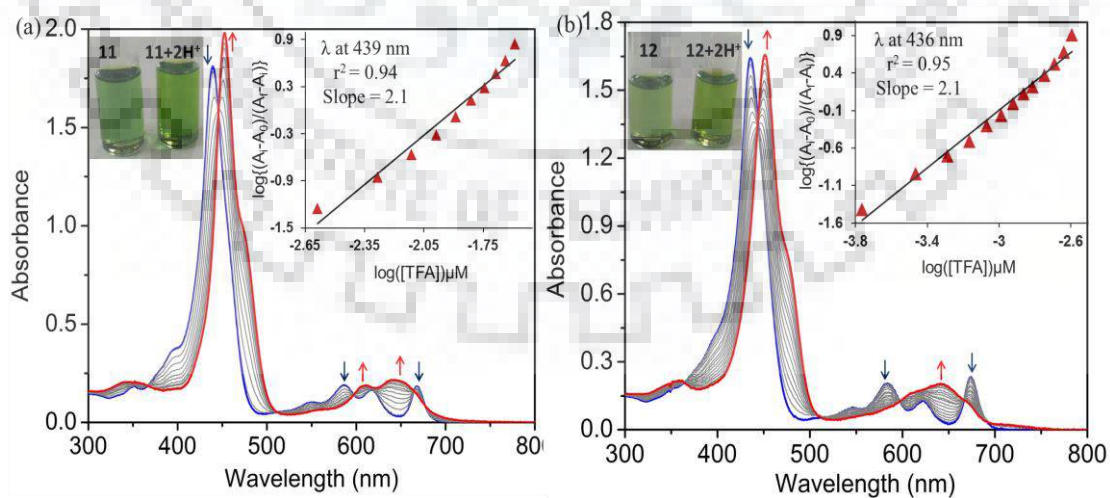
**Figure A20.** Plot of HOMO-LUMO Trend in  $\text{H}_2\text{DFCs}$ .



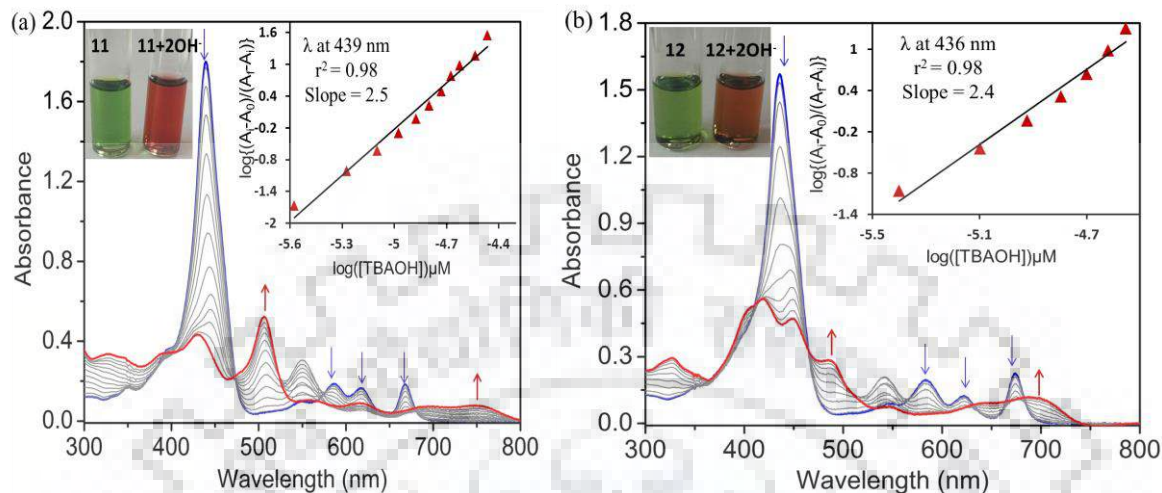
**Figure A21** UV-vis. Spectral Titrations of Synthesized H<sub>2</sub>DFCs (a) H<sub>2</sub>DFC(IND)<sub>2</sub> (**4**), (b) H<sub>2</sub>DFP(IND)<sub>2</sub> (**4a**), (c) H<sub>2</sub>DFC(IND)<sub>2</sub>Br<sub>2</sub> (**5**) and (d) H<sub>2</sub>DFC(IND)<sub>2</sub>Ph<sub>2</sub> (**6**) with TFA in CH<sub>2</sub>Cl<sub>2</sub>.



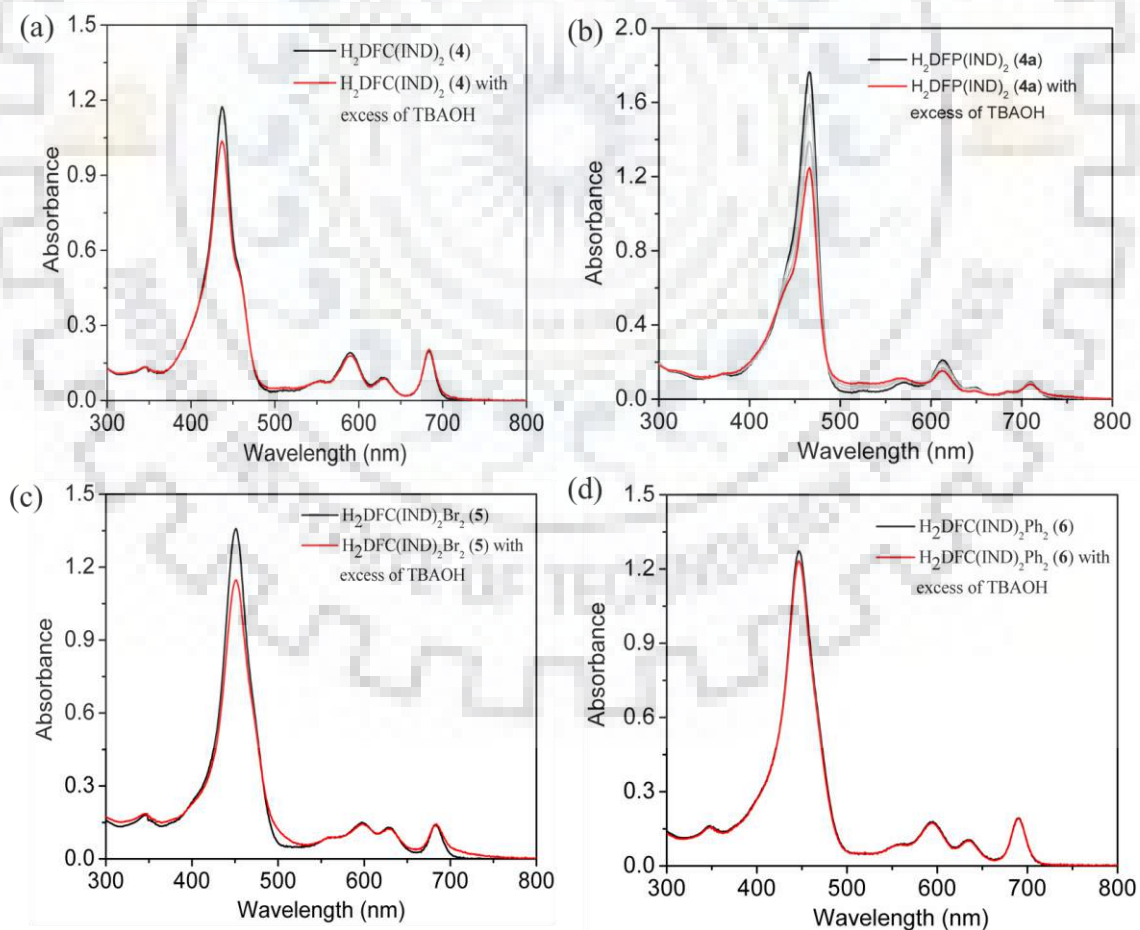
**Figure A22.** UV-vis. Spectral Titrations of Synthesized H<sub>2</sub>DFCs (a) H<sub>2</sub>DFC(MN)<sub>2</sub>Br<sub>2</sub> (**11**) and (b) H<sub>2</sub>DFC(MN)<sub>2</sub>Ph<sub>2</sub> (**12**) with TFA in CH<sub>2</sub>Cl<sub>2</sub>.



**Figure A23.** UV-vis. Spectral Titrations of Synthesized H<sub>2</sub>DFCs (a) H<sub>2</sub>DFC(MN)<sub>2</sub>Br<sub>2</sub> (**11**), (b) H<sub>2</sub>DFC(MN)<sub>2</sub>Ph<sub>2</sub> (**12**) with TBAOH in CH<sub>2</sub>Cl<sub>2</sub>.



**Figure A24.** UV-vis. Spectral Titrations of Synthesized H<sub>2</sub>DFCs (a) H<sub>2</sub>DFC(IND)<sub>2</sub> (**4**), (b) H<sub>2</sub>DFP(IND)<sub>2</sub> (**4a**), (c) H<sub>2</sub>DFC(IND)<sub>2</sub>Br<sub>2</sub> (**5**) and (d) H<sub>2</sub>DFC(IND)<sub>2</sub>Ph<sub>2</sub> (**6**) with TBAOH in CH<sub>2</sub>Cl<sub>2</sub>.



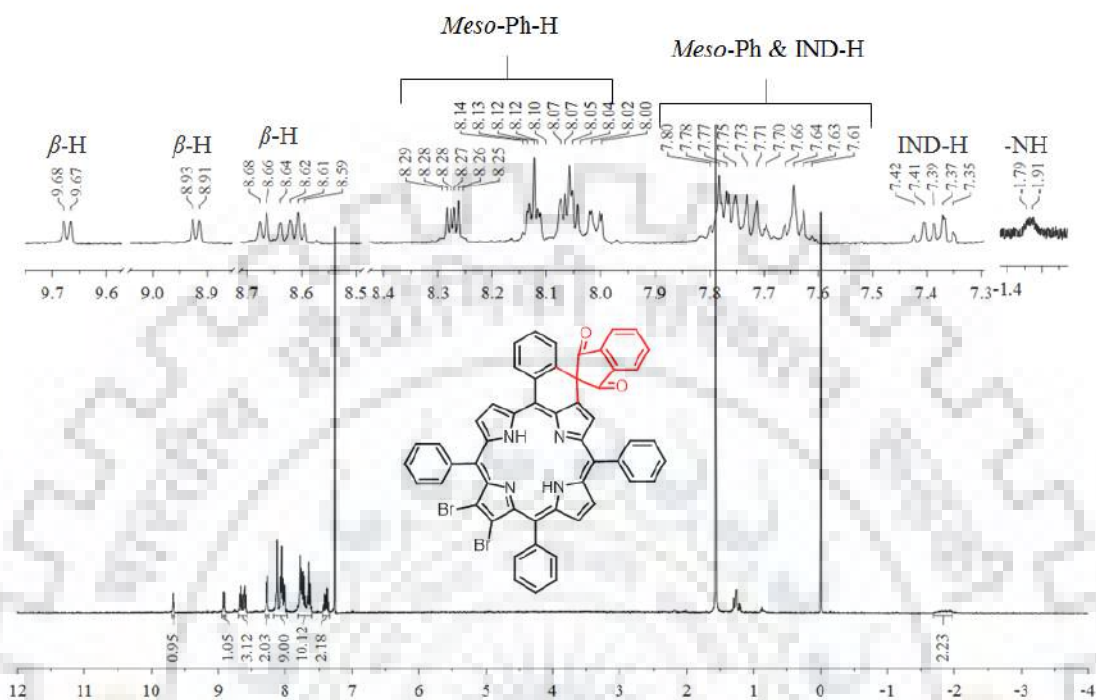
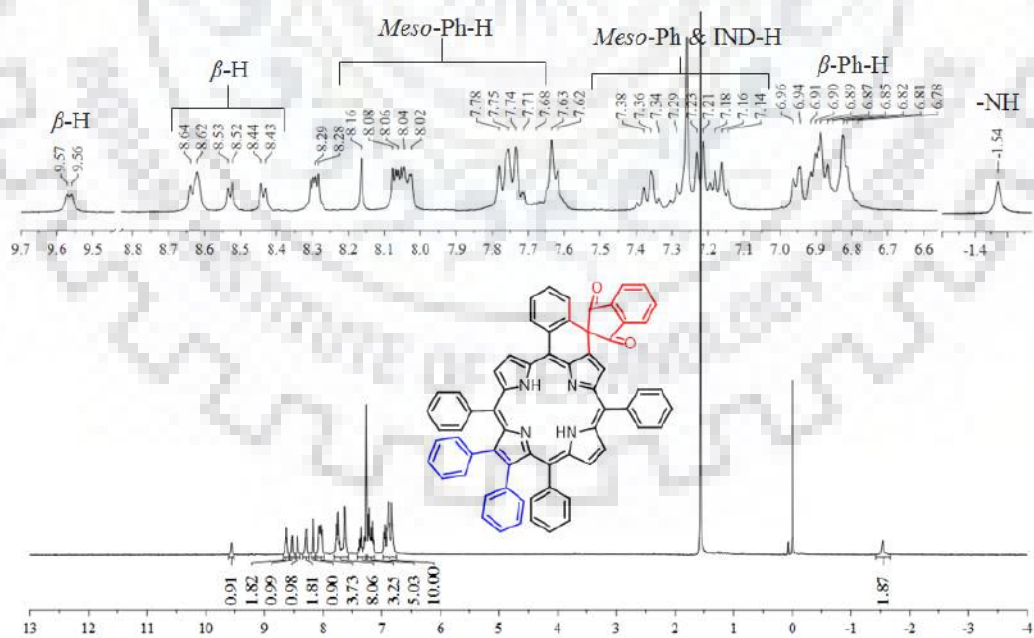


## APPENDIX-III

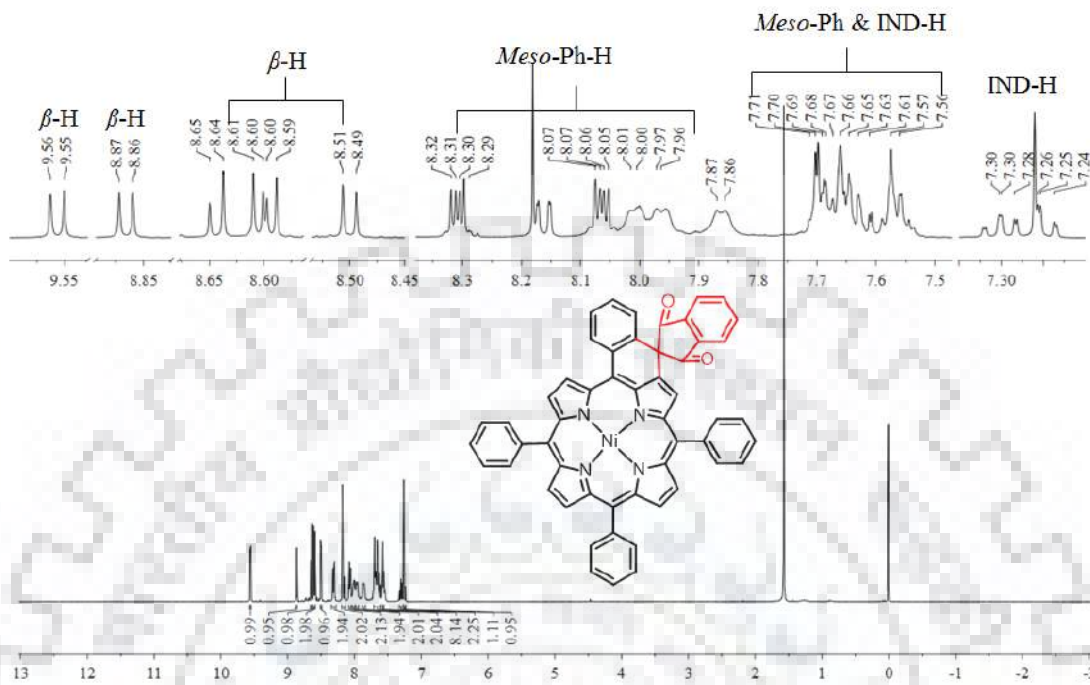
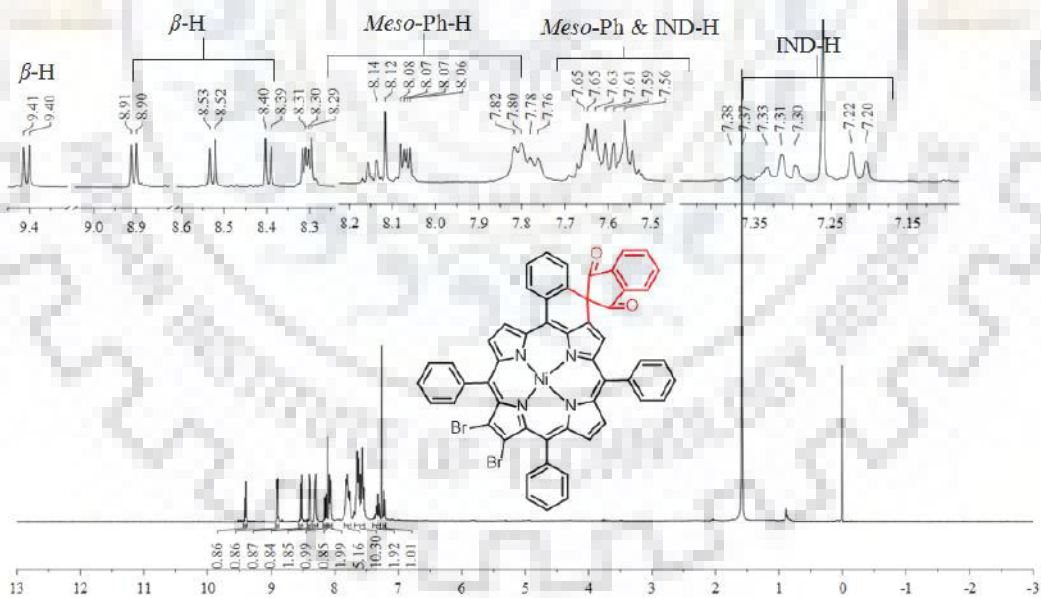
**One-Pot Synthesis of Ni(II) Monofused Porphyrins (NiMFPs) via Nickel  
Acetate Catalyzed Oxidation of Free Base *trans*-Chlorins**

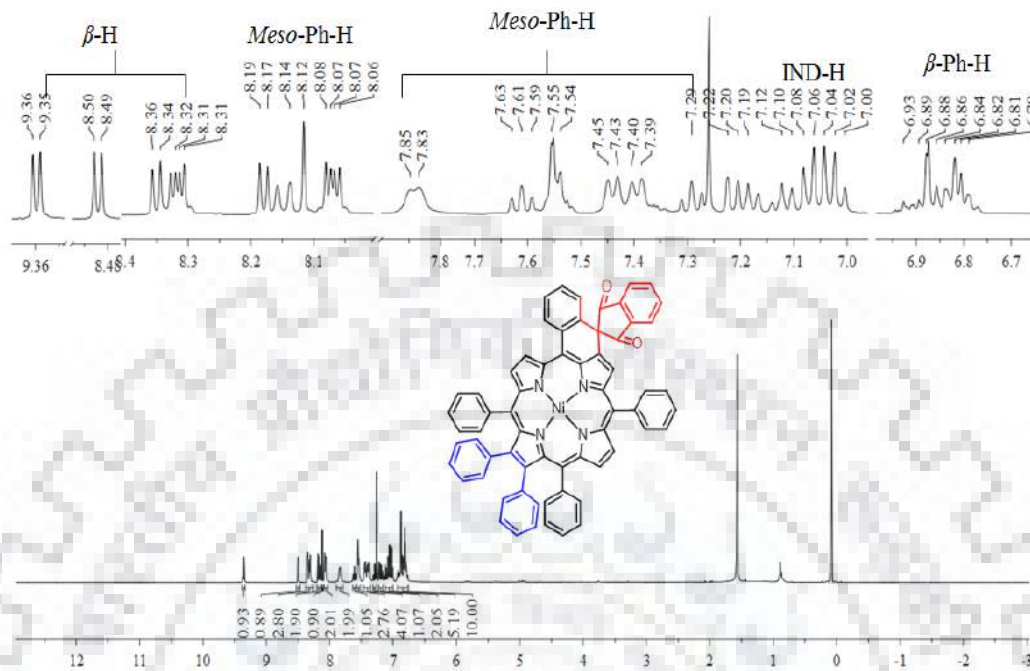
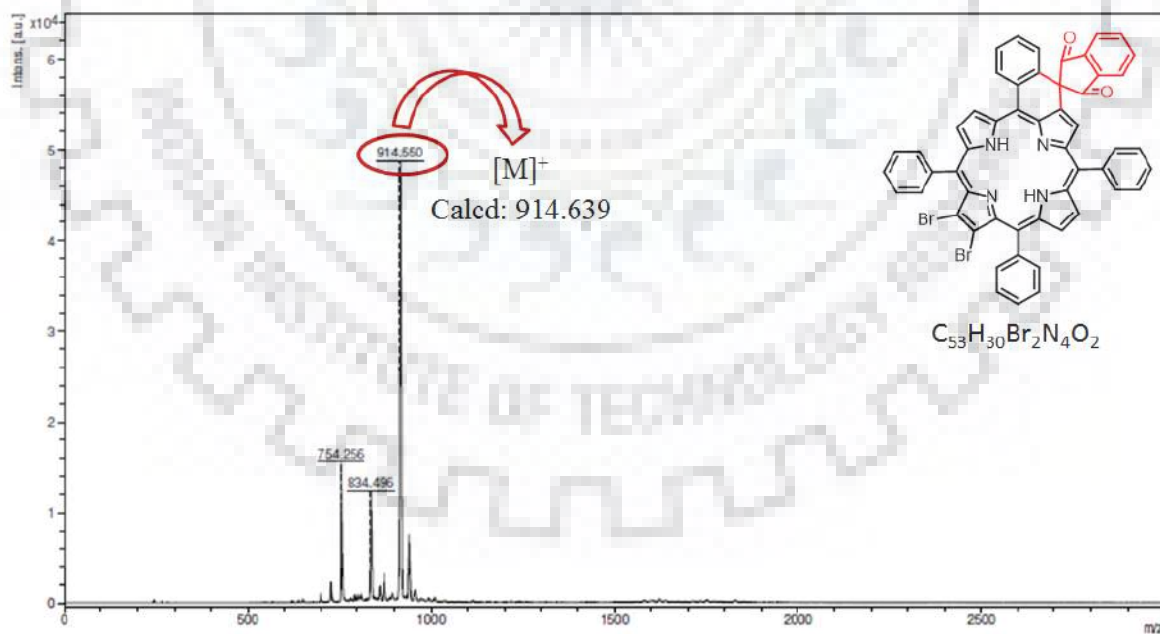
<b>Table of Contents</b>	<b>Page No.</b>
<b>Figure A1.</b> <sup>1</sup> H NMR Spectrum of H <sub>2</sub> MFP(IND)Br <sub>2</sub> ( <b>2</b> ) in CDCl <sub>3</sub> .	274
<b>Figure A2.</b> <sup>1</sup> H NMR Spectrum of H <sub>2</sub> MFP(IND)Ph <sub>2</sub> ( <b>3</b> ) in CDCl <sub>3</sub> .	274
<b>Figure A3.</b> <sup>1</sup> H NMR Spectrum of NiMFP(IND) ( <b>1b</b> ) in CDCl <sub>3</sub> .	275
<b>Figure A4.</b> <sup>1</sup> H NMR Spectrum of NiMFP(IND)Br <sub>2</sub> ( <b>2b</b> ) in CDCl <sub>3</sub> .	275
<b>Figure A5.</b> <sup>1</sup> H NMR Spectrum of NiMFP(IND)Ph <sub>2</sub> ( <b>3b</b> ) in CDCl <sub>3</sub> .	276
<b>Figure A6.</b> MALDI-TOF-MS Spectrum of H <sub>2</sub> MFP(IND)Br <sub>2</sub> ( <b>2</b> ) in CH <sub>2</sub> Cl <sub>2</sub> .	276
<b>Figure A7.</b> MALDI-TOF-MS Spectrum of H <sub>2</sub> MFP(IND)Ph <sub>2</sub> ( <b>3</b> ) in CH <sub>2</sub> Cl <sub>2</sub> .	277
<b>Figure A8.</b> MALDI-TOF-MS Spectrum of NiMFP(IND) ( <b>1b</b> ) in CH <sub>2</sub> Cl <sub>2</sub> .	277
<b>Figure A9.</b> MALDI-TOF-MS Spectrum of NiMFP(IND)Br <sub>2</sub> ( <b>2b</b> ) in CH <sub>2</sub> Cl <sub>2</sub> .	278
<b>Figure A10.</b> MALDI-TOF-MS Spectrum of NiMFP(IND)Ph <sub>2</sub> ( <b>3b</b> ) in CH <sub>2</sub> Cl <sub>2</sub> .	278
<b>Figure A11.</b> Displacement of the mean plane of the porphyrin core from the mean plane for (a) NiMFP(IND) ( <b>1a</b> ), (b) ZnMFP(IND) ( <b>1d</b> ), and (c) ZnMFP(IND)Ph <sub>2</sub> .	279
<b>Figure A12.</b> The top views [(a), (b), and (c)] and Side views [(d), (e), and (f)] of fully optimized geometries of synthesized free base mono-fused porphyrins.	279
<b>Figure A13.</b> The Frontier Molecular Orbitals (FMOs) of H <sub>2</sub> MFP(IND)Br <sub>2</sub> .	280
<b>Figure A14.</b> The Frontier Molecular Orbitals (FMOs) of H <sub>2</sub> MFP(IND)Ph <sub>2</sub> .	280
<b>Figure A15.</b> Comparative Absorption Spectra of Synthesized Compounds (a) CoMFP(IND)s, (b) NiMFP(IND)s, (c) CuMFP(IND)s, and (d) ZnMFP(IND)s in CH <sub>2</sub> Cl <sub>2</sub> .	281
<b>Figure A16.</b> The Comparative Emission Spectra of Synthesized Zn(II) Monofused Porphyrins ZnMFP(IND)s in CH <sub>2</sub> Cl <sub>2</sub> .	282
<b>Figure A17.</b> Comparative Cyclic Voltammograms of (a) H <sub>2</sub> MFP(IND)R <sub>2</sub> (b) CuMFP(IND)R <sub>2</sub> and (c) ZnMFP(IND)R <sub>2</sub> (where R = H, Br, Ph) in CH <sub>2</sub> Cl <sub>2</sub> Using 0.1 M TBAPF <sub>6</sub> .	283
<b>Table A1.</b> Electronic Absorption Data of Synthesized M(II) Mono-fused Porphyrins (M = Co, Ni, Cu) in CH <sub>2</sub> Cl <sub>2</sub> .	282

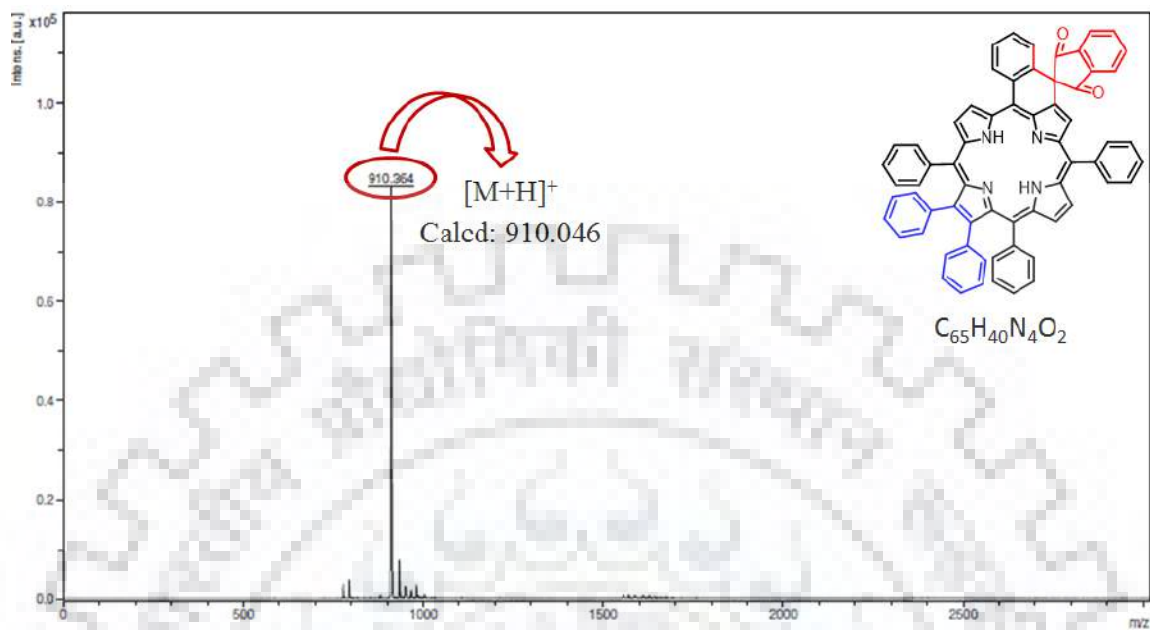
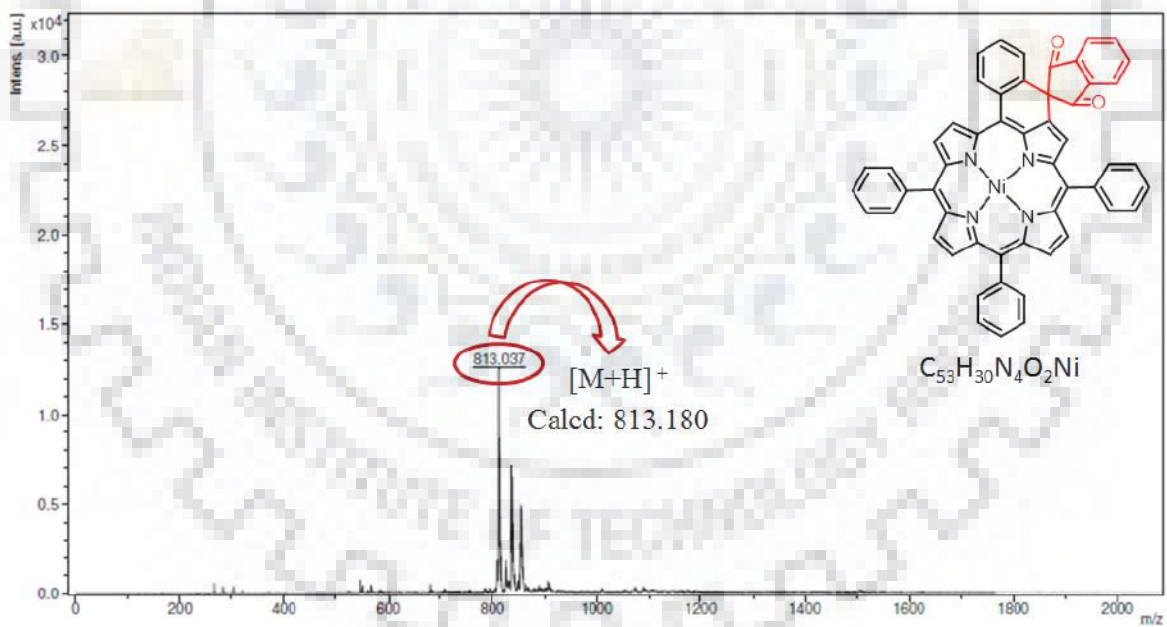


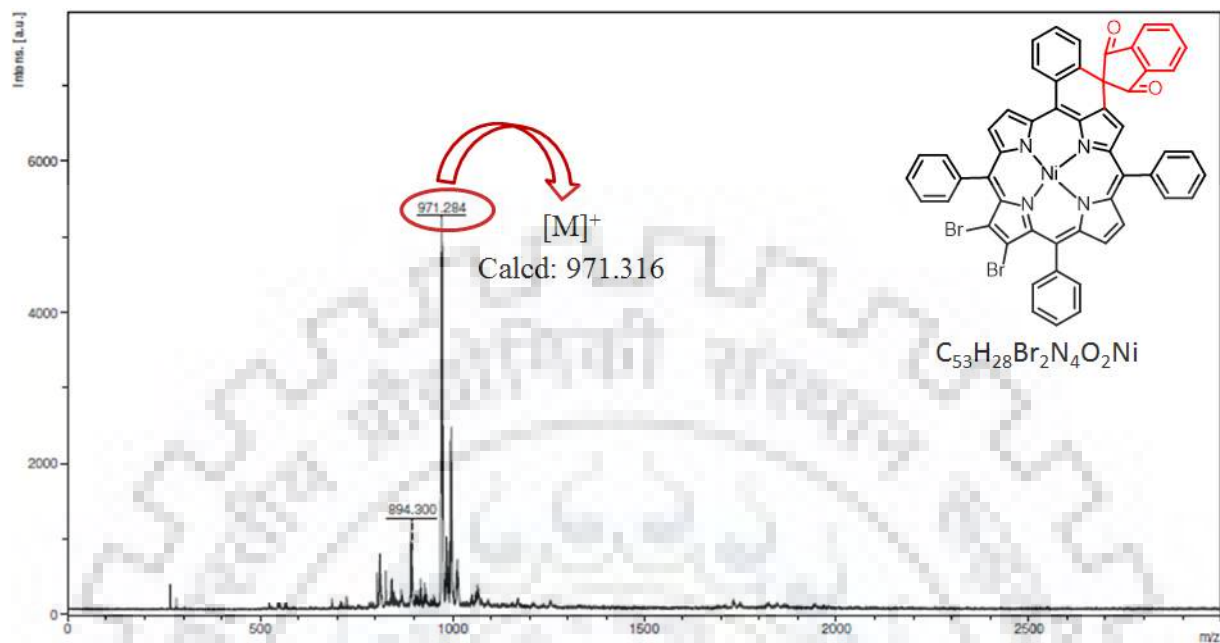
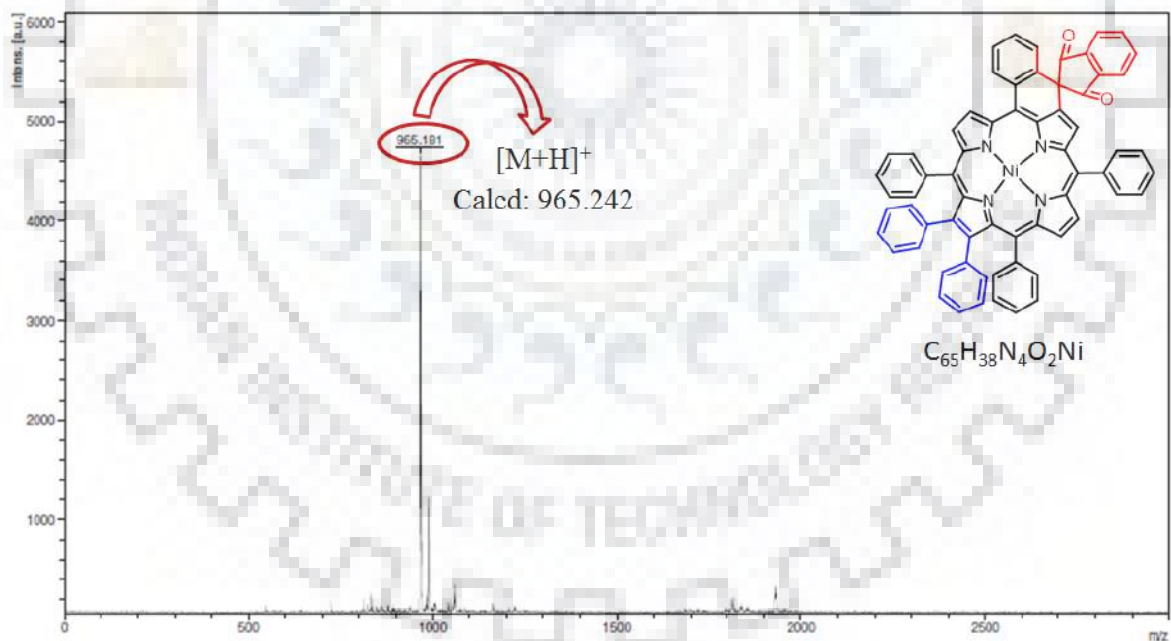
**Figure A1.**  $^1\text{H}$  NMR Spectrum of  $\text{H}_2\text{MFP}(\text{IND})\text{Br}_2$  (**2**) in  $\text{CDCl}_3$ .**Figure A2.**  $^1\text{H}$  NMR Spectrum of  $\text{H}_2\text{MFP}(\text{IND})\text{Ph}_2$  (**3**) in  $\text{CDCl}_3$ .



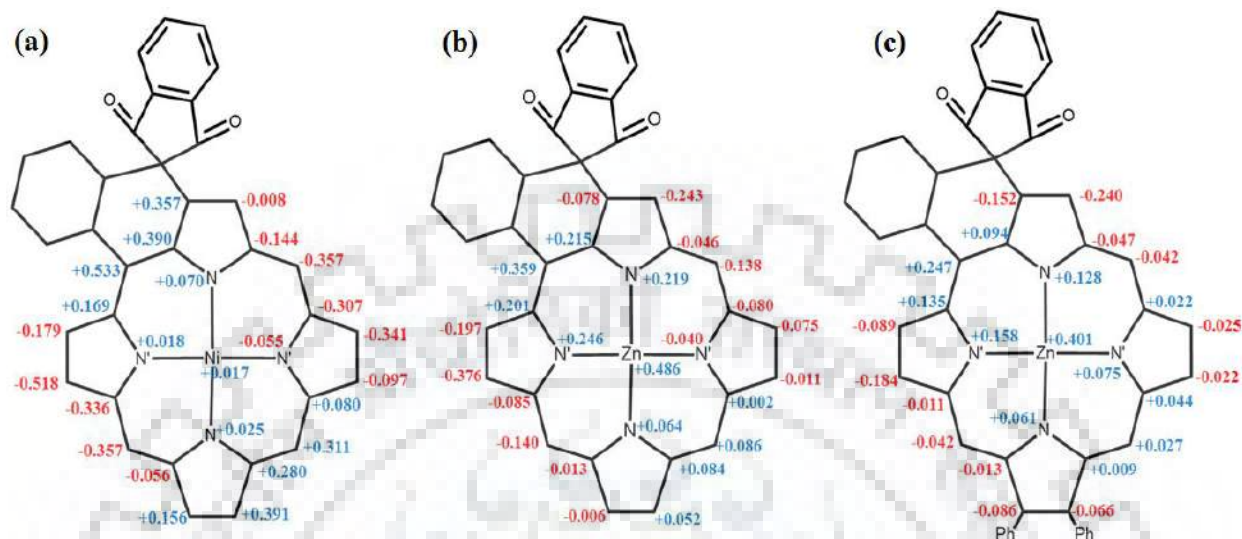
**Figure A3.**  $^1\text{H}$  NMR Spectrum of NiMFP(IND) (**1b**) in  $\text{CDCl}_3$ .**Figure A4.**  $^1\text{H}$  NMR Spectrum of NiMFP(IND)Br<sub>2</sub> (**2b**) in  $\text{CDCl}_3$ .

**Figure A5.**  $^1\text{H}$  NMR Spectrum of NiMFP(IND)Ph<sub>2</sub> (**3b**) in CDCl<sub>3</sub>.**Figure A6.** MALDI-TOF-MS Spectrum of H<sub>2</sub>MFP(IND)Br<sub>2</sub> (**2**) in CH<sub>2</sub>Cl<sub>2</sub>.

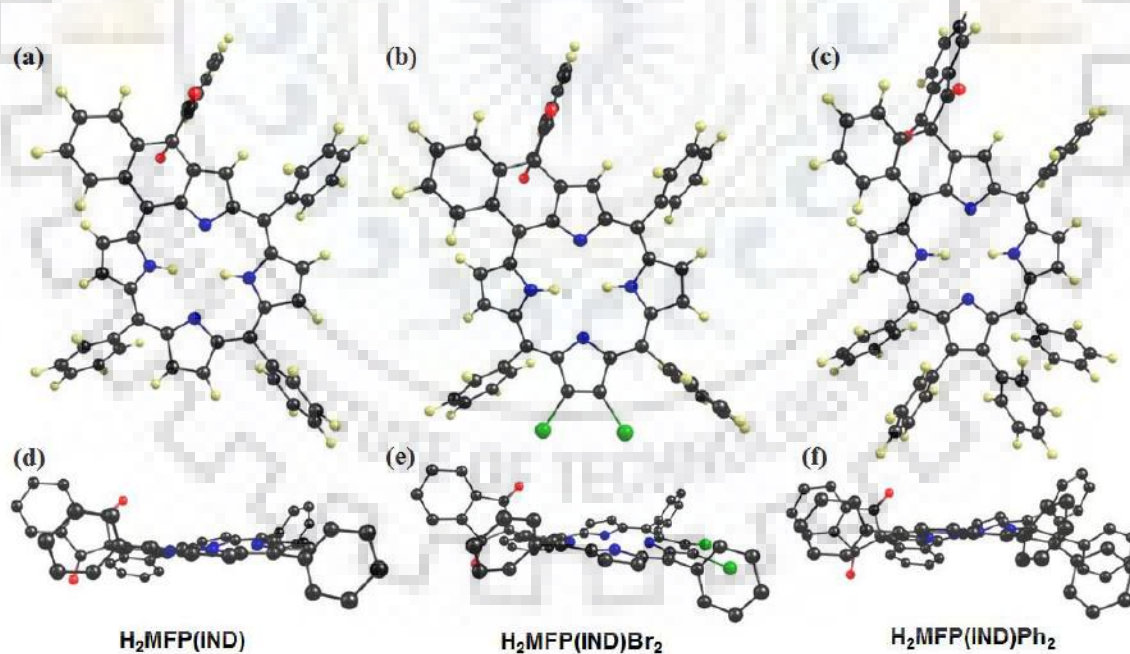
**Figure A7.** MALDI-TOF-MS Spectrum of H<sub>2</sub>MFP(IND)Ph<sub>2</sub> (**3**) in CH<sub>2</sub>Cl<sub>2</sub>.**Figure A8.** MALDI-TOF-MS Spectrum of NiMFP(IND) (**1b**) in CH<sub>2</sub>Cl<sub>2</sub>.

**Figure A9.** MALDI-TOF-MS Spectrum of NiMFP(IND)Br<sub>2</sub> (**2b**) in CH<sub>2</sub>Cl<sub>2</sub>.**Figure A10.** MALDI-TOF-MS Spectrum of NiMFP(IND)Ph<sub>2</sub> (**3b**) in CH<sub>2</sub>Cl<sub>2</sub>.

**Figure A11.** Displacement of the mean plane of the porphyrin core from the mean plane for (a) NIMFP(IND) (**1a**), (b) ZnMFP(IND) (**1d**), and (c) ZnMFP(IND)Ph<sub>2</sub>.

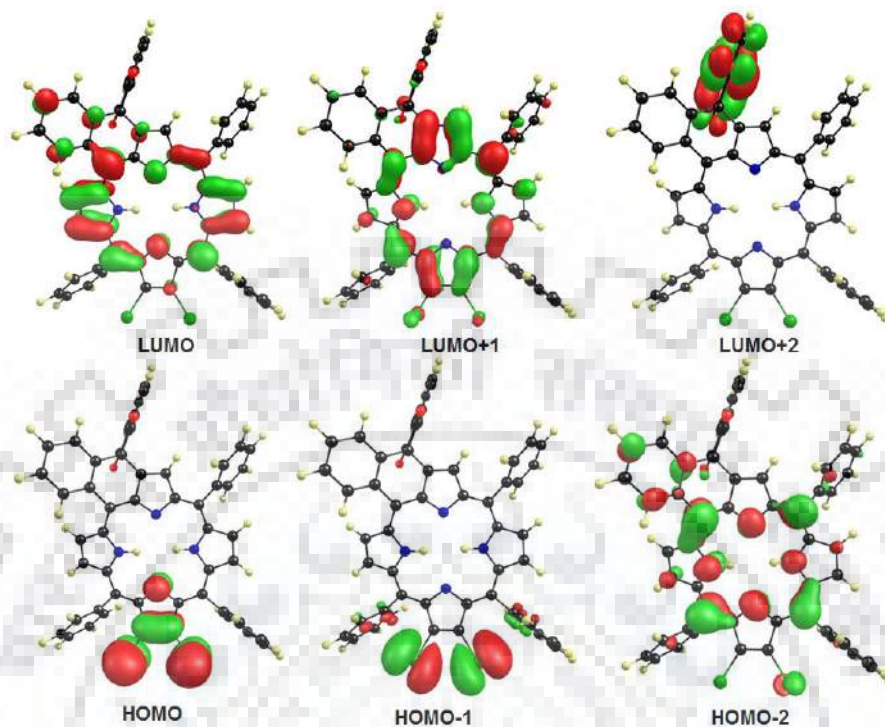


**Figure A12.** The top views [(a), (b), and (c)] and Side views [(d), (e), and (f)] of fully optimized geometries of synthesized free base mono-fused porphyrins.

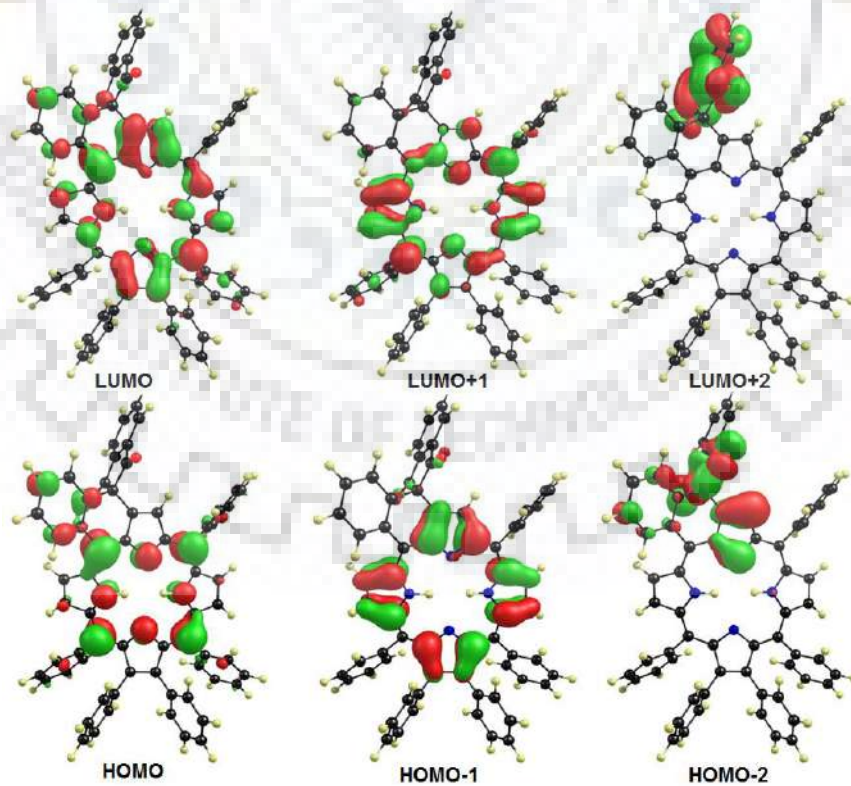




**Figure A13.** The Frontier Molecular Orbitals (FMOs) of H<sub>2</sub>MFP(IND)Br<sub>2</sub>.

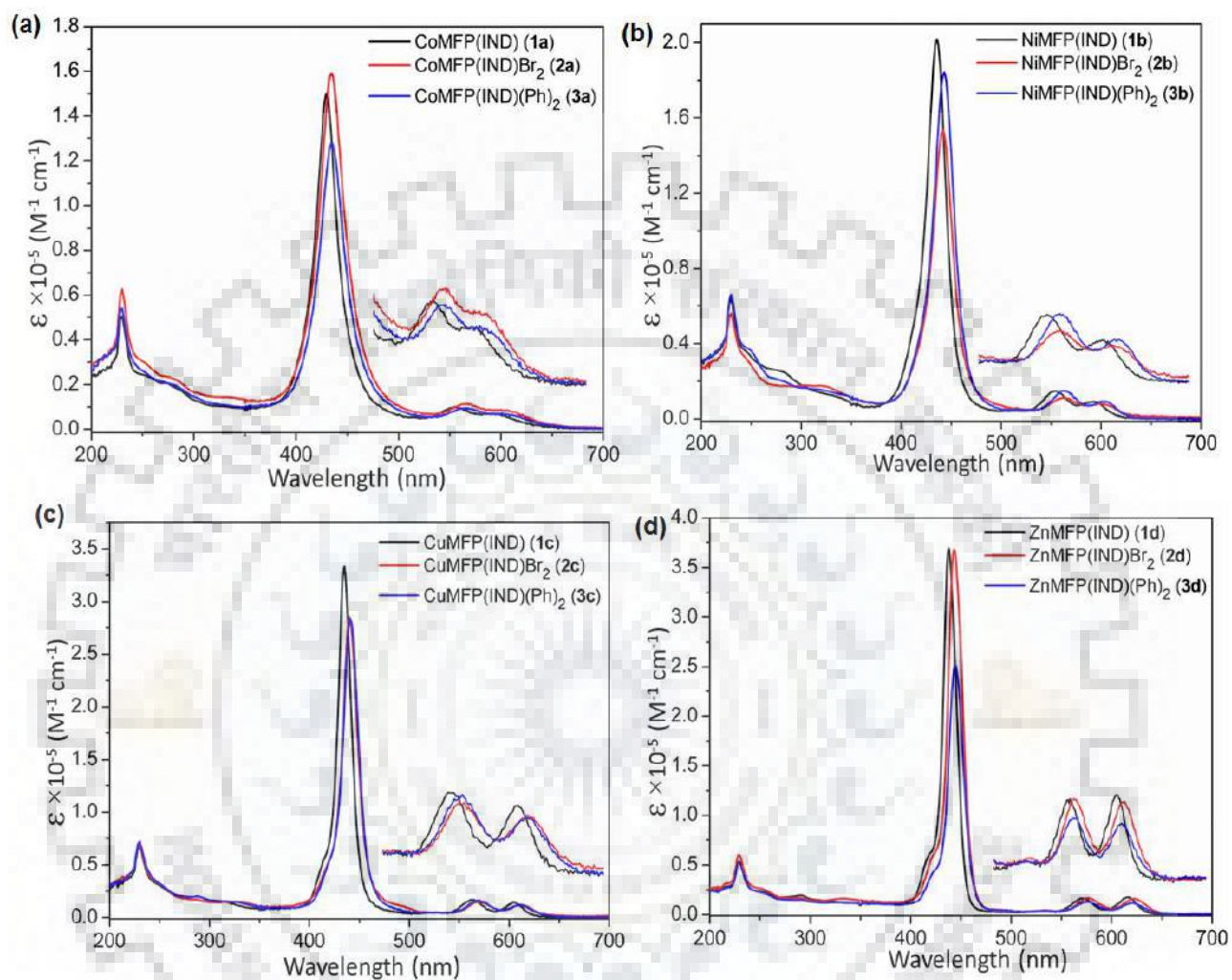


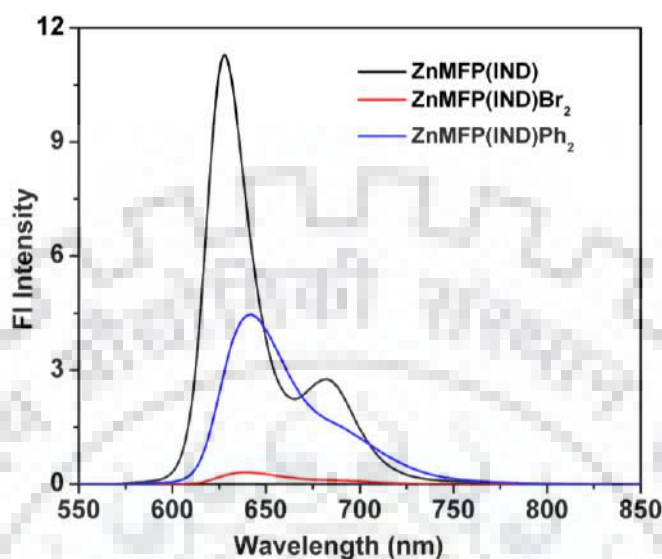
**Figure SA14.** The Frontier Molecular Orbitals (FMOs) of H<sub>2</sub>MFP(IND)Ph<sub>2</sub>.





**Figure A15.** Comparative Absorption Spectra of Synthesized Compounds (a) CoMFP(IND)s, (b) NiMFP(IND)s, (c) CuMFP(IND)s, and (d) ZnMFP(IND)s in  $\text{CH}_2\text{Cl}_2$ .

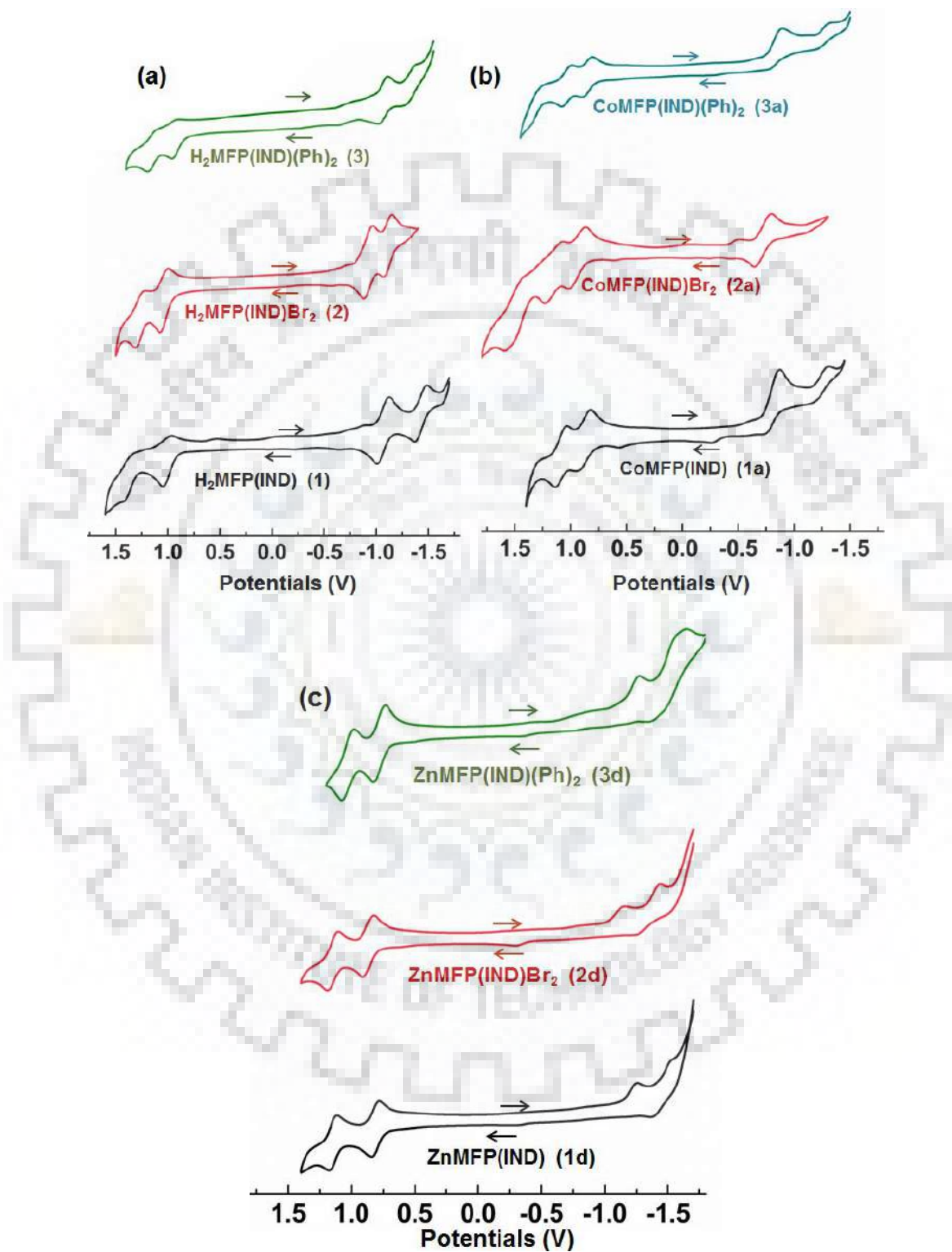


**Figure A16.** The Comparative Emission Spectra of Synthesized Zn(II) Monofused Porphyrins ZnMFP(IND)s in CH<sub>2</sub>Cl<sub>2</sub>.**Table A1.** Electronic Absorption Data of Synthesized M(II) Mono-fused Porphyrins (M = Co, Ni, Cu) in CH<sub>2</sub>Cl<sub>2</sub>.

Porphyrin	<sup>a</sup> λ <sub>abs</sub>	
	B band(s), nm	Q band(s), nm
CoTPP(NO <sub>2</sub> )	382(sh), 420(5.08)	540(4.03), 578(3.94)
CoMFP(IND) ( <b>1a</b> )	229(4.69), 429(5.18)	556(3.99), 596(3.84)
CoMFP(IND)Br <sub>2</sub> ( <b>2a</b> )	229(4.79), 434(5.20)	566(4.05), 606(3.93)
CoMFP(IND)Ph <sub>2</sub> ( <b>3a</b> )	229(4.72), 435(5.11)	567(3.97), 610(3.79)
NiTPP(NO <sub>2</sub> )	386(sh), 428(5.14)	539(4.07), 583(3.97)
NiMFP(IND) ( <b>1b</b> )	230(4.80), 435(5.30)	553(4.17), 592(3.97)
NiMFP(IND)Br <sub>2</sub> ( <b>2b</b> )	229(4.74), 441(5.18)	563(4.05), 602(3.90)
NiMFP(IND)Ph <sub>2</sub> ( <b>3b</b> )	229(4.81), 443(5.26)	562(4.17), 604(3.97)
CuTPP(NO <sub>2</sub> )	380(sh), 422(5.26)	547(4.15), 589(3.96)
CuMFP(IND) ( <b>1b</b> )	230(4.83), 434(5.52)	563(4.23), 605(4.16)
CuMFP(IND)Br <sub>2</sub> ( <b>2b</b> )	229(4.83), 440(5.46)	570(4.16), 612(4.08)
CuMFP(IND)Ph <sub>2</sub> ( <b>3b</b> )	229(4.85), 441(5.45)	570(4.22), 611(4.07)

<sup>a</sup>Values in parentheses refer to log ε.

**Figure A17.** Comparative Cyclic Voltammograms of (a)  $\text{H}_2\text{MFP(IND)R}_2$  (b)  $\text{CuMFP(IND)R}_2$  and (c)  $\text{ZnMFP(IND)R}_2$  (where  $\text{R} = \text{H, Br, Ph}$ ) in  $\text{CH}_2\text{Cl}_2$  Using 0.1 M  $\text{TBAPF}_6$ .

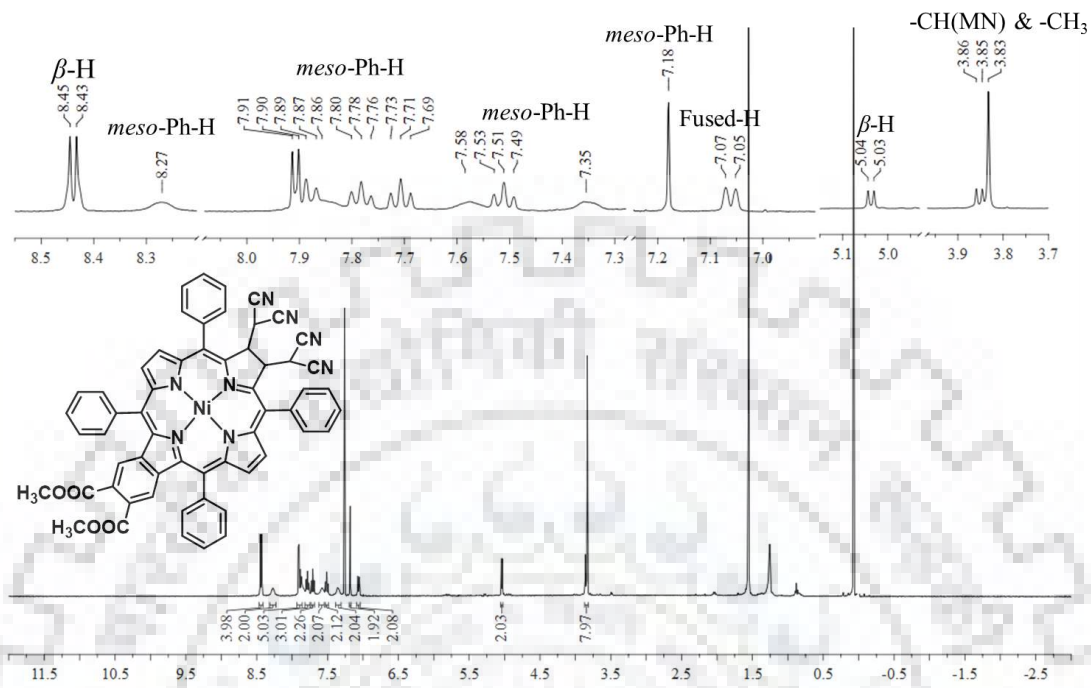
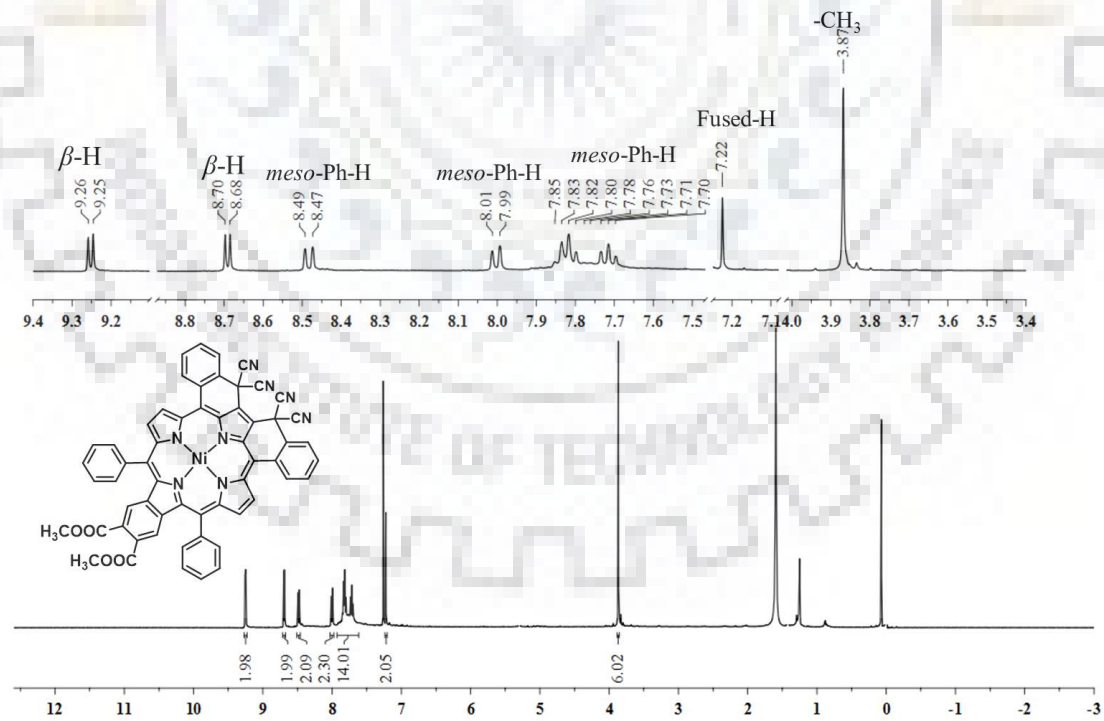




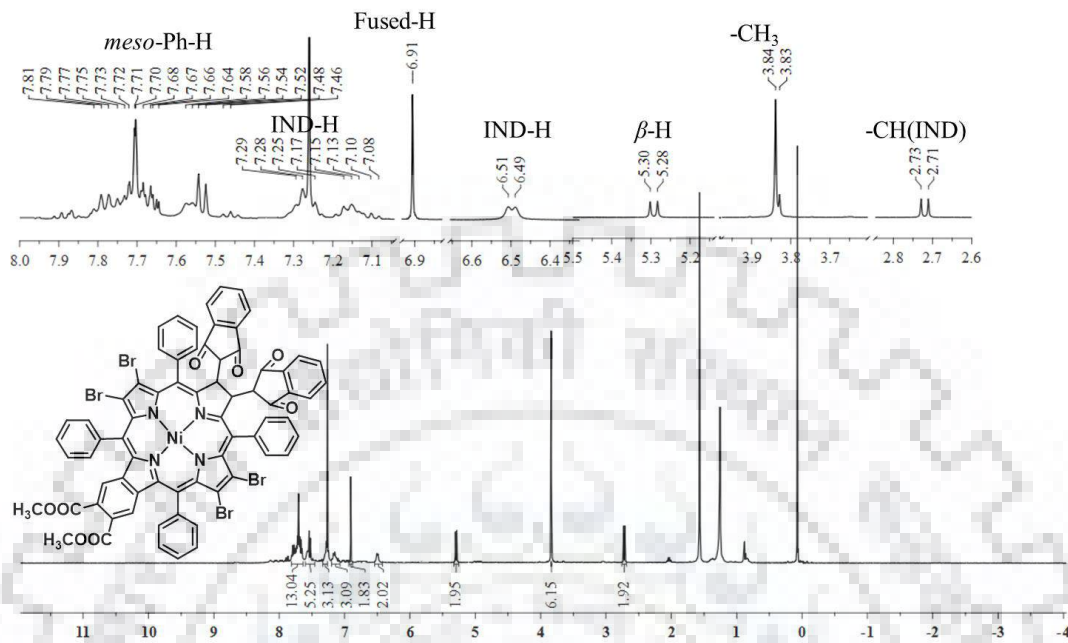
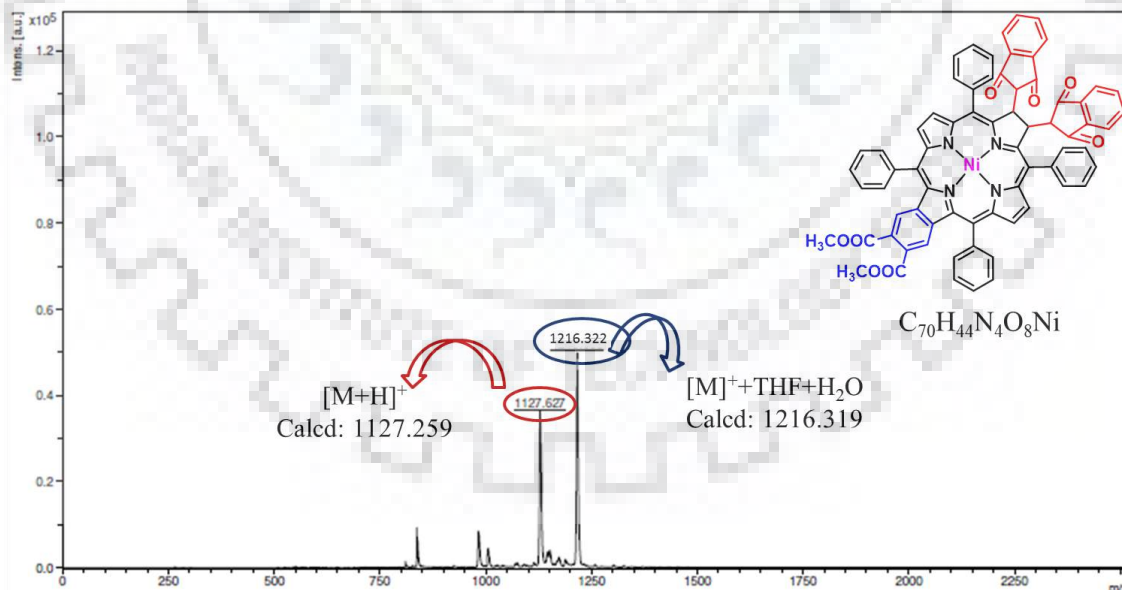
## APPENDIX-IV

## Triply Fused Porphyrins: Synthesis, Spectral, Electrochemical Redox and Anion Sensing Properties

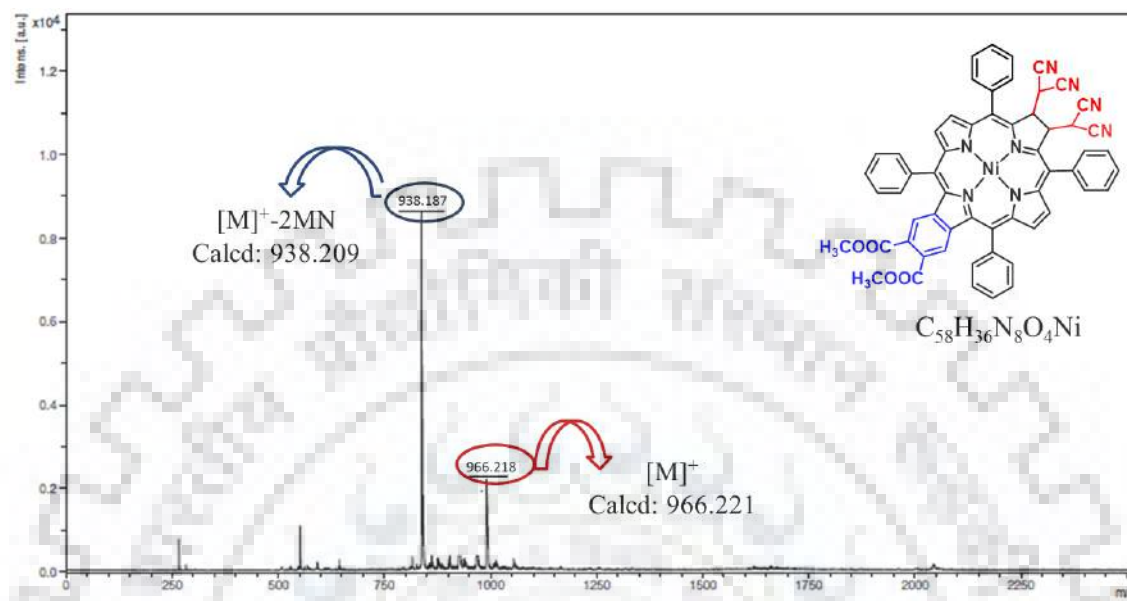
Table of Contents	Page No.
<b>Figure A1.</b> $^1\text{H}$ NMR Spectrum of NiTPC(MN) $_2$ (Benzo) ( <b>2</b> ) in $\text{CDCl}_3$ at 298 K.	286
<b>Figure A2.</b> $^1\text{H}$ NMR Spectrum of NiDFP(MN) $_2$ (Benzo) ( <b>4</b> ) in $\text{CDCl}_3$ at 298 K.	286
<b>Figure A3.</b> $^1\text{H}$ NMR Spectrum of NiTPCBr $_4$ (IND) $_2$ (Benzo) ( <b>5</b> ) in $\text{CDCl}_3$ at 298 K.	287
<b>Figure A4.</b> MALDI-TOF Mass Spectrum of NiTPC(IND) $_2$ (Benzo) ( <b>1</b> ).	287
<b>Figure A5.</b> MALDI-TOF Mass Spectrum of NiTPC(MN) $_2$ (Benzo) ( <b>2</b> ).	288
<b>Figure A6.</b> MALDI-TOF Mass Spectrum of NiDFP(MN) $_2$ (Benzo) ( <b>4</b> ).	288
<b>Figure A7.</b> MALDI-TOF Mass Spectrum of NiTPCBr $_4$ (IND) $_2$ (Benzo) ( <b>5</b> ).	289
<b>Figure A8.</b> Frontier Molecular Orbitals of NiTPC(IND) $_2$ (Benzo) ( <b>1</b> ).	289
<b>Figure A9.</b> Frontier Molecular Orbitals of NiTPC(MN) $_2$ (Benzo) ( <b>2</b> ).	290
<b>Figure A10.</b> Frontier Molecular Orbitals of NiDFP(MN) $_2$ (Benzo) ( <b>4</b> ).	290
<b>Figure A11.</b> Differential Pulse Voltammograms of Synthesized Compounds in $\text{CH}_2\text{Cl}_2$ .	291
<b>Figure A12.</b> UV-Visible Spectral Changes of (a) NiTPC(MN) $_2$ (Benzo) ( <b>1</b> ) with $\text{CN}^-$ ion; (b) NiTPCBr $_4$ (IND) $_2$ (Benzo) with Cyanide Ion in $\text{CH}_2\text{Cl}_2$ at 298 K.	291
<b>Figure A13.</b> Comparative UV-Visible Spectra of NiDFP(IND) $_2$ (Benzo) ( <b>3</b> ) With and Without Cyanide Ion $\text{CH}_2\text{Cl}_2$ at 298 K.	292

**Figure A1.**  $^1\text{H}$  NMR Spectrum of NiTPC(MN) $_2$ (Benzo) (**2**) in  $\text{CDCl}_3$  at 298 K.**Figure A2.**  $^1\text{H}$  NMR Spectrum of NiDFP(MN) $_2$ (Benzo) (**4**) in  $\text{CDCl}_3$  at 298 K.

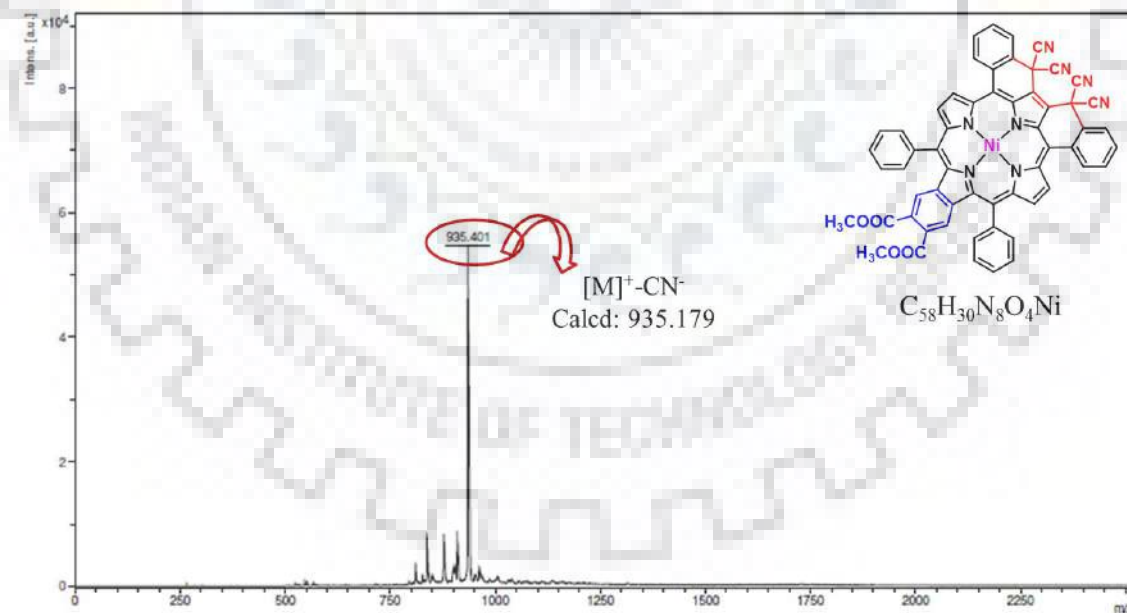


**Figure A3.**  $^1\text{H}$  NMR Spectrum of NiTPCBr<sub>4</sub>(IND)<sub>2</sub>(Benzo) (**5**) in CDCl<sub>3</sub> at 298 K.**Figure A4.** MALDI-TOF Mass Spectrum of NiTPC(IND)<sub>2</sub>(Benzo) (**1**) in Positive Ion Mode.

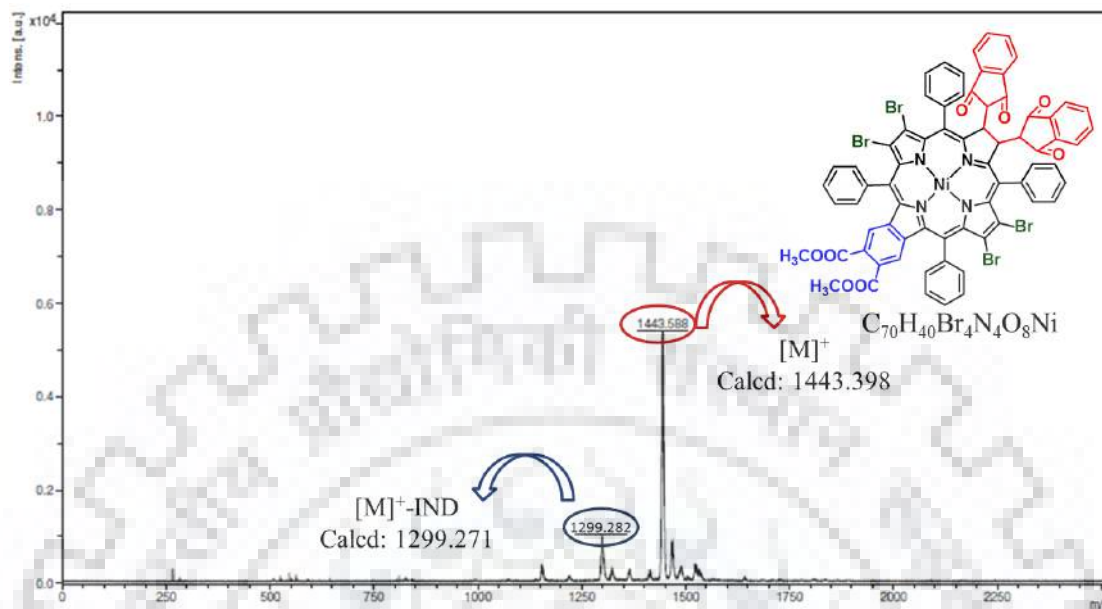
**Figure A5.** MALDI-TOF Mass Spectrum of NiTPC(MN)<sub>2</sub>(Benzo) (**2**) in Positive Ion Mode.



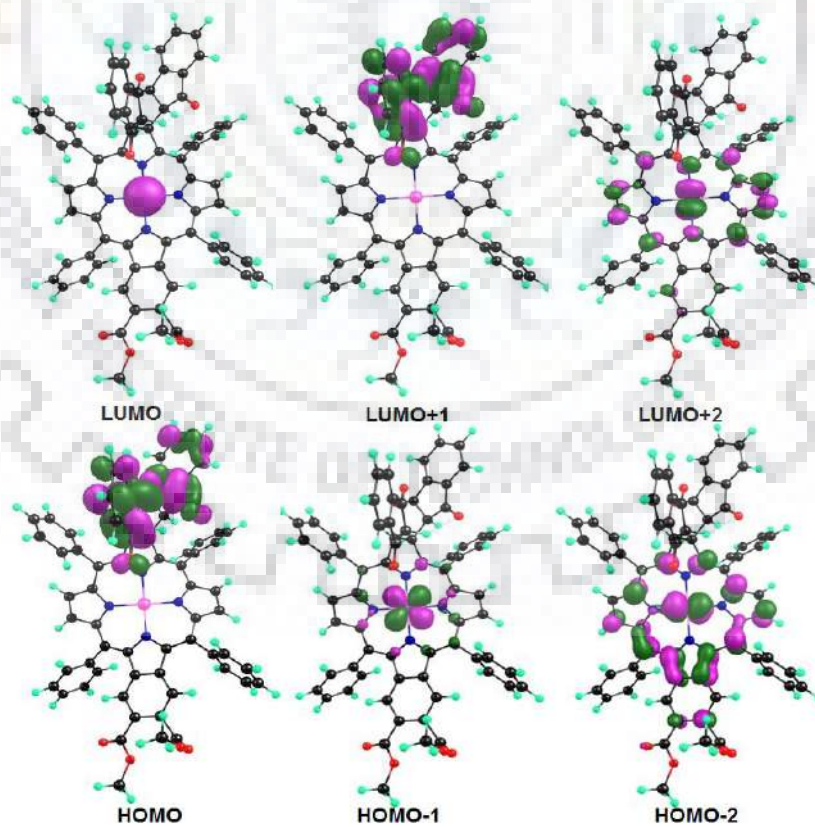
**Figure A6.** MALDI-TOF Mass Spectrum of NiDFP(MN)<sub>2</sub>(Benzo) (**4**) in Positive Ion Mode.



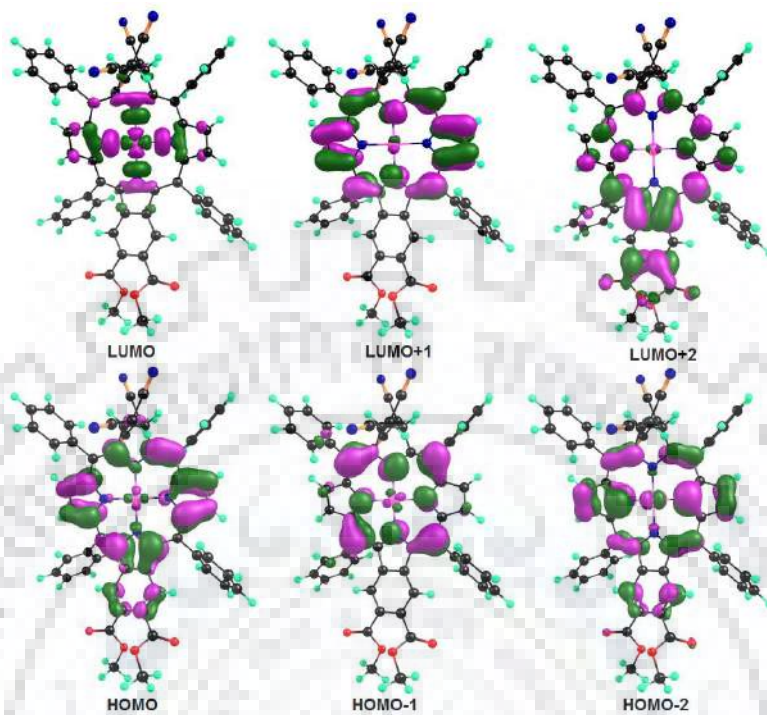
**Figure A7.** MALDI-TOF Mass Spectrum of NiTPCBr<sub>4</sub>(IND)<sub>2</sub>(Benzo) (**5**).



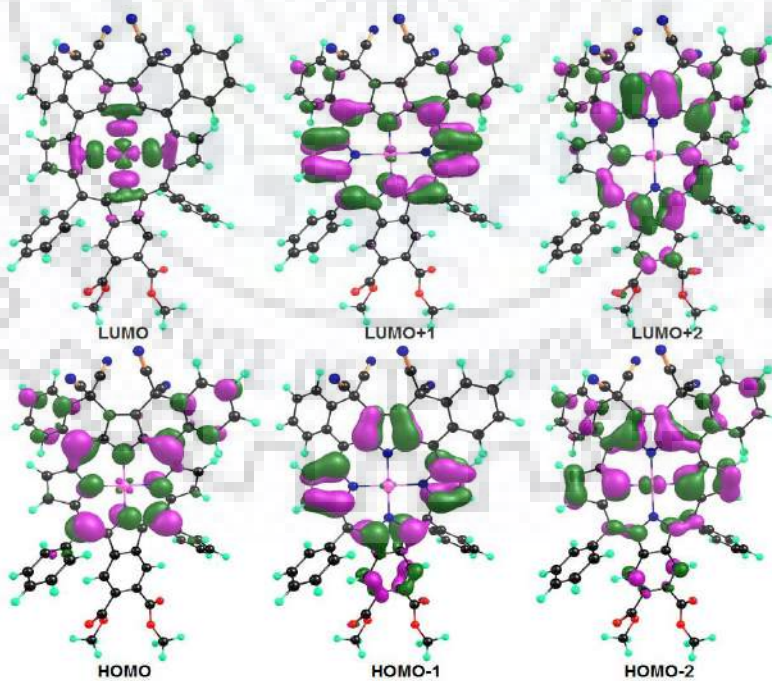
**Figure A8.** Frontier Molecular Orbitals of NiTPC(IND)<sub>2</sub>(Benzo) (**1**).



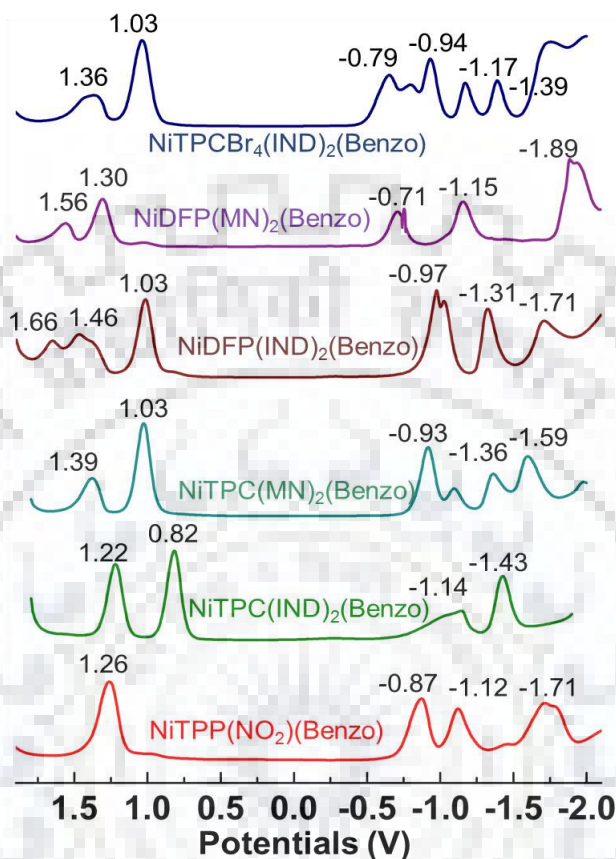
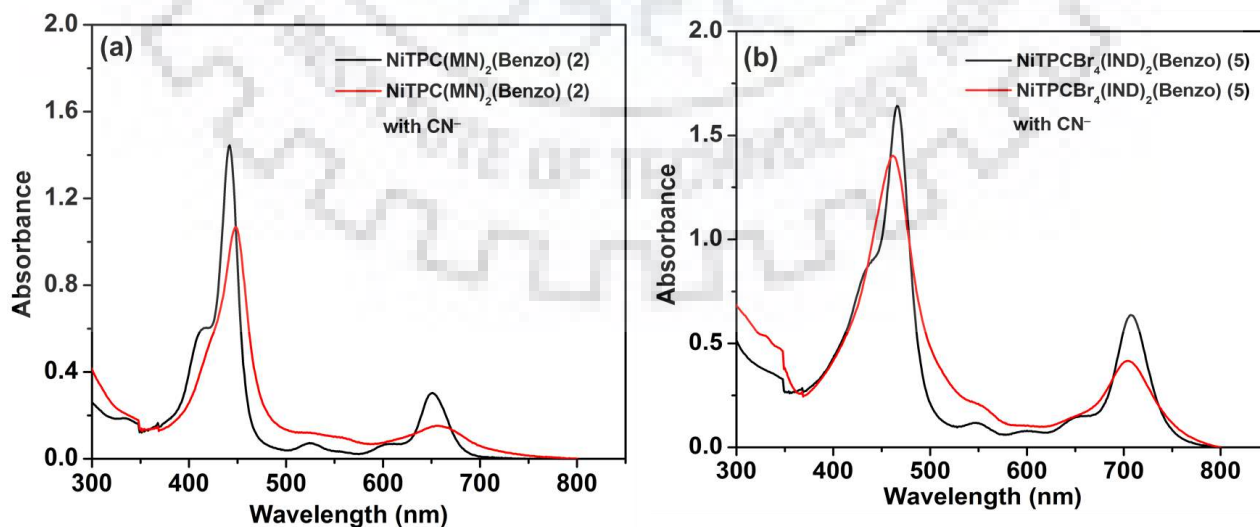
**Figure A9.** Frontier Molecular Orbitals of NiTPC(MN)<sub>2</sub>(Benzo) (2).



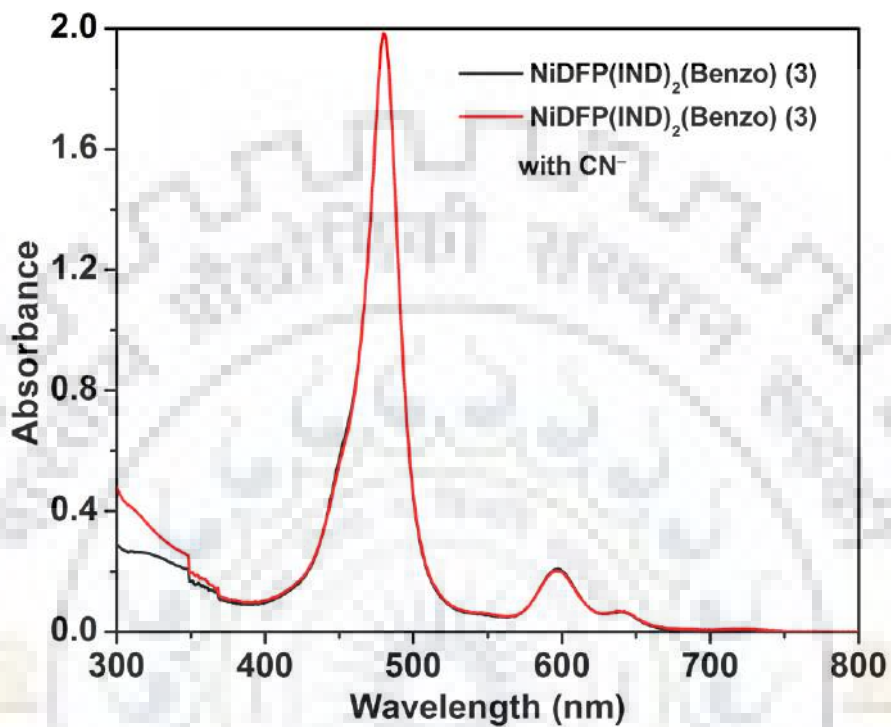
**Figure A10.** Frontier Molecular Orbitals of NiDFP(MN)<sub>2</sub>(Benzo) (4).





**Figure A11.** Differential Pulse Voltammograms of Synthesized Compounds in  $\text{CH}_2\text{Cl}_2$ .**Figure A12.** UV-Visible Spectral Changes of (a) NiTPC(MN)<sub>2</sub>(Benzo) (1) with  $\text{CN}^-$  ion; (b) NiTPCBr<sub>4</sub>(IND)<sub>2</sub>(Benzo) with Cyanide Ion in  $\text{CH}_2\text{Cl}_2$  at 298 K.

**Figure A13.** Comparative UV-Visible Spectra of NiDFP(IND)<sub>2</sub>(Benzo) (**3**) With and Without Cyanide Ion in CH<sub>2</sub>Cl<sub>2</sub> at 298K

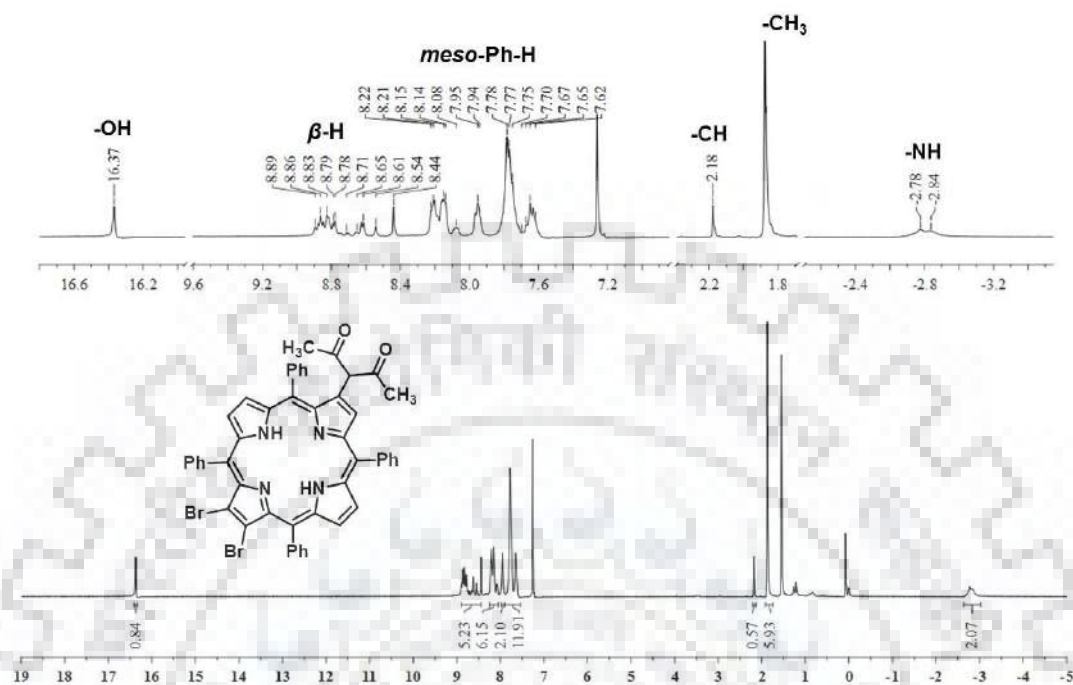
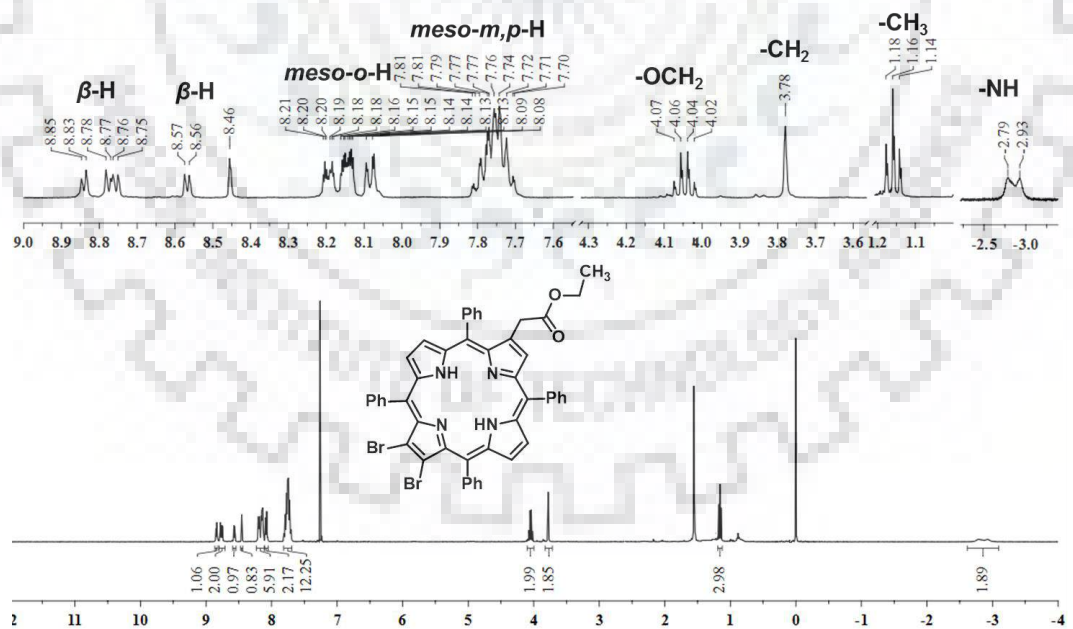


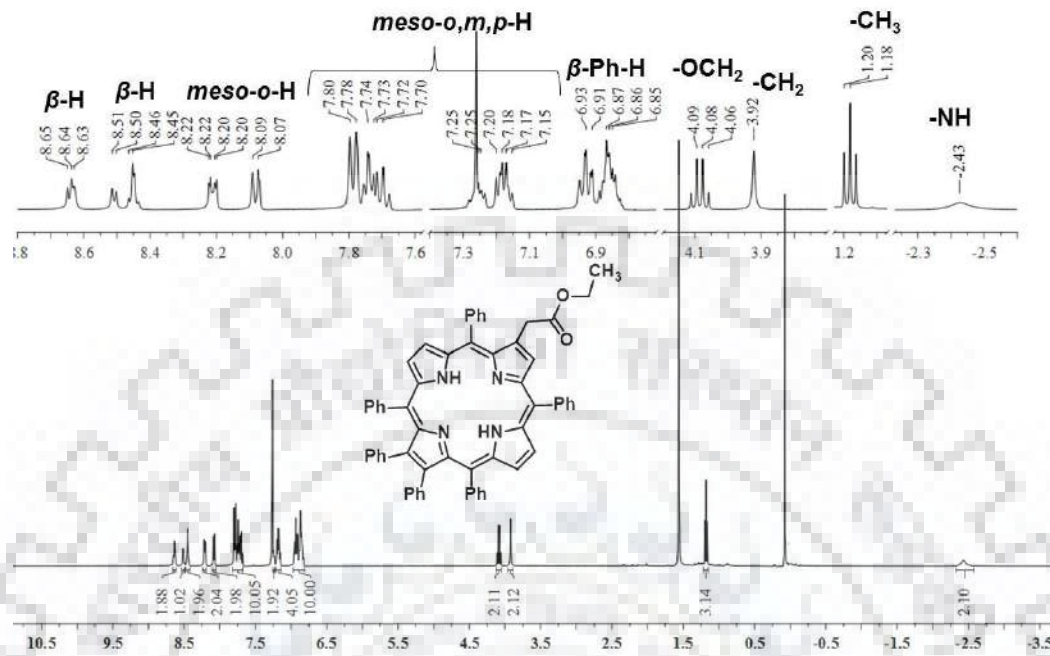
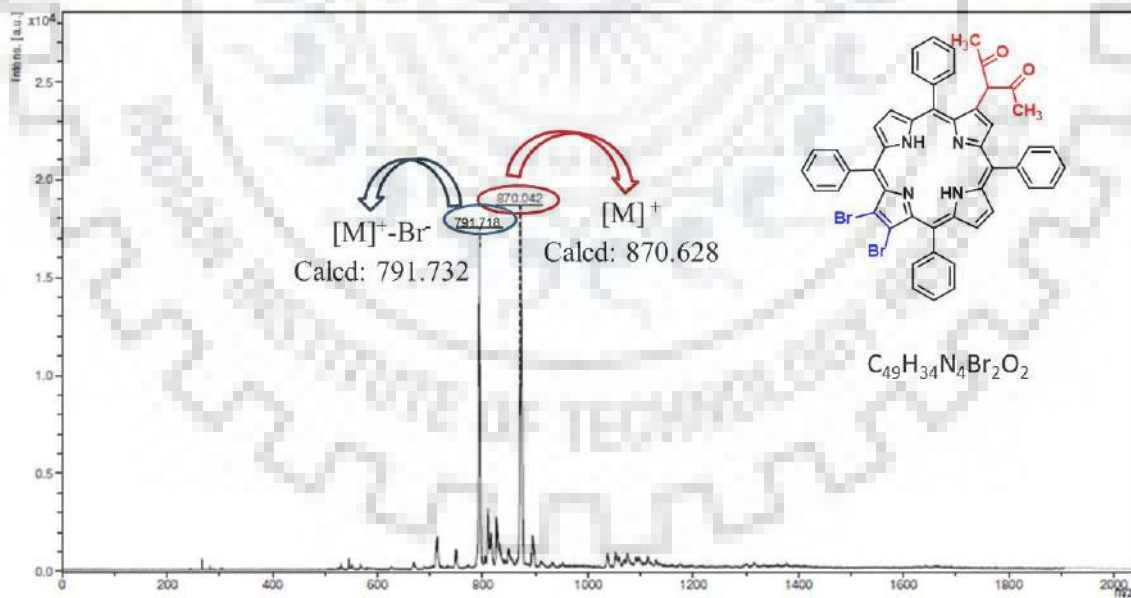


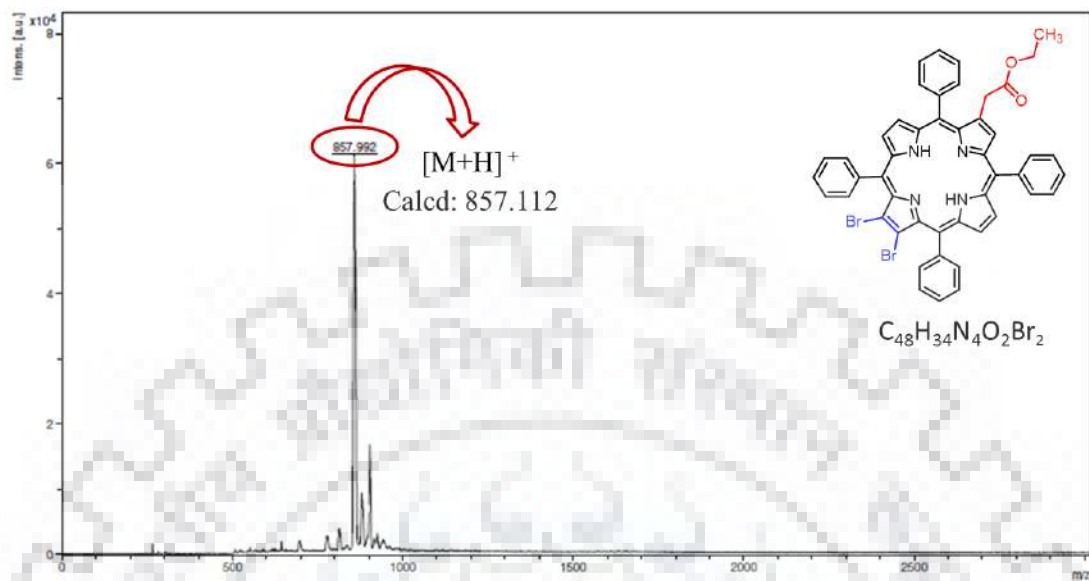
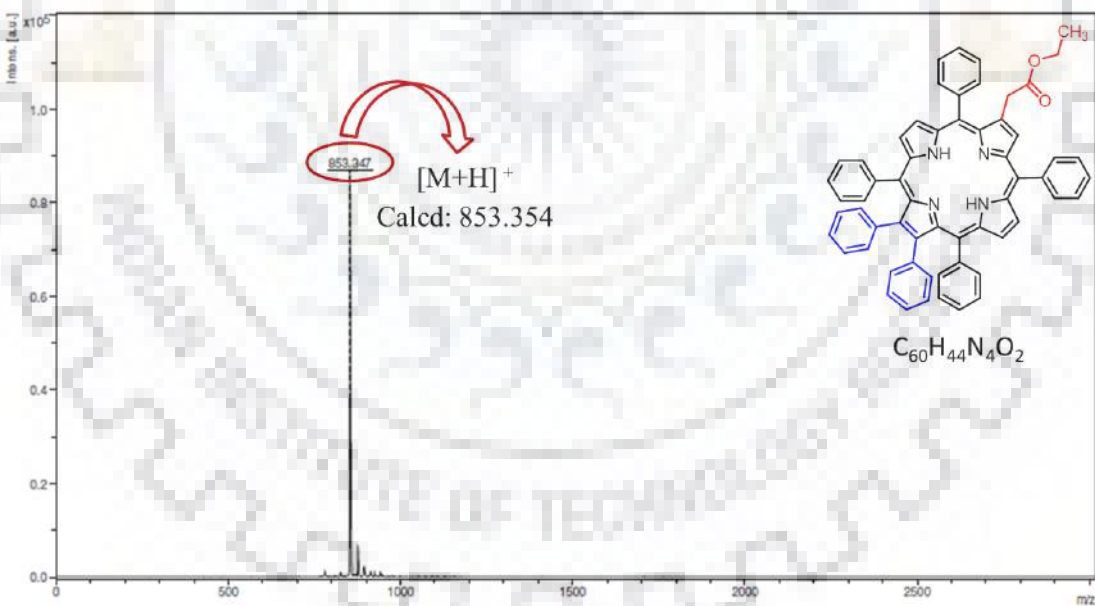
## APPENDIX-V

## Synthesis, Structural, Photophysical and Electrochemical Redox Studies of $\beta$ -Trisubstituted Porphyrins

Table of Contents	Page No.
<b>Figure A1.</b> $^1\text{H}$ NMR Spectrum of $\text{H}_2\text{TPP}[\text{CH}(\text{COCH}_3)_2]\text{Br}_2$ ( <b>1</b> ) in $\text{CDCl}_3$ at 298 K.	294
<b>Figure A2.</b> $^1\text{H}$ NMR Spectrum of $\text{H}_2\text{TPP}[\text{CH}_2\text{COOC}_2\text{H}_5]\text{Br}_2$ ( <b>3</b> ) in $\text{CDCl}_3$ at 298 K.	294
<b>Figure A3.</b> $^1\text{H}$ NMR Spectrum of $\text{H}_2\text{TPP}[\text{CH}_2\text{COOC}_2\text{H}_5]\text{Ph}_2$ ( <b>4</b> ) in $\text{CDCl}_3$ at 298 K.	295
<b>Figure A4.</b> MALDI-TOF Mass Spectrum of $\text{H}_2\text{TPP}[\text{CH}(\text{COCH}_3)_2]\text{Br}_2$ ( <b>1</b> ).	295
<b>Figure A5.</b> MALDI-TOF Mass Spectrum of $\text{H}_2\text{TPP}[\text{CH}_2\text{COOC}_2\text{H}_5]\text{Br}_2$ ( <b>3</b> ).	296
<b>Figure A6.</b> MALDI-TOF Mass Spectrum of $\text{H}_2\text{TPP}[\text{CH}_2\text{COOC}_2\text{H}_5]\text{Ph}_2$ ( <b>4</b> ).	296
<b>Figure A7.</b> Fully Optimized Geometries of Synthesized Free Base Porphyrins.	298
<b>Figure A8.</b> Frontier Molecular Orbitals of $\text{H}_2\text{TPP}[\text{CH}(\text{COCH}_3)_2]\text{Br}_2$ ( <b>1</b> ).	298
<b>Figure A9.</b> Frontier Molecular Orbitals of $\text{H}_2\text{TPP}[\text{CH}_2\text{COOC}_2\text{H}_5]\text{Br}_2$ ( <b>3</b> ).	299
<b>Figure A10.</b> Frontier Molecular Orbitals of $\text{H}_2\text{TPP}[\text{CH}_2\text{COOC}_2\text{H}_5]\text{Ph}_2$ ( <b>4</b> ).	299
<b>Figure A11.</b> (a) Comparative UV-Visible Spectra of Synthesized Zn(II) Porphyrins in $\text{CH}_2\text{Cl}_2$ . (b) Comparative Emission Spectra of Zn(II) Complexes in $\text{CH}_2\text{Cl}_2$ at 298 K.	300
<b>Figure A12.</b> Comparative UV-Visible Spectra of $\text{MTPP}(\text{X})_2(\text{R})$ (where $\text{M} = \text{Co}, \text{Ni}$ and $\text{Cu}$ ; $\text{X} = \text{Br}$ and $\text{Ph}$ ; $\text{R} = \text{CH}(\text{COCH}_3)_2$ and $\text{CH}_2\text{COOC}_2\text{H}_5$ ) in $\text{CH}_2\text{Cl}_2$ at 298 K.	300
<b>Figure A13.</b> Comparative Cyclic Voltammograms of Synthesized (a) Free Base Complexes, (b) Copper Complexes and (c) Zn(II) complexes in $\text{CH}_2\text{Cl}_2$ at 298 K using 0.1 M TBAPF <sub>6</sub> as Supporting Electrolyte.	302
<b>Table A1.</b> Crystal Structure Data of $\text{NiTPP}[\text{CH}(\text{COCH}_3)_2]\text{Br}_2$ ( <b>1b</b> ), $\text{H}_2\text{TPP}[\text{CH}_2\text{COOC}_2\text{H}_5]\text{Br}_2$ ( <b>3</b> ), and $\text{ZnTPP}[\text{CH}_2\text{COOC}_2\text{H}_5]\text{Ph}_2$ ( <b>4d</b> )	297
<b>Table A2.</b> Optical Absorption Spectral Data of Metal Complexes of Mixed $\beta$ -trisubstituted Porphyrins in $\text{CH}_2\text{Cl}_2$ .	301

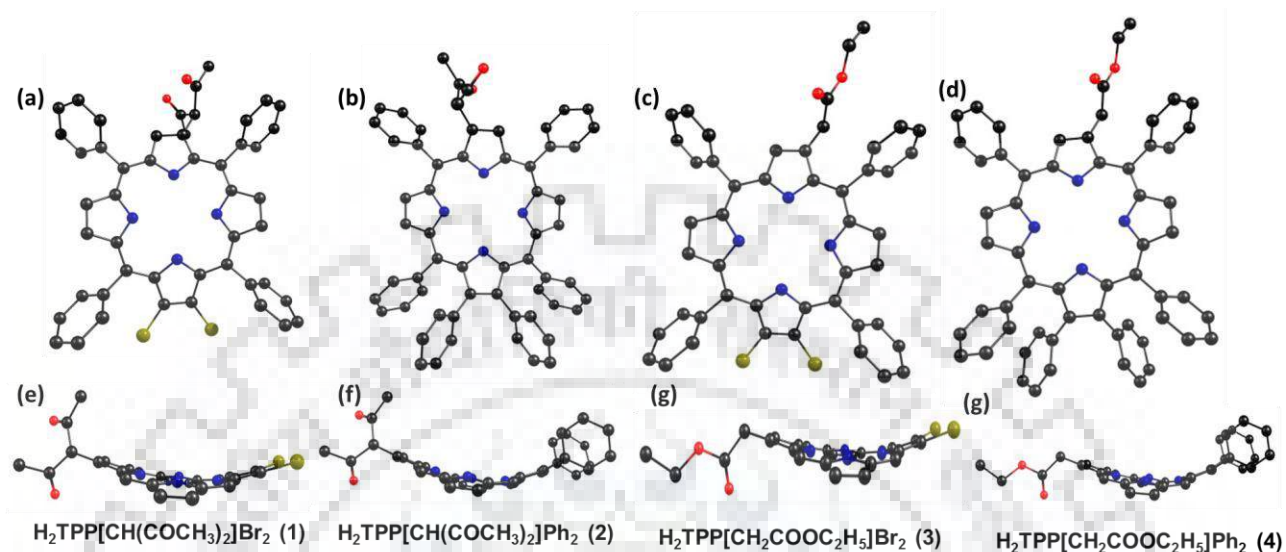
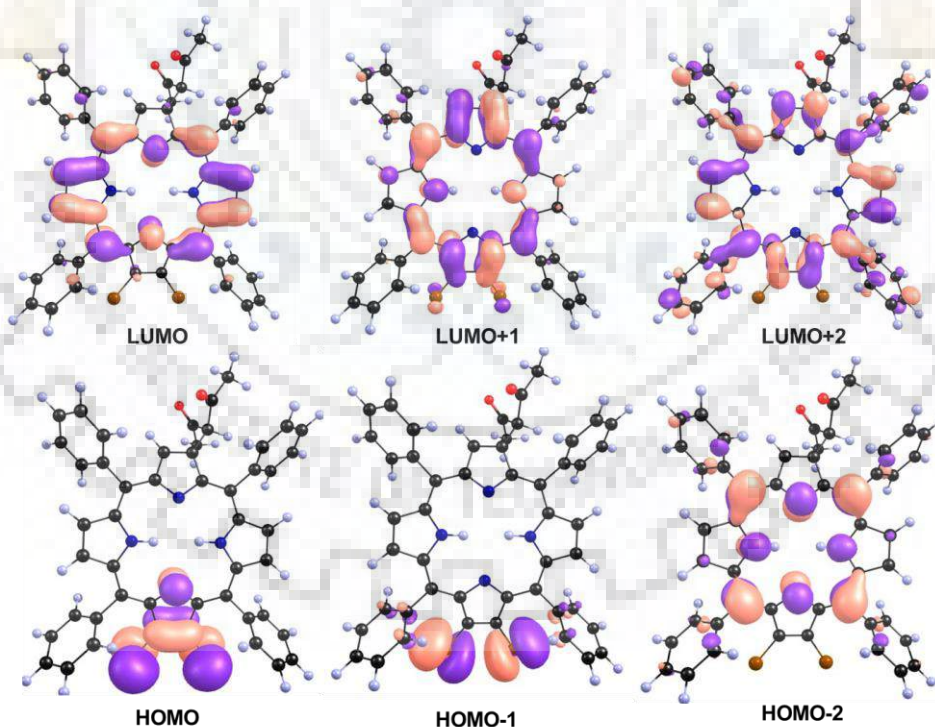
Figure A1.  $^1\text{H}$  NMR Spectrum of  $\text{H}_2\text{TPP}[\text{CH}(\text{COCH}_3)_2]\text{Br}_2$  (**1**) in  $\text{CDCl}_3$  at 298 K.Figure A2.  $^1\text{H}$  NMR Spectrum of  $\text{H}_2\text{TPP}[\text{CH}_2\text{COOC}_2\text{H}_5]\text{Br}_2$  (**3**) in  $\text{CDCl}_3$  at 298 K.

**Figure A3.**  $^1\text{H}$  NMR Spectrum of  $\text{H}_2\text{TPP}[\text{CH}_2\text{COOC}_2\text{H}_5]\text{Ph}_2$  (**4**) in  $\text{CDCl}_3$  at 298 K.**Figure A4.** MALDI-TOF Mass Spectrum of  $\text{H}_2\text{TPP}[\text{CH}(\text{COCH}_3)_2]\text{Br}_2$  (**1**).

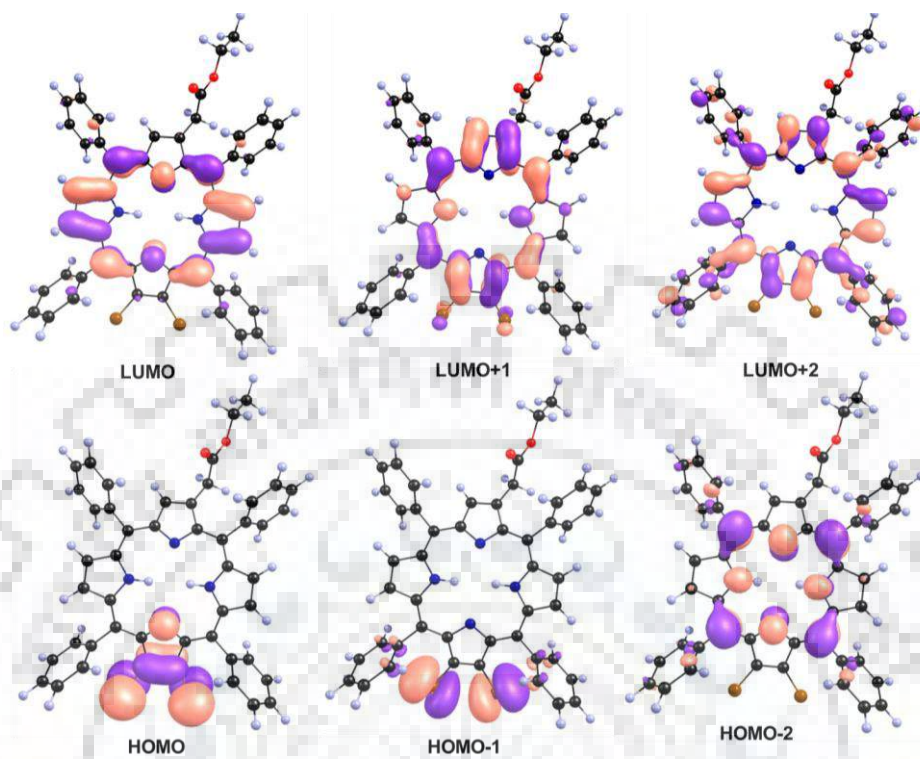
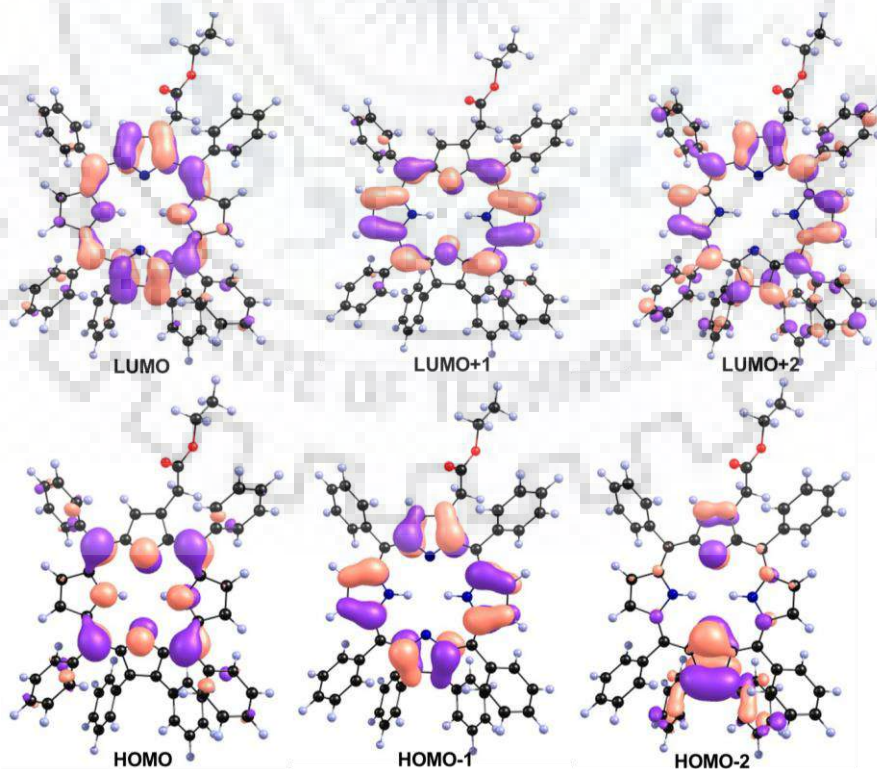
**Figure A5.** MALDI-TOF Mass Spectrum of  $H_2TPP[CH_2COOC_2H_5]Br_2$  (**3**).**Figure A6.** MALDI-TOF Mass Spectrum of  $H_2TPP[CH_2COOC_2H_5]Ph_2$  (**4**).

**Table A1.** Crystal Structure Data of NiTPP[CH(COCH<sub>3</sub>)<sub>2</sub>]<sub>2</sub>Br<sub>2</sub> (**1b**), H<sub>2</sub>TPP[CH<sub>2</sub>COOC<sub>2</sub>H<sub>5</sub>]<sub>2</sub>Br<sub>2</sub> (**3**), and ZnTPP[CH<sub>2</sub>COOC<sub>2</sub>H<sub>5</sub>]<sub>2</sub>Ph<sub>2</sub> (**4d**)

	NiTPP[CH(COCH <sub>3</sub> ) <sub>2</sub> ] <sub>2</sub> Br <sub>2</sub>	H <sub>2</sub> TPP[CH <sub>2</sub> COOC <sub>2</sub> H <sub>5</sub> ] <sub>2</sub> Br <sub>2</sub>	ZnTPP[CH <sub>2</sub> COOC <sub>2</sub> H <sub>5</sub> ] <sub>2</sub> Ph <sub>2</sub>
Empirical formula	C <sub>49</sub> H <sub>32</sub> Br <sub>2</sub> N <sub>4</sub> O <sub>2</sub> Ni	2(C <sub>48</sub> H <sub>34</sub> Br <sub>2</sub> N <sub>4</sub> O <sub>2</sub> )C <sub>7</sub> H <sub>8</sub>	C <sub>65</sub> H <sub>45</sub> N <sub>5</sub> O <sub>2</sub> Zn
Formula wt.	927.31	1809.32	990.43
Crystal system	triclinic	triclinic	triclinic
Space group	p-1	P1	p-1
<i>a</i> (Å)	11.8086(17)	12.531(5)	11.518(2)
<i>b</i> (Å)	13.0491(19)	13.572(5)	13.372(2)
<i>c</i> (Å)	13.862(2)	14.722(5)	17.496(3)
$\alpha$ (°)	72.580(5)	107.337(5)	102.002(9)
$\beta$ (°)	75.915(5)	108.420(5)	96.585(9)
$\gamma$ (°)	74.419(5)	104.393(5)	105.208(9)
Volume (Å <sup>3</sup> )	1932.1(5)	2098.9(13)	2502.4(8)
Z	2	1	2
D <sub>calcd.</sub> (mg/m <sup>3</sup> )	1.594	1.431	1.314
$\lambda$ (Å)	0.71073	0.71073	0.71073
T (K)	296(2)	293(2)	293(2)
No. of total reflns.	14188	21098	33620
No. of indepnt. reflns.	4192	7877	8127
R	0.0855	0.0595	0.0481
R <sub>w</sub>	0.2664	0.2191	0.1757
GOOF	1.133	0.992	1.156
CCDC	<b>1830111</b>	<b>1830110</b>	<b>1830112</b>

**Figure A7.** Fully Optimized Geometries of Synthesized Free Base porphyrins using B3LYP/6-31 G Basis Sets.**Figure A8.** Frontier Molecular Orbitals of  $\text{H}_2\text{TPP}[\text{CH}(\text{COCH}_3)_2]\text{Br}_2$  (1).



**Figure A9.** Frontier Molecular Orbitals of  $H_2TPP[CH_2COOC_2H_5]Br_2$  (3).**Figure A10.** Frontier Molecular Orbitals of  $H_2TPP[CH_2COOC_2H_5]Ph_2$  (4).

**Figure A11.** (a) Comparative UV-Visible Spectra of Synthesized Zn(II) Porphyrins in  $\text{CH}_2\text{Cl}_2$ . (b) Comparative Emission Spectra of Zn(II) Complexes in  $\text{CH}_2\text{Cl}_2$  at 298 K.

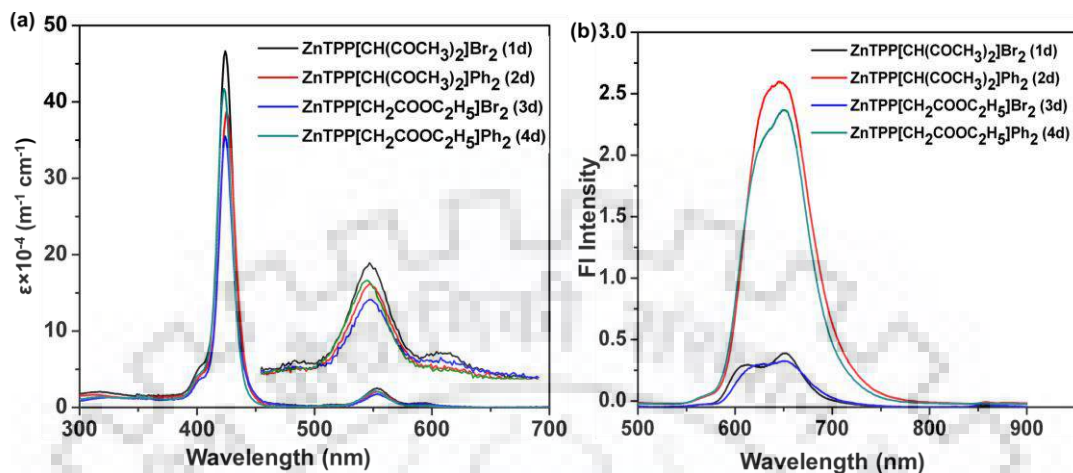


**Figure A12.** Comparative UV-Visible Spectra of MTPP(X)<sub>2</sub>(R) (where M = Co, Ni and Cu; X = Br and Ph; R = CH(COCH<sub>3</sub>)<sub>2</sub> and CH<sub>2</sub>COOC<sub>2</sub>H<sub>5</sub>) in  $\text{CH}_2\text{Cl}_2$  at 298 K.

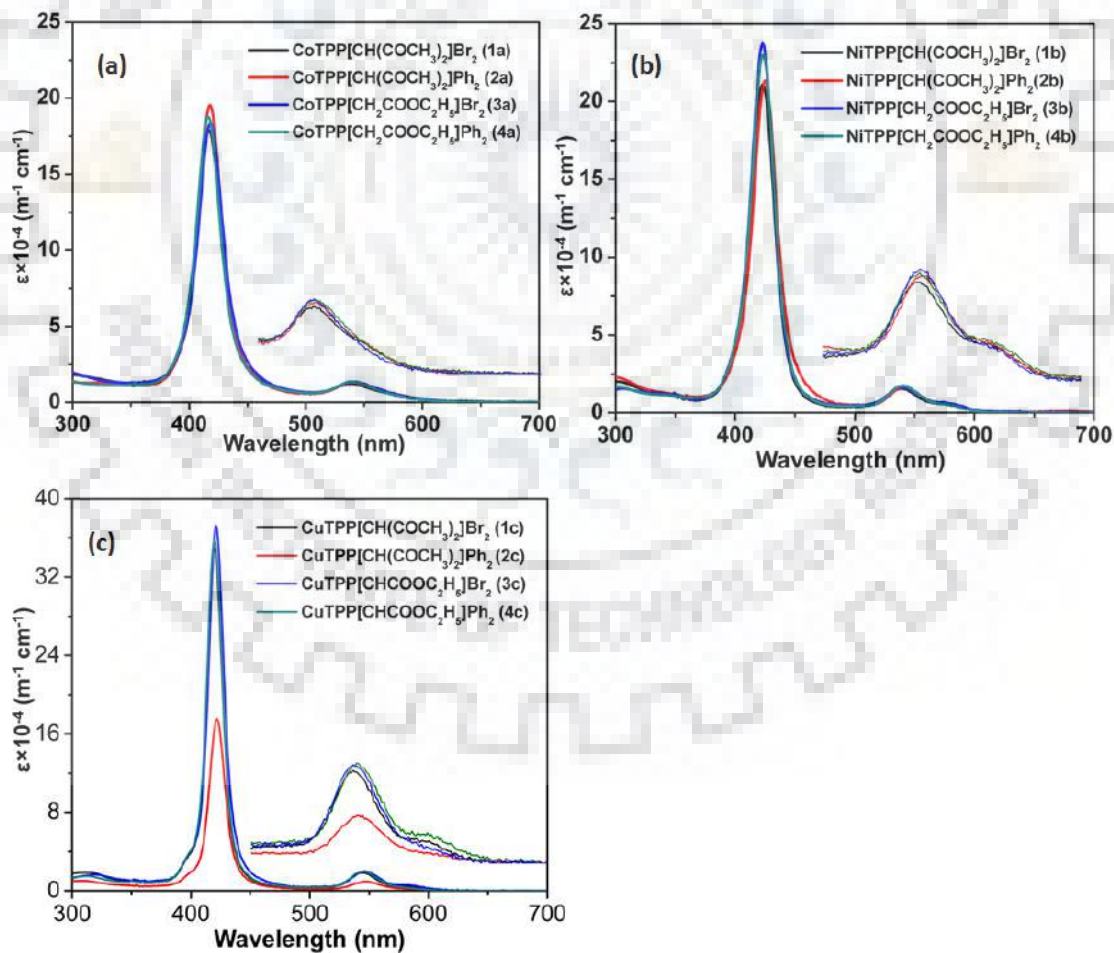
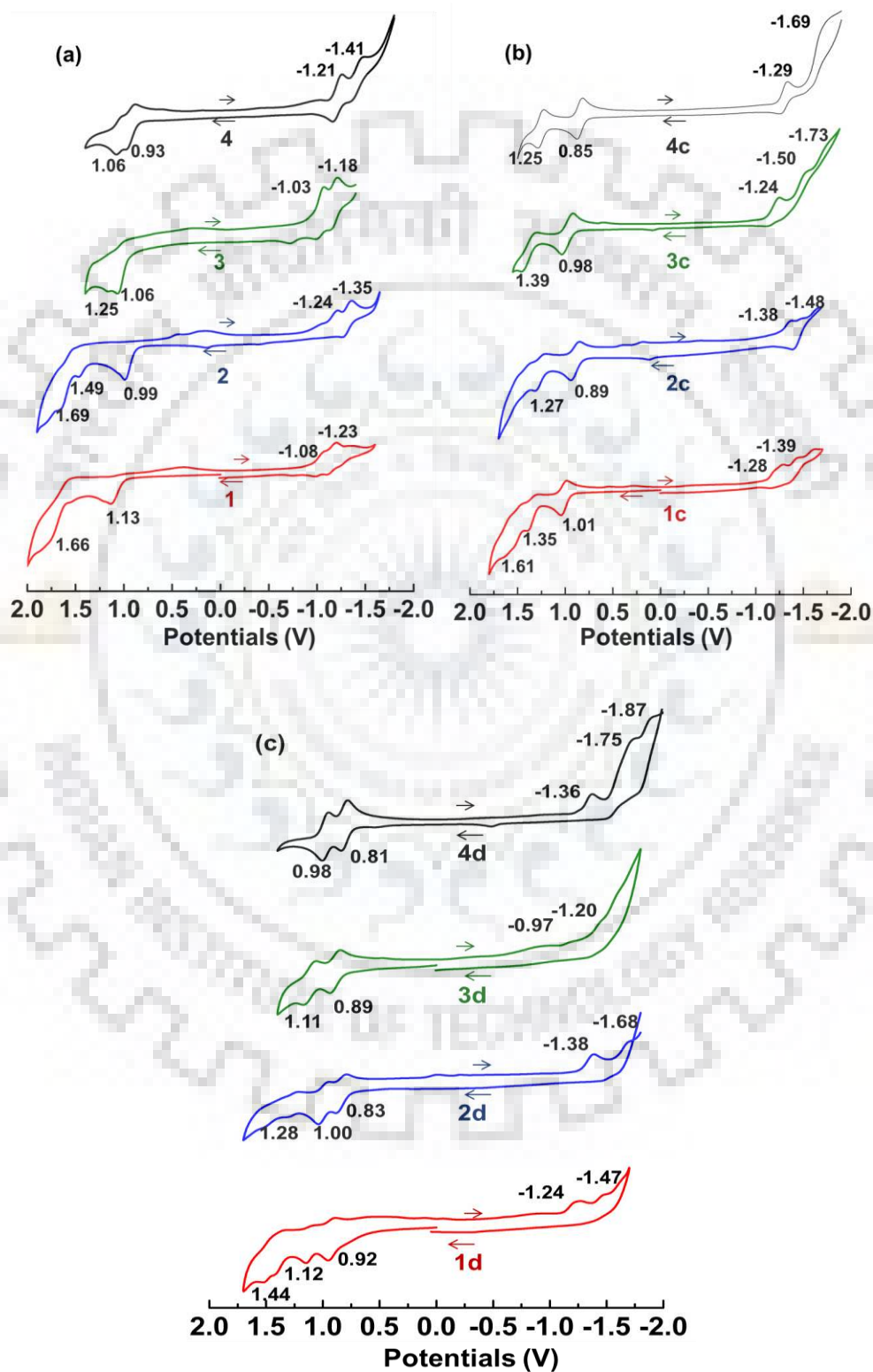


**Table A2.** Optical Absorption Spectral Data<sup>a</sup> of Metal Complexes of Mixed  $\beta$ -trisubstituted Porphyrins in CH<sub>2</sub>Cl<sub>2</sub>.

<b>Porphyrin</b>	<b>B band, nm</b>	<b>Q band(s), nm</b>	<b>FWHM</b>	<b><i>f</i></b>
CoTPP(NO <sub>2</sub> )Br <sub>2</sub>	431(5.04)	551(3.94), 595(4.02)		
CoTPP[CH(COCH <sub>3</sub> ) <sub>2</sub> ]Br <sub>2</sub> (1a)	417(5.25)	540(4.09)	29	0.015
CoTPP[CH <sub>2</sub> COOC <sub>2</sub> H <sub>5</sub> ]Br <sub>2</sub> (3a)	418(5.29)	541(4.12)	28	0.025
CoTPP(NO <sub>2</sub> )Ph <sub>2</sub>	434(4.98)	553(3.96), 593(3.98)		
CoTPP[CH(COCH <sub>3</sub> ) <sub>2</sub> ]Ph <sub>2</sub> (2a)	418(5.26)	540(4.13)	30	0.025
CoTPP[CH <sub>2</sub> COOC <sub>2</sub> H <sub>5</sub> ]Ph <sub>2</sub> (4a)	416(5.27)	539(4.13)	29	0.024
NiTPP(NO <sub>2</sub> )Br <sub>2</sub>	437(5.17)	548(4.02), 597(4.11)		
NiTPP[CH(COCH <sub>3</sub> ) <sub>2</sub> ]Br <sub>2</sub> (1b)	423(5.32)	539(4.19), 579(3.75)	26	0.025
NiTPP[CH <sub>2</sub> COOC <sub>2</sub> H <sub>5</sub> ]Br <sub>2</sub> (3b)	423(5.38)	540(4.23), 580(3.79)	25	0.028
NiTPP(NO <sub>2</sub> )Ph <sub>2</sub>	440(5.10)	550(4.04), 598(4.07)		
NiTPP[CH(COCH <sub>3</sub> ) <sub>2</sub> ]Ph <sub>2</sub> (2b)	425(5.33)	542(4.22), 580sh	27	0.027
NiTPP[CH <sub>2</sub> COOC <sub>2</sub> H <sub>5</sub> ]Ph <sub>2</sub> (4b)	423(5.36)	540(4.25), 579sh	26	0.027
CuTPP(NO <sub>2</sub> )Br <sub>2</sub>	430(5.23)	556(4.02), 600(4.05)		
CuTPP[CH(COCH <sub>3</sub> ) <sub>2</sub> ]Br <sub>2</sub> (1c)	420(5.54)	543(4.26), 583sh	17	0.027
CuTPP[CH <sub>2</sub> COOC <sub>2</sub> H <sub>5</sub> ]Br <sub>2</sub> (3c)	421(5.57)	545(4.29), 585sh	17	0.290
CuTPP(NO <sub>2</sub> )Ph <sub>2</sub>	432(5.18)	556(4.06), 601(4.00)		
CuTPP[CH(COCH <sub>3</sub> ) <sub>2</sub> ]Ph <sub>2</sub> (2c)	422(5.24)	547(3.98)	18	0.014
CuTPP[CH <sub>2</sub> COOC <sub>2</sub> H <sub>5</sub> ]Ph <sub>2</sub> (4c)	420(5.55)	545(4.29)	17	0.028

<sup>a</sup>Values in parentheses refers to log  $\epsilon$ , sh = shoulder

**Figure A13.** Comparative Cyclic Voltammograms of Synthesized (a) Free Base Complexes, (b) Copper Complexes and (c) Zn(II) Complexes in  $\text{CH}_2\text{Cl}_2$  at 298 K using 0.1 M  $\text{TBAPF}_6$  as Supporting Electrolyte.





## APPENDIX-VI

## Perhaloporphyrins: Synthesis, Structural, Electrochemical Redox and Anion Sensing Properties

Table of Contents	Page No.
<b>Figure A1.</b> The ORTEP Diagrams Showing Top Views of (a) CoTPP(NO <sub>2</sub> )Cl <sub>7</sub> .MeOH ( <b>1a</b> .MeOH), (b) ZnTPP(NO <sub>2</sub> )Cl <sub>7</sub> .Py ( <b>1d</b> .py) and (c) NiTPPCL <sub>8</sub> ( <b>2b</b> ).	305
<b>Figure A2.</b> The ORTEP Diagrams Showing Top (a) and Side (b) Views of 2,3,7,8,12,13,17,18-Octachloro- <i>meso</i> -tetraphenylporphyrin ( <b>2</b> ).	306
<b>Figure A3.</b> The Packing Diagram of (a) ZnTPP(NO <sub>2</sub> )Cl <sub>7</sub> .MeOH ( <b>1d</b> .MeOH) and (b) ZnTPPCL <sub>8</sub> .MeOH ( <b>2b</b> .MeOH).	306
<b>Figure A4.</b> Displacement of Porphyrin Core Atoms (in Angstroms) from the Mean Plane for CoTPP(NO <sub>2</sub> )Cl <sub>7</sub> .MeOH( <b>1a</b> .MeOH) (a), ZnTPP(NO <sub>2</sub> )Cl <sub>7</sub> .Py ( <b>1d</b> .Py) and NiTPPCL <sub>8</sub> ( <b>2b</b> ) (c), respectively.	307
<b>Figure A5.</b> <sup>1</sup> H NMR Spectrum of NiTPPCL <sub>8</sub> ( <b>2b</b> ) in CDCl <sub>3</sub> at 298 K.	311
<b>Figure A6.</b> Imino Protons Region of <b>1-4</b> in CDCl <sub>3</sub> at 298 K	311
<b>Figure A7.</b> The ESI-MS Spectrum of CoTPP(NO <sub>2</sub> )Cl <sub>7</sub> ( <b>2a</b> ) in CH <sub>3</sub> CN at 298 K.	312
<b>Figure A8.</b> The ESI-MS Spectrum of NiTPP(NO <sub>2</sub> )Cl <sub>7</sub> ( <b>2b</b> ) in CH <sub>3</sub> CN at 298 K.	312
<b>Figure A9.</b> The ESI-MS Spectrum of CuTPP(NO <sub>2</sub> )Cl <sub>7</sub> ( <b>2c</b> ) in CH <sub>3</sub> CN at 298 K.	313
<b>Figure A10.</b> The ESI-MS Spectrum of ZnTPP(NO <sub>2</sub> )Cl <sub>7</sub> ( <b>2d</b> ) in CH <sub>3</sub> CN at 298 K.	313
<b>Figure A11.</b> Electronic Absorption Spectra of (a) <b>1a</b> and <b>2a</b> , (b) <b>1b</b> and <b>2b</b> , and (c) <b>1c</b> and <b>2c</b> in Toluene at 298 K.	314
<b>Figure A12.</b> Comparative Cyclic Voltammograms of (a) <b>1a</b> and <b>2a</b> (b) <b>1b</b> and <b>2b</b> , (c) <b>1c</b> and <b>2c</b> in CH <sub>2</sub> Cl <sub>2</sub> with 0.1M TBAF <sub>6</sub> as the Supporting Electrolyte at a Scan Rate of 100 mV/s.	314
<b>Figure A13.</b> UV-Vis. Spectral Titrations of <b>2-4</b> with TFA in Toluene at 298 K.	315
<b>Figure A14.</b> UV-Vis. Spectral Titrations of <b>2-4</b> with TBAOH in Toluene at 298 K.	316
<b>Figure A15.</b> Colorimetric Responses of <b>2-4</b> while Adding Excess of Anions in Toluene.	317
<b>Figure A16.</b> UV-Vis Spectral Titrations of <b>2-4</b> while Increasing [CN <sup>-</sup> ] in Toluene at 298 K. Insets Show the Corresponding Hill plots.	319
<b>Figure A17.</b> Plots of ΔA at λ <sub>max</sub> vs [OAc <sup>-</sup> ] or [H <sub>2</sub> PO <sub>4</sub> <sup>-</sup> ] or [CN <sup>-</sup> ] for <b>1-4</b> Showing Sigmoidal Curve	319

Indicating the Positive Cooperative Behavior.

**Figure A18.** Fluorescence Spectral Titrations (FL quenching) of **1-4** while Increasing  $[F^-]$  in Toluene at 298 K. 320

**Figure A19.** DPV Traces of **1-4** in Absence and Presence of Excess of  $[F^-]$  in  $CH_2Cl_2$  Containing 0.1 M TBAPF<sub>6</sub> at 298 K. 321

**Figure A20:** UV-Visible Spectral Titrations of Planar Porphyrins (*meso*-Tetraphenylporphyrin ( $H_2TPP$ ) and 2,3,5,10,15,17,18,20-Octaphenylporphyrin ( $H_2TPP(Ph)_4$ ) and Nonplanar Porphyrins (2,3,12,13-Tetrabromo-*meso*-tetraphenylporphyrin ( $H_2TPPBr_4$ ) and 2,3,5,7,8,10,12,13,15,17,18,20-Dodecaphenylporphyrin ( $H_2TPP(Ph)_8$ )) while Increasing  $[F^-]$  in Toluene at 298 K. 322

**Figure A21.** Overlaid UV-Visible Spectra of **1-4** with Excess of *p*-Toluenesulphonic acid (PTSA), Piperidine and Fluoride Ions in Toluene 298 K. Herein, Piperidine forms 1:1 Host:Guest Complex with **1-4** in 1,2-Dichloroethane. 323

**Figure A22.** (a) UV-Vis Spectral Titrations of **3** with TBACl (0.008 M) in Toluene at 298 K. Inset Shows the Absorbance Changes in The Soret Region; (b) Hill Plot  $\log(A_i - A_0 / A_i - A_0) vs \log [Cl^-]$  Showing 1:1 Stoichiometry Indicated by Slope 1. 324

**Figure A23.** (a) Treatment of **1**• $2CN^-$  Complex with Aliquots of 1 mM Solution TFA at 298 K. (b) Reusability Test of Regenerated **1** with Aliquots of 8 mM Solution of  $CN^-$  Ions in Toluene at 298 K. 324

**Figure A24.** Axial Ligation of Pyridine to **2d** in Toluene at 298 K. 325

**Figure A25.** The Axial Ligation Studies of  $X^-$ , Where  $X = OAc^-$  (a),  $F^-$  (b), and  $PO_4^{3-}$  (c) Anions to **1d** ( $8.29 \times 10^{-6}$  M) in Toluene at 298 K. Insets Show plot  $[X^-]^2 vs [X^-]^2 / \Delta A$ . 325

**Figure A26.** Benesi-Hildebrand Plot Constructed for 1:1 Stoichiometric Ratio from the Titration Data of **1d** and **2d** with Cyanide Ion. 326

**Figure 27.** (a) Colorimetric Changes of **2a** with Tested Anions in Toluene at 298 K (Top). UV-Visible Spectral Changes of **2a** Upon Addition of Excess of Anions (Bottom). (b) UV-Visible Spectral Titration of **2a** ( $1.05 \times 10^{-5}$  M) Upon Sequential Addition of Cyanide Ion in Toluene. 326

**Figure A28.** (s) DPV (in V vs Ag/AgCl) Traces Recorded for **2a** and **2a**. $CN^-$  in  $CH_2Cl_2$  Containing 0.1 M TBAPF<sub>6</sub> with a Scan Rate of  $0.1 V s^{-1}$  at 298 K. (b) The Ratiometric Absorbance Changes ( $A_{483}/A_{440}$ ) of **2a** ( $1.05 \times 10^{-5}$  M) on Addition of 2 eq. of  $CN^-$  and 10 eq. of Other Anions. 327

**Figure A29.** The Pictorial representation of frontier molecular orbitals of (a)  $CoTPPCL_8$  (**2a**) (b)  $CoTPPCL_8.CN^-$  (**2a**. $CN^-$ ). 327



**Figure A30.** Theoretical UV-Visible Spectra of (a) **1a** and (b) **2a** Obtained by TD-DFT Calculations in Gas Phase. 328

**Figure A31.** Experimental UV-Vis. Spectrum (a) and Theoretical UV-Vis. Spectrum (b) of  $\text{CoTPP}(\text{Cl}_8, \text{CN}^-)$  (**2a.CN**). 328

**Table A1.** Crystal structure data of  $\text{CoTPP}(\text{NO}_2)\text{Cl}_7$ ,  $\text{NiTPP}(\text{Cl}_8)$ ,  $\text{ZnTPP}(\text{NO}_2)\text{Cl}_7$ , and  $\text{ZnTPP}(\text{Cl}_8)$  308

**Table A2.** Crystallographic Data and Selected Average Bond Length and Bond Angles of  $\text{H}_2\text{TPP}(\text{Cl}_8)$  (**2**). 309

**Table A3.** Selected Average Bond Lengths and Bond Angles of  $\text{CoTPP}(\text{NO}_2)\text{Cl}_8 \cdot \text{MeOH}$  (**1a**). $\text{MeOH}$ ,  $\text{NiTPP}(\text{Cl}_8)$  (**2b**),  $\text{ZnTPP}(\text{NO}_2)\text{Cl}_7 \cdot \text{MeOH}$ ,  $\text{ZnTPP}(\text{NO}_2)\text{Cl}_7 \cdot \text{Py}$ , and  $\text{ZnTPP}(\text{Cl}_8)$  (**2d**). 310

**Table A4.** Electronic Absorption Spectral Data of **1-4** in Presence of Excess of TFA, TBAOH and Various Anions in  $\text{CH}_2\text{Cl}_2$  at 298K. 318

**Figure A1.** The ORTEP Diagrams Showing Top Views of (a)  $\text{CoTPP}(\text{NO}_2)\text{Cl}_7 \cdot \text{MeOH}$  (**1a.MeOH**), (b)  $\text{ZnTPP}(\text{NO}_2)\text{Cl}_7 \cdot \text{Py}$  (**1d.py**) and (c)  $\text{NiTPP}(\text{Cl}_8)$  (**2b**).

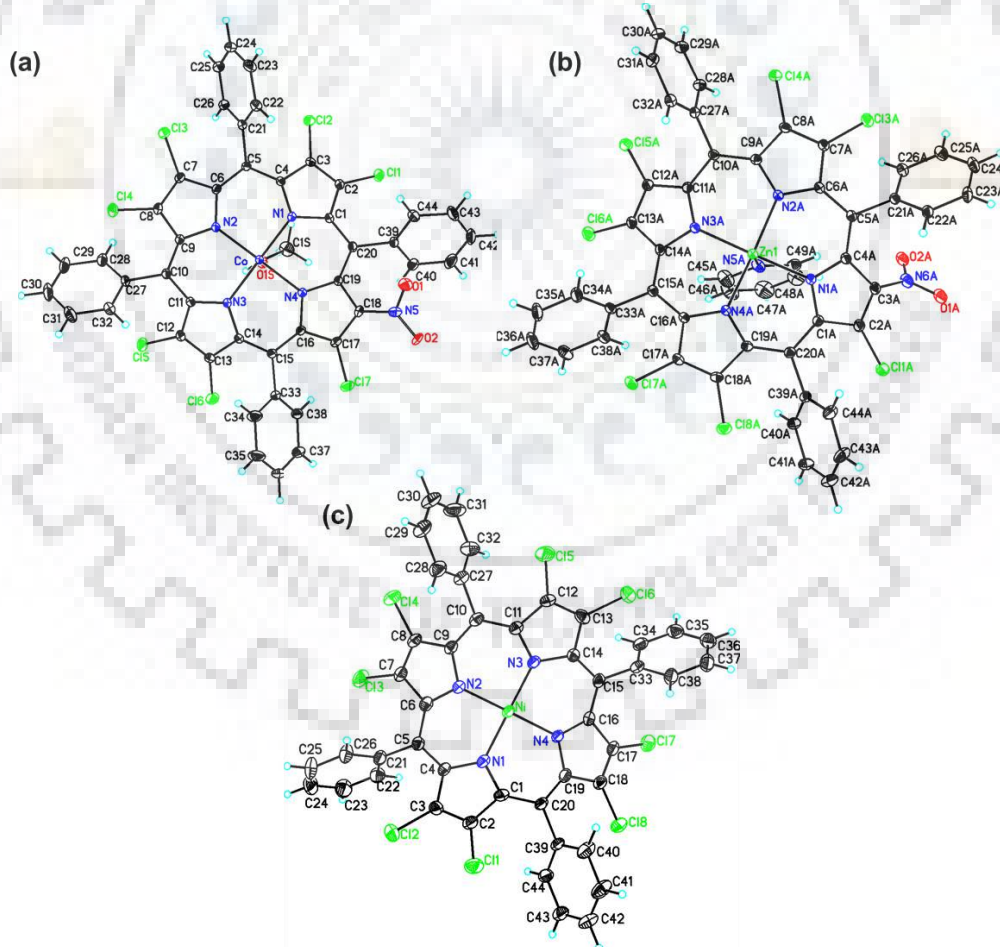


**Figure A2.** The ORTEP Diagrams Showing Top (a) and Side (b) Views of 2,3,7,8,12,13,17,18-Octachloro-*meso*-tetraphenylporphyrin (**2**).

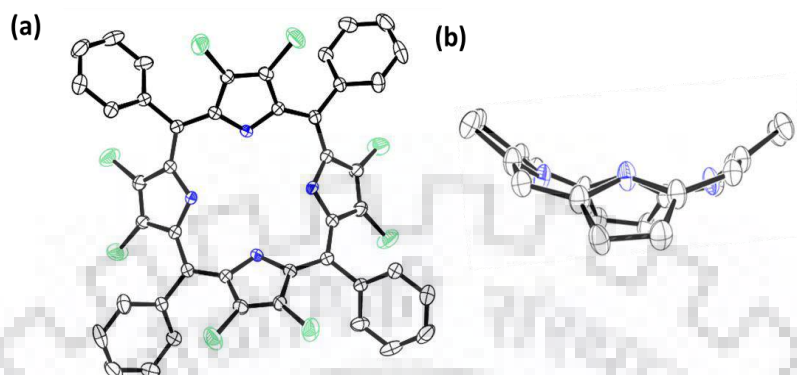


**Figure A3.** The Packing Diagram of (a) ZnTPP(NO<sub>2</sub>)Cl<sub>7</sub>.MeOH (**1d.MeOH**) and (b) ZnTPPCL<sub>8</sub>.MeOH (**2b.MeOH**).

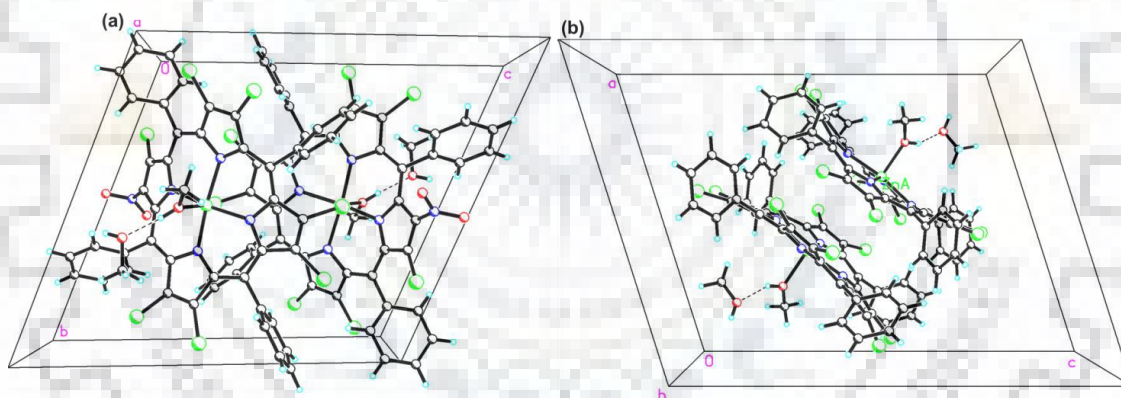


**Figure A4.** Displacement of Porphyrin Core Atoms (in Angstroms) from the Mean Plane for CoTPP(NO<sub>2</sub>)Cl<sub>7</sub>.MeOH (**1a**.MeOH) (a), ZnTPP(NO<sub>2</sub>)Cl<sub>7</sub>.Py (**1d**.Py) and NiTPPCl<sub>8</sub> (**2b**) (c), Respectively.

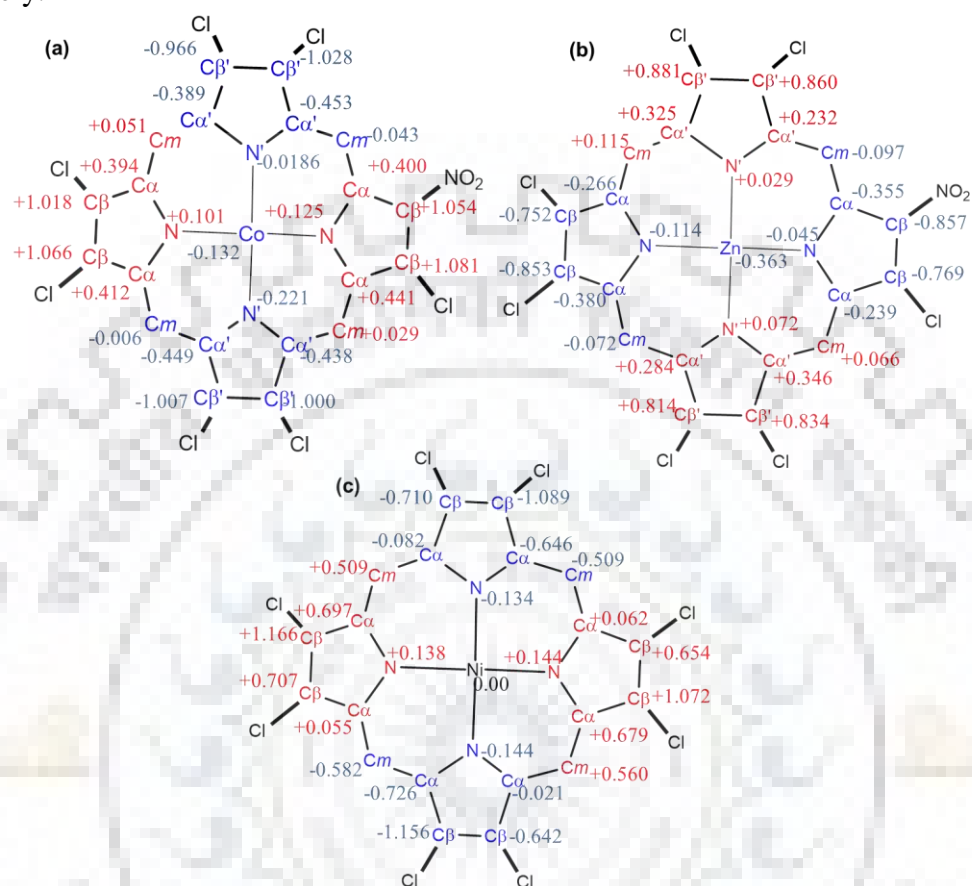


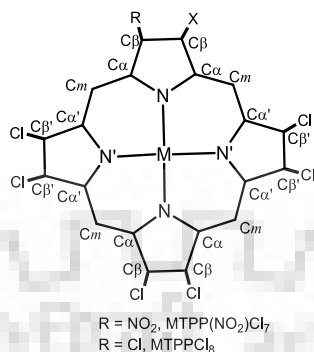
**Table A1.** Crystal Structures Data of CoTPP(NO<sub>2</sub>)Cl<sub>7</sub>, NiTPPCL<sub>8</sub>, ZnTPP(NO<sub>2</sub>)Cl<sub>7</sub>, and ZnTPPCL<sub>8</sub>

	<b>CoTPP(NO<sub>2</sub>)Cl<sub>7</sub></b>	<b>NiTPPCL<sub>8</sub></b>	<b>ZnTPP(NO<sub>2</sub>)Cl<sub>7</sub> .Py</b>	<b>ZnTPP(NO<sub>2</sub>)Cl<sub>7</sub> MeOH</b>	<b>ZnTPPCL<sub>8</sub> .MeOH</b>
Empirical formula	C <sub>46</sub> H <sub>28</sub> Cl <sub>7</sub> N <sub>5</sub> O <sub>4</sub> Co	C <sub>44</sub> H <sub>20</sub> Cl <sub>8</sub> N <sub>4</sub> Ni	C <sub>49</sub> H <sub>25</sub> Cl <sub>7</sub> N <sub>6</sub> O <sub>2</sub> Zn	C <sub>46</sub> H <sub>28</sub> Cl <sub>7</sub> .5N <sub>4</sub> .5O <sub>3</sub> Zn	C <sub>46</sub> H <sub>28</sub> Cl <sub>8</sub> N <sub>4</sub> O <sub>2</sub> Zn
Formula wt.	1021.81	946.95	1043.27	1022.97	1017.69
Crystal system	Monoclinic	Monoclinic	monoclinic	triclinic	monoclinic
Space group	P 21/n	P 21/n	P 21/c	P -1	P 21/n
<i>a</i> (Å)	16.157(2)	14.4657(7)	22.161(7)	10.4998(7)	15.706(3)
<i>b</i> (Å)	13.9906(17)	27.0627(14)	14.459(4)	14.4853(9)	14.352(3)
<i>c</i> (Å)	20.088(3)	10.7356(6)	29.775(9)	15.9272(11)	19.961(4)
<i>α</i> (°)	90.00	90.00	90.000(5)	110.246(6)	90°
<i>β</i> (°)	110.01(6)	111.244(3)	105.085(12)	97.020(6)	107.639°(11)
<i>γ</i> (°)	90.00	90.00	90.000(5)	103.619(5)	90°
Volume (Å <sup>3</sup> )	4266.8(10)	3917.2(4)	9212(5)	2153.0(3)	4288.2(15)
Z	4	4	8	2	4
D <sub>calc</sub> (mg/m <sup>3</sup> )	1.591	1.606	1.504	1.578	1.576
<i>λ</i> (Å)	0.71073	0.71073	0.71073	0.71073	0.71073
T (K)	100(2)	100(2)	100(2)	100(2)	296(2)
No. of total reflns.	52971	27312	71991	10605	61532
No. of indepnt. reflns.	8341	6843	16976	10605	11675
R	0.0538	0.0939	0.0484	0.1121	0.0444
R <sub>w</sub>	0.0932	0.1355	0.1054	0.2957	0.1040
GOOF	1.017	1.024	1.026	1.142	1.016
CCDC	<b>1585103</b>	<b>1585104</b>	<b>1585105</b>	<b>1585106</b>	<b>1585107</b>

**Table A2.** Crystallographic Data and Selected Average Bond Length and Bond Angles of H<sub>2</sub>TPPCl<sub>8</sub> (**2**).

H <sub>2</sub> TPPCl <sub>8</sub> ( <b>2</b> )		H <sub>2</sub> TPPCl <sub>8</sub> ( <b>2</b> )	
Empirical formula	C <sub>48</sub> H <sub>30</sub> N <sub>6</sub> Cl <sub>8</sub> O <sub>2</sub>	<b>Bond length (Å)</b>	
Formula wt.	1006.38	N-H	0.822(8)
Crystal system	Tetragonal	N-C <sub>α</sub>	1.355(10)
Space group	I 4 <sub>1</sub> /a	C <sub>α</sub> -C <sub>β</sub>	1.432(10)
<i>a</i> (Å)	19.880(3)	C <sub>β</sub> -C <sub>β</sub>	1.345(11)
<i>b</i> (Å)	19.880(4)	C <sub>α</sub> -C <sub>m</sub>	1.411(10)
<i>c</i> (Å)	13.1460(15)	$\Delta C_{\beta}$ (Å)	<b>1.2095</b>
$\alpha = \beta = \gamma$ (°)	90	$\Delta 24$ (Å)	<b>0.5695</b>
Volume (Å <sup>3</sup> )	5195.5(13)	<b>Bond angle (°)</b>	
Z	4	N-C <sub>α</sub> -C <sub>m</sub>	123.9(7)
D <sub>calc</sub> (mg/m <sup>3</sup> )	1.287	N-C <sub>α</sub> -C <sub>β</sub>	107.2(6)
$\lambda$ (Å)	0.71073	C <sub>α</sub> -C <sub>β</sub> -C <sub>β</sub>	107.5(6)
T (°C)	293 K	C <sub>β</sub> -C <sub>α</sub> -C <sub>m</sub>	128.5(7)
No. of total reflns.	1781	C <sub>α</sub> -C <sub>m</sub> -C <sub>α</sub>	120.6(6)
No. of indepnt. reflns.	1483	C <sub>α</sub> -N-C <sub>α</sub>	110.0(6)
R	0.0113		
R <sub>w</sub>	0.3293		
CCDC	1033576		

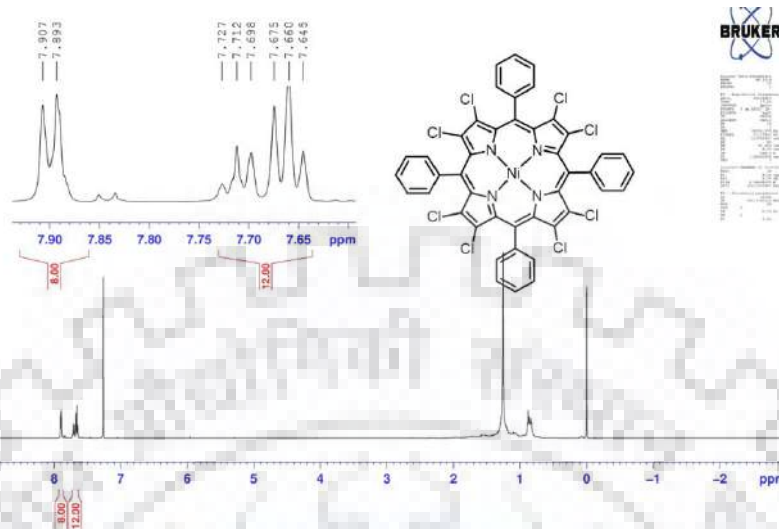
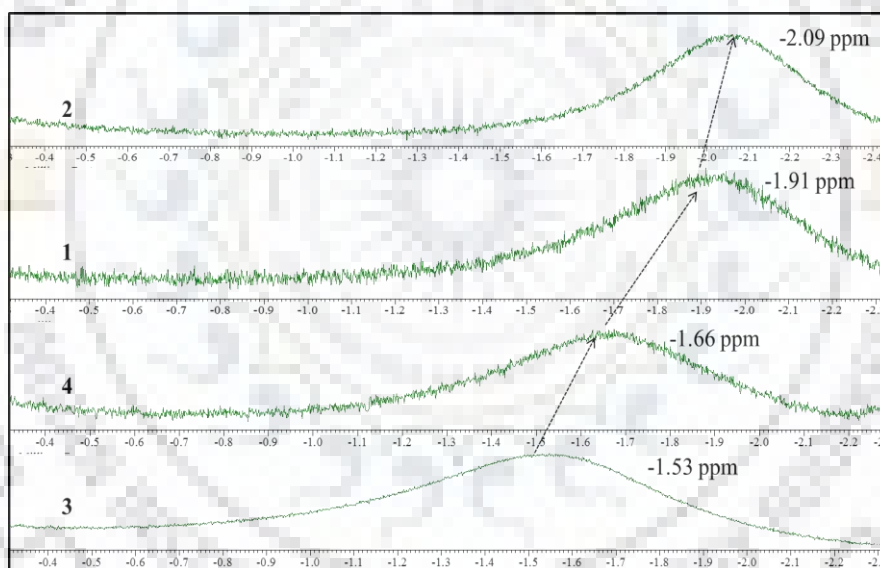
<sup>a</sup> $\Delta C_{\beta}$  = deviation of  $\beta$ -carbon atoms, <sup>b</sup> $\Delta 24$  = deviation of 24 core atoms

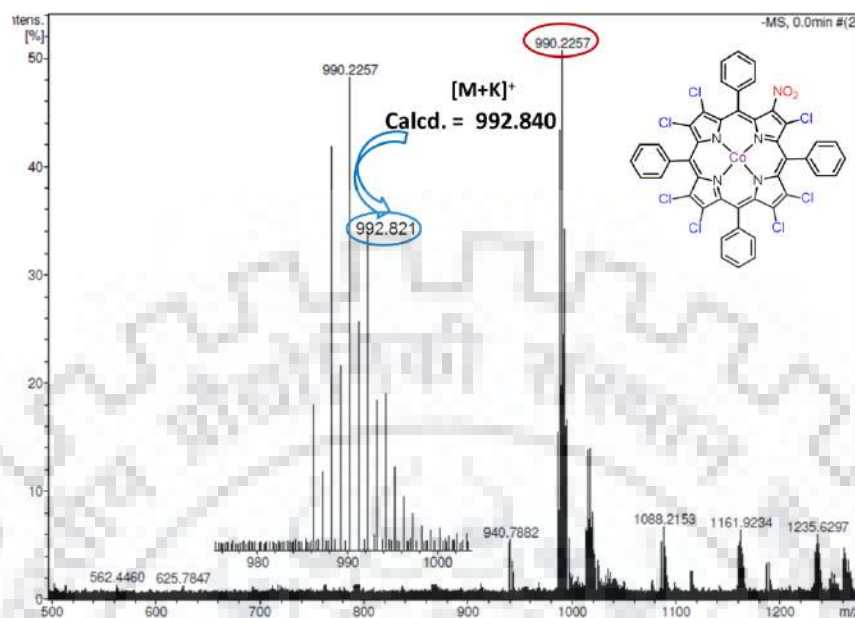
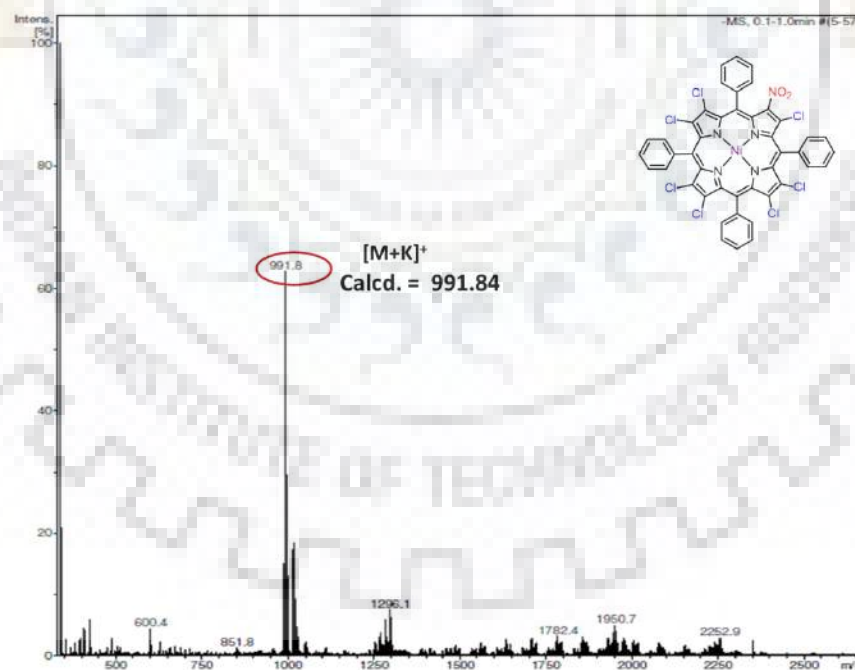
**Table A3.** Selected Average Bond Lengths and Bond Angles of CoTPP(NO<sub>2</sub>)Cl<sub>8</sub>.MeOH (**1a**).MeOH, NiTPPCl<sub>8</sub>(**2b**), ZnTPP(NO<sub>2</sub>)Cl<sub>7</sub>.MeOH, ZnTPP(NO<sub>2</sub>)Cl<sub>7</sub>.Py, and ZnTPPCl<sub>8</sub>(**2d**).

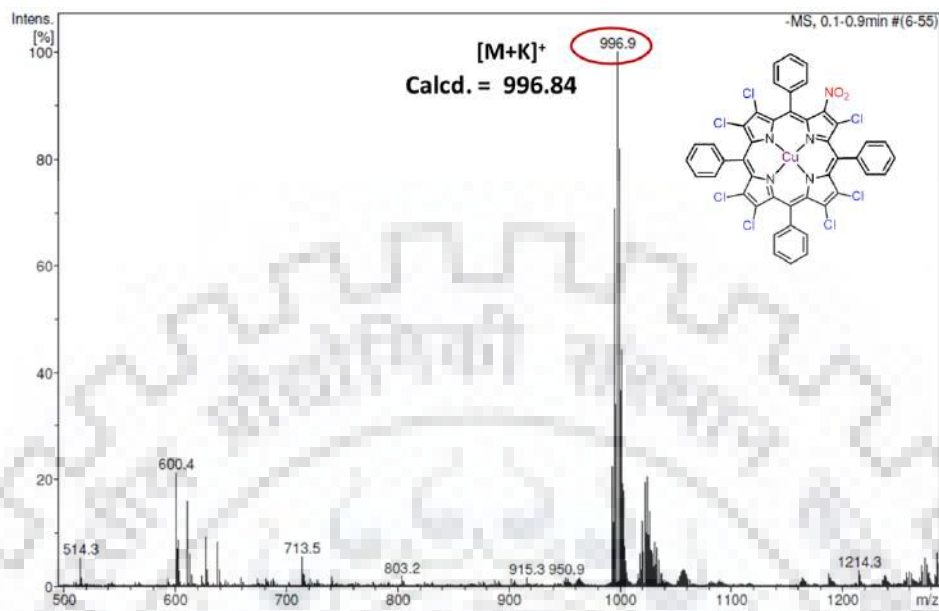
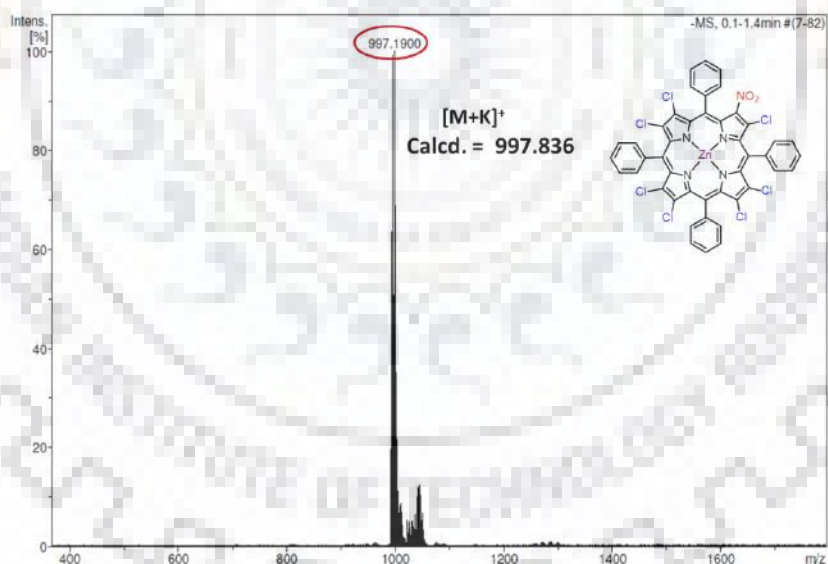
	CoTPP(NO <sub>2</sub> )Cl <sub>7</sub> ( <b>1a</b> )	NiTPPCl <sub>8</sub> ( <b>2b</b> )	ZnTPP(NO <sub>2</sub> )Cl <sub>7</sub> ( <b>1d</b> ).MeOH	ZnTPP(NO <sub>2</sub> )Cl <sub>7</sub> ( <b>1d</b> ).Py	ZnTPPCl <sub>8</sub> ( <b>2d</b> )
<b>Bond Lengths (Å)</b>					
M - N	1.959(2)	1.906(4)	2.057(4)	2.095(3)	2.075(4)
M - N'	1.945(2)	--	2.089(5)	2.099(3)	--
N - C <sub>α</sub>	1.379(4)	1.386(5)	1.373(6)	1.379(4)	1.378(4)
N' - C <sub>α</sub>	1.373(3)	--	1.369(5)	1.384(4)	--
C <sub>α</sub> - C <sub>β</sub>	1.441(3)	1.444(6)	1.448(7)	1.455(4)	1.452(4)
C <sub>α</sub> - C <sub>β'</sub>	1.439(3)	--	1.439(6)	1.454(4)	--
C <sub>β</sub> - C <sub>β'</sub>	1.340(3)	1.344(6)	1.323(9)	1.355(5)	1.353(4)
C <sub>β</sub> - C <sub>β''</sub>	1.341(3)	--	1.332(8)	1.356(4)	--
C <sub>α</sub> - C <sub>m</sub>	1.393(3)	1.393(6)	1.401(8)	1.412(4)	1.406(4)
C <sub>α</sub> - C <sub>m'</sub>	1.393(3)	--	1.388(7)	1.417(4)	--
$\Delta C_{\beta}$ <sup>a</sup>	<b>1.028</b>	<b>0.899</b>	<b>0.706</b>	<b>0.827</b>	<b>0.642</b>
$\Delta 24$ <sup>b</sup>	<b>0.515</b>	<b>0.536</b>	<b>0.343</b>	<b>0.402</b>	<b>0.313</b>
$\Delta M$	<b>0.132</b>	<b>0.00</b>	<b>0.305</b>	<b>0.363</b>	<b>0.228</b>
<b>Bond Angles (°)</b>					
N - M - N	165.59(8)	171.60(1)	162.09(2)	164.50(1)	166.96(9)
N' - M - N'	175.79(8)	--	167.39(2)	158.90(1)	--
M - N - C <sub>α</sub>	125.10(1)	125.20(3)	125.04(4)	122.10(2)	123.93(2)
M - N' - C <sub>α</sub>	125.20(2)	--	123.14(4)	125.12(2)	--
N - C <sub>α</sub> - C <sub>m</sub>	123.89(2)	123.79(4)	125.68(5)	124.48(3)	125.11(4)
N - C <sub>α</sub> - C <sub>m'</sub>	123.64(2)	--	124.72(5)	124.92(3)	--
N - C <sub>α</sub> - C <sub>β</sub>	108.37(2)	108.23(4)	107.15(5)	107.90(3)	108.06(2)
N - C <sub>α</sub> - C <sub>β'</sub>	108.57(2)	--	106.93(5)	107.84(3)	--
C <sub>β</sub> - C <sub>α</sub> - C <sub>m</sub>	127.37(2)	127.21(4)	126.98(5)	127.40(3)	126.67(3)
C <sub>β</sub> - C <sub>α</sub> - C <sub>m'</sub>	127.16(2)	--	127.74(5)	127.09(3)	--
C <sub>α</sub> - C <sub>β</sub> - C <sub>β'</sub>	107.79(2)	107.80(4)	108.33(5)	107.70(3)	107.69(3)
C <sub>α</sub> - C <sub>β</sub> - C <sub>β''</sub>	107.54(2)	--	108.09(5)	107.83(3)	--
C <sub>α</sub> - N - C <sub>α</sub>	107.19(2)	107.20(3)	108.86(5)	108.56(3)	108.33(2)
C <sub>α</sub> - N - C <sub>α'</sub>	107.05(2)	--	108.79(5)	108.48(3)	--
C <sub>α</sub> - C <sub>m</sub> - C <sub>α</sub>	121.28(2)	119.99(4)	124.59(5)	124.04(3)	125.10(3)

<sup>a</sup> $\Delta C_{\beta}$  = mean plane deviation of the  $\beta$ -pyrrole carbons <sup>b</sup> $\Delta 24$  = deviation of 24 core atoms

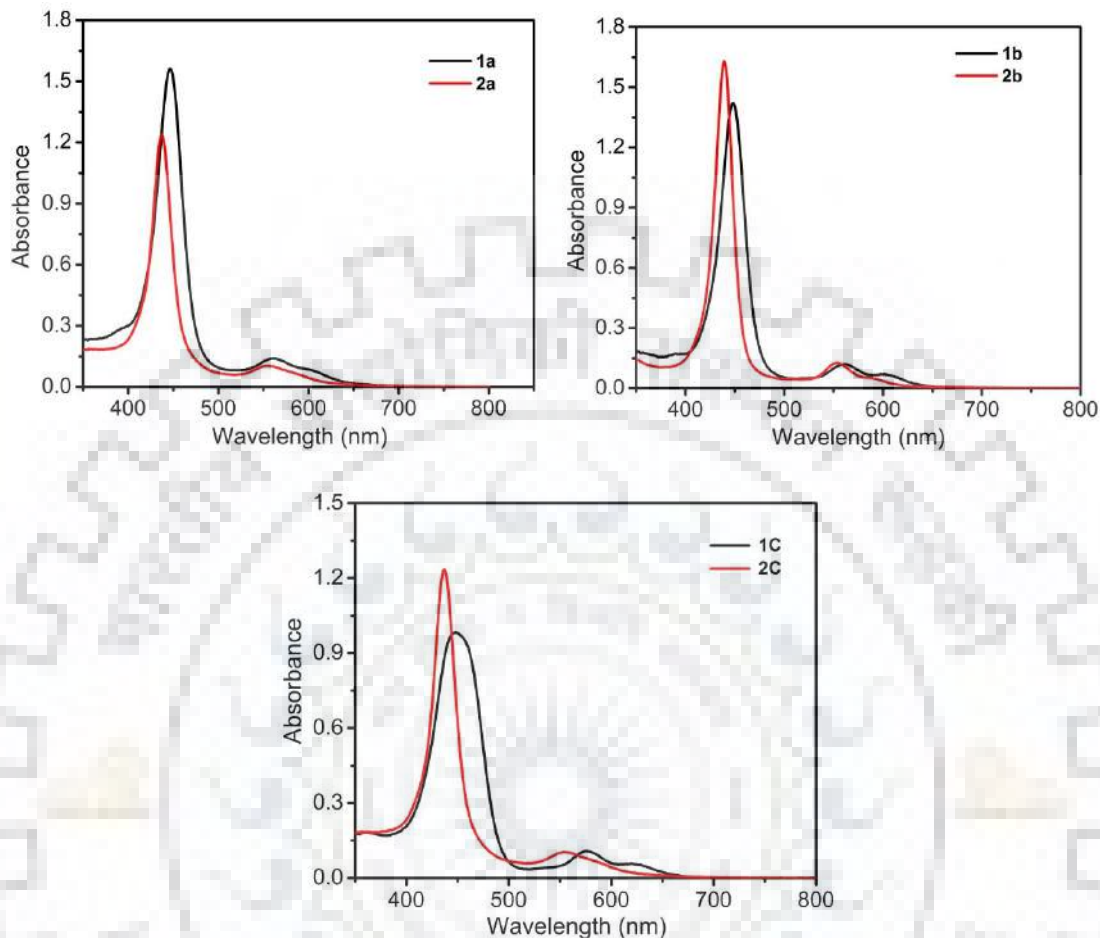


**Figure A5.**  $^1\text{H}$  NMR Spectrum of NiTPPCl<sub>8</sub> (**2b**) in CDCl<sub>3</sub> at 298 K.**Figure A6.** Imino Protons Region of **1-4** in CDCl<sub>3</sub> at 298 K.

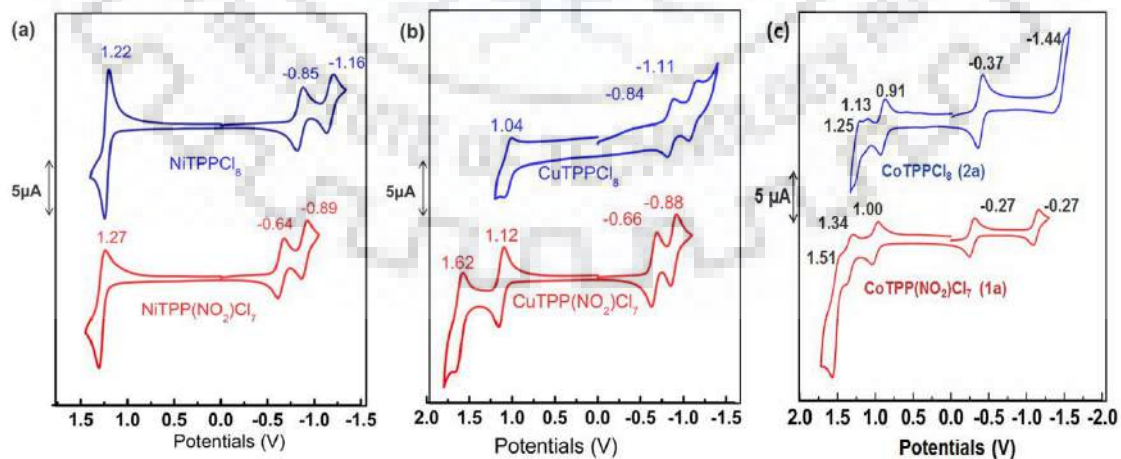
**Figure A7.** The ESI-MS Spectrum of CoTPP(NO<sub>2</sub>)Cl<sub>7</sub> (**2a**) in CH<sub>3</sub>CN at 298 K.**Figure A8.** The ESI-MS Spectrum of NiTPP(NO<sub>2</sub>)Cl<sub>7</sub> (**2b**) in CH<sub>3</sub>CN at 298 K.

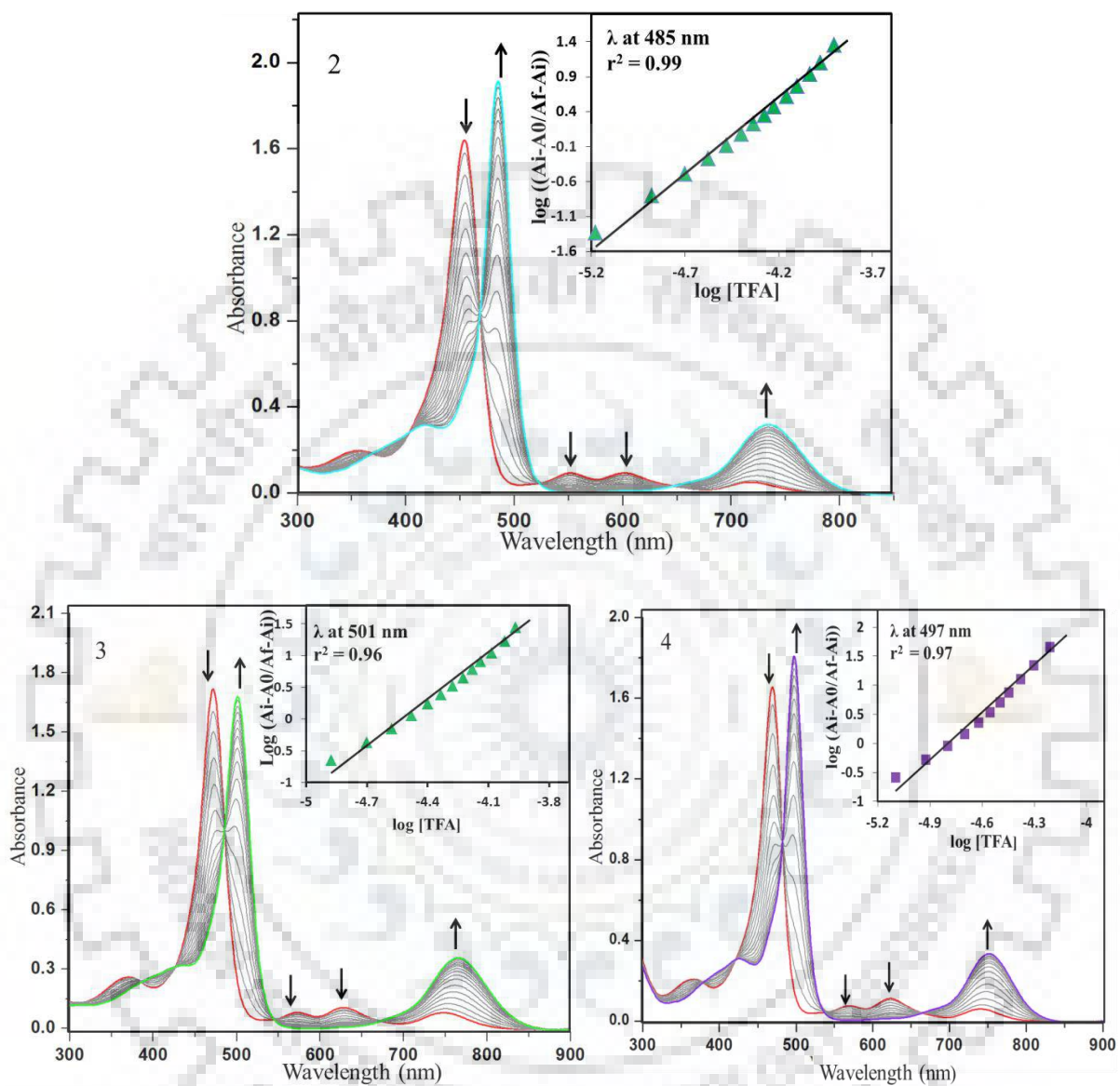
**Figure A9.** The ESI-MS Spectrum of CuTPP(NO<sub>2</sub>)Cl<sub>7</sub> (**2c**) in CH<sub>3</sub>CN at 298 K.**Figure A10.** The ESI-MS Spectra of ZnTPP(NO<sub>2</sub>)Cl<sub>7</sub> (**2d**) in CH<sub>3</sub>CN at 298 K.

**Figure A11.** Electronic Absorption Spectra of (a) **1a** and **2a**, (b) **1b** and **2b**, and (c) **1c** and **2c** in Toluene at 298 K



**Figure A12.** Comparative Cyclic voltammograms of (a) **1a** and **2a** (b) **1b** and **2b**, (c) **1c** and **2c** in  $\text{CH}_2\text{Cl}_2$  with 0.1M  $\text{TBAF}_6$  as the Supporting Electrolyte at a Scan Rate of 100 mV/s.



**Figure A13.** UV-vis. Spectral Titrations of 2-4 with TFA in Toluene at 298 K.

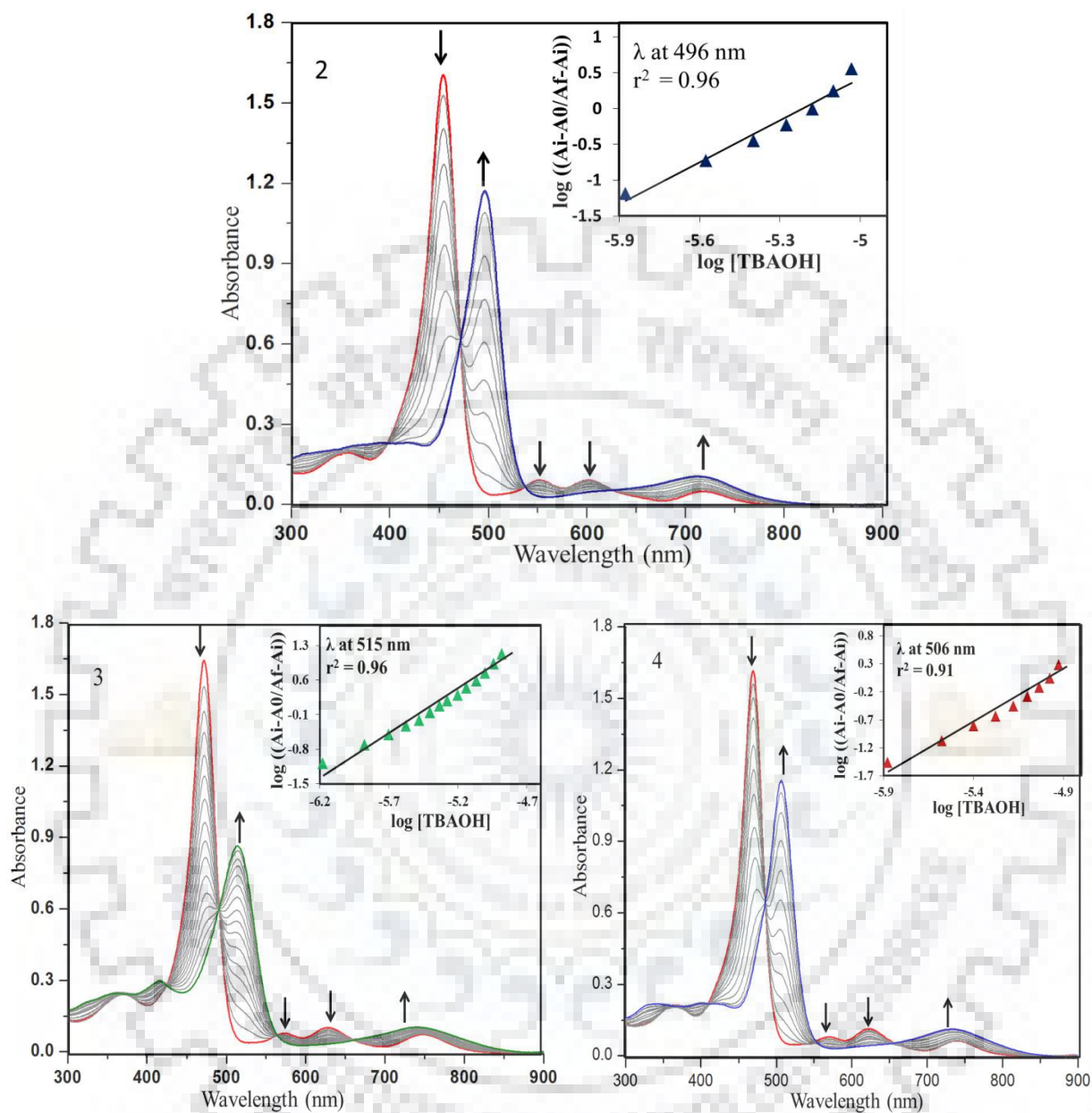
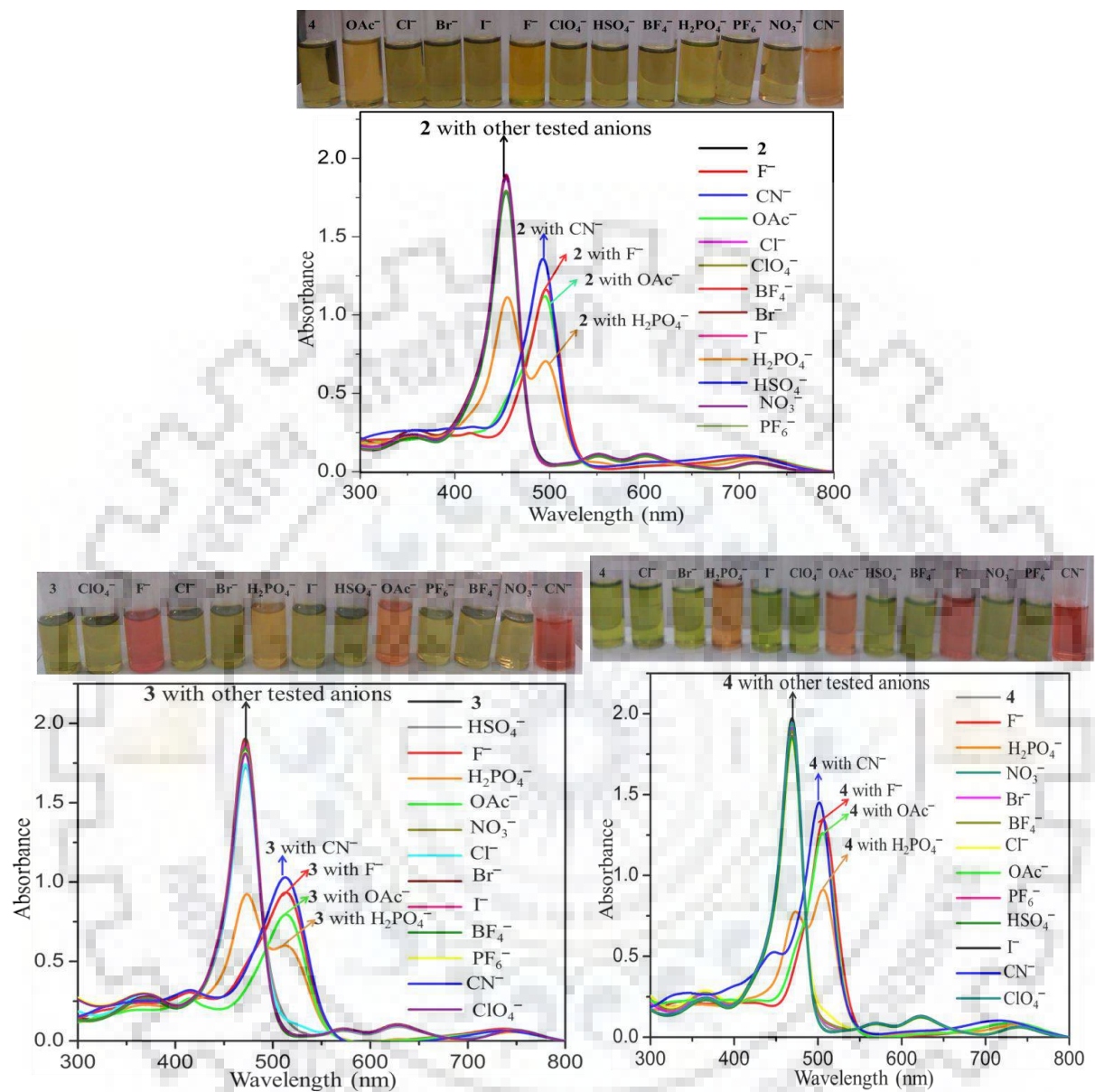
**Figure A14.** UV-vis. Spectral Titrations of **2-4** with TBAOH in Toluene at 298 K.



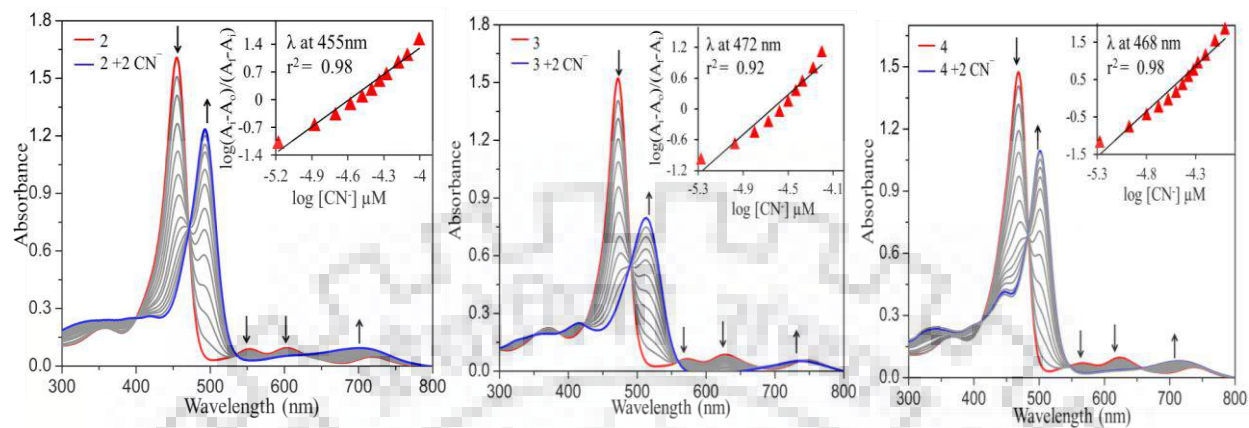
Figure A15. Colorimetric Responses of 2-4 while Adding Excess of Anions in Toluene.



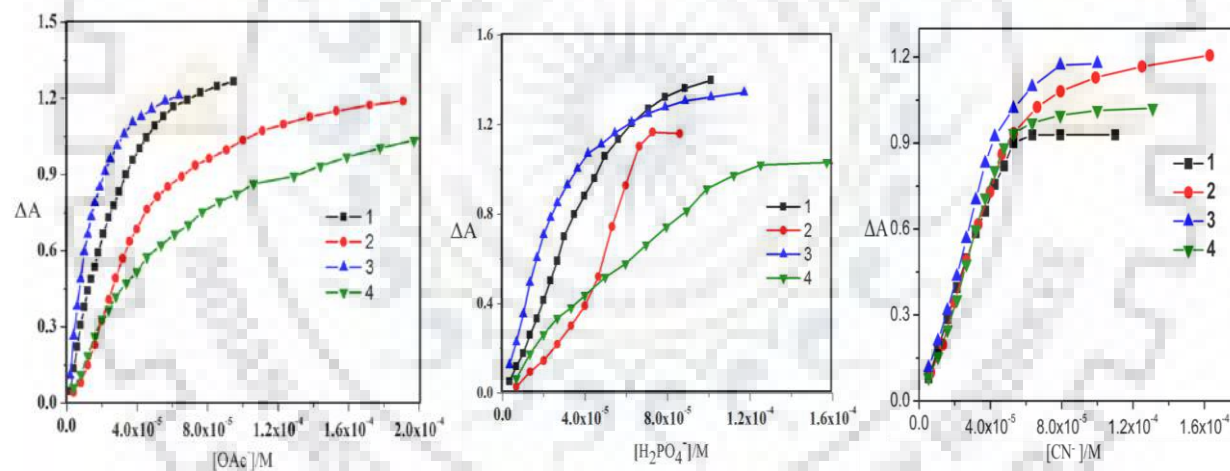
**Table A4.** Electronic Absorption Spectral Data of **1-4** in Presence of Excess of TFA, TBAOH and Various Anions in CH<sub>2</sub>Cl<sub>2</sub> at 298 K.

<b>Porphyrin</b>	<b>B band(s)</b>	<b>Q band</b>
<b>[1•2H]<sup>2+</sup></b>	491 (94.16)	754 (11.95)
<b>[2•2H]<sup>2+</sup></b>	415(22.14), 483 (151.99)	734 (24.90)
<b>[3•2H]<sup>2+</sup></b>	501 (93.75)	768 (7.99)
<b>[4•2H]<sup>2+</sup></b>	425(18.95), 495 (149.03)	750 (22.03)
<b>Deprotonation</b>		
<b>[1-2H]<sup>2-</sup></b>	409(17.69), 506 (47.81)	726 (4.01)
<b>[2-2H]<sup>2-</sup></b>	492 (87.13)	713(7.25)
<b>[3-2H]<sup>2-</sup></b>	414(15.94), 516 (50.21)	743(2.92)
<b>[4-2H]<sup>2-</sup></b>	401(15.55), 505 (88.66)	735 (6.11)
<b>Cyanide</b>		
<b>[1+2CN<sup>-</sup>]</b>	412(19.24), 506 (52.04)	720 (4.26)
<b>[2+2CN<sup>-</sup>]</b>	414(22.17), 492 (109.75)	713 (8.84)
<b>[3+2CN<sup>-</sup>]</b>	414(17.19), 514 (53.06)	740 (3.41)
<b>[4+2CN<sup>-</sup>]</b>	444(31.98), 503 (94.52)	723 (6.79)
<b>Fluoride</b>		
<b>[1+2F<sup>-</sup>]</b>	490(20.57), 506 (55.65)	721 (4.91)
<b>[2+2F<sup>-</sup>]</b>	492 (104.11)	710 (8.59)
<b>[3+2F<sup>-</sup>]</b>	414(1.35), 516 (56.87)	739 (3.75)
<b>[4+2F<sup>-</sup>]</b>	398(17.56), 504 (98.41)	731 (7.34)
<b>Acetate</b>		
<b>[1+2CH<sub>3</sub>COO<sup>-</sup>]</b>	410(22.07), 506 (58.50)	719 (5.22)
<b>[2+2CH<sub>3</sub>COO<sup>-</sup>]</b>	492 (77.95)	714 (7.04)
<b>[3+2CH<sub>3</sub>COO<sup>-</sup>]</b>	414(18.35), 516 (59.79)	737 (3.90)
<b>[4+2CH<sub>3</sub>COO<sup>-</sup>]</b>	472(53.79), 504 (88.60)	734 (6.76)
<b>Dihydrogenphosphate</b>		
<b>[1+2H<sub>2</sub>PO<sub>4</sub><sup>-</sup>]</b>	411(22.98), 506 (59.51)	721 (5.38)
<b>[2+2H<sub>2</sub>PO<sub>4</sub><sup>-</sup>]</b>	358(19.97), 456(73.95),492 (80.46)	716 (8.01)
<b>[3+2H<sub>2</sub>PO<sub>4</sub><sup>-</sup>]</b>	416(19.93), 516 (60.79)	741 (4.03)
<b>[4+2H<sub>2</sub>PO<sub>4</sub><sup>-</sup>]</b>	471(57.90), 504 (90.30)	734 (7.22)

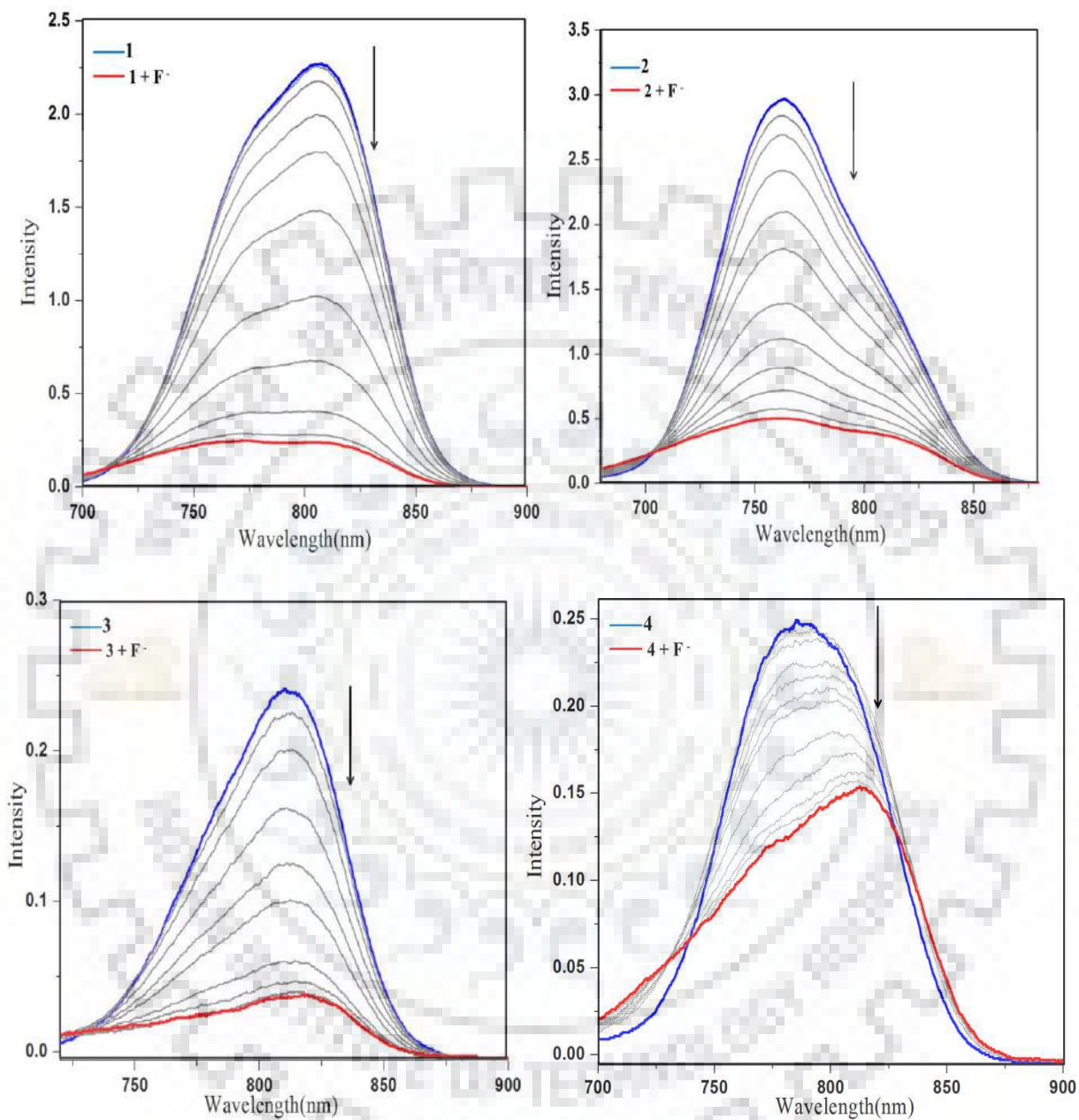
**Figure A16.** UV-Vis Spectral Titrations of **2-4** while Increasing  $[\text{CN}^-]$  in Toluene at 298 K. Insets Show the Corresponding Hill plots.



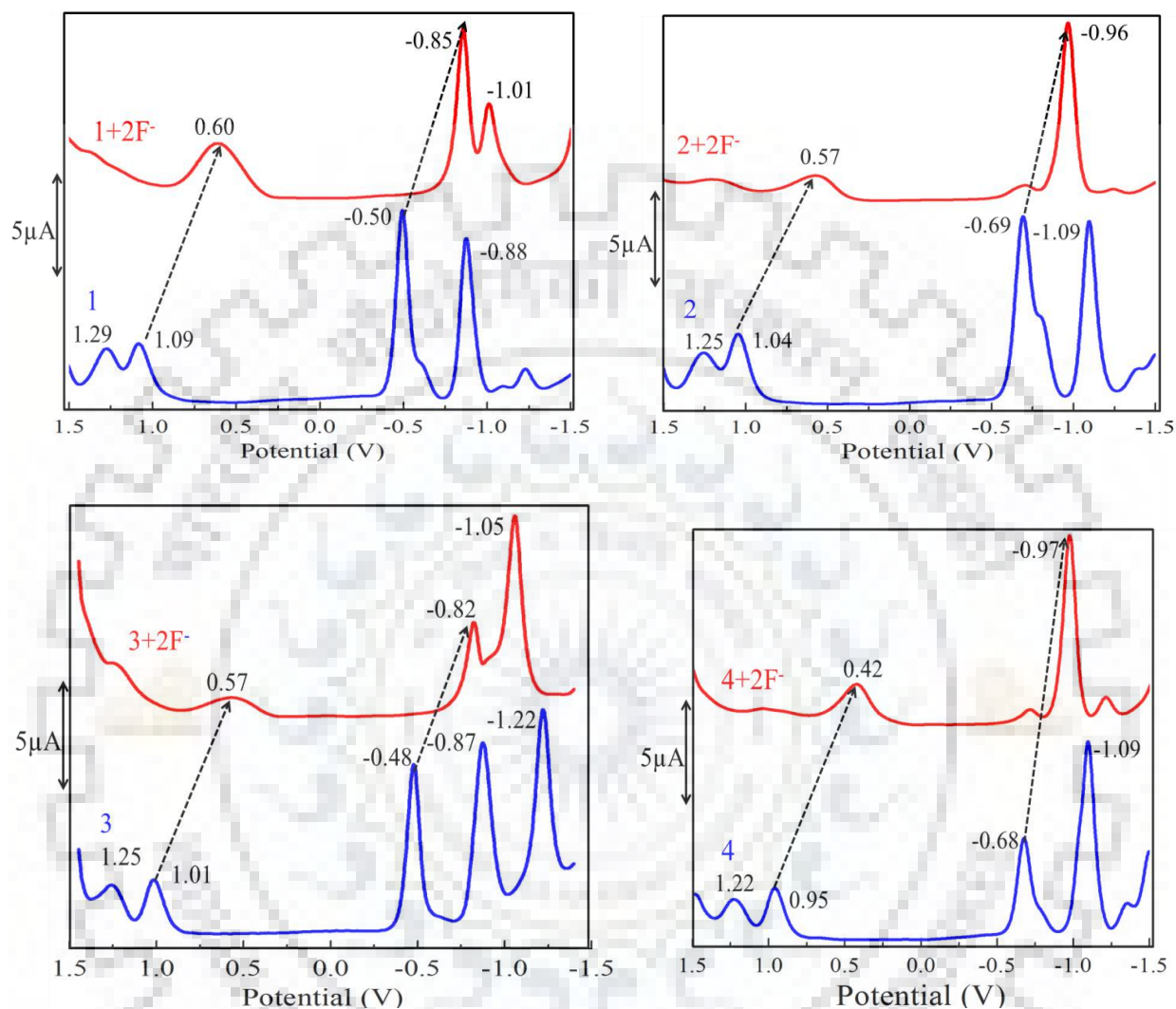
**Figure A17.** Plots of  $\Delta A$  at  $\lambda_{\text{max}}$  vs  $[\text{OAc}^-]$  or  $[\text{H}_2\text{PO}_4^-]$  or  $[\text{CN}^-]$  for **1-4** Showing Sigmoidal Curve Indicating the Positive Cooperative Behavior.



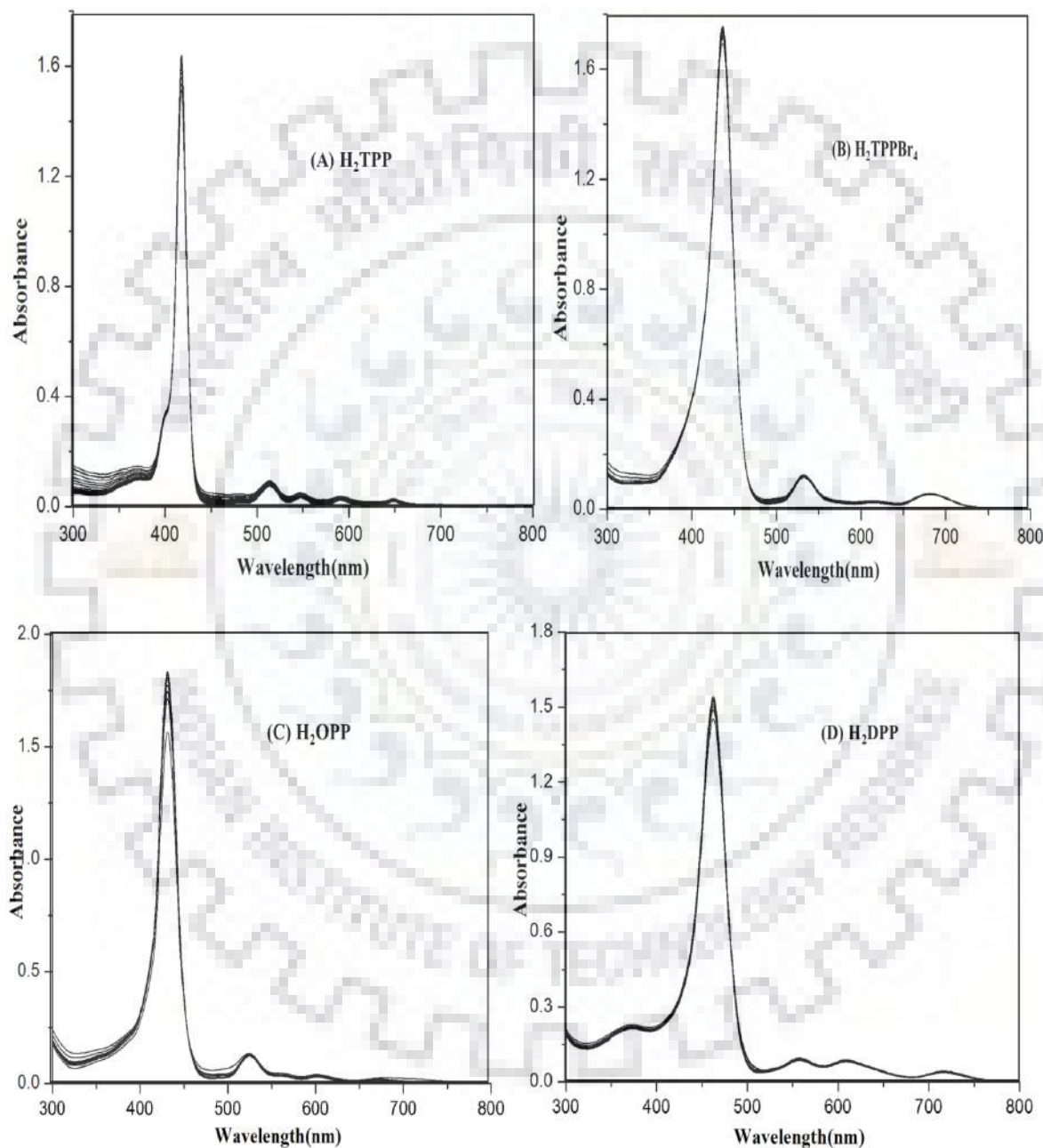
**Figure A18.** Fluorescence Spectral Titrations (FL quenching) of **1-4** while Increasing  $[F^-]$  in Toluene at 298 K.



**Figure A19.** DPV Traces of **1-4** in Absence and Presence of Excess of  $[F^-]$  in  $CH_2Cl_2$  Containing 0.1 M TBAPF<sub>6</sub> at 298 K.

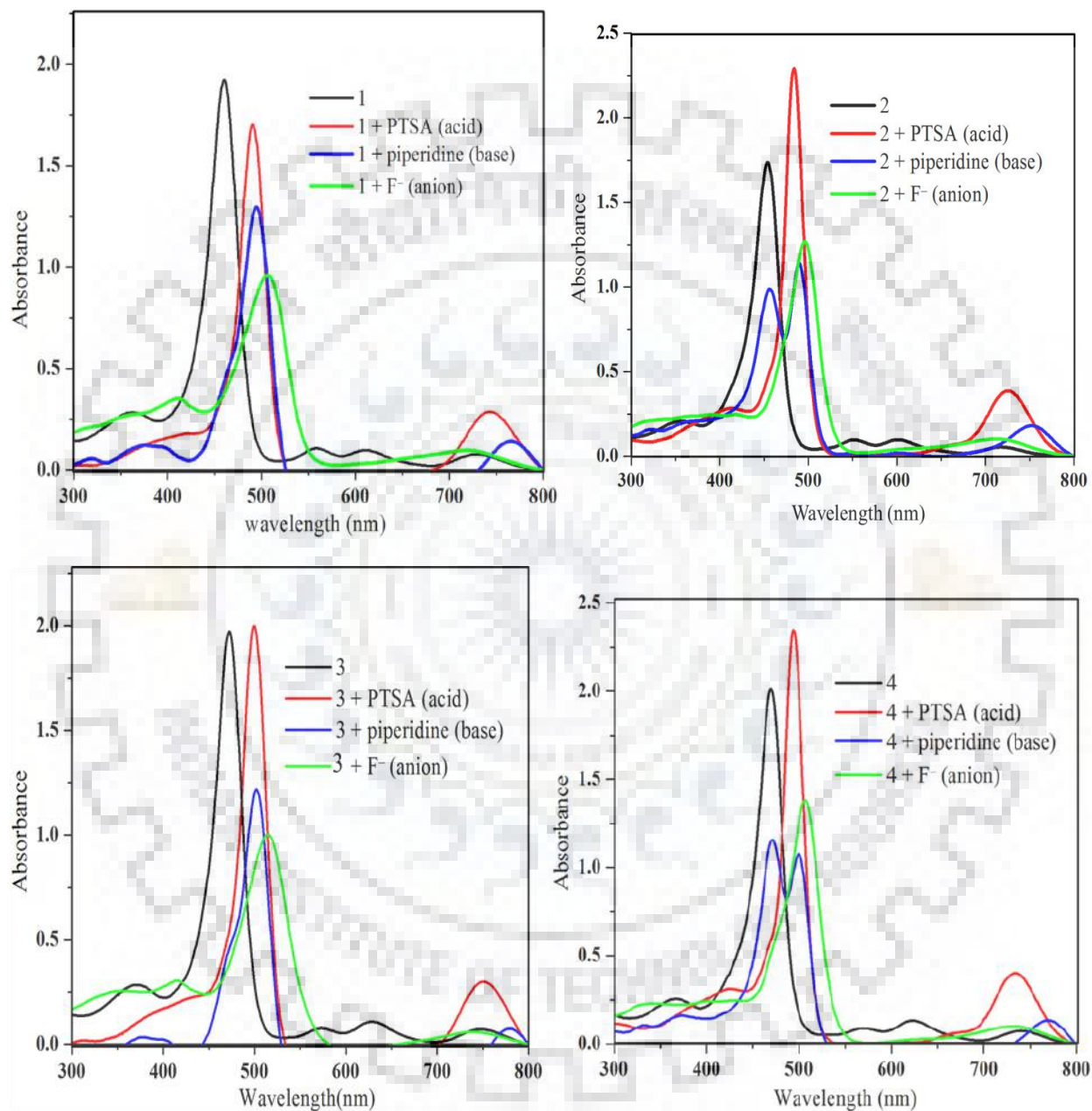


**Figure A20:** UV-Visible Spectral Titrations of Planar Porphyrins (*meso*-Tetraphenylporphyrin ( $H_2TPP$ ) and 2,3,5,10,15,17,18,20-Octaphenylporphyrin ( $H_2TPP(Ph)_4$ ) and Nonplanar Porphyrins (2,3,12,13-Tetrabromo-*meso*-tetraphenylporphyrin ( $H_2TPPBr_4$ ) and 2,3,5,7,8,10,12,13,15,17,18,20-Dodecaphenylporphyrin ( $H_2TPP(Ph)_8$ )) while Increasing  $[F^-]$  in Toluene at 298 K.

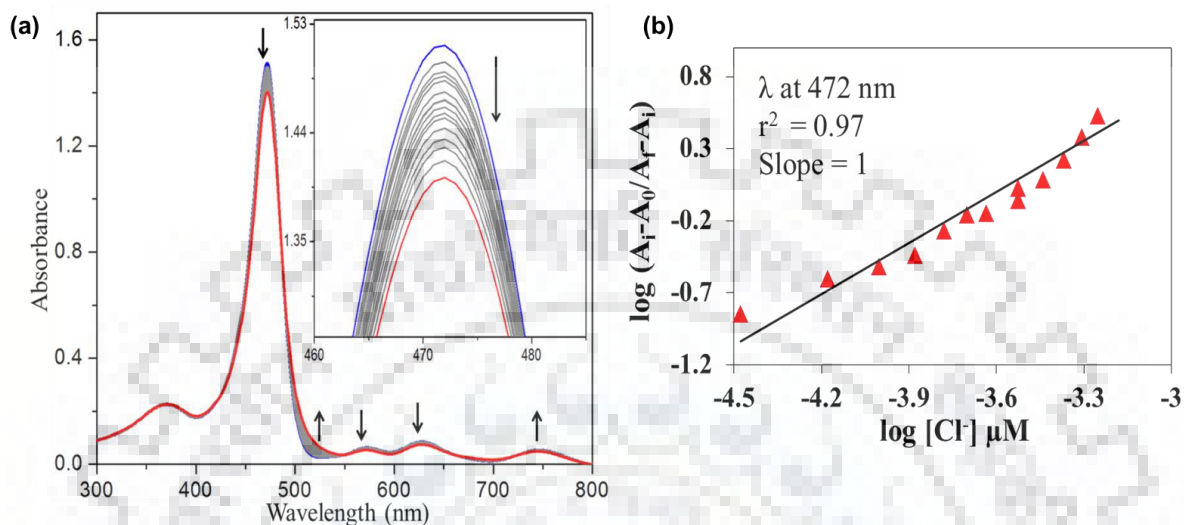




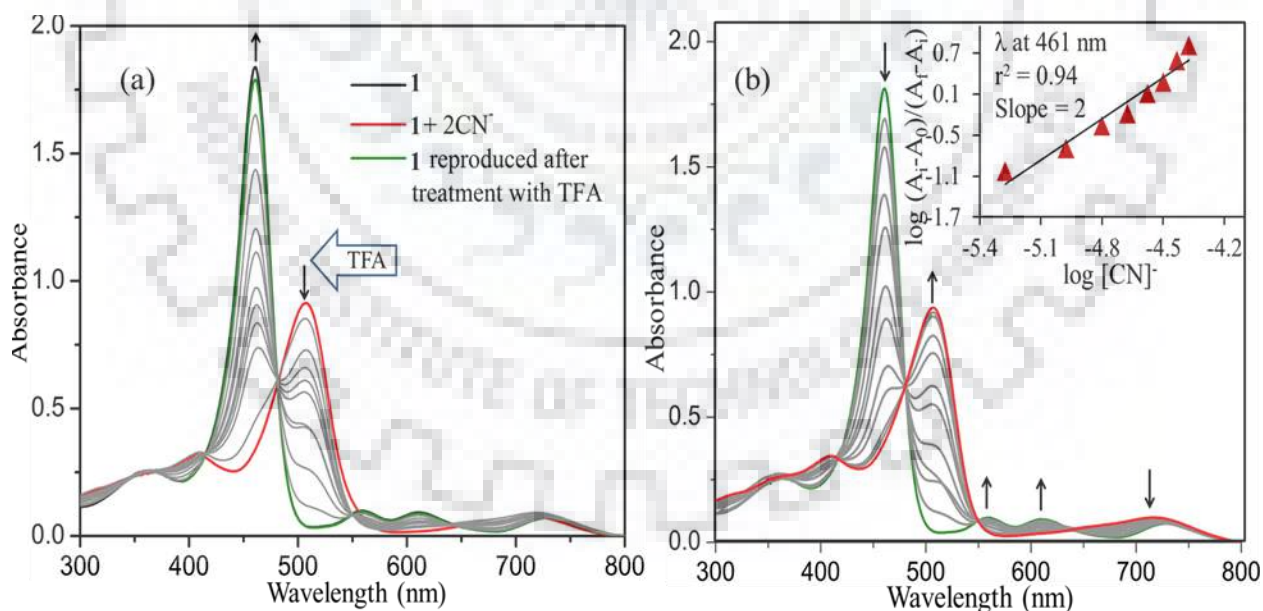
**Figure A21.** Overlaid UV-Visible Spectra of **1-4** with Excess of *p*-Toluenesulphonic acid (PTSA), Piperidine and Fluoride Ions in Toluene 298 K. Herein, Piperidine forms 1:1 Host:Guest Complex with **1-4** in 1,2-Dichloroethane as Reported in literature (*Ref.* Bhyrappa P.; Bhavana, *P. Chem. Phys. Lett.* **2002**, 357, 108).

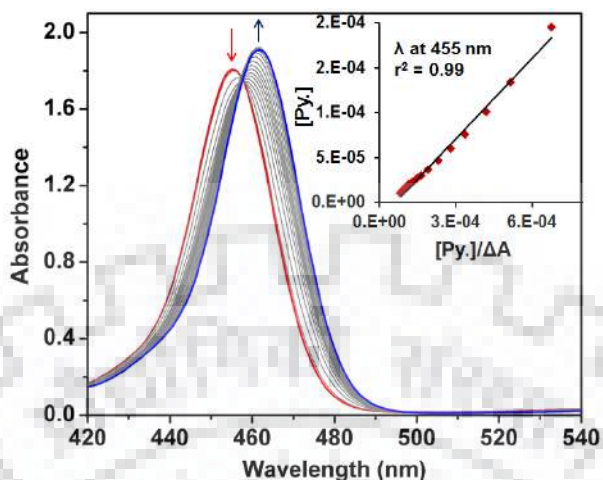
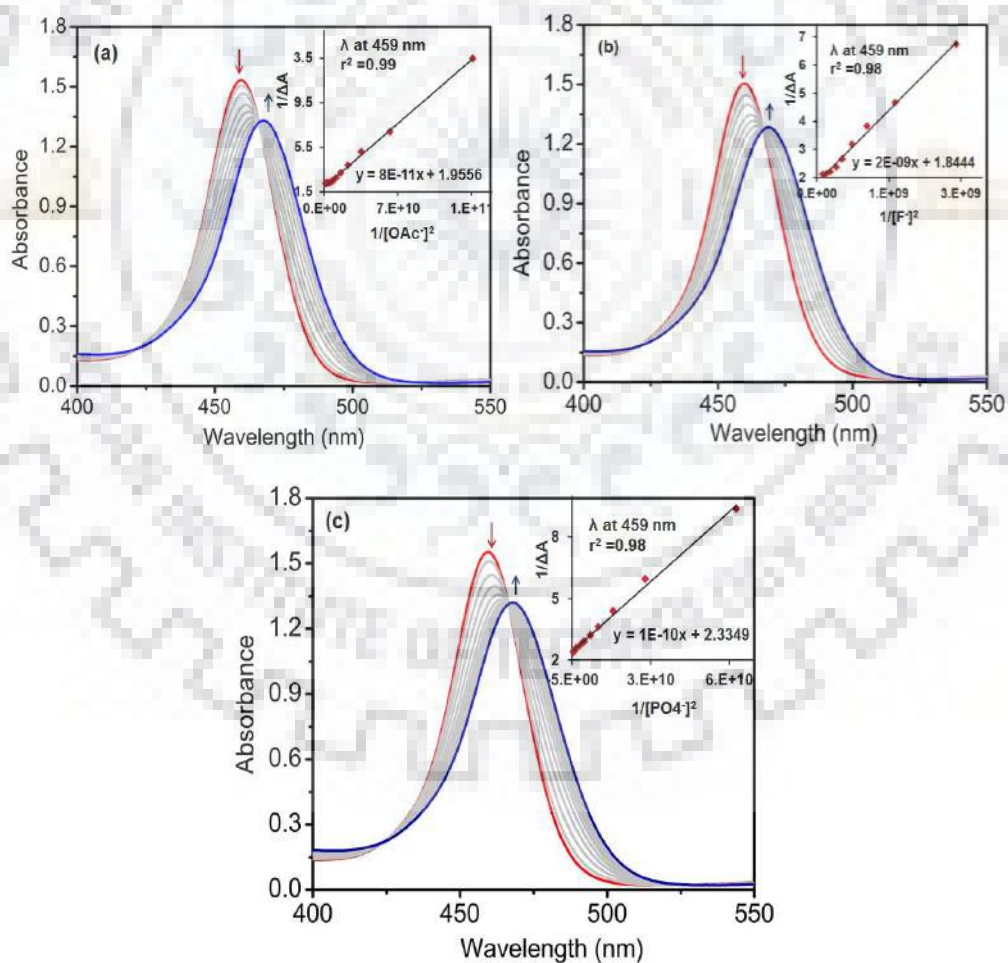


**Figure A22.** (a) UV-Vis Spectral Titrations of **3** with TBACl (0.008 M) in Toluene at 298 K. Inset Shows the Absorbance Changes in The Soret Region; (b) Hill Plot  $\log(A_i - A_0)/A_i - A_i$  vs  $\log[Cl^-]$  Showing 1:1 Stoichiometry Indicated by Slope 1.



**Figure A23.** (a) Treatment of  $1 \cdot 2CN^-$  Complex with Aliquots of 1 mM Solution TFA at 298 K. (b) Reusability Test of Regenerated **1** with Aliquots of 8 mM Solution of  $CN^-$  Ions in Toluene at 298 K.



**Figure A24.** Axial Ligation of Pyridine to **2d** in Toluene at 298 K.**Figure A25.** The Axial Ligation Studies of  $X^-$ , Where  $X = OAc^-$  (a),  $F^-$  (b), and  $PO_4^-$  (c) Anions to **1d** ( $8.29 \times 10^{-6}$  M) in Toluene at 298K. Insets Show plot  $[X]^{-2}$  vs  $[X]^{-2}/\Delta A$ .

**Figure A26.** Benesi-Hildebrand Plot Constructed for 1:1 Stoichiometric Ratio from the Titration Data of **1d** and **2d** with Cyanide Ion. Cyanide Binding is Not Accurately Modeled by This Plot Indicating That Binding Cannot be of 1:1 Stoichiometry.

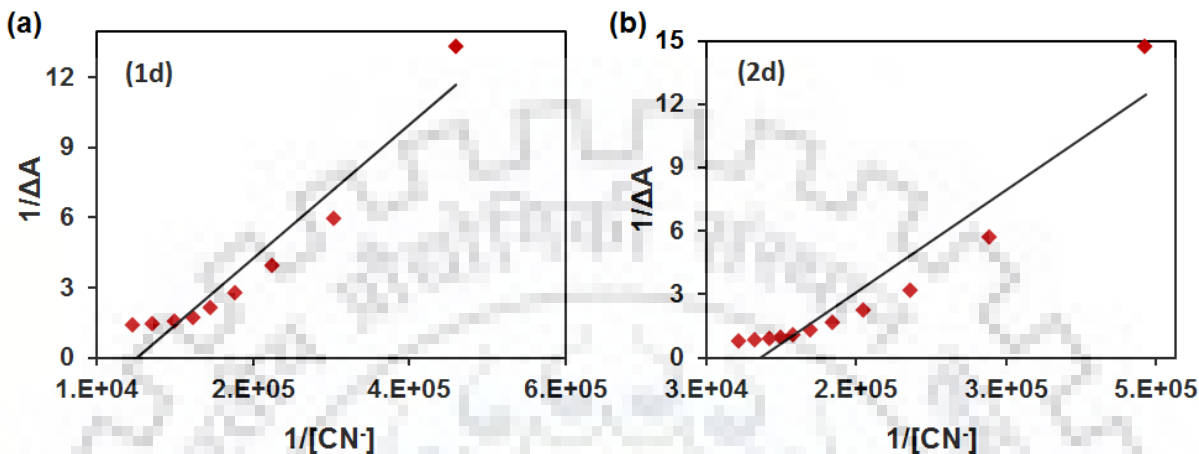


**Figure 27.** (a) Colorimetric Changes of **2a** with Tested Anions in Toluene at 298K (Top). UV-Visible Spectral Changes of **2a** Upon Addition of Excess of Anions (Bottom). (b) UV-Visible Spectral Titration of **2a** ( $1.05 \times 10^{-5}$  M) Upon Sequential Addition of Cyanide Ion in Toluene at 298 K. Inset Shows BH Plot between  $1/\Delta A$  and  $1/[CN^-]$ .

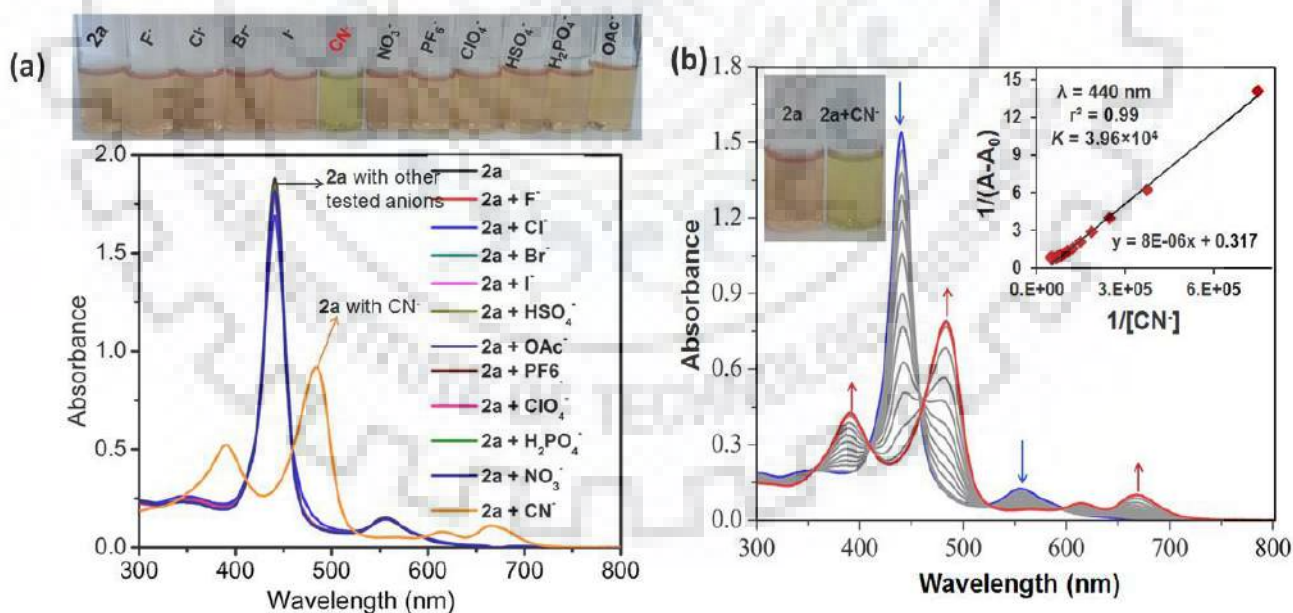




**Figure A28.** (s) DPV (in V vs Ag/ AgCl) Traces Recorded for **2a** and **2a.CN<sup>-</sup>** in CH<sub>2</sub>Cl<sub>2</sub> Containing 0.1 M TBAPF<sub>6</sub> with a Scan Rate of 0.1 V/s at 298 K. (b) The Ratiometric Absorbance Changes ( $A_{483}/A_{440}$ ) of **2a** ( $1.05 \times 10^{-5}$  M) on Addition of 2 eq. of CN<sup>-</sup> and 10 eq. of Other Anions.

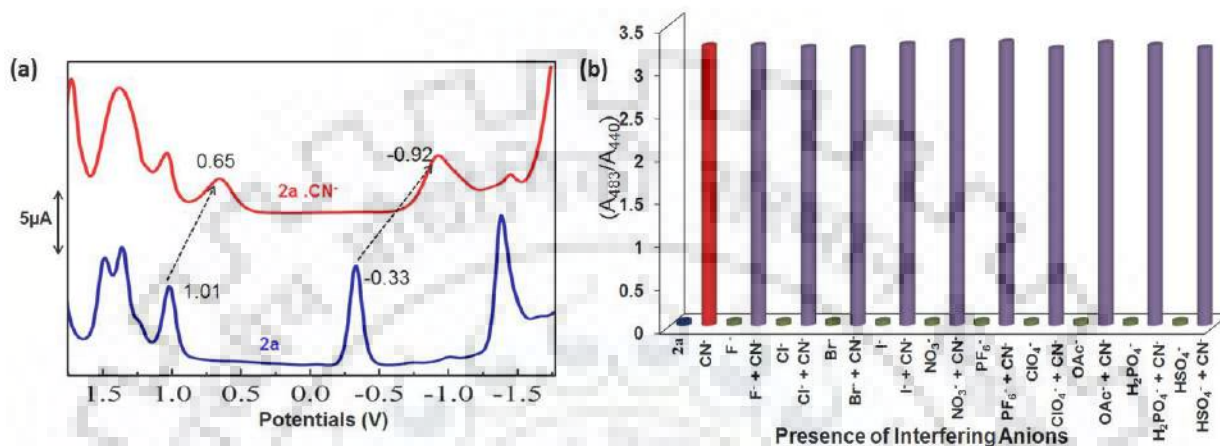


**Figure A29.** The Pictorial Representation of Frontier Molecular Orbitals of (a) CoTPPCl<sub>8</sub> (**2a**) (b) CoTPPCl<sub>8</sub>.CN<sup>-</sup> (**2a.CN<sup>-</sup>**).

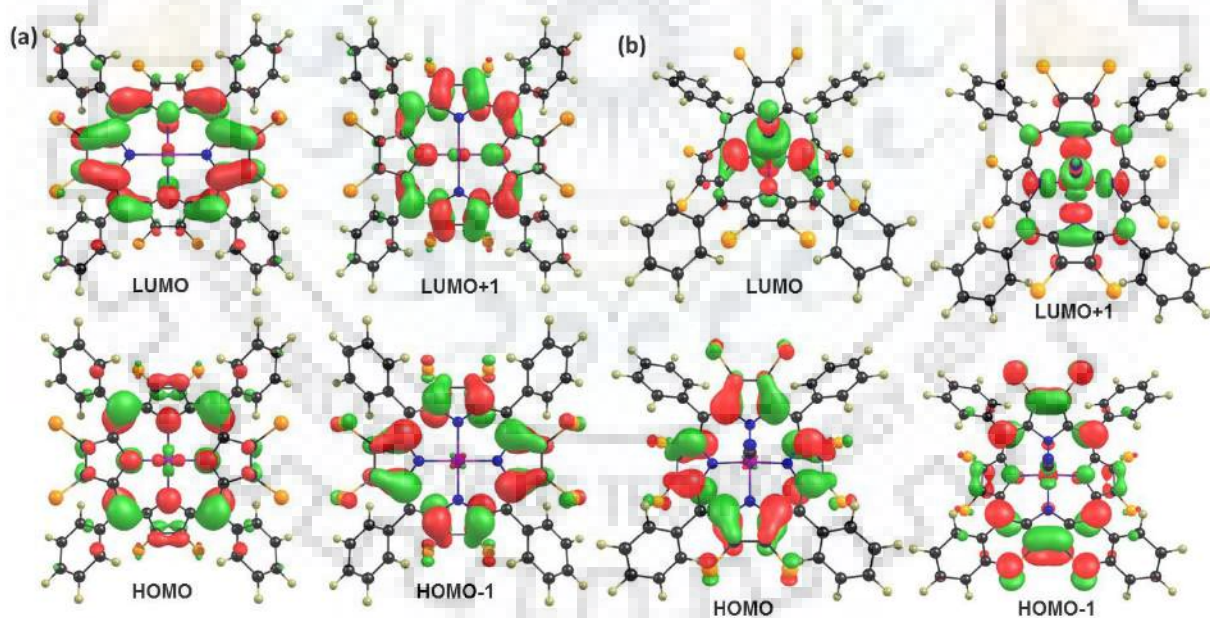


**Figure A30.** Theoretical UV-Visible Spectra of (a) **1a** and (b) **2a** Obtained by TD-DFT Calculations in Gas Phase.

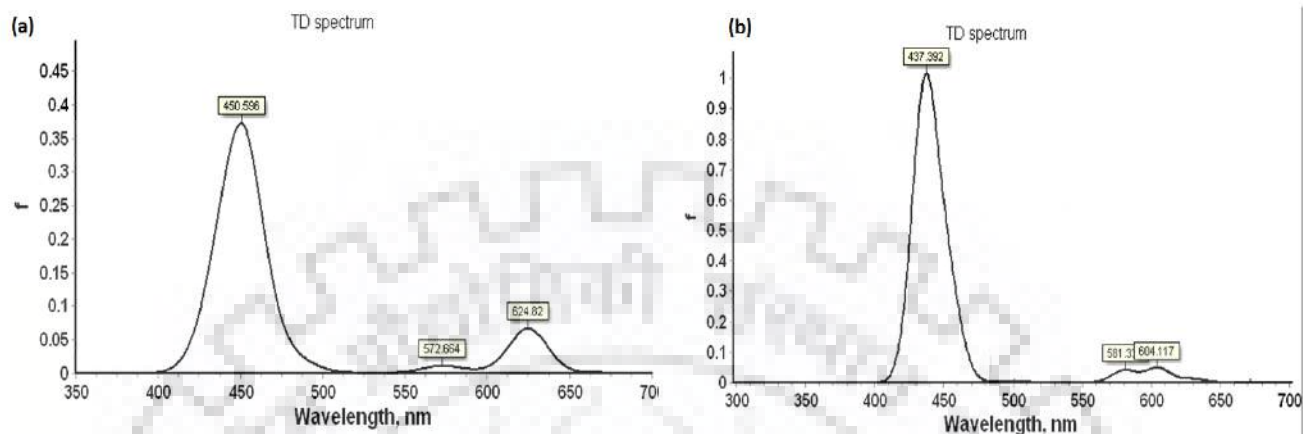


**Figure A31.** Experimental UV-Vis. Spectrum (a) and Theoretical UV-Vis. Spectrum (b) of  $\text{CoTPPCl}_8\cdot\text{CN}^-$  (**2a.CN**).

